frontiers | Research Topics

Plant cell wall in pathogenesis, parasitism and symbiosis, volume II

Edited by
Vincenzo Lionetti and Maïté Vicré

Published in
Frontiers in Plant Science

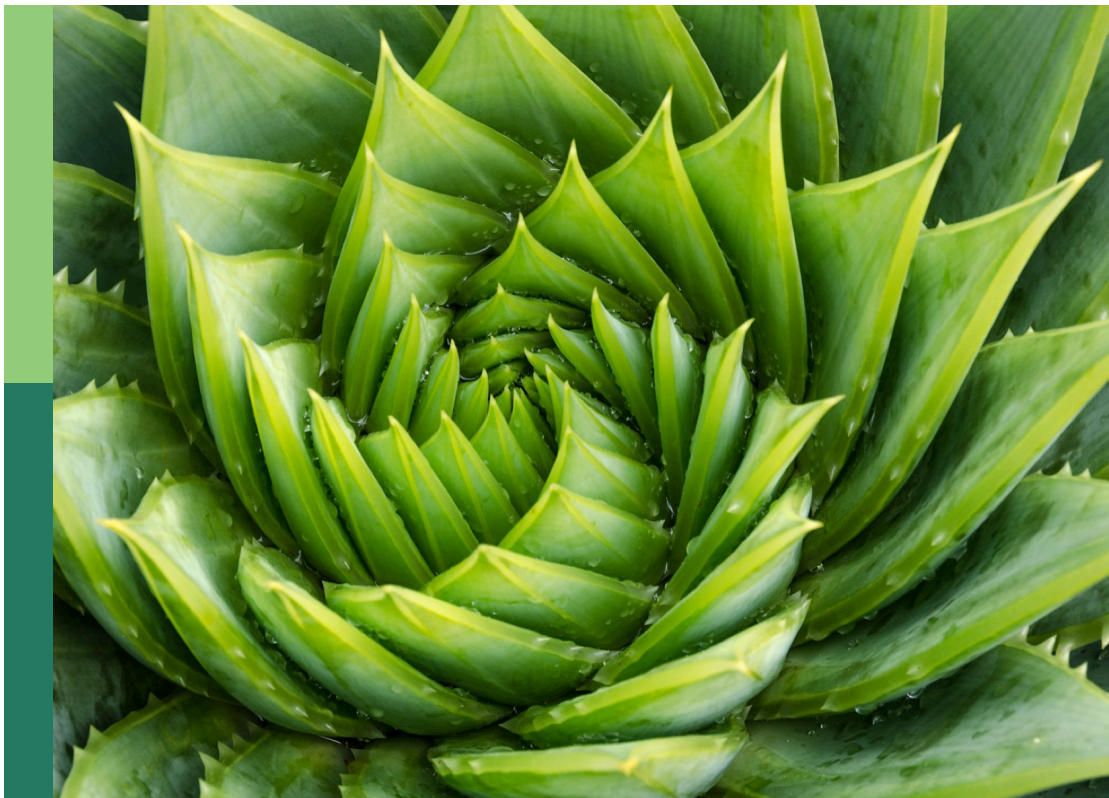

ISSN 1664-8714
ISBN 978-2-8325-2904-1
DOI 10.3389/978-2-8325-2904-1

About Frontiers

Frontiers is more than just an open access publisher of scholarly articles: it is a pioneering approach to the world of academia, radically improving the way scholarly research is managed. The grand vision of Frontiers is a world where all people have an equal opportunity to seek, share and generate knowledge. Frontiers provides immediate and permanent online open access to all its publications, but this alone is not enough to realize our grand goals.

Frontiers journal series

The Frontiers journal series is a multi-tier and interdisciplinary set of open-access, online journals, promising a paradigm shift from the current review, selection and dissemination processes in academic publishing. All Frontiers journals are driven by researchers for researchers; therefore, they constitute a service to the scholarly community. At the same time, the *Frontiers journal series* operates on a revolutionary invention, the tiered publishing system, initially addressing specific communities of scholars, and gradually climbing up to broader public understanding, thus serving the interests of the lay society, too.

Dedication to quality

Each Frontiers article is a landmark of the highest quality, thanks to genuinely collaborative interactions between authors and review editors, who include some of the world's best academicians. Research must be certified by peers before entering a stream of knowledge that may eventually reach the public - and shape society; therefore, Frontiers only applies the most rigorous and unbiased reviews. Frontiers revolutionizes research publishing by freely delivering the most outstanding research, evaluated with no bias from both the academic and social point of view. By applying the most advanced information technologies, Frontiers is catapulting scholarly publishing into a new generation.

What are Frontiers Research Topics?

Frontiers Research Topics are very popular trademarks of the *Frontiers journals series*: they are collections of at least ten articles, all centered on a particular subject. With their unique mix of varied contributions from Original Research to Review Articles, Frontiers Research Topics unify the most influential researchers, the latest key findings and historical advances in a hot research area.

Find out more on how to host your own Frontiers Research Topic or contribute to one as an author by contacting the Frontiers editorial office: frontiersin.org/about/contact

Plant cell wall in pathogenesis, parasitism and symbiosis, volume ii

Topic editors
Vincenzo Lionetti — Sapienza University of Rome, Italy
Maïté Vicré — Université de Rouen, France

Citation
Lionetti, V., Vicré, M., eds. (2023). *Plant cell wall in pathogenesis, parasitism and symbiosis, volume ii*. Lausanne: Frontiers Media SA.
doi: 10.3389/978-2-8325-2904-1

Table of contents

frontiers | Frontiers in Plant Science

TYPE Editorial
PUBLISHED 20 June 2023
DOI 10.3389/fpls.2023.1230438

OPEN ACCESS

EDITED AND REVIEWED BY
Prem Lal Kashyap,
Indian Institute of Wheat and Barley Research (ICAR), India

*CORRESPONDENCE
Vincenzo Lionetti
vincenzo.lionetti@uniroma1.it

RECEIVED 28 May 2023
ACCEPTED 06 June 2023
PUBLISHED 20 June 2023

CITATION
Vicré M and Lionetti V (2023) Editorial: Plant cell wall in pathogenesis, parasitism and symbiosis, Volume II.
Front. Plant Sci. 14:1230438.
doi: 10.3389/fpls.2023.1230438

Editorial: Plant cell wall in pathogenesis, parasitism and symbiosis, Volume II

Maïté Vicré[1] and Vincenzo Lionetti[2,3]*

[1]Univ Rouen Normandie, Laboratoire Glyco-MEV UR 4358, Rouen, France, [2]Dipartimento di Biologia e Biotecnologie "Charles Darwin", Sapienza Università di Roma, Rome, Italy, [3]Centro di Ricerca per le Scienze applicate alla Protezione dell'Ambiente e dei Beni Culturali (CIABC), Sapienza Università di Roma, Rome, Italy

KEYWORDS

cell wall remodeling, symbiosis, cell wall integrity, plant immunity, plant parasitism, plant cell wall

Editorial on the Research Topic
Plant cell wall in pathogenesis, parasitism and symbiosis, Volume II

A wide range of organisms that interact with plants must interface with the plant cell wall (CW) (Lionetti and Metraux, 2014). The view of the CW as only a static cellular barrier in these interactions is outdated. Cell wall polysaccharides, phenolic compounds, and proteins, in addition to regulating important growth and development processes, are also sources of elicitors that activate cell signaling pathways (Nguema-Ona et al., 2013). Surveillance mechanisms detect CW contacts with other organisms, and specific signaling pathways and responses are activated (Swaminathan et al., 2022) (Figure 1). During biotic interactions and abiotic stresses, the structure and composition of plant CW can be regulated at the biosynthetic level and through precise, continuous post-synthetic remodeling. As a consequence, the CW must be understood as a strategic space between organisms where intelligent and dynamic molecular strategies are implemented to overwhelm a fight or cooperate for specific physiological processes (Bacete et al., 2018; Castilleux et al., 2018; De Lorenzo et al., 2019).

Cell wall enzymes and their inhibitors play key roles in apoplastic metabolism (Rui and Dinneny, 2020). Invertases (INVs) and pectin methylesterases (PMEs) play essential roles in carbohydrate metabolism, stress responses, and sugar signaling (Bellincampi et al., 2014; Tauzin and Giardina, 2014; Del Corpo et al., 2020). In this collection, Coculo and Lionetti reviewed the roles of invertase inhibitors (INVI) and pectin methylesterase inhibitors (PMEI) belonging to the "Plant Invertase/Pectin Methylesterase Inhibitor Superfamily" (Lionetti et al., 2017). An updated overview of the specific activity of the characterized isoforms, their specific functions in plant physiology, and their applications in biotechnology is provided. After the pioneering work in 2007 (Lionetti et al., 2007), several piece of evidence supported the role of PMEIs in plant resistance to stresses (An et al., 2008; Liu et al., 2018). With a genome-wide analysis and transcriptomics of the *PMEI* genes in *Brassica napus*, Wang et al. identified several *BnPMEIs* as resistance gene candidates in response to *Sclerotinia sclerotiorum*, suggesting them as possible tools to breed new and improved genotypes more resistant to *Sclerotinia* stem rot.

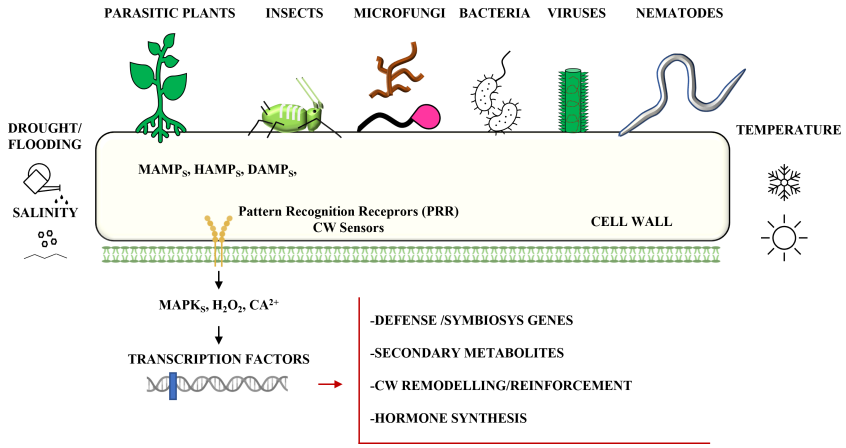

FIGURE 1
Schematic representation of the main systems of perception and responses related to the plant cell wall (CW) in the different biotic interactions. CW can play a central role in combined biotic and abiotic stress. Symbiont-induced CW modifications can improve plant development, nutrition, and tolerance to abiotic stresses. Abiotic stresses can alter CW composition, affecting efficient parasitism. M/H/DAMPS=Microbe/Herbivore/Damage Associated Molecular Patterns.

Specific CW changes can occur in the vicinity of plasmodesmata during viral infection (Lionetti et al., 2015; Stavolone and Lionetti, 2017). Viruses can modify pectin, callose, and structural proteins near plasmodesmata by increasing their size exclusion limit (Kozieł et al., 2021). López-González et al. addressed the little-explored impact of virus infections on secondary CW and plant development. The authors found a correlation between the developmental alterations induced in Arabidopsis by specific strains of turnip mosaic virus and specific changes in xylan and lignin biosynthesis. Although callose deposition is a response to both elicitors and pathogens, the mechanisms involved in its biosynthesis and degradation remain to be unraveled (German et al., 2023). Li et al. summarized the research progress on plant callose and its synthesizing enzymes in plant physiology.

Microfungi are also important etiological agents for plants (Doehlemann et al., 2017). The fungal pathogen *Sphaerulina musiva* causes stem canker with the consequent mortality of Populus trees. *Populus deltoides* can induce a lignified periderm to contain the pathogen, but the precise characterization of lignin changes in response to *S. musiva* infection is unknown. Bryant et al.identified a higher syringyl:guaiacil ratio, a higher Klason lignin content and lower p-hydroxybenzoate content in Septoria-infected *P. deltoides* trees compared to the healthy plant. This knowledge can favor biotechnological approaches aimed at improving the resilience and increasing the biomass yield of Populus for biofuel production.

Interesting contributions in this collection concern plant-parasite interactions. A fine-tuned re-arrangement of host CW is induced in response to infection by both plant-parasitic cyst nematodes and root-knot nematodes (Zhang et al., 2017; Bozbuga et al., 2018; Meidani et al., 2019). Veronico et al. found that drought stress affects CW metabolism in tomato roots, limiting feeding site development and reproduction of the nematode *Meloidogyne incognita*. Parasitic plants, such as Cuscuta species, severely damage economically important crops (Jhu and Sinha, 2022). These green parasites absorb resources through an invasive organ called the haustorium, which differentiates into vascular hyphae that establish a connection with the host plant's vasculature. The degradation and modification of host CWs allow haustorium to effectively invade host tissues. Yokoyama et al. propose that *Cuscuta campestris* APETALA2/ETHYLENE RESPONSE FACTORS (ERFs) can activate the transcription of the CW enzymatic genes in haustorium to favor its invasion of tobacco and *Arabidopsis* plants.

Plant CW is a field of molecular dialogues and agreements with symbiotic microbes to establish intimate interfaces for developmental coordination and nutrient exchange (Balestrini and Bonfante, 2014). Plants can establish mutualistic symbiosis with arbuscular mycorrhizal fungi, and phosphorus transfer across the CW specialized interfacial compartment is an important process in the mycorrhizal pathway (Begum et al., 2019). Exploiting the *Rhizophagus irregularis-Lotus japonicus* interaction, Nguyen and Saito showed that polyphosphate in fungal CWs and apoplastic phosphatases play an important role in phosphorus transfer at the symbiotic interface in arbuscules. Mycorrhizal fungi can be involved in mutualistic interactions during orchid seed germination (Põlme et al., 2018). Chen et al. identified several genes codifying CW structural proteins such as epidermis-specific secreted glycoprotein, proline-rich receptor-like protein, and leucine-rich repeat (LRR) extensin-like protein, which are particularly involved in the symbiosis of Tulasnella and Serendipita fungi with *Dendrobium officinale*.

Bioinoculants represent an environmentally-friendly agricultural practice to alleviate drought stress in crops (Kour et al., 2022). The work presented by Wilmowitz et al. indicates that the inoculation of maize seeds with *Glomus* sp. and *Bacillus* sp. can help to cope with drought stress, preventing inhibition of photosynthesis and disruption of redox balance. *Glomus* sp. and *Bacillus* sp. can modify pectin methylesterification and hemicellulose content of maize leaves, possibly leading to alleviation of the negative effects of drought.

These important contributions advance our understanding of the relationships between plants and the environment at the CW interface, which will be helpful to engineer biotechnological strategies for agriculture and bioenergy fields. As a closing remark, we are grateful to the authors and reviewers for their invaluable contributions to this Research Topic.

Author contributions

VL draft the editorial text. MV revised and approved the final version of the editorial. All authors approved the submitted version.

Funding

The research was supported by Sapienza University of Rome, Grants RM120172B78CFDF2, RM11916B7A142CF1, RG12117A898EABE0, RM122181424F1F42 and - Rome Technopole" - European Union Next-GenerationEU PNRR -RT12218451D2C509 to VL.

Conflict of interest

The authors declare that the research was conducted in the absence of any commercial or financial relationships that could be construed as a potential conflict of interest.

Publisher's note

References

An, S. H., Sohn, K. H., Choi, H. W., Hwang, I. S., Lee, S. C., and Hwang, B. K. (2008). Pepper pectin methylesterase inhibitor protein CaPMEI1 is required for antifungal activity, basal disease resistance and abiotic stress tolerance. *Planta* 228, 61–78. doi: 10.1007/s00425-008-0719-z

Bacete, L., Mélida, H., Miedes, E., and Molina, A. (2018). Plant cell wall-mediated immunity: cell wall changes trigger disease resistance responses. *Plant J.* 93, 614–636. doi: 10.1111/tpj.13807

Balestrini, R., and Bonfante, P. (2014). Cell wall remodeling in mycorrhizal symbiosis: a way towards biotrophism. *Front.Plant Sci.* 5. doi: 10.3389/fpls.2014.00237

Begum, N., Qin, C., Ahanger, M. A., Raza, S., Khan, M. I., Ashraf, M., et al. (2019). Role of arbuscular mycorrhizal fungi in plant growth regulation: implications in abiotic stress tolerance. *Front. Plant Sci.* 10. doi: 10.3389/fpls.2019.01068

Bellincampi, D., Cervone, F., and Lionetti, V. (2014). Plant cell wall dynamics and wall-related susceptibility in plant-pathogen interactions. *Front.Plant Sci.* 5, 228. doi: 10.3389/fpls.2014.00228

Bozbuga, R., Lilley, C. J., Knox, J. P., and Urwin, P. E. (2018). Host-specific signatures of the cell wall changes induced by the plant parasitic nematode, meloidogyne incognita. *Sci. Rep.* 8, 17302. doi: 10.1038/s41598-018-35529-7

Castilleux, R., Plancot, B., Ropitaux, M., Carreras, A., Leprince, J., Boulogne, I., et al. (2018). Cell wall extensins in root–microbe interactions and root secretions. *J. Exp. Bot.* 69, 4235–4247. doi: 10.1093/jxb/ery238

Del Corpo, D., Fullone, M. R., Miele, R., Lafond, M., Pontiggia, D., Grisel, S., et al. (2020). AtPME17 is a functional arabidopsis thaliana pectin methylesterase regulated by its PRO region that triggers PME activity in the resistance to botrytis cinerea. *Mol. Plant Pathol.* 21, 1620–1633. doi: 10.1111/mpp.13002

De Lorenzo, G., Ferrari, S., Giovannoni, M., Mattei, B., and Cervone, F. (2019). Cell wall traits that influence plant development, immunity, and bioconversion. *Plant J.* 97, 134–147. doi: 10.1111/tpj.14196

Doehlemann, G., Ökmen, B., Zhu, W., and Sharon, A. (2017). Plant pathogenic fungi. *Microbiol. Spectr.* 5, 5.1.14. doi: 10.1128/microbiolspec.FUNK-0023-2016

German, L., Yeshvekar, R., and Benitez-Alfonso, Y. (2023). Callose metabolism and the regulation of cell walls and plasmodesmata during plant mutualistic and pathogenic interactions. *Plant Cell Environ.* 46, 391–404. doi: 10.1111/pce.14510

Jhu, M.-Y., and Sinha, N. R. (2022). Parasitic plants: an overview of mechanisms by which plants perceive and respond to parasites. *Annu. Rev. Plant Biol.* 73, 433–455. doi: 10.1146/annurev-arplant-102820-100635

Kour, D., Khan, S. S., Kaur, T., Kour, H., Singh, G., Yadav, A., et al. (2022). Drought adaptive microbes as bioinoculants for the horticultural crops. *Heliyon* 8, e09493. doi: 10.1016/j.heliyon.2022.e09493

Kozieł, E., Otulak-Kozieł, K., and Bujarski, J. J. (2021). Plant cell wall as a key player during resistant and susceptible plant-virus interactions. *Front. Microbiol.* 12. doi: 10.3389/fmicb.2021.656809

Lionetti, V., Fabri, E., De Caroli, M., Hansen, A. R., Willats, W. G. T., Piro, G., et al. (2017). Three pectin methylesterase inhibitors protect cell wall integrity for arabidopsis immunity to botrytis. *Plant Physiol.* 173, 1844–1863. doi: 10.1104/pp.16.01185

Lionetti, V., and Metraux, J. P. (2014). Plant cell wall in pathogenesis, parasitism and symbiosis. *Front.Plant Sci.* 5. doi: 10.3389/fpls.2014.00612

Lionetti, V., Raiola, A., Camardella, L., Giovane, A., Obel, N., Pauly, M., et al. (2007). Overexpression of pectin methylesterase inhibitors in arabidopsis restricts fungal infection by botrytis cinerea. *Plant Physiol.* 143, 1871–1880. doi: 10.1104/pp.106.090803

Lionetti, V., Raiola, A., Cervone, F., and Bellincampi, D. (2015). How do pectin methylesterases and their inhibitors affect the spreading of tobamovirus? *Plant Signal.Behav.* 9, e972863. doi: 10.4161/15592316.2014.972863

Liu, N., Sun, Y., Pei, Y., Zhang, X., Wang, P., Li, X., et al. (2018). A pectin methylesterase inhibitor enhances resistance to verticillium Wilt1[OPEN]. *Plant Physiol.* 176, 2202–2220. doi: 10.1104/pp.17.01399

Meidani, C., Ntalli, N. G., Giannoutsou, E., and Adamakis, I.-D. S. (2019). Cell wall modifications in giant cells induced by the plant parasitic nematode meloidogyne incognita in wild-type (Col-0) and the fra2 arabidopsis thaliana katanin mutant. *Int. J. Mol. Sci.* 20, 5465. doi: 10.3390/ijms20215465

Nguema-Ona, E., Vicré-Gibouin, M., Cannesan, M.-A., and Driouich, A. (2013). Arabinogalactan proteins in root-microbe interactions. *Trends Plant Sci.* 18, 440–449. doi: 10.1016/j.tplants.2013.03.006

Põlme, S., Bahram, M., Jacquemyn, H., Kennedy, P., Kohout, P., Moora, M., et al. (2018). Host preference and network properties in biotrophic plant-fungal associations. *New Phytol.* 217, 1230–1239. doi: 10.1111/nph.14895

Rui, Y., and Dinneny, J. R. (2020). A wall with integrity: surveillance and maintenance of the plant cell wall under stress. *New Phytol.* 225, 1428–1439. doi: 10.1111/nph.16166

Stavolone, L., and Lionetti, V. (2017). Extracellular matrix in plants and animals: hooks and locks for viruses. *Front. Microbiol.* 8. doi: 10.3389/fmicb.2017.01760

Swaminathan, S., Lionetti, V., and Zabotina, O. A. (2022). Plant cell wall integrity perturbations and priming for defense. *Plants* 11, 3539. doi: 10.3390/plants11243539

Tauzin, A. S., and Giardina, T. (2014). Sucrose and invertases, a part of the plant defense response to the biotic stresses. *Front.Plant Sci.* 5. doi: 10.3389/fpls.2014.00293

Zhang, L., Lilley, C. J., Imren, M., Knox, J. P., and Urwin, P. E. (2017). The complex cell wall composition of syncytia induced by plant parasitic cyst nematodes reflects both function and host plant. *Front. Plant Sci.* 8. doi: 10.3389/fpls.2017.01087

frontiers in Plant Science

ORIGINAL RESEARCH
published: 20 September 2021
doi: 10.3389/fpls.2021.725939

Role of Cell Wall Polyphosphates in Phosphorus Transfer at the Arbuscular Interface in Mycorrhizas

Cuc Thi Nguyen[1,2] *and Katsuharu Saito*[1]*

[1]*Department of Bioscience and Food Production Science, Interdisciplinary Graduate School of Science and Technology, Shinshu University, Nagano, Japan,* [2]*Faculty of Agriculture and Forestry, Dalat University, Dalat, Vietnam*

Arbuscular mycorrhizal fungi provide plants with soil mineral nutrients, particularly phosphorus. In this symbiotic association, the arbuscular interface is the main site for nutrient exchange. To understand phosphorus transfer at the interface, we analyzed the subcellular localization of polyphosphate (polyP) in mature arbuscules of *Rhizophagus irregularis* colonizing roots of *Lotus japonicus* wild-type (WT) and H^+-ATPase *ha1-1* mutant, which is defective in phosphorus acquisition through the mycorrhizal pathway. In both, the WT and the *ha1-1* mutant, polyP accumulated in the cell walls of trunk hyphae and inside fine branch modules close to the trunk hyphae. However, many fine branches lacked polyP. In the mutant, most fine branch modules showed polyP signals compared to the WT. Notably, polyP was also observed in the cell walls of some fine branches formed in the *ha1-1* mutant, indicating phosphorus release from fungal cells to the apoplastic regions. Intense acid phosphatase (ACP) activity was detected in the periarbuscular spaces around the fine branches. Furthermore, double staining of ACP activity and polyP revealed that these had contrasting distribution patterns in arbuscules. These observations suggest that polyP in fungal cell walls and apoplastic phosphatases may play an important role in phosphorus transfer at the symbiotic interface in arbuscules.

Keywords: arbuscular mycorrhizal fungi, arbuscule, acid phosphatase, cell wall, H^+-ATPase, periarbuscular space, polyphosphate, two-compartment system

OPEN ACCESS

Edited by:
Juan Manuel Ruiz-Lozano, Consejo Superior de Investigaciones Científicas (CSIC), Spain

Reviewed by:
Qiang-Sheng Wu, Yangtze University, China
Tatsuhiro Ezawa, Hokkaido University, Japan

***Correspondence:**
Katsuharu Saito
saitok@shinshu-u.ac.jp

Specialty section:
This article was submitted to Plant Symbiotic Interactions, a section of the journal Frontiers in Plant Science

Received: *16 June 2021*
Accepted: *20 August 2021*
Published: *20 September 2021*

Citation:
Nguyen CT and Saito K (2021) Role of Cell Wall Polyphosphates in Phosphorus Transfer at the Arbuscular Interface in Mycorrhizas. Front. Plant Sci. 12:725939. doi: 10.3389/fpls.2021.725939

INTRODUCTION

Phosphorus is a crucial element for plant growth and development. Terrestrial plants absorb P as orthophosphate (Pi) from the soil solution. However, soil Pi is mainly present in immobile forms that are not directly available to plants (Pierzynski et al., 2005). Plants have evolved several mechanisms to overcome Pi-deficient conditions. One of the oldest adaptive strategies include formation of mutualistic symbiosis with arbuscular mycorrhizal (AM) fungi (Raghothama, 1999; Delaux et al., 2015; Field and Pressel, 2018). During symbiosis, host plants can acquire soil Pi *via* two pathways, the mycorrhizal pathway and the direct pathway. The mycorrhizal pathway is a route *via* AM fungal hyphae (Smith et al., 2003, 2011). In the direct pathway, Pi is directly taken up by plant roots. The mycorrhizal pathway is usually activated even in non-responsive AM plants, for which AM fungal colonization does not positively affect growth or P nutrition (Smith et al., 2003, 2004). The overall flow of P through the mycorrhizal

pathway includes: (1) P uptake from soil by AM fungal extraradical hyphae that extend far beyond the P depletion zone surrounding the root system; (2) long-distance P translocation through extraradical and intraradical hyphae; (3) P release from arbuscules that are the highly branched fungal structure formed in root cortical cell; and (4) P transfer into the host plant cells (Saito and Ezawa, 2016; Ezawa and Saito, 2018).

AM fungi absorb Pi from soil through the Pi transporters localized on the plasma membrane of extraradical hyphae (Harrison and van Buuren, 1995; Maldonado-Mendoza et al., 2001; Benedetto et al., 2005; Fiorilli et al., 2013; Xie et al., 2016). The Pi taken up is rapidly converted into polyphosphate (polyP) that is sequestered into tubular vacuoles (Rasmussen et al., 2000; Uetake et al., 2002; Ezawa et al., 2004; Viereck et al., 2004; Kuga et al., 2008; Hijikata et al., 2010; Kikuchi et al., 2014, 2016; Nayuki et al., 2014). PolyP is a linear polymer of Pi linked by high-energy phosphoanhydride bonds and likely to be synthesized by the vacuolar transporter chaperone (VTC) complex consisted of subunits VTC1, VTC2, and VTC4 using ATP as substrate (Tani et al., 2009; Tisserant et al., 2012; Kikuchi et al., 2014; Ezawa and Saito, 2018). P translocation in extraradical hyphae is bidirectional. However, the net flow of P toward intraradical hyphae that are the main sink for P (Nielsen et al., 2002; Viereck et al., 2004; Hijikata et al., 2010). A water potential gradient in AM fungal hyphae has been proposed as a driving force for long-distance translocation of P (Kikuchi et al., 2016). Once polyP is delivered to the intraradical hyphae, its chain length is shortened (Solaiman et al., 1999; Viereck et al., 2004; Ohtomo and Saito, 2005; Takanishi et al., 2009) in a reaction possibly catalyzed by fungal endopolyphosphatases. This depolymerized polyP in arbuscules may be a significant source of P for host plants (Solaiman and Saito, 2001; Takanishi et al., 2009). There is no doubt that arbuscules play a vital role in P supply through P release from fungal cells. However, the mechanism of P export from arbuscules remains unclear.

Conversely, the molecular mechanisms underlying plant's uptake of Pi released from arbuscules are well documented. Plant Pi transporter genes that are upregulated during AM symbiosis have been identified in many plant species reviewed in Chiu and Paszkowski (2019). In particular, the AM-specific transporter genes of the *Medicago truncatula PT4*/*Oryza sativa PT11* clade are conserved in all AM vascular plants (Yang et al., 2012; Delaux et al., 2015) and are strongly expressed in arbuscule-containing cortical cells (Harrison et al., 2002; Glassop et al., 2005; Nagy et al., 2005; Yang et al., 2012). Arbuscules are surrounded by host-derived periarbuscular membrane (PAM; Smith and Smith, 1990, 2011; Harrison, 1999) with localized MtPT4/OsPT11 proteins (Harrison et al., 2002; Kobae and Hata, 2010; Pumplin et al., 2012). Mutation of *MtPT4*, *OsPT11*, and their orthologs severely impairs symbiotic Pi uptake, indicating that AM-specific Pi transporters play a central role in the mycorrhizal pathway (Javot et al., 2007; Yang et al., 2012; Willmann et al., 2013; Xie et al., 2013; Watts-Williams et al., 2015). These Pi transporters are classified as H^+/Pi symporters and require H^+ electrochemical potential gradient across the PAM for Pi uptake from an apoplastic interface between the plant and fungus, the periarbuscular space (PAS), into a plant cell. PAS is an acidified compartment (Guttenberger, 2000) in which H^+-ATPase activity has been observed (Marx et al., 1982; Gianinazzi-Pearson et al., 1991). The *Medicago* HA1, rice HA1, and tomato HA8 proteins have been identified as AM-specific H^+-ATPases that are responsible for generating the H^+ gradient across PAS, contributing to symbiotic Pi uptake by AM-specific Pi transporters (Krajinski et al., 2014; Wang et al., 2014; Liu et al., 2020).

P release from AM fungus to PAS in arbuscule-containing cortical cells is a critical step in the mycorrhizal pathway. Mathematical modeling of AM fungus-plant nutrient exchange dynamics predicts that P is exported as Pi by fungal H^+-coupled Pi transporters localized in the plasma membrane of arbuscules (Schott et al., 2016; Dreyer et al., 2018). H^+-coupled Pi transporters expressed in intraradical hyphae have indeed been identified in AM fungi (Balestrini et al., 2007; Fiorilli et al., 2013; Xie et al., 2016). However, no evidence was found for Pi efflux into the PAS *via* these transporters. Ezawa and Saito (2018) postulated the involvement of the AM fungal SYG proteins (named after suppressor of yeast gpa1) in P release from arbuscules based on evidence that animal and plant SYG homologs mediate Pi export (Arpat et al., 2012; Giovannini et al., 2013). An alternative hypothesis is that polyP is directly exported to interfacial apoplasts around arbuscules (Saito and Ezawa, 2016). This hypothesis is supported by the observation that polyP is distributed in the cell walls of germ tubes and extraradical hyphae of AM fungi (Werner et al., 2007; Kuga et al., 2008). However, the precise distribution of polyP in arbuscules remains unclear. In this study, we determined the subcellular localization of polyP in arbuscules using 4′,6-diamidino-2-phenylindole (DAPI) staining (Tijssen et al., 1982) and by enzyme-affinity labeling with the polyP binding domain (PPBD) of *Escherichia coli* exopolyphosphatase PPX1 (Saito et al., 2005) to elucidate the role of polyP in P transfer at the symbiotic interface. In this analysis, we used *Lotus japonicus* with an AM-specific H^+-ATPase *HA1* mutation to analyze P dynamics in mature arbuscules. *Medicago*, rice, and tomato *ha1* mutants, similar to the *pt4*/*pt11* mutants, show a decrease in mature arbuscules due to degeneration of premature arbuscules (Krajinski et al., 2014; Wang et al., 2014; Liu et al., 2020). However, there is considerable variation in phenotype depending on the plant species and mutant alleles. Here, we analyzed polyP distribution in the *L. japonicus ha1-1* mutant that shows a relatively mild defect in arbuscule formation.

MATERIALS AND METHODS

Biological Materials and Growth Conditions

The *L. japonicus* homozygous *ha1-1* mutant line with a *LORE1* insertion in the *HA1* gene (gene ID: LotjaGi3g1v0066100.1 in the Lotus Base Gifu v1.2) and the wild-type (WT) segregant were selected from a heterozygous *LORE1* insertion line (plant ID: 30006854) that was obtained from Lotus Base.[1]

[1]https://lotus.au.dk/

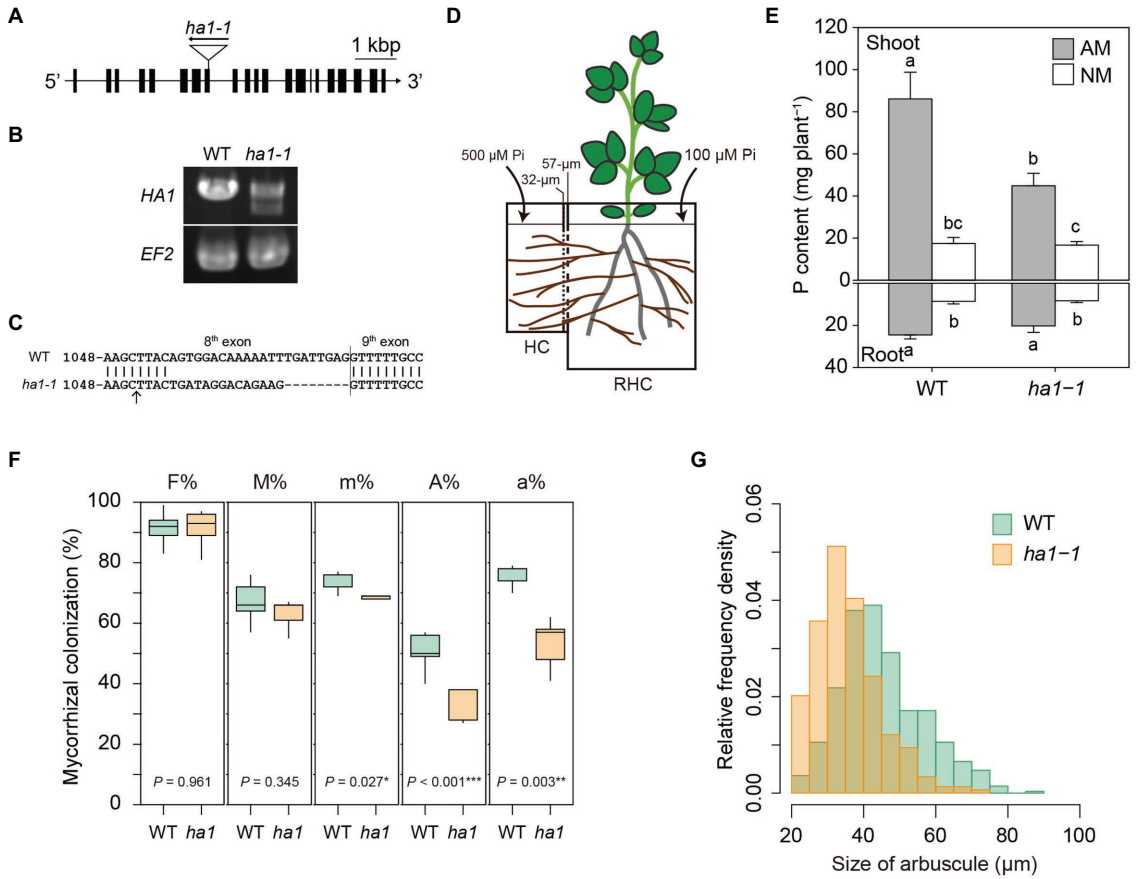

FIGURE 1 | Phenotype of the *ha1-1* mutant cultivated in the two-compartment system. **(A)** Exon-intron structure of the *HA1* gene, including the *ha1-1 LORE1* insertion site. **(B)** RT-PCR analysis of *HA1* in wild-type (WT) and *ha1-1* roots colonized by *Rhizophagus irregularis*. The elongation factor 2 (*EF2*) gene was amplified as the loading control. PCR was performed using 10 ng of cDNA as a template with 35 cycles. Similar results were obtained in three independent experiments. **(C)** Sequence comparison between WT and the *ha1-1 HA1* cDNAs showing frameshift indels in the *ha1-1* mutant transcript. The arrow indicates the *LORE1* insertion site. **(D)** The two-compartment system: the root-hyphal (RHC) and hyphal (HC) compartments were separated by 32- and 57-µM nylon meshes, allowing only hyphae of arbuscular mycorrhizal fungi to pass into the HC. The compartments were filled with autoclaved river sand. RHC was supplied with a half-strength Hoagland's solution containing a low phosphate (Pi) concentration (100 µM). HC was supplied with a nutrient solution with a high (500 µM) concentration of phosphate. **(E)** P content in shoots and roots of arbuscular mycorrhizal (AM) and non-mycorrhizal (NM) plants 4 weeks after inoculation. Error bars show SE ($n = 5$). For each plant part, bars topped by the same letter do not differ significantly at $p < 0.05$ on Tukey's multiple comparisons test. **(F)** Arbuscular mycorrhizal fungal colonization in WT and *ha1-1* roots. Mycorrhizal colonization was assessed according to method suggested by Trouvelot et al. (1986) after trypan blue staining. F%, frequency of mycorrhiza in the root system; M%, intensity of mycorrhizal colonization in the root system; m%, intensity of mycorrhizal colonization in the root fragments; A%, arbuscule abundance in the root system; and a%, arbuscule abundance in mycorrhizal parts of root fragments. The boxes show the first quartile, the median, and the third quartile; the whiskers reach 1.5 times the interquartile range ($n = 5$). p-values are based on Student's t-tests (*, $p < 0.05$; *, $p < 0.01$; **, $p < 0.001$). **(G)** Relative frequency density of arbuscule size. The lengths of the major axis of 549 WT and 297 *ha1-1* arbuscules randomly selected from >20 µM-long arbuscules stained with wheat germ agglutinin conjugated with Oregon Green 488 were measured. According to the two-sample Kolmogorov–Smirnov test, the size distribution was significantly different between the plant genotypes ($p < 0.001$).

Genotyping was performed using *HA1*-specific primers (**Supplementary Table S1**) combined with the P2 internal *LORE1* primer (Fukai et al., 2012; Urbański et al., 2012). A two-compartment culture system consisting of root-hyphal (RHC) and hyphal (HC) compartments was used to cultivate plants (**Figure 1**). The two compartments were separated by a three-layered barrier (Kobae et al., 2014) comprising an RHC filter (57 µM opening), a medial mesh (1 mM in thickness; 2 mM opening), and an HC filter (32 µM opening), which prevented plant roots from passing through but allowed AM fungal hyphae to pass. The compartments were filled with autoclaved river sand (particle size, 0.5–2.0 mM). *L. japonicus* seeds were surface sterilized with a hypochlorite solution, sown on a wetted filter paper in a Petri dish, and germinated at 26°C for 2 days in dark and 3 days in light. Seedlings were transplanted to RHC and inoculated with 500 spores of *Rhizophagus irregularis* DAOM 197198 (Mycorise, Premier Tech, Rivière-du-Loup, Canada) per plant. The inoculated and non-inoculated plants were grown in a growth chamber (photoperiod: 16 h, temperature: 26°C, and photosynthetic photon flux density: 150 µMol m^{-2} s^{-1}) for 4 weeks. RHC was supplied with a half-strength Hoagland's solution containing a low concentration of KH_2PO_4 (100 µM)

every 2 days to promote AM colonization. HC was provided with a high-nutrient solution with 500 μM KH_2PO_4 to enhance P translocation from the HC *via* AM fungal hyphae. The amount of applied fertilizer that did not flow from the HC into the RHC was determined before cultivation.

Cryostat Sectioning

Fresh mycorrhizal roots from at least three independent plants were cut into 5–10 mM fragments, placed in plastic molds, and covered with the O.C.T. compound (Sakura Finetek, Tokyo, Japan). The roots were frozen in dry ice-isopentane and stored at −80°C. The frozen roots were sectioned longitudinally at a thickness of 25–30 μM using a cryostat (Leica, Wetzlar, Germany). Cryosections were placed on an adhesive glass slide (Frontier, Matsunami, Osaka, Japan) and dried at room temperature for 60 min. These sections were used for DAPI staining and enzyme cytochemistry of phosphatase activity.

High-Pressure Freezing and Freeze-Substitution

Mycorrhizal roots from at least three independent plants of each genotype were cut into 5 mM fragments using a razor blade in a Petri dish on ice. The root fragments were placed in aluminum specimen carriers with 0.05 M sucrose as a cryoprotectant and then frozen using a Leica EM PACT2 high-pressure freezer. The frozen samples were temporarily maintained in liquid nitrogen and transferred into vials containing 1% glutaraldehyde in anhydrous acetone that was precooled to −80°C. The samples were freeze-substituted at −80°C for 48 h and gradually warmed to 4°C over a period of 21 h using a Leica EM AFS2. Roots were washed twice with anhydrous acetone for 15 min and twice with propylene oxide for 5 min at room temperature. The samples were infiltrated with Spurr's resin: propylene oxide mixture of ratios 1:2, 1:1, 2:1, 3:1, and 4:1 for 1 h in each mixture sequentially (Spurr's resin from Polysciences, PA, United States). Final soak was thrice in pure resin for 3 h, and samples were polymerized at 70°C for 12 h. The embedded roots were trimmed and sectioned longitudinally using an ultramicrotome. For fluorescence microscopy, semithin sections, approximately 200 nm thick, were cut with a knife (XAC, SYNTEC, Yokohama, Japan) and placed on an adhesive glass slide. For transmission electron microscopy (TEM), ultrathin sections of approximately 90 nm thickness were cut with a diamond knife (DiATOME, PA, United States) and picked up on nickel grids. These sections were immediately processed for polyP labeling.

PolyP Detection by DAPI Staining

Cryosections of fresh roots and semithin sections of resin-embedded roots were used for DAPI staining. Cryosections were washed gently with 70% ethanol, 25% ethanol, and distilled water (DW) sequentially for 3 min in each solution. Semithin sections were etched with 0.2% sodium ethoxide in ethanol for 5 min and then washed twice with 100% ethanol, 70% ethanol, and 25% ethanol sequentially for 3 min in each solution. Root samples were stained with 80 μg ml^{-1} DAPI in 70% ethanol for 60 min at room temperature in the dark. After washing with 70% ethanol and DW, the sections were mounted in DW and observed within 1 h. Fluorescence microscopy was performed using an Axio Imager D1 microscope (Carl Zeiss, Jena, Germany). DAPI-polyP fluorescence was excited with UV light, and the emitted fluorescence was detected using a long-pass filter, LP420. Digital images were captured with a digital CCD camera (AxioCam MRc5, Carl Zeiss) operated with AxioVision (Carl Zeiss). After randomly selecting images of mature arbuscules, the areas showing the DAPI-polyP signal in the arbuscules were measured using ImageJ software (Schneider et al., 2012).

PolyP Detection by Enzyme Affinity Labeling With PPBD

PolyP labeling using *E. coli* PPBD was performed according to the method described by Saito et al. (2005) and Kuga et al. (2008) with some modifications. For fluorescence microscopy, semithin sections of the resin-embedded roots were etched with 0.2% sodium ethoxide in ethanol for 5 min and then washed with 0.05% sodium ethoxide followed by 100% ethanol, 50% ethanol, and DW wash. The sections were blocked with 1% bovine serum albumin (BSA) in Tris-buffered saline (TBS) containing low concentrations of salts (TBS-low salt; 25 mM Tris-HCl pH 7.4, 13.7 mM sodium chloride, and 0.27 mM potassium chloride) for 10 min. Sections were first incubated in a mixture of 20 μg ml^{-1} PPBD, 10 μg ml^{-1} mouse anti-Xpress epitope antibody (#R910-25, Thermo Fisher Scientific, MA, United States), TBS-low salt, and 1% BSA for 2 h at room temperature. The sections were then washed with TBS-low salt buffer containing 0.05% Triton X-100, followed by TBS-low salt. Samples were incubated with a goat anti-mouse IgG antibody conjugated with Alexa Fluor 488 (#A28175, Thermo Fisher Scientific) diluted to ratio 1:100 in TBS-low salt containing 1% BSA for 1 h at room temperature. The sections were washed with TBS-low salt containing 0.05% Triton X-100, followed by TBS-low salt and DW. Alexa Fluor 488 fluorescence was excited with a band-pass filter BP470/40, and the emitted fluorescence was detected with BP525/50 using an epifluorescence microscope Axio Imager D1. Digital images were captured with a digital CCD camera (AxioCam MRm, Carl Zeiss) operated with AxioVision.

For TEM observation, ultrathin sections of the resin-embedded roots were etched with 0.2% sodium ethoxide in ethanol for 5 min. They were then washed with 0.02% sodium ethoxide, followed by 100% ethanol, 50% ethanol, and DW wash. Specimens were blocked with 1% BSA in phosphate-buffered saline (PBS) containing low concentrations of salts (PBS-low salt; 10 mM phosphate buffer pH 8.4, 13.7 mM sodium chloride, and 0.27 mM potassium chloride). They were then incubated in a mixture of 20 μg ml^{-1} PPBD, 10 μg ml^{-1} mouse anti-Xpress epitope antibody, PBS-low salt, and 1% BSA, and washed with PBS-low salt buffer containing 0.05% Triton X-100, followed by PBS-low salt. Samples were incubated with a goat anti-mouse IgG antibody conjugated with 6 nm colloidal gold (#115-195-146, Jackson ImmunoResearch Laboratories, PA, United States) diluted 1:20 in PBS-low salt buffer containing 1% BSA for 1 h at room temperature. The samples were washed with PBS-low salt

containing 0.05% Triton X-100, followed by PBS-low salt and DW wash. Specimens were stained with 50% TI-Blue (Nisshin EM, Tokyo, Japan) for 10 min, followed by lead citrate staining for 5 min, and observed using a TEM (JEOL, Tokyo, Japan) at an accelerating voltage of 80 kV. Negative controls were prepared by incubating sections without PPBD. Another negative control was prepared by incubating sections with an excessive competitor (100 mM tripolyphosphate) during the first reaction.

Enzyme Cytochemistry of Phosphatase Activity

Acid phosphatase (ACP) and neutral phosphatase (NTP) activity was detected using TEM with a cerium-based method (Dreyer et al., 2008) with some modifications. Root fragments (5–10 mM) were pre-fixed with 2.5% glutaraldehyde in 100 mM cacodylate buffer (pH 7.0) for 2 h on ice. The fragments were washed twice with cacodylate buffer for 30 min. Roots were further cut into 0.5 mM fragments. The fragments were sequentially incubated in a pre-incubation buffer [2 mM $CeCl_3$ in 100 mM acetate buffer (pH 4.6) and 100 mM Tris-HCl buffer (pH 7.4) for acid and NTP activity, respectively] for 1 h, a reaction buffer (1 mM β-glycerophosphate and 2 mM $CeCl_3$ in acetate or Tris-HCl buffer) for 30 min, a pre-incubation buffer for 15 min, and an acetate or Tris-HCl buffer for 15 min at 37°C. Samples were post-fixed with 1% OsO_4 in cacodylate buffer for 2 h on ice, followed by washing with DW thrice for 5 min. Roots were dehydrated with an ethanol series (20, 50, 70, 90, and 95% once and 100% thrice) for 20 min each at 4°C and incubated twice with propylene oxide for 5 min at room temperature. The samples were infiltrated with Spurr's resin:propylene oxide (1:2, 1:1, 2:1, 3:1, and 4:1) for 1 h in each step and thrice with pure resin for 3 h, and polymerized at 70°C for 12 h. Ultrathin sections on copper grids were stained with gadolinium acetate (Nakakoshi et al., 2011) and lead citrate and observed using a TEM at an accelerating voltage of 80 kV. Controls were prepared by incubating sections without β-glycerophosphate in the reaction buffer and without 2 mM $CeCl_3$ in the pre-incubation and reaction buffers.

The localization of phosphatase activity was also analyzed by fluorescence microscopy. Cryosections of mycorrhizal roots were fixed with 0.25% glutaraldehyde in PBS (pH 7.4) for 8 min at 4°C. They were then permeabilized by immersion in 25% ethanol in 100 mM acetate buffer (pH 4.6) and 100 mM Tris-HCl buffer (pH 7.4) for several seconds for ACP and NTP activity, respectively, and washed twice with the same buffer. The sections were incubated with 25 μM ELF97 phosphatase substrate (Thermo Fisher Scientific) in either acetate or Tris-HCl buffer for 30 min at room temperature in the dark and washed with the same buffer without the substrate. Fluorescence of the ELF97 reaction product was excited with UV, and the emitted fluorescence was detected with a long-pass filter, LP420, using an epifluorescence microscope Axio Imager D1 microscope.

For dual labeling of polyP accumulation and phosphatase activity, cryosections of mycorrhizal roots were sequentially washed with 70% ethanol, 25% ethanol, and DW. First, sections were labeled with 80 μg ml^{-1} DAPI in either 100 mM acetate buffer (pH 4.6) or 100 mM Tris-HCl buffer (pH 7.4) for 60 min at room temperature in the dark. The samples were then gently washed in either acetate buffer or Tris-HCl buffer. Subsequently, sections were incubated with 25 μM ELF97 in acetate buffer or Tris-HCl buffer for 30 min at room temperature in the dark. After the second labeling, the sections were mounted in DW, covered with a glass coverslip, and observed within 30 min. The fluorescence of the DAPI-polyP complex and the ELF97 reaction product was excited with UV, and the emitted fluorescence was detected with a long-pass filter, LP420, using the Axio Imager D1 microscope. Digital images were captured using an AxioCam MRc5 operated with AxioVision.

AM Fungal Colonization

Roots were cleared in a 10% (w/v) KOH solution at 90°C for 10 min, acidified with a 2% (v/v) HCl solution for 5 min, and then stained with 0.05% trypan blue in lactic acid at 90°C for 10 min. AM colonization was assessed using the method described by Trouvelot et al. (1986) with some modifications. Approximately 10 root fragments per plant were mounted on a slide and observed under a light microscope. The intensity of AM fungal colonization and arbuscule abundance in a field of view (diameter: 1.28 mM) was categorized into six and three classes, respectively. AM colonization parameters (F%, M%, m%, A%, and a%) were calculated based on the scores in 100 fields of view. To visualize the fine structure of AM fungal colonization, roots were also stained with wheat germ agglutinin (WGA) conjugated with Oregon Green 488 (Kojima et al., 2014). Fluorescent images of the mycorrhizal roots were captured using an Axio Imager D1 microscope equipped with a digital CCD camera AxioCam MRc5. The length of the major axis of arbuscules was measured with the AxioVision software.

Plant P Analysis

The plants were divided into shoots and roots and dried at 70°C for 48 h and were weighed after cooling in a desiccator. Dried samples were digested with sulfuric acid and hydrogen peroxide at 200°C for 2 h. P concentrations in the samples were determined using the acid-molybdate blue method (Watanabe and Olsen, 1965). The P content was calculated by multiplying each sample's dry weight by their P concentrations.

Gene Expression Analysis

Total RNA was isolated from roots using RNAiso Plus (Takara Bio, Shiga, Japan) combined with Fruit-mate (Takara Bio) according to the manufacturer's instructions. Contaminating genomic DNA was eliminated using a TURBO DNA-*free* kit (Thermo Fisher Scientific). cDNA was synthesized using a ReverTra Ace qPCR RT Kit (Toyobo, Osaka, Japan). Quantitative PCR was conducted using a StepOne Real-Time PCR System (Thermo Fisher Scientific) with a THUNDERBIRD SYBR qPCR Mix (TOYOBO). The primers used for qRT-PCR are listed in **Supplementary Table S1**. The *L. japonicus* elongation factor 2 gene and *R. irregularis EF1β* (Kobae et al., 2015) genes were used as internal controls for the expression analysis of plant and AM fungal genes, respectively. Melting curve analysis confirmed the presence of single peaks. Relative expression

levels were calculated using the $2^{-\Delta Ct}$ method (Schmittgen and Livak, 2008). All the reactions were performed using three biological replicates. RT-PCR was performed using *HA1*-specific primers (**Supplementary Table S1**) and 10 ng of cDNA template to confirm homozygous *LORE1* insertion lines at the transcript level, and the amplified products were sequenced.

Statistical Analyses

All statistical analyses were performed using the software R (version 4.0.0). The mycorrhizal colonization rate and relative gene expression values were logit-transformed ($\ln[p/1-p]$) and log-transformed, respectively, to avoid violating normality and homoscedasticity assumptions. To test the differences in mycorrhizal colonization and gene expression between WT and *ha1-1* mutants, data were analyzed using the Student's *t*-test. Tukey's HSD test was performed for multiple comparisons of P contents of plants. Relative frequency densities of arbuscule size and the percentage of arbuscule area showing DAPI-polyP signal were calculated using the MASS package in the software. The size distributions of WT and *ha1-1* mutants were compared using a two-sample Kolmogorov–Smirnov test. The proportion of mature and collapsed arbuscules in WT and *ha1-1* was analyzed using Fisher's exact test.

RESULTS

AM Phenotype of the *ha1-1* Mutant in *Lotus japonicus*

First, we investigated the effect of the mutation of *HA1* on P acquisition through the mycorrhizal pathway. A *L. japonicus* homozygous line carrying a *LORE1* insertion in exon 8 of the *HA1* gene was selected to obtain a *ha1* mutant, *ha1-1* (**Figure 1A**). RT-PCR analysis revealed that although *HA1* transcripts were observed in AM roots of the *ha1-1* mutant (**Figure 1B**), they had indels caused by putative abnormal splicing that created a frameshift and a premature stop codon 13 amino acids after the insertion (**Figure 1C**). To determine whether the *HA1* mutation affects P acquisition *via* the mycorrhizal pathway, we examined the P nutrition of the *ha1-1* mutant using a two-compartment system consisting of RHC and HC (**Figure 1D**). Under uninoculated conditions, plant's P nutrition did not differ between WT and *ha1-1* plants (**Figure 1E**). In the presence of AM fungi, P content increased in both genotypes. However, the positive effects on shoot P content were lower in the *ha1-1* mutant (average increase of 268%) than in the WT (average increase of 492%). These data demonstrate that P transfer from the AM fungus to the host *via* the mycorrhizal pathway was partially impaired in the *ha1-1* mutant. To examine the effects of *ha1-1* on hyphal development within roots, we assessed AM fungal colonization by staining mycorrhizal roots with trypan blue and WGA–Oregon Green 488. Quantitative analysis revealed that arbuscule densities (A% and a%) were moderately reduced in the mutant relative to the WT 4 weeks post-inoculation (**Figure 1F**). Furthermore, the arbuscules formed in *ha1-1* mutant roots were slightly smaller than those in WT roots (**Figure 1G**). However, the range of arbuscule sizes almost overlapped between the two genotypes. These results suggest that the *HA1* mutation induced a phase transition of the arbuscule life cycle from mature to degrading stage.

PolyP Localization in Arbuscules – DAPI Staining

We analyzed polyP accumulation in arbuscules by DAPI staining. Once DAPI binds to polyP, the complex emits yellow fluorescence under UV irradiation (Tijssen et al., 1982). Mycorrhizal root cryosections were DAPI-stained after polyP fixation and cell permeabilization with ethanol. We observed arrays of fully-developed arbuscules (mature arbuscules) and the patchy colonization of degenerating arbuscules which are small arbuscules with shrunken fine branches (**Figure 2A**). In most mature arbuscules formed in cortical cells, the fluorescent DAPI-polyP complex signal was confined to the central region, irrespective of the plant's genotype. The other region within the arbuscules, containing fine branches, exhibited non-specific blue fluorescence. In contrast, the entire hyphae of the degenerating arbuscules were stained with DAPI and fluoresced yellow. This type of arbuscules accounted for 57% of the total arbuscules formed in *ha1-1* mutants, which was 1.4-fold higher than that in the WT (**Figure 2B**). This result prompted us to examine whether the shift in size distribution toward small arbuscules in the mutant, as observed by WGA staining was due to the increased number of degenerating arbuscules. We measured the size of mature and degenerating arbuscules distinguished by the DAPI staining pattern. Overall, WGA staining reduced arbuscule size relative to DAPI, possibly due to cell shrinkage caused by fixation with Farmer's solution which contained ethanol and acetic acid (**Figure 1G** and **Figure 2C**). In both arbuscule types, the size distribution almost overlapped between the WT and the *ha1-1* mutant, but the median length was 5–8 μM shorter in the mutant (**Figure 2C**). Our DAPI staining data also suggested that *HA1* mutations caused early arbuscule degeneration.

Next, we focused on the distribution of polyP in mature arbuscules. It should be noted that the size of the DAPI-stained region in the arbuscules varied (**Figure 3A**). Quantitative analysis revealed that the distribution of the yellow fluorescent area relative to the entire mature arbuscule significantly differed between the WT and *ha1-1* (**Figure 3B**). In the WT, the most abundant size class was 0–5%; arbuscules with large DAPI-stained regions were infrequent. In contrast, the size distribution in the *ha1-1* mutant peaked at 10–15% with a higher right tail than the WT, indicating an expansion of the DAPI-polyP positive region.

To obtain more precise polyP localization in mature arbuscules, we analyzed semithin sections of resin-embedded AM roots. Arbuscules develop with repeated branching and narrowing of hyphal diameter from a thick trunk hypha to fine branches. Here, we define the fine branch module as a set of connected branches (**Figure 3C**). For arbuscules generated in WT roots, yellow fluorescence was detected in some fine branch modules located in the vicinity of the trunk hyphae (**Figure 3D**). The

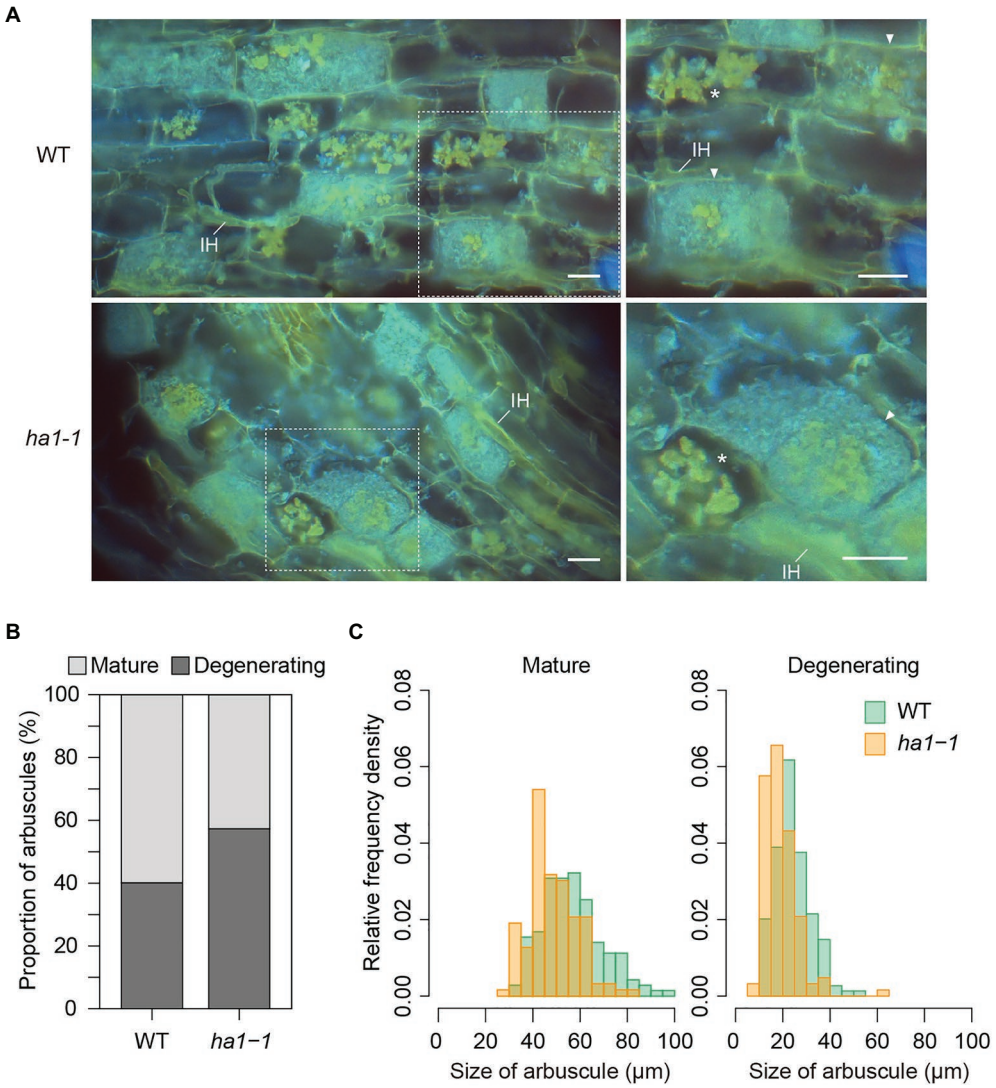

FIGURE 2 | Mature and degenerating arbuscules stained with 4′,6-diamidino-2-phenylindole (DAPI). **(A)** DAPI staining of arbuscules in wild-type (WT) and *ha1-1* roots of *Lotus japonicus*. Mycorrhizal roots were harvested 4 weeks after inoculation with *Rhizophagus irregularis*. Cryosections of fresh roots were stained with DAPI and observed using an epifluorescence microscope. The DAPI-polyP complex emits yellow fluorescence under UV irradiation. Blue fluorescence suggests non-specific DAPI binding to fungal hyphae. Right panels show the magnified images of dotted areas in the left panels. Mature arbuscules (arrowheads) and degenerating arbuscules (asterisks) are visible. IH: intraradical hypha. Scale bar = 20 μM. **(B)** Proportion of mature and degenerating arbuscules in WT and the *ha1-1* mutant. Small, shrunk arbuscules that entirely show intense yellow fluorescence by DAPI staining were considered as degenerating arbuscules. Mature arbuscules fully occupy plant cortical cells. The proportion was significantly different based on Fisher's exact test ($p < 0.001$, $n = 499$ and 562 in WT and *ha1-1*, respectively). **(C)** Relative frequency density of the size of mature and degenerating arbuscules formed in WT and *ha1-1*. The lengths of the major axis of arbuscules stained with DAPI were measured. The size distribution was significantly different between the plant genotypes according to the two-sample Kolmogorov-Smirnov test in each arbuscule type ($p < 0.001$). Mature arbuscule: $n = 143$ and 146; degenerating arbuscule: $n = 149$ and 125 in WT and *ha1-1*, respectively.

fluorescent signal was also visible around the periphery of the trunk hyphae where the cell wall was localized, but not inside these hyphae. Similarly, the *ha1-1* mutant displayed DAPI-polyP signals in fine branch modules in the central region of the arbuscule and cell walls of the trunk hyphae.

PolyP Localization in Arbuscules – PPBD Affinity Labeling

We further analyzed the subcellular localization of polyP using enzyme-affinity labeling with PPBD, which binds specifically to long-chain polyP (Saito et al., 2005), because the yellow fluorescence of DAPI is not specific only to polyP. PolyP was labeled in semithin sections of mycorrhizal roots with recombinant PPBD containing an epitope tag. The tag was then detected by indirect immunocytochemistry with an Alexa Fluor 488-conjugated secondary antibody and observed under a fluorescence microscope. In arbuscules formed in WT roots, a strong polyP signal was observed at the cell periphery of the trunk hyphae, possibly at the cell wall (**Figure 4**). Weak fluorescence was detected in plant and fungal nuclei, likely due to the low-affinity DNA-binding capability of

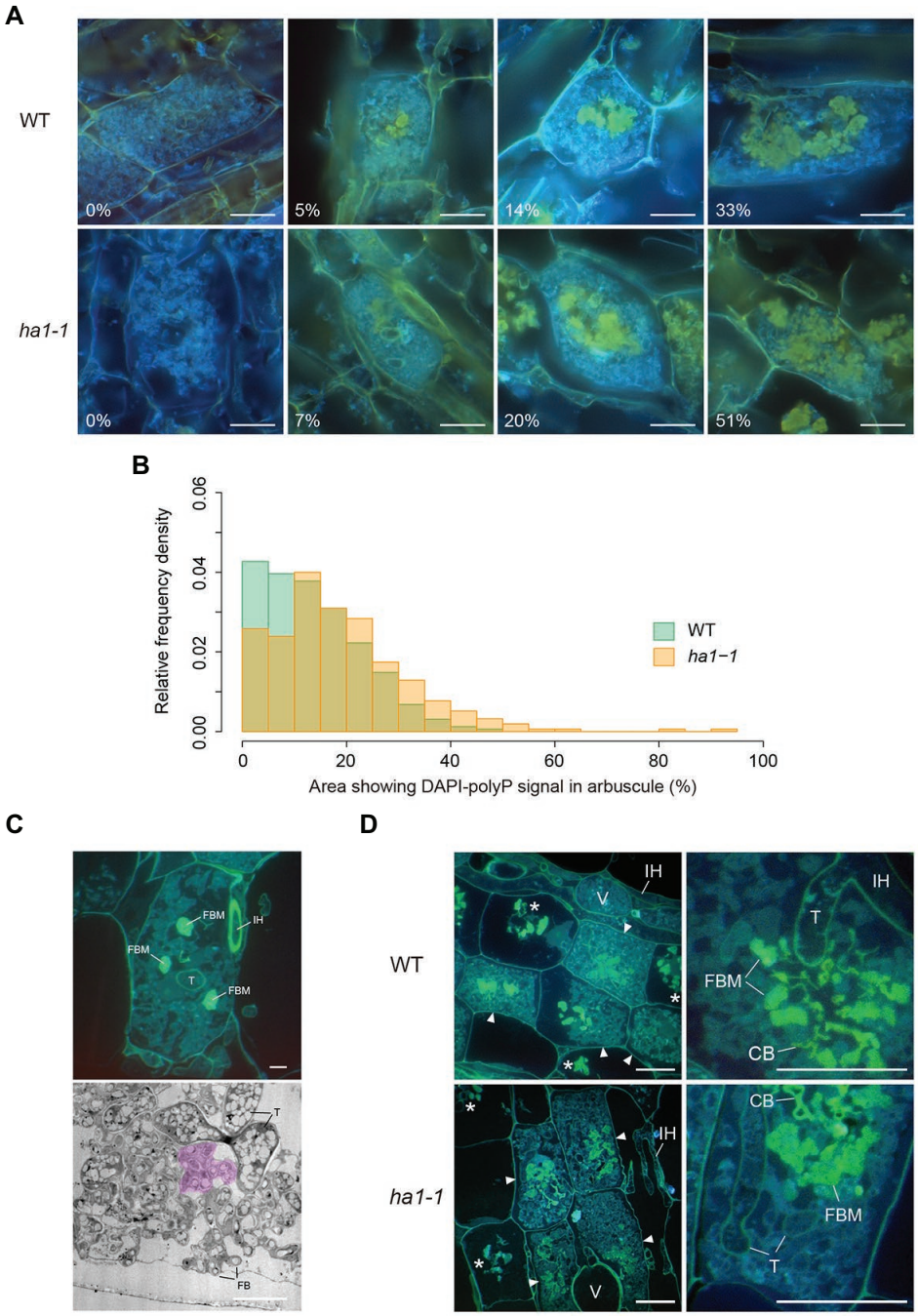

FIGURE 3 | Localization of polyphosphate (polyP) by DAPI staining. **(A)** Representative types of mature arbuscules stained with DAPI. Mycorrhizal roots of *L. japonicus* were harvested 4 weeks after inoculation with *R. irregularis*. Yellow fluorescence is observed in the central part of arbuscules. Percentages of arbuscule area showing yellow fluorescence signals are shown. Scale bars = 20 μM. **(B)** Relative frequency density of the area showing DAPI-polyP signal. The percentage of arbuscule area with signal was calculated. In total, 323 and 310 mature arbuscules were measured for wild-type (WT) and *ha1-1*, respectively. According to the two-sample Kolmogorov–Smirnov test, the size distribution was significantly different between the plant genotypes ($p < 0.001$). **(C)** Fine branch modules (FBM) in arbuscules. In the upper panel, semithin sections of mature arbuscules in resin-embedded WT roots were stained with DAPI and observed using an epifluorescence microscope. Strong yellow fluorescence was observed in several fine branch modules, a set of connected fine branches. The lower panel shows a transmission electron micrograph of fine branches and trunk hyphae of an arbuscule colonized in a WT cortical cell. Acid phosphatase (ACP) activity was detected by electron microscopic enzyme cytochemistry as black precipitates of the reaction product (cerium phosphate). The region colored in magenta is a putative FBM in which fine branches form a cluster. FB: fine branch, FBM: fine branch module, IH: intraradical hypha, T: trunk hypha. Scale bars = 5 μM. **(D)** DAPI staining of semithin sections of resin-embedded mycorrhizal roots. In the left panels, mature arbuscules (arrowheads) and degenerating arbuscules (asterisks) are shown. Right panels show magnified images of mature arbuscules. Fine branch modules (clusters of connected branches), trunk hyphae cell walls, and collapsed branches display yellow fluorescence. CB: collapsed branch, FBM: fine branch module, IH: intraradical hypha, T: trunk hypha, and V: vesicle. Scale bars = 20 μM.

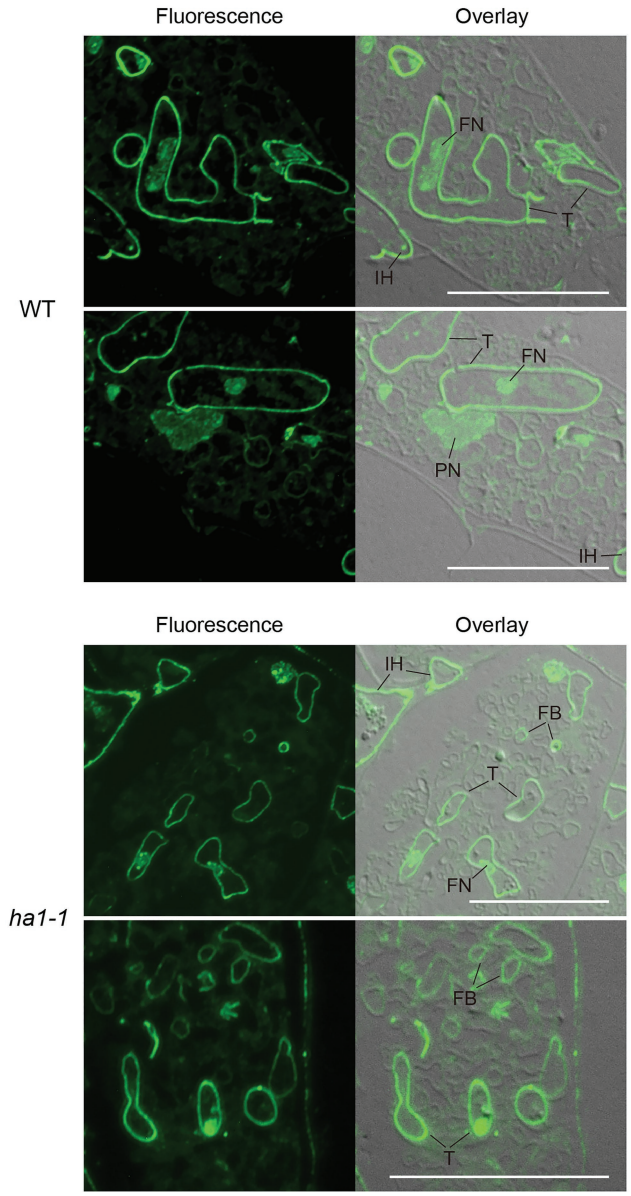

FIGURE 4 | Subcellular localization of polyP using polyphosphate (polyP) binding domain (PPBD) affinity labeling. Representative fluorescence images of polyP localization (left panels) and superimposed differential interference contrast (DIC) images (right panels) of arbuscule-containing cortical cells in wild-type and *ha1-1*. Sections were incubated with a PPBD-anti-Xpress antibody complex and, subsequently, an anti-mouse IgG antibody conjugated with Alexa Fluor 488. An intense fluorescence signal was observed in cell walls of trunk hyphae and intraradical hyphae in both genotypes. Signals were sometimes detected in fine branches in the mutant. FB, fine branch; FN, fungal nucleus; IH, intraradical hypha; PN, plant nucleus; and T, trunk hypha. Scale bars = 20 μM.

PPBD (Saito et al., 2005). There was no or very weak polyP signal in the fine branches throughout the cortical cells harboring arbuscules. This localization differed from the DAPI-polyP signal, which was associated with fine branch modules in the central region of arbuscules. These contradictory observations may result from a difference in polyP binding properties as DAPI can bind to short-chain polyP with at least 14 residues (Smith et al., 2018), but PPBD has an extremely low affinity for polyP shorter than 35 residues (Saito et al., 2005). In addition, polyP detected by DAPI was immobilized in ethanol. Conversely, the PPBD enzyme-affinity method included incubation in an aqueous solution that might have eluted some polyP from the sections. In the *ha1-1* mutant, the labeling pattern of fungal polyP was similar to that of the WT, in which the cell periphery of trunk hyphae was labeled (**Figure 4**). However, we found that polyP signals were occasionally present at the cell periphery of some fine branches.

PolyP localization was visualized by TEM using the enzyme-affinity method with gold-coupled secondary antibodies. In arbuscules formed in WT, the polyP signal was evenly distributed in the trunk cell wall, as observed with fluorescence microscopy (**Figures 5A–C**). Sparse labeling was observed sporadically within vacuoles of trunk hyphae (**Figure 5D**). However, there was no polyP signal in the fine branches (**Figures 5E–F**). In *ha1-1* roots, polyP localization was similar to that in the WT, with presence in the trunk hyphae fungal cell wall (**Figures 5G–H**). Interestingly, polyP signals were sometimes observed on the fine branch cell walls (**Figures 5I–J**). In particular, fine branches cut obliquely against the longitudinal axis showed prominent signals in their cell walls or their surrounding PAS (**Figures 5K–L**). In the negative controls, where sections of mycorrhizal roots were incubated in a reaction mixture without PPBD, no polyP signals were detected (**Supplementary Figure S1**). There was also no polyP signal when the PPBD polyP-binding site was masked with a high concentration of tripolyphosphate. In summary, enzyme-affinity labeling using PPBD revealed that in the WT, relatively long-chain polyP was mainly distributed in the trunk hyphae cell walls and absent in the fine branches. However, the *HA1* mutation led to polyP accumulation in some fine branch cell walls.

Localization of Phosphatase Activity in Arbuscule-Containing Cortical Cells

An interesting feature of polyP localization was its almost complete absence from fine branches at the periphery of cortical cells in WT and *ha1-1* (**Figure 3**). Dreyer et al. (2008) reported that ACP activity localizes at the interface between fungal cell walls and PAM. Generally, ACPs have broad substrate specificities for phosphate esters. To elucidate the spatial relationship between polyP and ACP in cells with arbuscules, we investigated the localization of ACP activity at the ultrastructural level (**Figure 6**). ACP activity was detected by incubating mycorrhizal roots in an acidic buffer containing the reaction substrate (β-glycerophosphate) and the co-precipitant (cerium salt) and observing the black precipitates of the reaction product (cerium phosphate) with TEM. High ACP activity was frequently detected in PAS around the fine branches in both WT and *ha1-1*, which was consistent with previous observations (Dreyer et al., 2008). Notably, most of the dense precipitates localized along the host-derived PAM and in small vesicles resembling the intramatrix compartment type I (IMC-I) or apoplastic vesicular structures (AVS; Ivanov et al., 2019; Roth et al., 2019). In contrast, only a few signals were associated with PAS around

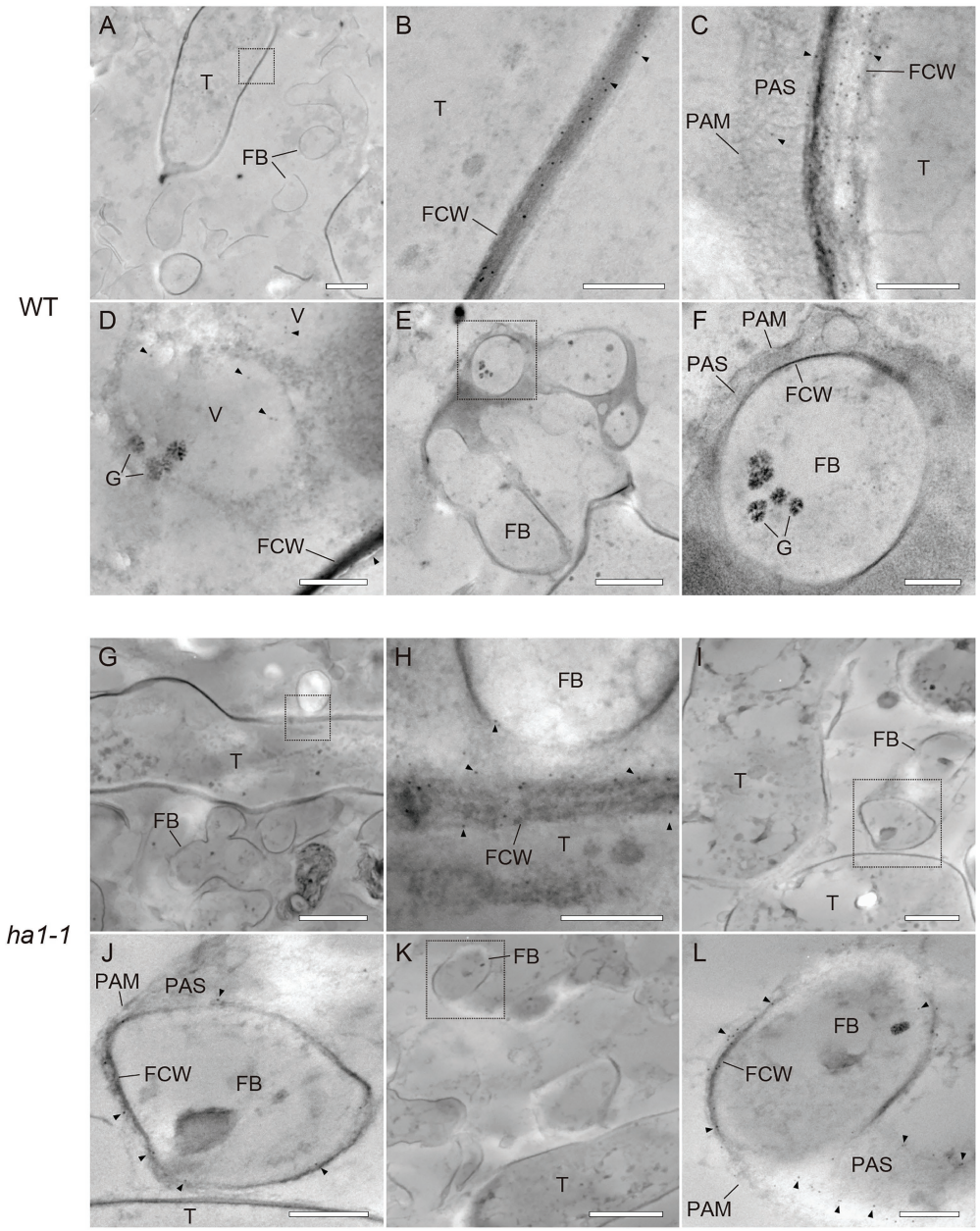

FIGURE 5 | Ultrastructural localization of polyphosphate (polyP) using polyP binding domain (PPBD) affinity labeling. Representative transmission electron micrographs showing polyP distribution (gold particle) in mycorrhizal roots of wild-type **(A–F)** and *ha1-1* **(G–L)**. Sections were incubated with a PPBD-anti-Xpress antibody complex and, subsequently, an anti-mouse IgG conjugated with 6-nm colloidal gold. Triangles show representative gold particles. **(A–C)** PolyP present in the trunk hyphae cell wall. **(D)** Occasional labeling in fungal vacuoles. **(E–F)** Fine branches lacking signal. **(G,H)** Signals were often detected in the trunk hyphae cell walls in the *ha1-1* roots. **(I–L)** Fine branch cell walls were sometimes labeled in *ha1-1*. Panels **(B,F,H,J,L)** show the magnified images of dotted areas in the previous panels. FB, fine branch; FCW, fungal cell wall; G, glycogen granule; PAM, periarbuscular membrane; PAS, periarbuscular space; T, trunk hypha; and V, vacuole. Scale bars = 500 nm.

the trunk hyphae in both WT and *ha1-1* cells. ACP activity was sometimes observed in fungal vacuoles. No dense cerium phosphate precipitate was observed in the control experiment lacking cerium salt (**Supplementary Figure S2**). In the control reaction without β-glycerophosphate, a few precipitates were observed in the fungal vacuoles, possibly due to a reaction with endogenous vacuole substrates. Next, we investigated the localization of NTP activity in the *ha1-1* mutant because the acidification around arbuscules diminishes in *ha1* cortical cells (Krajinski et al., 2014; Liu et al., 2020). NTP activity localization was similar to ACP activity with signals along the PAM and in small vesicles present in the PAS surrounding fine branches (**Figure 7**), as previously reported (Jeanmaire et al., 1985).

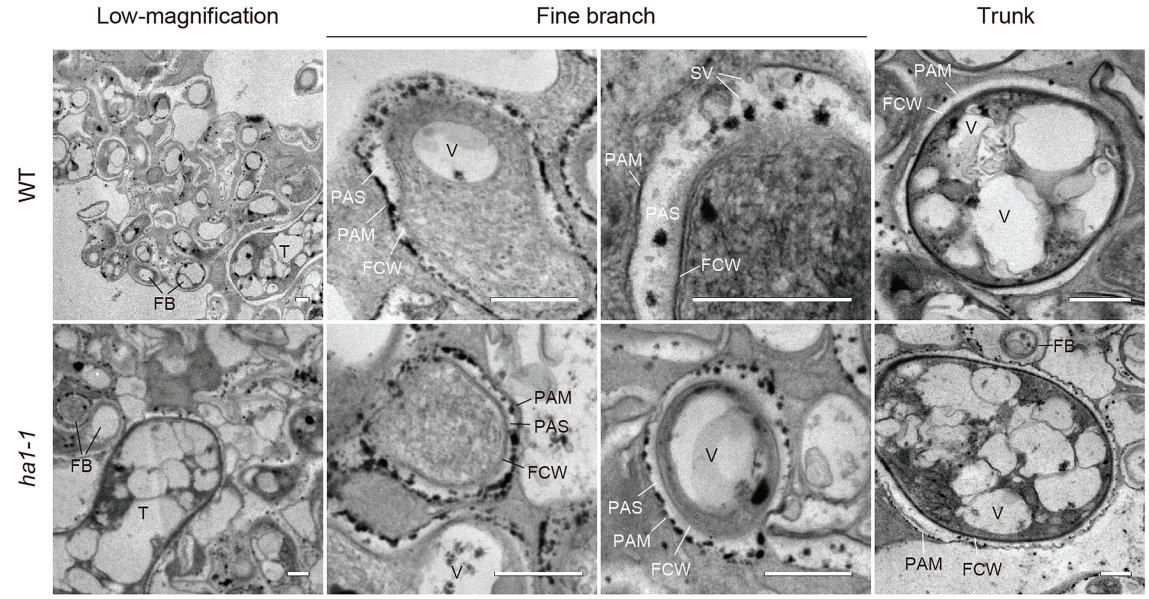

FIGURE 6 | Electron microscopic enzyme cytochemistry of acid phosphatase (ACP) activity in arbuscule-containing cortical cells. Representative transmission electron micrographs showing ACP activity in arbuscule-containing cortical cells of wild-type and *ha1-1* roots colonized by *R. irregularis*. Fine branches and trunk hyphae of an arbuscule colonized in a cortical cell are shown. ACP activity was detected as black precipitates of the reaction product (cerium phosphate) by incubating mycorrhizal roots in acetate buffer (pH 4.6) containing β-glycerophosphate and cerium chloride. FB, fine branch; FCW, fungal cell wall; PAM, periarbuscular membrane; PAS, periarbuscular space; SV, small vesicle; T, trunk hypha; and V, vacuole. Scale bars = 500 nm.

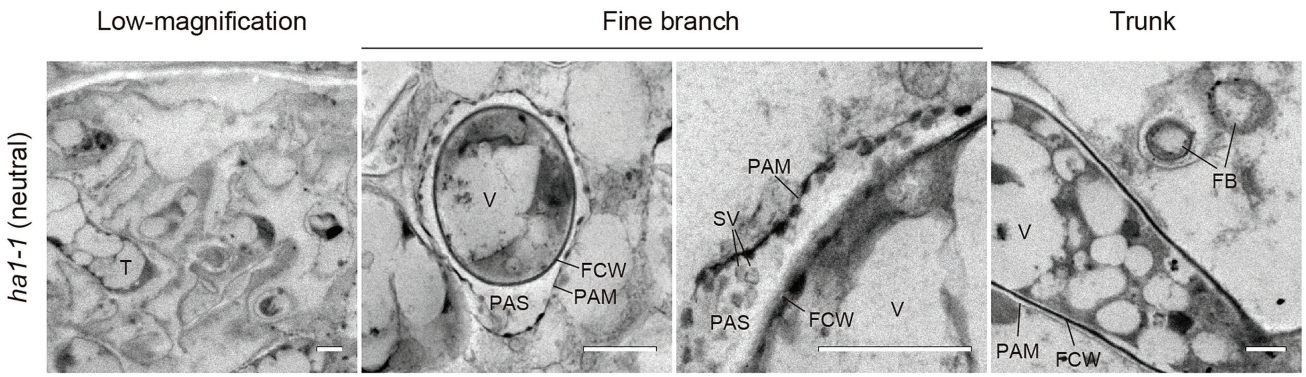

FIGURE 7 | Electron microscopic enzyme cytochemistry of neutral phosphatase (NTP) activity. Transmission electron micrographs showing NTP activity in arbuscule-containing cortical cells of the *ha1-1* roots colonized by *R. irregularis*. NTP activity was detected as black precipitates of the reaction product (cerium phosphate) by incubating mycorrhizal roots in Tris-HCl buffer (pH 7.4) containing β-glycerophosphate and cerium chloride. Fine branches and trunk hyphae of an arbuscule colonized in a cortical cell are shown. FB, fine branch; FCW, fungal cell wall; PAM, periarbuscular membrane; PAS, periarbuscular space; SV, small vesicle; T, trunk hypha; and V, vacuole. Scale bars = 500 nm.

To further study the relationship between phosphatase activity and polyP accumulation, we detected phosphatase activity and polyP signals simultaneously by enzyme cytochemistry using the ELF97 phosphatase substrate and DAPI staining, respectively. ELF97 forms fine precipitates after hydrolysis of its phosphate ester bond by non-specific phosphatases, emitting yellow-green fluorescence at the site of phosphatase activity (Haugland, 2005). First, ACP and NTP activities were visualized in a typical mature arbuscule by single ELF97 staining in WT and *ha1-1* roots, respectively (**Figure 8A**). In the WT, ACP activity was present throughout the arbuscule but was excluded from its central region. Similarly, NTP activity was detected in arbuscules in the mutant but the central region without phosphatase activity was larger than that in the WT. Next, we performed double labeling of phosphatase activity and polyP. The localization of phosphatase activity (green) and polyP (yellow) was distinct based on different emission colors using a long-pass filter, albeit showing weak and different color signals compared to the single staining (**Figure 8B**). Double labeling showed that polyP was present in the center of arbuscules, and phosphatase

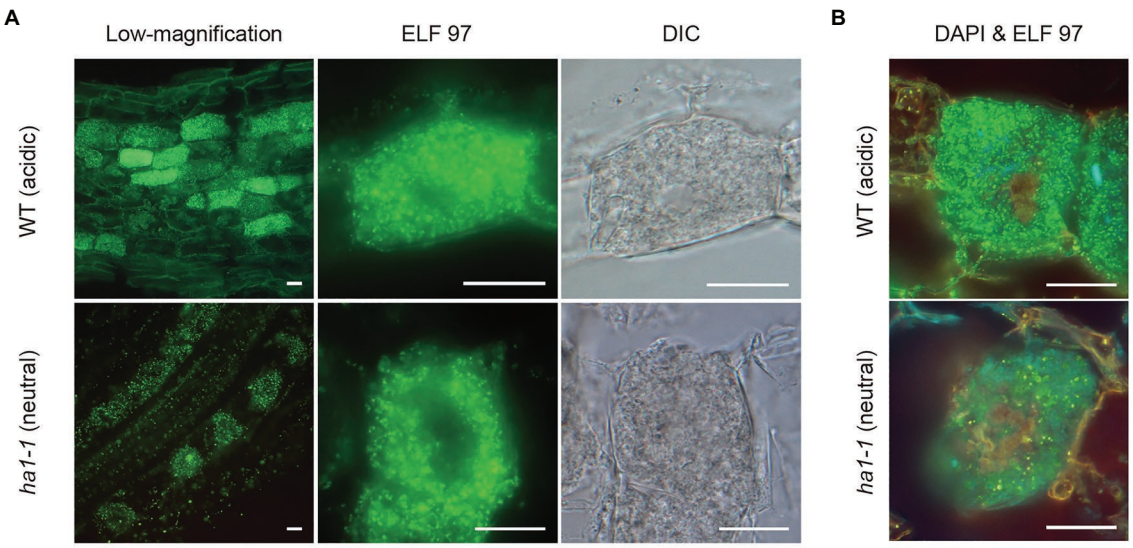

FIGURE 8 | Enzyme cytochemistry of phosphatase activity in arbuscule-containing cortical cells using ELF97. **(A)** Representative fluorescence images of acid and neutral phosphatase activity in wild-type (WT) and *ha1-1*, respectively. Green fluorescence of the ELF97 reaction product indicates phosphatase activity. Arbuscule structure was observed under a DIC microscope. **(B)** Double labeling using DAPI and ELF97 of WT and *ha1-1* under acidic and neutral conditions, respectively. The color balance was adjusted to discriminate between DAPI-polyP complex and the ELF97 reaction product fluorescence. Yellow-orange and green fluorescence indicate polyP and phosphatase activity, respectively. Scale bars = 20 μM.

activity localized in the surrounding regions. Thus, polyP and phosphatase activity showed opposite localization in both WT and *ha1-1* cells.

Gene Expression Analysis

We investigated whether the *HA1* mutation affected gene expression related to plant Pi uptake and fungal polyP metabolism during AM symbiosis. The levels of the phosphate transporter *PT1*, likely to function in the direct pathway due to its downregulation during mycorrhization (Maeda et al., 2006), were slightly elevated in *ha1-1* roots compared to the WT (**Figure 9A**), which may reflect a partial block in P translocation *via* the mycorrhizal pathway. Transcripts of other phosphate transporters, including AM-specific *PT4* (Guether et al., 2009a; Takeda et al., 2009), accumulated equally in the mycorrhizal roots of both genotypes. Similarly, the *ha1-1* mutation did not affect the expression of AM marker genes, AM-specific ammonium transporter *AMT2;2* (Guether et al., 2009b) and glycerol-3-phosphate acyltransferase *RAM2* (Wang et al., 2012). Fungal endopolyphosphatase genes *PPN1*, *PPN2*, and *PPN3* were downregulated in AM fungi colonizing the mutant, whereas the VTC genes involved in polyP synthesis were not affected (**Figure 9B**).

DISCUSSION

P transfer across the symbiotic interface is an important process in the mycorrhizal pathway. However, it has been challenging to elucidate this process, possibly due to rapid P movement from the AM fungus to the host. In this study, we sought to clarify the intermediate process of P transfer by visualizing polyP localization in arbuscules of *R. irregularis* formed in *L. japonicus* WT and the *ha1-1* mutant.

PPBD affinity-labeling for specifically detecting long-chain polyP demonstrated that polyP was predominantly distributed in cell walls of trunk hyphae in arbuscules formed in WT, but fine branch cell walls lacked a polyP signal. Since intense ACP activities were found in PAS around fine branches, the absence of polyP in the fine branch cell walls could be explained by the degradation of polyP in fungal cell walls by apoplastic ACP. Supporting this idea, the *ha1-1* mutant, in which the mycorrhizal pathway was partially suppressed, showed polyP localization in some cell walls of the fine branches. Based on our observations, we propose a hypothesis for P transfer at AM fungus-host interface in which polyP is released into the cell walls of fine branches and then immediately subjected to hydrolysis by ACP located in the PAS. The liberated Pi is delivered to host cells by symbiotic Pi transporters driven by the H^+ gradient generated across the PAM by the HA1 H^+-ATPase (Javot et al., 2007; Yang et al., 2012; Willmann et al., 2013; Xie et al., 2013; Krajinski et al., 2014; Wang et al., 2014; Watts-Williams et al., 2015; Liu et al., 2020). However, because the mechanism of polyP release into the fungal cell wall is unknown and it remains unclear whether the apoplastic ACP can catalyze polyP hydrolysis, we cannot rule out the possibility that polyP is hydrolyzed in AM fungal hyphae and the liberated Pi is exported to the PAS *via* an unidentified Pi exporter.

Moreover, polyP signals were observed within several fine branch modules close to the trunk hyphae by DAPI staining. The fine branch modules with polyP were slightly expanded in the *ha1-1* mutant. Around these fine branch modules, no phosphatase activity was observed by double staining with ELF97 and DAPI. It might be anticipated that P metabolism

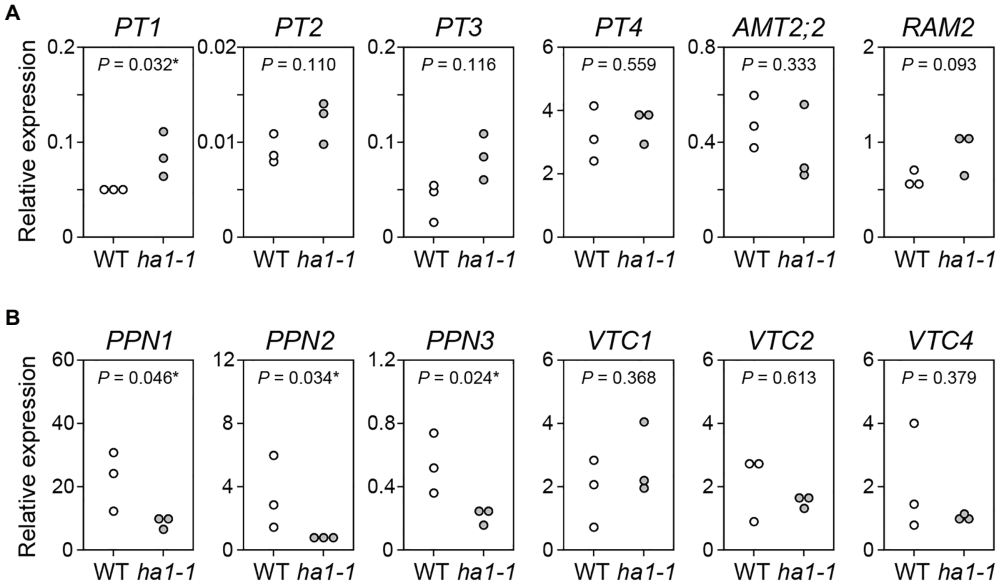

FIGURE 9 | Gene expression analysis. **(A)** Expression of *L. japonicus* genes encoding phosphate transporters (*PT1–PT4*), ammonium transporter (*AMT2;2*), and AM-specific glycerol-3-phosphate acyltransferase *RAM2* gene in mycorrhizal roots of the wild-type and *ha1-1* 4 weeks after inoculation with *R. irregularis*. Expression levels were normalized based on the amount of *L. japonicus EF2*. **(B)** Expression of *R. irregularis* genes encoding endopolyphosphatases (*PPN1–PPN3*) and vacuolar transporter chaperones (*VTC1*, *VTC2*, and *VTC4*) in mycorrhizal roots. The *R. irregularis EF1β* gene was used as an internal control. *p*-values are based on Student's *t*-test (*, $p < 0.05$).

and export are suppressed in these fine branch modules, leading to the accumulation of polyP. This is consistent with our finding that the expression levels of endopolyphosphatase genes were reduced in AM fungi colonizing the *ha1-1* mutant, although whether polyphosphatase activity is decreased in DAPI-stained fine branch modules stained is unknown.

A remarkable feature of arbuscule polyP is its localization in the fungal cell walls. The polyP chain appears to be relatively long, as detected by the PPBD enzyme affinity method. PolyP distribution in cell walls has also been observed in germ tubes and extraradical hyphae of AM fungi and mycelia of a wide range of fungal species (Mucoromycota, Dikarya, and Chytridiomyceta; Werner et al., 2007; Kuga et al., 2008). However, little is known about the molecular mechanisms underlying polyP accumulation in fungal cell walls. A possible mechanism is that polyP might be loaded into intracellular vesicles and released into the extracellular space *via* exocytosis. Alternatively, the VTC complex might be redistributed to the plasma membrane and then synthesize polyP. The yeast VTC2, a subunit of VTC complexes, is observed at the cell periphery along the plasma membrane under high Pi conditions, although it is localized in vacuoles in a low-Pi medium (Hothorn et al., 2009). How polyP is released across the fungal plasma membrane and the role of cell wall polyP in fungal physiology are important questions to be explored in future studies.

Extensive polyP accumulation in arbuscules has been observed in plant mutants of Pi transporter genes related to symbiotic P uptake. Arbuscules formed in *M. truncatula PT4* mutant and RNAi lines (Javot et al., 2007) and in *L. japonicus PT3* RNAi lines (Funamoto et al., 2007) were almost entirely stained with toluidine blue and DAPI, respectively, indicating that polyP accumulation extended to fine branches in the marginal regions of the arbuscule. However, the *ha1-1* mutant had DAPI-polyP signals in only some fine branch modules located at the arbuscule center. Similarly, *ha1-1* phenotypes in P uptake through the mycorrhizal pathway and early arbuscule degradation were not as severe as in *pt* or other *ha1* mutants (Javot et al., 2007; Krajinski et al., 2014; Wang et al., 2014; Liu et al., 2020). The *ha1-1* mutation may have partial ATPase activity. In both *ha1-1* and WT roots, arbuscule fine branch modules close to a trunk hypha displayed strong DAPI-polyP fluorescent signals but were not labeled with PPBD. Considering the differences in polyP chain length affinity between DAPI and PPBD (Saito et al., 2005; Smith et al., 2018), relatively short-chain polyPs are likely to accumulate in that region. In the *ha1-1* mutant, fine branch modules stained with DAPI were increased and expanded to the periphery of arbuscules. A similar pattern of polyP accumulation was observed in RNAi lines of the AM-inducible Pi transporter *PT3* (Funamoto et al., 2007). The P flow in arbuscules appear to be initially disrupted in the fine branches close to the trunk hypha, which is observed as polyP accumulation. Subsequently, the disruption of the P flow may be extended to fine branches in other regions.

We also found that ACP activity and polyP have opposite localization in mature arbuscules. Funamoto et al. (2007) observed a similar spatial relationship between alkaline phosphatase (ALP) activity and polyP distribution. ALPs in AM fungi (Gianinazzi-Pearson and Gianinazzi, 1978; Kojima et al., 1998; Aono et al., 2004) can hydrolyze monophosphate

esters but not pyrophosphate bonds in polyP (Ezawa et al., 1999; Liu et al., 2013). Therefore, the reduced accumulation of polyP at sites of intense ALP activity could result from a change in P metabolism indirectly mediated by fungal ALPs (Saito and Ezawa, 2016). ACP has a broad substrate specificity for various phosphate compounds. Some plant ACPs can potentially hydrolyze polyP (Ezawa and Yoshida, 1994; Ezawa et al., 2005; Huang et al., 2018). Enzyme histochemical analyses have demonstrated intense ACP activity in arbuscules, particularly in PAM (Van Aarle et al., 2005; Dreyer et al., 2008). In our study, ACP activity detected in PAS was often associated with host-derived PAM and small vesicles resembling IMC-I or AVS, possibly due to PAM outgrowth (Ivanov et al., 2019; Roth et al., 2019). This observation suggests that ACP in the apoplastic region originates from the plant cells. However, the corresponding proteins have not been identified in the host plants. Several AM-inducible phosphatase genes are candidates for encoding ACPs present in PAS. In soybean, two out of 35 purple ACP genes are upregulated in AM roots (Li et al., 2012). The AM-inducible soybean purple ACP gene, *GmPAP33*, is expressed in arbuscule-containing cortical cells and is involved in arbuscule degeneration *via* phospholipid hydrolysis (Li et al., 2019). The AM-inducible marigold purple ACP TpPAP1, which differs from GmPAP33 in subclass, displays a broad substrate specificity and can catalyze polyP degradation (Ezawa and Yoshida, 1994; Ezawa et al., 2005). Further research, including mutant analysis, is needed to clarify whether these purple ACPs are responsible for ACP activity in PAS.

DATA AVAILABILITY STATEMENT

The original contributions presented in the study are included in the article/**Supplementary Material**, further inquiries can be directed to the corresponding author.

AUTHOR CONTRIBUTIONS

CN conducted all experiments and wrote the first draft. CN and KS analyzed the data, designed the experiments, and contributed to the final manuscript. All authors contributed to the article and approved the submitted version.

FUNDING

This work was supported by the Science and Technology Research Promotion Program for Agriculture, Forestry, and Fisheries, the Food industry (26036A) from the Ministry of Agriculture, Forestry, and Fisheries of Japan (KS), and a Grant-in-Aid for Scientific Research (15H01751) from the Japan Society for the Promotion of Science (KS).

ACKNOWLEDGMENTS

We thank the Centre for Carbohydrate Recognition and Signalling, Aarhus University, Denmark, for providing the seeds of *LORE1* insertional mutagenesis lines. We appreciate Reika Oguchi (Shinshu University) for her technical assistance, and Tatsuhiro Ezawa (Hokkaido University) and Yukari Kuga (Hiroshima University) for discussions and comments on the work. We also thank the Research Center for Supports to Advanced Science, Shinshu University. We would like to thank Editage for English language editing.

SUPPLEMENTARY MATERIAL

The Supplementary Material for this article can be found online at: https://www.frontiersin.org/articles/10.3389/fpls.2021.725939/full#supplementary-material

REFERENCES

Aono, T., Maldonado-Mendoza, I. E., Dewbre, G. R., Harrison, M. J., and Saito, M. (2004). Expression of alkaline phosphatase genes in arbuscular mycorrhizas. *New Phytol.* 162, 525–534. doi: 10.1111/j.1469-8137.2004.01041.x

Arpat, A. B., Magliano, P., Wege, S., Rouached, H., Stefanovic, A., and Poirier, Y. (2012). Functional expression of PHO1 to the Golgi and *trans*-Golgi network and its role in export of inorganic phosphate. *Plant J.* 71, 479–491. doi: 10.1111/j.1365-313X.2012.05004.x

Balestrini, R., Gómez-Ariza, J., Lanfranco, L., and Bonfante, P. (2007). Laser microdissection reveals that transcripts for five plant and one fungal phosphate transporter genes are contemporaneously present in arbusculated cells. *Mol. Plant-Microbe Interact.* 20, 1055–1062. doi: 10.1094/MPMI-20-9-1055

Benedetto, A., Magurno, F., Bonfante, P., and Lanfranco, L. (2005). Expression profiles of a phosphate transporter gene (*GmosPT*) from the endomycorrhizal fungus *Glomus mosseae*. *Mycorrhiza* 15, 620–627. doi: 10.1007/s00572-005-0006-9

Chiu, C. H., and Paszkowski, U. (2019). Mechanisms and impact of symbiotic phosphate acquisition. *Cold Spring Harb. Perspect. Biol.* 11:a034603. doi: 10.1101/cshperspect.a034603

Delaux, P.-M., Radhakrishnan, G. V., Jayaraman, D., Cheema, J., Malbreil, M., Volkening, J. D., et al. (2015). Algal ancestor of land plants was preadapted for symbiosis. *Proc. Natl. Acad. Sci. U. S. A.* 112, 13390–13395. doi: 10.1073/pnas.1515426112

Dreyer, B., Pérez-Gilabert, M., Olmos, E., Honrubia, M., and Mort, A. (2008). Ultrastructural localization of acid phosphatase in arbusculate coils of mycorrhizal *Phoenix canariensis* roots. *Physiol. Plant.* 132, 503–513. doi: 10.1111/j.1399-3054.2007.01034.x

Dreyer, I., Spitz, O., Kanonenberg, K., Montag, K., Handrich, M., Ahmad, S., et al. (2018). Nutrient exchange in arbuscular mycorrhizal symbiosis from a thermodynamic point of view. *New Phytol.* 222, 1043–1053. doi: 10.1111/nph.15646

Ezawa, T., Cavagnaro, T. R., Smith, S. E., Smith, F. A., and Ohtomo, R. (2004). Rapid accumulation of polyphosphate in extraradical hyphae of an arbuscular mycorrhizal fungus as revealed by histochemistry and a polyphosphate kinase/luciferase system. *New Phytol.* 161, 387–392. doi: 10.1046/j.1469-8137.2003.00966.x

Ezawa, T., Hayatsu, M., and Saito, M. (2005). A new hypothesis on the strategy for acquisition of phosphorus in arbuscular mycorrhiza: up-regulation of secreted acid phosphatase gene in the host plant. *Mol. Plant-Microbe Interact.* 18, 1046–1053. doi: 10.1094/MPMI-18-1046

Ezawa, T., Kuwahara, S., Sakamoto, K., Yoshida, T., and Saito, M. (1999). Specific inhibitor and substrate specificity of alkaline phosphatase expressed in the symbiotic phase of the arbuscular mycorrhizal fungus, *Glomus etunicatum*. *Mycologia* 91, 636–641. doi: 10.1080/00275514.1999.12061062

Ezawa, T., and Saito, K. (2018). How do arbuscular mycorrhizal fungi handle phosphate? New insights into fine-tuning of phosphate metabolism. *New Phytol.* 220, 1116–1121. doi: 10.1111/nph.15187

Ezawa, T., and Yoshida, T. (1994). Characterization of phosphatase in marigold roots infected with vesicular-arbuscular mycorrhizal fungi. *Soil Sci. Plant Nutr.* 40, 255–264. doi: 10.1080/00380768.1994.10413299

Field, K. J., and Pressel, S. (2018). Unity in diversity: structural and functional insights into the ancient partnerships between plants and fungi. *New Phytol.* 220, 996–1011. doi: 10.1111/nph.15158

Fiorilli, V., Lanfranco, L., and Bonfante, P. (2013). The expression of *GintPT*, the phosphate transporter of *Rhizophagus irregularis*, depends on the symbiotic status and phosphate availability. *Planta* 237, 1267–1277. doi: 10.1007/s00425-013-1842-z

Fukai, E., Soyano, T., Umehara, Y., Nakayama, S., Hirakawa, H., Tabata, S., et al. (2012). Establishment of a *Lotus japonicus* gene tagging population using the exon-targeting endogenous retrotransposon *LORE1*. *Plant J.* 69, 720–730. doi: 10.1111/j.1365-313X.2011.04826.x

Funamoto, R., Saito, K., Oyaizu, H., Saito, M., and Aono, T. (2007). Simultaneous *in situ* detection of alkaline phosphatase activity and polyphosphate in arbuscules within arbuscular mycorrhizal roots. *Funct. Plant Biol.* 34, 803–810. doi: 10.1071/FP06326

Gianinazzi-Pearson, V., and Gianinazzi, S. (1978). Enzymatic studies on the metabolism of vesicular-arbuscular mycorrhiza II. Soluble alkaline phosphatase specific to mycorrhizal infection in onion roots. *Physiol. Plant Pathol.* 12, 45–53. doi: 10.1016/0048-4059(78)90017-6

Gianinazzi-Pearson, V., Smith, S. E., Gianinazzi, S., and Smith, F. A. (1991). Enzymatic studies on the metabolism of vesicular-arbuscular mycorrhizas. V. Is H^+-ATPase a componenet of ATP-hydrolysing enzyme activities in plant-fungus interfaces? *New Phytol.* 117, 61–74. doi: 10.1111/j.1469-8137.1991.tb00945.x

Giovannini, D., Touhami, J., Charnet, P., Sitbon, M., and Battini, J.-L. (2013). Inorganic phosphate export by the retrovirus receptor XPR1 in metazoans. *Cell Rep.* 3, 1866–1873. doi: 10.1016/j.celrep.2013.05.035

Glassop, D., Smith, S. E., and Smith, F. W. (2005). Cereal phosphate transporters associated with the mycorrhizal pathway of phosphate uptake into roots. *Planta* 222, 688–698. doi: 10.1007/s00425-005-0015-0

Guether, M., Balestrini, R., Hannah, M., He, J., Udvardi, M. K., and Bonfante, P. (2009a). Genome-wide reprogramming of regulatory networks, transport, cell wall and membrane biogenesis during arbuscular mycorrhizal symbiosis in *Lotus japonicus*. *New Phytol.* 182, 200–212. doi: 10.1111/j.1469-8137.2008.02725.x

Guether, M., Neuhäuser, B., Balestrini, R., Dynowski, M., Ludewig, U., and Bonfante, P. (2009b). A mycorrhizal-specific ammonium transporter from *Lotus japonicus* acquires nitrogen released by arbuscular mycorrhizal fungi. *Plant Physiol.* 150, 73–83. doi: 10.1104/pp.109.136390

Guttenberger, M. (2000). Arbuscules of vesicular-arbuscular mycorrhizal fungi inhabit an acidic compartment within plant roots. *Planta* 211, 299–304. doi: 10.1007/s004250000324

Harrison, M. J. (1999). Molecular and cellular aspects of the arbuscular mycorrhizal symbiosis. *Annu. Rev. Plant Physiol. Plant Mol. Biol.* 50, 361–389. doi: 10.1146/annurev.arplant.50.1.361

Harrison, M. J., Dewbre, G. R., and Liu, J. Y. (2002). A phosphate transporter from *Medicago truncatula* involved in the acquisition of phosphate released by arbuscular mycorrhizal fungi. *Plant Cell* 14, 2413–2429. doi: 10.1105/tpc.004861

Harrison, M. J., and Van Buuren, M. L. (1995). A phosphate transporter from the mycorrhizal fungus *Glomus versiforme*. *Nature* 378, 626–629. doi: 10.1038/378626a0

Haugland, R.P. (ed.). (2005). *The Handbook - A Guide to Fluorescent Probes and Labeling Technologies*. USA: Invitrogen.

Hijikata, N., Murase, M., Tani, C., Ohtomo, R., Osaki, M., and Ezawa, T. (2010). Polyphosphate has a central role in the rapid and massive accumulation of phosphorus in extraradical mycelium of an arbuscular mycorrhizal fungus. *New Phytol.* 186, 285–289. doi: 10.1111/j.1469-8137.2009.03168.x

Hothorn, M., Neumann, H., Lenherr, E. D., Wehner, M., Rybin, V., Hassa, P. O., et al. (2009). Catalytic core of a membrane-associated eukaryotic polyphosphate polymerase. *Science* 324, 513–516. doi: 10.1126/science.1168120

Huang, R., Wan, B., Hultz, M., Diaz, J. M., and Tang, Y. (2018). Phosphatase-mediated hydrolysis of linear polyphosphates. *Environ. Sci. Technol.* 52, 1183–1190. doi: 10.1021/acs.est.7b04553

Ivanov, S., Austin, J., Berg, R. H., and Harrison, M. J. (2019). Extensive membrane systems at the host-arbuscular mycorrhizal fungus interface. *Nat. Plants* 5, 194–203. doi: 10.1038/s41477-019-0364-5

Javot, H., Penmetsa, R. V., Terzaghi, N., Cook, D. R., and Harrison, M. J. (2007). A *Medicago truncatula* phosphate transporter indispensable for the arbuscular mycorrhizal symbiosis. *Proc. Natl. Acad. Sci. U. S. A.* 104, 1720–1725. doi: 10.1073/pnas.0608136104

Jeanmaire, C., Dexheimer, J., Marx, C., Gianinazzi, S., and Gianinazzipearson, V. (1985). Effect of vesicular-arbuscular mycorrhizal infection on the distribution of neutral phosphatase activities in root cortical cells. *J. Plant Physiol.* 119, 285–293. doi: 10.1016/S0176-1617(85)80095-X

Kikuchi, Y., Hijikata, N., Ohtomo, R., Handa, Y., Kawaguchi, M., Saito, K., et al. (2016). Aquaporin-mediated long-distance polyphosphate translocation directed towards the host in arbuscular mycorrhizal symbiosis: application of virus-induced gene silencing. *New Phytol.* 211, 1202–1208. doi: 10.1111/nph.14016

Kikuchi, Y., Hijikata, N., Yokoyama, K., Ohtomo, R., Handa, Y., Kawaguchi, M., et al. (2014). Polyphosphate accumulation is driven by transcriptome alterations that lead to near-synchronous and near-equivalent uptake of inorganic cations in an arbuscular mycorrhizal fungus. *New Phytol.* 204, 638–649. doi: 10.1111/nph.12937

Kobae, Y., and Hata, S. (2010). Dynamics of periarbuscular membranes visualized with a fluorescent phosphate transporter in arbuscular mycorrhizal roots of rice. *Plant Cell Physiol.* 51, 341–353. doi: 10.1093/pcp/pcq013

Kobae, Y., Kawachi, M., Saito, K., Kikuchi, Y., Ezawa, T., Maeshima, M., et al. (2015). Up-regulation of genes involved in *N*-acetylglucosamine uptake and metabolism suggests a recycling mode of chitin in intraradical mycelium of arbuscular mycorrhizal fungi. *Mycorrhiza* 25, 411–417. doi: 10.1007/s00572-014-0623-2

Kobae, Y., Tomioka, R., Tanoi, K., Kobayashi, N. I., Ohmori, Y., Nishida, S., et al. (2014). Selective induction of putative iron transporters, *OPT8a* and *OPT8b*, in maize by mycorrhizal colonization. *Soil Sci. Plant Nutr.* 60, 843–847. doi: 10.1080/00380768.2014.949854

Kojima, T., Hayatsu, M., and Saito, M. (1998). Intraradical hyphae phosphatase of the arbuscular mycorrhizal fungus, *Gigaspora margarita*. *Biol. Fertil. Soils* 26, 331–335. doi: 10.1007/s003740050384

Kojima, T., Saito, K., Oba, H., Yoshida, Y., Terasawa, J., Umehara, Y., et al. (2014). Isolation and phenotypic characterization of *Lotus japonicus* mutants specifically defective in arbuscular mycorrhizal formation. *Plant Cell Physiol.* 55, 928–941. doi: 10.1093/pcp/pcu024

Krajinski, F., Courty, P.-E., Sieh, D., Franken, P., Zhang, H., Bucher, M., et al. (2014). The H^+-ATPase HA1 of *Medicago truncatula* is essential for phosphate transport and plant growth during arbuscular mycorrhizal symbiosis. *Plant Cell* 26, 1808–1817. doi: 10.1105/tpc.113.120436

Kuga, Y., Saito, K., Nayuki, K., Peterson, R. L., and Saito, M. (2008). Ultrastructure of rapidly-frozen and freeze-substituted germ tubes of an arbuscular mycorrhizal fungus and localization of polyphosphate. *New Phytol.* 178, 189–200. doi: 10.1111/j.1469-8137.2007.02345.x

Li, C., Gui, S., Yang, T., Walk, T., Wang, X., and Liao, H. (2012). Identification of soybean purple acid phosphatase genes and their expression responses to phosphorus availability and symbiosis. *Ann. Bot.* 109, 275–285. doi: 10.1093/aob/mcr246

Li, C., Zhou, J., Wang, X., and Liao, H. (2019). A purple acid phosphatase, *GmPAP33*, participates in arbuscule degeneration during AM symbiosis in soybean. *Plant Cell Environ.* 42, 2015–2027. doi: 10.1111/pce.13530

Liu, J., Chen, J., Xie, K., Tian, Y., Yan, A., Liu, J., et al. (2020). A mycorrhiza-specific H^+-ATPase is essential for arbuscule development and symbiotic phosphate and nitrogen uptake. *Plant Cell Environ.* 43, 1069–1083. doi: 10.1111/pce.13714

Liu, Q., Parsons, A. J., Xue, H., Jones, C. S., and Rasmussen, S. (2013). Functional characterisation and transcript analysis of an alkaline phosphatase from the arbuscular mycorrhizal fungus *Funneliformis mosseae*. *Fungal Genet. Biol.* 54, 52–59. doi: 10.1016/j.fgb.2013.02.009

Maeda, D., Ashida, K., Iguchi, K., Chechetka, S. A., Hijikata, A., Okusako, Y., et al. (2006). Knockdown of an arbuscular mycorrhiza-inducible phosphate transporter gene of *Lotus japonicus* suppresses mutualistic symbiosis. *Plant Cell Physiol.* 47, 807–817. doi: 10.1093/pcp/pcj069

Maldonado-Mendoza, I. E., Dewbre, G. R., and Harrison, M. J. (2001). A phosphate transporter gene from the extra-radical mycelium of an arbuscular mycorrhizal fungus *Glomus intraradices* is regulated in response to phosphate in the environment. *Mol. Plant-Microbe Interact.* 14, 1140–1148. doi: 10.1094/MPMI.2001.14.10.1140

Marx, C., Dexheimer, J., Gianinazzi-Pearson, V., and Gianinazzi, S. (1982). Enzymatic studies on the metabolism of vesicular-arbuscular mycorrhizas. IV. Ultracytoenzymological evidence (ATPase) for active transfer processes in the host-arbscule interface. *New Phytol.* 90, 37–43. doi: 10.1111/j.1469-8137.1982.tb03238.x

Nagy, R., Karandashov, V., Chague, V., Kalinkevich, K., Tamasloukht, M. B., Xu, G., et al. (2005). The characterization of novel mycorrhiza-specific phosphate transporters from *Lycopersicon esculentum* and *Solanum tuberosum* uncovers functional redundancy in symbiotic phosphate transport in solanaceous species. *Plant J.* 42, 236–250. doi: 10.1111/j.1365-313X.2005.02364.x

Nakakoshi, M., Nishioka, H., and Katayama, E. (2011). New versatile staining reagents for biological transmission electron microscopy that substitute for uranyl acetate. *J. Electron Microsc.* 60, 401–407. doi: 10.1093/jmicro/dfr084

Nayuki, K., Chen, B. D., Ohtomo, R., and Kuga, Y. (2014). Cellular imaging of cadmium in resin sections of arbuscular mycorrhizas using synchrotron micro X-ray fluorescence. *Microbes Environ.* 29, 60–66. doi: 10.1264/jsme2.ME13093

Nielsen, J. S., Joner, E. J., Declerck, S., Olsson, S., and Jakobsen, I. (2002). Phospho-imaging as a tool for visualization and noninvasive measurement of P transport dynamics in arbuscular mycorrhizas. *New Phytol.* 154, 809–819. doi: 10.1046/j.1469-8137.2002.00412.x

Ohtomo, R., and Saito, M. (2005). Polyphosphate dynamics in mycorrhizal roots during colonization of an arbuscular mycorrhizal fungus. *New Phytol.* 167, 571–578. doi: 10.1111/j.1469-8137.2005.01425.x

Pierzynski, G. M., Mcdowell, R. W., and Sims, J. T. (2005). "Chemistry, cycling, and potential movement of inorganic phosphorus in soils," in *Phosphorus: Agriculture and the Environment*. eds. J. T. Sims and A. N. Sharpley (Madison, WI: American Society of Agronomy, Crop Science Society of America, Soil Science Society of America, Inc.), 53–86.

Pumplin, N., Zhang, X., Noar, R. D., and Harrison, M. J. (2012). Polar localization of a symbiosis-specific phosphate transporter is mediated by a transient reorientation of secretion. *Proc. Natl. Acad. Sci. U. S. A.* 109, E665–E672. doi: 10.1073/pnas.1110215109

Raghothama, K. G. (1999). Phosphate acquisition. *Annu. Rev. Plant Physiol. Plant Mol. Biol.* 50, 665–693. doi: 10.1146/annurev.arplant.50.1.665

Rasmussen, N., Lloyd, D. C., Ratcliffe, R. G., Hansen, P. E., and Jakobsen, I. (2000). ^{31}P NMR for the study of P metabolism and translocation in arbuscular mycorrhizal fungi. *Plant Soil* 226, 245–253. doi: 10.1023/A:1026411801081

Roth, R., Hillmer, S., Funaya, C., Chiapello, M., Schumacher, K., Lo Presti, L., et al. (2019). Arbuscular cell invasion coincides with extracellular vesicles and membrane tubules. *Nat. Plants* 5, 204–211. doi: 10.1038/s41477-019-0365-4

Saito, K., and Ezawa, T. (2016). "Phosphorus metabolism and transport in arbuscular mycorrhizal symbiosis," in *Molecular Mycorrhizal Symbiosis*. ed. F. Martin (New Jersey: John Wiley & Sons, Inc.), 197–216.

Saito, K., Ohtomo, R., Kuga-Uetake, Y., Aono, T., and Saito, M. (2005). Direct labeling of polyphosphate at the ultrastructural level in *Saccharomyces cerevisiae* by using the affinity of the polyphosphate binding domain of *Escherichia coli* exopolyphosphatase. *Appl. Environ. Microbiol.* 71, 5692–5701. doi: 10.1128/AEM.71.10.5692-5701.2005

Schmittgen, T. D., and Livak, K. J. (2008). Analyzing real-time PCR data by the comparative C_t method. *Nat. Protoc.* 3, 1101–1108. doi: 10.1038/nprot.2008.73

Schneider, C. A., Rasband, W. S., and Eliceiri, K. W. (2012). NIH image to ImageJ: 25 years of image analysis. *Nat. Methods* 9, 671–675. doi: 10.1038/nmeth.2089

Schott, S., Valdebenito, B., Bustos, D., Gomez-Porras, J. L., Sharma, T., and Dreyer, I. (2016). Cooperation through competition—dynamics and microeconomics of a minimal nutrient trade system in arbuscular mycorrhizal symbiosis. *Front. Plant Sci.* 7, 912. doi: 10.3389/fpls.2016.00912

Smith, S. A., Wang, Y., and Morrissey, J. H. (2018). DNA ladders can be used to size polyphosphate resolved by polyacrylamide gel electrophoresis. *Electrophoresis* 39, 2454–2459. doi: 10.1002/elps.201800227

Smith, S. E., Jakobsen, I., Grønlund, M., and Smith, F. A. (2011). Roles of arbuscular mycorrhizas in plant phosphorus nutrition: interactions between pathways of phosphorus uptake in arbuscular mycorrhizal roots have important implications for understanding and manipulating plant phosphorus acquisition. *Plant Physiol.* 156, 1050–1057. doi: 10.1104/pp.111.174581

Smith, S. E., and Smith, F. A. (1990). Structure and function of the interfaces in biotrophic symbioses as they relate to nutrient transport. *New Phytol.* 114, 1–38. doi: 10.1111/j.1469-8137.1990.tb00370.x

Smith, S. E., and Smith, F. A. (2011). Roles of arbuscular mycorrhizas in plant nutrition and growth: new paradigms from cellular to ecosystem scales. *Annu. Rev. Plant Biol.* 62, 227–250. doi: 10.1146/annurev-arplant-042110-103846

Smith, S. E., Smith, F. A., and Jakobsen, I. (2003). Mycorrhizal fungi can dominate phosphate supply to plants irrespective of growth responses. *Plant Physiol.* 133, 16–20. doi: 10.1104/pp.103.024380

Smith, S. E., Smith, F. A., and Jakobsen, I. (2004). Functional diversity in arbuscular mycorrhizal (AM) symbioses: the contribution of the mycorrhizal P uptake patheway is not correlated with mycorrhizal responses in growth or total P uptake. *New Phytol.* 162, 511–524. doi: 10.1111/j.1469-8137.2004.01039.x

Solaiman, M. Z., Ezawa, T., Kojima, T., and Saito, M. (1999). Polyphosphates in intraradical and extraradical hyphae of an arbuscular mycorrhizal fungus, *Gigaspora margarita*. *Appl. Environ. Microbiol.* 65, 5604–5606. doi: 10.1128/AEM.65.12.5604-5606.1999

Solaiman, M. Z., and Saito, M. (2001). Phosphate efflux from intraradical hyphae of *Gigaspora margarita in vitro* and its implication for phosphorus translocation. *New Phytol.* 151, 525–533. doi: 10.1046/j.0028-646x.2001.00182.x

Takanishi, I., Ohtomo, R., Hayatsu, M., and Saito, M. (2009). Short-chain polyphosphate in arbuscular mycorrhizal roots colonized by *Glomus* spp.: a possible phosphate pool for host plants. *Soil Biol. Biochem.* 41, 1571–1573. doi: 10.1016/j.soilbio.2009.04.002

Takeda, N., Sato, S., Asamizu, E., Tabata, S., and Parniske, M. (2009). Apoplastic plant subtilases support arbuscular mycorrhiza development in *Lotus japonicus*. *Plant J.* 58, 766–777. doi: 10.1111/j.1365-313X.2009.03824.x

Tani, C., Ohtomo, R., Osaki, M., Kuga, Y., and Ezawa, T. (2009). ATP-dependent but proton gradient-independent polyphosphate-synthesizing activity in extraradical hyphae of an arbuscular mycorrhizal fungus. *Appl. Environ. Microbiol.* 75, 7044–7050. doi: 10.1128/AEM.01519-09

Tijssen, J. P. F., Beekes, H. W., and Van Steveninck, J. (1982). Localization of polyphosphates in *Saccharomyces fragilis*, as revealed by 4′,6-diamidino-2-phenylindole fluorescence. *Biochim. Biophys. Acta* 721, 394–398. doi: 10.1016/0167-4889(82)90094-5

Tisserant, E., Kohler, A., Dozolme-Seddas, P., Balestrini, R., Benabdellah, K., Colard, A., et al. (2012). The transcriptome of the arbuscular mycorrhizal fungus *Glomus intraradices* (DAOM 197198) reveals functional tradeoffs in an obligate symbiont. *New Phytol.* 193, 755–769. doi: 10.1111/j.1469-8137.2011.03948.x

Trouvelot, A., Kough, J. L., and Gianinazzi-Pearson, V. (1986). "Mesure du taux de mycorhization VA d'un systeme radiculaire. Recherche de methodes d'estimation ayant une signification fonctionnelle" in *Physiological and Genetical Aspects of Mycorrhizae*. eds. V. Gianinazzi-Pearson and S. Gianinazzi (Paris: INRA Press), 217–221.

Uetake, Y., Kojima, T., Ezawa, T., and Saito, M. (2002). Extensive tubular vacuole system in an arbuscular mycorrhizal fungus, *Gigaspora margarita*. *New Phytol.* 154, 761–768. doi: 10.1046/j.1469-8137.2002.00425.x

Urbański, D. F., Małolepszy, A., Stougaard, J., and Andersen, S. U. (2012). Genome-wide *LORE1* retrotransposon mutagenesis and high-throughput insertion detection in *Lotus japonicus*. *Plant J.* 69, 731–741. doi: 10.1111/j.1365-313X.2011.04827.x

Van Aarle, I. M., Cavagnaro, T. R., Smith, S. E., Smith, F. A., and Dickson, S. (2005). Metabolic activity of *Glomus intraradices* in *Arum*- and *Paris*-type arbuscular mycorrhizal colonization. *New Phytol.* 166, 611–618. doi: 10.1111/j.1469-8137.2005.01340.x

Viereck, N., Hansen, P. E., and Jakobsen, I. (2004). Phosphate pool dynamics in the arbuscular mycorrhizal fungus *Glomus intraradices* studied by *in vivo* ^{31}P NMR spectroscopy. *New Phytol.* 162, 783–794. doi: 10.1111/j.1469-8137.2004.01048.x

Wang, E., Schornack, S., Marsh, J. F., Gobbato, E., Schwessinger, B., Eastmond, P., et al. (2012). A common signaling process that promotes mycorrhizal and

oomycete colonization of plants. *Curr. Biol.* 22, 2242–2246. doi: 10.1016/j.cub.2012.09.043

Wang, E., Yu, N., Bano, S. A., Liu, C., Miller, A. J., Cousins, D., et al. (2014). A H^+-ATPase that energizes nutrient uptake during mycorrhizal symbioses in rice and *Medicago truncatula*. *Plant Cell* 26, 1818–1830. doi: 10.1105/tpc.113.120527

Watanabe, F. S., and Olsen, S. R. (1965). Test of an ascorbic acid method for determining phosphorus in water and $NaHCO_3$ extracts from soil. *Soil Sci. Soc. Am. J.* 29, 677–678. doi: 10.2136/sssaj1965.03615995002900060025x

Watts-Williams, S. J., Jakobsen, I., Cavagnaro, T. R., and Grønlund, M. (2015). Local and distal effects of arbuscular mycorrhizal colonization on direct pathway pi uptake and root growth in *Medicago truncatula*. *J. Exp. Bot.* 66, 4061–4073. doi: 10.1093/jxb/erv202

Werner, T. P., Amrhein, N., and Freimoser, F. M. (2007). Specific localization of inorganic polyphosphate (poly P) in fungal cell walls by selective extraction and immunohistochemistry. *Fungal Genet. Biol.* 44, 845–852. doi: 10.1016/j.fgb.2007.01.008

Willmann, M., Gerlach, N., Buer, B., Polatajko, A., Nagy, R., Koebke, E., et al. (2013). Mycorrhizal phosphate uptake pathway in maize: vital for growth and cob development on nutrient poor agricultural and greenhouse soils. *Front. Plant Sci.* 4:533. doi: 10.3389/fpls.2013.00533

Xie, X., Huang, W., Liu, F., Tang, N., Liu, Y., Lin, H., et al. (2013). Functional analysis of the novel mycorrhiza-specific phosphate transporter AsPT1 and PHT1 family from *Astragalus sinicus* during the arbuscular mycorrhizal symbiosis. *New Phytol.* 198, 836–852. doi: 10.1111/nph.12188

Xie, X., Lin, H., Peng, X., Xu, C., Sun, Z., Jiang, K., et al. (2016). Arbuscular mycorrhizal symbiosis requires a phosphate transceptor in the *Gigaspora margarita* fungal symbiont. *Mol. Plant* 9, 1583–1608. doi: 10.1016/j.molp.2016.08.011

Yang, S.-Y., Grønlund, M., Jakobsen, I., Grotemeyer, M. S., Rentsch, D., Miyao, A., et al. (2012). Nonredundant regulation of rice arbuscular mycorrhizal symbiosis by two members of the *PHOSPHATE TRANSPORTER1* gene family. *Plant Cell* 24, 4236–4251. doi: 10.1105/tpc.112.104901

Conflict of Interest: The authors declare that the research was conducted in the absence of any commercial or financial relationships that could be construed as a potential conflict of interest.

Publisher's Note: All claims expressed in this article are solely those of the authors and do not necessarily represent those of their affiliated organizations, or those of the publisher, the editors and the reviewers. Any product that may be evaluated in this article, or claim that may be made by its manufacturer, is not guaranteed or endorsed by the publisher.

frontiers in Plant Science

ORIGINAL RESEARCH
published: 08 October 2021
doi: 10.3389/fpls.2021.741050

The Effects of *Turnip Mosaic Virus* Infections on the Deposition of Secondary Cell Walls and Developmental Defects in Arabidopsis Plants Are Virus-Strain Specific

OPEN ACCESS

Edited by:
José Díaz,
University of A Coruña, Spain

Reviewed by:
Venura Herath,
University of Peradeniya, Sri Lanka
Javier Veloso,
University of A Coruña, Spain

***Correspondence:**
Fernando Ponz
fponz@inia.es

Specialty section:
This article was submitted to Plant Pathogen Interactions, a section of the journal Frontiers in Plant Science

Received: *14 July 2021*
Accepted: *13 September 2021*
Published: *08 October 2021*

Citation:
López-González S, Gómez-Mena C, Sánchez F, Schuetz M, Samuels AL and Ponz F (2021) The Effects of Turnip Mosaic Virus Infections on the Deposition of Secondary Cell Walls and Developmental Defects in Arabidopsis Plants Are Virus-Strain Specific. Front. Plant Sci. 12:741050. doi: 10.3389/fpls.2021.741050

Silvia López-González[1], Concepción Gómez-Mena[2], Flora Sánchez[1], Mathias Schuetz[3], A. Lacey Samuels[3] and Fernando Ponz[1]*

[1]Centro de Biotecnología y Genómica de Plantas, Universidad Politécnica de Madrid-Centro Nacional Instituto Nacional de Investigación y Tecnología Agraria y Alimentaria, CSIC, Madrid, Spain, [2]Instituto de Biología Molecular y Celular de Plantas, Universitat Politècnica de València-Consejo Superior de Investigaciones Científicas, Valencia, Spain, [3]Department of Botany, University of British Columbia, Vancouver, BC, Canada

Two isolates of Turnip mosaic virus (UK 1 and JPN 1), representative of two different viral strains, induced differential alterations on secondary cell wall (SCW) development in *Arabidopsis thaliana*, suggesting cell-type specific effects of these viral infections. These potential effects were analyzed in inflorescence stems and flowers of infected plants, together with other possible cellular effects of the infections. Results obtained from macroscopic and histochemical analyses showed that infection with either virus significantly narrowed stem area, but defects in SCW were only found in JPN 1 infections. In flowers, reduced endothecium lignification was also found for JPN 1, while UK 1 infections induced severe floral cell and organ development alterations. A transcriptomic analysis focused on genes controlling and regulating SCW formation also showed notable differences between both viral isolates. UK 1 infections induced a general transcriptional decrease of most regulatory genes, whereas a more complex pattern of alterations was found in JPN 1 infections. The role of the previously identified viral determinant of most developmental alterations, the P3 protein, was also studied through the use of viral chimeras. No SCW alterations or creeping habit growth were found in infections by the chimeras, indicating that if the P3 viral protein is involved in the determination of these symptoms, it is not the only determinant. Finally, considerations as to the possibility of a taxonomical reappraisal of these TuMV viral strains are provided.

Keywords: turnip mosaic virus, secondary cell wall, developmental alterations, viral strains, viral chimeras

INTRODUCTION

Viruses often induce disease symptoms in the infected host, which in plants include mottles or mosaics, yellowing, or stunted growth. These general symptoms have long been recognized, are easily observed and well documented. The underlying molecular and cellular mechanisms are not fully understood, although they are the subject of a sustained research, reviewed in detail a few years ago (Culver and Padmanabhan, 2007; Pallás and García, 2011). However, less information is available on those disease symptoms affecting specific developmental traits. Plant development is mostly post-embryonic, consisting of phases with marked transitions (Huijser and Schmid, 2011), consequently virus infections of plants have increased chances to affect traits that are characteristic of the developmental phase, as compared with organisms with an embryonic development.

In previous work, we have established a system that allows focusing on some of these developmental traits. Infections of *Arabidopsis thaliana* with *Turnip mosaic virus* (TuMV, a potyvirus) alter a number of developmental stages that we identified in practically all plant organs in a comparative analysis between virus strains (Sánchez et al., 2015). Notable differential alterations affected the elongation and erection of the main inflorescence stem, and inflorescence branching pattern. Thus, plants infected with the viral isolate UK 1 were not able to elongate a stem, or produced only a very short stem with no flowers, or a few sterile ones. Those infected with isolate JPN 1 elongated a creeping inflorescence stem, which is unable to maintain upright growth. The derived inflorescence was highly branched, giving the plants a bushy global appearance with the intertwined branches forming a net just over the rosettes. The viral protein P3 is associated with the elongation trait (López-González et al., 2020). No information is available about the viral determinant of the creeping and branching.

The developmental alterations described above are strongly suggestive of an impact of the TuMV infections on the normal formation of the cell walls of the plant main vertical axis cells. Cell walls are critical players in mediating upwards plant growth, physical structure, and global morphogenesis, in highly regulated processes (Houston et al., 2016). Both primary and secondary cell walls (SCWs) play roles in growth and physical structure, although those plant cells developing SCWs are mainly responsible for the latter. The cell and molecular biology of SCW deposition and regulation have been recently reviewed (Meents et al., 2018; Zhong et al., 2019). Since the infection by TuMV has a strong impact on Arabidopsis global morphogenesis, in this work, we have focused on the effects of the virus on SCW formation and composition, and in the transcriptomics of the genes involved in the regulation of their formation. This work deciphers the relationship between virus infections and their impact on plant SCWs.

MATERIALS AND METHODS

Plant Growth Conditions and Virus Inoculations

Arabidopsis thaliana Col-0 plants were grown under controlled conditions: 21°C (day)/18°C (night) in 16-and 8-h cycles. Plants were inoculated at stage 1.08 (Boyes et al., 2001) with crude sap from virus-infected plants with TuMV UK 1 or TuMV JPN 1. In certain experiments, plants were inoculated with viral chimeras which interchange genomic fragments of the two strains. The description of the constructions of these chimeras and the inoculations to Arabidopsis plants have been previously published (Sánchez et al., 2015).

Histological Analyses

Flower stalks from Arabidopsis (20 days post inoculation) were cut 1 cm above the base and embedded in 7% (w/v) low melting point agarose following the protocol described (Pradhan Mitra and Loqué, 2014). Agarose blocks were sectioned using a vibratome (Leica VT1200 S). Cross sections were stained with toluidine blue [0.05% (w/v)] or HCl-phloroglucinol staining solution [10% phloroglucinol in absolute ethanol (w/v) with the addition of concentrated HCl before use], or freshly mounted and imaged for lignin autofluorescence. Sections were treated with 0.01% calcofluor white M2r (Sigma) for cellulose visualization. Slides were observed with an optical microscope (Nikon Eclipse E600).

Flower buds were submerged in FAE solution [4% formaldehyde (v/v), 5% acetic acid (v/v), and 50% ethanol(v/v)], placed under vacuum for 10 min and incubated overnight at 4°C. Samples were dehydrated in alcohol and embedded in acrylic resin (Technovit 7,100; Kulzer). For histological analysis, 1-μm transversal sections of the floral buds were obtained and stained with 0.05% toluidine blue in 0.1 M phosphate buffer at pH 6.8 (O'Brien et al., 1964). Slides were observed with an optical microscope (Nikon Eclipse E600).

Immunohistochemistry

For xylan immunostaining, flower stalks from mature Arabidopsis were cut 1 cm above the base and fixed with FAE for 1 h and washed with TBST solution [10 mM Tris–HCl (pH 7.0), 0.25 M NaCl, and 0.1% (w/v) Tween 20]. The sections were blocked with 0.2 M PBS containing 5% (w/v) bovine serum albumin for 1 h at room temperature, followed by incubation with anti-xylan LM10 rat monoclonal antibody (Plant Probes; (McCartney et al., 2005)) at 1:50 dilution overnight at 4°C with gentle shaking. Tissue samples were washed three times with TBST and incubated with anti-rat antibody conjugated to Alexa 488 (Invitrogen) at 1:100 dilution at room temperature for 1 h. Imaging of stalk longitudinal sections was performed on Laser Scanning Microscope Leica TCS SP8 using conventional GFP settings (488/509).

Scanning Electron Microscopy

Fresh samples were deep-frozen in slush nitrogen and attached to the specimen holder of a CryoTrans 1,500 Cryo-Preparation System (Oxford 127 Instruments, UK) interfaced with a JEOL JSM-5410 scanning electron microscope. Samples were gold-coated and observed at an accelerating voltage of 15 keV.

Gene Expression Analysis

Total RNA from stem longitudinal sections were extracted using the RNAeasy mini kit (Qiagen) following the manufacturer's instructions. Buffer-inoculated plants were used as a control. For the analysis, the first internode starting from the rosettes was taken, the same part of the plant used for the histological analyses. To avoid possible cross-contaminations, a clean mortar and pestle was used for each treatment. cDNA was synthesized using the kit High Capacity RNA-to-cDNA (Life Technologies), according to the manufacturer's instructions. Primers for RT-qPCR were designed using Primer3Plus (**Supplementary Table S1**). RT-qPCR was performed in a LightCycler 480 System (Roche), using LightCycler 480 SYBR green I master (Roche), following manufacturer's instructions. Cycling conditions for amplifications were as follows. Initial activation step of 95°C for 5 min followed by 45 cycles of 95°C for 10 s, 60°C for 10 s, and 72°C for 15 s. Changes in gene expression were determined using the $2^{-\Delta\Delta CT}$ method (Livak and Schmittgen, 2001). Data were relativized to 1, thus errors in the controls were calculated using the Standard Deviation/Mock CT Average. Results were expressed as fold change relative to the housekeeping gene *Actin 8* (*AT1G49240*). The experiments were carried out in triplicate for each data point. In detail: Three-four plants (stems) were used to prepare one biological replica. In total, 10–12 plants per treatment were used, and there were three biological replicas. For each biological replica, three technical replicates were loaded in the plate. This experiment was done twice, with different biological material, and the results were similar.

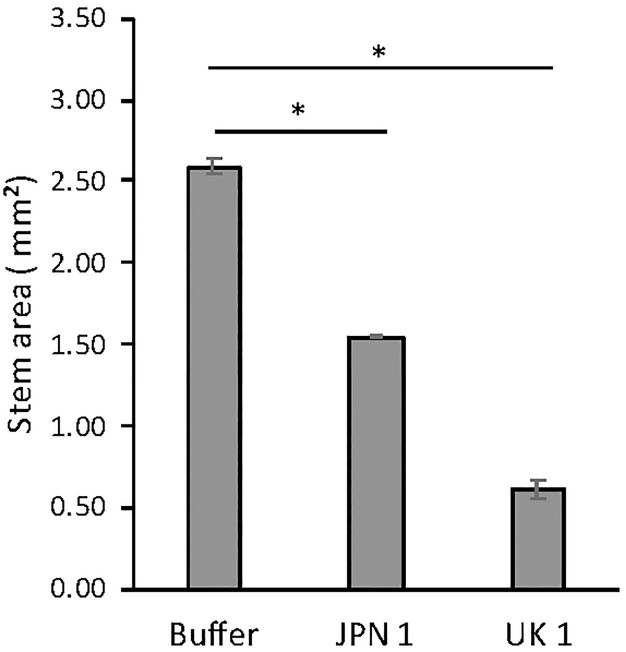

FIGURE 1 | Inflorescence stem areas of non-infected and TuMV-infected Arabidopsis plants, showing statistically significant differences (marked with and asterisk) between infected and non-infected plants (see text for experimental details). The statistical analysis was a student's *t*-test comparing Mock and JPN 1, and Mock and UK 1 ($p < 0.05$).

RESULTS

TuMV Infections Affect Arabidopsis Secondary Growth, Generating Narrow Stalks

The possible effect of TuMV infections on the inflorescence stem of Arabidopsis plants was assessed by comparing the cross-sectional areas of stems from the basal region (first internode) at 20 days after infection (dai). In control (buffer-inoculated) plants, the sections were done 5 cm above the rosette. UK 1-inoculated plants normally did not elongate 5 cm, so these stems were sampled just below the first internode. The areas were obtained by image analysis of microscope examinations, using the software Fiji. Compared to control plants, both the JPN 1-and UK 1-inoculated had significantly reduced stem areas (**Figure 1**). The area was reduced from $2.59 \pm 0.04\,mm^2$ for the buffer-inoculated control stems to 1.54 ± 0.01 for JPN 1 and 0.61 ± 0.06 for UK 1 (mean + SEM). These results clearly showed that TuMV infections with either viral strain led to thinner inflorescence stems.

Histochemical Analyses of the Virus-Infected Narrow Stems Reveal Viral Strain-Specific Alterations in Lignin SCW Deposition and in Stem Cell Sizes

We reasoned that important alterations in the composition/deposition of the stem SCWs of virus-infected plants could be underlying their reduction in diameter, so we approached their characterization by means of histochemical analyses. The presence of lignin in the secondary walls was assessed by phloroglucinol-HCl staining (**Figure 2**, upper row). In contrast to buffer-inoculated controls and plants infected with the UK-1 strain, where lignin stained SCW of the vascular bundles and interfascicular fibers in purple red, lignin deposition was absent or very low in JPN 1-infected SCWs (**Figure 2**). Analogous results were obtained when the stems were stained with Toluidine Blue (**Supplementary Figure S1**). Lignin was also directly visualized under UV light (**Figure 2**, middle row), which revealed lignin was present in xylem vessels, but not in xylary fibers or interfascicular fibers in the JPN 1-infected stems. This is probably a major reason for their lack of rigidity and high stalk fragility. No such lignin alteration was found in UK 1-infected stalks, which had a lignin deposition similar to buffer-inoculated plants. A major difference, however, was found in the cell sizes in the UK 1-infected (note the different sizes of the 100 µm bar in the Figure). In UK-1 plants, this is an important cause for the reduced stem areas of these plants.

Calcofluor staining was also performed to analyze possible alterations in the deposition of cellulose, callose, or other β-glucans. No major alterations for these wall components in virus-infected plants were found (**Figure 2**, bottom row), although the differences in cell sizes were also evident.

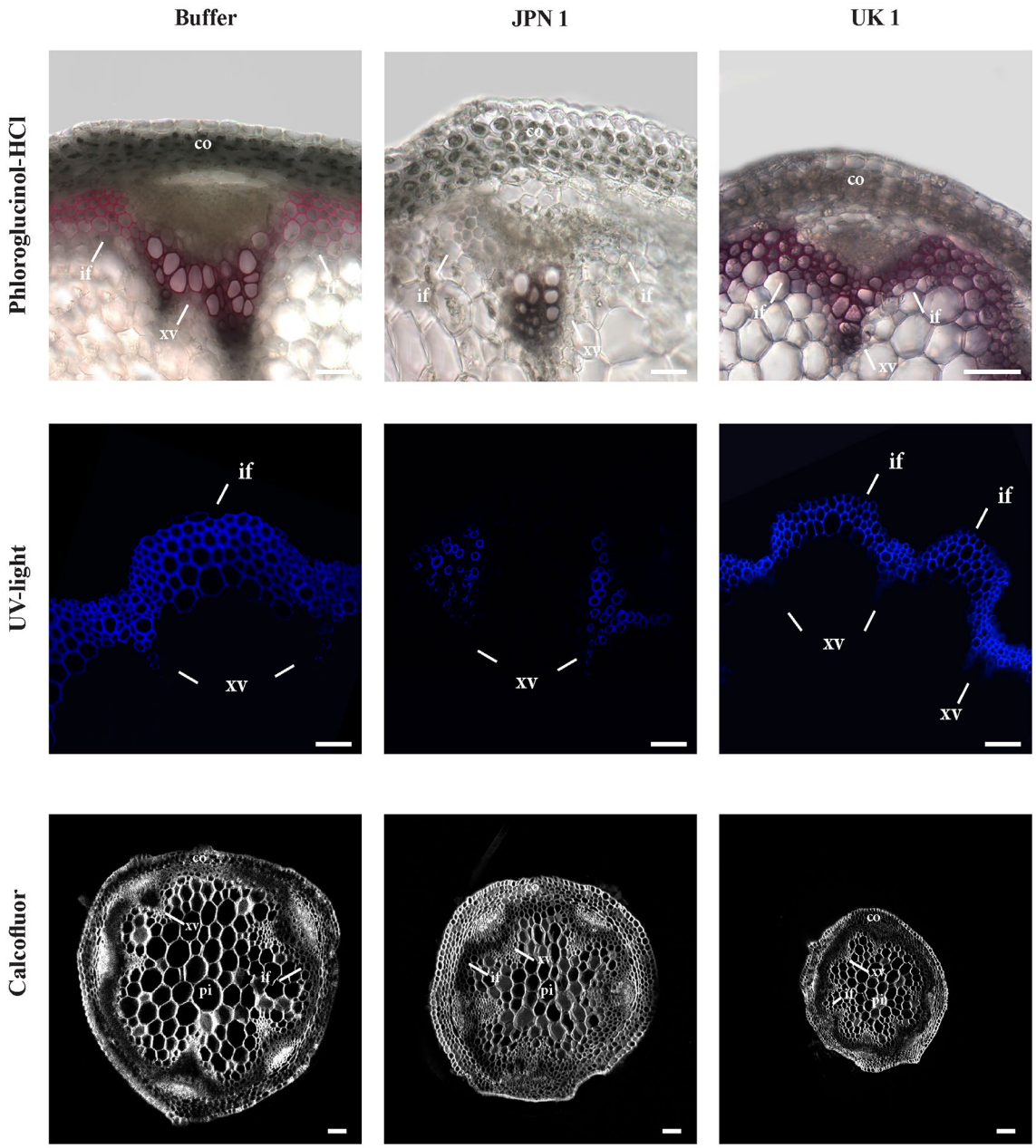

FIGURE 2 | Lignin histochemical analyses of the secondary cell walls (SCWs) of the inflorescence stems from plants mock-inoculated (buffer) or inoculated with either TuMV strain (JPN 1 or UK (1). **Top row** shows lignin staining with phloroglucinol; **middle row** shows lignin intrinsic fluorescence upon ultraviolet excitation (UV light); and **bottom row** shows cellulose staining with Calcofluor. Bars indicate 100 μm. The cortex (co), xylem vessels (xv), and interfascicular fibers (if) are marked with letters. Note the lack of differentiation in the interfascicular fibers of JPN 1.

Viral Strain-Specific Xylan Alterations Revealed by Immunofluorescence

A monoclonal antibody to xylan (LM10; (McCartney et al., 2005)) was used to analyze possible alterations in this important hemicellulose component of SCWs (**Figure 3**). The UV visualization of LM10 localization with a fluorescent secondary antibody showed a major lack of xylan in JPN 1-infected plants, with sparse fluorescent signal present only in the xylem vessels, and either no or irregular fluorescence in interfascicular fibers. No relevant xylan-label differences were found between the UK 1-plants and the buffer-inoculated, indicating a situation similar to the one found for lignin. The absence of xylan, and possibly of other hemicellulose components, would be contributing to the fragility and non-rigid inflorescence stems from JPN 1-infected plants, together with the lignin deficiency.

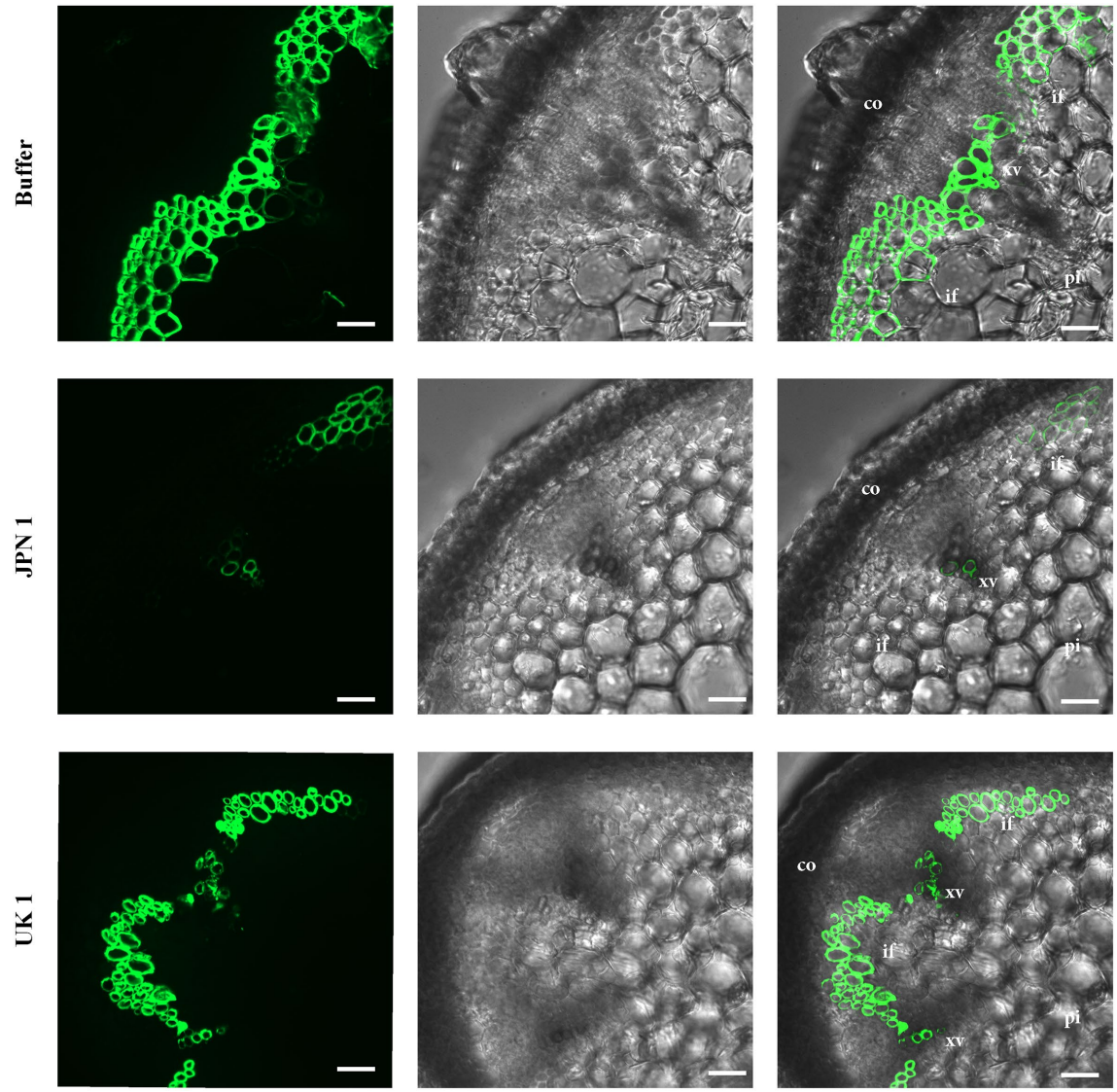

FIGURE 3 | Xylan immunohistochemical analysis. The presence of xylan was revealed by its recognition by the monoclonal antibody LM10, followed by the reaction with a fluorescent secondary antibody. Xylan is only weakly detected in the xylem in TuMV strain JPN 1-infected plants **(middle row)** compared to buffer control **(top)** or strain UK 1 **(bottom)**. In the third column, the fluorescence images are superimposed on the bright field shown in the second column. The cortex (co), xylem vessels (xv), interfascicular fibers (if), and pith (pi) are marked with letters.

The Viral Determinant for Inflorescence Stem Elongation Alone Does Not Determine the Creeping Habit of JPN 1-Infected Plants

The infection of Arabidopsis by the TuMV isolates leads to alterations in the inflorescence stem development. In the case of UK 1, the lack of stem elongation is the most dramatic one, whereas JPN 1 infections lead to fragile, non-erect stems conferring a creeping habit to the plant. The viral non-structural protein P3 was identified initially as the determinant for the lack of elongation in UK 1-infected Arabidopsis plants (Sánchez et al., 2015). Later, this determinant was finely mapped to the amino acid at position 279 of the protein (López-González et al., 2020). However, the determinant for the JPN 1-induced creeping phenotype has not been identified so far. Considering the differential intracellular ER-associated movement dynamics of the P3 proteins of the two isolates (López-González et al., 2020), we hypothesized that disrupted development of cells with thick cell walls could also be mediated by the P3 protein.

To tackle this issue, we used the same viral chimera approach described previously (Sánchez et al., 2015), where the P3 cistron was interchanged between the two isolates. The viral chimeras were Ch. U(2511-3767)J, where the JPN 1 P3 was inserted into the UK 1 strain and Ch. J(2511-3767)U, which was the reverse with UK 1 as the donor inserted into JPN 1. These chimeras were inoculated to Arabidopsis plants and the creeping

habit trait was examined. As predicted, interchanging the P3 viral proteins changed the elongation trait, and plants infected by Ch. J(2511-3767)U, which is mostly JPN 1 with a UK 1 P3, did not elongate a stem, whereas the reciprocal chimera Ch. U(2511-3767)J did. Surprisingly, in opposition to its parent isolate JPN 1, plants infected with the Ch. U(2511-3767)J chimera did not show a creeping habit and produced an erect stalk (**Figure 4**). This discarded the P3 protein as the sole viral determinant, although did not discard the possibility of its implication in the trait in a joint action with other factor(s), as yet unidentified.

The visual observation of the phenotypes of plants infected with the viral chimeras was complemented with a histochemical analysis to assess possible alterations in the stem development and SCWs. The results shown in **Figure 5** revealed that lignin and xylan-label of SCWs were similar among the controls and chimeras. These results indicate that JPN 1 P3 by itself is not enough determinant within the viral genome to induce the SCWs alterations but is required for them because the alterations disappear with UK 1 P3.

Gene Expression Analysis of the Master Genes Regulating SCW Biosynthesis in TuMV-Infected Arabidopsis Plants

The biosynthesis of the SCW is a highly complex process regulated at several levels (McCahill and Hazen, 2019). Among these levels, the transcriptional one is central and has been the subject of intense research over the last two decades or so (Yamaguchi et al., 2011; Schuetz et al., 2013; Ohtani and Demura, 2019). A global view of the regulation at the transcriptional level reveals a network of feed-forward loops affecting both regulatory genes (transcription factors, TFs) and metabolic genes (Taylor-Teeples et al., 2015). Occupying a central position in the network is TFs MYB46 and MYB83. These are involved in the regulation of the TFs that regulate the expression of the genes required to biosynthesize the structural components of SCWs. Upstream of MYB46 and MYB83 are the master switches for determining fiber, protoxylem, and metaxylem differentiation. The master regulators for fiber cell fate differentiation are SND1/NST3 and NST1 (Zhong et al., 2006; Mitsuda et al., 2007). For xylem vessels in Arabidopsis, VND7 triggers protoxylem and VND6 triggers metaxylem tracheary cell fate, respectively (Kubo et al., 2005; Yamaguchi et al., 2011). We therefore decided to evaluate the expression of these transcription factors. Moreover, due to the observed lack of xylan accumulation in JPN 1 inflorescence stems, we also evaluated the expression of the *IRX9* and *IRX10* genes which encode glycosyltransferases involved in the synthesis of the xylan backbone. *INTERFASCICULAR FIBERLESS* (*IFL1)* was also analyzed because Arabidopsis mutant *ifl1* closely mimics the loss of fibers phenotype seen in JPN 1 (Zhong and Ye, 1999). This gene, also called *REVOLUTA* (Ratcliffe et al., 2000),

FIGURE 4 | Phenotypes of Arabidopsis plants inoculated with viral chimeras (Sánchez et al., 2015) between TuMV isolates UK 1 and JPN 1, centered in the P3 region of the viral genome. The chimeras used for inoculation are shown in the panels.

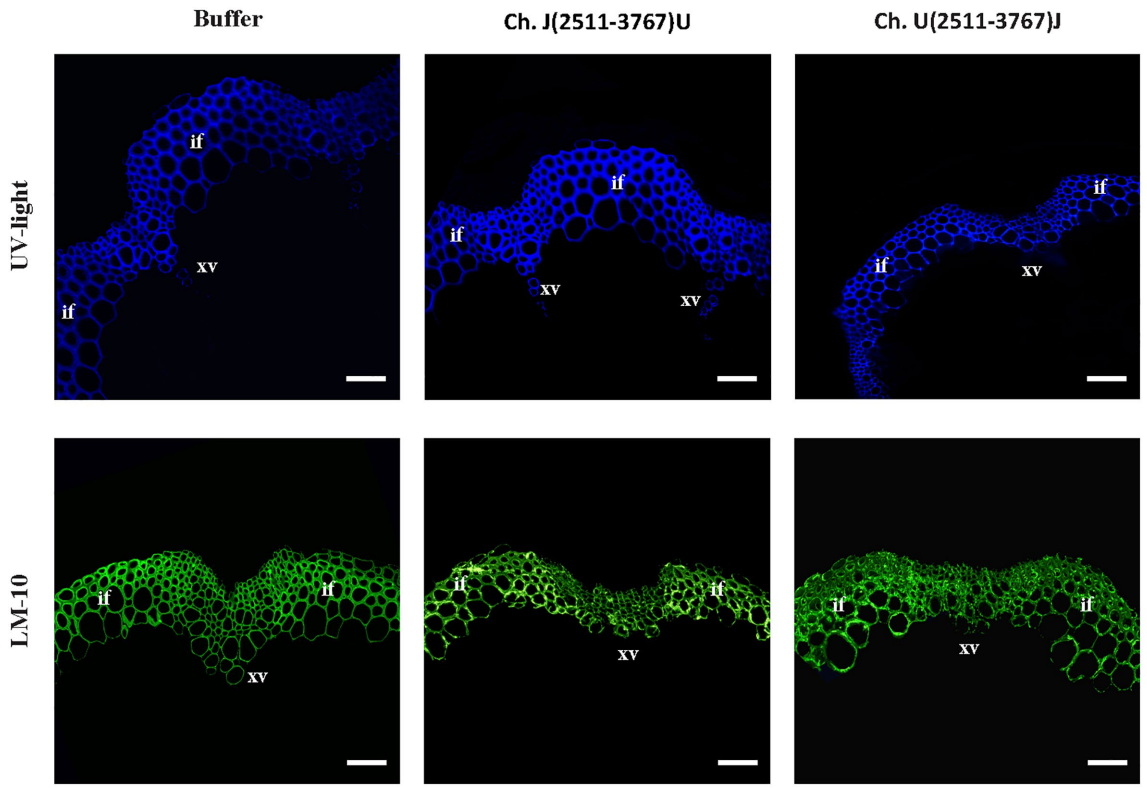

FIGURE 5 | Visualization of lignin by UV **(upper row)** and xylan (monoclonal antibody LM 10, **bottom row**) in the inflorescence stem SCW of buffer-inoculated or TuMV chimeras centered in the P3 region of the viral genome. Bars indicate 100 μm. Xylem vessels (xv) and interfascicular fibers (if) are marked.

encodes a TF of the class III HD-ZIP family with complex roles in plant development (Ramachandran et al., 2017).

The results obtained after RT-qPCR of the genes encoding the TFs and enzymes mentioned above are shown in **Figure 6**. A first global view of the virus-induced transcriptomic alterations notes that UK 1 had a higher quantitative impact on the expression of almost all genes under analysis, which is not surprising given the impaired elongation of the stem in these plants. This included both downregulation and a surprising upregulation in *IRX10*. In plants infected with JPN 1, where the fiber development was impaired (**Figures 2, 3**), the fiber master regulator *SND1/NST3* was the most strongly downregulated gene. The two xylan biosynthetic genes analyzed (*IRX9* and *IRX10*) were also decreased in these lines, consistent with the loss of LM10 staining seen in **Figure 3**. The vascular-related NAC domain TF genes (*VND6* and *VND7*) had the opposite behavior, increasing with JPN 1 and decreasing with UK 1. This may reflect the relatively normal xylem vessels seen in JPN 1, in contrast to the fiber phenotype, and the decreased vasculature in the poorly elongated UK 1. The results obtained are consistent with the phenotypic and microscopic observations of TuMV-infected Arabidopsis plants, since they reveal the high impact that TuMV infections have on the expression of the main genes involved in the regulation of the SCW formation.

The Impact of TuMV Infections on Plant Fertility Is Also Viral Strain Specific and Can Be Related to Reduced Endothecium Lignification for JPN 1-Infected Flowers

Arabidopsis reproductive development is largely affected by TuMV infections with both JPN 1 and UK 1 isolates, although the alterations are usually more striking in UK 1-infected plants (Sánchez et al., 2015). JPN 1-infected plants produce a reduced amount of pollen, whereas UK 1-infected plants mostly remain non-fertile. The light microscopy observations sustaining these effects have now been deepened to further detail by scanning electron microscopy (SEM) examinations (**Figure 7**). In comparison with buffer-inoculated plants (**Figures 7A,D**), flowers from JPN 1-infected plants showed shorter stamens and lower amount of pollen (**Figures 7B,E**). Petal and stamen development did not elongate in UK 1-inoculated plants showing signs of premature senescence (**Figures 7C,F**). In these plants, anthers remain immature and pollen is not usually seen (**Figure 7F**).

Following development of male gametophytes (pollen grains) within the anther, successful plant reproduction requires the dehiscence of the anther to release the mature pollen. Anther dehiscence entails the development of lignified secondary walls in endothecial cells (Goldberg et al., 1993). We assessed endothecium lignification of anthers by means of histological section of flowers at

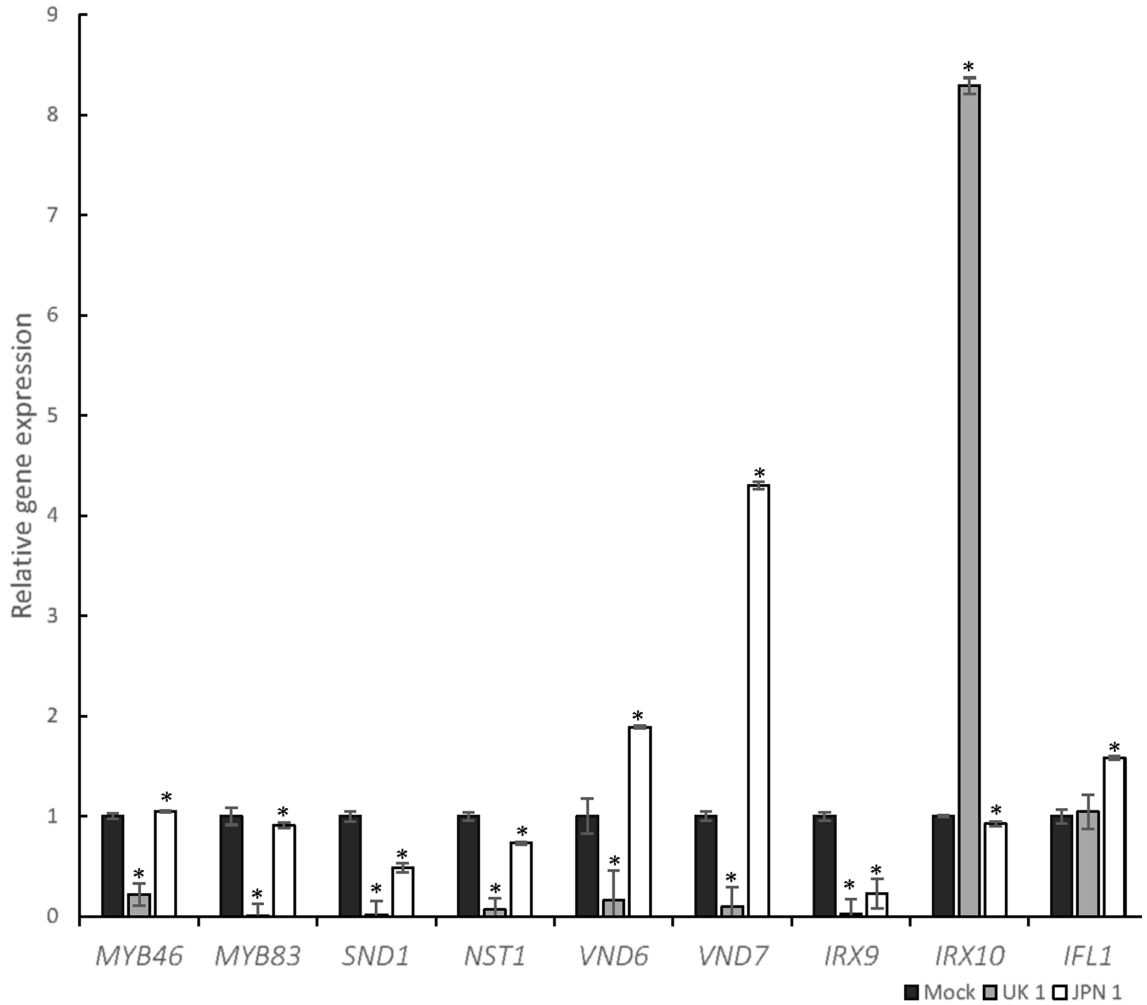

FIGURE 6 | Transcriptomic analysis of selected genes involved in SCW biosynthesis after TuMV infection. The graph shows the results of RT-qPCR of selected genes, represented as relative gene expression in JPN-1-infected or UK-1-infected strains of TuMV, compared to mock-inoculated plants. Comparisons are pairwise of each virus-infected and mock-inoculated. Genes analyzed and color-coded bars are shown in the figure. Asterisk indicates a significant difference compared with wild type (*$p < 0.05$ by *t*-test). Error bars show standard deviation.

anthesis. The flowers from buffer-inoculated plants showed a continuous layer of lignified cells in the endothecium below the epidermis, degradation of septum cells, and release of pollen grains (**Figure 7G**). Anthers from JPN 1-inoculated plants showed reduced endothecium lignification, although some dehiscence occurred and the anthers were able to release the pollen to some extent (**Figure 7H**). In contrast, the anther from UK 1-inoculated plants rarely dehisced, the epidermis and endothecium layers were not clearly differentiated and showed signs of degeneration. Moreover, pollen grains showed internal defects and signs of degradation (**Figure 7I**).

Thus, JPN 1 isolate has a specific effect on SCW lignification also during reproductive development, whereas UK 1 has a general effect on flower development that compromises plant fertility.

DISCUSSION

A role for virus-induced modifications of plant cell wall structure has long been recognized. Plant viruses encode proteins (movement proteins, MPs) whose main function is to promote and mediate virus intercellular movement, thus propagating the infection to still uninfected cells (Dorokhov et al., 2020; Kumar and Dasgupta, 2021). In order to move, viruses need to overcome the formidable barrier of the wall and mostly do it by increasing the size exclusion limit (SEL) of wall-crossing plasmodesmata. This increase implies modification of the cell wall, mostly through MP-induced degradation of the callose regulating the SEL of plasmodesmata. In addition to this well-known phenomenon, recent work has proposed cell wall modifications by regulation of cell wall structural proteins. However, these modifications, very recently reviewed (Kozieł et al., 2021), affect the primary cell wall and do not have a

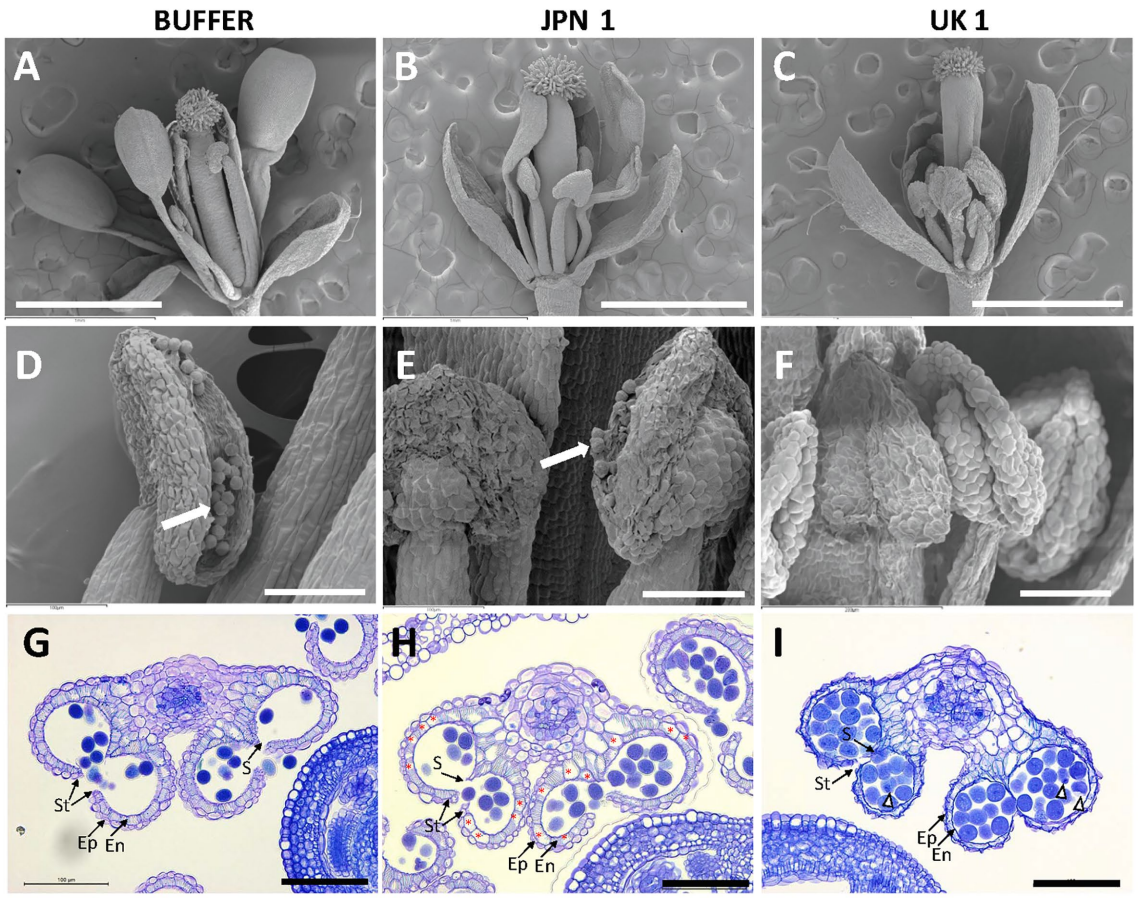

FIGURE 7 | Phenotypes of flowers from control buffer-inoculated and two strains of TuMV-infected Arabidopsis plants. Scanning electron micrographs of flowers at anthesis **(A-C)** and flower anthers **(D-F)**. Pollen grains are visible in **D** and **E** (arrows). Transversal sections of anthers from flowers at anthesis stained with toluidine blue **(G-I)**. Non-infected mock plants show strong lignification of the endothecium. Endothecium cells showing absence of lignification are marked by asterisks in **H**. Abnormal pollen grains are marked by arrow heads. Scale bars indicate: 1 mm in **A-C** and 100 μm in **D-I**. Epidermis (Ep); endothecium (En); stomium (St); and septum (S).

direct impact on specific plant developmental traits. The work described in this paper deals with effects of virus infections on the SCW, a topic unexplored so far, and their reflection on plant development.

The effects of TuMV infections on Arabidopsis developmental traits, previously described (Sánchez et al., 2015), are most dramatic on the elongation, erection, fragility, and branching of the inflorescence stem, and on flower fertility. A simple quantitative analysis of the inflorescence stem areas showed that they were significantly narrower in infected plants, suggesting some virus effect on the correct formation of the thick SCW deposited on specialized cells of the stem. One of the TuMV strains (JPN 1) induced significantly less area reduction than the other (UK 1), indicating likely differential effects. The presumed differences were confirmed upon histochemical analyses of stem cuts. Different staining approaches uncovered that lignin deposition was deeply altered in xylary fibers or interfascicular fibers of JPN 1-infected plants. Similar alterations were found for xylan deposition. On the contrary, and somewhat unexpectedly, none of these alterations were found in UK 1-infected plants, which bore the narrowest stems. However, stained UK 1 cells appeared as abnormally small in the analyses, which indicated severe impairment in cell development, and fully justified the strong stem area reduction. Our first microscopic observations of the effects of TuMV on stem development (Sánchez et al., 2015) had already detected a cellular basis of the alterations, including size. Those analyses and the present ones are not directly comparable because they were done on early developing stems, whereas now fully developed ones (first internode above the rosette) were analyzed. However, important cell alterations could already be found then, now confirmed and expanded, which are on the basis of the macroscopic developmental defects in stem elongation and erection. The SCW defects imposed by JPN 1 would justify the lack of upright growth and fragility in stems that, nevertheless, are able to elongate. A more general cell developmental defect seems to be causing the lack of stem elongation in UK-1 infected plants.

The defects in flower development and fertility had also been already noticed in our previous work. Like for the

inflorescence stem, the new microscopic analyses shed light on the cellular basis of the alterations. Very few flowers (if any) form in the practically stemless UK 1-infected plants. Their petals and stamens barely elongate, and their anthers do not release visible pollen, or do it in minute amounts. The SEM analyses provided further details and revealed a general alteration in the development of the different flower organs and pollen maturity in UK 1-infected plants. In the case of the JPN 1-infected, important defects in the SCW formation could be identified, especially in endothecium cells, which showed a low lignification degree. There seems to be a good correlation between the defects in SCW and the decrease in pollen release in the JPN 1-infected, whereas the almost absolute absence of pollen in UK 1-infected plants appears to be more related to pollen grain degradation and lack of clear differentiation of endothecial cells, again compatible with more general plant developmental defects.

A previous transcriptomic analysis performed on total RNA of the aerial part of UK 1-infected plants (Sánchez et al., 2015) revealed massive changes in plants which had already reached stage 5.1 of development (Boyes et al., 2001), affecting the transcription level of over 1,000 genes, a result fully compatible with an interpretation of alterations affecting multiple levels and pathways in plant development. The situation is quite different in JPN 1-infected plants, which showed transcriptional alterations in just over 60 genes at a similar developmental stage, indicating that developmental alterations induced by JPN 1 are less massive, probably affecting mostly just specific development aspects. As shown by our new analyses, one of these aspects is SCW deposition, both in the inflorescence stem and the endothecial cells of the flowers.

The new transcriptomic analysis focused on genes involved in stem SCW formation in the first internode of TuMV-infected plants. Significant changes were found in the genes analyzed, yet with different patterns for the two viral strains. In the case of UK 1, the expression of most regulatory genes (transcription factors, TFs) dropped down drastically, with the only exception of *IFL1*, which is not a TF only and specifically involved in the control of SCW formation. Rather, its role is more related to general patterning control, mostly through the control of auxin biosynthesis and fluxes (Brandt et al., 2014). In UK 1-infected plants, even though no obvious histological defects were found in SCW, the strong decrease found in specific SCW-controlling genes indicates that the process of SCW deposition is also part of the global developmental alteration. Maybe some other aspect of its regulation could be playing a role. Remarkable opposite alterations were found in the expression of the two biosynthetic genes analyzed (*IRX9* and *IRX10*). Most likely, a compensatory effect underlies this result. In JPN 1-infected plants, a completely different view was obtained. Here, the expression of the two TFs involved in fiber cell fate differentiation is the most decreased, in line with the fiber SCW impairment in these plants. No major differences were found for the two central *MYB* controlling genes, suggesting that the most relevant origins of the alterations found lie somewhere else, at the level of cell-type determination. This view is reinforced by the increase in the expression of the VND TFs (*VND6* and *VND7*), involved in protoxylem and metaxylem determination, considering that no important defects were found in the xylem vasculature in JPN 1-infected plants. Transcription of the biosynthetic genes is decreased, especially *IRX9*, in line with the SCW alterations found. *IFL1* transcription increased, but the interpretation of this result is less obvious given its more general role.

In an effort to link the SCW defects found in this work, and the possibly related creeping habit trait of JPN 1-infected plants, a study involving viral chimeras was undertaken. The approach taken was centered on the viral P3 protein, given its determinant role for the lack of stem elongation in UK 1-infected plants (Sánchez et al., 2015; López-González et al., 2020). The results obtained allowed further dissection of the TuMV-induced developmental alterations. Interchanging the P3 coding regions of both viral strains in their respective infectious clones confirmed again the involvement of this viral protein in stem elongation. However, the characteristic creeping habit of the JPN 1-infected was not found in plants infected with chimera Ch. U(2511-3767)J, in which the P3 of JPN 1 replaced the UK 1 P3. Instead, plants with normal erect inflorescence stems were obtained. The histological inspection of plants infected with this viral chimera, or with its reverse Ch. J(2511-3767)U, revealed no alterations in SCW composition induced by any of the chimeras. So, the results indicate that UK 1 P3 in a TuMV genome is enough to arrest elongation (in fact a single a.a. in the protein is the determinant), although it does not affect SCW composition, but a simple replacement of UK 1 P3 with JPN 1 P3 is not enough to induce a creeping habit, nor to affect SCW composition. Thus, defects in SCW composition and a creeping habit appear as two linked characteristics, as expected, but elongation and upright growth can happen together in TuMV-infected plants. They must then be seen as two different and unlinked characteristics of JPN 1-infected plants. It follows that if the P3 protein is a determinant of a creeping habit, it is only a partial one, requiring the concerted action of another, still unidentified, extra viral determinant.

How the effects of the two TuMV strains on plant and cell development and SCW formation relate to the subcellular localization and behavior of their P3 proteins, is still a question to be answered. TuMV P3 is a peripheral ER-membrane protein which undergoes a process of ER-streaming toward the cell periphery, a process related to its role as a protein involved in viral intercellular movement (López-González et al., 2020). This is common to the P3 proteins of both viral strains, but they also exhibit important differences. One is the much faster rate of ER-streaming in UK 1. A single amino acid at position 279 is the responsible for both streaming rate and the arrest of stem elongation, strongly suggesting that these are two associated processes. Another important difference is the co-localization of P3 with another viral protein, 6K2. In addition to its ER localization, UK 1 P3 can be found co-localizing together with 6K2 in ER-derived 6K2-induced vesicles and chloroplasts in the nuclear periphery. This association is not found for JPN 1 P3. As mentioned above, the typical UK 1 stemless

and sterile flower phenotypes go together with the UK 1 P3 subcellular behavior, but the new results show that SCW composition or final cell deposition is not altered in these plants. Rather, important defects in cell size and/or maturation are found. It is not obvious to envision how the typical subcellular behavior of UK 1 P3 can have such an important effect on plant developmental traits, at both macroscopic and cellular levels. ER-streaming is common to both P3 proteins, and their difference in speed does not seem "*a priori*" a factor so important to justify them. It is possible that its association with the 6K2-induced vesicles promotes much more important rearrangements in the intracellular endomembrane system than in the case of JPN 1 P3, and this could be at the basis of all subsequent defects. It is a point requiring further investigation. As to JPN 1 P3, we had previously suggested that its subcellular behavior could be linked to the creeping habit of the infected plants, but the new results with the viral chimeras show that this is not the case. The defects in SCW are found but, as mentioned above, these are not only influenced by the presence of a JPN 1 P3. Again, further work is needed to identify additional viral factors.

A final consideration concerning the different behaviors of TuMV strains is worth remarking. UK 1 and JPN 1 are considered as representative of two strains, not so closely genetically related, originally named MB and MR and also renamed as World B and Asian BR, respectively (Ohshima et al., 2002; Sánchez et al., 2003; Tomimura et al., 2003). In the recent years, several pieces of evidence have been found supporting the view that different TuMV strains (and maybe even different viral isolates within a strain) establish quite different relationships with the infected host. Thus, not only the different subcellular behavior of the P3 protein, but also the different impact of the infections on plant development and/or SCW formation discussed in this paper happen. Non-host resistance range also differs between strains (Sardaru et al., 2018), and recent important differences have been recently described for the interaction of the P1 viral protein with the host protein G3BP-2, leading to relevant differences in the formation of stress granules (Reuper and Krenz, 2021). How these relevant differences in the biology of intimate interactions with the host should be taken into account for the taxonomical differentiation between strains of viral species, will need to be considered in the future. Perhaps, these biological differences should be enough to consider them as separated viral species.

DATA AVAILABILITY STATEMENT

The original contributions presented in the study are included in the article/**Supplementary Material**, further inquiries can be directed to the corresponding author.

AUTHOR CONTRIBUTIONS

SL-G and CG-M run the experiments. FS, MS, and AS supervised different parts of the experimental work. FP conceived the work with the help of the other authors, supervised the whole work, and wrote the script with contributions from the other authors. All authors read and approved the final form of the script.

FUNDING

The work at the CBGP was funded by several INIA grants. During the course of the work SL-G was funded by a predoctoral FPI-INIA fellowship/contract. We thank the Spanish Ministry of Science for the Severo Ochoa Excellence Accreditations to the CBGP (SEV-2016-0672).

ACKNOWLEDGMENTS

We thank Lucía Zurita for her excellent technical assistance.

SUPPLEMENTARY MATERIAL

The Supplementary Material for this article can be found online at: https://www.frontiersin.org/articles/10.3389/fpls.2021.741050/full#supplementary-material

Supplementary Figure S1 | Toluidine-blue lignin histochemical analyses of the secondary cell walls of the inflorescence stems. The virus or buffer inoculum are indicated. Bars indicate 100 μm. The cortex(co), xylem vessels (xv), and interfascicular fibres (if) are marked with letters. The results with Toluidine-blue reinforce those shown in **Figure 2**.

REFERENCES

Boyes, D. C., Zayed, A. M., Ascenzi, R., McCaskill, A. J., Hoffman, N. E., Davis, K. R., et al. (2001). Growth stage-based phenotypic analysis of Arabidopsis: a model for high throughput functional genomics in plants. *Plant Cell* 13, 1499–1510. doi: 10.1105/tpc.010011

Brandt, R., Cabedo, M., Xie, Y., and Wenkel, S. (2014). Homeodomain leucine-zipper proteins and their role in synchronizing growth and development with the environment. *J. Integr. Plant Biol.* 56, 518–526. doi: 10.1111/jipb.12185

Culver, J. N., and Padmanabhan, M. S. (2007). Virus-induced disease: altering host physiology one interaction at a time. *Annu. Rev. Phytopathol.* 45, 221–243. doi: 10.1146/annurev.phyto.45.062806.094422

Dorokhov, Y. L., Sheshukova, E. V., Byalik, T. E., and Komarova, T. V. (2020). Diversity of plant virus movement proteins: what do they have in common? *PRO* 8:1547. doi: 10.3390/pr8121547

Goldberg, R. B., Beals, T. P., and Sanders, S. M. (1993). Anther development: basic principles and practical applications. *Plant Cell* 5, 1217–1229. doi: 10.1105/tpc.5.10.1217

Houston, K., Tucker, M. R., Chowdhury, J., Shirley, N., and Little, A. (2016). The plant cell wall: A complex and dynamic structure as revealed by the

responses of genes under stress conditions. *Front. Plant Sci.* 7:984. doi: 10.3389/fpls.2016.00984

Huijser, P., and Schmid, M. (2011). The control of developmental phase transitions in plants. *Development* 138, 4117–4129. doi: 10.1242/dev.063511

Kozieł, E., Otulak-Kozieł, K., and Bujarski, J. J. (2021). Plant cell wall as a key player during resistant and susceptible plant-virus interactions. *Front. Microbiol.* 12:656809. doi: 10.3389/fmicb.2021.656809

Kubo, M., Udagawa, M., Nishikubo, N., Horiguchi, G., Yamaguchi, M., Ito, J., et al. (2005). Transcription switches for protoxylem and metaxylem vessel formation. *Genes Dev.* 19, 1855–1860. doi: 10.1101/gad.1331305

Kumar, G., and Dasgupta, I. (2021). Variability, functions and interactions of plant virus movement proteins: what do we know so far? *Microorganisms* 9:695. doi: 10.3390/microorganisms9040695

Livak, K. J., and Schmittgen, T. D. (2001). Analysis of relative gene expression data using real-time quantitative PCR and the $2^{-\Delta\Delta CT}$ method. *Methods* 25, 402–408. doi: 10.1006/meth.2001.1262

López-González, S., Navarro, J. A., Pacios, L. F., Sardaru, P., Pallás, V., Sánchez, F., et al. (2020). Association between flower stalk elongation, an *Arabidopsis* developmental trait, and the subcellular location and movement dynamics of the nonstructural protein P3 of *turnip mosaic virus*. *Mol. Plant Pathol.* 21, 1271–1286. doi: 10.1111/mpp.12976

McCahill, I. W., and Hazen, S. P. (2019). Regulation of cell wall thickening by a medley of mechanisms. *Trends Plant Sci.* 24, 853–866. doi: 10.1016/j.tplants.2019.05.012

McCartney, L., Marcus, S. E., and Knox, J. P. (2005). Monoclonal antibodies to plant cell wall xylans and arabinoxylans. *J. Histochem. Cytochem.* 53, 543–546. doi: 10.1369/jhc.4B6578.2005

Meents, M. J., Watanabe, Y., and Samuels, A. L. (2018). The cell biology of secondary cell wall biosynthesis. *Ann. Bot.* 121, 1107–1125. doi: 10.1093/aob/mcy005

Mitsuda, N., Iwase, A., Yamamoto, H., Yoshida, M., Seki, M., Shinozaki, K., et al. (2007). NAC transcription factors, NST1 and NST3, are key regulators of the formation of secondary walls in woody tissues of *Arabidopsis*. *Plant Cell* 19, 270–280. doi: 10.1105/tpc.106.047043

O'Brien, T. P., Feder, N., and McCully, M. E. (1964). Polychromatic staining of plant cell walls by toluidine blue O. *Protoplasma* 59, 368–373. doi: 10.1007/BF01248568

Ohshima, K., Yamaguchi, Y., Hirota, R., Hamamoto, T., Tomimura, K., Tan, Z., et al. (2002). Molecular evolution of *turnip mosaic virus*: evidence of host adaptation, genetic recombination and geographical spread. *J. Gen. Virol.* 83, 1511–1521. doi: 10.1099/0022-1317-83-6-1511

Ohtani, M., and Demura, T. (2019). The quest for transcriptional hubs of lignin biosynthesis: beyond the NAC-MYB-gene regulatory network model. *Curr. Opin. Biotechnol.* 56, 82–87. doi: 10.1016/j.copbio.2018.10.002

Pallás, V., and García, J. A. (2011). How do plant viruses induce disease? Interactions and interference with host components. *J. Gen. Virol.* 92, 2691–2705. doi: 10.1099/vir.0.034603-0

Pradhan Mitra, P., and Loqué, D. (2014). Histochemical staining of *Arabidopsis thaliana* secondary cell wall elements. *J. Vis. Exp.* 87:e51381. doi: 10.3791/51381

Ramachandran, P., Carlsbecker, A., Etchells, J. P., and Turner, S. (2017). Class III HD-ZIPs govern vascular cell fate: An HD view on patterning and differentiation. *J. Exp. Bot.* 68, 55–69. doi: 10.1093/jxb/erw370

Ratcliffe, O. J., Riechmann, J. L., and Zhang, J. Z. (2000). *INTERFASCICULAR FIBERLESS1* is the same gene as *REVOLUTA*. *Plant Cell* 12, 315–317. doi: 10.1105/tpc.12.3.315

Reuper, H., and Krenz, B. (2021). Comparison of two turnip mosaic virus P1 proteins in their ability to co-localize with the *Arabidopsis thaliana* G3BP-2 protein. *Virus Genes* 57, 233–237. doi: 10.1007/s11262-021-01829-w

Sánchez, F., Manrique, P., Mansilla, C., Lunello, P., Wang, X., Rodrigo, G., et al. (2015). Viral strain-specific differential alterations in *Arabidopsis* developmental patterns. *Mol. Plant-Microbe Interact.* 28, 1304–1315. doi: 10.1094/MPMI-05-15-0111-R

Sánchez, F., Wang, X., Jenner, C. E., Walsh, J. A., and Ponz, F. (2003). Strains of *turnip mosaic potyvirus* as defined by the molecular analysis of the coat protein gene of the virus. *Virus Res.* 94, 33–43. doi: 10.1016/S0168-1702(03)00122-9

Sardaru, P., Sinausía, L., López-González, S., Zindovic, J., Sánchez, F., and Ponz, F. (2018). The apparent non-host resistance of Ethiopian mustard to a radish-infecting strain of *turnip mosaic virus* is largely determined by the C-terminal region of the P3 viral protein. *Mol. Plant Pathol.* 19, 1984–1994. doi: 10.1111/mpp.12674

Schuetz, M., Smith, R., and Ellis, B. (2013). Xylem tissue specification, patterning, and differentiation mechanisms. *J. Exp. Bot.* 64, 11–31. doi: 10.1093/jxb/ers287

Taylor-Teeples, M., Lin, L., De Lucas, M., Turco, G., Toal, T. W., Gaudinier, A., et al. (2015). An *Arabidopsis* gene regulatory network for secondary cell wall synthesis. *Nature* 517, 571–575. doi: 10.1038/nature14099

Tomimura, K., Gibbs, A. J., Jenner, C. E., Walsh, J. A., and Ohshima, K. (2003). The phylogeny of *turnip mosaic virus*; comparisons of 38 genomic sequences reveal a Eurasian origin and a recent 'emergence' in East Asia. *Mol. Ecol.* 12, 2099–2111. doi: 10.1046/j.1365-294X.2003.01881.x

Yamaguchi, M., Mitsuda, N., Ohtani, M., Ohme-Takagi, M., Kato, K., and Demura, T. (2011). VASCULAR-RELATED NAC-DOMAIN 7 directly regulates the expression of a broad range of genes for xylem vessel formation. *Plant J.* 66, 579–590. doi: 10.1111/j.1365-313X.2011.04514.x

Zhong, R., Cui, D., and Ye, Z. H. (2019). Secondary cell wall biosynthesis. *New Phytol.* 221, 1703–1723. doi: 10.1111/nph.15537

Zhong, R., Demura, T., and Ye, Z. H. (2006). SND1, a NAC domain transcription factor, is a key regulator of secondary wall synthesis in fibers of *Arabidopsis*. *Plant Cell* 18, 3158–3170. doi: 10.1105/tpc.106.047399

Zhong, R., and Ye, Z. H. (1999). *IFL*$_1$, a gene regulating interfascicular fiber differentiation in Arabidopsis, encodes a homeodomain-leucine zipper protein. *Plant Cell* 11, 2139–2152. doi: 10.1105/tpc.11.11.2139

Conflict of Interest: The authors declare that the research was conducted in the absence of any commercial or financial relationships that could be construed as a potential conflict of interest.

Publisher's Note: All claims expressed in this article are solely those of the authors and do not necessarily represent those of their affiliated organizations, or those of the publisher, the editors and the reviewers. Any product that may be evaluated in this article, or claim that may be made by its manufacturer, is not guaranteed or endorsed by the publisher.

frontiers in Plant Science

REVIEW
published: 25 March 2022
doi: 10.3389/fpls.2022.863892

The Plant Invertase/Pectin Methylesterase Inhibitor Superfamily

*Daniele Coculo and Vincenzo Lionetti**

Dipartimento di Biologia e Biotecnologie "C. Darwin", Sapienza Università di Roma, Rome, Italy

Invertases (INVs) and pectin methylesterases (PMEs) are essential enzymes coordinating carbohydrate metabolism, stress responses, and sugar signaling. INVs catalyzes the cleavage of sucrose into glucose and fructose, exerting a pivotal role in sucrose metabolism, cellulose biosynthesis, nitrogen uptake, reactive oxygen species scavenging as well as osmotic stress adaptation. PMEs exert a dynamic control of pectin methylesterification to manage cell adhesion, cell wall porosity, and elasticity, as well as perception and signaling of stresses. INV and PME activities can be regulated by specific proteinaceous inhibitors, named INV inhibitors (INVIs) and PME Inhibitors (PMEIs). Despite targeting different enzymes, INVIs and PMEIs belong to the same large protein family named "Plant Invertase/Pectin Methylesterase Inhibitor Superfamily." INVIs and PMEIs, while showing a low aa sequence identity, they share several structural properties. The two inhibitors showed mainly alpha-helices in their secondary structure and both form a non-covalent 1:1 complex with their enzymatic counterpart. Some PMEI members are organized in a gene cluster with specific PMEs. Although the most important physiological information was obtained in *Arabidopsis thaliana*, there are now several characterized INVI/PMEIs in different plant species. This review provides an integrated and updated overview of this fascinating superfamily, from the specific activity of characterized isoforms to their specific functions in plant physiology. We also highlight INVI/PMEIs as biotechnological tools to control different aspects of plant growth and defense. Some isoforms are discussed in view of their potential applications to improve industrial processes. A review of the nomenclature of some isoforms is carried out to eliminate confusion about the identity and the names of some INVI/PMEI member. Open questions, shortcoming, and opportunities for future research are also presented.

Keywords: pectin methylesterase inhibitors, invertase inhibitors, sucrose metabolism, CW integrity, degree of methylesterification, plant growth and defence, biotechnological applications

OPEN ACCESS

Edited by:
Andreia Figueiredo, University of Lisbon, Portugal

Reviewed by:
Bruce Kohorn, Bowdoin College, United States
Leonor Castro Guerra-Guimarães, University of Lisbon, Portugal

***Correspondence:**
Vincenzo Lionetti
vincenzo.lionetti@uniroma1.it

Specialty section:
This article was submitted to Plant Pathogen Interactions, a section of the journal Frontiers in Plant Science

Received: *27 January 2022*
Accepted: *02 March 2022*
Published: *25 March 2022*

Citation:
Coculo D and Lionetti V (2022) The Plant Invertase/Pectin Methylesterase Inhibitor Superfamily. Front. Plant Sci. 13:863892. doi: 10.3389/fpls.2022.863892

INTRODUCTION

Plant Invertase/Pectin Methyl Esterase Inhibitors (INV/PMEIs; PF04043)[1] belong to a large protein superfamily acting in the tight post-transcriptional regulation of Invertases (INVs) and Pectin methylesterases (PMEs), two classes of enzymes with distinct enzymatic activities in carbohydrate metabolism (**Figure 1**; Gough et al., 2001). INVI/PMEIs are highly represented

[1]http://pfam.xfam.org/family/PF04043

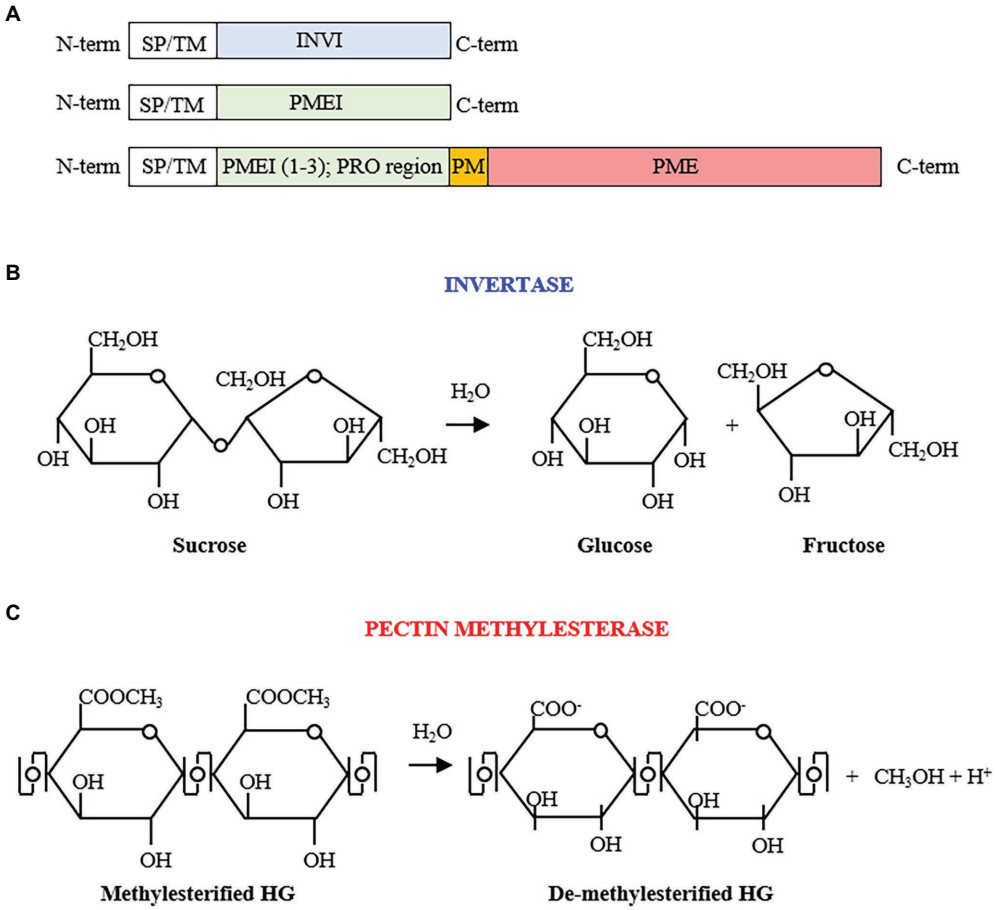

FIGURE 1 | (A) Invertase inhibitor (INVI) and pectin methylesterase inhibitor (PMEI) structural organizations. The INVI/PMEIs domain are preceded by a signal peptide (SP) or a transmembrane domain (TM) for the targeting to the endomembrane system leading to the different subcellular localization. PMEI/INVIs can possess one, both, and neither of these motifs. Some PMEIs (from 1 to 3 isoforms; also named PRO region) can be clustered with a C-terminal PME. **(B)** Sucrose hydrolysis by invertase activity yielding glucose and fructose. **(C)** De-methylesterification of homogalacturonan (HG) by pectin methylesterases, with consequent production of negatively charged carboxyl groups, methanol, and protons.

in different plant species (**Table 1**). Plant INVs (also known as β-fructosidases), convert the sucrose into its building blocks, fructose and glucose, central molecules for carbohydrate translocation, metabolism, and sensing in higher plants (**Figure 1B**; Roitsch and González, 2004). INVs play different roles in organ development, carbohydrate partitioning, sugar signaling, and response to biotic and abiotic stresses (Ruan et al., 2010; Tauzin and Giardina, 2014; Liao et al., 2020). Acid INVs and neutral/alkaline INVs were identified, showing different pH optima and subcellular compartments. The Acid INVs, belonging to gH32 (glycoside hydrolase family 32),[2] shows an optimum pH of 3.5–5.0 and can be divided in cell wall (CW) and vacuolar (V) INVs. Neutral/alkaline INVs show an optimum pH of 6.8–9.0, belong to gH100, and appear to be localized to the cytosol, mitochondrion, plastids, and nucleus. The INV activity can be post-transcriptionally controlled by INV Inhibitor (INVI; **Figures 1A, 2A,B, 3**). Based on the subcellular site where their activity is exerted, CW- and V-INVIs (previously named also Inhibitor of β-Fructosidases; C/VIFs) can be distinguished (Rausch and Greiner, 2004; **Figure 3**). The first INVI was described more than 40 years ago in potato plants (*Solanum tuberosum*; Pressey, 1966). Although INVIs have been reported for various plant species, little is known about their roles in plant physiology (Bate et al., 2004; Raiola

Abbreviations: Ac, *Actinidia chinensis*; At, *Arabidopsis thaliana*; CIF1, Cell Wall Inhibitor of β-Fructosidase; C/VIFs, Cell Wall/Vacuolar Inhibitor of β-Fructosidases; CW, Cell Wall; CWDEs, Cell Wall Degrading Enzymes; CW-INV, Cell Wall Invertase; CW-INVI, Cell Wall Invertase Inhibitor; EDA, embryo sac development arrest; ERF, Ethylene Responsive Element Binding Factor; FER, FERONIA; GH, Glycoside Hydrolase family; GL, GLABRA; Gm, *Glycine max*; HG, Homogalacturonan; HMS, Highly Methyl Esterified Seeds; INV, Invertase; INVI, Invertase Inhibitor; ISR, Induced Systemic Resistance; JA, Jasmonic Acid; LUH/MUM, Leunig Homolog/Mucilage Modified; Ma, *Musa acuminata*; MYB, Myeloblastosis; *ozs2*, overly Zinc sensitive 2; PME, Pectin Methylesterase; PMEI, Pectin Methylesterase Inhibitor; Sl, *Solanum lycopercsicum*; STK, Seedstick; TMV, Tobacco Mosaic Virus; TVCV, Turnip Vein Clearing Virus; UNE, Unfertilized Embryo Sac; V-INV, Vacuolar Invertase; Vv, *Vitis vinifera*; WAK, Wall Associated Kinase; Zm, *Zea mays*.

[2]www.cazy.org

TABLE 1 | INVI/PMEIs assignments in different plant species genomes.

Species	Common name	Number of proteins
Actinidia chinensis Hongyang		109
Aegilops tauschii		94
Amborella trichopoda		40
Aquilegia coerulea		63
Arabidopsis lyrata	Lyrate rockcress	132
Arabidopsis thaliana	Thale cress	125
Brachypodium distachyon	Stiff brome	60
Brassica rapa	Field mustard	167
Capsella rubella		130
Carica papaya	Papaya	54
Citrus clementina		75
Citrus sinensis	Sweet orange	78
Cucumis sativus	Cucumber	62
Eucalyptus grandis	Rose gum	46
Fragaria vesca	Wild strawberry	82
Glycine max	Soybean	163
Gossypium raimondii		152
Hordeum vulgare	Domesticated barley	68
Linum usitatissimum	Flax	160
Lotus japonicus		69
Malus domestica	Apple	144
Manihot esculenta	Cassava	100
Medicago truncatula	Barrel medic	171
Mimulus guttatus	Spotted monkey flower	115
Musa acuminata	Wild Malaysian banana	58
Musa balbisiana	Balbis banana	88
Nicotiana benthamiana		160
Oryza sativa	Rice	81
Panicum virgatum	Switchgrass	131
Phaseolus vulgaris	French bean	104
Phoenix dactylifera	Date palm	13
Phyllostachys heterocyclavar	Kikko-chiku	30
Physcomitrella patens		12
Picea abies	Norway spruce	53
Picea sitchensis	Sitka spruce	5
Pinus taeda	Loblolly pine	82
Populus trichocarpa	Black cottonwood	118
Prunus persica	Peach	70
Ricinus communis	Castor bean	71
Selaginella moellendorffii		13
Setaria italica	Foxtail millet	67
Solanum lycopersicum	Tomato	86
Solanum pimpinellifolium	Currant tomato	86
Solanum tuberosum	Potato	113
Sorghum bicolor	Sorghum	73
Thellungiella halophila		105
Theobroma cacao	Cacao	72
Triticum aestivum	Bread wheat	95
Triticum urartu		85
Vitis vinifera	Wine grape	21
Zea mays	Maize	76
Zea mays	Maize	79

Source: https://supfam.mrc-lmb.cam.ac.uk/SUPERFAMILY/index.html

et al., 2004; Reca et al., 2008; Zhang et al., 2010; Lionetti et al., 2015b).

A member of INVI/PMEI family can be classified as PME Inhibitor (PMEI) if it is able to inhibit a PME activity (**Figures 1A–C, 2C,D**, **4**). The first PMEI, named AcPMEI, was discovered in ripe fruit of kiwi (*Actinidia chinensis*; Balestrieri et al., 1990). PMEs (CE8, Carbohydrate Esterase) catalyze the de-methylesterification of pectin, releasing free carboxyl ester groups, protons, and methanol (**Figure 1C**). PMEs are encoded by large multigene families in many plant species (Pelloux et al., 2007; Harholt et al., 2010). Until now, these enzymes were linked to the modulation of the degree and pattern of methylesterification of homogalacturonan (HG), the major component of pectin secreted in a highly methylesterified form to the CW (**Figure 4**). The degree of methylesterification constitutes an important factor influencing stiffness and hydration status of the pectic matrix (Catoire et al., 1998; Willats et al., 2001). The current knowledge on the mode of de-methylesterification of the single plant PME isoforms remains scarce. The existence of different methylester distributions on HG *in vivo* suggests the involvement of multiple PME isoforms with different action patterns. A blockwise de-methylesterification results in the production of adjacent free galacturonic acid units that can form calcium crosslinks between HG chains, known as "egg-box" structures, resulting in pectin stiffening (Limberg et al., 2000; Wu et al., 2018). Instead, the random de-methylesterification results in the removal of one methylester group at a time from various non-contiguous residues on the HG chains exposing the polymer to the activity of pectinolytic enzymes (Limberg et al., 2000). While this latter mechanism has been demonstrated for PMEs of microbial origin, plant PMEs with a random de-methylesterification have not been identified so far. PME isoforms finely tune the degree and pattern of methylesterification during multiple developmental processes, such as stomata function (Amsbury et al., 2016; Huang et al., 2017), cell adhesion (Lionetti et al., 2014a; Daher and Braybrook, 2015), organ development, and phyllotactic patterning (Peaucelle et al., 2011b; Senechal et al., 2014). Plant PMEs also play a critical role in multiple plant–microbe interactions and stress responses (Lionetti et al., 2012). An immunity triggered PME activity, driven by specific PME isoforms, is exploited against pathogens (Bethke et al., 2014; Del Corpo et al., 2020). This activity is triggered to modulate pectin methylesterification in *Arabidopsis thaliana* against fungi, such as *Botrytis cinerea* and *Alternaria brassicicola*, bacteria, such as *Pseudomonas syringae*, and viruses like *turnip vein clearing virus* (*TVCV*; Bethke et al., 2014; Lionetti et al., 2014b, 2015a, 2017). Moreover, PMEI activity and pectin methylesterification status play important roles during plant resistance to abiotic stresses (Wu et al., 2018).

A PMEI can be transcribed independently or in pairs with a Type I PME as one polycistronic messenger RNA which resembles an operon-like gene cluster (**Figure 1A**; Boycheva et al., 2014). In these PMEI-PMEs clusters, PMEI region (also referred to as PRO region, PRO domain, or PMEI-like region) can be separated from the PME domain by specific subtilisin-like serine proteases (subtilases) before excretion of PME domain or later into the apoplast during different physiological processes (Figueiredo et al., 2018; Schaller et al., 2018). Different evidence indicates that in these clusters, PMEI domain acts as an intramolecular inhibitor of PME enzymatic activity (Bosch et al., 2005; Wolf et al., 2009; Del Corpo et al., 2020). Other works indicate that PMEI domain can be required for the targeting of PMEs toward the CW (Wolf et al., 2009) or that it could work as intramolecular chaperone in the regulation

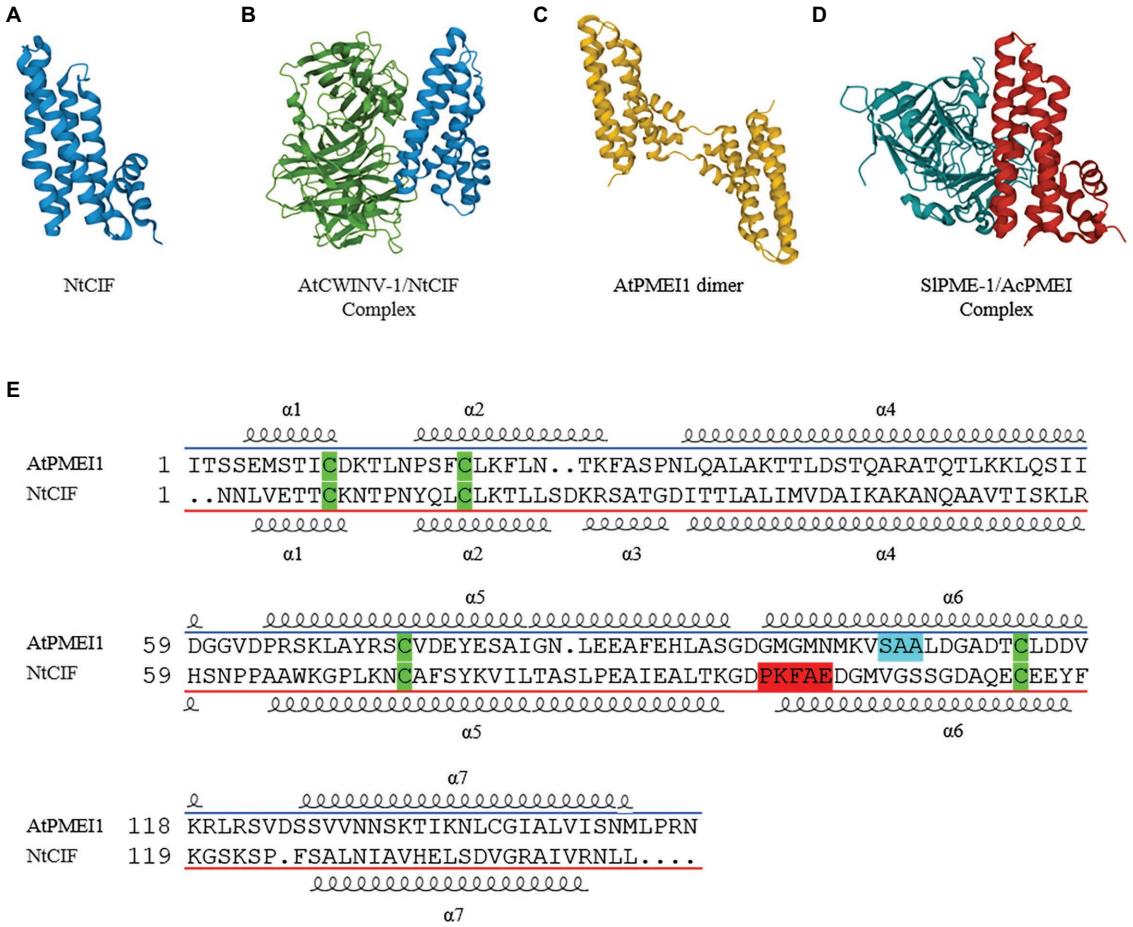

FIGURE 2 | Crystal structure of different INVI/PMEI isoforms alone or in complex with their enzymatic counterpart. **(A)** NtCIF (PDB ID; 1RJ1) and **(B)** NtCIF in complex with AtCWINV-1 (PDB ID; 2XQR). **(C)** AtPMEI1 dimer (PDB ID; IX8Z) and **(D)** AcPMEI in complex with SlPME-1 (PDB ID; 1Xg2). **(E)** Sequence Comparison of AtPMEI1 and NtCIF. The most conserved motifs are highlighted in light blue for PMEI and in red for INVI. The four cysteine conserved in both inhibitors are highlighted in green. The α symbols followed by numbers indicates the different alpha-helices.

of PME folding (Micheli, 2001). Further investigation is needed to understand the subcellular action of both independent and PME-clustered PMEIs.

Gene structure and sequence analyses show that the origin of the independently expressed PMEIs may be derived from the neofunctionalization of the PMEI domain from the PMEI-PME genes (Wang et al., 2013). PMEI-PME clusters evolved during the divergence of moss from charophytes, while independent PMEIs appear later in land plants. The physiological reasons which prompted plants to initially evolve a coordinated expression of the enzyme with its inhibitor counterpart and, later, to involve also a PME inhibition using independent PMEIs, deserves further investigation. Most likely, both PMEI-PMEs clusters and independent PMEIs were fundamental factors finely tuning the pectin methyl-esterification in the CW remodeling that emerged as necessary in land plants. The existence of specific pairs between PMEIs and PMEs has been hypothesized based on data obtained *in vitro* (**Table 2**). A single PMEI can inhibit multiple plant PMEs and the PMEI characterized up to now are unable to inhibit microbial PMEs (Lionetti, 2015; Lionetti et al., 2015b). The bacterial enzymes show much longer turns that protrude out of the β-helix making its putative active site cleft deeper and narrower than that of plant PMEs, a feature that could prevent the approach of the inhibitor to the active site of the enzyme (D'Avino et al., 2003).

From a structural point of view, PMEIs and INVIs, despite having a low aa sequence identity (20–30%), they share several structural properties. The three-dimensional structures of AtPMEI1 from Arabidopsis and of a CW-INVI from tobacco (*Nicotiana tabacum*; NtCIF) were elucidated (Hothorn et al., 2004a,b; **Figures 2A,C**). Both fold in a four-helix bundle structure preceded by an N-terminal extension thought to play an important role during the enzymatic inhibition. Both inhibitors hold four conserved cysteine residues typically engaged in the formation of two disulfide bridges, important to stabilize both two α helices of the hairpin loop and two α helices of the four-helical bundle structure. The structure of AtPMEI1 (**Figure 2C**) is composed of a four-helix bundle that arranges the helical components in an up-down–up-down topology with disulfide bridges. The N-terminal region, composed of two

short and distorted helices, extends outside the central domain, forming a hairpin. The orientation of this hairpin allows the extensive contacts with the α-hairpin of a neighboring molecule forming an active dimer in solution. The N-terminal region of AtPMEI1 was proposed to be crucial for the interaction with a PME from Carrot (*Daucus carota*; Hothorn et al., 2004b). Although this model does not fit with the crystallographic data regarding the complex between AcPMEI and SlPME-1 of tomato (*Solanum lycopercsicum*; **Figure 2D**; Di Matteo et al., 2005), where the N-terminal region of AcPMEI does not establish contact with PME, it cannot be excluded that the two inhibitors use two different modes of interaction. AcPMEI interacts with PME at the level of the active site by forming a stoichiometric 1:1 complex in which the inhibitor covers the shallow cleft of the enzyme where the putative active site is located (Di Matteo et al., 2005; Ciardiello et al., 2008). The four-helix bundle of AcPMEI packs roughly perpendicular to the parallel β-helix of SlPME-1, and three of these helices (and not an helix of the N-terminal extension as proposed for AtPMEI1) interact with SlPME-1 in proximity of the putative active site (Di Matteo et al., 2005). The crystal structure of the complex between the AtCWINV-1 from Arabidopsis and the NtCIF was also elucidated (**Figures 2A,B**; Hothorn et al., 2010). The structure revealed that the four-helix bundle of NtCIF binds primarily in the substrate-binding cleft of the five-bladed β-propeller module of invertase. PME and INV activities and their complexes with their respective inhibitors are pH sensitive (Hothorn et al., 2010; Bonavita et al., 2016; Hocq et al., 2017b). There is no information available on the three-dimensional structure of PMEI-PME clusters.

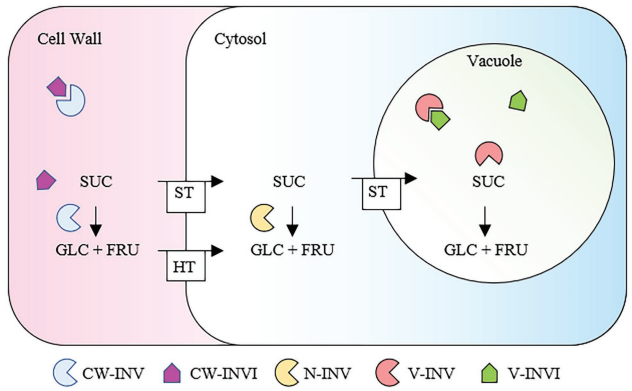

FIGURE 3 | Subcellular localization and activities of INVs and INVIs. Sucrose can be cleaved in the apoplast by a CW-INV in glucose and fructose, which are transported into the cytoplasm by a hexose transporter. Sucrose can also be directly loaded by specific sucrose transporters into the cytosol or in the vacuole where it is cleaved by neutral invertase (N-INV; or sucrose synthase) or V-INV, respectively. The hexoses generated by INV activity can serve as substrate for growth as well as can regulate gene expression during growth and defense. Modulations of INVs by INVIs are dependent from different environmental stimuli and can influence different physiological processes. FRU, fructose; glc, glucose; SUC, Sucrose. ST, Sucrose Transporter; HT, Hexose Transporter.

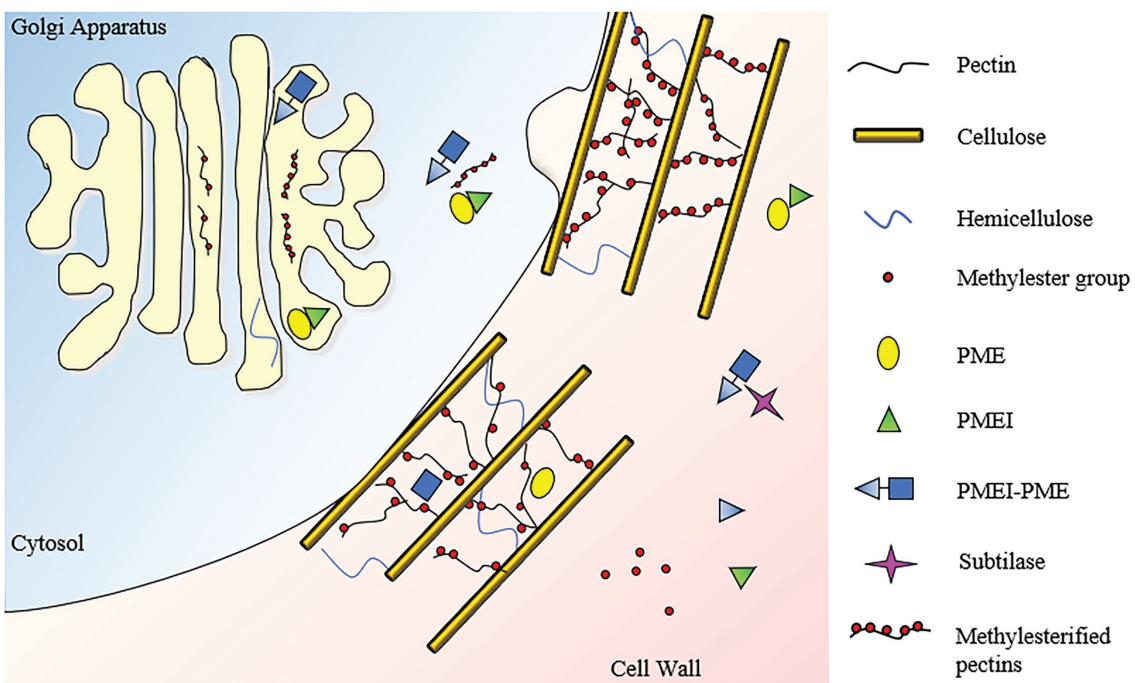

FIGURE 4 | Subcellular localization and activities of PMEI-PMEs and PMEIs. HG is methylesterified in the golgi apparatus, where PMEIs can avoid a premature pectin de-methylesterification by PME, which could cause a pectin jellification. Pectin is secreted in the apoplast in a high methylesterified form. In this compartment, a fine-tuning of PME activity is exerted by independent and clustered PMEIs to regulate the degree and pattern of pectin methylesterification in various plant physiology processes. Subtilisin-like proteases (Subtilases) can degrade the processing motif of PMEI-PME catalyzing the separation of the inhibitor from the PME domain.

TABLE 2 | Arabidopsis INVI-PMEI independent protein isoforms.

	Gene ID	AGI code	Symbol	Possible interactor	Function	Literature
1	837879	At1g02550				
2	837458	At1g09360				
3	837459	At1g09370				
4	837620	At1g10770				
5	6240451	At1g11362				
6	7922417	At1g11593				
7	838054	At1g14890				
8	838929	At1g23205				
9	838944	At1g23350			Plant stresses	Coolen et al., 2019
10	841214	At1g47960	AtCW-INVI1, AtC/VIF1		Seed germination, Root length, Plant-pathogen interaction, Salt susceptibility	Link et al., 2004; Siemens et al., 2011; Su et al., 2016; Yang et al., 2020
11	841219	At1g48010				
12	841220	At1g48020	AtPMEI1	ATPPME1, AtPMEI-PME17, AtPMEI-PME3, AtPMEI-PME16	Plant growth, Pavement cells morphogenesis, Plant-pathogen interaction	Wolf et al., 2003; Raiola et al., 2004; Lionetti et al., 2007; Lin et al., 2021
13	6240492	At1g50325				
14	841456	At1g50340				
15	841904	At1g54620				
16	841939	At1g54980				
17	842026	At1g55770				
18	842062	At1g56100	AtPMEI14		Mucilage release	Shi et al., 2018; Ding et al., 2021
19	842117	At1g56620	AtPMEI16		Mucilage release	Shi et al., 2018; Ding et al., 2021
20	842370	At1g60760				
21	842574	At1g62760	AtPMEI10		Salt susceptibility, Plant-pathogen interaction,	Jithesh et al., 2012; Lionetti et al., 2017
22	842576	At1g62770	AtPMEI9	AtPME3	CW integrity, Root growth	Sorek et al., 2015; Hocq et al., 2017b
23	843391	At1g70540	EDA24		Embryo sac	Pagnussat et al., 2005
24	843409	At1g70720				
25	814690	At2g01610				
26	815562	At2g10970				
27	816026	At2g15345				
28	3768435	At2g31425				
29	817701	At2g31430	AtPMEI5		Seed germination, Seedling emergence, Plant growth	Wolf et al., 2012; Müller et al., 2013; Jonsson et al., 2021
30	6241279	At2g31432				
31	819319	At2g47050				
32	819347	At2g47340				
33	819380	At2g47670	AtPMEI6		Mucilage release	Saez-Aguayo et al., 2013
34	3768856	At3g05741	AtPMEI15		Mucilage release	Shi et al., 2018; Ding et al., 2021
35	820471	At3g12880				
36	820970	At3g17130	AtPMEI8		CW integrity, Root growth	Sorek et al., 2015, p. 16
37	820971	At3g17140				
38	820972	At3g17150				
49	5008004	At3g17152				
40	820981	At3g17220	AtPMEI2	ATPPME1, AtPMEI-PME3, AtPMEI-PME16	Plant growth, Plant-pathogen interaction	Wolf et al., 2003; Raiola et al., 2004; Tian et al., 2006; Lionetti et al., 2007
41	820982	At3g17225				
42	28719277	At3g17227				
43	820983	At3g17230				
44	6240965	At3g27999				
45	819850	At3g36659				
46	823892	At3g47380	AtPMEI11		Plant-pathogen interaction	Lionetti et al., 2017
47	823921	At3g47670				
48	824095	At3g49330				
49	824734	At3g55680				
50	825391	At3g62180				
51	825457	At3g62820				
52	828192	At4g00080	UNE11		Embryo sac	Pagnussat et al., 2005
53	7922364	At4g00872				
54	827589	At4g02250				

(Continued)

TABLE 2 | Continued

	Gene ID	AGI code	Symbol	Possible interactor	Function	Literature
55	828628	At4g25250	AtPMEI4	AtPMEI-PME3; AtPMEI-PME17	Root growth	Pelletier et al., 2010
56	6240679	At4g03945				
57	827253	At4g15750	AtPMEI13		Mucilage release	Shi et al., 2018; Ding et al., 2021
58	828566	At4g24640	APPB1			Holmes-Davis et al., 2005
59	828628	At4g25250				
60	828629	At4g25260	AtPMEI7	AtPMEI-PME3		Sénéchal et al., 2015
61	832197	At5g20740	AtPMEI3		Phyllotaxis, Rhyzotaxis, Pavement cells morphogenesis	Peaucelle et al., 2008; Haas et al., 2020; Wachsman et al., 2020
62	832508	At5g24370				
63	833851	At5g38610				
64	834739	At5g46930				
65	834740	At5g46940				
66	834741	At5g46950	InvINH2			Zuma et al., 2018
67	834742	At5g46960	AtPMEI12		Plant-pathogen interaction	Lionetti et al., 2017; Zuma et al., 2018
68	834743	At5g46970				
69	834744	At5g46980				
70	834745	At5g46990				
71	835067	At5g50030				
72	835068	At5g50040				
73	835069	At5g50050				
74	835070	At5g50060				
75	835071	At5g50070				
76	835226	At5g51520				
77	836355	At5g62340				
78	836356	At5g62350				
79	836357	At5g62360	AtPMEI17		Salt and Aphid tolerance, Freezing susceptibility	Chen et al., 2018; Silva-Sanzana et al., 2019
80	836583	At5g64620	AtCW/V-INVI2; AtC/VIF2		Plant-pathogen interaction	Link et al., 2004; Siemens et al., 2011

A PMEI or an INVI can hold specific features in their amino acid sequence (**Figure 2E**). PMEI has a conserved Threonine residue, previously demonstrated to strengthen the interaction with PME at the acidic apoplastic pH, a typical Serine, Alanine, Alanine (SAA) amino acid motif in α6 helix, and a C-terminal hydrophobic region of six amino acids involved in the stabilization of the four-helical bundle structure of the protein (Di Matteo et al., 2005). Instead, the amino acid motif Proline, Lysine, Phenylalanine (PKF) in α6 helix, as well as the contiguous Alanine and glutamic Acid (AE) residues are the sequence fingerprints highly conserved in INVIs and critical for INVI-INV interaction. Both INVIs residues, important for the formation of the complex with INVs, and the distortion of INVI α2 helix could be responsible for the lack of interaction between INVI and PME (Di Matteo et al., 2005). Unfortunately, these features do not always help to understand the identity of an isoform. For example, PKF motif is absent in AtC/VIF2 (Link et al., 2004).

THE ARABIDOPSIS INVI/PMEI SUPERFAMILY

Most of the knowledge on the role of INVI/PMEIs in plant physiology has so far been gained by studying *A. thaliana*, the annual dicotyledonous plant, served as a model for physiological studies in many laboratories. For this reason, this review will deal specifically with all Arabidopsis isoforms, integrating them with data obtained in other species. We identified *in silico* 125 INVI/PMEIs in Arabidopsis, 80 independent INVI/PMEIs, and 45 PMEI-PME clusters (**Tables 1–3**). Given the need to verify the type of inhibitory activity, the INVI-PMEIs members cannot be pre-numbered as for other families. The name of various members was assigned by the scientific community based on the chronological order they were characterized. However, confusion about the identity and the names of some INVI/PMEI member begins to appear in literature. For example, both PMEI and INVI functions have been proposed for the same AgI code. At5g46960, although named *InvINH1,* its INVI activity has never been demonstrated (Zuma et al., 2018). Rather, At5g46960 is the *AtPMEI12*, which possess the SAA amino acid motif and influences PME activity, the degree of pectin methylesterification, and the HG integrity in Arabidopsis during *B. cinerea* infection (Lionetti et al., 2017). Also, two different isoforms were named with the same name. This is the case of At4g15750 and At5g62360 isoforms both called *AtPMEI13* by different authors (Chen et al., 2018; Shi et al., 2018; Silva-Sanzana et al., 2019). To avoid confusion and respecting the chronology of publications, we rename At5g62360 as *AtPMEI17*. Moreover, the lack of symbol for At3g60730 and At2g26450 led us to name them, respectively, *AtPMEI-PME65* and *AtPMEI-PME66*. Also unfortunately, the

TABLE 3 | Arabidopsis INVI-PMEI protein isoforms clustered with a PME.

	Gene ID	AGI code	PME Symbol	New symbol	Function	Paper
1	838078	At1g02810	AtPME7	AtPMEI-PME7	Probable pseudogene	Dedeurwaerder et al., 2008
2	837701	At1g11580	AtPME18; AtPME-PCRA	AtPMEI-PME18	Root growth, Plant-pathogen interaction	Micheli et al., 1998, p. 3; De-la-Peña et al., 2008; Lionetti et al., 2017; Stefanowicz et al., 2021
3	837702	At1g11590	AtPME19	AtPMEI-PME19		
4	838928	At1g23200	AtPME6, HIgHLY METHYL ESTERIFIED SEEDS (HMS)	AtPMEI-PME6	Stomatal function, Embryo development, Mucilage release	Levesque-Tremblay et al., 2015; Amsbury et al., 2016
5	841820	At1g53830	AtPME2	AtPMEI-PME2	Callus formation	Xu et al., 2018
6	841821	At1g53840	AtPME1	AtPMEI-PME1		
7	817184	At2g26440	AtPME12	AtPMEI-PME12		
8	817185	At2g26450	No number	AtPMEI-PME66		
9	818907	At2g43050	AtPME16; ATPMEPCRD	AtPMEI-PME16		
10	819130	At2g45220	AtPME17	AtPMEI-PME17	Root growth, Plant-pathogen interaction	Senechal et al., 2014; Del Corpo et al., 2020
11	819317	At2g47030	AtPME4; VgDH1	AtPMEI-PME4	Pollen tube growth	Jiang et al., 2005
12	819318	At2g47040	AtPME5; VgD1	AtPMEI-PME5	Pollen tube growth	Jiang et al., 2005
13	819368	At2g47550	AtPME20	AtPMEI-PME20		
14	819727	At3g05610	AtPME21	AtPMEI-PME21		
15	819728	At3g05620	AtPME22	AtPMEI-PME22		
16	819867	At3g06830	AtPME23	AtPMEI-PME23		
17	820240	At3g10710	AtPME24; RHS12	AtPMEI-PME24	Root hair development	Won et al., 2009; Cheong et al., 2019
18	820241	At3g10720	AtPME25	AtPMEI-PME25		
19	820650	At3g14300	AtPME26; ATPMEPCRC	AtPMEI-PME26		
20	820651	At3g14310	AtPME3	AtPMEI-PME3	Seed germination, Root development, Pavement cells morphogenesis, Plant-pathogen interactions, Metal tolerance	Micheli et al., 1998; Hewezi et al., 2008; Raiola et al., 2011; Weber et al., 2013; Guénin et al., 2017; Lin et al., 2021
21	822422	At3g27980	AtPME30	AtPMEI-PME30	Beneficial bacterial recruitment, Plant-pathogen interaction	Lakshmanan et al., 2013; Zehra et al., 2021
22	823402	At3g43270	AtPME32	AtPMEI-PME32		
23	823894	At3g47400	AtPME33	AtPMEI-PME33		
24	824083	At3g49220	AtPME34	AtPMEI-PME34	Transpiration, Heat tolerance	Huang et al., 2017; Wu et al., 2017
25	825070	At3g59010	AtPME35	AtPMEI-PME35	Mechanical strength of stem	Hongo et al., 2012, p. 35
26	825244	At3g60730	No number	AtPMEI-PME65		
27	825390	At3g62170	AtPME37; VgDH2	AtPMEI-PME37	Pollen tube growth	Jiang et al., 2005
28	828218	At4g00190	PME38	AtPMEI-PME38	Probable pseudogene	Dedeurwaerder et al., 2008
29	827708	At4g02300	AtPME39	AtPMEI-PME39		
30	828067	At4g02320	AtPME40	AtPMEI-PME40		
31	828064	At4g02330	AtPME41; ATPMEPCRB	AtPMEI-PME41	Chilling tolerance	Qu et al., 2011
32	825703	At4g03930	AtPME42	AtPMEI-PME42		
33	827282	At4g15980	AtPME43	AtPMEI-PME43		
34	829458	At4g33220	AtPME44	AtPMEI-PME44		
35	829459	At4g33230	AtPME45	AtPMEI-PME45		
36	830378	At5g04960	AtPME46	AtPMEI-PME46	Metal tolerance	Geng et al., 2017
37	830379	At5g04970	AtPME47	AtPMEI-PME47		
38	830836	At5g09760	AtPME51	AtPMEI-PME51		
39	832209	At5g20860	AtPME54	AtPMEI-PME54		
40	832850	At5g27870	AtPME28	AtPMEI-PME28		
41	834977	At5g49180	AtPME58	AtPMEI-PME58	Mucilage release	Turbant et al., 2016
42	835223	At5g51490	AtPME59	AtPMEI-PME59		
43	835224	At5g51500	AtPME60	AtPMEI-PME60		
44	835418	At5g53370	AtPME61; ATPMEPCRB	AtPMEI-PME61		
45	836585	At5g64640	AtPME64	AtPMEI-PME64		

AtPMEI-PME17 isoform was considered an independent PMEI in different papers (Leyva-González et al., 2012; Takahashi et al., 2019). We propose to rename Type I PMEs, by adding the PMEI-tag in front of PME (PMEI-PMEs; **Table 3**) to allow the scientific community to immediately recognize a PMEI co-expressed with a PME. We will begin to discuss the findings on PMEIs, given the greater amount of data available compared to INVIs.

PME INHIBITORS

To date, 17 INVI/PMEI isoforms were already identified as independent PMEI in Arabidopsis, although only AtPMEI1, AtPMEI2, and AtPMEI7 were purified and their activities verified. The inhibitory activity of the PMEI region in the PMEI-PME cluster was demonstrated for AtPMEI-PME17 (Del Corpo et al., 2020). The remaining isoforms were considered PMEIs because their transgenic overexpression or mutation leads to an alteration of PME activity and/or of the pectin methylesterification, with consequences in different plant physiology processes (**Figures 5, 6**). From here on, considerations on the role of PMEI-PMEs will be understood as actions of the enzyme controlled by the inhibitor in the specific cluster.

PMEIs Assist Pollen Tube Growth During Fertilization and Embryogenesis

Pollen tube tip growth in the transmitting tract is crucial for reproductive success of plants. Pollen tube elongation is driven by secretion of pectic material and a gradient of degree of pectin methylesterification along the pollen tube axis provides the plasticity and rigidity requested for pollen tube growth (Parre and geitmann, 2005). PME and PMEI can play multiple roles in this process in different species (Bosch and Hepler, 2005; Zhang et al., 2010; Rocchi et al., 2011). AtPMEI1 and AtPMEI2 transcripts are particularly expressed in flower tissues suggesting a role of these inhibitors during flower formation or during the reproductive process. Both proteins interact with, and inhibit *in vitro*, different PMEs indicating a large spectrum of recognition for the PMEIs (**Table 2**; Raiola et al., 2004; Lionetti et al., 2007; Röckel et al., 2008). An interesting role in the regulation of the dynamics of pectin metabolism in polar pollen cell growth was demonstrated for AtPMEI2 (Röckel et al., 2008). AtPMEI2 showed a polarized accumulation at the pollen tube apex favored by a local PMEI endocytosis at the flanks of the tip. By reducing blockwise de-methylesterification and Ca^{2+}-mediated pectin crosslinks, the localized AtPMEI2 accumulation at pollen tube apex favors CW extensibility and polar growth. Also, AtPMEI-PME5, AtPMEI-PME4, and AtPMEI-PME37 clusters are highly expressed during pollen tube growth (Jiang et al., 2005). A controlled AtPMEI-PME5 activity by PMEI domain could modulate pectin

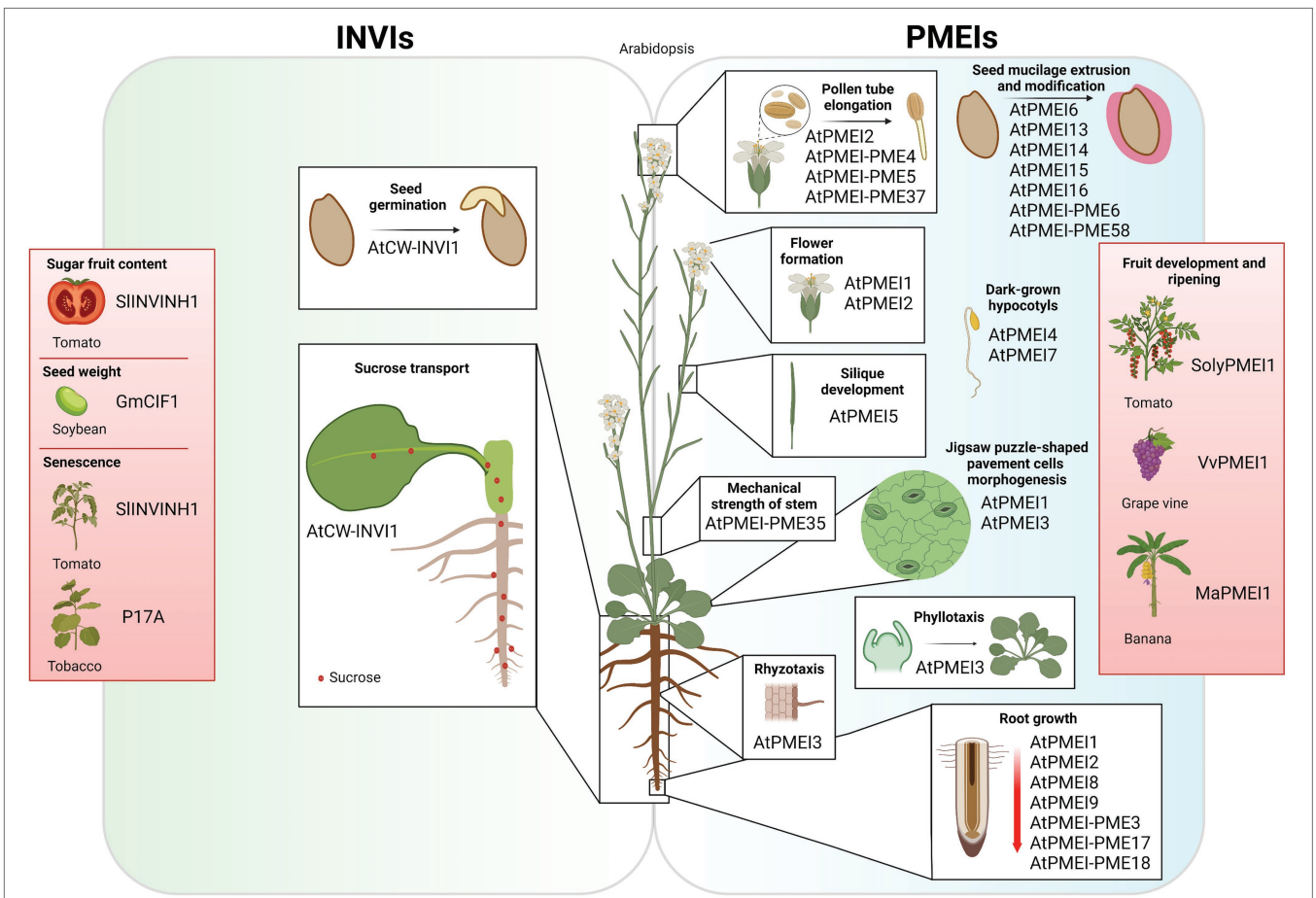

FIGURE 5 | Overview of INVIs and PMEIs functions in plant growth and development. INVIs control seed germination, sugar transport in roots; senescence and sugar fruit content. PMEIs play multiple roles in several physiological processes, such as pollen tube elongation, seed mucilage extrusion, and modification, flowering transition, silique development, mechanical strength of stem, phyllotaxis, rhyzotaxis, pavement cells morphogenesis, hypocotyl growth in the dark, and root growth, and they are also involved in fruit development and ripening.

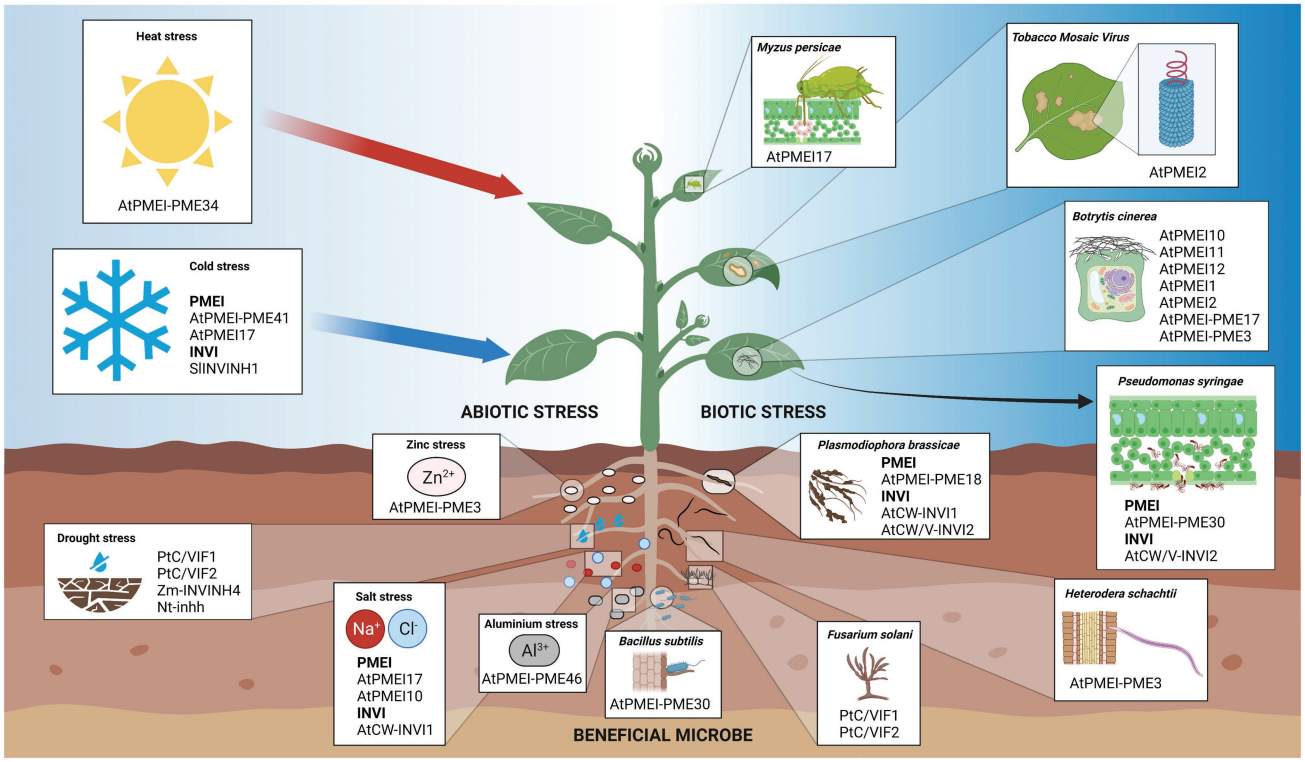

FIGURE 6 | Schematic representation of the involvement of INVI/PMEI members in plant-environment interactions. Plants face different pathogens and pests, such as bacteria, nematodes, fungi, viruses, and insects as well as multiple abiotic stresses. Different INVI/PMEI members have a pivotal role plant-microbe associations beneficial to the host plant like also during multiple plant-pathogen interactions. PMEIs and INVIs are also involved in plant responsiveness to different abiotic stresses and in heavy metal tolerance.

methylesterification of the transmitting tract cells to assist pollen tube movement toward the ovules.

The remodeling of pectin methylesterification play important roles in embryogenesis (Cruz-Valderrama et al., 2018; Pérez-Pérez et al., 2019). AtPMEI12 is expressed in the micropylar endosperm that surrounds the embryo and its prolonged expression suppressed embryo growth in Arabidopsis, most likely, by disturbing pectin methylesterification homeostasis (Zuma et al., 2018). AgL62 and FIS2 are required to regulate the expression of AtPMEI12 in the syncytial endosperm (Hoffmann et al., 2022). AtPMEI-PME6 is required for cell wall loosening in the embryo to facilitate cell expansion (Levesque-Tremblay et al., 2015).

PMEIs Regulate Pectin Extensibility During Emergence, Formation, and Growth of Different Organs

Precise spatiotemporal modifications of CW composition and structure are critical for cell expansion and shape (Somerville et al., 2004). Pectin remodeling underlie changes in CW elasticity in organ initiation and differentiation (Hocq et al., 2017a; Shin et al., 2021). The phyllotaxis in the Arabidopsis shoot apical meristem is accompanied by a pectic de-methylesterification in subepidermal tissue layers which is strictly controlled by AtPMEI3 (Peaucelle et al., 2008, 2011a). The *AtPMEI3* overexpression in Arabidopsis produced, throughout the meristem dome, a significant reduction of "egg-box" structures, the development of shorter cells, and loss of growth asymmetry leading to an altered primordia outgrowth. Also in rhyzotaxis, AtPMEI3 expression, acting on pectin methylesterification, influences the functionality of the root clock for lateral root formation (Wachsman et al., 2020).

The jigsaw puzzle-shaped pavement cells of the leaf epidermis serve as an attractive model to investigate the mechanisms for cell–cell coordination of cell shapes (Yang, 2008). Pectin nanofilament expansion drives morphogenesis in plant epidermal cells (Haas et al., 2020). Plant overexpressing AtPMEI1 or AtPMEI3 showed defects in interdigitation and lobe formation in the pavement cells of the leaf epidermis indicating that the pectin methylesterification can influence plant cell morphogenesis (Haas et al., 2020; Lin et al., 2021). Auxin-induced callus formation is considered as a cell reprogramming process for *in vitro* regeneration of plants. Transgenic plants overexpressing AtPMEI-PME2 developed callus-like structures in the roots when grown on medium without exogenous auxin indicating that this cluster participates in the cell reprogramming during callus formation (Xu et al., 2018).

The Arabidopsis dark-grown hypocotyls and root growth were extensively used as models to study pectin modifications during organ elongation (Hocq et al., 2017b). The growth of hypocotyls in the dark is biphasic, with an initial slow and

synchronous growth and a subsequent growth acceleration that propagates rapidly from the base to the top of the hypocotyls. AtPMEI4 controls the timing of the growth acceleration modulating the PME activity and pectin de-methylesterification (Pelletier et al., 2010). *AtPMEI4* overexpression showed an increased concentrations of methylesterified pectins and a delay of growth acceleration. AtPMEI7 was also detected in apoplastic proteins extracted from dark-grown hypocotyl although its role in this process remain to be demonstrated (Sénéchal et al., 2015).

Modulation of PMEIs expression can have different effects on root and root hair growth. A decrease in PME activity correlated with an increased root length in *atpmei-pme17* mutants and in plant overexpressing *AtPMEI1*, *AtPMEI2*, or *AtPMEI9* compared to controls (Lionetti et al., 2007, 2010; Wolf et al., 2012; Senechal et al., 2014, p. 17; Hocq et al., 2017b). On the contrary, a *pmei4* mutant and a AtPMEI-PME3 overexpressor, both expressing an elevated PME activity in Arabidopsis root CWs, showed an increased root length (Hewezi et al., 2008; Senechal et al., 2015). Specific PMEI-PME interactions and their regulation could underlie the contrasting root phenotypes observed in the transgenic plants. AtPMEI1 can inhibit the AtPMEI-PME17 activity *in vitro* (Del Corpo et al., 2020). AtPMEI7 expressed in *Escherichia coli* can form *in vitro* a pH-dependent reversible complex with AtPMEI-PME3 (Sénéchal et al., 2017). Indirect evidence indicates that AtPMEI4/AtPMEI-PME17, AtPMEI4/AtPMEI-PME3 and AtPMEI9/AtPMEI-PME3 interactions are likely to occur *in vivo* (Senechal et al., 2015; Hocq et al., 2017b). The inhibition capacity of AtPMEI4 was predicted to be highly pH-dependent, for the presence of key protonatable amino acids interacting with AtPMEI-PME3. *AtPMEI5* overexpression in Arabidopsis caused root waiving in seedlings and strong defects in adult plants like fusion of cauline leaf and shoot as well as strongly impaired silique development (Wolf et al., 2012; Müller et al., 2013). These effects were related to brassinosteroids as part of a compensatory response against the loss of CW integrity, triggered by an imbalance in pectin methylesterification. Moreover, the AtPMEI5 overexpressors germinate earlier and faster compared to control suggesting that pectin methylesterification is essential for the temporal regulation of radicle emergence in endospermic seeds by altering the mechanical properties of the CWs (Muller et al., 2013). Interestingly, *AtPMEI5* overexpression also revealed a correlation between HG methylesterification and auxin distribution in cell elongation that induce hypocotyl bending required for seedling emergence (Jonsson et al., 2021). AtPMEI8 and AtPMEI9 were identified during a suppressor screen for genetic suppressors of *cobra*, an Arabidopsis mutant with a reduced root length associated to defects in cellulose formation and an increased ratio of unesterified/esterified pectin (Sorek et al., 2015). *AtPMEI8* and *AtPMEI9* expression is exaggerated in mutants with CW defects. The overexpression of *AtPMEI8* and *AtPMEI9* increases the amount of pectin methylesterification in the *cob-6* mutant at the wild-type levels and partially restore the cobra root growth suggesting that pectin methylesterification is a significant factor for CW integrity. AtPMEI-PME3 is ubiquitous in Arabidopsis tissues and it was involved in multiple physiological processes like adventitious rooting, root hair production, and seed germination (Guénin et al., 2011, 2017). AtPMEI-PME24 plays a role in root hair development and it can be inhibited by the non-proteinaceous PME inhibitor phenylephrine (Won et al., 2009; Cheong et al., 2019).

Lignin in secondary CW is considered the main component influencing the mechanical strength of the stem. Interestingly, the de-methylesterification of the primary CW can play a role in CW stiffening for mechanical support of the Arabidopsis inflorescence stem (Hongo et al., 2012). A loss-of-function mutant of AtPMEI-PME35 showed a pendant stem phenotype and an increased deformation rate of the stem.

PMEI in Fruit Development, Ripening, and Postharvest Fruit Processes

Fruit development and ripening require a combined, sequential, and synergistic action of a range of CW degrading enzymes (CWDEs; Wang et al., 2018). Advanced softening during ripening is a limiting factor in fruit shelf life and storage (Brummell and Harpster, 2001). The role of PME in fruit ripening was intensively examined in tomato. PME activity can affect pectin structure during ripening and fruit processing and it can also be a potential enhancers of ascorbic acid production (Tieman et al., 1992; Gaffe et al., 1994; Tieman and Handa, 1994; Thakur et al., 1996; Rigano et al., 2018). PMEIs can modulate PME activity and pectin methylesterification in different stages of fruit life. Several inhibitors were identified and characterized from the fruits of different species, like AcPMEI in Kiwi (Balestrieri et al., 1990), SolyPMEI1 in Tomato (Reca et al., 2012), MaPMEI1 in Banana (*Musa acuminata*; Srivastava et al., 2012) and VvPMEI1 in grapevine (*Vitis vinifera*; Lionetti et al., 2015b). The *AcPMEI*, *SolyPMEI,* and *MaPMEI1* expressions increase as the fruits ripen to finely control pectin de-methylesterification in softening during ripening. Differently, VvPMEI1 control PME activity at early phases of grape berry development to assist a rapid cell growth and to maintain pulp firmness, by preventing precocious pectin degradation and grape berry softening.

Different evidence indicates PMEI activity as a valid tool in food processes (Sørensen et al., 2004). PME is physiologically released into the juice during processing, and it is considered a juice clarifying enzyme. PME activity, by triggering the formation of "egg-box" structures, causes the precipitation of pectins and cloud loss in juice, one of the major problems in fruit juice manufacturing industries (Bazaraa et al., 2020). The thermal inhibition of PME activity might be a solution but it can negatively affect the nutritional quality of the juice. The addition of PMEI during the process was demonstrated to reduce phase separation improving juice quality (Castaldo et al., 1991; Sørensen et al., 2004; Bellincampi et al., 2005). PME activity can represent also a postharvest problem in grape fermentation and distillation processes, inducing a high methanol content in spirits (Botelho et al., 2020). PMEI can reduce methanol formation in grape must and marc as well as in products derived by fermentation and distillation (Lante et al., 2008; Zocca et al., 2008).

PMEIs Modulate Seed Mucilage Extrusion and the Mucilage Degree of Methylesterification

The mucilage secretory cells present in the epidermal layer of the seed coat are responsible for mucilage production and release (Francoz et al., 2015). The release and function of mucilage are affected by PME activity (Rautengarten et al., 2008), and several evidence indicate that this activity requires a fine regulation by PMEIs. AtPMEI6 is specifically expressed in seed coat epidermal cells and *pmei6* mutants showed a delayed mucilage release (Saez-Aguayo et al., 2013). The analysis of PME activity in soluble mucilage from *pmei6* and 35S:PMEI6 transgenic plants indicates that AtPMEI6 inhibits endogenous PME activities. The level of *AtPMEI6* expression in transformants correlated with the level of methylesterified HG revealed using antibodies recognizing HG methylesterification status. This evidence leads to conclude that AtPMEI6 controls CW integrity of seed coat epidermal cells by preventing HG de-methylesterification for a correct seed mucilage release. Mechanistic insights indicate that the AtPMEI6-dependent partially methylesterified HG pattern represents an amphiphilic polysaccharidic platform necessary for PEROXIDASE36-specific anchoring, useful to loosen the outer periclinal wall domains of mucilage secretory cells, necessary for mucilage extrusion (Kunieda et al., 2013; Francoz et al., 2019).

AtPMEI13, AtPMEI14, AtPMEI15, and AtPMEI16 are other four independent mucilage-related PMEIs (Shi et al., 2018; Ding et al., 2021). *pmei13* and *pmei14* mutants but not *pmei15* mutant showed an increased PME activity and a reduced degree of methylesterification in the seed mucilage. AtPMEI15 might play only a minimal role in HG de-methylesterification or it could also be an INVI. AtPMEI14 protein seems dedicated to the modulation of pectin de-methylesterification in the mucilage after its release because any discernible mucilage extrusion defects were detected in the *pmei14* mutant. The expression of *AtPMEI6*, *AtPMEI14,* and *AtPMEI16*, like also other pectin modifying enzymes can be activated by the transcriptional factors GLABRA2 (GL2), *LEUNIG_HOMOLOG/MUCILAGE MODIFIED1* (*LUH/MUM1*), *SEEDSTICK* (*STK*), and MYELOBLASTOSIS 52 (MYB52; Saez-Aguayo et al., 2013; Ezquer et al., 2016; Ding et al., 2021). The Arabidopsis ETHYLENE RESPONSIVE ELEMENT BINDING FACTOR 4 (ERF4) and the MYB52 transcription factors interact and play antagonistic roles in the regulation of pectin de-methylesterification in seed mucilage. ERF4 directly suppresses the expression of *AtPMEI13*, *AtPMEI14*, *ATPMEI15* and suppresses *AtPMEI6* indirectly by antagonizing MYB52 function, giving rise to positive regulation of pectin de-methylesterification during seed development (Ding et al., 2021). Also the clusters AtPMEI-PME6 and AtPMEI-PME58 were associated to HG modification during mucilage release (Levesque-Tremblay et al., 2015; Turbant et al., 2016). AtPMEI-PME6 is required for mucilage extrusion while AtPMEI-PME58 activity participates in the regulation of interactions between HG and other polymers (probably rhamnogalacturonan I) during the formation of the mucilage adherent layer.

PMEIs Are Involved in Multiple Biotic and Abiotic Stresses

A fine modulation of PME activity and pectin methylesterification is exerted to face biotic and abiotic stresses (Lionetti et al., 2012; Bellincampi et al., 2014). Plants involve a spatiotemporal modulation of PME activity against multiple pathogens to trigger defense response in several ways (Bethke et al., 2014; Lionetti, 2015; Del Corpo et al., 2020). PMEs can induce the formation of the "egg-box" structures, resulting in pectin stiffening (Limberg et al., 2000). Moreover, PME activity can favor the production of damage-associated molecular patterns. For instance, PMEs can promote the release or perception of de-methylesterified oligogalacturonides, able to trigger plant immunity (Osorio et al., 2008, 2011; Ferrari et al., 2013; Kohorn et al., 2014). De-methylesterification of pectin by PMEs can also generate the alarm signal methanol (Hann et al., 2014). Methanol and oligogalacturonides are able to trigger a defensive priming in plants (Dorokhov et al., 2012; Komarova et al., 2014; Gamir et al., 2021; Giovannoni et al., 2021). Moreover, the pathogen recognition receptors Wall Associated Kinase 1 (WAK1), WAK2, and FERONIA (FER) preferentially bind to de-methylesterified pectins (Decreux and Messiaen, 2005; Kohorn et al., 2014; Feng et al., 2018; Guo et al., 2018; Lin et al., 2021). Independent and clustered PMEIs were involved in plant immunity, at different times during microbial infection. Intriguingly, INVI/PMEIs families show gene duplications, which are frequent in stress-related genes and are beneficial for survival in challenging environments (Oh et al., 2012; Kalunke et al., 2015). *atpmei-pme17* mutants exhibited increased susceptibility to *B. cinerea* indicating that AtPMEI-PME17 cluster contributes to trigger PME activity against *B. cinerea* (Del Corpo et al., 2020). *AtPMEI-PME17* expression is regulated by defense signaling pathways suggesting its involvement for early defense response. At later stages of infection, an extensive PME mediated de-methylesterification of pectin could favor pectin degradation by microbial CWDE. This effect can be restrained by the expression of independent PMEIs (Lionetti et al., 2017). at*pmei10*, at*pmei11*, and at*pmei12* mutants showed increased PME activity, decreased pectin degree of methylesterification, and increased susceptibility to infection indicating that AtPMEI10, AtPMEI11, and AtPMEI12 can be exploited late during *Botrytis* infection to lock an extensive decrease of pectin methylesterification to defend pectin integrity. Intriguingly, the evidence that AtPMEI11 is induced by oligogalacturonides suggests a system of amplification of the pectin protection during immunity. Consistently, the overexpression of *AtPMEI1* and *AtPMEI2* in Arabidopsis induced a high degree of pectin methylesterification that correlated with a low susceptibility to *B. cinerea* (Lionetti et al., 2007). Similar results were obtained also in other pathosystems and also in monocots where the pectin level is low (An et al., 2008; Volpi et al., 2011; Liu et al., 2018). It must be emphasized that PMEI overexpression is free of disease resistance/developmental growth trade-offs observed in plants with engineered CWs (Pontiggia et al., 2020; Ha et al., 2021). Rather, PMEI overexpressors had a higher biomass yield and can improve tissue saccharification in bioconversion (Lionetti et al., 2010, 2014a; Francocci et al., 2013). Early aphid infestation induces an increase in PME activity,

methanol emissions, and HG de-methylesterification (Silva-Sanzana et al., 2019). at*pmei17* mutants (named pmei13 mutants in the original article) are significantly more susceptible to the green peach aphid (*Myzus persicae*) compared to control in terms of settling preference, phloem access, and phloem sap drainage. AtPMEI17 seems particularly effective in plant–aphid interaction, since aphid feeding activities were not altered in AtPMEI6 overexpressors.

Induced Systemic Resistance (ISR) triggered by microbial bio-agents showed strong potential for biocontrol against phytopathogens (Zehra et al., 2021). Interestingly, the beneficial microbe *Bacillus subtilis* manipulate PME activity in root to improve own colonization while promoting plant resistance to leaf microbes (Lakshmanan et al., 2013). Roots of *atpmei-pme30* mutant inoculated with showed increased bacterial root colonization and foliar protection against the pathogen *P. syringae*.

Also, pathogens can exploit plant PMEI-PMEs to create an optimal cellular environment for their own survival. The ubiquitous AtPMEI-PME3 seems particularly targeted. AtPMEI-PME3 is exploited by *B. cinerea* and *Pectobacterium carotovorum* as susceptibility factor required for tissue degradation and colonization (Raiola et al., 2011). Cyst nematodes use own CWDEs, such as cellulases and pectinases to breach the CW for their root penetration and migration (Bohlmann and Sobczak, 2014). A cellulose binding domain-containing protein released by the sugar beet cyst nematode *Heterodera schachtii* into Arabidopsis tissues interacts with AtPMEI-PME3 to aid cyst nematode parasitism (Hewezi et al., 2008). PME activity, by reducing the level of pectin methylesterification can improve the accessibility of other CWDEs to CW polymers, assisting syncytium development. The cellulose binding domain-containing protein could interact with AtPMEI-PME3 in the cytoplasm followed by a potential joint export into the CW. The PMEI region of AtPMEI-PME3 could protect pectin in the golgi apparatus from premature de-methylesterification. CW remodeling of Arabidopsis root cells is also exploited by the obligate biotrophic *Plasmodiophora brassicae*, a protist pathogen that causes clubroot disease in brassica species (Stefanowicz et al., 2021). A pectin de-methylesterification mediated by AtPMEI-PME18 can favor the release of resting spores of the fungus. Intriguingly, AtPMEI-PME18 showed both PME and ribosome-inactivating proteins activity (De-la-Peña et al., 2008). Intriguingly, AtPMEI-PME18 activity could be manipulated by *P. brassicae* to kill host cells to its advantage since ribosome-inactivating proteins were previously considered as "suicidal agent," exploited from plant to contain the spread of pathogens (Bonness et al., 1994; Park et al., 2004). Also, the viruses like Tobacco Mosaic Virus (TMV), *Turnip vein clearing virus* (TVCV), *Cauliflower mosaic virus*, and *Chinese wheat mosaic virus* can exploit the interaction between a own movement protein and a PME for cell-to-cell movement (Chen et al., 2000; Chen and Citovsky, 2003). PME-dependent formation of methanol and PME-dependent enhancement of RNA silencing also influences viral cell-to-cell movement (Dorokhov et al., 2006, 2012). A tobacco PMEI (FN432040) is a methanol-inducible gene involved in defense reactions. The overexpression of AtPMEI2 in Arabidopsis and AcPMEI in tobacco contrasts the cell-to-cell and systemic movement of tobamoviruses (Lionetti et al., 2014b, 2015a).

The ability of plants to sense and maintain pectin integrity is important for salt tolerance (Yan et al., 2018; Liu et al., 2021). A fine control of different PME isoforms could modulate the ion-binding capacities of CWs to cope with salt stress (Pilling et al., 2004). AtPMEI17 positively contributes to salt tolerance in Arabidopsis (Chen et al., 2018; Liu et al., 2021). *AtPMEI17* overexpression showed decreased PME activity, increased pectin methylesterification, and an improved seeds germination, root growth and survival rate under salt stress compared to control. Instead, AtPMEI10 is a negative regulator of salinity tolerance (Jithesh et al., 2012). *Atpmei10* mutants upon NaCl treatment showed enhanced root growth and biomass yield and a reduced salt stress.

The ubiquitous AtPMEI-PME3 was also involved in basal metal tolerance to Zinc (Weber et al., 2013). A defective proteolytic cleavage of PMEI domain from catalytic part of AtPMEI-PME3 cluster *in ozs2* (overly zinc sensitive 2) mutant, causes a root hypersensitivity to zinc. The PME activity, by producing free carboxylic groups, could potentially favor the binding of metal cations to CW thereby lowering their uptake into the symplast. Similarly, AtPMEI-PME46 mediated de-methylesterification reduces aluminum binding to CWs and hence alleviating aluminum-induced root growth inhibition (Geng et al., 2017).

Pectin contents, PME activity, and pectin methylesterification are dynamically regulated during plant acclimation to temperature stresses (Solecka et al., 2008; Baldwin et al., 2014). Under chilling stress PME activity can increase the stiffness of CWs, increasing cold and freezing tolerance for the plant (Qu et al., 2011). AtPMEI-PME41 is proposed to modulate the chilling tolerance by modifying the mechanical properties of CW though the brassinosteroid signaling. AtPMEI17 (named AtPMEI13 in the original article) negatively contributes to Arabidopsis freezing tolerance (Chen et al., 2018). However, AtPMEI17 overexpressors showed longer roots under less severe cold conditions, suggesting a role of this inhibitor in balancing the trade-off between freezing tolerance and growth maintenance under low-temperature conditions. AtPMEI-PME34 can regulate the rate of transpiration during the heat response (Huang et al., 2017; Wu et al., 2017). This cluster is highly expressed in guard cell where it contributes to regulate CW flexibility and heat tolerance, promoting stomatal movement.

INV INHIBITORS

The first INVI was identified and biochemically characterized in potato (Schwimmer et al., 1961). Later, INVI isoforms were also identified in tobacco, maize (*Zea mays*), tomato, potato, soybean (*glycine max*), and Arabidopsis (Greiner et al., 1998; Bate et al., 2004; Reca et al., 2008; Liu et al., 2010; Su et al., 2016; Tang et al., 2017). To date, only two INVI/PMEI genes were annotated to encode INVIs in *A. thaliana.* These genes, originally termed AtC/VIF1 and AtC/VIF2, were cloned in *E. coli*, their activity characterized *in vitro* and identified as INVIs (Link et al., 2004). AtC/VIF1 exhibited an apoplastic

localization and inhibited a large proportion of CW-INV activity in Arabidopsis (Su et al., 2016). The situation is less clear for AtC/VIF2, which inhibited both V-INV and CW-INV activity, but the affinity for V-INV activity was about 10-fold higher than that for CW-INV activity (Link et al., 2004). However, AtC/VIF2 clearly localized in the cell wall. To standardize the nomenclature of the INVI/PMEI superfamily and enjoying a broader view of information, we rename these two proteins as AtCW-INVI1 and AtCW/V-INVI2, respectively. Unlike PMEIs, the physiological information on INVIs in Arabidopsis is scarce. The contribution to understanding their roles comes mainly from experiments carried out in other plant species (**Figures 5, 6**).

INVIs Affect Seed Germination, Seedling Growth, Senescence, and Sugar Content in Fruits

Some INVIs can regulate cell elongation and division. In Arabidopsis, AtCW-INVI1 can influence sugar metabolism and transport in seeds and roots. *atcw-invi1* mutant showed a faster seed germination and an increased root length in seedlings compared to control (Su et al., 2016). CW-INV activity can support cell division of the endosperm and embryo during early kernel development (Bate et al., 2004). Zm-INVINH1 is a maize CW-INVI that localizes specifically to the embryo surrounding regions. Zm-INVINH1 activity could compartmentalize invertase activity within the early kernel to allow the endosperm and embryo to follow distinct developmental programs.

CW-INVs play roles also in seed filling and fruit set in a wide range of plant species (Zanor et al., 2009; Wang and Ruan, 2012; Li et al., 2013; Liao et al., 2020). The control of INV activity by CW-INVIs is part of sugar unloading from phloem to fruits. In tomato, a knock-down expression of the apoplastic SlINVINH1 by RNAi technology caused an improvement in seed filling and sugar content in fruits (Jin et al., 2009). Later, a tomato knock-out for SlINVINH1 obtained using genome editing technology increases sugar content of tomato fruit without decrease fruit weight (Kawaguchi et al., 2021). Also in soybean, the suppression of the apoplastic *GmCIF1* improves seed weight (Tang et al., 2017). Also, fruit ripening seems affected by the balance between CW and V-INV activity. The repression of the vacuolar *SlVIF* by RNA interference delayed tomato fruit ripening and its overexpression increased ethylene production and led to a precocious color shift, due to elevated lycopene accumulation (Qin et al., 2016). Manipulation of INVI-INV interactions represents a promising strategy to increase crop production and to produce crops with a high sugar content in fruits.

Leaf senescence is characterized by a nutrient relocation from leaves to other parts of the plant and the cytokinins delay senescence affecting source–sink relations (Guo et al., 2021). Different CW-INVIs were correlated to senescence. Silencing the *SlINVINH1* expression in tomato increases apoplastic INV activity and delays leaf senescence (Jin et al., 2009). Consistently, the expression of the INVI *P17A* in tobacco under control of a cytokinin-inducible promoter causes the loss of cytokinin-induced delay in senescence (Balibrea Lara et al., 2004).

INVIs Play Roles During Biotic and Abiotic Stresses

Invertase activity and its post-translational modulation by INVIs are part of immune responses against microbes, especially in the apoplast (Tauzin and Giardina, 2014). The downregulation of AtCW/V-INVI2 expression and activity in Arabidopsis source leaves in response to infection by *P. syringae*, de-represses invertase activity as part of the plant defense response (Bonfig et al., 2010). However, invertase activity can also be exploited by pathogens in the root. Invertase gene expression is upregulated in root galls developed by *P. brassicae* in Arabidopsis (Siemens et al., 2011). The overproduction of AtCW-INVI1 and AtCW/V-INVI2 in Arabidopsis transgenic lines caused a reduced invertase activity in the root, a lower sucrose import into infected cells, leading to a reduced clubroot symptoms. The expressions of the two apoplastic *PtC/VIF1* and *PtC/VIF2* are strongly induced in the root of *Populus trichocarpa* against different stress cues including fusarium wilt (*Fusarium solani*), drought, abscisic acid, wound, and senescence (Su et al., 2020). A *Nicotiana attenuata* CW-INVI, named NaCWII, is strongly upregulated in a JA-dependent manner to increase secondary metabolite biosynthesis in *Manduca sexta*-attacked plants (Ferrieri et al., 2015).

Cold stress limits productivity and adversely affects plant growth and development. The content of sugars with an osmoprotective function increased during cold treatment (Janská et al., 2010). During chilling stress, tomato plants de-repress INV activity in the apoplast by controlling *SlINVINH1*expression (Xu et al., 2017). Cold storage of potato tubers prevent sprouting and pathogenesis favoring the maintenance of supply throughout the year. However, cold induces a breakdown of starch to sucrose that is ultimately cleaved into glucose and fructose by acid invertases, leading to a tuber sweetening (Mckenzie et al., 2013). Cold-induced sweetening is a serious postharvest problem for potato compromising tuber quality. The ectopic expression of different V-INVIs in potato tubers prevents cold-induced sweetening by capping the activities of V-INVs (Greiner et al., 1999; Brummell et al., 2011; Liu et al., 2013; Mckenzie et al., 2013).

Stomatal movement is critical in plant response to drought and V-INV activity is correlated with stomatal aperture under normal and drought conditions (Ni, 2012). The ectopic expression of the tobacco V-INVI, *Nt-inhh*, under the control of an ABA-sensitive and guard cell-specific promoter AtRab18 conferred enhanced drought tolerance in Arabidopsis and tomato (Chen et al., 2016). More recently, the drought-responsive apoplastic Zm-INVINH4 was identified and characterized in maize (Chen et al., 2019). Moreover, Arabidopsis salt tolerance can be influenced by At*CW-INVI1* (Yang et al., 2020). Transgenic plant overexpressing At*CW-INVI1* showed enhanced sensitivity to ABA and reduced tolerance to salt.

UNDEFINED INVI/PMEIs AND THEIR POSSIBLE ROLES

Some knowledge was collected for INVI/PMEI members from now on presented. However, new experiments are needed to

define their PMEI or INVI activity and to elucidate their roles in plant physiology. A INVI/PMEI isoforms, named AppB1 (At4g24640) was previously associated to pollen development (Holmes-Davis et al., 2005). A large-scale mutant screen in *A. thaliana* led to the identification of two INVI/PMEI mutants with defects in female gametophyte development and function (Pagnussat et al., 2005). The mutant embryo sac development arrest 24 (EDA 24) fails in polar nuclei fusion during the embryo sac development while the mutant unfertilized embryo sac 11 (UNE11) is affected in embryo sac fertilization. At5g46950 (named InvINH2) is an endosperm-specific INVI-PMEI, but its specific activity remain still to be characterized (Zuma et al., 2018). A genome wide association study supported by quantitative trait loci mapping identified the INVI/PMEI At1g23350 as a candidate gene for the response to drought/*B. cinerea* sequential double-stress combination (Coolen et al., 2019).

CONCLUSION AND PERSPECTIVE

Data obtained on the pattern of expression, specific activity, and related physiological effects deepen our knowledge of INVI/PMEI roles in plant growth and defense and allow to engineer precise biotechnological applications. A stage-specific manipulation of INVI/PMEIs *in planta* could be used as biotechnological strategy to control the fruit growth and postharvest fruit softening. INVI/PMEI represent also genetic sources to generate crop varieties, either by traditional breeding or by genetic engineering, with a durable resistance to stresses and/or with a high crop yield. The revision allowed to eliminate various inaccuracies in the nomenclature of INVI/PMEI members, providing a clear tool for future studies. We emphasize the importance of verifying the inhibitory activity of new members of the superfamily not yet characterized, before assigning them an identity. Some shortcomings on the family certainly emerge, especially on the physiological role of INVIs, and several questions remain unanswered. Although a vacuolar, cytosolic or apoplastic function was suggested for some INVI/PMEI isoforms, further investigation is needed to understand their subcellular action and processing. Future research could also try to reveal the dynamics of inhibition as well as the fate of the inhibitors after performing their function. Moreover, PMEIs were linked to the modulation of the degree and pattern of methylesterification of HG. However, an interesting and not yet tested hypothesis is that some PME and PMEI isoforms could be dedicated to xylogalacturonan or rhamnogalacturonans, which are other pectic polysaccharides showing some degree of methylesterification. PMEIs, like also other apoplastic factor as pH and calcium concentration could influence not only the degree but also the pattern of methylesterification. Studies aimed at identifying the three-dimensional structure of PMEI-PMEs could provide important information useful to clarify the role of PMEIs in these clusters. New knowledge on the interactions between specific PMEI and PME isoforms and on the inhibition features in PMEI-PMEs isoforms will be necessary to understand the dynamics of the control of PME activity in plant physiology.

AUTHOR CONTRIBUTIONS

DC and VL collected data from literature and prepared figures and revised the paper. VL designed and wrote the manuscript. All authors contributed to the article and approved the submitted version.

FUNDING

The work was supported by Sapienza University of Rome, Grants RM120172B78CFDF2 and RM11916B7A142CF1 to VL and AR12117A8A4A1ADC to DC and LV.

ACKNOWLEDGMENTS

Figures 5, 6 were created with biorender.com.

REFERENCES

Amsbury, S., Hunt, L., Elhaddad, N., Baillie, A., Lundgren, M., Verhertbruggen, Y., et al. (2016). Stomatal function requires pectin de-methyl-esterification of the guard cell wall. *Curr. Biol.* 26, 2899–2906. doi: 10.1016/j.cub.2016.08.021

An, S. H., Sohn, K. H., Choi, H. W., Hwang, I. S., Lee, S. C., and Hwang, B. K. (2008). Pepper pectin methylesterase inhibitor protein CaPMEI1 is required for antifungal activity, basal disease resistance and abiotic stress tolerance. *Planta* 228, 61–78. doi: 10.1007/s00425-008-0719-z

Baldwin, L., Domon, J.-M., Klimek, J. F., Fournet, F., Sellier, H., Gillet, F., et al. (2014). Structural alteration of cell wall pectins accompanies pea development in response to cold. *Phytochemistry* 104, 37–47. doi: 10.1016/j.phytochem.2014.04.011

Balestrieri, C., Castaldo, D., Giovane, A., Quagliuolo, L., and Servillo, L. (1990). A glycoprotein inhibitor of pectin methylesterase in kiwi fruit (*Actinidia chinensis*). *Eur. J. Biochem.* 193, 183–187. doi: 10.1111/j.1432-1033.1990.tb19321.x

Balibrea Lara, M. E., Gonzalez Garcia, M.-C., Fatima, T., Ehness, R., Lee, T. K., Proels, R., et al. (2004). Extracellular invertase is an essential component of cytokinin-mediated delay of senescence. *Plant Cell* 16, 1276–1287. doi: 10.1105/tpc.018929

Bate, N. J., Niu, X., Wang, Y., Reimann, K. S., and Helentjaris, T. G. (2004). An invertase inhibitor from maize localizes to the embryo surrounding region during early kernel development. *Plant Physiol.* 134, 246–254. doi: 10.1104/pp.103.027466

Bazaraa, W. A., Ammar, A. S., and Aqlan, A. M. (2020). Effects of kiwi's pectin methylesterase inhibitor, nanomilling and pasteurization on orange juice quality. *Food Sci. Nutr.* 8, 6367–6379. doi: 10.1002/fsn3.1886

Bellincampi, D., Cervone, F., and Lionetti, V. (2014). Plant cell wall dynamics and wall-related susceptibility in plant-pathogen interactions. *Front. Plant Sci.* 5:228. doi: 10.3389/fpls.2014.00228

Bellincampi, D., Cervone, F., Raiola, A., Camardella, L., Balestrieri, C., De Lorenzo, G., et al. (2005). Pectin methylesterase inhibitors for the preparation of fruit juices and derivative. Patent No. WO2005005470A2. Available at: https://patents.google.com/patent/WO2005005470A2/en

Bethke, G., Grundman, R. E., Sreekanta, S., Truman, W., Katagiri, F., and Glazebrook, J. (2014). *Arabidopsis* PECTIN METHYLESTERASES contribute to immunity against *Pseudomonas syringae*. *Plant Physiol.* 164, 1093–1107. doi: 10.1104/pp.113.227637

Bohlmann, H., and Sobczak, M. (2014). The plant cell wall in the feeding sites of cyst nematodes. *Front. Plant Sci.* 5:89. doi: 10.3389/fpls.2014.00089

Bonavita, A., Carratore, V., Ciardiello, M. A., Giovane, A., Servillo, L., and D'Avino, R. (2016). Influence of pH on the structure and function of kiwi pectin methylesterase inhibitor. *J. Agric. Food Chem.* 64, 5866–5876. doi: 10.1021/acs.jafc.6b01718

Bonfig, K. B., Gabler, A., Simon, U. K., Luschin-Ebengreuth, N., Hatz, M., Berger, S., et al. (2010). Post-translational derepression of invertase activity in source leaves via down-regulation of invertase inhibitor expression is part of the plant defense response. *Mol. Plant* 3, 1037–1048. doi: 10.1093/mp/ssq053

Bonness, M. S., Ready, M. P., Irvin, J. D., and Mabry, T. J. (1994). Pokeweed antiviral protein inactivates pokeweed ribosomes; implications for the antiviral mechanism. *Plant J.* 5, 173–183. doi: 10.1046/j.1365-313X.1994.05020173.x

Bosch, M., Cheung, A. Y., and Hepler, P. K. (2005). Pectin methylesterase, a regulator of pollen tube growth. *Plant Physiol.* 138, 1334–1346. doi: 10.1104/pp.105.059865

Bosch, M., and Hepler, P. (2005). Pectin methylesterases and pectin dynamics in pollen tubes. *Plant Cell* 17, 3219–3226. doi: 10.1105/tpc.105.037473

Botelho, G., Anjos, O., Estevinho, L. M., and Caldeira, I. (2020). Methanol in grape derived, fruit and honey spirits: a critical review on source, quality control, and legal limits. *PRO* 8:1609. doi: 10.3390/pr8121609

Boycheva, S., Daviet, L., Wolfender, J.-L., and Fitzpatrick, T. B. (2014). The rise of operon-like gene clusters in plants. *Trends Plant Sci.* 19, 447–459. doi: 10.1016/j.tplants.2014.01.013

Brummell, D. A., Chen, R. K. Y., Harris, J. C., Zhang, H., Hamiaux, C., Kralicek, A. V., et al. (2011). Induction of vacuolar invertase inhibitor mRNA in potato tubers contributes to cold-induced sweetening resistance and includes spliced hybrid mRNA variants. *J. Exp. Bot.* 62, 3519–3534. doi: 10.1093/jxb/err043

Brummell, D. A., and Harpster, M. H. (2001). Cell wall metabolism in fruit softening and quality and its manipulation in transgenic plants. *Plant Mol. Biol.* 47, 311–339. doi: 10.1023/A:1010656104304

Castaldo, D., Lovoi, A., Quagliuolo, L., Servillo, L., Balestrieri, C., and Giovane, A. (1991). Orange juices and concentrates stabilization by a proteic inhibitor of pectin methylesterase. *J. Food Sci.* 56, 1632–1634. doi: 10.1111/j.1365-2621.1991.tb08658.x

Catoire, L., Pierron, M., Morvan, C., du Penhoat, C. H., and Goldberg, R. (1998). Investigation of the action patterns of pectinmethylesterase isoforms through kinetic analyses and NMR spectroscopy. Implications In cell wall expansion. *J. Biol. Chem.* 273, 33150–33156. doi: 10.1074/jbc.273.50.33150

Chen, J., Chen, X., Zhang, Q., Zhang, Y., Ou, X., An, L., et al. (2018). A cold-induced pectin methyl-esterase inhibitor gene contributes negatively to freezing tolerance but positively to salt tolerance in *Arabidopsis*. *J. Plant Physiol.* 222, 67–78. doi: 10.1016/j.jplph.2018.01.003

Chen, M.-H., and Citovsky, V. (2003). Systemic movement of a tobamovirus requires host cell pectin methylesterase. *Plant J.* 35, 386–392. doi: 10.1046/j.1365-313X.2003.01818.x

Chen, S.-F., Liang, K., Yin, D.-M., Ni, D.-A., Zhang, Z.-G., and Ruan, Y.-L. (2016). Ectopic expression of a tobacco vacuolar invertase inhibitor in guard cells confers drought tolerance in *Arabidopsis*. *J. Enzyme Inhib. Med. Chem.* 31, 1381–1385. doi: 10.3109/14756366.2016.1142981

Chen, L., Liu, X., Huang, X., Luo, W., Long, Y., Greiner, S., et al. (2019). Functional characterization of a drought-responsive invertase inhibitor from maize (*Zea mays* L.). *Int. J. Mol. Sci.* 20:4081. doi: 10.3390/ijms20174081

Chen, M. H., Sheng, J., Hind, G., Handa, A. K., and Citovsky, V. (2000). Interaction between the tobacco mosaic virus movement protein and host cell pectin methylesterases is required for viral cell-to-cell movement. *EMBO J.* 19, 913–920. doi: 10.1093/emboj/19.5.913

Cheong, M. S., Lee, D. Y., Seo, K. H., Choi, G.-H., Song, Y. H., Park, K. H., et al. (2019). Phenylephrine, a small molecule, inhibits pectin methylesterases. *Biochem. Biophys. Res. Commun.* 508, 320–325. doi: 10.1016/j.bbrc.2018.11.117

Ciardiello, M. A., D'Avino, R., Amoresano, A., Tuppo, L., Carpentieri, A., Carratore, V., et al. (2008). The peculiar structural features of kiwi fruit pectin methylesterase: amino acid sequence, oligosaccharides structure, and modeling of the interaction with its natural proteinaceous inhibitor. *Proteins* 71, 195–206. doi: 10.1002/prot.21681

Coolen, S., Van Pelt, J. A., Van Wees, S. C. M., and Pieterse, C. M. J. (2019). Mining the natural genetic variation in *Arabidopsis thaliana* for adaptation to sequential abiotic and biotic stresses. *Planta* 249, 1087–1105. doi: 10.1007/s00425-018-3065-9

Cruz-Valderrama, J. E., Jiménez-Durán, K., Zúñiga-Sánchez, E., Salazar-Iribe, A., Márquez-Guzmán, J., and Gamboa-deBuen, A. (2018). Degree of pectin methyl esterification in endosperm cell walls is involved in embryo bending in *Arabidopsis thaliana*. *Biochem. Biophys. Res. Commun.* 495, 639–645. doi: 10.1016/j.bbrc.2017.11.077

D'Avino, R., Camardella, L., Christensen, T. M. I. E., Giovane, A., and Servillo, L. (2003). Tomato pectin methylesterase: Modeling, fluorescence, and inhibitor interaction studies—comparison with the bacterial (*Erwinia chrysanthemi*) enzyme. *Proteins* 53, 830–839. doi: 10.1002/prot.10487

Daher, F. B., and Braybrook, S. A. (2015). How to let go: pectin and plant cell adhesion. *Front. Plant Sci.* 6:523. doi: 10.3389/fpls.2015.00523

Decreux, A., and Messiaen, J. (2005). Wall-associated kinase WAK1 interacts with cell wall pectins in a calcium-induced conformation. *Plant Cell Physiol.* 46, 268–278. doi: 10.1093/pcp/pci026

Dedeurwaerder, S., Menu-Bouaouiche, L., Mareck, A., Lerouge, P., and Guerineau, F. (2008). Activity of an atypical *Arabidopsis thaliana* pectin methylesterase. *Planta* 229, 311–321. doi: 10.1007/s00425-008-0831-0

Del Corpo, D., Fullone, M. R., Miele, R., Lafond, M., Pontiggia, D., Grisel, S., et al. (2020). AtPME17 is a functional *Arabidopsis thaliana* pectin methylesterase regulated by its PRO region that triggers PME activity in the resistance to *Botrytis cinerea*. *Mol. Plant Pathol.* 21, 1620–1633. doi: 10.1111/mpp.13002

De-la-Peña, C., Badri, D. V., and Vivanco, J. M. (2008). Novel role for pectin methylesterase in *Arabidopsis*: a new function showing ribosome-inactivating protein (RIP) activity. *Biochim. Biophys. Acta Gen. Subj.* 1780, 773–783. doi: 10.1016/j.bbagen.2007.12.013

Di Matteo, A., Giovane, A., Raiola, A., Camardella, L., Bonivento, D., Lorenzo, G. D., et al. (2005). Structural basis for the interaction between pectin methylesterase and a specific inhibitor protein. *Plant Cell* 17, 849–858. doi: 10.1105/tpc.104.028886

Ding, A., Tang, X., Yang, D., Wang, M., Ren, A., Xu, Z., et al. (2021). ERF4 and MYB52 transcription factors play antagonistic roles in regulating homogalacturonan de-methylesterification in Arabidopsis seed coat mucilage. *Plant Cell* 33, 381–403. doi: 10.1093/plcell/koaa031

Dorokhov, Y. L., Frolova, O. Y., Skurat, E. V., Ivanov, P. A., Gasanova, T. V., Sheveleva, A. A., et al. (2006). A novel function for a ubiquitous plant enzyme pectin methylesterase: the enhancer of RNA silencing. *FEBS Lett.* 580, 3872–3878. doi: 10.1016/j.febslet.2006.06.013

Dorokhov, Y. L., Komarova, T. V., Petrunia, I. V., Frolova, O. Y., Pozdyshev, D. V., and Gleba, Y. Y. (2012). Airborne signals from a wounded leaf facilitate viral spreading and induce antibacterial resistance in neighboring plants. *PLoS Pathog.* 8:e1002640. doi: 10.1371/journal.ppat.1002640

Ezquer, I., Mizzotti, C., Nguema-Ona, E., Gotté, M., Beauzamy, L., Viana, V. E., et al. (2016). The developmental regulator SEEDSTICK controls structural and mechanical properties of the Arabidopsis seed coat. *Plant Cell* 28, 2478–2492. doi: 10.1105/tpc.16.00454

Feng, W., Kita, D., Peaucelle, A., Cartwright, H. N., Doan, V., Duan, Q., et al. (2018). The FERONIA receptor kinase maintains cell-wall integrity during salt stress through Ca2+ signaling. *Curr. Biol.* 28, 666.e5–675.e5. doi: 10.1016/j.cub.2018.01.023

Ferrari, S., Savatin, D. V., Sicilia, F., Gramegna, G., Cervone, F., and De Lorenzo, G. (2013). Oligogalacturonides: plant damage-associated molecular patterns and regulators of growth and development. *Front. Plant Sci.* 4:49. doi: 10.3389/fpls.2013.00049

Ferrieri, A. P., Arce, C. C. M., Machado, R. A. R., Meza-Canales, I. D., Lima, E., Baldwin, I. T., et al. (2015). A *Nicotiana attenuata* cell wall invertase inhibitor (NaCWII) reduces growth and increases secondary metabolite biosynthesis in herbivore-attacked plants. *New Phytol.* 208, 519–530. doi: 10.1111/nph.13475

Figueiredo, J., Silva, M. S., and Figueiredo, A. (2018). Subtilisin-like proteases in plant defence: the past, the present and beyond. *Mol. Plant Pathol.* 19, 1017–1028. doi: 10.1111/mpp.12567

Francocci, F., Bastianelli, E., Lionetti, V., Ferrari, S., De Lorenzo, G., Bellincampi, D., et al. (2013). Analysis of pectin mutants and natural accessions of *Arabidopsis* highlights the impact of de-methyl-esterified homogalacturonan on tissue saccharification. *Biotechnol. Biofuels* 6:163. doi: 10.1186/1754-6834-6-163

Francoz, E., Ranocha, P., Burlat, V., and Dunand, C. (2015). *Arabidopsis* seed mucilage secretory cells: regulation and dynamics. *Trends Plant Sci.* 20, 515–524. doi: 10.1016/j.tplants.2015.04.008

Francoz, E., Ranocha, P., Le Ru, A., Martinez, Y., Fourquaux, I., Jauneau, A., et al. (2019). Pectin demethylesterification generates platforms that anchor peroxidases to remodel plant cell wall domains. *Dev. Cell* 48, 261.e8–276.e8. doi: 10.1016/j.devcel.2018.11.016

Gaffe, J., Tieman, D. M., and Handa, A. K. (1994). Pectin methylesterase isoforms in tomato (*Lycopersicon esculentum*) tissues (effects of expression of a pectin methylesterase antisense gene). *Plant Physiol.* 105, 199–203. doi: 10.1104/pp.105.1.199

Gamir, J., Minchev, Z., Berrio, E., García, J. M., De Lorenzo, G., and Pozo, M. J. (2021). Roots drive oligogalacturonide-induced systemic immunity in tomato. *Plant Cell Environ.* 44, 275–289. doi: 10.1111/pce.13917

Geng, X., Horst, W. J., Golz, J. F., Lee, J. E., Ding, Z., and Yang, Z.-B. (2017). LEUNIG_HOMOLOG transcriptional co-repressor mediates aluminium sensitivity through PECTIN METHYLESTERASE46-modulated root cell wall pectin methylesterification in *Arabidopsis*. *Plant J.* 90, 491–504. doi: 10.1111/tpj.13506

Giovannoni, M., Lironi, D., Marti, L., Paparella, C., Vecchi, V., Gust, A. A., et al. (2021). The *Arabidopsis thaliana* LysM-containing receptor-Like kinase 2 is required for elicitor-induced resistance to pathogens. *Plant Cell Environ.* 44, 3775–3792. doi: 10.1111/pce.14192

Gough, J., Karplus, K., Hughey, R., and Chothia, C. (2001). Assignment of homology to genome sequences using a library of hidden Markov models that represent all proteins of known structure. *J. Mol. Biol.* 313, 903–919. doi: 10.1006/jmbi.2001.5080

Greiner, S., Krausgrill, S., and Rausch, T. (1998). Cloning of a tobacco apoplasmic invertase inhibitor. Proof of function of the recombinant protein and expression analysis during plant development. *Plant Physiol.* 116, 733–742. doi: 10.1104/pp.116.2.733

Greiner, S., Rausch, T., Sonnewald, U., and Herbers, K. (1999). Ectopic expression of a tobacco invertase inhibitor homolog prevents cold-induced sweetening of potato tubers. *Nat. Biotechnol.* 17, 708–711. doi: 10.1038/10924

Guénin, S., Hardouin, J., Paynel, F., Müller, K., Mongelard, G., Driouich, A., et al. (2017). AtPME3, a ubiquitous cell wall pectin methylesterase of *Arabidopsis thaliana*, alters the metabolism of cruciferin seed storage proteins during post-germinative growth of seedlings. *J. Exp. Bot.* 68, 1083–1095. doi: 10.1093/jxb/erx023

Guénin, S., Mareck, A., Rayon, C., Lamour, R., Assoumou Ndong, Y., Domon, J.-M., et al. (2011). Identification of pectin methylesterase 3 as a basic pectin methylesterase isoform involved in adventitious rooting in *Arabidopsis thaliana*. *New Phytol.* 192, 114–126. doi: 10.1111/j.1469-8137.2011.03797.x

Guo, H., Nolan, T. M., Song, G., Liu, S., Xie, Z., Chen, J., et al. (2018). FERONIA receptor kinase contributes to plant immunity by suppressing jasmonic acid signaling in *Arabidopsis thaliana*. *Curr. Biol.* 28, 3316.e6–3324.e6. doi: 10.1016/j.cub.2018.07.078

Guo, Y., Ren, G., Zhang, K., Li, Z., Miao, Y., and Guo, H. (2021). Leaf senescence: progression, regulation, and application. *Mol. Hortic.* 1:5. doi: 10.1186/s43897-021-00006-9

Ha, C. M., Rao, X., Saxena, G., and Dixon, R. A. (2021). Growth–defense trade-offs and yield loss in plants with engineered cell walls. *New Phytol.* 231, 60–74. doi: 10.1111/nph.17383

Haas, K. T., Wightman, R., Meyerowitz, E. M., and Peaucelle, A. (2020). Pectin homogalacturonan nanofilament expansion drives morphogenesis in plant epidermal cells. *Science* 367, 1003–1007. doi: 10.1126/science.aaz5103

Hann, C. T., Bequette, C. J., Dombrowski, J. E., and Stratmann, J. W. (2014). Methanol and ethanol modulate responses to danger- and microbe-associated molecular patterns. *Front. Plant Sci.* 5:550. doi: 10.3389/fpls.2014.00550

Harholt, J., Suttangkakul, A., and Scheller, H. V. (2010). Biosynthesis of pectin. *Plant Physiol.* 153, 384–395. doi: 10.1104/pp.110.156588

Hewezi, T., Howe, P., Maier, T. R., Hussey, R. S., Mitchum, M. G., Davis, E. L., et al. (2008). Cellulose binding protein from the parasitic nematode *Heterodera schachtii* interacts with *Arabidopsis* pectin methylesterase: cooperative cell wall modification during parasitism. *Plant Cell* 20, 3080–3093. doi: 10.1105/tpc.108.063065

Hocq, L., Pelloux, J., and Lefebvre, V. (2017a). Connecting homogalacturonan-type pectin remodeling to acid growth. *Trends Plant Sci.* 22, 20–29. doi: 10.1016/j.tplants.2016.10.009

Hocq, L., Sénéchal, F., Lefebvre, V., Lehner, A., Domon, J.-M., Mollet, J.-C., et al. (2017b). Combined experimental and computational approaches reveal distinct pH dependence of pectin methylesterase inhibitors. *Plant Physiol.* 173, 1075–1093. doi: 10.1104/pp.16.01790

Hoffmann, T., Shi, X., Hsu, C.-Y., Brown, A., Knight, Q., Courtney, L. S., et al. (2022). The identification of type I MADS box genes as the upstream activators of an endosperm-specific invertase inhibitor in *Arabidopsis*. *BMC Plant Biol.* 22:18. doi: 10.1186/s12870-021-03399-3

Holmes-Davis, R., Tanaka, C. K., Vensel, W. H., Hurkman, W. J., and McCormick, S. (2005). Proteome mapping of mature pollen of *Arabidopsis thaliana*. *Proteomics* 5, 4864–4884. doi: 10.1002/pmic.200402011

Hongo, S., Sato, K., Yokoyama, R., and Nishitani, K. (2012). Demethylesterification of the primary wall by PECTIN METHYLESTERASE35 provides mechanical support to the *Arabidopsis* stem. *Plant Cell* 24, 2624–2634. doi: 10.1105/tpc.112.099325

Hothorn, M., D'Angelo, I., Márquez, J. A., Greiner, S., and Scheffzek, K. (2004a). The invertase inhibitor Nt-CIF from tobacco: a highly thermostable four-helix bundle with an unusual N-terminal extension. *J. Mol. Biol.* 335, 987–995. doi: 10.1016/j.jmb.2003.10.066

Hothorn, M., Van den Ende, W., Lammens, W., Rybin, V., and Scheffzek, K. (2010). Structural insights into the pH-controlled targeting of plant cell-wall invertase by a specific inhibitor protein. *Proc. Natl. Acad. Sci. U. S. A.* 107, 17427–17432. doi: 10.1073/pnas.1004481107

Hothorn, M., Wolf, S., Aloy, P., Greiner, S., and Scheffzek, K. (2004b). Structural insights into the target specificity of plant invertase and pectin methylesterase inhibitory proteins. *Plant Cell* 16, 3437–3447. doi: 10.1105/tpc.104.025684

Huang, Y.-C., Wu, H.-C., Wang, Y.-D., Liu, C.-H., Lin, C.-C., Luo, D.-L., et al. (2017). PECTIN METHYLESTERASE34 contributes to heat tolerance through its role in promoting stomatal movement. *Plant Physiol.* 174, 748–763. doi: 10.1104/pp.17.00335

Janská, A., Maršík, P., Zelenková, S., and Ovesná, J. (2010). Cold stress and acclimation – what is important for metabolic adjustment? *Plant Biol.* 12, 395–405. doi: 10.1111/j.1438-8677.2009.00299.x

Jiang, L., Yang, S.-L., Xie, L.-F., Puah, C. S., Zhang, X.-Q., Yang, W.-C., et al. (2005). VANGUARD1 encodes a pectin methylesterase that enhances pollen tube growth in the *Arabidopsis* style and transmitting tract. *Plant Cell* 17, 584–596. doi: 10.1105/tpc.104.027631

Jin, Y., Ni, D.-A., and Ruan, Y.-L. (2009). Posttranslational elevation of Cell Wall invertase activity by silencing its inhibitor in tomato delays leaf senescence and increases seed weight and fruit hexose level. *Plant Cell* 21, 2072–2089. doi: 10.1105/tpc.108.063719

Jithesh, M. N., Wally, O. S. D., Manfield, I., Critchley, A. T., Hiltz, D., and Prithiviraj, B. (2012). Analysis of seaweed extract-induced transcriptome leads to identification of a negative regulator of salt tolerance in *Arabidopsis*. *HortScience* 47, 704–709. doi: 10.21273/HORTSCI.47.6.704

Jonsson, K., Lathe, R. S., Kierzkowski, D., Routier-Kierzkowska, A.-L., Hamant, O., and Bhalerao, R. P. (2021). Mechanochemical feedback mediates tissue bending required for seedling emergence. *Curr. Biol.* 31, 1154–1164.e3. doi: 10.1016/j.cub.2020.12.016

Kalunke, R. M., Tundo, S., Benedetti, M., Cervone, F., De Lorenzo, G., and D'Ovidio, R. (2015). An update on polygalacturonase-inhibiting protein (PGIP), a leucine-rich repeat protein that protects crop plants against pathogens. *Front. Plant Sci.* 20:146. doi: 10.3389/fpls.2015.00146

Kawaguchi, K., Takei-Hoshi, R., Yoshikawa, I., Nishida, K., Kobayashi, M., Kusano, M., et al. (2021). Functional disruption of cell wall invertase inhibitor by genome editing increases sugar content of tomato fruit without decrease fruit weight. *Sci. Rep.* 11:21534. doi: 10.1038/s41598-021-00966-4

Kohorn, B. D., Kohorn, S. L., Saba, N. J., and Martinez, V. M. (2014). Requirement for pectin methyl esterase and preference for fragmented over native Pectins for wall-associated kinase-activated, EDS1/PAD4-dependent stress response in Arabidopsis. *J. Biol. Chem.* 289, 18978–18986. doi: 10.1074/jbc.M114.567545

Komarova, T. V., Sheshukova, E. V., and Dorokhov, Y. L. (2014). Cell wall methanol as a signal in plant immunity. *Front. Plant Sci.* 5:101. doi: 10.3389/fpls.2014.00101

Kunieda, T., Shimada, T., Kondo, M., Nishimura, M., Nishitani, K., and Hara-Nishimura, I. (2013). Spatiotemporal secretion of PEROXIDASE36 is required for seed coat mucilage extrusion in Arabidopsis. *Plant Cell* 25, 1355–1367. doi: 10.1105/tpc.113.110072

Lakshmanan, V., Castaneda, R., Rudrappa, T., and Bais, H. P. (2013). Root transcriptome analysis of *Arabidopsis thaliana* exposed to beneficial *Bacillus subtilis* FB17 rhizobacteria revealed genes for bacterial recruitment and plant defense independent of malate efflux. *Planta* 238, 657–668. doi: 10.1007/s00425-013-1920-2

Lante, A., Zocca, F., Spettoli, P., Lomolino, G., Raiola, A., Bellincampi, D., et al. (2008). Use of a protein inhibitor of pectin methylesterase for reducing methanol formation in grape must and marc, and process therefor. Patent No. WO2008104555A1. Available at: https://patents.google.com/patent/WO2008104555A1/en:Method

Levesque-Tremblay, G., Müller, K., Mansfield, S. D., and Haughn, G. W. (2015). HIGHLY METHYL ESTERIFIED SEEDS is a pectin methyl esterase involved in embryo development. *Plant Physiol.* 167, 725–737. doi: 10.1104/pp.114.255604

Leyva-González, M. A., Ibarra-Laclette, E., Cruz-Ramírez, A., and Herrera-Estrella, L. (2012). Functional and transcriptome analysis reveals an acclimatization strategy for abiotic stress tolerance mediated by Arabidopsis NF-YA family members. *PLoS One* 7:e48138. doi: 10.1371/journal.pone.0048138

Li, B., Liu, H., Zhang, Y., Kang, T., Zhang, L., Tong, J., et al. (2013). Constitutive expression of cell wall invertase genes increases grain yield and starch content in maize. *Plant Biotechnol. J.* 11, 1080–1091. doi: 10.1111/pbi.12102

Liao, S., Wang, L., Li, J., and Ruan, Y.-L. (2020). Cell wall invertase is essential for ovule development through sugar signaling rather Than provision of carbon nutrients. *Plant Physiol.* 183, 1126–1144. doi: 10.1104/pp.20.00400

Limberg, G., Korner, R., Buchholt, H. C., Christensen, T. M., Roepstorff, P., and Mikkelsen, J. D. (2000). Analysis of different de-esterification mechanisms for pectin by enzymatic fingerprinting using endopectin lyase and endopolygalacturonase II from *A. niger*. *Carbohydr. Res.* 327, 293–307. doi: 10.1016/S0008-6215(00)00067-7

Lin, W., Tang, W., Pan, X., Huang, A., Gao, X., Anderson, C. T., et al. (2021). *Arabidopsis* pavement cell morphogenesis requires FERONIA binding to pectin for activation of ROP GTPase signaling. *Curr. Biol.* 32, 497.e4–507.e4. doi: 10.1016/j.cub.2021.11.030

Link, M., Rausch, T., and Greiner, S. (2004). In *Arabidopsis thaliana*, the invertase inhibitors AtC/VIF1 and 2 exhibit distinct target enzyme specificities and expression profiles. *FEBS Lett.* 573, 105–109. doi: 10.1016/j.febslet.2004.07.062

Lionetti, V. (2015). PECTOPLATE: the simultaneous phenotyping of pectin methylesterases, pectinases, and oligogalacturonides in plants during biotic stresses. *Front. Plant Sci.* 6:331. doi: 10.3389/fpls.2015.00331

Lionetti, V., Cervone, F., and Bellincampi, D. (2012). Methyl esterification of pectin plays a role during plant-pathogen interactions and affects plant resistance to diseases. *J. Plant Physiol.* 169, 1623–1630. doi: 10.1016/j.jplph.2012.05.006

Lionetti, V., Cervone, F., and De Lorenzo, G. (2014a). A lower content of de-methylesterified homogalacturonan improves enzymatic cell separation and isolation of mesophyll protoplasts in *Arabidopsis*. *Phytochemistry* 112, 188–194. doi: 10.1016/j.phytochem.2014.07.025

Lionetti, V., Fabri, E., De Caroli, M., Hansen, A. R., Willats, W. G., Piro, G., et al. (2017). Three pectin methyl esterase inhibitors protect cell wall integrity for immunity to Botrytis. *Plant Physiol.* 173, 1844–1863. doi: 10.1104/pp.16.01185

Lionetti, V., Francocci, F., Ferrari, S., Volpi, C., Bellincampi, D., Galletti, R., et al. (2010). Engineering the cell wall by reducing de-methyl-esterified homogalacturonan improves saccharification of plant tissues for bioconversion. *Proc. Natl. Acad. Sci. U. S. A.* 107, 616–621. doi: 10.1073/pnas.0907549107

Lionetti, V., Raiola, A., Camardella, L., Giovane, A., Obel, N., Pauly, M., et al. (2007). Overexpression of pectin methylesterase inhibitors in *Arabidopsis* restricts fungal infection by *Botrytis cinerea*. *Plant Physiol.* 143, 1871–1880. doi: 10.1104/pp.106.090803

Lionetti, V., Raiola, A., Cervone, F., and Bellincampi, D. (2014b). Transgenic expression of pectin methylesterase inhibitors limits tobamovirus spread in tobacco and *Arabidopsis*. *Mol. Plant Pathol.* 15, 265–274. doi: 10.1111/mpp.12090

Lionetti, V., Raiola, A., Cervone, F., and Bellincampi, D. (2015a). How do pectin methylesterases and their inhibitors affect the spreading of tobamovirus? *Plant Signal. Behav.* 9:e972863. doi: 10.4161/15592316.2014.972863

Lionetti, V., Raiola, A., Mattei, B., and Bellincampi, D. (2015b). The grapevine VvPMEI1 gene encodes a novel functional pectin Methylesterase inhibitor associated to grape berry development. *PLoS One* 10:e0133810. doi: 10.1371/journal.pone.0133810

Liu, X., Lin, Y., Liu, J., Song, B., Ou, Y., Zhang, H., et al. (2013). StInvInh2 as an inhibitor of StvacINV1 regulates the cold-induced sweetening of potato tubers by specifically capping vacuolar invertase activity. *Plant Biotechnol. J.* 11, 640–647. doi: 10.1111/pbi.12054

Liu, X., Song, B., Zhang, H., Li, X.-Q., Xie, C., and Liu, J. (2010). Cloning and molecular characterization of putative invertase inhibitor genes and their possible contributions to cold-induced sweetening of potato tubers. *Mol. Gen. Genomics.* 284, 147–159. doi: 10.1007/s00438-010-0554-3

Liu, N., Sun, Y., Pei, Y., Zhang, X., Wang, P., Li, X., et al. (2018). A pectin Methylesterase inhibitor enhances resistance to verticillium Wilt1[OPEN]. *Plant Physiol.* 176, 2202–2220. doi: 10.1104/pp.17.01399

Liu, J., Zhang, W., Long, S., and Zhao, C. (2021). Maintenance of Cell Wall integrity under high salinity. *Int. J. Mol. Sci.* 22:3260. doi: 10.3390/ijms22063260

Mckenzie, M. J., Chen, R. K. Y., Harris, J. C., Ashworth, M. J., and Brummell, D. A. (2013). Post-translational regulation of acid invertase activity by vacuolar invertase inhibitor affects resistance to cold-induced sweetening of potato tubers. *Plant Cell Environ.* 36, 176–185. doi: 10.1111/j.1365-3040.2012.02565.x

Micheli, F. (2001). Pectin methylesterases: cell wall enzymes with important roles in plant physiology. *Trends Plant Sci.* 6, 414–419. doi: 10.1016/S1360-1385(01)02045-3

Micheli, F., Holliger, C., Goldberg, R., and Richard, L. (1998). Characterization of the pectin methylesterase-like gene AtPME3: a new member of a gene family comprising at least 12 genes in *Arabidopsis thaliana*. *Gene* 220, 13–20. doi: 10.1016/S0378-1119(98)00431-4

Muller, K., Levesque-Tremblay, G., Bartels, S., Weitbrecht, K., Wormit, A., Usadel, B., et al. (2013). Demethylesterification of cell wall pectins in *Arabidopsis* plays a role in seed germination. *Plant Physiol.* 161, 305–316. doi: 10.1104/pp.112.205724

Müller, K., Levesque-Tremblay, G., Fernandes, A., Wormit, A., Bartels, S., Usadel, B., et al. (2013). Overexpression of a pectin methylesterase inhibitor in *Arabidopsis thaliana* leads to altered growth morphology of the stem and defective organ separation. *Plant Signal. Behav.* 8:e26464. doi: 10.4161/psb.26464

Ni, D. A. (2012). Role of vacuolar invertase in regulating *Arabidopsis* stomatal opening. *Acta Physiol. Plant.* 34, 2449–2452. doi: 10.1007/s11738-012-1036-5

Oh, D.-H., Dassanayake, M., Bohnert, H. J., and Cheeseman, J. M. (2012). Life at the extreme: lessons from the genome. *Genome Biol.* 13:241. doi: 10.1186/gb4003

Osorio, S., Bombarely, A., Giavalisco, P., Usadel, B., Stephens, C., Araguez, I., et al. (2011). Demethylation of oligogalacturonides by FaPE1 in the fruits of the wild strawberry *Fragaria vesca* triggers metabolic and transcriptional changes associated with defence and development of the fruit. *J. Exp. Bot.* 62, 2855–2873. doi: 10.1093/jxb/erq465

Osorio, S., Castillejo, C., Quesada, M. A., Medina-Escobar, N., Brownsey, G. J., Suau, R., et al. (2008). Partial demethylation of oligogalacturonides by pectin methyl esterase 1 is required for eliciting defence responses in wild strawberry (*Fragaria vesca*). *Plant J.* 54, 43–55. doi: 10.1111/j.1365-313X.2007.03398.x

Pagnussat, G. C., Yu, H.-J., Ngo, Q. A., Rajani, S., Mayalagu, S., Johnson, C. S., et al. (2005). Genetic and molecular identification of genes required for female gametophyte development and function in *Arabidopsis*. *Development* 132, 603–614. doi: 10.1242/dev.01595

Park, S.-W., Vepachedu, R., Sharma, N., and Vivanco, J. M. (2004). Ribosome-inactivating proteins in plant biology. *Planta* 219, 1093–1096. doi: 10.1007/s00425-004-1357-8

Parre, E., and Geitmann, A. (2005). Pectin and the role of the physical properties of the cell wall in pollen tube growth of *Solanum chacoense*. *Planta* 220, 582–592. doi: 10.1007/s00425-004-1368-5

Peaucelle, A., Braybrook, S. A., Le Guillou, L., Bron, E., Kuhlemeier, C., and Höfte, H. (2011a). Pectin-induced changes in cell wall mechanics underlie organ initiation in *Arabidopsis*. *Curr. Biol.* 21, 1720–1726. doi: 10.1016/j.cub.2011.08.057

Peaucelle, A., Louvet, R., Johansen, J. N., Höfte, H., Laufs, P., Pelloux, J., et al. (2008). Arabidopsis phyllotaxis is controlled by the methyl-esterification status of cell-wall pectins. *Curr. Biol.* 18, 1943–1948. doi: 10.1016/j.cub.2008.10.065

Peaucelle, A., Louvet, R., Johansen, J. N., Salsac, F., Morin, H., Fournet, F., et al. (2011b). The transcription factor BELLRINGER modulates phyllotaxis by regulating the expression of a pectin methylesterase in *Arabidopsis*. *Development* 138, 4733–4741. doi: 10.1242/dev.072496

Pelletier, S., Van Orden, J., Wolf, S., Vissenberg, K., Delacourt, J., Ndong, Y. A., et al. (2010). A role for pectin de-methylesterification in a developmentally regulated growth acceleration in dark-grown *Arabidopsis* hypocotyls. *New Phytol.* 188, 726–739. doi: 10.1111/j.1469-8137.2010.03409.x

Pelloux, J., Rustérucci, C., and Mellerowicz, E. J. (2007). New insights into pectin methylesterase structure and function. *Trends Plant Sci.* 12, 267–277. doi: 10.1016/j.tplants.2007.04.001

Pérez-Pérez, Y., Carneros, E., Berenguer, E., Solís, M.-T., Bárány, I., Pintos, B., et al. (2019). Pectin de-methylesterification and AGP increase promote Cell Wall Remodeling and are required During somatic embryogenesis of *Quercus suber*. *Front. Plant Sci.* 9:1915. doi: 10.3389/fpls.2018.01915

Pilling, J., Willmitzer, L., Bücking, H., and Fisahn, J. (2004). Inhibition of a ubiquitously expressed pectin methyl esterase in *Solanum tuberosum* L. affects plant growth, leaf growth polarity, and ion partitioning. *Planta* 219, 32–40. doi: 10.1007/s00425-004-1204-y

Pontiggia, D., Benedetti, M., Costantini, S., De Lorenzo, G., and Cervone, F. (2020). Dampening the DAMPs: how plants maintain the homeostasis of cell wall molecular patterns and avoid hyper-immunity. *Front. Plant Sci.* 11:2010. doi: 10.3389/fpls.2020.613259

Pressey, R. (1966). Separation and properties of potato invertase and invertase inhibitor. *Arch. Biochem. Biophys.* 113, 667–674. doi: 10.1016/0003-9861(66)90246-3

Qin, G., Zhu, Z., Wang, W., Cai, J., Chen, Y., Li, L., et al. (2016). A tomato vacuolar invertase inhibitor mediates sucrose metabolism and influences fruit ripening. *Plant Physiol.* 172, 1596–1611. doi: 10.1104/pp.16.01269

Qu, T., Liu, R. F., Wang, W., An, L. Z., Chen, T., Liu, G. X., et al. (2011). Brassinosteroids regulate pectin methylesterase activity and AtPME41 expression in *Arabidopsis* under chilling stress. *Cryobiology* 63, 111–117. doi: 10.1016/j.cryobiol.2011.07.003

Raiola, A., Camardella, L., Giovane, A., Mattei, B., De Lorenzo, G., Cervone, F., et al. (2004). Two *Arabidopsis thaliana* genes encode functional pectin methylesterase inhibitors11The industrial utilization of *Arabidopsis* and kiwi PMEIs is patent pending it, no. RM2003A000346. *FEBS Lett.* 557, 199–203. doi: 10.1016/S0014-5793(03)01491-1

Raiola, A., Lionetti, V., Elmaghraby, I., Immerzeel, P., Mellerowicz, E. J., Salvi, G., et al. (2011). Pectin methylesterase is induced in Arabidopsis upon infection and is necessary for a successful colonization by necrotrophic pathogens. *Mol. Plant-Microbe Interact.* 24, 432–440. doi: 10.1094/MPMI-07-10-0157

Rausch, T., and Greiner, S. (2004). Plant protein inhibitors of invertases. *Biochim. Biophys. Acta* 1696, 253–261. doi: 10.1016/j.bbapap.2003.09.017

Rautengarten, C., Usadel, B., Neumetzler, L., Hartmann, J., Bussis, D., and Altmann, T. (2008). A subtilisin-like serine protease essential for mucilage release from *Arabidopsis* seed coats. *Plant J.* 54, 466–480. doi: 10.1111/j.1365-313X.2008.03437.x

Reca, I. B., Brutus, A., D'Avino, R., Villard, C., Bellincampi, D., and Giardina, T. (2008). Molecular cloning, expression and characterization of a novel apoplastic invertase inhibitor from tomato (*Solanum lycopersicum*) and its use to purify a vacuolar invertase. *Biochimie* 90, 1611–1623. doi: 10.1016/j.biochi.2008.04.019

Reca, I. B., Lionetti, V., Camardella, L., D'Avino, R., Giardina, T., Cervone, F., et al. (2012). A functional pectin methylesterase inhibitor protein (SolyPMEI) is expressed during tomato fruit ripening and interacts with PME-1. *Plant Mol. Biol.* 79, 429–442. doi: 10.1007/s11103-012-9921-2

Rigano, M. M., Lionetti, V., Raiola, A., Bellincampi, D., and Barone, A. (2018). Pectic enzymes as potential enhancers of ascorbic acid production through the D-galacturonate pathway in Solanaceae. *Plant Sci.* 266, 55–63. doi: 10.1016/j.plantsci.2017.10.013

Rocchi, V., Janni, M., Bellincampi, D., Giardina, T., and D'Ovidio, R. (2011). Intron retention regulates the expression of pectin methylesterase inhibitor (Pmei) genes during wheat growth and development. *Plant Biol.* 14, 365–373. doi: 10.1111/j.1438-8677.2011.00508.x

Röckel, N., Wolf, S., Kost, B., Rausch, T., and Greiner, S. (2008). Elaborate spatial patterning of cell-wall PME and PMEI at the pollen tube tip involves PMEI endocytosis, and reflects the distribution of esterified and de-esterified pectins. *Plant J.* 53, 133–143. doi: 10.1111/j.1365-313X.2007.03325.x

Roitsch, T., and González, M.-C. (2004). Function and regulation of plant invertases: sweet sensations. *Trends Plant Sci.* 9, 606–613. doi: 10.1016/j.tplants.2004.10.009

Ruan, Y.-L., Jin, Y., Yang, Y.-J., Li, G.-J., and Boyer, J. S. (2010). Sugar input, metabolism, and signaling mediated by invertase: roles in development, yield potential, and response to drought and heat. *Mol. Plant* 3, 942–955. doi: 10.1093/mp/ssq044

Saez-Aguayo, S., Ralet, M.-C., Berger, A., Botran, L., Ropartz, D., Marion-Poll, A., et al. (2013). PECTIN METHYLESTERASE INHIBITOR6 promotes *Arabidopsis* mucilage release by limiting methylesterification of homogalacturonan in seed coat epidermal cells. *Plant Cell* 25, 308–323. doi: 10.1105/tpc.112.106575

Schaller, A., Stintzi, A., Rivas, S., Serrano, I., Chichkova, N. V., Vartapetian, A. B., et al. (2018). From structure to function - a family portrait of plant subtilases. *New Phytol.* 218, 901–915. doi: 10.1111/nph.14582

Schwimmer, S., Makower, R. U., and Rorem, E. S. (1961). Invertase & invertase inhibitor in potato. *Plant Physiol.* 36, 313–316. doi: 10.1104/pp.36.3.313

Senechal, F., Graff, L., Surcouf, O., Marcelo, P., Rayon, C., Bouton, S., et al. (2014). *Arabidopsis* PECTIN METHYLESTERASE17 is co-expressed with and processed by SBT3.5, a subtilisin-like serine protease. *Ann. Bot.* 114, 1161–1175. doi: 10.1093/aob/mcu035

Sénéchal, F., Habrylo, O., Hocq, L., Domon, J.-M., Marcelo, P., Lefebvre, V., et al. (2017). Structural and dynamical characterization of the pH-dependence of the pectin methylesterase–pectin methylesterase inhibitor complex. *J. Biol. Chem.* 292, 21538–21547. doi: 10.1074/jbc.RA117.000197

Sénéchal, F., L'Enfant, M., Domon, J.-M., Rosiau, E., Crépeau, M.-J., Surcouf, O., et al. (2015). Tuning of pectin methylesterification: pectin methylesterase inhibitor 7 modulates the processive activity of co-expressed pectin methylesterase 3 in a pH-dependent manner. *J. Biol. Chem.* 290, 23320–23335. doi: 10.1074/jbc.M115.639534

Senechal, F., Mareck, A., Marcelo, P., Lerouge, P., and Pelloux, J. (2015). Arabidopsis PME17 activity can be controlled by pectin methylesterase inhibitor4. *Plant Signal. Behav.* 10:e983351. doi: 10.4161/15592324.2014.983351

Shi, D., Ren, A., Tang, X., Qi, G., Xu, Z., Chai, G., et al. (2018). MYB52 negatively regulates pectin Demethylesterification in seed coat mucilage. *Plant Physiol.* 176, 2737–2749. doi: 10.1104/pp.17.01771

Shin, Y., Chane, A., Jung, M., and Lee, Y. (2021). Recent advances in understanding the roles of pectin as an active participant in plant Signaling networks. *Plants* 10:1712. doi: 10.3390/plants10081712

Siemens, J., González, M.-C., Wolf, S., Hofmann, C., Greiner, S., Du, Y., et al. (2011). Extracellular invertase is involved in the regulation of clubroot disease in *Arabidopsis thaliana*. *Mol. Plant Pathol.* 12, 247–262. doi: 10.1111/j.1364-3703.2010.00667.x

Silva-Sanzana, C., Celiz-Balboa, J., Garzo, E., Marcus, S. E., Parra-Rojas, J. P., Rojas, B., et al. (2019). Pectin methylesterases modulate plant homogalacturonan status in defenses against the aphid *Myzus persicae*. *Plant Cell* 31, 1913–1929. doi: 10.1105/tpc.19.00136

Solecka, D., Żebrowski, J., and Kacperska, A. (2008). Are pectins involved in cold acclimation and de-acclimation of winter oil-seed rape plants? *Ann. Bot.* 101, 521–530. doi: 10.1093/aob/mcm329

Somerville, C., Bauer, S., Brininstool, G., Facette, M., Hamann, T., Milne, J., et al. (2004). Toward a systems approach to understanding plant cell walls. *Science* 306, 2206–2211. doi: 10.1126/science.1102765

Sorek, N., Szemenyei, H., Sorek, H., Landers, A., Knight, H., Bauer, S., et al. (2015). Identification of MEDIATOR16 as the Arabidopsis COBRA suppressor MONGOOSE1. *Proc. Natl. Acad. Sci. U. S. A.* 112, 16048–16053. doi: 10.1073/pnas.1521675112

Sørensen, J. F., Kragh, K. M., Sibbesen, O., Delcour, J., Goesaert, H., Svensson, B., et al. (2004). Potential role of glycosidase inhibitors in industrial biotechnological applications. *Biochim. Biophys. Acta Proteins Proteom.* 1696, 275–287. doi: 10.1016/j.bbapap.2003.09.016

Srivastava, S., Gupta, S. M., Sane, A. P., and Nath, P. (2012). Isolation and characterization of ripening related pectin methylesterase inhibitor gene from banana fruit. *Physiol. Mol. Biol. Plants* 18, 191–195. doi: 10.1007/s12298-012-0102-1

Stefanowicz, K., Szymanska-Chargot, M., Truman, W., Walerowski, P., Olszak, M., Augustyniak, A., et al. (2021). *Plasmodiophora brassicae*-triggered cell enlargement and loss of cellular integrity in root systems are mediated by pectin demethylation. *Front. Plant Sci.* 12:1569. doi: 10.3389/fpls.2021.711838

Su, T., Han, M., Min, J., Zhou, H., Zhang, Q., Zhao, J., et al. (2020). Functional characterization of invertase inhibitors PtC/VIF1 and 2 revealed their involvements in the defense response to fungal pathogen in *Populus trichocarpa*. *Front. Plant Sci.* 10:1654. doi: 10.3389/fpls.2019.01654

Su, T., Wolf, S., Han, M., Zhao, H., Wei, H., Greiner, S., et al. (2016). Reassessment of an *Arabidopsis* cell wall invertase inhibitor AtCIF1 reveals its role in seed germination and early seedling growth. *Plant Mol. Biol.* 90, 137–155. doi: 10.1007/s11103-015-0402-2

Takahashi, D., Gorka, M., Erban, A., Graf, A., Kopka, J., Zuther, E., et al. (2019). Both cold and sub-zero acclimation induce cell wall modification and changes in the extracellular proteome in *Arabidopsis thaliana*. *Sci. Rep.* 9:2289. doi: 10.1038/s41598-019-38688-3

Tang, X., Su, T., Han, M., Wei, L., Wang, W., Yu, Z., et al. (2017). Suppression of extracellular invertase inhibitor gene expression improves seed weight in soybean (*Glycine max*). *J. Exp. Bot.* 68, 469–482. doi: 10.1093/jxb/erw425

Tauzin, A. S., and Giardina, T. (2014). Sucrose and invertases, a part of the plant defense response to the biotic stresses. *Front. Plant Sci.* 5:293. doi: 10.3389/fpls.2014.00293

Thakur, B. R., Singh, R. K., Tieman, D. M., and Handa, A. K. (1996). Tomato product quality from transgenic fruits with reduced pectin methylesterase. *J. Food Sci.* 61, 85–87. doi: 10.1111/j.1365-2621.1996.tb14731.x

Tian, G.-W., Chen, M.-H., Zaltsman, A., and Citovsky, V. (2006). Pollen-specific pectin methylesterase involved in pollen tube growth. *Dev. Biol.* 294, 83–91. doi: 10.1016/j.ydbio.2006.02.026

Tieman, D. M., and Handa, A. K. (1994). Reduction in pectin Methylesterase activity modifies tissue integrity and cation levels in ripening tomato (*Lycopersicon esculentum* Mill.) fruits. *Plant Physiol.* 106, 429–436. doi: 10.1104/pp.106.2.429

Tieman, D. M., Harriman, R. W., Ramamohan, G., and Handa, A. K. (1992). An antisense pectin methylesterase gene alters pectin chemistry and soluble solids in tomato fruit. *Plant Cell* 4, 667–679. doi: 10.2307/3869525

Turbant, A., Fournet, F., Lequart, M., Zabijak, L., Pageau, K., Bouton, S., et al. (2016). PME58 plays a role in pectin distribution during seed coat mucilage extrusion through homogalacturonan modification. *J. Exp. Bot.* 67, 2177–2190. doi: 10.1093/jxb/erw025

Volpi, C., Janni, M., Lionetti, V., Bellincampi, D., Favaron, F., and D'Ovidio, R. (2011). The ectopic expression of a pectin methyl esterase inhibitor increases pectin methyl esterification and limits fungal diseases in wheat. *Mol. Plant-Microbe Interact.* 24, 1012–1019. doi: 10.1094/MPMI-01-11-0021

Wachsman, G., Zhang, J., Moreno-Risueno, M. A., Anderson, C. T., and Benfey, P. N. (2020). Cell wall remodeling and vesicle trafficking mediate the root clock in *Arabidopsis*. *Science* 370, 819–823. doi: 10.1126/science.abb7250

Wang, L., and Ruan, Y.-L. (2012). New insights into roles of cell wall invertase in early seed development revealed by comprehensive spatial and temporal expression patterns of *GhCWIN1* in cotton. *Plant Physiol.* 160, 777–787. doi: 10.1104/pp.112.203893

Wang, D., Yeats, T. H., Uluisik, S., Rose, J. K. C., and Seymour, G. B. (2018). Fruit softening: revisiting the role of pectin. *Trends Plant Sci.* 23, 302–310. doi: 10.1016/j.tplants.2018.01.006

Wang, M., Yuan, D. J., Gao, W. H., Li, Y., Tan, J. F., and Zhang, X. L. (2013). A comparative genome analysis of PME and PMEI families reveals the evolution of pectin metabolism in plant cell walls. *PLoS One* 8:e72082. doi: 10.1371/journal.pone.0085650

Weber, M., Deinlein, U., Fischer, S., Rogowski, M., Geimer, S., Tenhaken, R., et al. (2013). A mutation in the *Arabidopsis thaliana* cell wall biosynthesis gene pectin methylesterase 3 as well as its aberrant expression cause hypersensitivity specifically to Zn. *Plant J.* 76, 151–164. doi: 10.1111/tpj.12279

Willats, W. G., Orfila, C., Limberg, G., Buchholt, H. C., van Alebeek, G. J., Voragen, A. G., et al. (2001). Modulation of the degree and pattern of methyl esterification of pectic homogalacturonan in plant cell walls: implications for pectin methyl esterase action, matrix properties and cell adhesion. *J. Biol. Chem.* 276, 19404–19413. doi: 10.1074/jbc.M011242200

Wolf, S., Grsic-Rausch, S., Rausch, T., and Greiner, S. (2003). Identification of pollen-expressed pectin methylesterase inhibitors in *Arabidopsis*. *FEBS Lett.* 555, 551–555. doi: 10.1016/S0014-5793(03)01344-9

Wolf, S., Mravec, J., Greiner, S., Mouille, G., and Hofte, H. (2012). Plant cell wall homeostasis is mediated by Brassinosteroid feedback signaling. *Curr. Biol.* 22, 1732–1737. doi: 10.1016/j.cub.2012.07.036

Wolf, S., Rausch, T., and Greiner, S. (2009). The N-terminal pro region mediates retention of unprocessed type-I PME in the Golgi apparatus. *Plant J.* 58, 361–375. doi: 10.1111/j.1365-313X.2009.03784.x

Won, S.-K., Lee, Y.-J., Lee, H.-Y., Heo, Y.-K., Cho, M., and Cho, H.-T. (2009). cis-Element- and transcriptome-based screening of root hair-specific genes and their functional characterization in *Arabidopsis*. *Plant Physiol.* 150, 1459–1473. doi: 10.1104/pp.109.140905

Wu, H.-C., Bulgakov, V. P., and Jinn, T.-L. (2018). Pectin methylesterases: cell wall remodeling proteins are required for plant response to heat stress. *Front. Plant Sci.* 9:1612. doi: 10.3389/fpls.2018.01612

Wu, H.-C., Huang, Y.-C., Stracovsky, L., and Jinn, T.-L. (2017). Pectin methylesterase is required for guard cell function in response to heat. *Plant Signal. Behav.* 12:e1338227. doi: 10.1080/15592324.2017.1338227

Xu, C., Cao, H., Xu, E., Zhang, S., and Hu, Y. (2018). Genome-wide identification of *Arabidopsis* LBD29 target genes reveals the molecular events behind auxin-induced cell reprogramming during callus formation. *Plant Cell Physiol.* 59, 749–760. doi: 10.1093/pcp/pcx168

Xu, X., Hu, Q., Yang, W., and Jin, Y. (2017). The roles of cell wall invertase inhibitor in regulating chilling tolerance in tomato. *BMC Plant Biol.* 17:195. doi: 10.1186/s12870-017-1145-9

Yan, J., He, H., Fang, L., and Zhang, A. (2018). Pectin methylesterase31 positively regulates salt stress tolerance in *Arabidopsis*. *Biochem. Biophys. Res. Commun.* 496, 497–501. doi: 10.1016/j.bbrc.2018.01.025

Yang, Z. (2008). Cell polarity Signaling in *Arabidopsis*. *Annu. Rev. Cell Dev. Biol.* 24, 551–575. doi: 10.1146/annurev.cellbio.23.090506.123233

Yang, W., Chen, S., Cheng, Y., Zhang, N., Ma, Y., Wang, W., et al. (2020). Cell wall/vacuolar inhibitor of fructosidase 1 regulates ABA response and salt tolerance in *Arabidopsis*. *Plant Signal. Behav.* 15:1744293. doi: 10.1080/15592324.2020.1744293

Zanor, M. I., Osorio, S., Nunes-Nesi, A., Carrari, F., Lohse, M., Usadel, B., et al. (2009). RNA interference of LIN5 in tomato confirms its role in controlling brix content, uncovers the influence of sugars on the levels of fruit hormones, and demonstrates the importance of sucrose cleavage for Normal fruit development and fertility. *Plant Physiol.* 150, 1204–1218. doi: 10.1104/pp.109.136598

Zehra, A., Raytekar, N. A., Meena, M., and Swapnil, P. (2021). Efficiency of microbial bio-agents as elicitors in plant defense mechanism under biotic stress: a review. *Curr. Res. Microb. Sci.* 2:100054. doi: 10.1016/j.crmicr.2021.100054

Zhang, G. Y., Feng, J., Wu, J., and Wang, X. W. (2010). BoPMEI1, a pollen-specific pectin methylesterase inhibitor, has an essential role in pollen tube growth. *Planta* 231, 1323–1334. doi: 10.1007/s00425-010-1136-7

Zocca, F., Lomolino, G., Spettoli, P., and Lante, A. (2008). A study on the relationship between the volatile composition of moscato and prosecco grappa and enzymatic activities involved in its production. *J. Federat. Inst. Brew.* 114, 262–269. doi: 10.1002/j.2050-0416.2008.tb00337.x

Zuma, B., Dana, M. B., and Wang, D. (2018). Prolonged expression of a putative invertase inhibitor in micropylar endosperm suppressed embryo growth in Arabidopsis. *Front. Plant Sci.* 9:61. doi: 10.3389/fpls.2018.00061

Conflict of Interest: The authors declare that the research was conducted in the absence of any commercial or financial relationships that could be construed as a potential conflict of interest.

Publisher's Note: All claims expressed in this article are solely those of the authors and do not necessarily represent those of their affiliated organizations, or those of the publisher, the editors and the reviewers. Any product that may be evaluated in this article, or claim that may be made by its manufacturer, is not guaranteed or endorsed by the publisher.

frontiers | Frontiers in Plant Science

ORIGINAL RESEARCH
published: 15 April 2022
doi: 10.3389/fpls.2022.817185

Water Stress Differentially Modulates the Expression of Tomato Cell Wall Metabolism-Related Genes in *Meloidogyne incognita* Feeding Sites

Pasqua Veronico†, Laura Cristina Rosso†, Maria Teresa Melillo, Elena Fanelli, Francesca De Luca, Aurelio Ciancio, Mariantonietta Colagiero and Isabella Pentimone*

Istituto per la Protezione Sostenibile delle Piante, Consiglio Nazionale delle Ricerche, Bari, Italy

OPEN ACCESS

Edited by:
Shahid Siddique, University of California, Davis, United States

Reviewed by:
Eric Nguema-Ona, Centre Mondial de l'Innovation Roullier, France
Krzysztof Wieczorek, University of Natural Resources and Life Sciences Vienna, Austria

***Correspondence:**
Laura Cristina Rosso
laura.rosso@ipsp.cnr.it

† These authors have contributed equally to this work and share first authorship

Specialty section:
This article was submitted to Plant Pathogen Interactions, a section of the journal Frontiers in Plant Science

Received: *17 November 2021*
Accepted: *02 March 2022*
Published: *15 April 2022*

Citation:
Veronico P, Rosso LC, Melillo MT, Fanelli E, De Luca F, Ciancio A, Colagiero M and Pentimone I (2022) Water Stress Differentially Modulates the Expression of Tomato Cell Wall Metabolism-Related Genes in Meloidogyne incognita Feeding Sites. Front. Plant Sci. 13:817185. doi: 10.3389/fpls.2022.817185

Microscopic observations and transcriptomic RNA-Seq analyses were applied to investigate the effect of water stress during the formation of tomato galls formation 1 and 2 weeks after inoculation with the root-knot nematode *Meloidogyne incognita*. Water stress affected root growth and the nematode ability to mount an efficient parasitism. The effects of water stress on the feeding site development were already observed at 1 week after nematode inoculation, with smaller giant cells, delayed development, and thinner cell walls. These features suggested changes in the expression levels of genes involved in the feeding site formation and maintenance. Gene Ontology (GO) enrichment and expression patterns were used to characterize differentially expressed genes. Water stress modified the expression profile of genes involved in the synthesis, degradation, and remodeling of the cell wall during the development of nematode feeding site. A comparison of gene expression with unstressed galls revealed that water stress intensified the up or downregulation of most genes. However, it particularly influenced the expression pattern of *expansin A11* (Solyc04g081870.4.1), *expansin-like B1*(Solyc08g077910.3.1), a *pectin acetylesterase* (Solyc08g005800.4.1), and the *pectin methylesterase pmeu1* (Solyc03g123630.4.1) which were upregulated in unstressed galls and repressed by water stress, at both sampling times. The expression of most members of the genes involved in cell wall metabolism, i.e., those coding for Csl, fasciclin, and COBRA proteins, were negatively influenced. Interestingly, alteration in the expression profiles of most dirigent protein genes (DIRs) and upregulation of five gene coding for Casparian strip domain protein (CASP)-like proteins were found. Gene expression analysis of galls from water stressed plants allowed us to better understand the molecular basis of *M. incognita* parasitism in tomato. Specific genes, including those involved in regulation of cellulose synthesis and lignification process, require further study to develop defense strategies against root-knot nematodes.

Keywords: water stress, *Meloidogyne incognita*, tomato, feeding site, cell wall, transcriptome

INTRODUCTION

Plants are continuously exposed to a broad range of environmental stresses during their entire life cycle. Stresses include both abiotic factors, such as drought, salinity, heat, or cold, and biotic factors, such as bacteria, viruses, fungi, or nematodes. Both types of stress can have a devastating impact on plant growth and yield under field conditions (Suzuki et al., 2014). Plants developed a complex morphological and molecular response system to prevent and/or tolerate stress damages and survive (Lamers et al., 2020). Most efficient mechanisms involve the recognition of stress-related features (either chemical or physical) by dedicated receptors and the transduction and the propagation of the signal by downstream players, resulting in cellular responses characterized by an alteration of the expression of a variety of genes. The response of plants to simultaneous biotic and abiotic stresses is distinct for individual stresses, and not merely additive (Atkinson and Urwin, 2012; Ramegowda and Senthyl-Kumar, 2015). For example, the combination of water deficit and plant-parasitic nematodes is a realistic threat under field conditions and could drastically impact crop productivity. Drought stress itself generates physiological changes in higher plants, including loss of turgor, osmotic adjustment, and reduced leaf water potential (Le Gall et al., 2015). These changes are associated with increases in endogenous abscisic acid (ABA), which plays a role in regulating drought stress responses in plants (Schachtman and Goodger, 2008; Cutler et al., 2010). On the other hand, nematode infection can exacerbate or counteract the effects of water stress on plants, as root parasitism greatly influences the plant-water relations (Atkinson et al., 2013).

Root-knot nematodes *Meloidogyne* spp. have an intimate relationship with their hosts as they derive nutrients directly from living root cells. Therefore, factors that alter plant growth, such as water shortage, may also alter the root-nematode interaction.

Motile second stage juveniles (J2) of root-knot nematodes penetrate roots in a region behind tips, along the elongation zone. By migrating intercellularly, they reach the differentiating vascular cylinder. Here, the invading nematodes select some parenchyma cells where they induce and maintain, with their secretions, a specialized feeding site (FS). Selected root cells then differentiate into hypertrophied, multinucleate, and metabolically active giant cells (GCs) (Gheysen and Mitchum, 2011). GCs serve as an exclusive food source for the nematode to develop into a reproductive female. Symptoms of root infection include proliferation of the cells surrounding GCs, consequent vascular alterations, hypertrophy of endodermis, and cortex that ultimately generate swollen roots tissues known as galls (Gheysen and Mitchum, 2011). At the cellular level, the changes that occur during the formation of the nematode FS are complex and include hormonal metabolism adjustment, transcription factors modulation, cytoskeleton rearrangement, and modifications of the cell wall metabolism (Shukla et al., 2018). Cell wall metabolism includes cell wall biogenesis and cell wall remodeling. In nematode FS, the cell wall undergoes complex modifications involving a reorganization of the wall extension and various synthesis and degradation-related processes (Sobczak et al., 2011).

The cell wall plays a fundamental role in plant defense as it provides structural support during development and represents the first line of defense against pathogens, parasites, and abiotic stressors including drought (Underwood, 2012; Ricardi et al., 2014).

Information provided by different omics data analyses and functional characterization of individual genes in response to drought showed a modulation of several genes involved in cell wall metabolism. Modulation of cellulose synthesis in Arabidopsis (Chen et al., 2005) and the overexpression of expansin genes in several plant species (Guo et al., 2011; Xu et al., 2014; Liu et al., 2019) lead to improved drought tolerance and higher survival rates. Similar findings were found with other genes, i.e., *pectin methylesterase* (Wormit and Usadel, 2018) or *xyloglucan endotransglucosylase/hydrolase* (XTH), in transgenic Arabidopsis and tomato, respectively (Cho et al., 2006; Choi et al., 2011).

Tomato (*Solanum lycopersicon*) represents an excellent model to study the host–nematode interactions due to the availability of routinely well-annotated genome reference. Moreover, despite its large-scale cultivation and industrial value, it is still sensitive to severe stresses of abiotic and biotic nature (Kissoudis et al., 2016). In the present study, we evaluated how water stress impacts *Meloidogyne incognita* parasitism in tomato. This knowledge could be highly informative in plant protection due to the importance of root-knot nematodes as pests and to the effects of climate change that is expected to alter precipitation regimes toward more frequent and severe drought events. To date, few studies have been carried out on transcriptome analyses under combined abiotic and biotic stresses. By using microscopic observation of GCs and in depth transcriptomic (RNA-Seq) analyses, we show here that water stress affects the ability of nematodes to mount an efficient parasitism by limiting the FS development and nematode reproduction. Additionally, we describe differentially expressed genes (DEGs) responsive to combined stresses and genes mainly involved in cell wall modifications during GC development in galls of normally watered and water-stressed plants.

MATERIALS AND METHODS

Plants, Growth Conditions, and Water Stress Treatment

Seeds of tomato (*Solanum lycopersicum* cv. 'San Marzano nano') were kept for germination in quartz sand in a growth chamber at 25°C and then transplanted to 10 ml pots containing soil-sand mixture (3:1). The seedlings were grown in a growth chamber under controlled conditions at 25°C, with a light intensity of 150 $\mu mol/m^2/s$ and a 16 h:8 h light/dark cycle and watered with Long Ashton solution containing 300 μM phosphate. After 20 days, 40 plants were transferred in plastic pots filled with 800 g of sandy soil and watered with filtered tap water (twice a week) and Long Ashton solution (once a week). After 20 days, the plants were divided into four groups: (i) regularly watered (treatment "C," control plants), (ii) regularly irrigated and to be inoculated with *M. incognita* J2 (treatment "RKN"), (iii)

subjected to a water stress (treatment "WS"), and (iv) subjected to water stress and to be inoculated with *M. incognita* (treatment "RKN_WS"). Ten replicates for each group have been used and arranged in a randomized block design. The experiment was carried out according to Balestrini et al. (2019). Before treatments, the pots were weighed. Plants from the groups C and RKN were regularly watered throughout the entire experimental period (**Supplementary Figure 1A**), whereas those to be stressed (WS and RKN_WS) were not watered until they showed stress symptoms, i.e., leaves were folded up due to loss of turgidity, if pots weighted about 200 g less than their initial weight, and/or a loss previously described to be needed to reach a moderate water stress condition (Volpe et al., 2018). From this moment, the plants received the amounts of water or nutritive solution needed to keep their last weight in order to maintain a moderate stress level (**Supplementary Figure 1B**).

Nematode Infection Assay

A pure population of the root-knot nematode *M. incognita* race 2 was multiplied on tomato (cv. Roma) in a growth chamber. Egg masses were hand-picked from infested roots and kept for hatching in water in a growth chamber at 25°C. Freshly hatched J2 were used for inoculation.

Each plant from the RKN and RKN_WS groups was inoculated with 1,200 freshly hatched J2 according to the scheme reported in **Supplementary Figures 1A,B**. The plants were maintained in a growth chamber at 25°C. Plants from all treatments were harvested 62 and 69 days after sowing [corresponding to 7- and 14-days post-nematode inoculation (dpi) for RKN and RKN_WS treatments]. Soil was washed from roots, and the height and the fresh root and shoot weights were subsequently measured. Nematode infection was evaluated by counting the number of galls per plant with a stereomicroscope.

Morphological and Morphometric Analyses

Galls collected at 7 and 14 dpi from normally watered (RKN) and water-stressed (RKN_WS) roots were hand-dissected under a stereomicroscope and fixed in a mixture of 1.5% glutaraldehyde and 3% paraformaldehyde (Sigma-Aldrich), dehydrated in an ethanol series, and embedded in acrylic resin LR White (Sigma, St. Louis, MO, United States) (Melillo et al., 2014). Cell structures, i.e., nuclei and cell walls, were visualized by toluidine blue staining. Embedded galls were cut in serial cross sections (2.5 μm thick) through their length, then stained briefly with 1% toluidine blue in 1% borax solution and mounted in Depex. The sections of 30 galls from three different plants (ten galls per plants), both from normally watered and water-stressed roots at 7 and 14 dpi, were observed using Leica DM 4,500 B light microscope (Leica Microsystems, Milan, Italy). The FS images were recorded by a Leica DFC 450C camera. Gall diameters were measured by using the line tool provided by the ImageJ basic package[1]. The two largest GCs were selected for each FS at 7 and 14 dpi, and their area was measured with ImageJ. The average size area and standard error for a minimum of 50 GCs were also measured from the gall sections at each time point.

Cellulose distribution was visualized by Calcofluor white staining. The dye was prepared by adding 100 μl of stock solution (FLUKA, Sigma-Aldrich; Calcofluor white M2R 1 g L^{-1}, Evans blue 0.5 g L^{-1}) to 1 ml of water. Evans blue in the solution allows to quench background fluorescence. The sections (2.5 μm thick) were stained in this solution for 5 min at room temperature and protected by light, washed with water, and mounted in glycerol. Samples were observed with a Leica DM 4500 B using an A filter cube (excitation filter: 340–380 nm and detection filter LP 430 nm).

RNA Extraction, RNA-Seq Library Preparation, and Sequencing

For RNA-Seq experiments, visible galls and corresponding portions of roots from non-inoculated plants were collected. For C, RKN, WS, and RKN_WS samples, each plant was considered as a biological replicate. For each sample and collection time (7 and 14 days/dpi), two independent biological replicates were performed, except for WS and RKN_WS at 7 days/dpi where three replicates were considered due to a lower amount of developed roots. Samples were immediately stored at −80°C until further use. Root tissues (100 mg) were powdered in liquid nitrogen. Total RNA was extracted and purified using the RNeasy Plant Mini Kit (Qiagen, Milan, Italy) following the manufacturer's protocol. RNA quantity and quality was determined with a Nanodrop 2,000 spectrophotometer (Thermo Fisher Scientific Inc., Wilmington, DE, United States) and a Bioanalyzer 2,100 (Agilent Technologies, Santa Clara, CA, United States). cDNA libraries preparation and sequencing were performed by Identity Governance and Administration (IGA) Technology Services (Udine, Italy). The libraries were sequenced on an Illumina HiScanSQ, generating single reads 75 nt in length.

RNA-Seq Data Analysis and Differential Gene Expression Quantification

Raw sequences were processed for quality check using the "RNA-seq analysis" functions included in CLC Genomics Workbench software v.10.1 (QIAGEN, Aarhus, Denmark[2]). Adapters, indexes, and genomic sequences added during the sequencing process were removed. Filtered reads from each sample were then aligned to the reference genome of *S. lycopersicum* (Genome version SL4.0 and Annotation ITAG4.0[3]) using CLC (similarity parameter = 0.8; identity parameter = 0.8; mismatch/insertion/deletion penalties = 2/3/3; multi-position matches allowed) and employed to quantify the abundance of all tomato transcripts, measured as Reads Per Kilobase Million (RPKM) (Mortazavi et al., 2008) and Transcripts Per Million (TPM) (Wagner et al., 2012). A multiple correlation test (Pearson's correlation) on RPKM values for all pairwise combinations was performed for preliminary batch comparisons of replicates and experimental conditions. Principal

[1]http://imagej.nih.gov/ij/

[2]http://www.clcbio.com

[3]https://solgenomics.net/organism/Solanum_lycopersicum/genome/

Component Analysis (PCA) was also performed to analyze the variation sources in the dataset. Differential expression analysis was performed with the CLC statistical tools, applying the Generalized Linear Model (GLM) which corrects differences in library size between the samples, over-dispersion caused by biological variability, and the effects of confounding factors. Differentially expressed genes (DEGs) were evaluated at each time points (7 and 14 dpi) comparing the RPKM expression values of every gene for each sample group against the reference group (normally watered uninoculated roots, treatment C). The gene expression level was considered significant when it displayed at least a two-fold change (Fc), with a p-value ≤ 0.05 and TPM value ≥ 5. The terms "upregulation" and "downregulation" were used to indicate transcript expression levels (Fc ≥ 2 or Fc ≤ -2, respectively) higher or lower than those observed in the reference. The DEGs were then submitted to functional analysis. Heatmaps were constructed with TPM mean values using online available tools[4] (**Supplementary Table 1**).

Functional Analysis of Tomato Differentially Expressed Genes

Enrichment analysis was performed using AgriGO ver.2.0[5] (Tian et al., 2017) in order to identify, in each DEG selected set (RKN_WS vs. C at 7 and 14 dpi), the over-represented GO categories. Through enrichment analysis, molecular functions and biological processes over-represented with a statistical significance (Fisher's Exact Test: p-value ≤ 0.05; Hochberg FDR ≤ 0.05) were considered. The *S. lycopersicum* cDNA libraries ITAG3.2 and ITAG4.0 version[6] were used as reference. The Venn/Euler diagram online tool[7] was used to show DEGs that were unique and common for each condition.

Identification of cell wall metabolism-related DEGs was carried out by comparing RKN_WS transcriptome with a local cell wall database created by consulting available *S. lycopersicum* UniProtKB[8] and SolGenomics[9] databases. Used terms were as follows: cell wall organization or biogenesis, cell wall biosynthesis, and plant cell structures.

cDNA Synthesis and Real-Time Quantitative PCR Analyses

The expression of 10 DEGs (**Supplementary Table 2**) involved in stress response and cell wall metabolism was analyzed using quantitative reverse transcription-PCR (RT-qPCR) to validate the RNA-Seq results. Plant tissue collection and RNA extraction were performed as previously described. cDNA was synthesized from 0.5 mg of DNase-treated RNA using oligo(dT) primers and a reverse transcription kit (Promega Corporation, Madison, WI, United States).

Real-time PCR assays were performed on an Aria device (Agilent Technologies Inc., Santa Clara, CA, United States) in 20-μl reaction mixtures containing 0.4 μM of each gene-specific primer, 10 μl of GoTaq qPCR Master Mix (Promega), and 1 μl (50 ng) of template cDNA. Specific qRT-PCR primers were designed on available sequences of *S. lycopersicum* SL4.0 (see Text Footnote 3) using Primer3 and an online basic local alignment search tool (BLAST)[10] (**Supplementary Table 2**). The amplification specificity was confirmed by a single peak in the dissociation curve at the end of the PCR and a single band in agarose gel electrophoresis. Gene expression was calculated using AriaMx version 1.6 software and expressed as a relative quantitation to the normalizer gene actin (BT013524).

Statistical Analyses

Data were subjected to analysis of variance (ANOVA) and significant differences among treatments were analyzed by applying a least-significant difference test ($p < 0.05$) for morphometric parameters and Turkey's pairwise test ($p < 0.05$) for RT-qPCR validation data. Values between treatments and untreated and uninfected control were compared at each time point. The number of galls per plant and the GC area measurements at 14 dpi were statistically analyzed by Student's t-test ($p < 0.01$). Statistical analyses were performed using Plot IT software version 3.20i and Past 4.03 (Hammer et al., 2001). Box plot graphics were produced with R using library *ggplot2* ver. 3.3.3 (RStudio, PBC version 4.0.5).

RESULTS

Effects of Water Stress on Tomato Growth and Pathogenesis Rating

In this study, tomato plants were firstly subjected to a moderate water stress before root-knot nematode infection. Plants from group RKN_WS (water stressed and infected) were inoculated with *M. incognita* J2, and sampling was performed at 7 and 14 dpi. Plants from group WS (water stressed) were harvested 7 and 14 days after they reached the condition of moderate water stress. Plants from groups C (normally watered and uninfected) and RKN (normally watered and infected) were regularly watered along the experimental period (**Supplementary Figures 1A,B**). The aim was to understand the water stress-related responses in roots infested by *M. incognita*. Comparisons of WS vs. C plants and RKN_WS vs. RKN plants showed that water stress significantly ($p < 0.05$) decreased tomato plant heights at both times (**Table 1**). Likewise, shoot fresh weight was significantly reduced by water stress both in WS and RKN_WS plants compared to regular watering (C and RKN) (**Table 1**). Water stress affected root growth, particularly at 14 days, when a severe weight reduction (by 73%) was observed in WS plants compared to C (**Table 1**). The effect of nematode parasitism (RKN vs. C) on fresh root weight was clearly appreciable due to the presence of galls on RKN plants (**Table 1**). Water stress affected nematode infection, causing a severe decrease in the number of galls per plant (RKN_WS vs. RKN; $p < 0.01$) both at 7 and 14 dpi (around −84%) (**Table 1**). Moreover, a significant reduction in

[4]http://www.heatmapper.ca/expression/

[5]http://bioinfo.cau.edu.cn/agriGO/

[6]https://solgenomics.net/organism/Solanum_lycopersicum/genome/

[7]http://bioinformatics.psb.ugent.be/webtools/Venn/

[8]http://geneontology.org

[9]https://solcyc.solgenomics.net/pwy-search.shtml

[10]https://www.ncbi.nlm.nih.gov/tools/primer-blast/

TABLE 1 | Effect of water stress on tomato vegetative growth and *M. incognita* infection.

Recording time	Treatments	Height (cm)	Fresh shoot weight (g)	Fresh root weight (g)	Galls/plant	Gall diam. (μ m)	GC area (μ m^2)
7 days	C	30.83 ± 0.31^b	20.95 ± 1.48^b	3.33 ± 0.47^{ab}			
	RKN	31.67 ± 0.80^b	24.49 ± 0.36^c	5.81 ± 0.27^c	209 ± 22	245 ± 9	10462 ± 903
	WS	22.67 ± 0.80^a	10.53 ± 0.57^a	2.47 ± 0.09^a			
	RKN_WS	21.25 ± 0.73^a	10.36 ± 0.35^a	3.15 ± 0.20^a	34 ± 3**	176 ± 6**	5247 ± 290**
14 days	C	32.50 ± 1.15^b	24.74 ± 2.41^b	6.52 ± 0.52^b			
	RKN	35.00 ± 2.13^b	27.21 ± 2.01^b	8.59 ± 0.63^c	276 ± 17	253 ± 14	24071 ± 1319
	WS	20.00 ± 0.73^a	5.63 ± 0.56^a	1.75 ± 0.05^a			
	RKN_WS	20.17 ± 1.01^a	5.96 ± 0.50^a	2.14 ± 0.12^a	46 ± 10**	208 ± 11*	10297 ± 658**

Data recorded 7 and 14 days after nematode infection.
*C, normally watered and uninfected; RKN, unstressed and M. incognita infected; WS, water-stressed; RKN_WS, water-stressed and M. incognita infected plants. Values are means from six replicates ± SD. Same letters represent values that are not significantly different according to Duncan's Multiple Range Test ($p < 0.05$). Asterisks *, ** indicate significant differences according to Student's t-test $p < 0.05$ or < 0.01 respectively.*

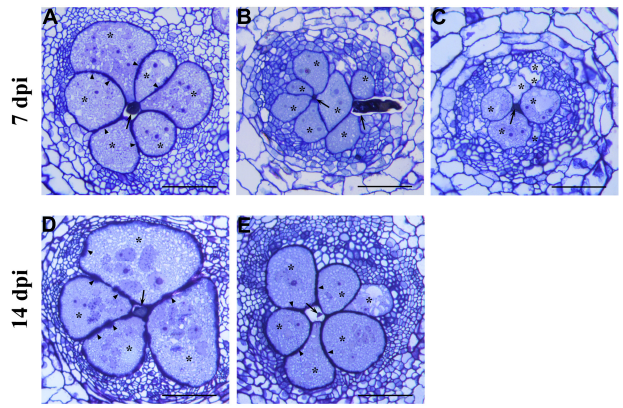

FIGURE 1 | Histological analysis of giant cells (GCs) induced by *Meloidogyne incognita* in normally watered (RKN) and water-stressed (RKN_WS) tomato roots at 7- and 14-day post inoculation (dpi). Cross sections (2.5 μm) were stained with toluidine blue and observed at light microscope. **(A)** Well developed and metabolically active giant cells in RKN roots at 7 dpi. **(B,C)** Feeding sites in RKN_WS galls at 7 dpi. **(B)** GCs look similar to those in unstressed gall but are smaller in size. **(C)** GCs contain large vacuoles and cytoplasm poorly active showing a delay in their development. Cell walls in all RKN_WS feeding sites at 7 dpi are thinner than those in RKN galls. **(D)** GCs in RKN galls at 14 dpi show a large expansion with increase in cell wall thickness and density of cytoplasm. **(E)** GCs in RKN_WS galls at 14 dpi look significantly smaller but similar in appearance to GCs in unstressed galls. *, GCs; arrow, nematode; arrowhead, thickened cell walls; scale bar, 100 μm.

the diameter of galls both at 7 and 14 dpi was observed in RKN_WS as compared with RKN (**Table 1**).

Nematode Feeding Site Development

Morphological changes in GC development were analyzed in RKN_WS plants and compared to those in RKN roots. Detailed observations were carried out on serial cross sections of galls at 7 and 14 dpi. Measurements of the GC area revealed that the cells in RKN_WS were consistently less expanded than in RKN roots both at 7 and 14 dpi (−50 and −57%, respectively; $p < 0.01$) (**Table 1**).

Histological observations were performed to monitor possible alterations in the development of the nematode FS. At 7 dpi, the RKN galls showed large multinucleate GCs mostly occupying the vascular cylinder area (**Figure 1A**). They showed a conspicuous number of nuclei, several small vacuoles, and a dense, granular, metabolically active cytoplasm. Unevenly thickened cell walls could also be noted (**Figure 1A**). At 14 dpi (**Figure 1D**), the vascular cylinder was entirely occupied by GCs with uniformly dense and granular cytoplasm and scarce vacuolation, allowing the provision of nutrients for nematode development. Cell wall thickening was observed in all GCs. Numerous sections of RKN_WS galls at 7 dpi consistently showed that many GCs had an appearance comparable with that of unstressed GCs, although they were significantly smaller (**Figure 1B**). A number of GCs showed large vacuoles typical of the early infection and poorly active cytoplasm, revealing a significant delay in development (**Figure 1C**). In all observed GCs, the cell walls were thinner than those in RKN galls. At 14 dpi, the GCs in RKN_WS galls were shown to have dense cytoplasm and thickened walls, a similar feature to those in unstressed galls though their size remained considerably smaller (**Figure 1E**).

RNA-Seq and Transcriptomic Profiles of Tomato Galls in Response to Water Stress

Sequencing analyses were performed on 7 and 14 dpi galls from RKN and RKN_WS tomato plants vs. the respective C plants. The aim was to gain insights into the molecular mechanisms that are affected by water stress within the nematode FS.

Over 220 million high quality 75-bp single reads were generated across all sampled roots at 7 dpi and about 174 million at 14 dpi (ranging from 38 up to 65 million per sample) (**Supplementary Table 3**). The sequences were deposited in FASTQ format in the Short Read Archive (SRA) of National Centre for Biotechnology Information (NCBI) and are available under BioProject accession PRJNA734743.

In total, 70–94% of good-quality reads were mapped onto the *S. lycopersicum* genome (SL4.0 assembly) across all samples (**Supplementary Table 3**). A high Pearson's correlation coefficient (r) was observed between RPKM values for each set of sample replicates sequenced (average $r = 0.94$ at 7 dpi and $r = 0.90$ at 14 dpi).

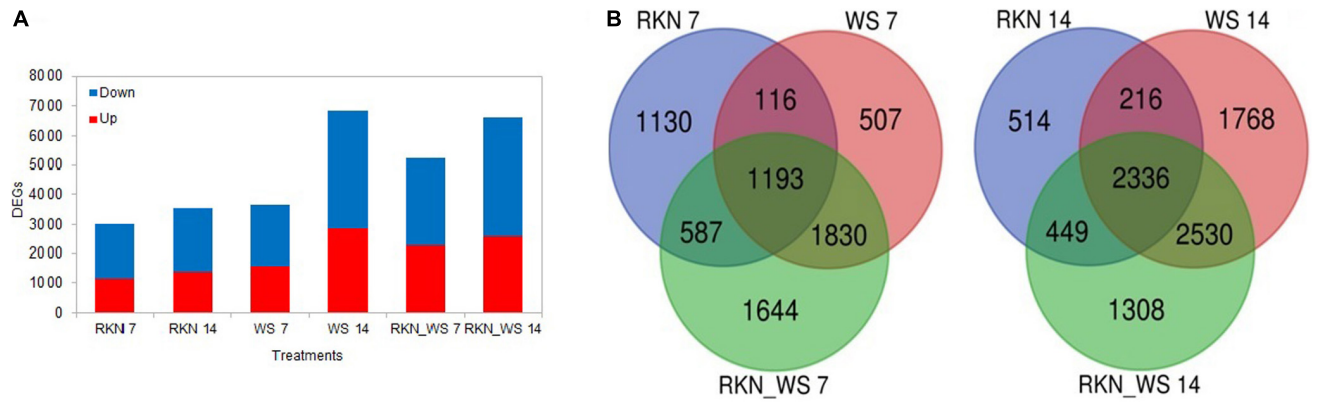

FIGURE 2 | Differentially expressed genes (DEGs) in normally watered and *M. incognita* infected (RKN), water-stressed (WS) and water-stressed and *M. incognita* infected plants (RKN_WS), compared to uninfected and normally watered control (C) (Fold change ≥ 2 or ≤–2, *p*-value ≤ 0.05 and TPM ≥ 5). **(A)** Number of DEGs for each treatment and sampling time. Bars represent total number of up (red) and downregulated (blue) genes compared to the respective C at 7 and 14 dpi. **(B)** Venn diagrams showing exclusive and common DEGs for each experimental condition.

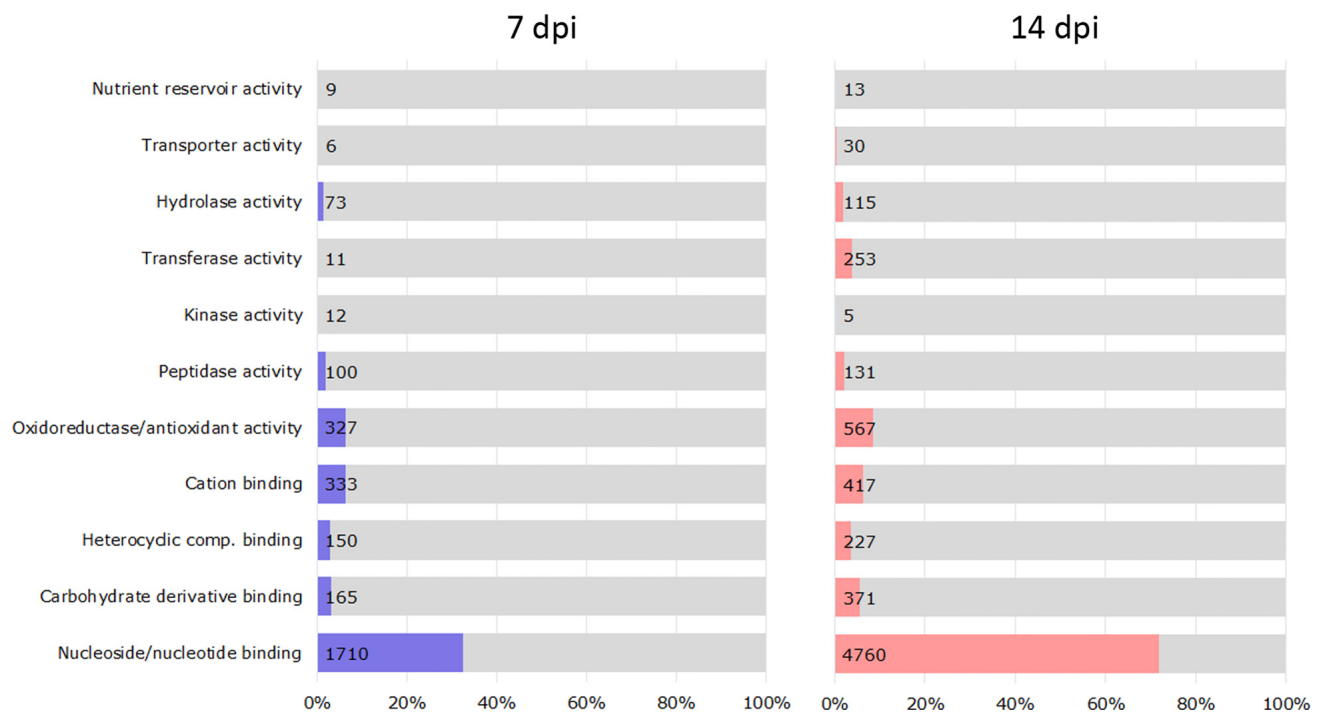

FIGURE 3 | Classification of DEGs based on enriched molecular function in RKN_WS at 7 and 14 dpi. The vertical axis indicates molecular function information, and the horizontal axis indicates the number and percentages of genes enriched in each category. Values were calculated respect to total RKN_WS DEGs [Fold change ≥ 2 or ≤–2, *p*-value ≤ 0.05 and transcripts per million (TPM) ≥ 5].

The percent of DEGs relative to the reference tomato transcriptome (34.075 protein coding genes in ITAG4.0) evaluated at each time points (7 and 14 dpi) increased for stressed plants in the sampling time and, when compared to the reference normally watered, uninfected roots (treatment C). This fraction increased after 14 days, raising from 9, 11, and 15% at 7 dpi to 10, 20, and 19% at 14 dpi for RKN, WS, and RKN_WS, respectively. For each treatment, downregulated transcripts always exceeded the upregulated ones (**Figure 2A**).

Comparative analysis across treatments showed that 37, 14, and 31% of DEGs at 7 dpi and 15, 26, and 20% at 14 dpi were exclusive for treatments RKN, WS, and RKN_WS, respectively. The percentage of DEGs common to all conditions were 39, 33, and 23% at 7 dpi and 66, 34, and 35% at 14 dpi for RKN, WS, and RKN_WS, respectively (**Figure 2B** and **Supplementary Table 4**).

TABLE 2 | Gene Ontology (GO) analysis summary: molecular functions were enriched (p-value ≤ 0.05) for differentially expressed genes (DEGs) during water stress and *M. incognita* infection (RKN_WS vs. C) at 7 and 14 dpi.

Molecular function	Term	Description	7 dpi	14 dpi
Nucleoside/nucleotide binding	GO:0000166	Nucleotide binding		–
	GO:0001882	Nucleoside binding	–	±
	GO:0017076	Purine nucleotide binding	–	±
	GO:0001883	Purine nucleoside binding	–	±
	GO:0030554	Adenyl nucleotide binding	–	±
	GO:0032549	Ribonucleoside binding	–	±
	GO:0032550	Purine ribonucleoside binding	–	±
	GO:0032553	Ribonucleotide binding	–	±
	GO:0032555	Purine ribonucleotide binding	–	±
	GO:0032559	Adenyl ribonucleotide binding	–	±
	GO:0035639	Purine ribonucleoside triphosphate binding	–	±
	GO:1901265	Nucleoside phosphate binding		–
	GO:0005524	ATP binding	–	±
	GO:0097367	Carbohydrate derivative binding	–	–
Heterocyclic comp. binding	GO:0020037	Heme binding	–	–
	GO:0046906	Tetrapyrrole binding	–	–
Ion binding	GO:0046914	Transition metal ion binding	±	±
	GO:0005506	Iron ion binding	–	–
	GO:0008270	Zinc ion binding	+	+
	GO:0005509	Calcium ion binding	–	–
Oxidoreductase/antioxidant activity	GO:0016209	Antioxidant activity	–	–
	GO:0016491	Oxidoreductase activity	–	–
	GO:0016684	Oxidoreductase act., acting on peroxide as acceptor	–	–
	GO:0016701	Oxidoreductase act., acting on single donors with incorporation of molecular oxygen	–	–
	GO:0004601	Peroxidase activity	–	–
	GO:0015035	Protein disulfide oxidoreductase activity		–
	GO:0004097	Catechol oxidase activity	–	
Peptidase activity	GO:0008236	Serine−type peptidase activity	–	–
	GO:0004252	Serine−type endopeptidase activity	–	
	GO:0070008	Serine−type exopeptidase activity	–	–
	GO:0004185	Serine-type carboxypeptidase activity		–
	GO:0070001	Aspartic-type peptidase activity	–	–
	GO:0004190	Aspartic-type endopeptidase activity	–	–
	GO:0004866	Endopeptidase inhibitor activity		–
Kinase activity	GO:0008443	Phosphofructokinase activity	–	
	GO:0003872	6−phosphofructokinase activity	–	
	GO:0000155	Phosphorelay sensor kinase activity		+
Transferase activity	GO:0046912	Transferase act., transferring acyl groups, acyl groups converted into alkyl on transfer		–
	GO:0016762	Xyloglucan:xyloglucosyl transferase activity	–	–
Hydrolase activity	GO:0004553	Hydrolase act., hydrolyzing *O*-glycosyl compounds	–	–
	GO:0017171	Serine hydrolase activity	–	–
Transporter activity	GO:0090484	Drug transporter activity		–
	GO:0015238	Drug transmembrane transporter activity	–	–
	GO:0045735	Nutrient reservoir activity	–	–

Differentially Expressed Genes Validation by Reverse Transcription-PCR

Ten genes were selected within the up and downregulated DEGs and analyzed by RT-qPCR at 7 and 14 days to evaluate the quality of gene expression profiles by RNA-Seq. The expression pattern of *Polyphenol oxidase* (Solyc08g074630.2.1), *1-aminocyclopropane-1-carboxylate oxidase* (aco5) (Solyc07g026650.3.1), *Heat stress transcription factor B-2b* (Solyc08g080540.3.1), *17.4 kDa class III heat shock protein* (Solyc03g123540.3.1), *Oleosin* (Solyc03g112440.1.1), *COBRA-like protein* (Solyc03g114900.3.1), *LEXYL2* (Solyc01g104950.4.1), *Fasciclin-like arabinogalactan protein 2* (Solyc07g045440.1.1), *Xyloglucan endotransglucosylase/hydrolase 6* (Solyc11g066270.3.1), and *Auxin response factor 9B*

(Solyc08g008380.4.1) are shown in **Supplementary Figures 1**, **2**. The expression trends obtained by RT-qPCR were consistent with the results observed by RNA-Seq, confirming the reliability of the DEGs data produced.

Responses of Abscisic Acid-Related Genes in Water-Stressed Roots and Galls

Dehydration induces transcriptional regulation of abscisic acid (ABA) biosynthetic genes (Xiong and Zhu, 2003) and plant responses to this hormone (Fujita et al., 2011). In order to verify the efficacy of the applied water stress, the expression level of genes associated with ABA synthesis and response were monitored (**Supplementary Figure 4**). Water stress significantly affected the expression of *NCED1* which encodes the 9-*cis*-epoxycarotenoid-dioxygenase (EC 1.13.11.51). This gene was downregulated in WS roots and RKN_WS galls with respect to C roots. Likewise, *AO3,* which encodes for an aldehyde oxidase (EC 1.2.3.1) key enzyme in the ABA biosynthesis, was downregulated in both WS roots and RKN_WS galls. These results could be peculiar of a late response as the samplings were carried out several days after the imposition of water stress. Indeed, several studies have shown that, at the onset of water stress, ABA increases largely within a few hours, then drops rapidly to a pre-stress value (Cohen et al., 1999). On the other hand, ABA-responsive genes were upregulated upon water-stress. The tomato dehydrin gene *TAS14* is clearly induced by water stress in WS roots and in RKN_WS galls, whereas in RKN galls, the expression was slightly lower than in control roots. Solyc03g116390.2.1, a coding for a late embryogenesis abundant (LEA) protein, was already shown to be inducible by water stress (Gong et al., 2010) along with other two LEA genes (Solyc12g098900.1.1, Solyc10g078770.1.1) that were significantly upregulated in WS and RKN_WS conditions at both times of observation. The upregulation of these marker genes confirmed the effect of the imposed stress.

Effect of Water Stress and Nematode Infection on Tomato Transcriptome

We examined DEGs (5,254 at 7 dpi and 6,623 at 14 dpi) in the RKN_WS condition to investigate the effect of combined stress on plants (**Supplementary Tables 5**, **6**). A GO enrichment analysis showed that the functional categories significantly enriched in each time sampling were as follows: binding of nucleosides/nucleotides, carbohydrates, heterocyclic compounds, and cations; and oxidoreductase/antioxidant, peptidase, kinase, transferase, hydrolase, transporter, and nutrient reservoir activities (**Figure 3**). Most of them were downregulated both at 7 and 14 dpi (**Table 2**).

Changes due to the persistence of the stress conditions were found for functions ascribed to nucleoside/nucleotide binding and phosphorelay sensor kinase activity, which showed upregulation after 14 dpi. DEGs that downregulated at 14 dpi included Ca ion binding, protein disulfide oxidoreductase activity, serine-type carboxypeptidase activity, endopeptidase inhibitor activity, transferase activity transferring acyl groups, and drug transporter activity (**Table 2**). Among enriched biological processes, we found 34 and 53 downregulated and 8 and 49 upregulated GO terms at 7 and 14 dpi, respectively (**Supplementary Table 7**). The processes associated with cell wall organization or biogenesis were mostly downregulated and showed differences in enriched GO terms and number of DEGs (**Figure 4**).

Focusing on DEGs exclusive for RKN_WS treatment were previously shown in **Figure 2B**, i.e., 1,644 and 1,308 at 7 and 14 dpi, respectively, wherein 733 and 517 genes were upregulated while 715 and 595 genes were specifically downregulated in 7- and 14-days old galls, respectively (**Figure 5A**).

The analysis indicated that 196 genes, with around 58% upregulated and 42% downregulated, were common to both times of observation (**Figure 5A**). Interestingly, three genes (Solyc03g123860.4.1, Receptor-like protein kinase; Solyc04g076300.4.1, Mechanosensitive ion channel protein 2, chloroplastic; Solyc02g078760.1.1, hypothetical protein) were upregulated at 7 dpi but downregulated at 14 dpi. Four genes (Solyc06g070900.3.1, TCP transcription factor 17; Solyc12g087860.3.1, RING/U-box superfamily protein; Solyc05g006340.3.1, Transducin/WD40 repeat-like superfamily protein; Solyc06g072690.3.1, Mitotic-spindle organizing protein 1B) were downregulated at 7 dpi, while upregulated at 14 dpi.

Insights into DEGs shared between RKN_WS and RKN galls, shown in **Figure 2B**, i.e., 587 and 449 at 7 and 14 dpi, respectively, revealed that 74 transcripts were common for both times, whereas 513 and 375 were exclusive at 7 at 14 dpi, respectively (**Figure 5B**). Among the 513 DEGs, 29% and 71% were, respectively, up and downregulated. The analysis evidenced that water stress changed completely the expression of 19 (from down to up) and 15 (from up to down) genes (**Supplementary Table 8**). Some of them were involved in signaling receptor, oxidoreductase, transporter, and transcription factor activities. Particularly, the transcription of Solyc04g072070.3.1, the encoding for a WRKY_transcription_factor_55, and upregulation in nematode parasitized roots were inhibited (from 4.4 to −5.18-fold) in galls under water stress (**Supplementary Table 8**). A further regulatory element markedly affected by water stress was Solyc06g053610.3.1 and the encoding for a R2R3MYB_transcription_factor 14, which changed its expression from down in RKN to up in RKN_WS (−3.5 to 2.6-fold) at 7 dpi. Among the 375 DEGs at 14 dpi, 52 and 48% were, respectively, up and downregulated. Three of them changed from down to up and one from up to down under water stress (**Supplementary Table 8**). Overall, the time of water deprivation affected the intensity of expression without causing changes in gene trends (**Supplementary Table 8**).

Water Stress Modulation of Genes Related to Cell Wall Metabolism in Nematode Feeding Site

Due to the morphology changes observed in nematode FS upon water stress and the GO biological process enrichment, we focalized on genes involved in cell wall biosynthesis, degradation, re-modeling, and extension. Response to water stress was firstly examined in galls of water-stressed plants (RKN_WS) in

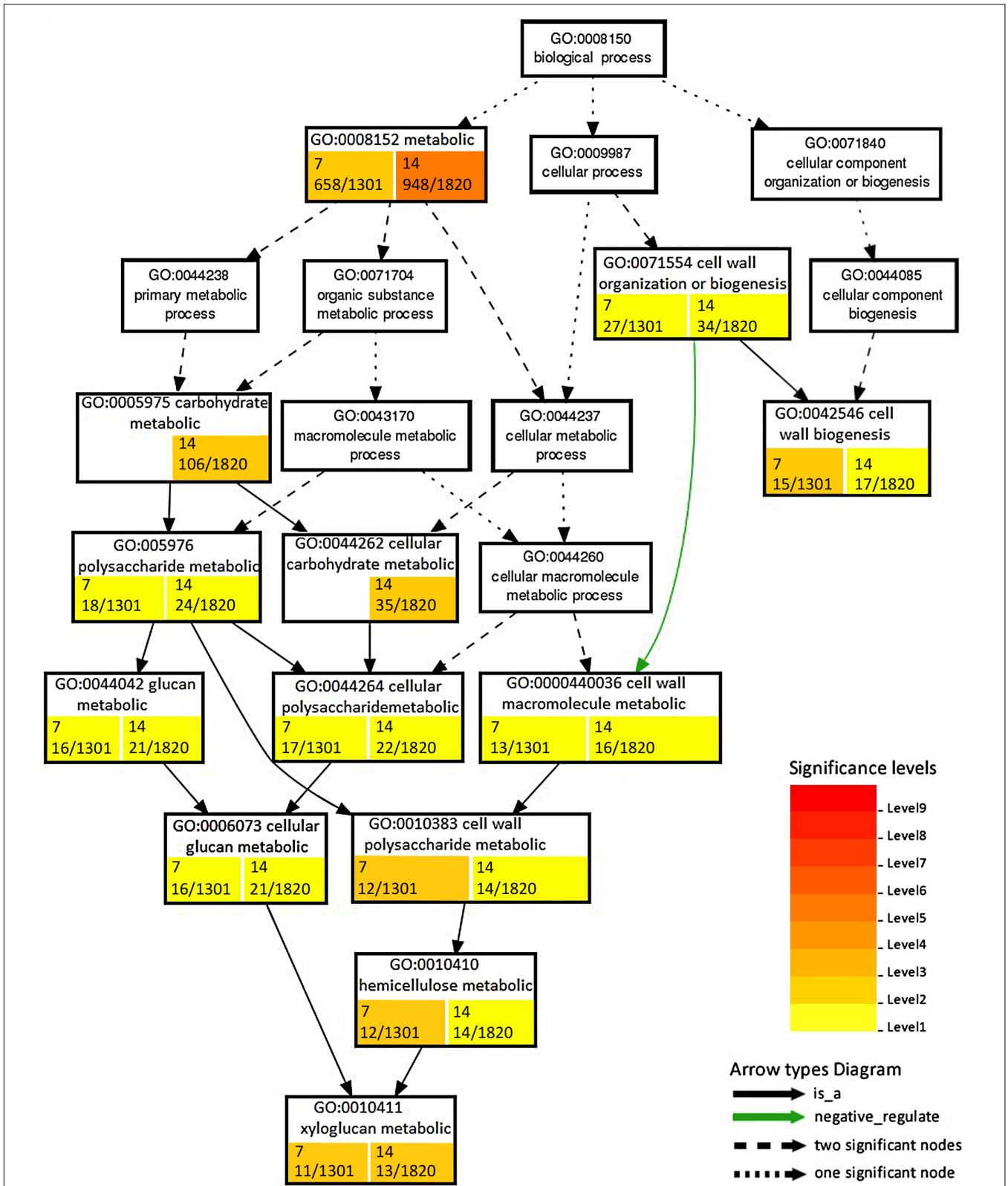

FIGURE 4 | Enrichment analysis of RKN_WS DEGs using Gene Ontology (GO) terms in the "Biological process" related to cell wall. Number of DEGs ascribed to each GO category with respect to total DEGs considered in the analysis are shown in colored box at 7 and 14 dpi. Color is proportional to the level of significance, as indicated by the scale in the legend.

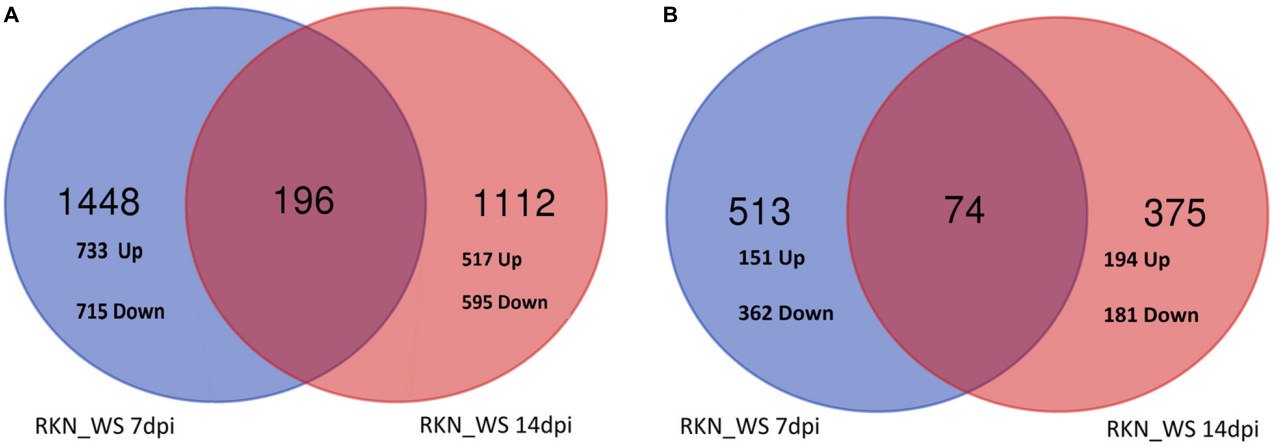

FIGURE 5 | Venn analysis of RKN_WS DEGs exclusive **(A)** and in common with RKN **(B)**, along the two sampling times.

comparison with the normally watered and uninfected control roots (**Supplementary Tables 9**, **10**). Based on this analysis, 246 (63 upregulated and 183 downregulated) and 288 (55 upregulated and 233 downregulated) DEGs were found in 7- and 14-day-old RKN_WS galls, respectively (**Supplementary Table 11**). Among them, 181 were present at both infection times. Most DEGs were downregulated with a small number of upregulated genes (**Supplementary Table 12**). Moreover, only 7 genes showed an opposite regulation between 7- and 14-day-old RKN_WS galls. Four genes, Solyc06g009190.4.1 (Pectinesterase), Solyc11g071470.1.1 (Transferase), Solyc01g080010.2.1 (Xyloglucan endoglucanase inhibitor), and Solyc06g060970.2.1 (Expansin-like B1) were upregulated at 7 dpi but downregulated at 14 dpi. Three genes, Solyc06g060170.3.1 (Pectin lyase-like superfamily protein), Solyc12g008530.2.1 (Pectinesterase), and Solyc06g062580.3.1 (Beta-galactosidase), were downregulated at 7 dpi but upregulated at 14 dpi (**Supplementary Tables 9**, **10**).

Seventy-one out of the 181 DEGs found in both 7- and 14-day-old RKN_WS galls were also present in RKN galls both at 7 and 14 dpi (**Table 3**) with the same trend, although with different intensity.

Expression of Feeding Site Genes Involved in Cell Wall Biogenesis

Expression of genes related to cell wall metabolism in RKN_WS were compared to that of the other conditions. Analysis showed that most members of the large cellulose synthase (CesA) and the cellulose synthase-like (Csl) enzyme families were downregulated either in unstressed or stressed galls. The only exception was *CesA* Solyc11g005560.3.1 which was upregulated at 7 and 14 dpi with a higher level of expression at 14 dpi and found in both types of FS (**Figure 4**). In addition, we found that water stress repressed the expression of the *Csl* genes Solyc08g006310.3.1, Solyc09g075550.3.1, and Solyc12g014430.2.1 that were upregulated at 7 dpi in RKN galls. On the other hand, Solyc03g005450.3.1 was induced by water stress in RKN_WS galls at 14 dpi (**Supplementary Tables 9**, **10**).

We also found that fasciclin-like arabinogalactan proteins (FLAs), cell wall structural glycoproteins that mediate cellulose deposition and cell wall development, were differentially expressed in all stress conditions evaluated. In RKN_WS galls, we found 10 DEGs coding for FLAs 1, 2, 4, 9, 11, and 12. Water stress suppressed their expression, and the negative effect was, in some cases, enhanced by the nematode presence (**Figure 6**). A striking example is Solyc12g006110.3.1, coding for FLA 2, which was downregulated by 551.9 times in RKN_WS with respect to control, and around 55 times with respect to water-stressed and uninfected roots (WS). Likewise, comparison of the expression trends between RKN and RKN_WS galls highlighted an increased downregulation during the double stress condition at both 7 and 14 dpi. In particular, Solyc07g045440.1.1 showed an opposite expression trend at 7 dpi (from 2.02-fold upregulation in RKN to −3.64-fold downregulation in RKN_WS compared to control) (**Figure 6** and **Supplementary Table 1**). Solyc07g045440.1.1 was selected for RT-qPCR validation, and the results confirmed RNA-seq data for all conditions and tested times (**Supplementary Figure 2B**). In addition, Solyc10g005960.1.1, Solyc01g091530.4.1, and Solyc09g007650.3.1, which were upregulated in RKN galls at 7 dpi, were significantly repressed by water stress (**Figure 6** and **Supplementary Table 1**).

Likewise, water stressed galls showed differential expression of regulatory elements. COBRA proteins play an important role in the cellular architecture and root growth, acting through the organization of cellulose microfibrils orientation. Five *COBRA-like* genes (Solyc01g065530.3.1, Solyc02g065765.1.1, Solyc03g114890.4.1, Solyc03g114900.3.1, and Solyc09g075540.1.1) were found downregulated in RKN_WS galls both at 7 and 14 dpi (**Figure 6** and **Supplementary Tables 9**, **10**). Comparing RKN_WS with RKN galls, the major change was observed for Solyc03g114890.4.1, whose expression was sixfold more inhibited upon water stress at 14 dpi. Moreover, two transcripts encoding COBRA proteins, Solyc02g089120.4.1 and Solyc03g070440.4.1, were upregulated in RKN_WS galls at 14 dpi. In addition, their level of expression was higher than in RKN galls (**Figure 6** and **Supplementary Table 1**).

TABLE 3 | DEGs related to the cell wall in common between galls from treatments RKN_WS and RKN at 7 and 14 dpi.

Transcript ID	RKN_WS		RKN		Description
	7	14	7	14	
Solyc11g007970.2.1	−1503.76	−4575.84	−12.14	−77.36	4-coumarate–CoA ligase-like 5
Solyc08g068190.3.1	−36.65	−33.43	−8.84	−1697.71	Aldehyde dehydrogenase
Solyc12g007030.3.1	−3.49	−5.32	−2.08	−3.52	Aldehyde dehydrogenase
Solyc02g089170.4.1	−14.58	−139.15	−755.63	−580.39	Alpha−1, 4-glucan-protein synthase
Solyc02g065740.3.1	−22.11	−1200.09	−1753.08	−20.71	Alpha-1, 4-glucan-protein synthase
Solyc07g053640.1.1	2.69	3.67	4.69	2.57	Arabinogalactan-protein
Solyc02g078950.4.1	−8.78	−2936.24	−17.34	−9.53	Beta-galactosidase
Solyc03g019890.3.1	3.3	2.74	4.8	2.63	Beta-galactosidase 7
Solyc07g063390.3.1	−4.68	−3.64	−2.62	−2.94	Beta-glucosidase 16
Solyc01g101120.4.1	4.86	4.03	2.7	2.35	Carbohydrate-binding X8 domain
Solyc09g010200.4.1	−56.74	−5256.02	−2.46	−8.65	Casparian strip membrane protein 1
Solyc04g011480.3.1	−1271.02	−410.76	−23.02	−352.85	CASP-like protein
Solyc02g069730.3.1	16.16	4.67	24.92	7.74	CASP-like protein
Solyc04g051270.2.1	−619.38	−338.07	−531.08	−290.68	CASP-like protein
Solyc11g012590.3.1	3.72	12.01	−2.6	3.85	CASP-like protein
Solyc08g082640.2.1	−3.72	−5.13	−14.47	−4.31	Cellulose synthase
Solyc01g059900.4.1	−5472.7	−7306.08	−4687.24	−64.79	Dirigent protein
Solyc02g032030.1.1	−1788.43	−991.41	−6.68	−852.18	Dirigent protein
Solyc08g081780.1.1	−146.45	−2188.99	−14.31	−9.24	Dirigent protein
Solyc10g008900.3.1	−31.18	−1160.22	−965.99	−997.72	Dirigent protein
Solyc02g083980.3.1	−2.47	−2.14	−5.81	−2.87	Endoglucanase
Solyc08g076640.1.1	−33.29	−3189.76	−1739.85	−69.24	Eukaryotic aspartyl protease family protein
Solyc01g079920.3.1	−1096.42	−886.28	−938.83	−761.85	Eukaryotic aspartyl protease family protein
Solyc08g076630.3.1	−9.34	−1078.72	−20.97	−10.53	Eukaryotic aspartyl protease family protein
Solyc05g012730.1.1	−24.07	−106.8	−5.45	−8.29	Exostosin-like
Solyc08g080060.4.1	−14.47	−579.84	−748.84	−498.99	Expansin
Solyc10g084780.3.1	−27.35	−920.38	−1495.87	−792.06	Expansin
Solyc06g051800.3.1	5.35	1.95	10.48	2.96	Expansin 1
Solyc10g086520.2.1	−11.37	−17.84	−5.72	−6.54	Expansin 6
Solyc12g089380.2.1	−70.45	−43.41	−2362.07	−3055.95	Expansin 8
Solyc05g007830.3.1	8.59	5.24	9.76	4.76	Expansin 12
Solyc06g005560.4.1	8.75	9.46	14.28	12.86	Expansin 9
Solyc01g107220.2.1	−3.87	−5.17	−27.75	−9.61	Extensin-2-like
Solyc11g065910.1.1	−79.94	−223.25	−52.11	−101.94	Extensin-2-like
Solyc03g082790.4.1	−11424.49	−12747.98	−9801.77	−70.53	Extensin-like 54
Solyc01g005850.2.1	−6.12	−9.68	−5.14	−30.13	Extensin-like protein Dif54
Solyc01g097680.2.1	−1006.4	−3158.2	−105.17	−20.03	Extensin-like protein Dif10
Solyc02g030220.1.1	−59.08	−103.67	−48.94	−1116.38	Extensin-like protein Dif10
Solyc03g082770.1.1	−30.11	−28.61	−793.28	−687.37	Extensin-like protein Dif10
Solyc12g100080.1.1	−1178.66	−2207.66	−1010.44	−24.33	Extensin-like protein Ext1
Solyc12g100110.1.1	−1571.56	−4183.64	−1346.01	−64.78	Extensin-like protein Ext1
Solyc12g006110.3.1	−551.93	−16555.46	−8.2	−42.99	Fasciclin-like arabinogalactan protein 2
Solyc02g088500.1.1	−3.5	−2.64	−3.74	−2.84	Glycosyltransferase
Solyc12g010200.2.1	−3.17	−3.26	−3.92	−2.05	Hexosyltransferase
Solyc07g005760.3.1	−2.85	−9.09	−3.65	−4.58	Hydroxycinnamoyl CoA quinate transferase
Solyc02g084990.3.1	2.22	2.32	4.76	3.14	Mannan endo-1, 4-beta-mannosidase
Solyc12g013750.2.1	2.04	3.46	2.25	3.51	Mannan endo-1, 4-beta-mannosidase 1
Solyc05g055490.3.1	−294.21	−1593.95	−18.07	−5.29	Monocopper oxidase-like protein SKU5
Solyc06g007960.4.1	−9.39	−95.01	−6.06	−23.13	*O*-methyltransferase
Solyc03g111690.4.1	8.29	11.28	10.17	11.1	Pectate lyase
Solyc12g019440.3.1	−835.8	−564.02	−715.09	−11.69	Pectin acetylesterase

(Continued)

TABLE 3 | (Continued)

Transcript ID	RKN_WS		RKN		Description
	7	14	7	14	
Solyc01g094970.4.1	5.34	2.67	3.58	4.9	Pectin lyase-like superfamily protein
Solyc12g019120.2.1	−912.6	−749.48	−780.44	−644.87	Pectin lyase-like superfamily protein
Solyc05g005040.4.1	−15.47	−13.52	−7.44	−26.71	Pectin lyase-like superfamily protein
Solyc08g014560.3.1	−688.93	−2452.14	−2174.11	−2107.82	Pectin lyase-like superfamily protein
Solyc12g019130.3.1	−1288.08	−640.72	−1103.89	−551.62	Pectin lyase-like superfamily protein
Solyc12g019140.3.1	−225.89	−1854.83	−3320.17	−21.48	Pectin lyase-like superfamily protein
Solyc03g083840.3.1	−110.35	−4658.06	−4732.88	−4007.47	Pectinesterase
Solyc02g014300.2.1	−26.69	−2090.67	−1339.11	−340.42	Pectinesterase
Solyc12g008530.2.1	−3.16	2.07	−7.19	2.9	Pectinesterase
Solyc10g018320.1.1	−302.97	−423.08	−259.08	−364.13	Plant invertase/pectin methylesterase inhibitor superfamily protein
Solyc03g083660.1.1	−340.41	−1016.1	−291.57	−873.43	Plant invertase/pectin methylesterase inhibitor superfamily protein
Solyc03g083710.1.1	−17.35	−48.38	−5.36	−7.51	Plant invertase/pectin methylesterase inhibitor superfamily protein
Solyc05g005540.4.1	−26.85	−15486.03	−4.19	−29.06	Polygalacturonase-1 non-catalytic subunit beta
Solyc12g056960.2.1	−6.22	−54.19	−2.07	−2.59	Putative glucan 1, 3-beta-glucosidase
Solyc04g076660.3.1	4.18	5.29	7.15	2.85	Rhamnogalacturonate lyase family protein
Solyc03g097500.3.1	21.72	2.06	9.06	3.39	Transferase
Solyc11g071470.1.1	4.17	−3.7	3.61	−2.86	Transferase
Solyc01g080010.2.1	21.95	−2.51	9.65	−2.27	Xyloglucan endoglucanase inhibitor
Solyc12g007250.1.1	−529.09	−824.11	−453.18	−708.43	Xyloglucan endotransglucosylase/hydrolase
Solyc11g040140.2.1	−16.18	−3466.93	−2050.1	−2981	Xyloglucan endotransglucosylase/hydrolase

Values indicate the fold change respect to uninfected and unstressed control plants.

Solyc03g114900.3.1 was validated by RT-qPCR and results were consistent with RNA-Seq data for all conditions and tested times (**Supplementary Figure 2C**).

Among the genes involved in phenylpropanoid pathway, we found that *4-coumarate-CoA ligase* (4CL), *hydroxycinnamoyl CoA quinate transferase* (HCT), *Caffeoyl-CoA O-methyltransferase* (CCoAMT), *Cinnamyl alcohol dehydrogenase* (CAD), and *cinnamoyl-CoA reductase 2* (CCR2) were downregulated at 7 and 14 dpi in galls of stressed and normally watered plants (**Supplementary Tables 9**, **10**). We also found changes in expression of genes involved in the regulation of lignification. Eight dirigent proteins genes (*DIR*), ensuring the stereoselectivity of coniferyl alcohol dimerization and likely mediating the free radical coupling of monolignol plant phenols to yield lignans and lignins, were differentially expressed in response to both biotic and abiotic stress (**Supplementary Tables 9**, **10**). Solyc04g010270.1.1, Solyc06g075630.4.1, Solyc07g042300.1.1, and Solyc12g097090.3.1 were downregulated at both times of observation when compared to C and RKN. In particular, Solyc12g097090.3.1 and Solyc04g010270.1.1 were, respectively, 250- and 20-fold more downregulated with respect to RKN at 7 dpi (**Figure 6** and **Supplementary Table 1**). In addition, Solyc06g054320.1.1 and Solyc10g084440.3.1 were upregulated at 14 dpi (**Supplementary Tables 9**, **10**). DIR proteins interact in some way with Casparian strip domain proteins (CASPs). The latter constitutes a protein complex directing transport across the plasma membrane and recruiting proteins required for Casparian strip (CS) formation and lignification. Our data showed that three CASPs (Solyc04g005620.3.1, Solyc05g007790.3.1, and Solyc10g083250.2.1) were downregulated by nematode infection, particularly at 14 dpi, and that combined stresses enhanced their downregulation. By contrast, we found five CASP-like proteins that were upregulated in RKN_WS galls at both times of observation (**Figure 6** and **Supplementary Tables 9**, **10**).

Expression of Genes Involved in Cell Wall Remodeling

Water stress downregulated most of the gene coding for endo-β-1,4-glucanases (EGase, EC 3.2.1.4) and involved in many processes requiring cell wall modifications. Despite this, it triggered a higher expression of an *EGase* (Solyc12g055980.1.1) in 7-day-old RKN_WS galls (**Figure 4**). In addition, we found that *EGase cel 8* (Solyc08g082250.3.1), known to be induced by nematode infection in syncytia and giant cells in several plant-nematode interactions (Sobczak et al., 2011), was over-expressed at 7 dpi during the *M. incognita*-tomato interaction in both unstressed and stressed galls, with an expression level higher in presence of nematode only (**Supplementary Tables 9**, **10**).

Analysis of gene expression in RKN_WS galls also showed changes in abundance of several pectin esterase coding genes (**Supplementary Tables 9**, **10**). In particular, Solyc11g070187.1.1 and Solyc11g070175.1.1 were upregulated both at 7 and 14 dpi, whereas Solyc03g083840.3.1, Solyc02g014300.2.1, Solyc09g075350.4.1, Solyc09g075330.4.1, Solyc03g083360.3.1, and Solyc03g123620.4.1 were downregulated at 7 and 14 dpi. Only Solyc06g009190.4.1 was upregulated at 7 dpi and downregulated at 14 dpi, whereas Solyc12g008530.2.1 (downregulated at 7 dpi) was upregulated at 14 dpi (**Figure 6** and

Supplementary Tables 9, **10**). In general, the expression patterns of pectin esterase genes observed for RKN_WS galls were similar to those of RKN galls (**Table 3**).

Several genes belonging to the pectin lyase-like superfamily, whose members hydrolyze methylated pectin, showed differential expression in RKN_WS galls (**Supplementary Tables 9**, **10**). In particular, two genes (Solyc01g094970.4.1 and Solyc05g005170.4.1) were upregulated at both 7 and 14 dpi, and seven (Solyc08g082170.4.1, Solyc12g019120.2.1, Solyc05g005040.4.1, Solyc12g019140.3.1, Solyc08g014560.3.1, Solyc06g060170.3.1, and Solyc12g019130.3.1) were downregulated at both 7 and 14 dpi (**Figure 6** and **Supplementary Tables 9**, **10**). Expression of the aforementioned genes showed the same trend in RKN galls, except for Solyc08g082170.4.1 which was repressed by water stress in RKN_WS galls at 7 dpi compared to galls of normally watered plants (**Figure 6** and **Supplementary Table 1**).

Polygalacturonases and pectate lyases are unable to degrade methylated pectin as they can only work once the pectin is demethylated or deacetylated by pectin methylesterases or acetylesterases. In water-stressed galls, these genes were downregulated at both times of observation except for the pectin acetyl esterase gene Solyc08g075020.3.1 which was upregulated at 7 dpi (**Figure 6**). Interestingly, a *pectin acetylesterase* (Solyc08g005800.4.1) and the *pectin methylesterase pmeu1* (Solyc03g123630.4.1), which were downregulated in response to water stress, were upregulated in RKN galls at 7 dpi (**Figure 6** and **Supplementary Table 1**).

Moreover, genes coding for polygalacturonases were downregulated at both 7 and 14 dpi in RKN_WS and in RKN galls. Among genes coding for pectate lyases, two (Solyc09g008380.3.1 and Solyc03g111690.4.1) were upregulated in RKN_WS galls at 7 dpi, and Solyc03g111690.4.1 was also up-regulated at 14 dpi (**Figure 6**). Another three genes coding for pectate lyase were downregulated in 14-day-old RKN_WS galls (**Supplementary Tables 9**, **10**). Our results showed that the expression of a *xyloglucan endotransglucosylase-hydrolase 6* (Solyc11g066270.3.1) was affected by water stress as the gene, upregulated in RKN galls, and was downregulated in RKN_WS at 7 dpi (**Figure 6** and **Supplementary Table 1**). Likewise, another gene coding for a xyloglucan endotransglucosylase-hydrolase (Solyc09g008320.4.1), which was up-regulated in RKN galls at 7 dpi, was down-regulated in response to water stress at both 7 and 14 dpi (**Figure 6** and **Supplementary Table 1**).

Plant cell wall hemicellulose components, arabinoxylans and xylans, are subject to modification during plant growth and development. We found that *LEXYL2* (Solyc01g104950.4.1) coding for a α-l-arabinofuranosidase, belonging to glycoside hydrolase (GH) family 3 with both α-L arabinofuranosidase and β-xylosidase activities, was downregulated at 14 dpi in RKN and RKN_WS galls. By contrast, at 7 dpi it was upregulated in RKN and downregulated in RKN_WS galls, suggesting a role of LEXYL2 in the early stage of nematode FS development which was negatively affected by water stress (**Figure 6** and **Supplementary Table 1**). The expression of this gene was validated by RT-qPCR, and values were significant ($p < 0.05$) compared with control and trends were consistent with RNA-Seq data (**Supplementary Figure 2A**).

Also, the expression analysis of members of the expansin families revealed five downregulated and three upregulated genes at both 7 and 14 dpi in RKN_WS galls. *Expansin 9* (Solyc06g005560.4.1) and *expansin 12* (Solyc05g007830.3.1) were specifically activated, whereas *expansin 6* (Solyc10g086520.2.1) and *expansin 8* (Solyc12g089380.2.1) were repressed in water-stressed galls compared to control plants (**Table 3**). These genes showed the same expression trend in RKN galls. By contrast, expansin A11 (Solyc04g081870.4.1) and expansin-like B1 (Solyc08g077910.3.1) showed opposite expression patterns in the different type of FS. Particularly, upregulated in 7 dpi RKN galls and repressed by water stress in 7- and 14-day-old RKN_WS galls (**Figure 6** and **Supplementary Table 1**). The expression of expansin 1 (Solyc06g051800.3.1) in nematode FS was affected by water stress. Although upregulated compared to C plants, it had a lower level of expression (about twofold less) in comparison to RKN galls at 7 dpi (data not shown).

Distribution of Cellulose in Feeding Site

For the study of cellulose distribution, we used Calcofluor white (**Figure 7**), which stains cellulose, callose, and other β-glucans (Hughes and McCully, 1975). When excited with UV light, calcofluor white produces a blue fluorescence of cellulosic walls (Kitin et al., 2020). The presence of cellulose was detectable in vessel walls of both RKN and RKN_WS galls (**Figures 7A′–D′**). By contrast, a stronger signal was only detected along the GC walls in RKN both at 7 and 14 dpi (**Figures 7A′,C′**).

DISCUSSION

The current study shows the combination of morphological features and mRNA-Seq data during the tomato-*M. incognita* interaction under a concomitant water stress.

Meloidogyne spp. establish a permanent FS by inducing multinucleate hypertrophied GCs which reach their maximum size within 2 weeks. GC wall surface presents ingrowths that interface with xylem cells to increase the plasmalemma surface area and support increased nutrient uptake (Rodiuc et al., 2014). The transfer of nutrients to nematodes involves regulation of water flux into GCs (Baldacci-Cresp et al., 2015). Cell wall thickening and loosening is required to allow GC expansion and to provide mechanical support to maintain cell shape in response to high osmotic pressure (Gheysen and Mitchum, 2009). It has been demonstrated that the nematode nutrient acquisition through GCs relies on the formation of *de novo* formed vascular tissues, and that both primary and secondary cell walls are deposited both in GCs and vascular tissues (Kyndt et al., 2013).

In our study, the decreased tomato growth in aboveground plant parts and roots was a clear response to water stress which could be correlated with endogenous ABA accumulation (Sharp and Davies, 1989). Furthermore, a worsened nematode penetration rate was observed, as demonstrated by the drastic reduction in the number of galls at both sampling times. An increase in endogenous ABA at the onset of drought

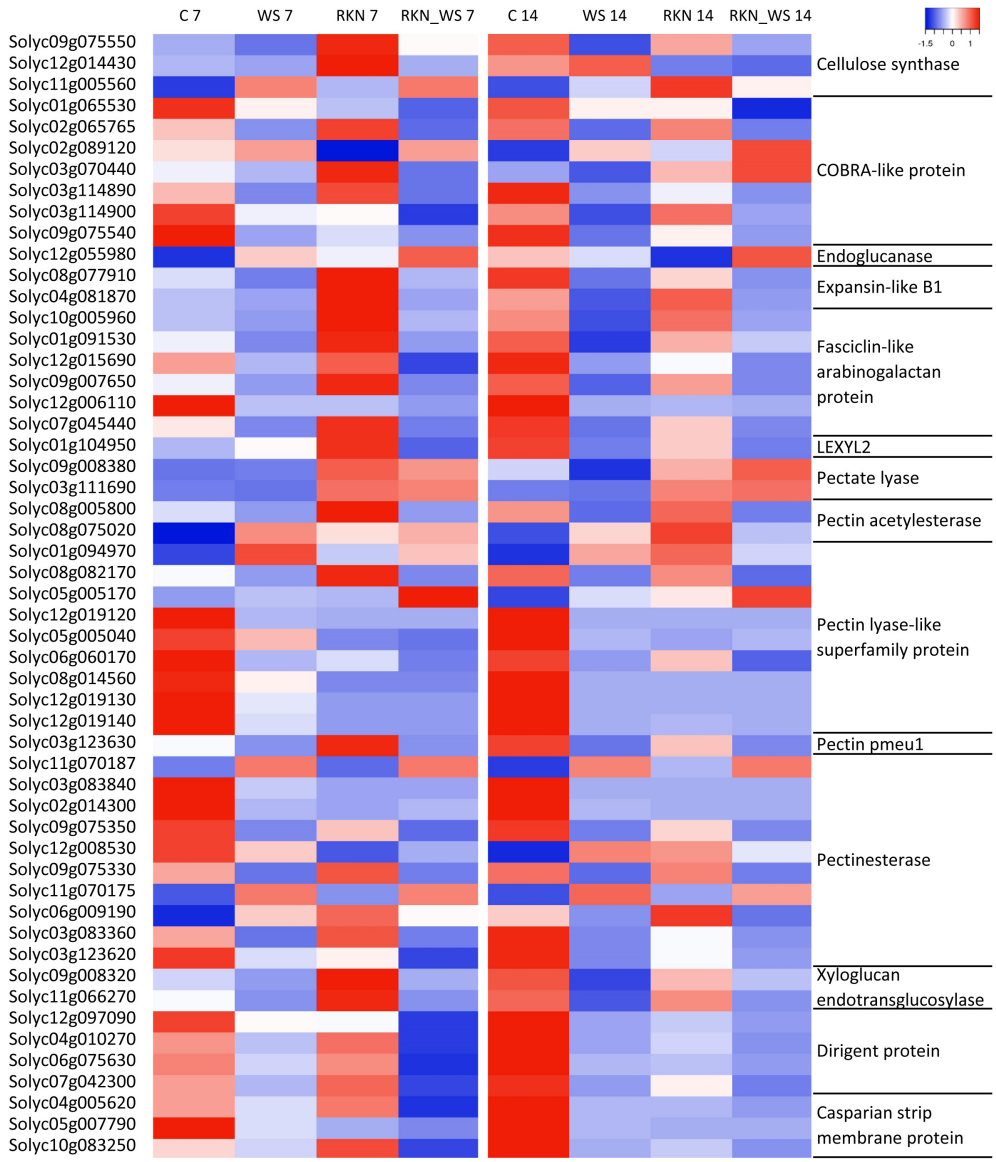

FIGURE 6 | Gene expression patterns of subsets of DEGs associated with cell wall in tomato. The heatmap represents TPM mean values of subsets selected in water stressed roots inoculated with *M. incognita* (RKN_WS) with statistically significant differences (p-value ≤ 0.05) for almost one condition. Each row represents a gene, and each column represents an experimental condition at 7 and 14 dpi. Labels on the left and right sides of the heatmap show the Solyc id and annotation, respectively. The color key scale values range from −1 (lowest TPM number) to 1 (highest TPM number).

stress (Cohen et al., 1999) might have stimulated resistance to *M. incognita* in tomato. ABA plays a complex role in the plant's defense response while it promotes resistance in some plant–pathogen interactions, whereas it increases susceptibility in others (Asselbergh et al., 2007; Ton et al., 2009). Reports on the direct influence of ABA on plant responses to nematode attack remain controversial. Experiments with exogenous ABA revealed that ABA plays a negative role in rice defense against the migratory nematode *Hirschmanniella oryzae* in roots (Nahar et al., 2012). Nevertheless, Karimi et al. (1995) reported a lower reproduction of *M. incognita* on potato roots of ABA-treated plants. In our study, the effects of water stress on the FS development at 7 dpi were remarkable. The GCs were smaller and delayed in development, and their walls were thinner compared to those of the GCs in normally watered plants. In time, the GCs in stressed plants looked similar to those in the 14 dpi normally watered ones, although they continued to be smaller. These changes could be orchestrated by ABA which has a role in prevention of cell-wall loosening (Gimeno-Gilles et al., 2009) and/or secondary cell wall formation (Liu et al., 2021; Yu et al., 2021). In this context, we tried to characterize the transcriptomic landscape of nematode FS and its adaptation in response to water stress in 7- and 14-day-old galls. The expression analysis was carried out in whole tomato galls, including GCs,

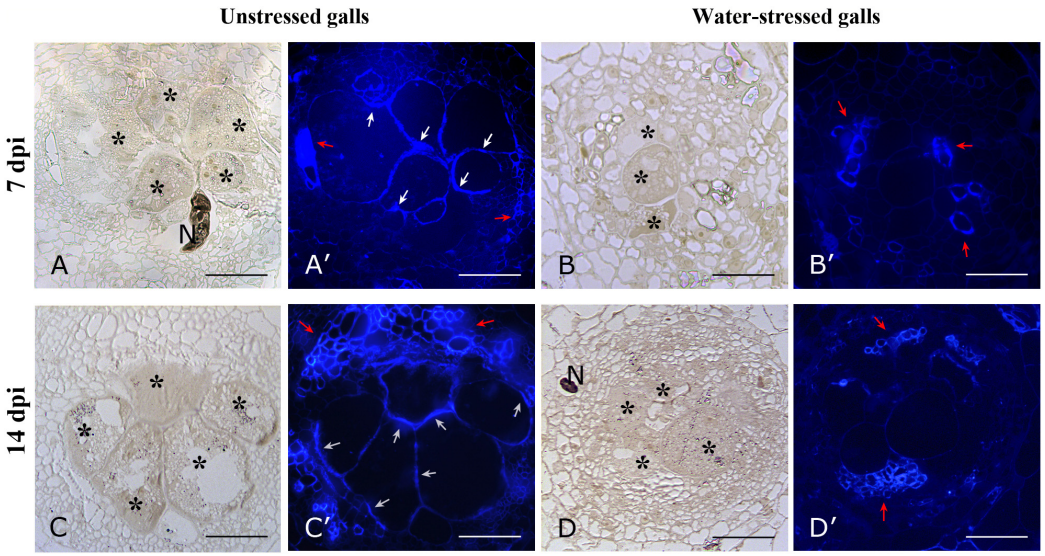

FIGURE 7 | Bright field and fluorescence microscope images of cellulose distribution in cross sections of unstressed (RKN) and water-stressed (RKN_WS) galls stained with Calcofluor-white. Blue fluorescence was present on cellulosic walls of GCs and vessels of unstressed galls at 7 **(A′)** and 14 dpi **(C′)**. No signals were detectable on GCs walls of water-stressed galls both at 7 and 14 dpi **(B′,D′)**, only xylem vessels showed fluorescence. Bright field images of corresponding sections of unstressed **(A,C)** and water-stressed galls **(B,D)**. Asterisks indicate GCs; N, nematode; white arrow, cellulosic cell walls; red arrow, vessels; scale bar, 100 μm.

neighboring cells, and vascular tissues, therefore reflecting the changes occurring during the tomato-*M. incognita* interaction.

Enrichment analysis allowed to highlight that the persistence of the water stress condition triggers the modulation of genes involved in specific cellular functions and biological processes. In particular, GO categories, such as binding, kinase and transporter activities, and cell wall related processes, showed different trends along the experimental conditions. Thus, we focused our attention on those transcripts involved in cell wall synthesis and modification during gall formation. The plant cell wall is a complex and dynamic structure with an important role in cell and organ growth and intercellular communication. It also provides mechanical strength to withstand turgor pressure and reacts to different biotic and abiotic stresses to allow proper development and differentiation of plant tissues and organs (Houston et al., 2016).

Cell Wall Biogenesis in Galls Induced by *M. incognita*

The cell walls consist of primary and secondary walls whose typical components are cellulose, non-cellulosic, and pectic polysaccharides, enzymatic and catalytic proteins, phenolic compounds, and water. A number of studies report that cellulose biosynthesis can be altered in response to water deficit, as shown by the decreased level of cellulose content in several different species (Le Gall et al., 2015). We found that the distribution of cellulose resulted in altered nematode FS of plants subjected to water stress. The fluorescent dye only highlighted cellulose in GC walls of unstressed galls. Moreover, our expression analyses confirmed that genes involved in cellulose biosynthesis had a different expression pattern in response to water stress during the FS development. Generally, water stress repressed the expression of genes belonging to the Csl family. In particular, the dramatic downregulation of *cellulose synthase-like* Solyc07g043390.4.1 triggered by water stress mainly at 14 dpi could be associated to a reduced FS growth. This finding is in agreement with Choe et al. (2021) who reported that downregulation of this gene by tomato yellow leaf curl virus infection caused a stunted growth phenotype in tomato. Moreover, Solyc07g043390.4.1-silenced tomato plants displayed changes in stem anatomy with cell size reduction and inhibition of secondary xylem (Choe et al., 2021). This suggests that this *cellulose synthase-like gene* plays a critical role in cell wall metabolism in different tomato tissues.

Among many genes involved in cellulose synthesis and deposition, members of the COBRA multigene superfamily act in the assembly of cellulose micro-fibrils at least by partially modulating cellulose crystallinity (Liu et al., 2013) and by regulating the orientation of cell expansion (Schindelman et al., 2001). COBRA encodes an extracellular glycosylphosphatidylinositol (GPI)- anchored protein which is stably associated with the plasma membrane by its GPI-anchor and is required for cell wall synthesis and morphogenesis (Gillmor et al., 2005). Each COBRA member is active in diverse biological processes during cell expansion and cell wall biosynthesis (Roudier et al., 2005). This is also confirmed in our data, with some genes downregulated and others upregulated during the root-*M. incognita* interaction. Interestingly, water stress intensified these effects. Thus, the differential regulation observed for COBRA genes in stressed gall suggests that they are specifically responsive to water stress and could be directly involved in modifications of the cell wall through changes in the orientation of cellulose micro-fibrils.

Furthermore, in our transcriptome analysis, three genes (Solyc10g005960.1.1, Solyc01g091530.4.1, and Solyc09g007650.3.1) coding for Fasciclin-like arabinogalactan proteins (FLAs) were specifically upregulated during the tomato-*M. incognita* interaction. FLAs are a subclass of arabinogalactan proteins (AGPs) that play a role in secondary cell wall assembly and may physically interact with the cellulose synthase complex. They are characterized by containing one or two FAS1 (fasciclin-like) domains and at least one AGP module, and often contain a C-terminal GPI anchor signal peptide. Plants may express some FLAs with GPI for maintaining the integrity of the plasma membrane and others that are not GPI-anchored for mediating cell expansion (Johnson et al., 2003). According to a recent study, GPI-anchored function might also be involved in host–pathogen interactions (Wu et al., 2020). All tomato upregulated FLAs showed a potential C-terminal GPI-modification site (predicted by big-PI Plant Predictor[11]). In unstressed FS, the accumulation of fasciclins could promote cell wall expansion. This latter, in turn, can provide a greater surface area for water absorption and nutrient uptake, thus ensuring nematode development. Moreover, FLAs are also involved in signaling as they can control the transcriptional program for cell wall formation (Huang et al., 2013). In this regard, knock down of FLA6 in *Populus* resulted in a decrease of lignin and cellulose content in the xylem and in a downregulation of some xylem-specific genes associated with cellulose and lignin biosynthesis (Wang et al., 2015). Under water stress, the expression levels of tomato FLAs appeared dramatically decreased. Therefore, alterations in FLAs' transcript abundance upon water stress could induce changes in expression of other genes involved in cell wall metabolism and presumably affect its chemical composition. Similar evidence was found for two AGP in *Pinus taeda* (No and Loopstra, 2000), which was likely an effect of growth inhibition induced by drought.

Our results also showed a general downregulation of genes involved in monolignol biosynthesis in both unstressed and water-stressed FS. These results were consistent with previous findings observed during *M. incognita*-tomato interaction (Veronico et al., 2018) where repression of some gene functioning in the core of phenylpropanoid pathway and in lignin biosynthesis was found in galls at 7 dpi. Similarly, a global downregulation of phenylpropanoid pathway was reported in rice (Kyndt et al., 2012) and poplar (Baldacci-Cresp et al., 2016) galls and in micro-dissected GCs in both tomato and Arabidopsis (Portillo et al., 2013). The root-knot nematodes likely repress the host defense mechanism to facilitate infection and to establish appropriate gall and GC formation.

Interestingly, our data revealed for the first time an alteration in the expression profiles of most DIR proteins in tomato-*M. incognita* interaction which is likely involved in the production of lignin and lignan (Davin and Lewis, 2000) and therefore participate in plant defense (Paniagua et al., 2017). *DIR* genes were downregulated in response to nematode parasitism and water stress. Considering these results, it is conceivable that DIR proteins could mediate the spatial control of lignin deposition during gall development and in response to water stress.

Dirigent proteins are also required for the correct patterning of lignin deposition in CS (Hosmani et al., 2013), a ring-like cell wall structure in the root endodermis of vascular plants. It is composed of a lignin polymer that is tightly adhered to the plasma membrane and spans the apoplastic space between adjacent endodermal cells. In this way, a barrier that seals the apoplastic pathway in and out of the endodermis is generated and is thus thought to be crucial for selective nutrient uptake, exclusion of pathogens, and many other processes (Enstone et al., 2002). A family of transmembrane proteins called CASPs drives CS formation by accumulating at the appropriate membrane locations (Roppolo et al., 2011). Second-stage endodermis differentiation proceeds with the suberization of entire cell walls where suberin forms a barrier for uptake from the apoplast into the cell interior. In the present study, the expression of many transcript coding for enzymes involved in suberin biosynthesis, including fatty acid hydroxylases, a β-ketoacyl-CoA synthase, fatty acyl-CoA reductases, and long-chain acyl-CoA synthases (data not shown), was activated in tomato upon *M. incognita* parasitism. Meanwhile, expression of genes involved in CS formation was particularly decreased in 14-day-old galls, consistent with what has been found in Arabidopsis by Holbein et al. (2019). Intriguingly, water stress induced a remarkable downregulation of CASP genes from 7 dpi in RKN_WS galls and a concomitant strong activation of genes involved in suberin biosynthesis. These results could reflect changes in root tissues induced by nematodes during various parasitic stages, i.e., endodermis degradation during later stages of FS development and consequent periderm formation (Holbein et al., 2019). However, the sharp downregulation of CASPs at 7 dpi in RKN_WS is a confirmation of how the lignification process is altered by water stress. Therefore, we can speculate that defects in CS formation with simultaneous loss of nutrients could impair nematode development as supported by microscopic observations of smaller FS. In contrast, we found five CASP-like proteins exclusively upregulated in galls of water stressed plants, mainly at 7 dpi. Recent studies revealed that this endodermal barrier can play a central role in mediating signaling to control growth and to respond to external environment (Dinneny, 2014; Vermeer et al., 2014). Therefore, our findings offer cues to further explore the distinguished role of the CS protein family genes in growth, development, and environmental challenges.

Cell Wall Remodeling in Galls Induced by *M. incognita*

Cell growth and expansion of nematode FS are mediated by the upregulation of gene encoding proteins that promote wall loosening, such as expansins, pectate lyases, pectin methylesterases, and glucanases (Griesser and Grundler, 2008; Wieczorek et al., 2014; Shukla et al., 2018). Plant expansins are also implicated in responses to many abiotic stresses, such as drought, salinity, cold, heat, and oxidative stress (Marowa et al., 2016), indicating that these proteins constitute

[11]https://mendel.imp.ac.at/gpi/cgi-bin/gpi_pred_plants.cgi

a common component in the response of plants to stress. They act by weakening the hydrogen bonds between cell wall polysaccharides (McQueen-Mason and Cosgrove, 1994). Our data highlighted the involvement of expansins in the processes that require the expansion and degradation of cell walls. Most gene coding for these proteins were differentially expressed compared to control plants both in unstressed and stressed galls, but mainly in response to nematode parasitism. However, water stress particularly repressed expansin A11 (Solyc04g081870.4.1) and expansin-like B1 (Solyc08g077910.3.1), which were over-expressed in unstressed galls. Interestingly, expansin 1 (Solyc06g051800.3.1), although upregulated upon infection, had a lower level of expression at 7 dpi in stressed galls. Arabidopsis EXPA1 (Jammes et al., 2005) and a poplar homolog to the Arabidopsis *EXPA1* (Baldacci-Cresp et al., 2016) were upregulated during gall development, confirming the hypothesis that these enzymes play a role in the establishment of root-knot nematode parasitism as already suggested in tomato for LeEXPA5 (Gal et al., 2006). In agreement with other plant-microbe interactions (Gal et al., 2006; Dermatsev et al., 2010; Abuqamar et al., 2013), our findings suggest that the decreased expression of some expansin and expansin-like genes could reduce cell wall-loosening activity, resulting in stiffer walls that impede the physical penetration and proliferation of *M. incognita* in tomato.

Likewise, water stress also modified the expression profile of genes involved in the degradation and remodeling of cell wall. In particular, their involvement could be associated with the gall development stage. Although several genes showed the same trend of expression between unstressed and stressed galls, some were specifically up or downregulated by water stress, and this behavior underwent a shift during FS development. Several alterations concerned the genes involved in pectin degradation. Pectins form a hydrated gel, allowing polymer slippage during cell wall growth and facilitate elongation. Interestingly, our findings showed that the gene coding for *pectin acetylesterase* (Solyc08g005800.4.1) and for *pectin methylesterase pmeu1* (Solyc03g123630.4.1), upregulated in FS of normally watered plants, were downregulated in response to water stress. PME3 *Arabidopsis thaliana* mutants overexpressing this gene were more susceptible to the cyst nematode *Heterodera schachtii*, while a knockout mutant showed the opposite effect (Hewezi et al., 2008). Therefore, this allows us to speculate their importance for the establishment of nematode parasitism.

The cell wall of giant cells contains high ester pectic homogalacturonan, xyloglucan, and pectic arabinan (Bozbuga et al., 2018) which are responsible for the flexible properties of FS cell walls. Major cell wall polysaccharides arabinan and arabinoxylan, deriving from arabinose, have an important role in cellular attachment (Iwai et al., 2001) and wall flexibility (Moore et al., 2008). A recent study conducted in young tomato fruit, in which cell wall reconstitution actively occurs, reported an upregulation of α-*l-arabinofuranosidase LeXYL2* (Miyohashi et al., 2021). Authors suggested that this enzyme may contribute to the temporal loosening of the rigid structure that is required for fruit enlargement. We found downregulation of *LEXYL2* in RKN_WS with respect to RKN. Likewise, water stress negatively affected expression of two different genes coding for xyloglucan endotransglucosylase-hydrolases which were upregulated in RKN galls. These enzymes, involved in xyloglucan modification and cell expansion, have also been reported to be upregulated in *Populus-M. incognita* interaction (Baldacci-Cresp et al., 2020). Evidently, water stress modifies processes related to polysaccharide polymerization and/or the mechanism involved in the development of FS where cell enlargement is required. This could explain the changes in the morphology of FS upon water stress.

CONCLUSION

This investigation provides novel insights on how water stress modulated tomato response during nematode FS development. These data highlighted that water stress particularly affects genes involved in cell wall metabolism which are important for the successful establishment of parasitism. These findings offer interesting cues for a better understanding of the role of differentially modulated genes during the formation of *M. incognita* GCs. These genes could be potential targets for biotechnological strategies aimed at providing new varieties resistant to root-knot nematodes.

DATA AVAILABILITY STATEMENT

The original contributions presented in the study are publicly available. This data can be found here: National Center for Biotechnology Information (NCBI) BioProject database under accession number PRJNA734743.

AUTHOR CONTRIBUTIONS

AC, MTM, LR, and PV conceived and designed the research. PV, LR, EF, and MC performed the molecular biology experiments and data analysis. MTM performed the histopathology and morphological analyses. IP carried out the bioinformatics analyses. LR and PV wrote the manuscript. AC, FD, EF, and MTM provided editorial advice and revised the manuscript. All authors read and approved the final manuscript.

FUNDING

This study was partially funded by the AQUA project (Progetto Premiale, Consiglio Nazionale delle Ricerche).

SUPPLEMENTARY MATERIAL

The Supplementary Material for this article can be found online at: https://www.frontiersin.org/articles/10.3389/fpls.2022.817185/full#supplementary-material

REFERENCES

Abuqamar, S., Ajeb, S., Sham, A., Enan, M. R., and Iratni, R. (2013). A mutation in the expansin-like A2 gene enhances resistance to necrotrophic fungi and hypersensivity to abiotic stress in *Arabidopsis thaliana*. *Mol. Plant Pathol.* 14, 813–827. doi: 10.1111/mpp.12049

Asselbergh, B., Curvers, K., Franca, S. C., Audenaert, K., Vuylsteke, M., Van Breusegem, F., et al. (2007). Resistance to Botrytis cinerea in sitiens, an abscisic acid-deficient tomato mutant, involves timely production of hydrogen peroxide and cell wall modifications in the epidermis. *Plant Physiol.* 144, 1863–1877. doi: 10.1104/pp.107.099226

Atkinson, N. J., Liley, C. J., and Urwin, P. E. (2013). Identification of genes involved in the response of *Arabidopsis* to simultaneous biotic and abiotic stresses. *Plant Physiol*. 162, 2028–2041. doi: 10.1104/pp.113.222372

Atkinson, N. J., and Urwin, P. E. (2012). The interaction between plant biotic and abiotic stresses: from genes to the field. *J. Exp. Bot.* 63, 3523–3543. doi: 10.1093/jxb/ers100

Baldacci-Cresp, F., Behr, M., Kohler, A., Badalato, N., Morreel, K., Goeminne, G., et al. (2020). Molecular changes concomitant with vascular system development in mature galls induced by root-knot nematodes in the model tree host *Populus tremula x P. alba*. *Int. J. Mol. Sci.* 21:406. doi: 10.3390/ijms21020406

Baldacci-Cresp, F., Maucourt, M., Deborde, C., Pierre, O., Moing, A., Brouquisse, R., et al. (2015). Maturation of nematode-induced galls in *Medicago truncatula* is related to water status and primary metabolism modifications. *Plant Sci.* 232, 77–85. doi: 10.1016/j.plantsci.2014.12.019

Baldacci-Cresp, F., Sacré, P. Y., Twyffels, L., Mol, A., Vermeersch, M., Ziemons, E., et al. (2016). Poplar root-knot nematode interaction: a model for perennial woody species. *Mol. Plant Microbe Interact.* 29, 560–572. doi: 10.1094/MPMI-01-16-0015-R

Balestrini, R., Rosso, L. C., Veronico, P., Melillo, M. T., De Luca, F., Fanelli, E., et al. (2019). Transcriptomal response to water deficit and nematode infection in mychorrizal tomato roots. *Front. Microbiol.* 10:1807. doi: 10.3389/fmicb.2019.01807

Bozbuga, R., Lilley, C. J., Knox, J. P., and Urwin, P. E. (2018). Host-specific signatures of the cell wall changes induced by the plant parasitic nematode, Meloidogyne incognita. *Sci. Rep.* 8:17302. doi: 10.1038/s41598-018-35529-7

Chen, Z., Hong, X., Zhang, H., Wang, Y., Li, X., Zhu, J. K., et al. (2005). Disruption of the cellulose synthase gene, AtCesA8/IRX1, enhances drought and osmotic stress tolerance in *Arabidopsis*. *Plant J.* 43, 273–283. doi: 10.1111/j.1365-313X.2005.02452.x

Cho, S. K., Kim, J. E., Park, J.-A., Eom, T. J., and Kim, W. T. (2006). Constitutive expression of abiotic stress-inducible hot pepper CaXTH3, which encodes a xyloglucan endotransglucosylase/hydrolase homolog, improves drought and salt tolerance in transgenic Arabidopsis plants. *FEBS Lett.* 580, 3136–3144. doi: 10.1016/j.febslet.2006.04.062

Choe, S., ChoI, B., Kang, J. H., and Seo, J. K. (2021). Tolerance to tomato yellow leaf curl virus in transgenic tomato overexpressing a cellulose synthase–like gene. *Plant Biotechnol. J.* 19, 657–659. doi: 10.1111/pbi.13539

Choi, J. Y., Seo, Y. S., Kim, S. J., Kim, W. T., and Shin, J. S. (2011). Constitutive expression of CaXTH3, a hot pepper xyloglucan endotransglucosylase/hydrolase, enhanced tolerance to salt and drought stresses without phenotypic defects in tomato plants (Solanum lycopersicum cv. Dotaerang). *Plant Cell Rep.* 30, 867–877. doi: 10.1007/s00299-010-0989-3

Cohen, A., Moses, M. S., Plant, A. L., and Bray, E. A. (1999). Multiple mechanisms control the expression of abscisic acid (ABA)-requiring genes in tomato plants exposed to soil water deficit. *Plant Cell Environ.* 22, 989–998. doi: 10.1046/j.1365-3040.1999.00474.x

Cutler, S. R., Rodriguez, P. L., Finkelstein, R. R., and Abrams, S. R. (2010). Abscisic acid: emergence of a core signalling network. *Annu. Rev. Plant Biol.* 61, 651–679. doi: 10.1146/annurev-arplant-042809-112122

Davin, L. B., and Lewis, N. G. (2000). Dirigent proteins and dirigent sites explain the mystery of specificity of radical precursor coupling in lignan and lignin biosynthesis. *Plant Physiol.* 123, 453–461. doi: 10.1104/pp.123.2.453

Dermatsev, V., Weingarten-Baror, C., Resnick, N., Gadkar, V., Wininger, S., Kolotilin, I., et al. (2010). Microarray analysis and functional tests suggest the involvement of expansins in the early stages of symbiosis of the mychorrizal fungus *Glomus intraradices* on tomato (*Solanum lycopersicon*). *Mol. Plant Pathol.* 11, 121–135. doi: 10.1111/j.1364-3703.2009.00581.x

Dinneny, J. R. (2014). A gateway with a guard: how the endodermis regulated growth through hormone signalling. *Plant Sci.* 214, 14–19. doi: 10.1016/j.plantsci.2013.09.009

Enstone, D. E., Peterson, C. A., and Ma, F. S. (2002). Root endodermis and exodermis: Structure, function, and responses to the environment. *J. Plant Growth Reg.* 21, 335–351. doi: 10.1007/s00344-003-0002-2

Fujita, Y., Fujita, M., Shinozaki, K., and Yamaguchi-Shinozaki, K. (2011). ABA-mediated transcriptional regulation in response to osmotic stress in plants. *J Plant Res.* 124, 509–525. doi: 10.1007/s10265-011-0412-3

Gal, T. Z., Aussenberg, E. R., Burdman, S., KapulniK, Y., and Koltai, H. (2006). Expression of a plant expansin is involved in the establishment of root-knot nematode parasitism in tomato. *Planta* 224, 155–162. doi: 10.1007/s00425-005-0204-x

Gheysen, G., and Mitchum, M. G. (2009). "Molecular insights in susceptible plant response to nematode infection," in *Plant Cell Monographs-Cell Biology of Plant Nematode Parasitism*, eds R. H. Berg and C. G. Taylor (Berlin: Springer), 45–81. doi: 10.1007/978-3-540-85215-5_3

Gheysen, G., and Mitchum, M. G. (2011). How nematodes manipulate plant development pathways for infection. *Curr. Opin. Plant Biol.* 14, 415–421. doi: 10.1016/j.pbi.2011.03.012

Gillmor, C. S., Lukowitz, W., Brininstool, G., Sedbrook, J. C., Hamann, T., Poindexter, P., et al. (2005). Glycosylphosphatidylinositol-anchored proteins are required for cell wall synthesis and morphogenesis in Arabidopsis. *Plant Cell* 17, 1128–1140. doi: 10.1105/tpc.105.031815

Gimeno-Gilles, C., Lelievre, E., Viau, L., Malik-Ghulama, M., Ricoult, C., Niebel, A., et al. (2009). ABA-mediated inhibition of germination is related to the inhibition of genes encoding cell-wall biosynthetic and architecture: modifying enzymes and structural proteins in *Medicago truncatula* embryo axis. *Mol. Plant* 2, 108–119. doi: 10.1093/mp/ssn092

Gong, P., Zhang, J., Li, H., Yang, C., Zhang, C., Zhang, X., et al. (2010). Transcriptional profiles of drought-responsive genes in modulating transcription signal transduction, and biochemical pathways in tomato. *J. Exp. Bot.* 61, 3563–3575. doi: 10.1093/jxb/erq167

Griesser, M., and Grundler, F. M. W. (2008). Quantification of tomato expansins in nematode feeding sites of cyst and root-knot nematodes. *J. Plant Dis. Protect.* 115, 263–272. doi: 10.1007/bf03356275

Guo, W., Zhao, J., Li, X., Qin, L., Yan, X., and Liao, H. (2011). A soybean β-expansin gene GmEXPB2 intrinsically involved in root system architecture responses to abiotic stresses. *Plant J.* 66, 541–552. doi: 10.1111/j.1365-313X.2011.04511.x

Hammer, Ø, Harper, D. A. T., and Ryan, P. D. (2001). PAST: Paleontological statistics software package for education and data analysis. *Palaeontol. Electron* 4:9.

Hewezi, T., Howe, P., Maier, T. R., Hussey, R. S., Goellner Mitchum, M., Davis, E. L., et al. (2008). Cellulose binding protein from the parasitic nematode *Heterodera schachtii* interacts with Arabidopsis pectin methylesterase: Cooperative cell wall modification during parasitism. *Plant Cell* 20, 3080–3093. doi: 10.1105/tpc.108.063065

Holbein, J., Franke, R. B., Marhavı, P., Fujita, S., Górecka, M., Sobczak, M., et al. (2019). Root endodermal barrier system contribute to defence against plant-parasitic cyst and root-knot nematodes. *Plant J.* 100, 221–236. doi: 10.1111/tpj.14459

Hosmani, P. S., Kamiya, T., Danku, J., Naseer, S., Geldner, N., Guerinot, M. L., et al. (2013). Dirigent domain-containing protein is part of the machinery required for formation of the lignin-based Casparian strip in the root. *Proc. Natl. Acad. Sci.* 110, 1498–1503. doi: 10.1073/pnas.1308412110

Houston, K., Tucker, M. R., Chowdhury, J., Shirley, N., and Little, A. (2016). The plant cell wall: a complex and dynamic structure as revealed by the responses of genes under stress conditions. *Front. Plant Sci.* 7:984. doi: 10.3389/fpls.2016.00984

Huang, G. Q., Gong, S. Y., Xu, W. L., Li, W., Li, P., Zhang, C. J., et al. (2013). A fasciclin-like arabinogalactan protein, GhFla1, is involved in fiber initiation and elongation of cotton. *Plant Physiol.* 161, 1278–1290. doi: 10.1104/pp.112.203760

Hughes, J., and McCully, M. E. (1975). The use of an optical brightener in the study of plant structure. *Stain Technol.* 50, 319–329. doi: 10.3109/10520297509117082

Iwai, H., Ishii, T., and Satoh, S. (2001). Absence of arabinan in the side chains of the pectic polysaccharides strongly associated with cell walls of *Nicotiana*

plumbaginifolia nonorganogenic callus with loosely attached constituent cells. *Planta* 213, 907–915. doi: 10.1007/s004250100559

Jammes, F., Lecomte, P., de Almeida-Engler, J., Bitton, F., Martin-Magniette, M. L., Renou, J. P., et al. (2005). Genome-wide expression profiling of the host response to root-knot nematode infection in *Arabidopsis*. *Plant J*. 44, 447–458. doi: 10.1111/j.1365-313X.2005.02532.x

Johnson, K. L., Jones, B. J., Bacic, A., and Shultz, C. J. (2003). The fasciclin-like arabinogalactan proteins of Arabidopsis. A multigene family of putative cell adhesion molecules. *Plant Physiol.* 133, 1911–1925. doi: 10.1104/pp.103.031237

Karimi, M., Van Montagu, M., and Gheysen, G. (1995). Exogenous application of abscisic acid to potato plants suppresses reproduction of *Meloidogyne incognita*. *Mededelingen van de Faculteit Landbouwkundige en Toegepaste Biologische Wetenschappen, Universiteit Gent* 60, 1033–1035.

Kissoudis, C., Sunarti, S., Van de Wiel, C., Visser, R. G. F., van der Linden, C. G., and Bai, Y. (2016). Responses to combined abiotic and biotic stress in tomato are governed by stress intensity and resistance mechanism. *J. Exp. Bot*. 67, 5119–5132. doi: 10.1093/jxb/erw285

Kitin, P., Nakaba, S., Hunt, C. G., Lim, S., and Funada, R. (2020). Direct fluorescence imaging of lignocellulosic and suberized cell walls in roots and stems. *AoB Plants* 12:19. doi: 10.1093/aobpla/plaa032

Kyndt, T., Nahar, K., Haegeman, A., De Vleesschauwer, D., Hofte, M., and Gheysen, G. (2012). Comparing systemic defence-related gene expression changes upon migratory and sedentary nematode attack in rice. *Plant Biol.* 14, 73–82.

Kyndt, T., Vieira, P., Gheysen, G., and De Almeida-Engler, J. (2013). Nematode feeding sites: unique organs in plant roots. *Planta* 238, 807–818. doi: 10.1007/s00425-013-1923-z

Lamers, J., van der Meer, T., and Testerink, C. (2020). How plants sense and respond to stressful environments. *Plant Physiol.* 182, 1624–1635. doi: 10.1104/pp.19.01464

Le Gall, H., Philippe, F., Domon, J. M., Gillet, F., Pelloux, J., and Rayon, C. (2015). Cell wall metabolism in response to abiotic stress. *Plants* 4, 112–166. doi: 10.3390/plants4010112

Liu, L., Shang-Guan, K., Zhang, B., Liu, X., Yan, M., Zhang, L., et al. (2013). Brittle Culm1, a COBRA-like protein, functions in cellulose assembly through binding cellulose microfibrils. *PLoS Genet.* 9:e1003704. doi: 10.1371/journal.pgen.1003704

Liu, C., Yu, H., Rao, X., Li, L., and Dixon, R. A. (2021). Abscisic acid regulates secondary cell-wall formation and lignin deposition in *Arabidopsis thaliana* through phosphorylation of NST1. *Proc. Natl. Acad. Sci* 118:e2010911118. doi: 10.1073/pnas.2010911118

Liu, Y., Zhang, L., Hao, W., Zhang, L., Liu, Y., and Chen, L. (2019). Expression of two α-type expansins from *Ammopiptanthus nanus* in *Arabidopsis thaliana* enhance tolerance to cold and drought stresses. *Int. J. Mol. Sci.* 20:5255. doi: 10.3390/ijms20215255

Marowa, P., Ding, A., and Kong, Y. (2016). Expansins: roles in plant growth and potential applications in crop improvement. *Plant Cell Rep.* 35, 949–965. doi: 10.1007/s00299-016-1948-4

McQueen-Mason, S. J., and Cosgrove, D. J. (1994). Disruption of hydrogen-bonding between plant cell wall polymers by proteins that induce wall extension. *Proc. Natl. Acad. Sci. USA*. 91, 6574–6578. doi: 10.1073/pnas.91.14.6574

Melillo, M. T., Leonetti, P., and Veronico, P. (2014). Benzothiadiazole effect in the compatible tomato-*Meloidogyne incognita* interaction: changes in giant cell development and priming of two root anionic peroxidases. *Planta* 240, 841–854. doi: 10.1007/s00425-014-2138-7

Miyohashi, F., Yukihisa, S., Kaminishi, A., Soga, A., Yoshida, M., Kamiyoshihara, Y., et al. (2021). Expression of α-L-Arabinofuranosidase Genes at Ripening Initiation Potentially Contributes to the Difference in Flesh Juiciness Between Processing and Fresh Tomatoes. *Hortic. J.* 90, 130–137. doi: 10.2503/hortj.UTD-218

Moore, J. P., Farrant, J. M., and Driouich, A. (2008). A role for pectin-associated arabinans in maintaining the flexibility of the plant cell wall during water deficit stress. *Plant Signal. Behav*. 3, 102–104. doi: 10.4161/psb.3.2.4959

Mortazavi, A., Williams, B. A., McCue, K., Schaeffer, L., and Wold, B. (2008). Mapping and quantifying mammalian transcriptomes by RNA-Seq. Nat. Methods 5, 621–628. doi: 10.1038/nmeth.1226

Nahar, K., Kyndt, T., Nzogela, Y. B., and Gheysen, G. (2012). Abscisic acid interacts antagonistically with classical defence pathways in rice–migratory nematode interaction. *New Phytol.* 196, 901–913. doi: 10.1111/j.1469-8137.2012.04310.x

No, E. G., and Loopstra, C. A. (2000). Hormonal and developmental regulation of two arabinogalactan-proteins in xylem of loblolly pine (*Pinus taeda*). *Physiol. Plant*. 110, 524–529. doi: 10.1111/j.1399-3054.2000.1100415.x

Paniagua, C., Bilkova, A., Jackson, P., Dabravolski, S., Riber, W., Didi, V., et al. (2017). Dirigent proteins in plants: modulating cell wall metabolism during abiotic and biotic stress exposure. *J. Exp. Bot.* 68, 3287–3301. doi: 10.1093/jxb/erx141

Portillo, M., Topping, J., Emiliozzi, M., Solano, R., Resnick, N., García-Casado, G., et al. (2013). Distinct and conserved transcriptomic changes during nematode-induced giant cell development in tomato compared with Arabidopsis: a functional role for gene repression. *New Phytol.* 197, 1276–1290.

Ramegowda, V., and Senthyl-Kumar, M. (2015). The interactive effects of simultaneous biotic and abiotic stresses on plants: Mechanistic understanding from drought and pathogen combination. *J. Plant Physiol.* 176, 47–54. doi: 10.1016/j.jplph.2014.11.008

Ricardi, M. M., Gonzales, R. M., Zhong, S., Dominguez, P. G., Duffy, T., Turjansky, P. G., et al. (2014). Genome-wide data (ChIP-seq) enabled identification of cell wall-related and aquaporin genes as targets of tomato ASR1, a drought stress-responsive transcription factor. *BMC Plant Biol*. 14:29. doi: 10.1186/1471-2229-14-29

Rodiuc, N., Vieira, P., Banora, M. Y., and Engler, J. D. (2014). On the track of transfer cell formation by specialized plant-parasitic nematodes. *Front. Plant Sci*. 5:160. doi: 10.3389/fpls.2014.00160

Roppolo, D., De Rybel, B., Tendon, V. D., Pfister, A., Alassimone, J., Vermeer, J. E. M., et al. (2011). A novel protein family mediates Casparian strip formation in the endodermis. *Nature* 473, 380–383. doi: 10.1038/nature10070

Roudier, F., Fernandez, A. G., Fujita, M., Himmelspach, R., Borner, G. H., Schindelman, G., et al. (2005). COBRA, an Arabidopsis extracellular glycosyl-phosphatidyl inositol-anchored protein, specifically controls highly anisotropic expansion through its involvement in cellulose microfibril orientation. *Plant Cell* 17, 1749–1763. doi: 10.1105/tpc.105.031732

Schachtman, D. P., and Goodger, Q. D. (2008). Chemical Root to Shoot Signaling under Drought. *Trends Plant Sci.* 13, 281–287. doi: 10.1016/j.tplants.2008.04.003

Schindelman, G., Morikami, A., Jung, J., Baskin, T. I., Carpita, N. C., Derbyshire, P., et al. (2001). COBRA encodes a putative GPI-anchored protein, which is polarly localized and necessary for oriented cell expansion in Arabidopsis. *Genes Dev.* 15, 1115–1127. doi: 10.1101/gad.879101

Sharp, R. E., and Davies, W. J. (1989). "Regulation of growth and development of plants growing with a restricted supply of water," in *Plants Under Stress*, eds H. G. Jones, T. J. Flowers, and M. B. Jones (Cambridge, UK: Cambridge University Press), 71–93. doi: 10.1017/cbo9780511661587.006

Shukla, N., Yadav, R., Kaur, P., Rasmussen, S., Goel, S., Agarwal, M., et al. (2018). Transcriptome analysis of root-knot nematode (*Meloidogyne incognita*)-infected tomato (*Solanum lycopersicum*) roots reveals complex gene expression profiles and metabolic networks of both host and nematode during susceptible and resistance responses. *Mol. Plant Pathol.* 19, 615–633. doi: 10.1111/mpp.12547

Sobczak, M., Fudali-Alves, S. L., and Wieczorek, K. (2011). "Cell wall modifications induced by nematodes," in *Genomics and Molecular Genetics of Plant-Nematode Interactions*, eds J. Jones, G. Gheysen, and C. Fenoll (Dordrecht: Springer). 19, 395–422. doi: 10.1007/978-94-007-0434-3_19

Suzuki, N., Rivero, R. M., Shulaev, V., Blumwald, E., and Mittler, R. (2014). Abiotic and biotic stress combinations. *New Phytol.* 203, 32–43.

Tian, T., Yue, L., Hengyu, Y., Qi, Y., Xin, Y., Zhou, D., et al. (2017). agriGO v2.0: a GO analysis toolkit for the agricultural community, 2017 update. *Nucleic Acids Res*. 45, W122–W129. doi: 10.1093/nar/gkx382

Ton, J., Flors, V., and Mauch-Mani, B. (2009). The multifaceted role of ABA in disease resistance. *Trends Plant Sci.* 14, 310–317. doi: 10.1016/j.tplants.2009.03.006

Underwood, W. (2012). The plant cell wall: a dynamic barrier against pathogen invasion. *Front. Plant Sci.* 3:85. doi: 10.3389/fpls.2012.00085

Vermeer, J. E. M., von Wangenheim, D., Barberon, M., Lee, Y., Stelzer, E. H. K., Maizel, A., et al. (2014). A spatial accommodation by neighboring cell is required for organ initiation in *Arabidopsis*. *Science* 343, 178–183. doi: 10.1126/science.1245871

Veronico, P., Paciolla, C., Pomar, F., De Leonardis, S., Garcìa-Ulloa, A., and Melillo, M. T. (2018). Changes in lignin biosynthesis and monomer composition in response to benzothiadiazole and *Meloidogyne incognita* infection in tomato. *J. Plant Physiol.* 230, 40–50. doi: 10.1016/j.jplph.2018.07.013

Volpe, V., Chitarra, W., Cascone, P., Volpe, M. G., Bartolini, P., Moneti, G., et al. (2018). The association with two different arbuscular mycorrhizal fungi differently affects water stress tolerance in tomato. *Front. Plant Sci.* 9:1480. doi: 10.3389/fpls.2018.01480

Wang, H., Jiang, C., Wang, C., Yang, Y., Yang, L., Gao, X., et al. (2015). Antisense expression of the fasciclin-like arabinogalactan protein FLA6 gene in *Populus* inhibits expression of its homologous genes and alters stem biomechanics and cell wall composition in transgenic trees. *J. Exp. Bot.* 66, 1291–1302. doi: 10.1093/jxb/eru479

Wagner, G. P., Kin, K., and Lynch, V. J. (2012). Measurement of mRNA abundance using RNA-seq data: RPKM measure is inconsistent among samples. Theory Biosci. 131, 281–285. doi: 10.1007/s12064-012-0162-3

Wieczorek, K., El-Ashry, A., Quentin, M., Grundler, F. M. W., Favery, B., Seifert, G. J., et al. (2014). A distinct role of pectate lyases in the formation of feeding structures induced by cyst and root-knot nematodes. *Mol. Plant Microbe. Interact.* 27, 901–912. doi: 10.1094/MPMI-01-14-0005-R

Wormit, A., and Usadel, B. (2018). The multifaceted role of pectin methylesterase inhibitors (PMEIs). *Int. J. Mol. Sci.* 19:2878. doi: 10.3390/ijms19102878

Wu, X., Lai, Y., Lv, L., Ji, M., Han, K., Yan, D., et al. (2020). Fasciclin-like arabinogalactan gene family in *Nicotiana benthamiana*: genome-wide identification, classification and expression in response to pathogens. *BMC Plant Biol.* 20:305. doi: 10.1186/s12870-020-02501-5

Xiong, L., and Zhu, J. K. (2003). Regulation of abscisic acid biosynthesis. *Plant Physiol.* 133, 29–36. doi: 10.1104/pp.103.025395

Xu, Q., Xu, X., Shi, Y., Xu, J., and Huang, B. (2014). Transgenic tobacco plants overexpressing a grass PpEXP1 gene exhibit enhanced tolerance to heat stress. *PLoS One* 9:e100792. doi: 10.1371/journal.pone.0100792

Yu, D., Janz, D., Zienkiewicz, K., Herrfurth, C., Feussner, I., Chen, S., et al. (2021). Wood formation under severe drought invokes adjustment of the hormonal and transcriptional landscape in poplar. *Int. J. Mol. Sci.* 22:9899. doi: 10.3390/ijms22189899

Conflict of Interest: The authors declare that the research was conducted in the absence of any commercial or financial relationships that could be construed as a potential conflict of interest.

Publisher's Note: All claims expressed in this article are solely those of the authors and do not necessarily represent those of their affiliated organizations, or those of the publisher, the editors and the reviewers. Any product that may be evaluated in this article, or claim that may be made by its manufacturer, is not guaranteed or endorsed by the publisher.

frontiers | Frontiers in Plant Science

ORIGINAL RESEARCH
published: 06 May 2022
doi: 10.3389/fpls.2022.880600

Comparative Transcriptomics Analysis of the Symbiotic Germination of *D. officinale* (Orchidaceae) With Emphasis on Plant Cell Wall Modification and Cell Wall-Degrading Enzymes

Juan Chen[1], *Yanjing Tang*[1], *Annegret Kohler*[2], *Annie Lebreton*[2], *Yongmei Xing*[1], *Dongyu Zhou*[1], *Yang Li*[1], *Francis M. Martin*[2]* *and Shunxing Guo*[1]*

[1] *Key Laboratory of Bioactive Substances and Resource Utilization of Chinese Herbal Medicine, Ministry of Education, Institute of Medicinal Plant Development, Chinese Academy of Medical Sciences and Peking Union Medical College, Beijing, China,* [2] *Université de Lorraine, INRAE, UMR Interactions Arbres/Microorganismes, INRAE Grand Est - Nancy, Champenoux, France*

OPEN ACCESS

Edited by:
Raffaella Balestrini, National Research Council (CNR), Italy

Reviewed by:
Luca Nerva, Council for Agricultural and Economics Research (CREA), Italy
Silvia Perotto, University of Turin, Italy

***Correspondence:**
Francis M. Martin
francis.martin@inrae.fr
Shunxing Guo
sxguo1986@163.com

Specialty section:
This article was submitted to Plant Symbiotic Interactions, a section of the journal Frontiers in Plant Science

Received: *21 February 2022*
Accepted: *04 April 2022*
Published: *06 May 2022*

Citation:
Chen J, Tang Y, Kohler A, Lebreton A, Xing Y, Zhou D, Li Y, Martin FM and Guo S (2022) Comparative Transcriptomics Analysis of the Symbiotic Germination of D. officinale (Orchidaceae) With Emphasis on Plant Cell Wall Modification and Cell Wall-Degrading Enzymes. Front. Plant Sci. 13:880600. doi: 10.3389/fpls.2022.880600

Orchid seed germination in nature is an extremely complex physiological and ecological process involving seed development and mutualistic interactions with a restricted range of compatible mycorrhizal fungi. The impact of the fungal species' partner on the orchids' transcriptomic and metabolic response is still unknown. In this study, we performed a comparative transcriptomic analysis between symbiotic and asymbiotic germination at three developmental stages based on two distinct fungi (*Tulasnella* sp. and *Serendipita* sp.) inoculated to the same host plant, *Dendrobium officinale*. Differentially expressed genes (DEGs) encoding important structural proteins of the host plant cell wall were identified, such as epidermis-specific secreted glycoprotein, proline-rich receptor-like protein, and leucine-rich repeat (LRR) extensin-like protein. These DEGs were significantly upregulated in the symbiotic germination stages and especially in the protocorm stage (stage 3) and seedling stage (stage 4). Differentially expressed carbohydrate-active enzymes (CAZymes) in symbiotic fungal mycelium were observed, they represented 66 out of the 266 and 99 out of the 270 CAZymes annotated in *Tulasnella* sp. and *Serendipita* sp., respectively. These genes were speculated to be involved in the reduction of plant immune response, successful colonization by fungi, or recognition of mycorrhizal fungi during symbiotic germination of orchid seed. Our study provides important data to further explore the molecular mechanism of symbiotic germination and orchid mycorrhiza and contribute to a better understanding of orchid seed biology.

Keywords: comparative transcriptome, *Tulasnella* sp., *Serendipita* sp., CAZymes, symbiotic germination

INTRODUCTION

On Earth, ∼90% of angiosperm plants can form a mycorrhizal symbiosis with more than 50,000 fungal species belonging to Ascomycota, Basidiomycota, Glomeromycotina and Mucoromycotina (Bruns et al., 2018; Tedersoo et al., 2020). The most ubiquitous mycorrhizal type are arbuscular mycorrhizae (AM, 72%), orchid mycorrhizae (ORM, 10%), ectomycorrhizae (ECM, 2%), and ericoid mycorrhizal (ERM, 1.4%) (Genre et al., 2020). Similar to ancient AM, the orchid mycorrhiza also partakes in endosymbioses with specific intracellular structures, but orchid plants have lost the ability to form arbuscular mycorrhizal symbiosis and represent clear symbiosis switches that have occurred during plant evolution (Radhakrishnan et al., 2020). Orchid mycorrhizal fungi transfer carbohydrates to their hosts, especially during the early germination and seedling stages, whereas other types of mycorrhizal fungi (e.g., AM) primarily transport inorganic matter to host plants (Cameron et al., 2006; Parniske, 2008).

Because of their highly ornamental and medicinal value, orchid plants around the world are facing serious extinction so there is an urgent need to conserve them. The *Dendrobium* genus is one of the largest genera in the orchid family, and many species, such as *Dendrobium officinale,* are traditionally used in Chinese medicine. Orchid seeds generally lack endosperm and rely on mycorrhizal fungi to provide essential nutrients for germination, protocorm growth, and even adult plant development (Rasmussen et al., 2015). Most studies indicate that symbiotic germination is an effective technique for orchid conservation and ecological restoration in natural habitats (Phillips et al., 2020; Shao et al., 2021). In recent years, a large number of orchid mycobionts have been identified worldwide. These identifications, mainly based on molecular biology approaches such as high-throughput sequencing, have shown that the diversity and composition of orchid mycorrhizal fungi are related to plant species, geographical distribution, nutrition type, ecotype, and even developmental stage (Xing et al., 2015; Jacquemyn et al., 2017; Freestone et al., 2021). The most common orchid mycorrhizal fungi are saprotrophic basidiomycetes of the Ceratobasidiaceae, Tulasnellaceae, and Serendipitaceae families, which were previously assigned to asexual rhizoctonias (Rasmussen, 2002; Dearnaley, 2007; Smith and Read, 2008; Li et al., 2021). Yet, many mycoheterotrophic orchids have been reported to be associated with ectomycorrhizal fungi (Taylor and Bruns, 1997; Suetsugu et al., 2020). Some orchids are associated with root endophytes (Selosse et al., 2021). Although great progress has been made on the mycorrhizal diversity, specificity, and ecological dynamics of orchid-fungal association, orchids and their mycorrhizal partner are underexplored compared to the well-studied AM and ECM (Jacquemyn et al., 2015; McCormick et al., 2018; Li et al., 2021; Ventre Lespiaucq et al., 2021; Wang et al., 2021). Several important works have tried to elucidate the morphological and metabolic changes during the symbiotic process (Smith and Read, 2008; Ghirardo et al., 2020), nutrients exchange (Bougoure et al., 2010; Kuga et al., 2014; Dearnaley and Cameron, 2017; Suetsugu et al., 2020), genes or proteins expression (Balestrini et al., 2014; Perotto et al., 2014; Chen et al., 2017, 2020; Fochi et al., 2017; Adamo et al., 2020; Favre-Godal et al., 2020; Valadares et al., 2021) and common and unique trait of mycorrhizal symbiosis (Genre et al., 2020). Recently, the expression analysis of calcium and calmodulin-dependent protein kinase gene CCaMK, homologs of AM-related genes in orchids, suggested orchids possess, at least in part, the molecular mechanisms common to AM plants (Miura et al., 2018). However, the orchid mycorrhizal process was speculated to have unique characteristics due to the different taxonomic and genetic features of the partners. Thus, additional work is needed to fully understand orchid mycorrhizal biology.

The germination of orchid seeds is extremely complex as they are obligated to associate with mycorrhizal fungi for carbon source supply and are moreover influenced by abiotic factors. Although the fungal function for nutrition supply to the seed germination has been speculated and verified in early studies (Smith and Read, 2008), little information regarding the symbiotic molecular mechanism, especially in the establishment of symbiotic processes and functional pathways, is available. Before mycorrhizal fungi reach their full symbiotic functionality (to stimulate seed germination), the penetration and development of an extensive contact surface between the plant and fungal cells are essential, as this is where the transport and exchange of nutrients occur between plant cells and fungi take place (Balestrini and Bonfante, 2014; Rich et al., 2014). It has been demonstrated that high carbon transfer occurs in the interface between host roots and the AM fungal partner (Vandenkoornhuyse et al., 2007) and recently, a sucrose transporter has been documented to mediate sucrose import at the symbiotic interface for carbon allocation of heterotrophic *Gastrodia elata* with *Armillaria* (Ho-Pl Garo et al., 2021). Plant cell walls are thought to play a central role in mycorrhizal symbiosis. It was confirmed that the penetration of the fungus into the cortical cell of the orchid triggers the change of the plant's cytoskeleton (Uetake et al., 1996). The actin cytoskeleton also undergoes major modifications in cortical cells and the dynamic of the cytoskeleton in orchid mycorrhizal protocorms has been described in detail in early studies (Uetake and Peterson, 1998). Moreover, observations and immunolocalization by electron microscopy indicated that components such as xyloglucans, proteins rich in hydroxyproline (HRGPs), and arabinogalactan proteins (AGPs) are localized in the cell wall and interfacial matrix near the fungal cell wall during fungal colonization in the embryonic cells of orchid seeds (Li et al., 2018).

Moreover, increasing comparative genomics analysis of mycorrhizal and saprophytic fungi have attempted to create toolkits of mycorrhizal symbiosis from a fungal perspective. Large-scale genome sequencing of fungi of different lifestyles, including mycorrhizal fungi and saprotrophic, endophytic, and pathogenic species, has also demonstrated that the transition of fungal lifestyles from saprophyte to symbiosis involves widespread losses of lignin- and cellulose-acting degrading enzymes and the diversification of novel lineage-specific genes induced by symbiosis (Kohler et al., 2015; Miyauchi et al., 2020). However, orchid mycobionts in Tulasnellaceae, Serendipitaceae, and Ceratobasidiaceae possess large sets of carbohydrate-active enzymes (CAZymes) acting on cellulose, hemicellulose,

and pectins that support their saprotrophic ability (transfer carbohydrates to their hosts), especially during the early stage of seed germination; thus, the nutritional strategies of orchid plant and the characteristics of their mycorrhizal fungi likely dictate to some extent the specificity for symbiotic association (Miyauchi et al., 2020).

During fungal colonization in orchid seeds or roots, fungal hyphae must penetrate into the cell walls of the epidermis or root hairs to enter cortical cells (Chen et al., 2014; Favre-Godal et al., 2020). Meanwhile, fungi release a wide range of extracellular enzymes to degrade plant cell walls (e.g., CAZy glycoside hydrolases, GH families) or secrete effector proteins to inhibit plant defense and help them achieve successful colonization (e.g., Small Secreted proteins, SSPs) (Pellegrin et al., 2015; Feldman et al., 2020; Tanaka and Kahmann, 2021). Furthermore, several SSPs have been identified as fungal effectors that play key roles in ECM, AM, and EM symbiosis (Plett et al., 2014; Casarrubia et al., 2018; Zeng et al., 2020). Recently, Adamo et al. (2020) attempted to elucidate the behavior of saprotrophic fungi in orchid mycorrhiza from expression changes of the fungal genes encoding degrading enzymes of the plant cell wall (PCW) between saprotrophic growth and mycorrhizal symbiosis of *Tulasnella calospora* and suggesting fungal PCW-degrading enzymes is finely regulated during saprotrophic growth and in symbiosis, often with a different regulation in the two orchid species. Thus, the role of the fungal PCW degrading enzymes in orchid symbiotic interactions are need to be addressed furtherly.

Thus, to further investigate the molecular responses of plants to mycorrhizal fungal colonization during the symbiotic germination of orchid seeds, we performed a comparative transcriptomic analysis between symbiotic and asymbiotic germination trials at three developmental stages based on two different fungi (*Tulasnella* sp. or *Serendipita* sp.), which were inoculated on the same host plant. We emphasize (i) plant gene expression changes related to plant cell wall biosynthesis, and structure modification, as well as (ii) the expression profile of fungal genes related to plant/fungal cell wall degradation (i.e., CAZymes). We aimed to (1) understand the molecular responses at the transcriptional level of *D. officinale* seeds after inoculation with two different fungal species and identify the core plant and fungal gene sets involved in symbiotic germination and (2) analyze the possible role of fungal genes encoding CAZymes which are known to be important for AM and ECM mycorrhizal establishment in orchid mycorrhizae.

MATERIALS AND METHODS

Seed Sample Collection

Mature and indehiscent *D. officinale* capsules were collected from an artificial cultivation greenhouse in Jinhua, Zhejiang Province, in November 2018. The obtained capsules were dried naturally at room temperature (25°C) for ∼1 week. Next, seeds were cleaned from capsule debris, mixed, and stored in wax paper on silica gel at 4°C. Two mycorrhizal fungi, *Tulasnella* sp. (strain no. S6) and *Serendipita* sp. (strain no. 12825), were isolated from the roots of *Dendrobium* spp. and deposited in the Institute of Medicinal Plant Development, Chinese Academy of Medical Science. Free-living mycelium was cultivated on a PDA medium at 25°C in the dark.

Seed Germination Experiments

The seed germination experiment was designed as shown in **Figure 1**. Before sowing, the seeds were immersed in sterile water and allowed to stand for 1–2 h. Seeds in the bottom of the tube were chosen for subsequent experiments. First, the seeds were surface sterilized in 1% NaClO for 3 min, rinsed three times, and diluted with sterile water into a suitable seed suspension for sowing. For symbiotic germination, 400 μL of seed suspension was dispensed with a pipette onto a square of autoclaved nylon cloth (4 × 4 cm) on oatmeal agar plates (OMA, 0.25% oatmeal, and 1% agar, 20 ml in total) in a 9 cm petri dish, and then four 5 × 5 mm inocula of *Tulasnella* sp. S6 (or *Serendipita* sp. 12825) on PDA medium were placed in each OMA for coculture. For asymbiotic germination, only 400 μL of seed suspension was dropped onto the 1/2 MS culture medium. Plates were incubated at 25°C with a 12 h/12 h light-dark cycle. Seed germination and protocorm development were evaluated under a dissecting stereomicroscope every 2 days. The seed developmental stages were defined according to the previous study by Stewart and Zettler (2002).

Total RNA Extraction, Library Preparation, and Sequencing

Symbiotic (with *Tulasnella* sp. or *Serendipita* sp.), asymbiotic germination seeds at stage 2 (germination), stage 3 (protocorm), stage 4 (seedling), and free-living mycelium of both fungi were collected either immediately frozen in liquid nitrogen or stored at −80°C for RNA extraction. There are three biological replicates for each sample. Total RNA of 11 samples including three samples for asymbiotic, three symbiotic samples with *Tulasnella*, three symbiotic samples with *Serendipita* (stages 2, 3, and 4, respectively), and two free-living mycelium fungal samples *Tulasnella* sp. and *Serendipita* sp., respectively) was extracted using the RNeasy Plant Mini Kit (QIAGEN, Hilden, Germany), and the quality, integrity, and quantification of RNA were assessed following our previous study (Chen et al., 2017). Finally, 2 μg of high-quality total RNA (RNA Quality number, RON > 7) was used for stranded RNA sequencing library preparation. The library was constructed using a KC-Digital TM Stranded mRNA-seq Library Prep Kit for Illumina® (Kangce Technology Co., LTD, Wuhan, China) following the manufacturer's instructions. Duplication bias in PCR and sequencing steps were eliminated using a unique molecular identifier (UMI) of 8 random bases to label the preamplified cDNA molecules with this kit. The library products corresponding to 200–500 bps were enriched, quantified, and finally sequenced on an Illumina HiSeq 2500 sequencer (Illumina, San Diego CA, USA) using the paired-end (PE) 150 strategy (Kangce Technology Co., LTD, Wuhan, China).

Prior to assembly and mapping, the raw sequencing data were first filtered by Trimmomatic (version.36) (Bolger et al., 2014), and then the low-quality reads and the reads containing adapter were trimmed using default parameters (PE -phred33 ILLUMINACLIP:adaptor_file:2:30:5 LEADING:3

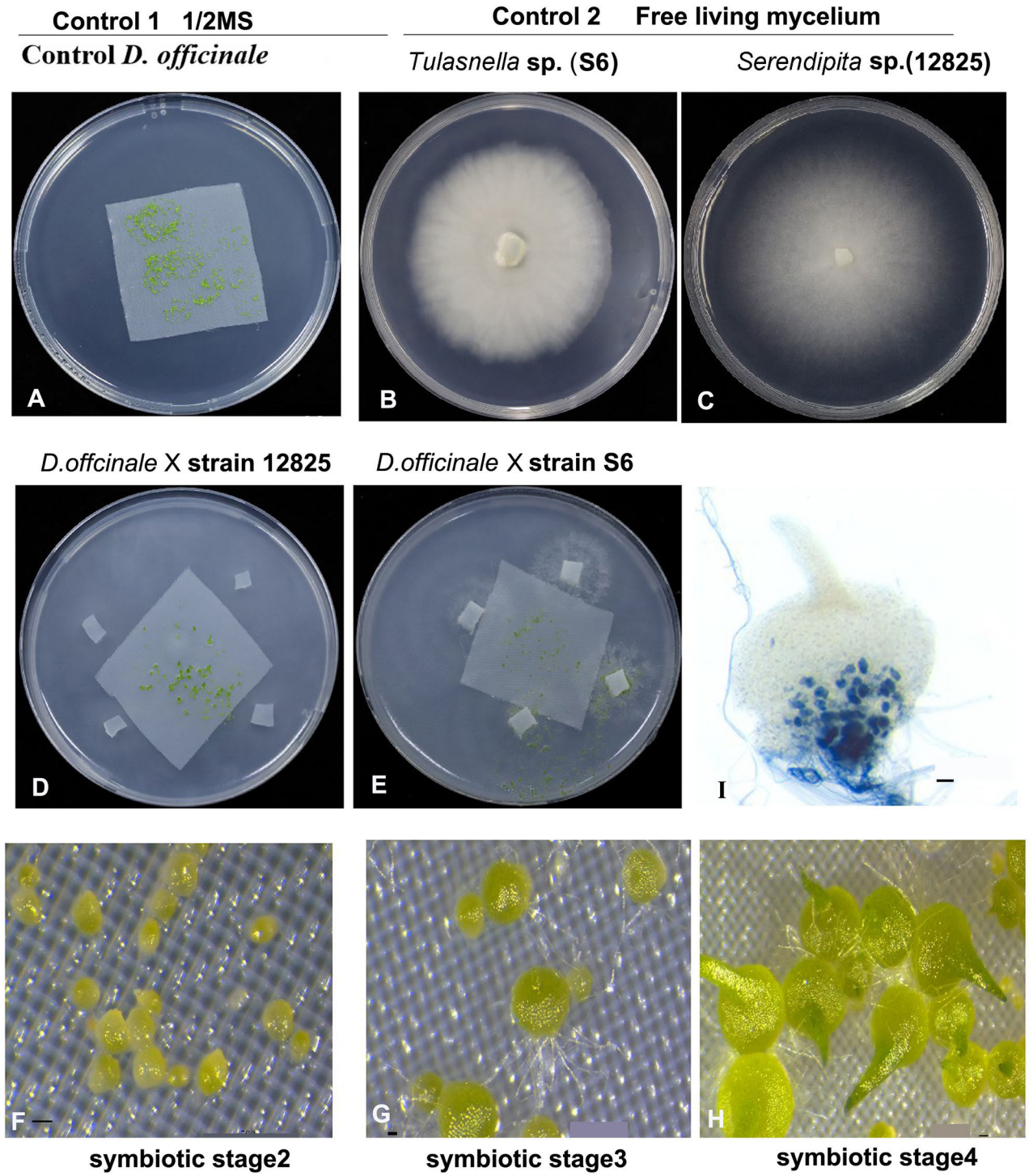

FIGURE 1 | Experiment designs for our study. Aymbiotic and symbiotic germination of medicinal orchid *Dendrobium officinale* inoculated with two mycorrhizal fungi *Tulasnella* sp. (S6) and *Serendipita* sp. (12825) at three development stages. **(A)** showing asymbiotic germination in 1/2 MS medium as control; **(B,C)** The free-living mycelium of two fungi on PDA medium, respectively. **(D–H)** showing the symbiotic germination assay with two fungal species, respectively. **(I)** Trypan blue staining showing the pelotons in embryo cell in symbiotic stage 4 of *D. officinale* seed inoculated with strain 12825. Scale bar = 20 μm in **(F–H)**, and 50 μm in **(I)**.

TRAILING:3 SLIDINGWINDOW:4:15 HEADCROP:0 MINLEN:36). Clean reads were further treated with in-house scripts to eliminate duplication bias introduced in library preparation and sequencing. Briefly, clean reads with the same UMI sequence were first clustered together, and then they were compared to each other using pairwise

alignment. Reads with sequence identity over 95% were extracted into a new subcluster. After all subclusters had been generated, multiple sequence alignment was performed to obtain one consensus sequence for each subcluster. Using these steps, any errors and biases introduced by PCR amplification or sequencing were eliminated. The de-duplicated consensus sequences with high quality were used for downstream analyses.

Analysis of *D. officinale* Transcriptomic Data

Genomics mapping and alignment program analysis were performed based on the reference genome of *Dendrobium catenatum* (https://www.ncbi.nlm.nih.gov/assembly/GCF_001605985.2) using STAR software (version 2.5.3a) with default parameters (Dobin et al., 2013; Dobin and Gingeras, 2015). Functional annotation of predicted genes was first performed using diamond Blastx in UniProt (Universal Protein) to obtain the protein ID, and then the annotation was searched in the database of Nr (NCBI non-redundant protein sequences), Pfam (Protein family), Rfam (RNA family), eggNog (evolutionary genealogy of genes: non-supervised orthologous groups), Gene Ontology (GO), and Kyoto Encyclopedia of Genes and Genomes (KEGG) using the same ID. Gene expression was qualified using the RSEM software package (RNA-Seq by Expectation-Maximization). Genes that were differentially expressed between groups were identified using the edgeR package (version 3.12.1) (Li and Dewey, 2011). The threshold for significantly differentially expressed genes (Robinson et al., 2010) (DEGs) was set at a fold change of $\geq$2 and an FDR corrected p-value < 0.05 (Robinson and Oshlack, 2010).

Analysis of Orchid Mycorrhizal Fungi *Tulasnella* sp. and *Serendipita* sp. Transcriptomic Data

Fungal *de novo* transcriptome assemblies were first reconstructed using Trinity based on the free-living mycelium of *Tulasnella* sp. (S6) and *Serendipita* sp. (12825), and the longest transcript was chosen as the unigene. Next, the unmapped reads of symbiotic samples (after mapping to the plant genome) were subjected to mapping analysis using the unigenes by Kangce Technology Co., Ltd., Wuhan, China, followed by Grabherr et al. (2011). Because we focused our analysis on the gene scale, further analysis was performed on Trinity unigenes, i.e., the longest isoform per Trinity gene. TransDecoder (version 5.5; http://transdecoder.sourceforge.net/) was used to identify putative coding regions from the assembled unigenes, and only the best-predicted protein was retained for each transcript (single_best_only option). Carbohydrate active enzyme (CAZyme) assignment was performed with dbCAN2 (Zhang et al., 2018) using HMMER, DIAMOND, and Hotpep prediction. Only domains detected by at least two tools were conserved.

RESULTS

Global Analysis of the Transcriptomic Data and Identification of Core Plant Gene Expression

Transcriptomic data were generated for the symbiotic germination of *D. officinale* seeds with the two mycorrhizal fungal species, asymbiotic germination seeds, and free-living mycelium of both fungi (**Figure 1**; **Table 1**). An average of 64.52% of the total 24,811 plant genes were detected to have transcriptional activity in at least one of the symbiotic germination stages (RPKM value $\geq$ 5) of *D. officinale* seeds inoculated with *Tulasnella* sp. A total of 1,287 genes were common differentially expressed (|fold change| $\geq$ 2; FDR <.05) within the three symbiotic germination stages compared to that of asymbiotic germination (**Figure 2A**). Similarly, an average of 66.6% of plant genes exhibited expression values (RPKM value $\geq$ 5) in at least one of the symbiotic samples of *D. officinale* seeds inoculated with *Serendipita* sp., and 1,943 plant genes were commonly differentially expressed in the three symbiotic stages compared to those of asymbiotic germination (**Figure 2B**). When we examined gene expression between both symbiotic germination groups of *D. officinale* inoculated with *Tulasnella* sp. and *Serendipita* sp., respectively, 1,003 common regulated plant genes were identified (**Figure 2C**). Among 1,003 differentially expressed genes (DEGs), 452 genes were upregulated in symbiotic groups and were clustered into nine clades based on expression profile (**Figure 3**; **Supplementary Table S1**). The genes with the highest expression level were primarily restricted to clusters I-V (**Figure 3**), and they displayed highly similar expression profiles in symbiotic plants inoculated with the two different mycorrhizal fungi, including the genes encoding a nodulin-like protein, Ras domain protein, sugar transporter, lysM domain protein, mannose-binding lectin, and histone-like transcription factor. These upregulated genes took part in molecular functions, biological processes, and cell components.

To further explore commonly expressed plant genes of *D. officinale* seeds induced by both fungal species, GO function and KEGG pathway enrichment analyses were performed (**Figure 4**). Compared to asymbiotic germination, all DEGs across various developmental stages of symbiotic *D. officinale* seeds were primarily enriched in organic or inorganic substance transport and sucrose, trehalose, and lipid synthesis and transport (**Figure 4A**). Several pathways, such as plant–pathogen interactions, plant hormone signal transduction, starch, and sucrose metabolism and phenylpropanoid biosynthesis, protein processing in the endoplasmic reticulum, lysosomes (for *Tulasnella* sp. pairs), and peroxisome (for *Serendipita* sp. pairs) were significantly enriched, and genes involved in these pathways exhibited a similar pattern in interaction with both *Tulasnella* sp. and *Serendipita* sp. (**Figures 4B,C**). Most genes in the plant-pathogen interaction pathway were encoded by calcium-binding proteins, calmodulin, LRR receptor-like, WRKY transcription factor, etc. The genes encoding auxin-responsive proteins and DELLA proteins (involved in plant hormone signal transduction) were significantly enriched during the

TABLE 1 | Samples information in our study.

Development stage of *D. officinale* seeds	Sample label				
	Asymbiotic	Symbiotic			
		+*Tulasnella* sp. (S6)		+*Serendipita* sp. (12825)	
	For plant or fungus (control)	For plant	For fungus	For plant	For fungus
Stage2 (germination)	D2	T2	Ft2	S2	Fs2
Stage3 (protocorm)	D3	T3	Ft3	S3	Fs3
Stage4 (seedling)	D4	T4	Ft4	S4	Fs4
Free-living mycelium for *Tulasnella* sp. (S6)	Ft				
Free-living mycelium for *Serendipita* sp. (12825)	Fs				

interaction between *D. officinale* seeds and their mycelia. Genes encoding trehalase, beta-amylase, pectinesterase, hexokinase, glucan endo-1,3-beta-glucosidase, etc., which are implicated in starch and sucrose metabolism, were also enriched in symbiotic germination from early germination to seedling formation. Twenty-five upregulated common expression genes of the host plant (fold change $\geq$ 5, FDR $\leq$ 0.05, compared to asymbiotic germination) are listed in **Supplementary Table S2**, and these genes typically encoded aquaporin-like, cytochrome P450, nodulin-like, glycoside hydrolases 35 (GH35), GH18, sugar transporter, etc.

When we compared gene expression at the same germination stage of *D. officinale* seeds between inoculation with *Tulasnella* sp. and *Serendipita* sp., we found more DEGs in the symbiotic protocorm stage (1,852 genes, stage 3) than in the germination stage (934 genes, stage 2), implicating the protocorm stage is likely a crucial stage responding to different fungal invasions during orchid mycorrhizal development. In total, 350 plant genes were identified as significantly differentially expressed in symbiotic seeds of *D. officinale* across all germination stages during interaction with *Tulasnella* sp. compared to those symbiotic with *Serendipita* sp. (**Figure 5**). GH17, GH79, UPD-glucoronsyl transferase, UbiA prenyltransferase, CYP450, nodulin-like, hydrophobic seed protein, etc., were significantly upregulated in *D. officinale* seeds inoculated with *Tulasnella*, and upregulated plant genes in various symbiotic stages inoculated with *Tulasnella* sp. were primarily enriched in plant hormone signal transduction and phenylpropanoid biosynthesis, especially during the initial germination stage and photosynthesis pathway, and were significantly enriched in the protocorm stage (**Figure 5**).

Genes Expression Involved in Plant Cell Wall Synthesis and Remodeling

We identified 15 common DEGs involved in plant cell wall constitution and remodeling at each symbiotic stages (**Table 2**) during seed germination of *D. officinale* inoculated with fungi. Among them, genes encoding epidermis-specific secreted glycoprotein, proline-rich receptor-like protein, and leucine-rich repeat (LRR) extensin-like protein were upregulated in the symbiotic stages and even more highly upregulated in the protocorm stage (stage 3) and seedling stage (stage 4). The gene encoding LRR extensin-like protein (LOC110096373) exhibited the highest expression of 20.2-fold in the protocorm stage of *D. officinale* seeds inoculated with *Serendipita* sp., and the gene encoding proline-rich receptor-like protein kinase displayed more highly upregulated expression with more than a 25-fold induction in the symbiotic stage compared to asymbiotic germination inoculated with either *Tulasnella* or *Serendipita* across the entire germination stage. Moreover, genes encoding enzymes that function in cell wall biosynthesis also displayed significantly differential expression between symbiotic and asymbiotic germination, such as cellulose syntheses, pectinacetylesterase, and pectinesterase. The gene encoding microtubule-associated protein RP was also significantly upregulated during symbiotic germination.

Fungal Gene Expression During Interaction With the Same Host Plant

Overview of Fungal Genes Expression During Seed Symbiotic Germination of *D. officinale*

With the seed germination process occurring in the symbiotic system, fungal mycelium in embryonic cells also underwent a series of morphological changes. Although the mycorrhizal infection in orchid protocorm could be a cyclic event and pelotons are supposed as short-lived structures (Smith and Read, 2008), our previous showed that in the early stage of seed germination (embryo enlargement, rupture of testa, stage 2), several fungal mycelia colonized the embryonic cells from the epidermal hair or suspensor, and the hyphae formed pelotons with protocorm development (stage 3). After protocorm formation, most invaded hyphae lost bioactivity and formed clumps that started to degenerate at stage 4 or 5 (seedling development), although the timepoint boundary was not entirely clear (Chen et al., 2014).

To analyze fungal gene expression, RNA-seq data were generated from fungi in symbiotic status, namely, colonized during three symbiotic germination stage samples (seed germination, stage 2; protocorm formation, stage 3, and seedling development stage 4) and compared to free-living mycelium (FLM). Assembly of the fungal transcriptome was based on our *de novo* sequencing of *Tulasnella* sp. (S6) and *Serendipita* sp.

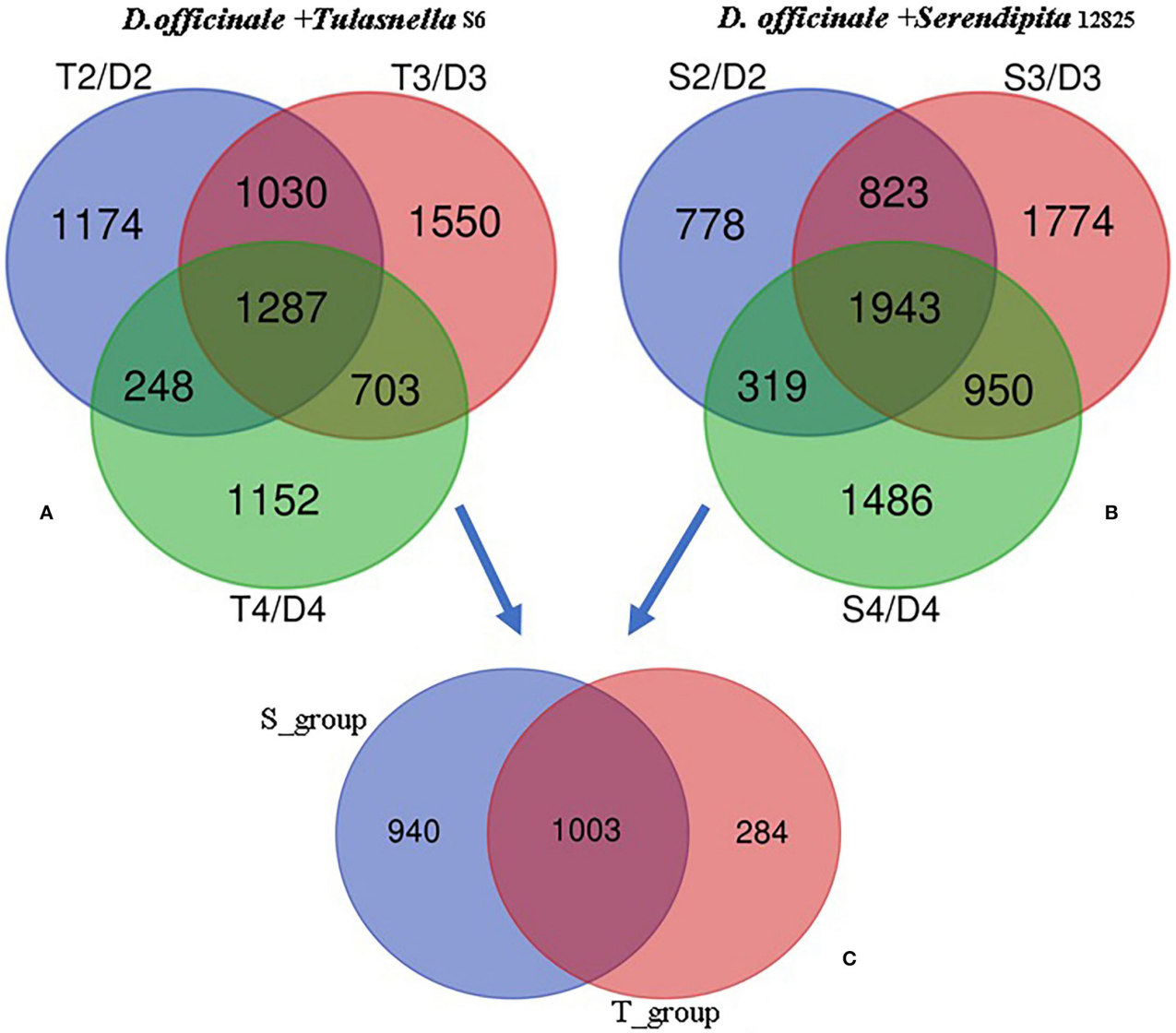

FIGURE 2 | Venn diagram showing the numbers of plant differentially expressed genes (DEGs) in the adjacent development stage of two symbiotic groups of *D. officinale* seeds with *Tulasnella* sp. (S6) and *Serendipita* sp. (12825), respectively. **(A,B)** DEGs at adjacent development stage during *D.officinale* seed with *Tulasnella* sp. **(A)** and *Serendipita* sp. **(B)** and compared to the same stage in asymbiotic germination; **(C)** 1,003 common differentially expressed plant genes across the three development stages (stages 2, 3, and 4) in symbiotic process with two different mycorrhizal fungi compared asymbiotic germination. D2, D3, and D4 mean asymbiotic germination stages 2, 3, and 4, respectively; S2, S3, and S4 mean stages 2, 3, and 4 in symbiotic germination with *Serendipita* sp., respectively, T2, T3, and T4 mean stages 2, 3, and 4 in symbiotic germination with *Tulasnella* sp., respectively.

(12825) due to the low species similarity with the published genome, but gene annotation was also performed with the reference genome of *Tulasnella calospora* AL13/4D (version 1; https://www.ncbi.nlm.nih.gov/assembly/GCA_000827465.1/) and *Serendipita vermifera* MAFF 305830 (version 1; https://www.ncbi.nlm.nih.gov/assembly/GCA_000827415.1/).

In the global expression analysis of *Tulasnella* sp. during interaction with *D. officinale* seeds, a total of 8,228, 7,939, and 6,034 genes exhibited transcriptional activities at the beginning of invasion (according to stage 2 of seed germination), peloton formation (stage 3), and peloton degradation stages (stage 4), respectively. Among them, 2,555 common upregulated genes were identified across the entire symbiotic process with *D. officinale* seeds (compared to FLM) (**Supplementary Figure S1**). Similarly, there were 4,630, 4,182, and 3,123 genes differentially expressed in symbiotic stages 2, 3, and 4, respectively, compared to FLM when *D. officinale* seeds were inoculated with *Serendipita* sp. (**Supplementary Figure S1**). Furthermore, 403 fungal genes were commonly upregulated in the symbiotic process across the three seed germination stages compared to the FLM of *Serendipita* sp. (**Supplementary Figure S1**). The number of DEGs in *Serendipita* sp. (403 common

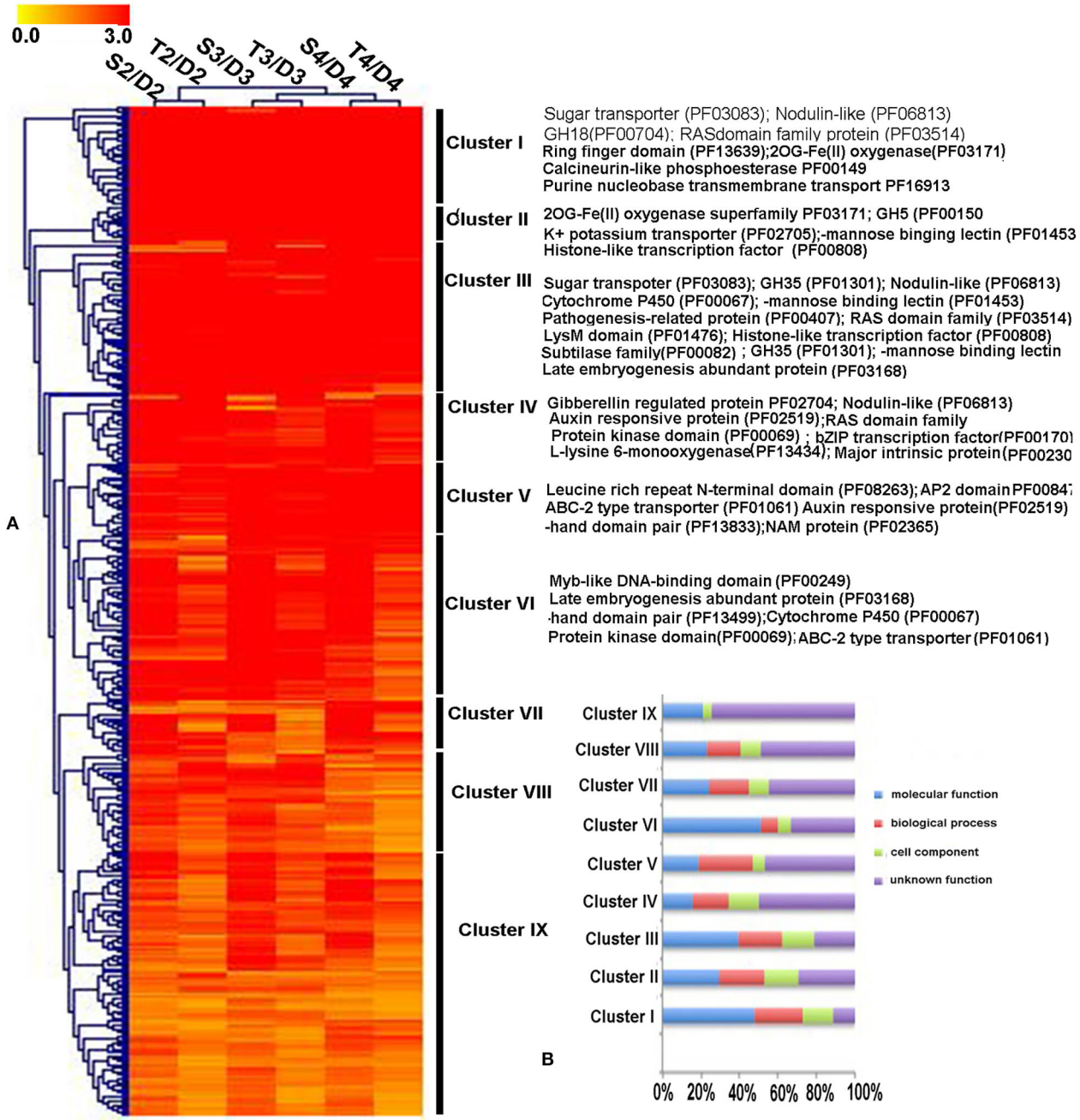

FIGURE 3 | The expression patterns and functional classification of 452 differentially upregulated expressed plant genes (DEGs) at least one symbiotic stage during *D. officinale* inoculated two mycorrhizal fungi. **(A)** Heatmap showing the expression level of up-regulated genes in symbiotic germination of *D. officinale.* Expression value was calculated based on Log_2 Fold change. Red color means a gene with a high expression value (Fold change ≥ 8) and yellow color means a gene with a relatively low expression value (Fold change ≥ 2). The function annotation of the representative genes with high expression (Cluster I-Cluster VI) was marked in the heatmap right. **(B)** GO functional category of the 452 up-regulated genes in nine clusters. D2, D3, and D4 mean asymbiotic germination stage2, stage3, and stage4, respectively; S2, S3, and S4 mean stages 2, 3, and 4 in symbiotic germination with *Serendipita* sp., respectively, T2, T3, and T4 means stages 2, 3, and 4 in symbiotic germination with *Tulasnella* sp., respectively. The detailed information of these genes is in **Supplementary Table S1**.

upregulated) was less than that of *Tulasnella* sp. (2,555 common upregulated genes). Functional analysis of the two upregulated fungal gene sets revealed that the most abundant genes with known functions played important roles in transcription, posttranslational modification, lipid transporter, and metabolism, carbohydrate transport and metabolism, amino acid transport, and metabolism, and RNA processing and modification (**Supplementary Figure S1**).

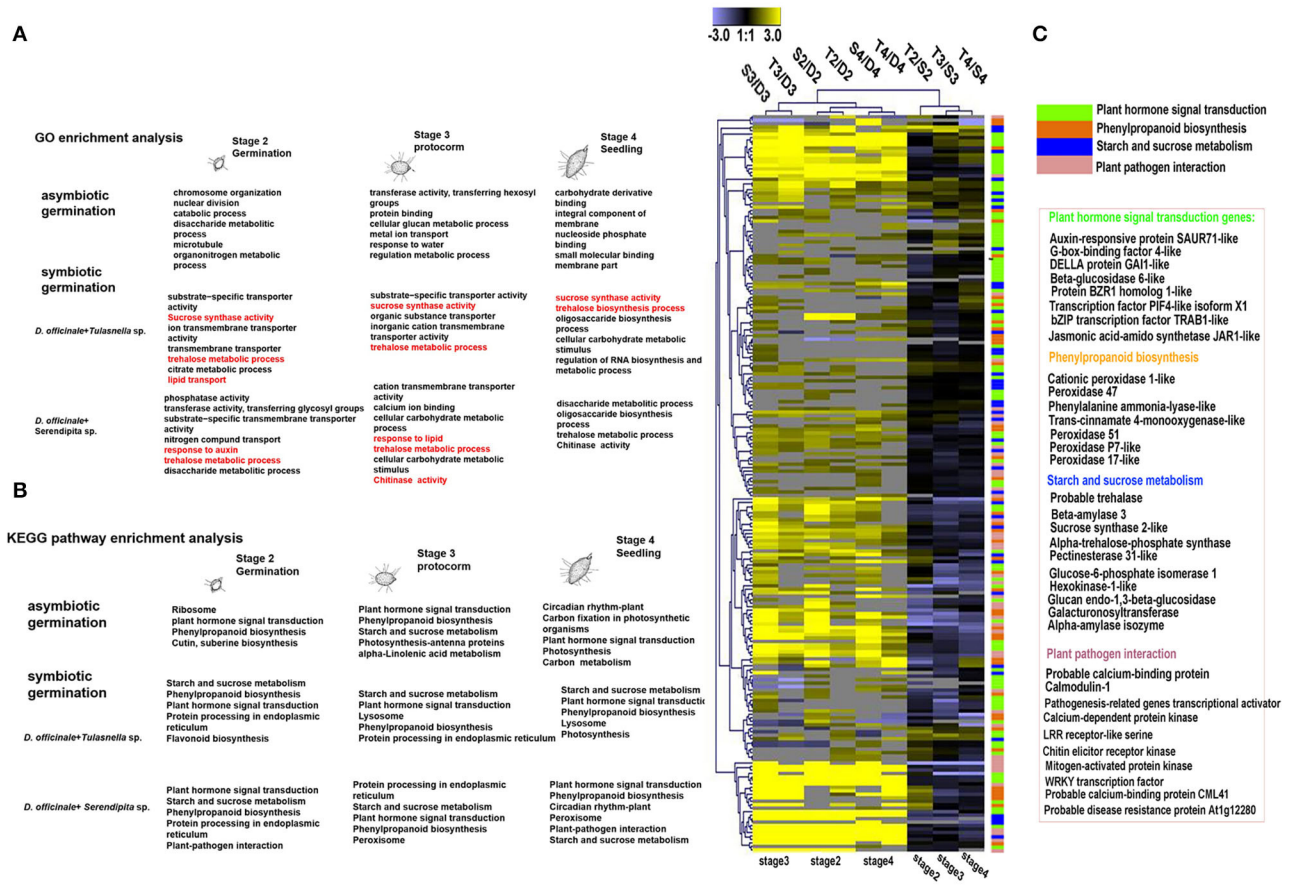

FIGURE 4 | KEGG and GO enrichment analysis of differentially expressed plant genes (DEGs) during germination of *D. officinale* seeds with two mycorrhizal fungi. **(A)** GO enrichment analysis; red color indicated that typical Go functional enrichment for these genes involved in symbiotic germination compared to asymbiotic germination. **(B)** KEGG pathway enrichment analysis showed that the significant enrichment pathway exists as overlaps between symbiotic and asymbiotic germination. It means these pathways could be most important during seed development. And the symbiotic germination with two fungal species have similar metabolic pathway but also display difference e.g., lysosome in *Tulasnella* sp.-*D.officinale* and peroxisome in *Serendipita* sp.- *D.officinale*; **(C)** heatmap showing the expression profile of genes in the significantly enriched four metabolic pathways during symbiotic germination of *D.officinale* (such as plant hormone signal transduction, phenylpropanoid biosynthesis, starch, and sucrose metabolism and plant-pathogen interaction); expression value was calculated based on Log2 Fold change. Significant expression changes were labeled in colors: blue represents down regulated and yellow represents up regulated. The functional annotation of representative genes in each enriched pathway was recorded in heatmap aside.

Expression Profile of Fungal Genes Encoding Carbohydrate- Active Enzymes

Based on our transcriptomic data, we identified 266 putative genes encoding CAZymes in the *Tulasnella* sp.×*D. officinale* symbiotic transcriptome, and among them, 66 genes were differentially expressed in at least one symbiotic stage compared to that of the FLM (**Figure 6**), including 3 carbohydrate-binding modules (CBM) family members (4 genes), 3 members of the carbohydrate esterase (CE) family (7 genes), 5 members of the auxiliary activity (AA) (7 genes), 13 glycoside hydrolase (GH) family members (20 genes), 14 glycosyltransferases (GT) family members (27 genes), and two pectin lyase members (PL35, PL8). Moreover, CBM43, CBM48, CBM13, CE8, AA2, AA9, GH1, GH79, GH38, and GH45 were upregulated in the entire symbiotic stage with more than 5-fold changes compared to that of the FLM.

Compared to the interaction between *Tulasnella* sp. × *D. officinale* seeds, the transcriptomics analysis of *Serendipita* sp. × *D. officinale* identified 270 putative genes encoding CAZymes. Among them, 99 genes were differentially expressed in the symbiotic stage (**Figure 6**). Genes encoding AA class proteins (21 genes for 7 members) targeted to pectin were significantly upregulated in symbiotic conditions by more than 5-fold compared to free living mycelium. In addition, genes in the GH family, such as GH15, GH17, GH3, GH5, GH38, GH47, and GT family members (GT2, GT22, and GT59), were upregulated in the symbiotic stage compared to FLM.

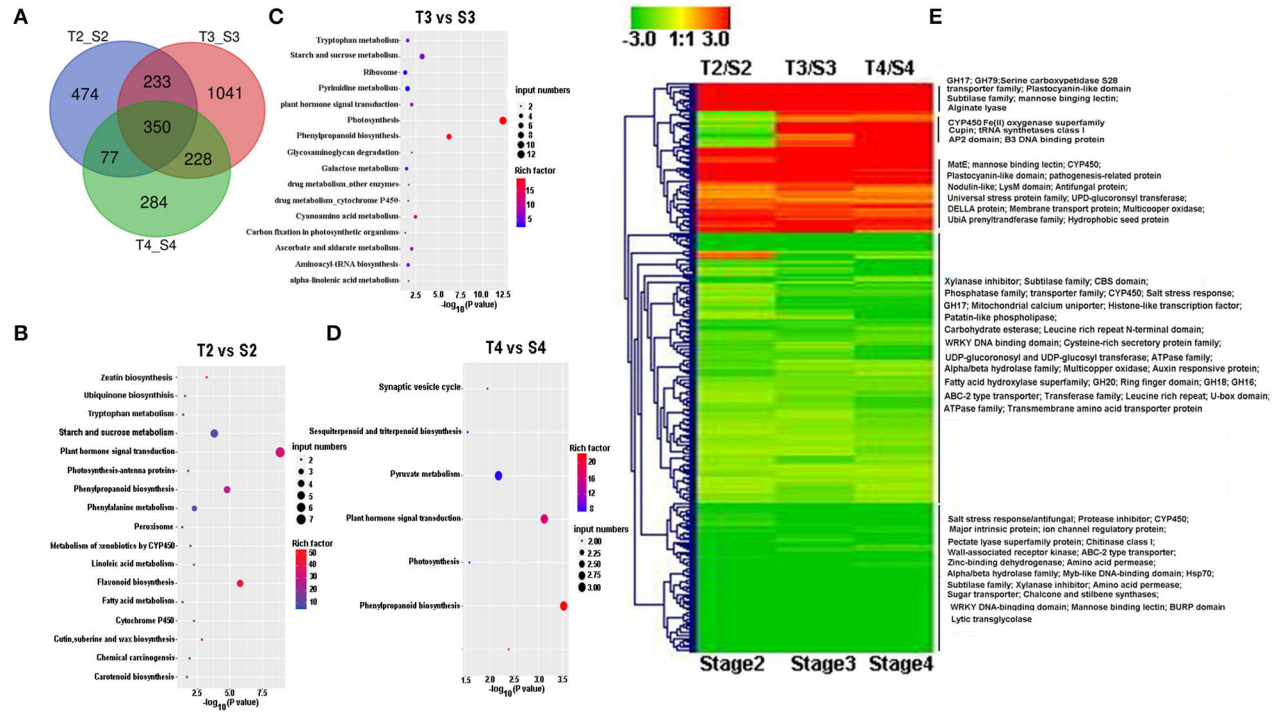

FIGURE 5 | Heatmp showing the differentially expressed genes (DEGs) between symbiotic germination at the same stage during *D. offcinale* inoculated with *Tulasnella* sp. (S6) and *Serendipita* sp. (12825). **(A)** The number of DEGs when *D. officinale* seed inoculated with *Tulasnella* sp. compared to with *Serendipita* sp. at the same development stage; **(B–D)** KEGG enrichment analysis of up-regulated DEGs at various germination stages during *D.officinale* symbiotic germination with two fungi. **(E)** Heatmap showing the expression pattern of 350 common differentially expressed genes in *D. officinale* × *Tulasnella* sp. compared to *D. officinale* × *Serendipita* sp. Expression value was calculated based on Log2 Fold change, red color means up-regulated expression and green color means down-regulated expression. S2, S3, and S4 mean stages 2, 3, and 4 in symbiotic germination with *Serendipita* sp., respectively, T2, T3, and T4 mean stages 2, 3, and 4 in symbiotic germination with *Tulasnella* sp., respectively.

Definition of a Core Gene Set Shared by *Tulasnella* sp. and *Serendipita* sp. During Interaction With the Same Host Plant

We hypothesized that the different mycorrhizal fungal species would share common gene expression patterns during interaction with seeds of the same host plant of *D. officinale*. To identify possible orthologous genes between the two mycorrhizal fungi, we performed a bidirectional BlastP analysis on *Tulasnella* sp. and *Serendipita* sp. at an e-value $< 10^{-5}$. Additionally, we performed homology analysis using BlastP search with the published *Tulasnella* (AL13/4D version 1) and *Serendipita* (MAFF 305830 v1.0) genomes for gene annotation.

We identified 4,954 genes (25.21%) that were orthologous between *Tulasnella* sp. (S6) and *Serendipita* sp. (12825) based on the fungal transcriptomics data. Among them, 1,682 genes were expressed in symbiotic *Serendipita* sp. and 2,464 genes were expressed in symbiotic *Tulasnella* sp. in at least one symbiotic stage during the interaction with *D. officinale* seeds. A total of 936 orthologous genes were shared between *Tulasnella* sp. (S6) and *Serendipita* sp. (12825) in at least one symbiotic stage during colonization in seeds of *D. officinale*. Most of these genes exhibited similar expression profiles. According to gene expression level, 936 orthologous genes were divided into five clusters (**Supplementary Figure S2**; **Supplementary Tables S2**, **S3**). For example, in cluster 1, genes were primarily upregulated in both fungi during early symbiotic stages with seeds (stage 2, starting germination), and most of these genes were involved in energy production and conservation, translation and posttranslational modification, amino acid transport, and metabolism and lipid transport and metabolism. Genes encoding a fungal transcriptional regulatory protein, chitin synthase, zinc finger protein, serine/threonine-protein kinase-related, ribosomal protein, transcription factor, sugar transporter, ABC transporter-like, and acyltransferase, which participate in signal transduction, posttranslational modification, lipid transport and metabolism (androgen and estrogen metabolism), were upregulated in symbiotic *Tulasnella* sp. but downregulated in symbiotic *Serendipita* sp. during the entire process of interaction with *D. officinale* seeds (cluster 2), especially during the germination and protocorm stages (stages 2 and 3), indicating strikingly different expression profiles. Genes encoding ribosomal protein, protein synthesis factor (translation, ribosomal structure, and biogenesis), aminotransferase, spermine synthase, methionine synthase, glutamate-5-semialdehyde dehydrogenase, etc. (amino acid metabolism) were significantly upregulated in symbiotic *Serendipita* sp. compared

TABLE 2 | Fifteen differentially expression plant genes involved in cell wall composition and remodeling during *D. officinale* symbiotic germination.

Geneid	logT2/D2	logT3/D3	logT4/D4	logS2/D2	logS3/D3	logS4/D4	Description
LOC110109313	4.31	5.00	3.24	4.60	6.05	4.13	Cellulose synthase-like protein D2
LOC110106368	−1.52	−3.72	−1.46	−3.27	−2.60	−1.75	Cellulose synthase-like protein G3
LOC110106369	−2.02	−2.00	1.21	−2.78	−1.83	1.40	Cellulose synthase-like protein G3
LOC110106370	−2.33	−2.18	−1.34	−3.44	−2.43	−1.94	Cellulose synthase-like protein G3
LOC110096247	1.15	1.63	1.09	1.28	2.30	1.62	Microtubule-associated protein RP
LOC110113646	−1.87	−2.84	−1.62	−2.23	−2.23	−1.12	Pectinesterase inhibitor 11-like
LOC110101432	−1.90	−3.42	−2.25	−2.21	−3.72	−3.19	Pectinesterase inhibitor 3-like
LOC110112046	1.27	1.05	2.38	1.53	1.03	2.20	Pectinesterase-like
LOC110101606	3.69	4.99	3.30	4.48	5.98	4.61	Probable pectinesterase
LOC110115556	2.05	2.47	2.40	2.44	1.47	1.67	Epidermis-specific secreted glycoprotein
LOC110113177	−1.18	−1.86	−1.70	−2.78	−3.17	−1.88	36.4 kDa proline-rich protein-like
LOC110094976	4.65	4.90	4.49	5.12	5.99	6.08	Proline-rich receptor-like protein kinase PERK1
LOC110093563	−1.03	−2.03	−1.95	−1.52	−1.04	−1.15	Extensin-2-like
LOC110103208	−2.78	−2.25	−2.24	−3.87	−1.22	−2.33	Extensin-3-like isoform X1
LOC110096373	2.89	2.65	2.12	3.51	4.34	3.45	Leucine-rich repeat extensin-like protein 5

to FLM but were not significantly differentially expressed in symbiotic *Tulasnella* sp. group (cluster 5). In addition, genes encoding rasGAP protein, Ca2+/calmodulin-dependent protein kinase, serine/threonine protein kinases (signal transduction mechanisms), sterol desaturase, and ergosterol biosynthesis protein (lipid metabolism) were upregulated in symbiotic *Serendipita* sp. compared to FLM. Notably, cluster 4 included 29 orthologous genes that were both upregulated in the two mycorrhizal fungi during interaction with *D. officinale* seeds in various symbiotic stages, especially in *Tulasnella* with the *D. officinale* seed group. These 29 genes primarily encode ubiquitin, short-chain dehydrogenase, ribosomal protein, histone, heat shock protein, glutathione S-transferase, carbohydrate-binding, ATPase, and amine oxidase, which are involved in carbohydrate metabolism, energy metabolism, and glutathione metabolism.

To further understand the potential function of fungal orthologous genes during interaction with orchid seeds, we analyzed the fungal genes encoding CAZymes, protease, lipase, and SSPs, which were reported to likely be involved in mycorrhizal symbiosis in previous studies. The results revealed a total of 126 of 936 commonly expressed orthologous genes encoding the three specific protein categories (61 proteases, 24 CAZymes, and 31 SPs), and the expression profiles of the two symbiotic fungi during seed symbiotic germination of *D. officinale* at different stages (stage 2, stage 3, and stage 4) were analyzed (**Figure 7**). Twenty-four CAZyme genes were differentially regulated at the transcriptional level in at least one symbiotic stage compared to FLM. Genes encoding AA9 were both highly upregulated at the early germination stage (fungal invasion and peloton formation) after inoculation with *Tulasnella* sp. or *Serendipita* sp. with more than 100-fold changes. The gene encoding AA1 was upregulated during the seedling stage (fungal peloton digestion) in *D. officinale* with *Serendipita* sp. and *Tulasnella* sp. Genes encoding GT66 and GT4 and AA family proteins (AA2, AA3, and AA6) were upregulated during the early stage of germination and the protocorm formation of seeds with *Serendipita*. Genes encoding GH family proteins (GH16, GH9, and GH5) were markedly upregulated in at least one stage of seed symbiotic germination with *Tulasnella* sp. Among the 31 SPs, the genes encoding peptides S8, peptides M28, and carbohydrate-binding WSC domain proteins, representing secreted proteins, were specifically upregulated in the symbiotic *Tulasnella* group with more than a 100-fold-change compared to FLM. GH61 was upregulated in the initial invasion stages (or early germination stage) during symbiotic germination in the two symbiotic fungi, and GH5 was highly upregulated in symbiotic *Serendipita*.

In orthologous and commonly expressed gene sets, genes encoding proteases, such as asparaginase, HMG-CoA, septin, ASF, and peptidase, were significantly upregulated in at least one germination stage interaction in either *Tulasnella* sp. or *Serendipita* sp. Genes encoding cytochrome b5 and major facilitator superfamily proteins were specifically upregulated in symbiotic *Tulasnella* compared to FLM, with more than a 100-fold-change, while ribosomal S7 and fatty acid hydroxylase were highly upregulated in symbiotic *Serendipita* sp.

DISCUSSION

Orchid mycorrhizal symbionts of *Tulasnella* and *Serendipita* are the most common mycorrhizal partners of green orchids and belong to the phylum Basidiomycota. Here, we compared to plant and fungal gene expression in *D. officinale* seeds inoculated with two taxonomically different orchid mycorrhizal species (*Tulasnella* sp. S6 and *Serendipita* sp. 12825) at the transcriptional level. The two mycorrhizal fungi stimulated seed germination (stage 2), protocorm formation (stage 3), and seedling development (stage 4-5) in *D. officinale*.

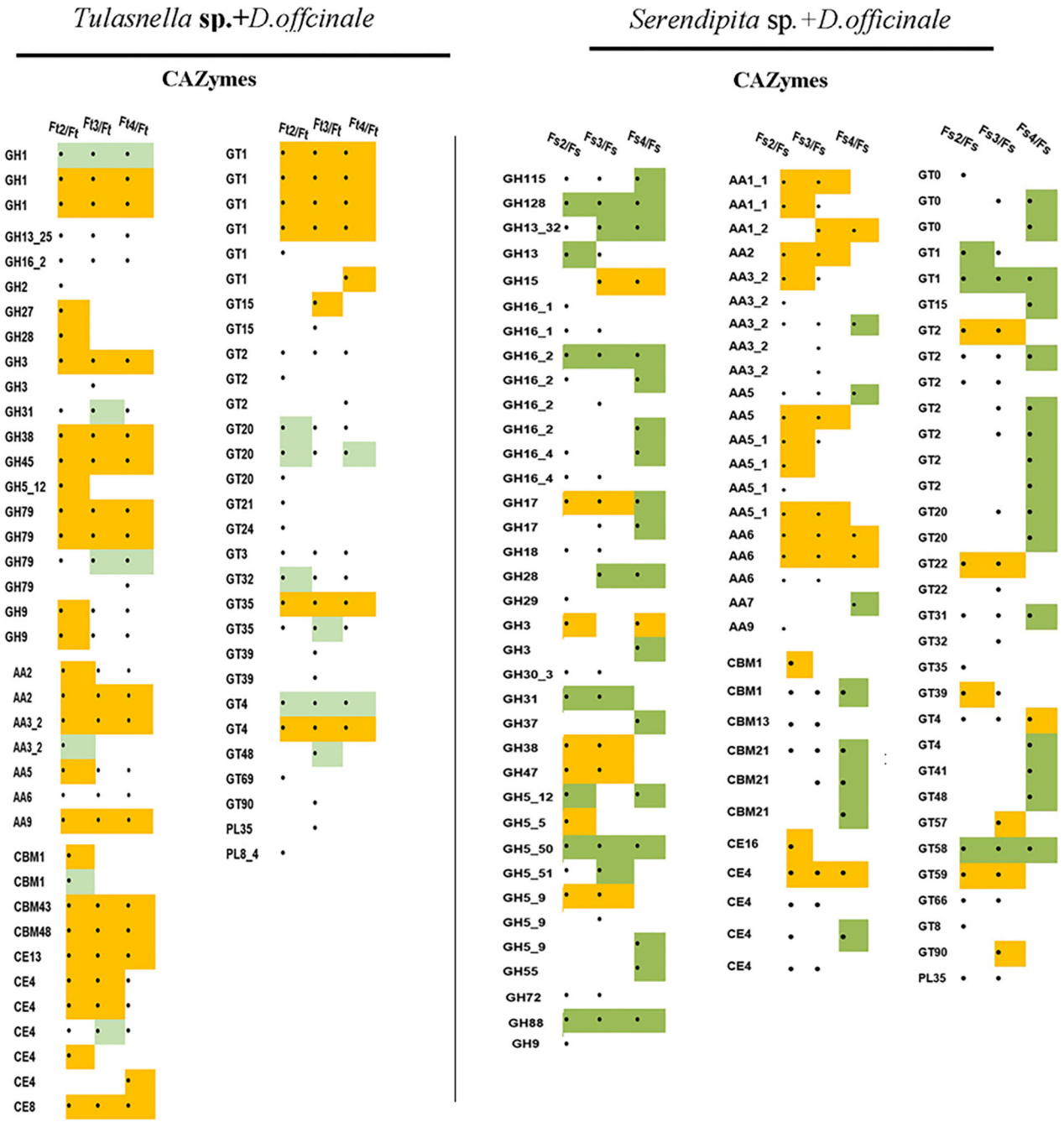

FIGURE 6 | Heatmap showing the expression profile of fungal DEGs encoding CAZyme proteins during symbiotic germination of *D.officinale* with *Tulasnella* sp. and *Serendipita* sp. • means genes differentially expression, blank means no significant differential expression; yellow color means genes up-regulated with fold change ≥ 5 and green color means genes down regulated with fold change ≥ 5. Ft2, Ft3, and Ft4 represent *Tulasnella* sp. in symbiotic statuses 2, 3, 4 stages while Fs2, Fs3, and Fs4 represent *Serendipita* sp. in symbiotic statuses 2, 3, and 4 stages (according to germination stage) and Ft and Fs means free-living mycelium of *Tulasnella* sp. and *Serendipita* sp., respectively.

Expression of Genes Related to Plant Cell Wall Biosynthesis and Remodeling

Our comparative transcriptomics analysis revealed that an important proportion of plant genes (>60%) were expressed during the symbiotic germination of *D. officinale*. Most exhibited similar expression profiles at the same symbiotic germination stage with different mycorrhizal fungi. Genes encoding universal stress protein, UbiA, aquaporin-like, cytochrome P450 family,

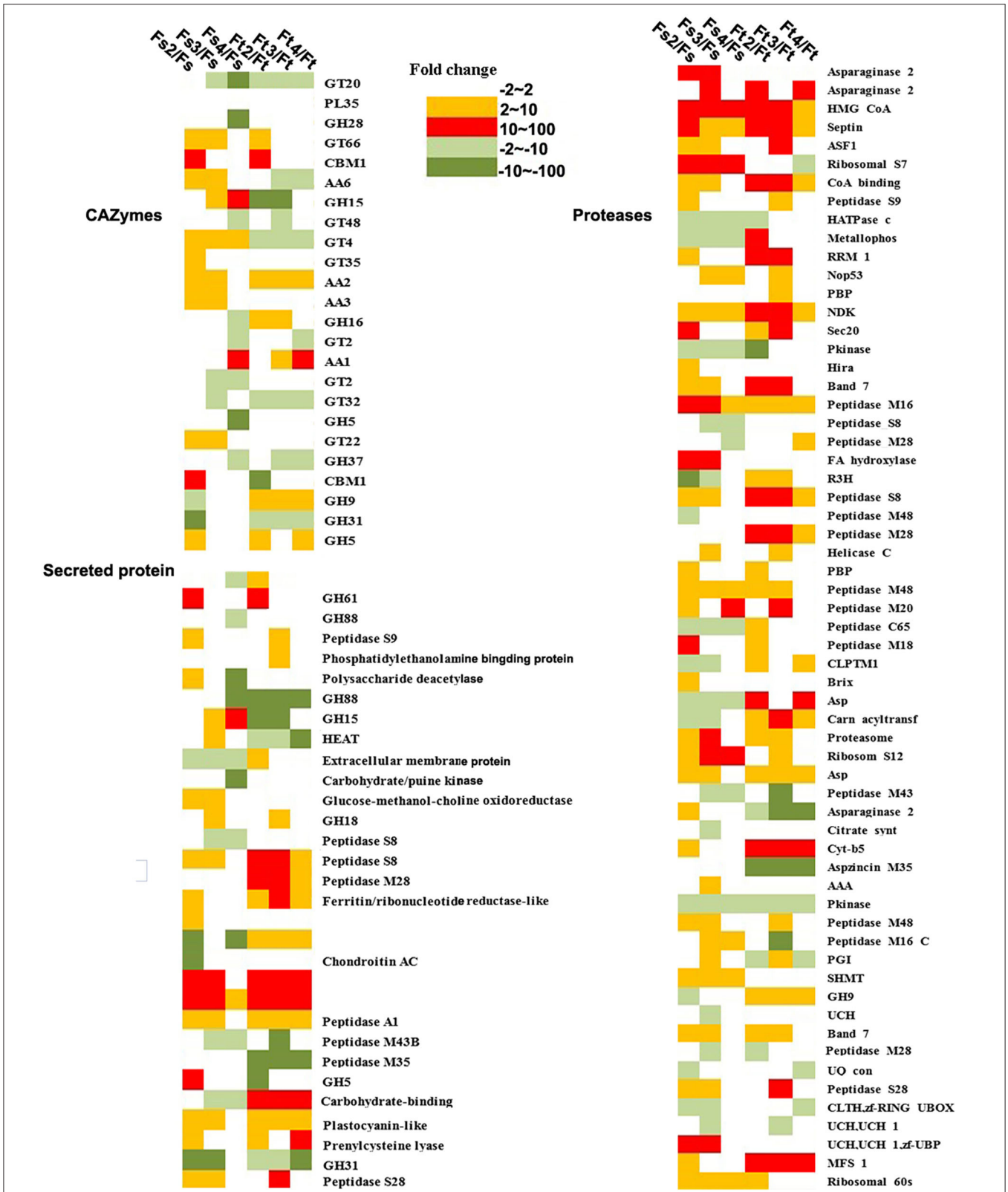

FIGURE 7 | Heatmap showing the expression profile of fungal orthologous genes encoding CAZyme, secreted proteins, and protease during symbiotic germination of *D. officinale* with *Tulasnella* sp. and *Serendipita* sp. The expression level was evaluated using fold change in different colors. Green color (dark green means expression level with fold change ≥ 10) means genes down-regulated expression and red and orange color means genes up-regulated expression (red color means expression level with fold change ≥ 10). Ft2, Ft3, and Ft4 represent *Tulasnella* sp. in symbiotic statuses 2, 3, 4 stages while Fs2, Fs3, and Fs4 represent *Serendipita* sp. in symbiotic statuses 2, 3, and 4 stages (according to germination stage) and Ft and Fs means free-living mycelium of *Tulasnella* sp. and *Serendipita* sp., respectively.

nodulin-like, plant lipid transfer protein; RAS domain family, and sugar (and other) transporter were significantly upregulated between the two mycorrhizal fungal combinations, indicating their common roles in the core mechanisms of symbiotic recognition, nutrition transport, or other aspects between the orchid host and the mycorrhizal fungi. These results are consistent with previous studies (Balestrini et al., 2014; Chen et al., 2017).

The plant cell wall is the headmost interface where interactions occur between the host plant and its mycobionts (Balestrini and Bonfante, 2014; Lionetti and Métraux, 2014). The plant cell wall is primarily composed of polysaccharides, such as cellulose, hemicelluloses, and pectins. In addition, there are some structural cell wall proteins characterized by highly repetitive sequence motifs, which are especially rich in specific amino acids, e.g., proline, glycine, and hydroxyproline glycoproteins, to modify the cell wall (Herger et al., 2019). In our present study, genes encoding epidermis-specific secreted glycoprotein, proline-rich receptor-like protein, leucine-rich repeat (LRR) extensin-like protein, and extensin-like protein were significantly upregulated during the symbiotic stage in *D. officinale* seeds after inoculation with *Tulasnella* sp. and *Serendipita* sp. Extensins are an abundant group of hydroxyproline-rich glycoproteins and are responsible for various processes, including embryonic development, root hair growth, cell wall assembly and structure, and biotic and abiotic stress responses (Castilleux et al., 2018). Most studies indicate that extensins exert their roles in plant defense by strengthening the cell wall, decreasing pathogen invasion, or facilitating the attachment of symbiotic organisms (Castilleux et al., 2021). In addition, new insights have been provided regarding the structure and role of extensins and their glycosylation in plant–microbe interactions using a set of anti-extensin-specific monoclonal antibodies (Castilleux et al., 2020), indicating that modeling of the cell wall architecture is likely to impact cell binding and pathogen colonization of roots. The extensins, especially arabinosylation, could even serve as markers of the plant immune response during plant-microbe interactions (Castilleux et al., 2018). In orchid symbiotic germination, previous studies revealed that the signals for the dynein monoclonal antibody JIM11 epitope were stronger in symbiotic *Dendrobium* protocorms than in asymbiotic ones and were primarily located in the plant walls and in special plant cells colonized by fungi rather than in the apical meristem. This indicated that the extensins were not only related to fungal attachment in a symbiotic relationship but were also likely critical for limiting fungal colonization in basal cells and preventing fungal spread inside the protocorms (Li et al., 2018). Regardless, our transcriptomics analysis indicated that the two mycorrhizal fungi both triggered plant genes encoding extensions to be significantly upregulated in the symbiotic stage during interaction with *D. officinale* seeds, consistent with the results of previous studies and further provided supported data.

Immunofluorescence labeling revealed that microtubules were altered and reorganized adjacent to the symbiosis interface after the fungus invaded root cells (Genre and Bonfante, 2002), although the ultrastructural changes were not illustrated in detail in the orchid mycorrhiza. In our study, the gene encoding microtubule-associated protein was upregulated in the symbiotic stage, indicating that cytoskeletal rearrangements likely occurred during the invasion of orchid seeds by the fungus. In addition, genes related to plant cell biosyntheses, such as those encoding cellulose synthase and pectinesterase, were significantly upregulated when inoculated with either *Tulasnella* sp. or *Serendipita* sp. compared to asymbiotic germination, indicating that plant cell wall biosynthesis and reinforcement was very active during the interaction between the mycorrhizal fungi and *D. officinale* seeds.

Fungal Gene Expression Related to Plant Cell Wall Degradation Enzymes

During interaction with the same host plant, *Tulasnella* sp. induced more genes involved in the symbiotic germination of *D. officinale* than did *Serendipita* sp. For example, during the initial invasion stage (correspondingly, the early germination stage), a total of 8,128 fungal genes in *Tulasnella* (5,268 up- and 2,960 downregulated) were differentially expressed compared to FLM, while there were 4,630 differentially expressed genes in *Serendipita* sp. (2,066 up to and 2,564 down). Although no genome information is available for either mycorrhizal fungus, using an overview of the reported genome of *Tulasnella calospora* (62.39 Mb, 19,635 genes) and *Serendipita vermifera* (38.09 Mb, 15,317 genes) (Kohler et al., 2015), we suspect that different taxon of mycorrhizal fungi could be contributed to the gene expression difference during interaction with the orchid plant to the extent.

In addition, we identified 4,954 orthologous genes based on the transcriptome of *Serendipita* sp. and *Tulasnella* sp. A total of 1,682 genes were expressed in symbiotic *Serendipita* sp. and 2,464 genes were expressed in symbiotic *Tulasnella* sp. compared to the FLM during interaction with *D. officinale* seeds (in at least a symbiotic condition). A total of 936 orthologous genes were commonly expressed, and most of the genes exhibited similar expression during mycorrhizal interactions with any mycobiont, suggesting that different mycorrhizal fungi shared a common set of genes involved in symbiotic responses.

CAZymes

Genome analysis revealed that orchid mycorrhizal symbionts had the largest set of CAZymes supporting their dual saprotrophic/symbiotic lifestyles (Martin et al., 2016). For example, *T. calospora* has 7 GH6, 27 GH7, and 33 LPMO genes for the degradation of crystalline cellulose (Kohler et al., 2015). Proteins with a cellulose-binding domain (CBM1) are also abundant in orchid mycorrhizal fungi (ORM). In our present study, 66 DEGs encoding CAZymes were identified in symbiotic *Tulasnella* sp., 99 genes encoding CAZymes were differentially expressed in symbiotic *Serendipita* sp., and AA family members, CBM, CE, and GH, were upregulated in symbiotic fungi compared with FLM. CBM 43 (β-1,3-glucanosyltransferase, former X8) and CBM48 (starch debranching enzymes) are not common in the known various fungal lifestyles, and their exact function in orchid mycorrhizal fungi is also unclear, but their significantly high expression in symbiotic *Tulasnella* sp. implies that they likely play a vital role in fungal cell wall construction because they are required for fungal cell wall component dual

β-(1,3)-glucan elongation and branching (Aimanianda et al., 2017). In addition, chitin deacetylases of the CE4 family were upregulated in symbiotic *Tulasnella* sp. and chitosan, the product of *Tulasnella* chitin deacetylases has been identified by metabolomic analyses in symbiotic orchid protocorms (Ghirardo et al., 2020). The role of CE4 is suspected to protect the fungal cell wall from acting by plant chitin or decreasing the plant defense responses when the fungal colonization transfers chitin to chitosan in the ECM (Veneault-Fourrey et al., 2014).

Genes encoding the lignin-degrading auxiliary enzyme AA class were also upregulated in symbiotic *Tulasnella* sp. and *Serendipita* compared to FLM, especially AA9, a family of fungal origin with only lytic polysaccharide monooxygenases (Vandhana et al., 2021). AA9 is a mono-copper enzyme family and participates in the degradation of lignocellulose via the oxidative cleavage of celluloses, cello-oligosaccharides, or hemicelluloses (Zhang, 2020). Zarattini et al. (2021) employed AA9 LPMO reaction products to trigger innate immune responses in the model plant *Arabidopsis thaliana* during fungal pathogenesis, while results on AA17 LPMO indicated that LPMO action would help overcome plant defense barriers (Sabbadin et al., 2021). Thus, the role of AA9 in orchid symbiotic germination needs to be further investigated. In addition, the glycoside hydrolase family GH5 and GH28 were recently confirmed to be involved in cell wall remodeling for ECM symbiosis as enzymatic effectors (Zhang et al., 2021). In our study, the expression of many glycoside hydrolase family members was induced in symbiotic tissue, such as genes encoding the hemicellulose-active enzyme GH3 (β-glucosidases), which were both upregulated in the symbiotic condition of the two fungi, indicating that they likely play a key role in orchid mycorrhizal establishment and development.

Of note, several genes encoding glycosyltransferases (GTs) were differentially expressed in symbiotic *Tulasnella* sp. or *Serendipita* sp. mycelium, and there were 9 GT family proteins (GT2, GT4, GT20, GT22, GT32, GT35, GT48, GT66) with induced expression among the 24 orthologous genes encoding CAZymes. Glycosyltransferases are enzymes that catalyze the transfer of sugar moieties from activating donor molecules to specific acceptor molecules, forming glycosidic bonds and are involved in the biosynthesis of diverse carbohydrates (http://www.cazy.org/GlycosylTransferase-family). A recent result indicated that GT2 likely participates in the synthesis of extracellular or outer cell wall polysaccharides, which play a key role in facilitating many interactions between plants and fungi by enabling hyphal growth on solid matrices (King et al., 2017). However, the exact function of glycosyltransferases in orchid mycorrhizae still needs to be characterized. Adamo et al. (2020) primarily explored the roles of CAZymes of orchid mycorrhizal fungi in the development of unsuccessful and successful interactions and suspected that the expression of some key CAZymes was related to OMF switches from symbiotic to saprotrophic growth. However, the mycorrhizal relationship is particularly complex in orchids, and successful mycrrhizal interactions between orchids and their symbionts can be controlled by a balance between fungal invasion and plant defense, balancing nutritional supply and demand; therefore, the specific nutritional strategy of orchids should be considered for mycorrhizal establishment.

In addition, *Tulasnella* and *Serendipita* possessed several CAZyme, but they display different expression profiles, indicating that their function could be different in fungal species. Moreover, only a few orthologous genes encoding CAZymes were identified. Among the 24 orthologous DEGs encoding CAZymes, most exhibited distinct expression profiles between *Tulasnella* and *Serendipita,* and only genes encoding GH5, AA1, AA2, CBM1, and GT66 were upregulated in at least one symbiotic stage in both *Tulasnella* and *Serendipita*. Thus, about function of CAZymes in different mycobionts during interaction with the host plant still need to be addressed furtherly in the future.

CONCLUSION

A high proportion of plant genes were induced, and most genes displayed similar expression profiles in *D. officinale* seeds inoculated with the two different fungal species of *Tulasnella* sp. and *Serendipita* sp., indicating that plant genes participate in symbiotic relationships, which might be conserved in orchid mycorrhizae. We also highlight the differences and similarities in fungal gene expression between *Tulasnella* sp. and *Serendipita* sp. during interactions with the same host plant. Comparative transcriptomics analyses identified a core set of orthologous genes between *Tulasnella* sp. and *Serendipita* sp. involved in symbiotic orchid germination. Most symbiosis-induced genes are restricted to a single fungal species. Several genes encoding CAZyme likely contribute to establishing orchid mycorrhizal interactions. The available transcriptome sequences of mycorrhizal fungi interactions with orchid plants represent foundational information for a better understanding of symbiosis development, the function of orchid mycorrhiza, and orchid seed biology.

DATA AVAILABILITY STATEMENT

The datasets presented in this study can be found in online repositories. The names of the repository/repositories and accession number(s) can be found below: National Center for Biotechnology Information (NCBI). SRA database BioProject database under accession number PRJNA805043.

AUTHOR CONTRIBUTIONS

JC, FM, and SG designed the experiments. YT and DZ performed the experiments. JC, YT, AK, AL, YL, and YX analyzed the data. FM discussed the result and gave great suggestions. JC wrote the manuscript draft and all authors revised and discussed it. All authors contributed to the article and approved the submitted version.

FUNDING

This work was funded by the National Natural Science Foundation of China (81973423) and the CAMS Innovation Fund for Medical Sciences (CIFMS) (2021-I2M-1-032).

SUPPLEMENTARY MATERIAL

The Supplementary Material for this article can be found online at: https://www.frontiersin.org/articles/10.3389/fpls.2022.880600/full#supplementary-material

Supplementary Figure S1 | Venn diagram showing the number of fungal genes differentially expressed across various symbiotic stages of *D. officinale* inoculated with *Tulasnella* sp. and *Serendipita* sp. **(A–D)**. **(E)** Functional classification of 2,555 co-upregulated fungal genes of *Tulasnella* sp. in symbiotic status compared to free living mycelium; **(F)** Functional classfication of 403 co-upregulated fungal genes of *Serendipita* sp. in symbiotic status compared to free-living mycelium.

Supplementary Figure S2 | Cluster analysis of 936 fungal orthologous differentially expressed genes. All genes analyzed were divided into five clusters. F_S2, F_S3, F_S3 means *Serendipita* sp. in symbiotic statuses 2, 3, and 4 stages, and F_T2, F_T3, and F_T4 means *Tulasnella* sp. in symbiotic statuses 2, 3, and4 stage (according to seed germination), Ft and Fs means free-living mycelium of *Tulasnella* sp. and *Serendipita* sp., respectively.

Supplementary Table S1 | Functional classification of 452 upregulated expressed plant genes across various symbiotic germination stages of *D.officinale* inoculated with *Tulasnella* sp. or *Serendipita* sp.

Supplementary Table S2 | 25 most up-regulated common expression plant genes across germination stage whatever inoculated with *Tulasnella* sp. and *Serendipita* sp. (Fold change $\geq$ 5).

Supplementary Table S3 | The KEGG pathway annotation of 936 orthologous expressed genes in 5 clusters.

REFERENCES

Adamo, M., Chialva, M., Calevo, J., Rose, S., Girlanda, M., Perotto, S., et al. (2020). The Dark side of orchid symbiosis: can *Tulasnella calospora* decompose host tissues? *Int. J. Mol. Sci.* 21, 3139. doi: 10.3390/ijms21093139

Aimanianda, V., Simenel, C., Garnaud, C., Clavaud, C., Tada, R., Barbin, L., et al. (2017). The dual activity responsible for the elongation and branching of beta-(1,3)-Glucan in the fungal cell wall. *MBio* 8, e00619–e00617. doi: 10.1128/mBio.00619-17

Balestrini, R., and Bonfante, P. (2014). Cell wall remodeling in mycorrhizal symbiosis: a way towards biotrophism. *Front. Plant Sci.* 5, 237. doi: 10.3389/fpls.2014.00237

Balestrini, R., Nerva, L., Sillo, F., Girlanda, M., and Perotto, S. (2014). Plant and fungal gene expression in mycorrhizal protocorms of the orchid *Serapias vomeracea* colonized by *Tulasnella calospora*. *Plant Signal. Behav.* 9, e977707. doi: 10.4161/15592324.2014.977707

Bolger, A. M., Lohse, M., and Usadel, B. (2014). Trimmomatic: A flexible trimmer for Illumina sequence data. *Bioinformatics* 30, 2114–2120. doi: 10.1093/bioinformatics/btu170

Bougoure, J. J., Brundrett, M. C., and Grierson, P. F. (2010). Carbon and nitrogen supply to the underground orchid, *Rhizanthella gardneri*. *New Phytol.* 186, 947–956. doi: 10.1111/j.1469-8137.2010.03246.x

Bruns, T. D., Corradi, N., Redecker, D., Taylor, J. W., and Öpik, M. (2018). Glomeromycotina: what is a species and why should we care? *New Phytol.* 220, 963–967. doi: 10.1111/nph.14913

Cameron, D. D., Leake, J. R., and Read, D. J. (2006). Mutualistic mycorrhiza in orchids: evidence from plant-fungus carbon and nitrogen transfers in the green-leaved terrestrial orchid *Goodyera repens*. *New Phytol.* 171, 405–416. doi: 10.1111/j.1469-8137.2006.01767.x

Casarrubia, S., Daghino, S., Kohler, A., Morin, E., Khouja, H. R., Daguerre, Y., et al. (2018). The hydrophobin-like OmSSP1 may be an effector in the ericoid mycorrhizal symbiosis. *Front. Plant Sci.* 9, 546. doi: 10.3389/fpls.2018.00546

Castilleux, R., Plancot, B., Gügi, B., Attard, A., Loutelier-Bourhis, C., Lefranc, B., et al. (2020). Extensin arabinosylation is involved in root response to elicitors and limits Oomycete colonization. *Ann. Bot.*125, 751–763. doi: 10.1093/aob/mcz068

Castilleux, R., Plancot, B., Ropitaux, M., Carreras, A., Leprince, J., Boulogne, I., et al. (2018). Cell wall extensins in root-microbe interactions and root secretions. *J. Exp. Bot.* 69, 4235–4247. doi: 10.1093/jxb/ery238

Castilleux, R., Plancot, B., Vicr,é, M., Nguema-Ona, E., and Driouich, A. (2021). Extensin, an underestimated key component of cell wall defence? *Ann. Bot.* 127, 709–713. doi: 10.1093/aob/mcab001

Chen, J., Liu, S. S., Kohler, A., Yan, B., Luo, H. M., Chen, X. M., et al. (2017). iTRAQ and RNA-seq analyses provide new insights into regulation mechanism of symbiotic germination of *Dendrobium officinale* seeds (Orchidaceae). *J. Proteome Res.* 16, 2174–2187. doi: 10.1021/acs.jproteome.6b00999

Chen, J., Wang, H., Liu, S. S., Li, Y. Y., and Guo, S. X. (2014). Ultrastructure of symbiotic germination of the orchid *Dendrobium officinale* with its mycobiont, *Sebacina* sp. *Aust. J. Bot.* 62, 229–234. doi: 10.1071/BT14017

Chen, J., Yan, B., Tang, Y., Xing, Y., Li, Y., Zhou, D., et al. (2020). Symbiotic and asymbiotic germination of *Dendrobium officinale* (Orchidaceae) respond differently to exogenous gibberellins. *Int. J. Mol. Sci.* 21, 6104. doi: 10.3390/ijms21176104

Dearnaley, J. D., and Cameron, D. D. (2017). Nitrogen transport in the orchid mycorrhizal symbiosis - further evidence for a mutualistic association. *New Phytol.* 213, 10–12. doi: 10.1111/nph.14357

Dearnaley, J. D. W. (2007). Further advances in orchid mycorrhizal research. *Mycorrhiza*. 17, 475–486. doi: 10.1007/s00572-007-0138-1

Dobin, A., Davis, C. A., Schlesinger, F., Drenkow, J., Zaleski, C., Jha, S., et al. (2013). STAR: Ultrafast universal RNA-seq aligner. *Bioinformatics* 29, 15–21. doi: 10.1093/bioinformatics/bts635

Dobin, A., and Gingeras, T. R. (2015). Mapping RNA-seq reads with STAR. *Curr Protoc Bioinform.* 51, 11.14.1–11.14.19. doi: 10.1002/0471250953.bi1114s51

Favre-Godal, Q., Gourguillon, L., Lordel-Madeleine, S., Gindro, K., and Choisy, P. (2020). Orchids and their mycorrhizal fungi: an insufficiently explored relationship. *Mycorrhiza* 30, 5–22. doi: 10.1007/s00572-020-00934-2

Feldman, D., Yarden, O., and Hadar, Y. (2020). Seeking the roles for fungal small-secreted proteins in affecting saprophytic lifestyles. *Front. Microbiol.* 11, 455. doi: 10.3389/fmicb.2020.00455

Fochi, V., Chitarra, W., Kohler, A., Voyron, S., Singan, V. R., Lindquist, E. A., et al. (2017). Fungal and plant gene expression in the *Tulasnella calospora-Serapias vomeracea* symbiosis provides clues about nitrogen pathways in orchid mycorrhizas. *New Phytol.* 213, 365–379. doi: 10.1111/nph.14279

Freestone, M. W., Swarts, N. D., Reiter, N., Tomlinson, S., Sussmilch, F. C., Wright, M. M., et al. (2021). Continental-scale distribution and diversity of *Ceratobasidium* orchid mycorrhizal fungi in Australia. *Ann. Bot.* 128, 329–343. doi: 10.1093/aob/mcab067

Genre, A., and Bonfante, P. (2002). Epidermal cells of a symbiosis-defective mutant of *Lotus japonicus* show altered cytoskeleton organisation in the presence of a mycorrhizal fungus. *Protoplasma* 219, 43–50. doi: 10.1007/s007090200004

Genre, A., Lanfranco, L., Perotto, S., and Bonfante, P. (2020). Unique and common traits in mycorrhizal symbioses. *Nat. Rev. Microbiol.* 18, 649–660. doi: 10.1038/s41579-020-0402-3

Ghirardo, A., Fochi, V., Lange, B., Witting, M., Schnitzler, J.-P., Perotto, S., et al. (2020). Metabolomic adjustments in the orchid mycorrhizal fungus *Tulasnella calospora* during symbiosis with *Serapias vomeracea*. *New Phytol.* 228, 1939–1952. doi: 10.1111/nph.16812

Grabherr, M. G., Haas, B. J., Yassour, M., Levin, J. Z., Thompson, D. A., Amit, I., et al. (2011). Full-length transcriptome assembly from RNA-Seq data without a reference genome. *Nat. Biotechnol.* 29, 644–652. doi: 10.1038/nbt.1883

Herger, A., Dünser, K., Kleine-Vehn, J., and Ringli, C. (2019). Leucine-rich repeat extensin proteins and their role in cell wall sensing. *Curr. Biol.* 29, R851–R858. doi: 10.1016/j.cub.2019.07.039

Ho-Pl Garo, T., Huertas, R. L., Tamayo-Navarrete, M. A. I., Blancaflor, E., Gavara, N., and Garc A-Garrido, J. M. (2021). A novel putative microtubule-associated protein is involved in arbuscule development during arbuscular mycorrhiza formation. *Plant Cell Physiol.* 62, 306–320. doi: 10.1093/pcp/pcaa159

Jacquemyn, H., Brys, R., Waud, M., Busschaert, P., and Lievens, B. (2015). Mycorrhizal networks and coexistence in species-rich orchid communities. *New Phytol.* 206, 1127–1134. doi: 10.1111/nph.13281

Jacquemyn, H., Waud, M., Brys, R., Lallemand, F., Courty, P. E., Robionek, A., et al. (2017). Mycorrhizal associations and trophic modes in coexisting orchids: an ecological continuum between auto- and mixotrophy. *Front. Plant Sci.* 8, 1497. doi: 10.3389/fpls.2017.01497

King, R., Urban, M., Lauder, R. P., Hawkins, N., Evans, M., Plummer, A., et al. (2017). A conserved fungal glycosyltransferase facilitates pathogenesis of plants by enabling hyphal growth on solid surfaces. *PLoS Pathog.* 13, e1006672. doi: 10.1371/journal.ppat.1006672

Kohler, A., Kuo, A., Nagy, L. G., Morin, E., Barry, K. W., Buscot, F., et al. (2015). Convergent losses of decay mechanisms and rapid turnover of symbiosis genes in mycorrhizal mutualists. *Nat. Genet.* 47, 410–415. doi: 10.1038/ng.3223

Kuga, Y., Sakamoto, N., and Yurimoto, H. (2014). Stable isotope cellular imaging reveals that both live and degenerating fungal pelotons transfer carbon and nitrogen to orchid protocorms. *New Phytol.* 202, 594–605. doi: 10.1111/nph.12700

Li, B., and Dewey, C. N. (2011). RSEM: accurate transcript quantification from RNA-Seq data with or without a reference genome. *BMC Bioinform.* 12, 323. doi: 10.1186/1471-2105-12-323

Li, T., Yang, W., Wu, S., Selosse, M. A., and Gao, J. (2021). Progress and prospects of mycorrhizal fungal diversity in Orchids. *Front. Plant Sci.* 12, 646325. doi: 10.3389/fpls.2021.646325

Li, Y. Y., Chen, X. M., Zhang, Y., Cho, Y. H., Wang, A. R., Yeung, E. C., et al. (2018). Immunolocalization and changes of hydroxyproline-rich glycoproteins during symbiotic germination of *Dendrobium officinale*. *Front. Plant Sci.* 9, 552. doi: 10.3389/fpls.2018.00552

Lionetti, V., and Métraux, J. P. (2014). Plant cell wall in pathogenesis, parasitism and symbiosis. *Front. Plant Sci.* 5, 612. doi: 10.3389/fpls.2014.00612

Martin, F., Kohler, A., Murat, C., Veneault-Fourrey, C., and Hibbett, D. S. (2016). Unearthing the roots of ectomycorrhizal symbioses. *Nat. Rev. Microbiol.* 14, 760–773. doi: 10.1038/nrmicro.2016.149

McCormick, M. K., Whigham, D. F., and Canchani-Viruet, A. (2018). Mycorrhizal fungi affect orchid distribution and population dynamics. *New Phytol.* 219, 1207–1215. doi: 10.1111/nph.15223

Miura, C.,Yamaguchi, K., Miyahara, R., Yamamoto, T., Fuji, M., Yagame, T., et al. (2018). The Mycoheterotrophic symbiosis between orchids and mycorrhizal fungi possesses major components shared with mutualistic plant-mycorrhizal symbioses. *Mol. Plant Microbe Interact.* 31, 1032–1047. doi: 10.1094/MPMI-01-18-0029-R

Miyauchi, S., Kiss, E., Kuo, A., Drula, E., Kohler, A., Sánchez-García, M., et al. (2020). Large-scale genome sequencing of mycorrhizal fungi provides insights into the early evolution of symbiotic traits. *Nat. Commun.* 11, 5125. doi: 10.1038/s41467-020-18795-w

Parniske, M. (2008). Arbuscular mycorrhiza: the mother of plant root endosymbioses. *Nat. Rev. Microbiol.* 6, 763–775. doi: 10.1038/nrmicro1987

Pellegrin, C., Morin, E., Martin, F. M., and Veneault-Fourrey, C. (2015). Comparative analysis of secretomes from ectomycorrhizal fungi with an emphasis on small-secreted proteins. *Front. Microbiol.* 6, 1278. doi: 10.3389/fmicb.2015.01278

Perotto, S., Rodda, M., Benetti, A., Sillo, F., Ercole, E., Rodda, M., et al. (2014). Gene expression in mycorrhizal orchid protocorms suggests a friendly plant-fungus relationship. *Planta* 239, 1337–1349. doi: 10.1007/s00425-014-2062-x

Phillips, R. D., Reiter, N., and Peakall, R. (2020). Orchid conservation: from theory to practice. *Ann. Bot.* 126, 345–362. doi: 10.1093/aob/mcaa093

Plett, J. M., Daguerre, Y., Wittulsky, S., Vayssières, A., Deveau, A., Melton, S. J., et al. (2014). Effector MiSSP7 of the mutualistic fungus *Laccaria bicolor* stabilizes the *Populus* JAZ6 protein and represses jasmonic acid (JA) responsive genes. *Proc. Natl. Acad. Sci. U. S. A.*111, 8299–8304. doi: 10.1073/pnas.1322671111

Radhakrishnan, G. V., Keller, J., Rich, M. K., Vernie, T., Mbadinga Mbadinga, D. L., Vigneron, N., et al. (2020). An ancestral signalling pathway is conserved in intracellular symbioses-forming plant lineages. *Nat. Plants* 6, 280–289. doi: 10.1038/s41477-020-0613-7

Rasmussen, H. N. (2002). Recent developments in the study of orchid mycorrhiza. *Plant Soil* 244, 149–163. doi: 10.1023/A:1020246715436

Rasmussen, H. N., Dixon, K. W., Jersáková, J., and Těšitelová, T. (2015). Germination and seedling establishment in orchids: a complex of requirements. *Ann. Bot.* 116, 391–402. doi: 10.1093/aob/mcv087

Rich, M. K., Schorderet, M., and Reinhardt, D. (2014). The role of the cell wall compartment in mutualistic symbioses of plants. *Front. Plant Sci.* 5, 238. doi: 10.3389/fpls.2014.00238

Robinson, M. D., McCarthy, D. J., and Smyth, G. K. (2010). edgeR: A Bioconductor package for differential expression analysis of digital gene expression data. *Bioinformatics* 26, 139–140. doi: 10.1093/bioinformatics/btp616

Robinson, M. D., and Oshlack, A. (2010). A scaling normalization method for differential expression analysis of RNA-seq data. *Genome Biol.* 11, R25. doi: 10.1186/gb-2010-11-3-r25

Sabbadin, F., Urresti, S., Henrissat, B., Avrova, A. O., Welsh, L. R., Lindley, P. J., et al. (2021). Secreted pectin monooxygenases drive plant infection by pathogenic oomycetes. *Science* 373, 774–779. doi: 10.1126/science.abj1342

Selosse, M. A., Petrolli, R., Mujica, M. I., Laurent, L., Perez-Lamarque, B., Figura, T., et al. (2021). The waiting room hypothesis revisited by orchids: were orchid mycorrhizal fungi recruited among root endophytes? *Ann. Bot.* 129, 259–270. doi: 10.1093/aob/mcab134

Shao, S. C., Luo, Y., and Jacquemyn, H. (2021). Successful reintroduction releases pressure on China's orchid species. *Trends Plant Sci.* 27, 211–213. doi: 10.1016/j.tplants.2021.11.018

Smith, S. E., and Read, D. J. (2008). *Mycorrhizal Symbiosis*. Cambridge: Elsevier.

Stewart, S. L., and Zettler L. W. (2002). Symbiotic germination of three semi-aquatic rein orchids (*Habenaria repens, H. quinqueseta, H. macroceratitis*) from Florida. *Aquatic Bot.* 72, 25–35. doi: 10.1016/S0304-3770(01)00214-5

Suetsugu, K., Matsubayashi, J., and Tayasu, I. (2020). Some mycoheterotrophic orchids depend on carbon from dead wood: novel evidence from a radiocarbon approach. *New Phytol.* 227, 1519–1529. doi: 10.1111/nph.16409

Tanaka, S., and Kahmann, R. (2021). Cell wall-associated effectors of plant-colonizing fungi. *Mycologia* 113, 247–260. doi: 10.1080/00275514.2020.1831293

Taylor, D. L., and Bruns, T. D. (1997). Independent, specialized invasions of ectomycorrhizal mutualism by two nonphotosynthetic orchids. *Proc. Natl. Acad. Sci. U. S. A.* 94, 4510–4515. doi: 10.1073/pnas.94.9.4510

Tedersoo, L., Bahram, M., and Zobel, M. (2020). How mycorrhizal associations drive plant population and community biology. *Science* 367, eaba1223. doi: 10.1126/science.aba1223

Uetake, Y., Farquhar, M. L., and Peterson, R. L. (1996). Changes in microtubule arrays in symbiotic orchid protocorms during fungal colonisation and senescence. *New Phytol.* 135, 701–709. doi: 10.1046/j.1469-8137.1997.00686.x

Uetake, Y., and Peterson, R. L. (1998). Association between microtubules and symbiotic fungal hyphae in protocorm cells of the orchid species, *Spiranthes sinensis*. *New Phytol.* 140, 715–722. doi: 10.1046/j.1469-8137.1998.00310.x

Valadares, R. B. S., Marroni, F., Sillo, F., Oliveira, R. R. M., Balestrini, R., and Perotto, S. (2021). A transcriptomic approach provides insights on the mycorrhizal symbiosis of the mediterranean orchid *Limodorum abortivum* in nature. *Plants* 10, 251. doi: 10.3390/plants10020251

Vandenkoornhuyse, P., Mahé, S., Ineson, P., Staddon, P., Ostle, N., Cliquet, J. B., et al. (2007). Active root-inhabiting microbes identified by rapid incorporation of plant-derived carbon into RNA. *Proc. Natl. Acad. Sci. U. S. A.* 104, 16970–16975. doi: 10.1073/pnas.0705902104

Vandhana, T. M., Reyre, J. L., Sushmaa, D., Berrin, J. G., Bissaro, B., and Madhuprakash, J. (2021). On the expansion of biological functions of lytic polysaccharide monooxygenases. *New Phytol.* 233, 2380–2396. doi: 10.1111/nph.17921

Veneault-Fourrey, C., Commun, C., Kohler, A., Morin, E., Balestrini, R., and Plett, J. (2014). Genomic and transcriptomic analysis of *Laccaria bicolor* CAZome reveals insights into polysaccharides remodelling during symbiosis establishment. *Fungal Genet. Biol.* 72, 168–181. doi: 10.1016/j.fgb.2014.08.007

Ventre Lespiaucq, A., Jacquemyn, H., Rasmussen, H. N., and Méndez, M. (2021). Temporal turnover in mycorrhizal interactions: a proof of concept with orchids. *New Phytol.* 230, 1690–1699. doi: 10.1111/nph.17291

Wang, D., Jacquemyn, H., Gomes, S. I. F., Vos, R. A., and Merckx, V. S. F. T. (2021). Symbiont switching and trophic mode shifts in Orchidaceae. *New Phytol.* 231, 791–800. doi: 10.1111/nph.17414

Xing, X., Gai, X., Liu, Q., Hart, M. M., and Guo, S. (2015). Mycorrhizal fungal diversity and community composition in a lithophytic and epiphytic orchid. *Mycorrhiza* 25, 289–296. doi: 10.1007/s00572-014-0612-5

Zarattini, M., Corso, M., Kadowaki, M. A., Monclaro, A., Magri, S., Milanese, I., et al. (2021). LPMO-oxidized cellulose oligosaccharides evoke immunity in *Arabidopsis* conferring resistance towards necrotrophic fungus *B. cinerea*. *Commun. Biol.* 4, 727. doi: 10.1038/s42003-021-02226-7

Zeng, T., Rodriguez-Moreno, L., Mansurkhodzaev, A., Wang, P., van den Berg, W., Gasciolli, V., et al. (2020). A lysin motif effector subverts chitin-triggered immunity to facilitate arbuscular mycorrhizal symbiosis. *New Phytol.* 225, 448–460. doi: 10.1111/nph.16245

Zhang, F., Labourel, A., Haon, M., Kemppainen, M., Da Silva Machado, E., and Brouilly, N. (2021). The ectomycorrhizal basidiomycete *Laccaria bicolor* releases a GH28 polygalacturonase that plays a key role in symbiosis establishment. *New Phytol.* 233, 2534–2547. doi: 10.1101/2021.09.24.461608

Zhang, H., Yohe, T., Huang, L., Entwistle, S., Wu, P., Yang, Z., et al. (2018). dbCAN2: a meta server for automated carbohydrate-active enzyme annotation. *Nucleic Acids Res.* 46, W95–W101. doi: 10.1093/nar/gky418

Zhang, R. (2020). Functional characterization of cellulose-degrading AA9 lytic polysaccharide monooxygenases and their potential exploitation. *Appl. Microbiol. Biotechnol.* 104, 3229–3243. doi: 10.1007/s00253-020-10467-5

Conflict of Interest: The authors declare that the research was conducted in the absence of any commercial or financial relationships that could be construed as a potential conflict of interest.

Publisher's Note: All claims expressed in this article are solely those of the authors and do not necessarily represent those of their affiliated organizations, or those of the publisher, the editors and the reviewers. Any product that may be evaluated in this article, or claim that may be made by its manufacturer, is not guaranteed or endorsed by the publisher.

frontiers | Frontiers in Plant Science

HYPOTHESIS AND THEORY
published: 06 July 2022
doi: 10.3389/fpls.2022.904313

Regulatory Modules Involved in the Degradation and Modification of Host Cell Walls During *Cuscuta campestris* Invasion

Ryusuke Yokoyama[1], Toshiya Yokoyama[2], Takeshi Kuroha[3], Jihwan Park[4], Koh Aoki[4] and Kazuhiko Nishitani[2]*

[1] Graduate School of Life Sciences, Tohoku University, Sendai, Japan, [2] Faculty of Science, Kanagawa University, Hiratsuka, Japan, [3] Division of Crop Genome Editing Research, Institute of Agrobiological Science, National Agriculture and Food Research Organization, Tsukuba, Japan, [4] Graduate School of Life and Environmental Sciences, Osaka Prefecture University, Sakai, Japan

Haustoria of parasitic plants have evolved sophisticated traits to successfully infect host plants. The degradation and modification of host cell walls enable the haustorium to effectively invade host tissues. This study focused on two *APETALA2/ETHYLENE RESPONSE FACTOR* (*ERF*) genes and a set of the cell wall enzyme genes principally expressed during the haustorial invasion of *Cuscuta campestris* Yuncker. The orthogroups of the TF and cell wall enzyme genes have been implicated in the cell wall degradation and modification activities in the abscission of tomatoes, which are currently the phylogenetically closest non-parasitic model species of *Cuscuta* species. Although haustoria are generally thought to originate from root tissues, our results suggest that haustoria have further optimized invasion potential by recruiting regulatory modules from other biological processes.

Keywords: parasitic, haustorium, cell wall, ERF, regulatory module

OPEN ACCESS

Edited by:
Vincenzo Lionetti, Sapienza University of Rome, Italy

Reviewed by:
Satoko Yoshida, Nara Institute of Science and Technology (NAIST), Japan
Kirsten Krause, UiT The Arctic University of Norway, Norway

****Correspondence:***
Ryusuke Yokoyama
ryusuke.yokoyama.d6@tohoku.ac.jp

Specialty section:
This article was submitted to Plant Pathogen Interactions, a section of the journal Frontiers in Plant Science

Received: *25 March 2022*
Accepted: *21 June 2022*
Published: *06 July 2022*

Citation:
Yokoyama R, Yokoyama T, Kuroha T, Park J, Aoki K and Nishitani K (2022) Regulatory Modules Involved in the Degradation and Modification of Host Cell Walls During Cuscuta campestris Invasion. Front. Plant Sci. 13:904313. doi: 10.3389/fpls.2022.904313

INTRODUCTION

Cuscuta species are one of the most widespread groups of parasitic plants that severely damage economically important crops, reducing yields (Westwood et al., 2010). Parasitic plants absorb resources from the host through an invasive organ called the haustorium (Dawson et al., 1994). Haustorium penetrates the host tissue and develops into search hyphae, which elongate within the host tissue. Search hyphae differentiate into vascular hyphae upon reaching the host vasculature, followed by the establishment of a vascular connection between the parasite and the host plant (Kaga et al., 2020; Park et al., 2022). A series of haustorium development processes are involved in a variety of molecular interactions between host plants and parasitic plants (Hegenauer et al., 2016, 2020). Thus, understanding the molecular basis of haustorium development is not only important from a crop production viewpoint but also of interest from a biological perspective (Shimizu and Aoki, 2019).

Abbreviations: TF, transcription factor; DREB, dehydration response element-binding factors; DEG, differentially expressed genes; TPM, transcripts per million; LMD, laser capture microdissection.

Recently, molecular research on *Cuscuta campestris* provided an invaluable basis for enhancing our knowledge of haustorium development and function. For example, Jhu et al. (2021) demonstrated that CcLBD25 is a crucial regulator of *C. campestris* haustorium development including haustorium initiation. Furthermore, three genes (*CcHB7*, *CcPMEI*, and *CcERF1*) were recently identified as putative key regulators of *C. campestris* haustorium organogenesis (Jhu et al., 2022). Previously, we also observed that *C. campestris* utilizes host-produced ethylene for the proper growth of search hyphae, and penetration into the host tissue is facilitated by the degradation and modification of host cell walls (Narukawa et al., 2021; Yokoyama et al., 2021). Additionally, we performed transcriptomic analysis using an *in vitro* induction system to characterize xylem vessel cell differentiation in the haustorium of *C. campestris* (Kaga et al., 2020). Several aspects of the haustorium have been evaluated, but the molecular-level understanding of haustorium development, especially regarding transcriptional regulation, remains incomplete.

To understand the transcriptional regulation of haustorium development, we comprehensively characterized the TFs involved in haustorium development. This study focused on two *APETALA2/ETHYLENE RESPONSE FACTOR* (*ERF*) genes that displayed a significant expression correlation with the cell wall enzyme genes during the haustorial invasion. The *C. campestris* ERFs are orthologous to tomato SlERF52, which regulates genes encoding abscission-associated cell wall enzymes (Nakano et al., 2014). In plants, abscission is generally defined as the process that detaches leaves or flower organs from the remainder of the plant body. In this process, cell wall degradation is facilitated by the activation of cell wall enzymatic genes, which are orthologous to the *C. campestris* cell wall enzyme genes involved in haustorial invasion (Yokoyama et al., 2021). Together, the *C. campestris* ERFs might activate the transcription of the cell wall enzymatic genes in haustorial invasion.

MATERIALS AND METHODS

Comparative Analysis of Gene Expression Profiles in Haustoria of *Cuscuta campestris* Parasitizing *Nicotiana tabacum* Stems and Non-living Materials

RNA-seq analysis was performed by using *C. campestris* stem coiling around rods made of non-living material (dried bamboo rod) or living material (stem of wild type *Nicotiana tabacum*). Seeds of *C. campestris* were germinated, grown for 7 days, and coiling was induced, as described previously (Hozumi et al., 2017). The time at which *C. campestris* coiled around the host *N. tabacum* stem was designated 0 h after coiling (hac). Samples of coiling stems of *C. campestris* were harvested at 0, 24, 48 hac, and total RNA was prepared as described previously (Shimizu et al., 2018). Sequencing libraries were constructed by using TruSeq RNA Library Preparation Kit v2, and read by using Illumina HiSeq 2500 platform (Illumina Inc., San Diego, CA, United States.) to obtain 100 nt-long single-end reads. Quality and read length distribution of the raw data in the FASTQ format were checked using FastQC.[1] Barcode removal and adapter sequence trimming was performed with the Trimmomatic (Bolger et al., 2014), followed by quality control (-q 20 -p 80). Mapping to *C. campestris* transcripts (Vogel et al., 2018) was performed by using HISAT2 and Stringtie (Pertea et al., 2015). Gene Ontology term enrichment analysis was performed by using web tool provided by The Arabidopsis Information Resource (TAIR).[2] Run data are registered in DDBJ Sequence Read Archive under accession numbers of DRR353312-DRR353329.

Cluster Analysis of Gene Expression Data in Haustorium Development in *Cuscuta campestris* Parasitizing *Arabidopsis thaliana*

We performed soft clustering analysis on gene sets defined as DEGs using Mfuzz (Futschik and Carlisle, 2005) based on TPM with the RNA-seq data generated previously by our group (Kaga et al., 2020). RNA-seq data were obtained from the DNA Data Bank of Japan (DDBJ) Sequence Read Archive.[3] A brief description of each sample is as follows. The *C. campestris* stems were harvested at 24 h after exposure to blue light and attachment to host. We designated "time 0 h after coiling" as the time point at which *C. campestris* completed coiling around the host (Hozumi et al., 2017). This stage probably corresponds to a pre-infective stage because expression of marker genes for an early infective "swelling stage" is not detected (Bawin et al., 2022). Additionally, the marker gene (e.g., Cc008373) for the early infective stage was specifically expressed at 12 hac. The exact timing when Cuscuta stem stops coiling movement around the host was determined based on the images captured by time lapse camera at 5-min intervals during the coiling and subsequent period. Tissue samples obtained at 0 hac consisted of the epidermis and cortex of the *C. campestris* at the contact site of the *Arabidopsis thaliana* (L.) Heynh inflorescence stem. Tissue samples obtained at 12, 42, and 54 hac were all derived from haustoria in the coiling regions of *C. campestris* lateral shoots parasitizing the *A. thaliana* stems. Tissue samples (n = 50) were transversely sectioned (100 μm) along the host stem axis, using a vibratome. Haustorial regions were excised and pooled from the transverse sections by LMD using the PALM MicroBeam (Carl Zeiss Microscopy GmbH). Total RNAs were isolated from 50 haustorial regions. Three biological replicates were prepared for each stage of the development. Tissue samples containing epidermal and cortical cells of *C. campestris* without contact with the *A. thaliana* stem were used as negative controls (-). The "flower" and "seedlings" samples were derived from *C. campestris* flower bud clusters and 7-day-old seedlings, respectively.

[1] https://www.bioinformatics.babraham.ac.uk/projects/fastqc/
[2] https://www.arabidopsis.org/tools/go_term_enrichment.jsp
[3] https://trace.ddbj.nig.ac.jp/dra/index_e.html/DRA009453

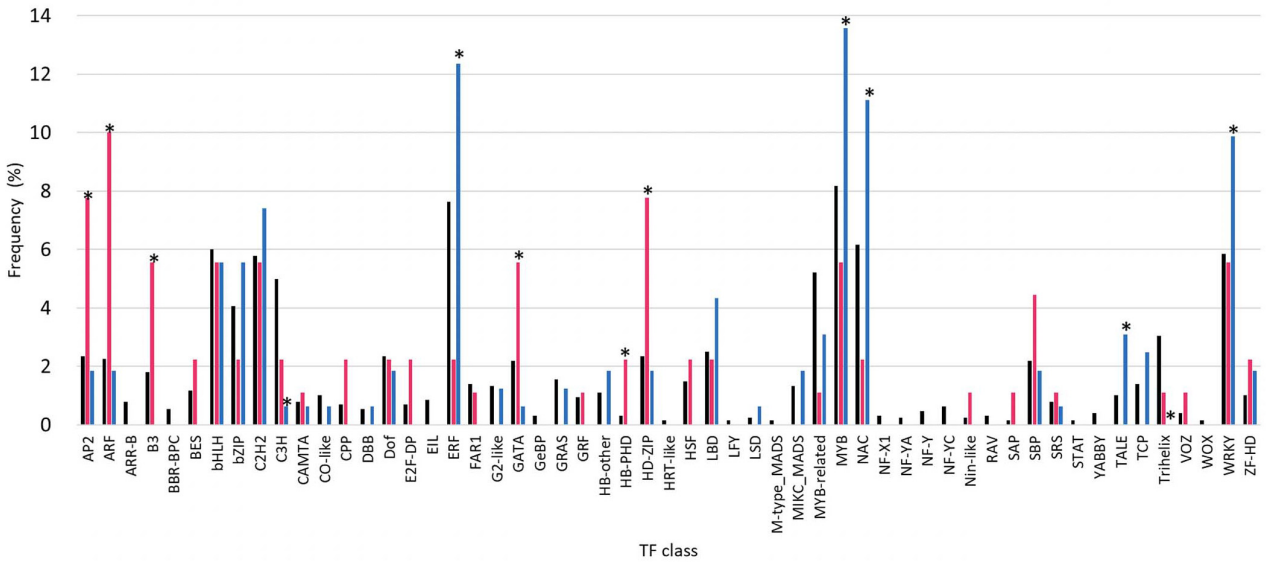

FIGURE 1 | Comparison of transcription factor (TF) expression in haustoria of *Cuscuta campestris* parasitizing *Nicotiana tabacum* stems and non-living materials. TF families were classified according to the identification and characterization of PlantTFDB (http://planttfdb.gao-lab.org). Black bars indicate the population of family genes in all the TF members of *C. campestris*. Red bars indicate the population of members that showed higher expression levels in *C. campestris* parasitizing *N. tabacum* stems than rods made of non-living material (dried bamboo sticks) at 24 and 48 hac, and progressively increased of expression levels from 0 to 48 hac (fold change (FC) > 2, comparing 0 hac vs. 48 hac), in each TF family. Blue bars indicate the population of members that showed lower expression levels in *C. campestris* parasitizing *N. tabacum* stems than bamboo sticks at 24 and 48 hac, and progressively decreased of expression levels from 0 to 48 hac [fold change (FC) < 0.5, comparing 0 hac vs. 48 hac], in each TF family. Asterisks indicate significant difference at 5% level of probability among members of each TF family.

Identification of Transcription Factors in *Cuscuta campestris*

A protein sequence dataset for *C. campestris* was downloaded from plaBiPD[4] (Vogel et al., 2018). The protein sequences for each TF family of *Solanum lycopersicum* L. were obtained from PlantTFDB.[5] BLASTP (e $\leq$ 1e−5) was performed to search for homologous proteins against the *C. campestris* protein sequence dataset using the protein sequences of TFs of *S. lycopersicum* as queries.

Phylogenetic Analysis and Characterization of *Cuscuta campestris* Ethylene Response Factors

Phylogenetic analysis was performed using the *C. campestris* and *S. lycopersicum* ERF protein sequences (Zhang et al., 2022). The amino acid sequences were aligned using the Gonnet matrix in Clustal 2.1. A phylogenetic tree was constructed using the iTOL online tool.[6] Conserved motifs of 10 ERF members of the subclade, including SlERF52, and consensus logos for the AP2/ERF domains were obtained using the software tool MEME.[7]

[4]https://www.plabipd.de
[5]http://planttfdb.gao-lab.org
[6]https://itol.embl.de
[7]http://meme.nbcr.net/meme/

Identification of *Cuscuta campestris* Orthologs of Tomato Abscission-Associated Transcription Factors

Cuscuta campestris orthologs of tomato abscission-associated TFs were identified based on a previous study (Ito and Nakano, 2015). BLASTP (e $\leq$ 1e−5) was performed to search for homologous proteins against the *C. campestris* protein sequence dataset, using the sequence data retrieved from the reference as queries. A graphical representation of the pairwise correlation between the haustorial expression patterns was constructed using the R package Corrplot.

RESULTS

Identification and Classification of Transcription Factor Genes in *Cuscuta campestris*

To comprehensively identify the TF genes in *C. campestris*, BLAST searches of the *C. campestris* database were performed using the protein sequences of the tomato TFs as queries. Tomato (*S. lycopersicum* L.) is currently the phylogenetically closest non-parasitic model species of the *Cuscuta* species and serves as a model for the family Solanaceae (Kimura and Sinha, 2008). We obtained tomato TF datasets from PlantTFDB,(see text footnote 5) a useful resource for the sequence and classification of plant TFs (Tian et al., 2019). A total of 1,283 *C. campestris* genes were

identified as potential TFs and then classified into 55 TF families (**Supplementary Table 1**).

Transcriptome Analysis of Transcription Factors Involved in the Interaction With the Host Plant *Nicotiana tabacum*

To examine the contribution of TFs to haustorium development involved in the interaction with the host, we performed the RNA-seq analysis to compare the expression levels of TFs of *C. campestris* stems coiling *N. tabacum* stems and a rod made of non-living materials. The results showed that their expression was influenced by the presence of host plant, although several types of the TF families had only the members with unchanging expression profiles (**Figure 1**). Among 1,283 TFs, 96 TFs showed significantly higher level of induction by the stem of living *N. tabacum* than non-living rod, while 180 TFs showed significantly lower level of induction. GO enrichment analysis demonstrated that GO terms such as regulation of cell differentiation (GO:0045595) and phyllome development (GO:0048827) were enriched uniquely among the TF genes which showed higher induction by living *N. tabacum*, and that defense response to fungus (GO:0050832), response to wounding (GO:0009611) and regulation of secondary cell wall biogenesis (GO:2000652) were enriched exclusively among the TF genes which showed lower induction by living *N. tabacum* (**Supplementary Table 2**).

Identification of Transcription Factor Genes Involved in Haustorium Development in *Cuscuta campestris* Parasitizing *Arabidopsis thaliana*

We investigated differentially expressed TF genes among different stages of haustorium development in *C. campestris* parasitizing the host plant *A. thaliana*. Using our previous comprehensive RNA-seq data for *C. campestris* haustorium development in combination with LMD (Kaga et al., 2020), clustering analysis was performed, and differentially expressed TF genes were identified in each cluster (**Figure 2**; **Supplementary Table 3**). The TF genes expressed in haustoria of *C. campestris* parasitizing *A. thaliana* coincided with those in *C. campestris* parasitizing *N. tabacum*, with some exceptions. The present results, associated with those of our previous reports, confirmed that TFs involved in vascular differentiation were predominantly expressed during the later stages of haustorium development (**Supplementary Table 4**; Kaga et al., 2020). We further characterized the TF genes predominantly expressed at the initial invasion stage (clusters 2 and 9 in **Figure 2B**), during which haustoria penetrated the host tissue by specific biochemical degradation and modification of host cell walls. The members of clusters 2 and 9 contained orthologs to Arabidopsis TFs involved in stress responses and developmental processes (**Supplementary Table 5**). However, we focused on *C. campestris* orthologous *SlERF52* genes because SlERF52 is known to regulate cell wall enzymatic activities in tomatoes (Nakano et al., 2014).

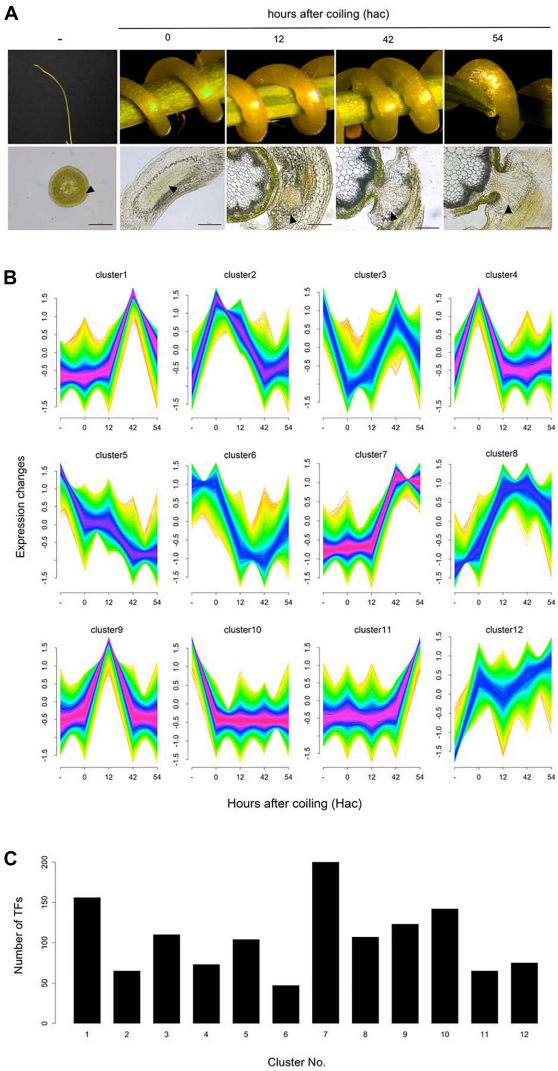

FIGURE 2 | Cluster analysis of differentially expressed genes during the haustorial invasion. **(A)** Images of the samples and the sections in each stage of haustorium development. Arrowheads indicate the tissue areas collected by laser microdissection. Scale bars: 200 μm. **(B)** Clustering analysis of differentially expressed genes (false discovery rate < 0.01) using Mfuzz. **(C)** Number of the transcription factors in each cluster.

Characterization of Orthologous SlERF52 in *Cuscuta campestris*

Ethylene response factors are unique transcriptional regulators with various functions in plants and are typically encoded by members of a multigene family. According to the classifications for Arabidopsis ERFs, the family members have been divided into ERF and DREB, which together comprise ten distinct groups (designated from I to X) (Sakuma et al., 2002; Nakano et al., 2006). To clarify the phylogenetic relationships between the genes in both tomato and *C. campestris* ERF families, we performed multiple alignment analyses using amino acid sequences of the ERF family members and constructed a phylogenetic tree

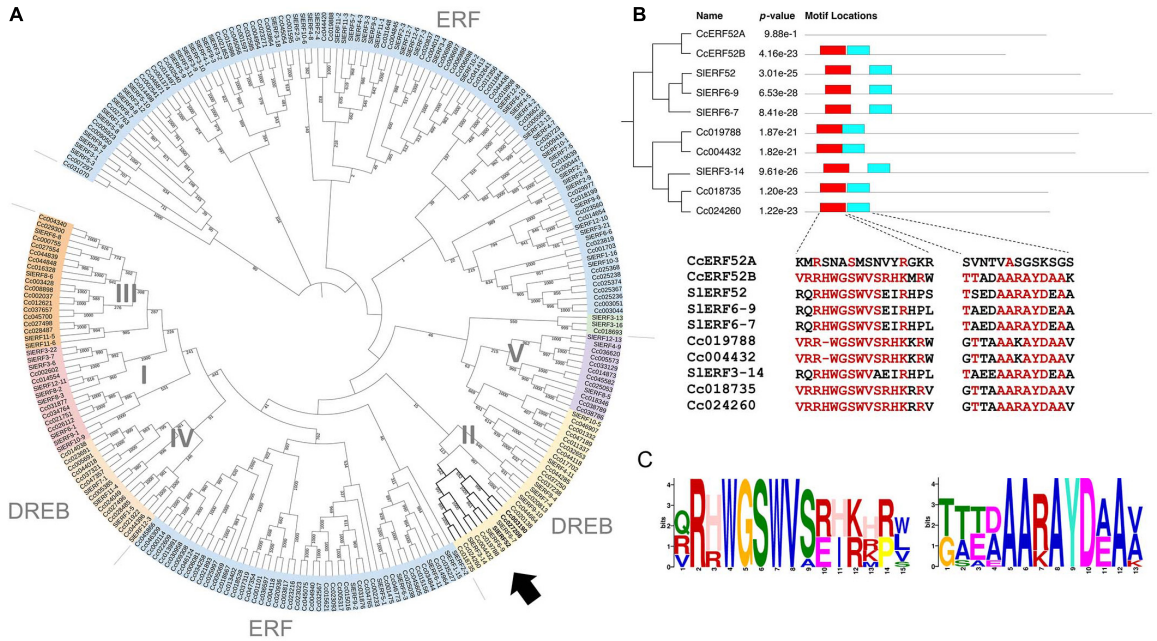

FIGURE 3 | Phylogenetic analysis and conserved protein domain of the *C. campestris* SlERF52 orthologous genes. **(A)** Phylogenetic relationships of the ERF proteins from *C. campestris* and tomato. The phylogenetic tree was constructed by iTOL (https://itol.embl.de). Arrow indicates the subclade, which includes SlERF52. **(B)** The domain organization and conserved protein domain of the ERF genes in the subclade including SlERF52. The two conserved sequences within the AP2/ERF domain (shown in red and light blue boxes) are shown in the lower panel. Red letters indicate conserved amino acid residues present in more than 50% of the aligned sequences. **(C)** The logo of two sequence motifs is shown by red and light blue boxes shown in panel **(B)**. The height of the superposition reflects the conservatism of the sequence, and the height of each marker reflects the frequency that amino acid residue appears.

based on the alignment (**Figure 3A**). In this analysis, two *C. campestris* members (Cc003190 and Cc027208, hereinafter called CcERF52A and CcERF52B, respectively) branched into a single clade, which included SlERF52 in DREB group II. Interestingly, the alignment indicated that the AP2/ERF domains of CcERF52A possessed sparse homology to the consensus sequence (**Figures 3B,C**).

Expression of CcERF52A and CcERF52B in Development of Haustorium

CcERF52A and *CcERF52B* were predominantly expressed at the initial invasion stage, during which haustorium penetrated the host tissue (**Figure 4A**). The expression patterns of *CcERF52A* and *CcERF52B* were consistent with those of the cell wall enzyme genes encoding endo-β-1,4-glucanases, polygalacturonases and pectin methylesterases (**Figure 4B**). Interestingly, the expression of *CcERF52A* and *CcERF52B* was not detected in the flower bud cluster (**Figure 4A**), indicating that these orthologs specifically function as transcriptional regulators of haustorial invasion. Additionally, our previous transcriptome analysis which used *in vitro* system indicated that interaction of *Cuscuta* with host tissues enhanced the expression levels of *CcERF52A* and *CcERF52B* during the invasion stage (**Supplementary Figure 1**; Kaga et al., 2020). We also selected the tomato abscission-associated regulators based on a model originally presented by Ito and Nakano (2015), and identified some *C. campestris* orthologs of these regulators, such as *Jointless*, *BI*, *REV* (**Supplementary Table 6**). However, no significant correlation was observed between the expression patterns of these regulators and cell wall genes encoding enzymes during haustorial invasion (**Figure 4B**).

DISCUSSION

The acquisition of haustoria is a critical evolutionary process for the establishment of plant parasitism. Sun et al. (2018) showed that many orthologous genes that are principally expressed in *Cuscuta* haustorium are also principally expressed in the roots of phylogenetically related autotrophic plant species. This suggests that *Cuscuta* haustorium evolution may have occurred by changing the expression mode of genes involved in root development. Similarly, comparative transcriptome analyses of root parasitic plants revealed that parasitism genes, which were defined as having enhanced expression in haustoria, are primarily derived from root tissue (Yang et al., 2015). The root is a highly specialized organ for the uptake and transfer of water and solutes, and is, therefore, a useful source for the evolutionary acquisition of haustorial function as a feeding organ. In the root parasitic plants, haustoria are generated from the apex of the primary root or lateral root extensions, supporting the idea that the haustorial structure evolved through changes in root development (Yoshida et al., 2016).

On the other hand, haustoria have evolved various sophisticated traits for parasitism. For example, haustoria develop into search hyphae that elongate *via* tip growth within

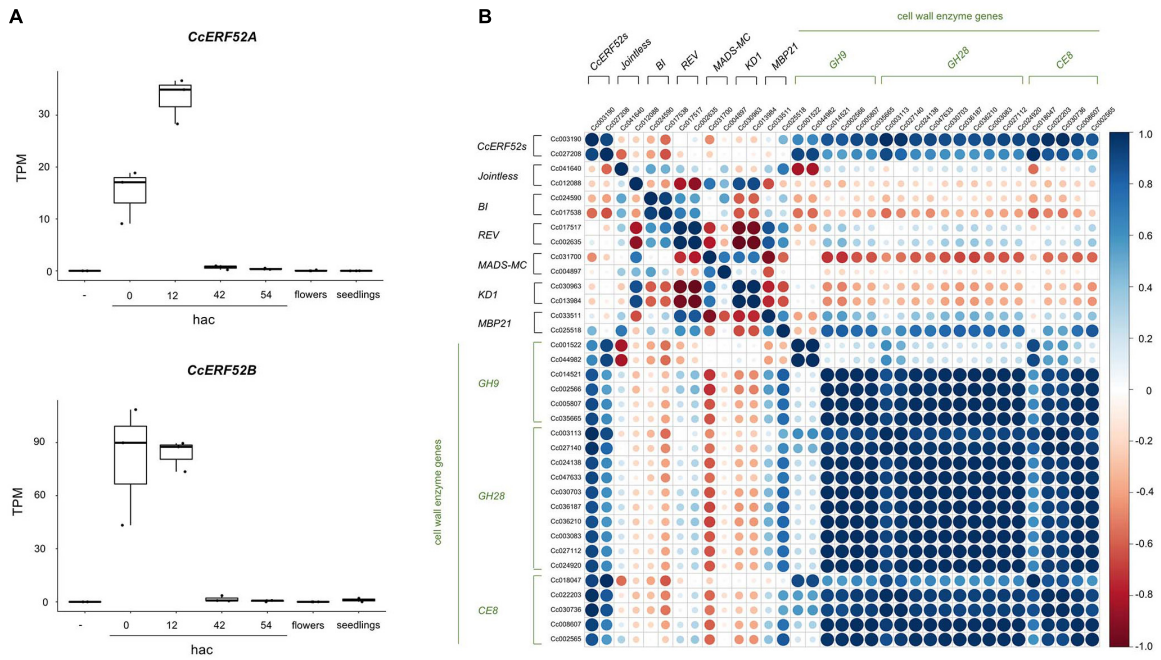

FIGURE 4 | Characterization of *CcERF52A* and *CcERF52B* expression. **(A)** Expression patterns of the *C. campestris SlERF52* orthologous genes during the haustorial invasion. The abundance of the transcripts in each stage of haustorial invasion, flower bud clusters (shown as flowers), and seedlings were measured by mapping RNA-Seq reads and expressed as TPM. "-" indicates the epidermal and cortical cells of *C. campestris* without contact with the host plant. **(B)** Correlation analysis of the *C. campestris* orthologous regulator and cell wall enzyme genes, which are implicated in abscission of tomato, in different stages of haustorium development. Pearson correlation analysis was conducted using the Corrplot package in R. GH9, GH28, and CE include endo-β-1,4-glucanases, polygalacturonases and pectin methylesterases, respectively.

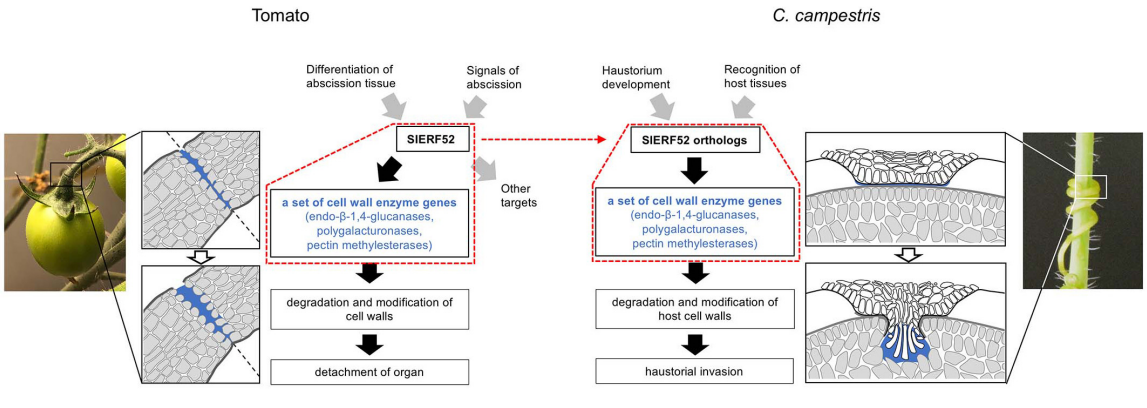

FIGURE 5 | Model showing SlERF52-dependent regulatory module for the degradation and modification of cell walls in tomato abscission and *C. campestris* haustorial invasion. Red dot frames indicate SlERF52-dependent regulatory module. Transcriptional regulation in tomatoes is based on a model originally presented by Ito and Nakano (2015).

the host tissue. The elongation of search hyphae is like the intrusive growth of pollen tubes in the flowers (Vaughn, 2003; Yang et al., 2015). This similarity is supported by the haustorial expression of *C. campestris* orthologous genes, which are expressed in the flowers of related non-parasitic plants (Yang et al., 2015; Sun et al., 2018).

Haustorial invasion is also facilitated by mechanical action and by biochemical degradation and modification of host cell walls (Nagar et al., 1984; Olsen et al., 2016; Hozumi et al., 2017). Many genes encoding cell wall degrading and modifying enzymes were upregulated haustorium (Ranjan et al., 2014; Ikeue et al., 2015; Jhu et al., 2022). Furthermore, the dynamics of cell wall components were observed by the penetration of haustorium into the host tissue (Johnsen et al., 2015; Hozumi et al., 2017). Previously, we identified the cell wall enzyme genes principally expressed during the haustorial invasion of *C. campestris* and suggested that the orthogroups of these cell wall enzyme genes have been implicated in the abscission of

closely autotrophic plants (Yokoyama et al., 2021). Because plant cell wall enzymes work collaboratively as a unique group for each biological event (Yokoyama, 2020), the haustoria of *Cuscuta* species may have recruited a unique set of cell wall enzyme genes that are involved in abscission. Identification of the *C. campestris* orthologous *SlERF52s* supports that the evolutionary acquisition of cell wall enzymatic activities in *Cuscuta haustoria* is related to changes in the transcriptional regulation of abscission processes since SlERF52 regulates the expression of a set of abscission-associated cell wall enzyme genes in tomato (**Figure 5**). More interestingly, the expression levels of *CcERF52A* and *CcERF52B* were significantly enhanced under the presence of the host tissues. We previously demonstrated that the host-produced ethylene is required for the proper growth of search hyphae in *C. haustoria* (Narukawa et al., 2021). In tomatoes, the expression levels of *SlERF52* are unlikely to be affected by ethylene production during abscission (Nakano et al., 2014). In *C. haustoria*, however, transcriptional regulation of *CcERF52A* and *CcERF52B* might be directly or indirectly linked to the regulatory network involving the ethylene pathway for elongation of search hyphae. Host recognition by haustoria is hypothesized to trigger the activation of multiple cascades and facilitate effective penetration into the host tissue.

We found other *C. campestris* orthologous regulators, including the earlier regulators that regulate abscission in tomatoes. However, we did not find a significant positive expression correlation between these orthologous regulators and cell wall enzyme genes during haustorium development. This result suggests that the haustorium of *Cuscuta* evolutionarily recruited only specific SlERF52-dependent regulatory mechanisms for the degradation and modification of cell walls (**Figure 5**). In tomatoes, it was successfully demonstrated that suppression of *SlERF52* decreased the transcript levels of particular cell wall enzyme genes (Nakano et al., 2014). Further in-depth investigations, including loss-of-function mutation, will be required to similarly show that CcERF52A and CcERF52B target the orthogroup of the cell wall enzyme genes in *C. campestris*. Since stable gene knockout approaches for *Cuscuta* plants is currently not available, it has not been possible to access *in vivo* function of CcERF52A and CcERF52B. However, it has recently been reported that the host-derived siRNAs could successfully down-regulate target gene transcription in *C. campestris*, *via* a host-induced gene silencing (HIGS) system (Jhu et al., 2022). One of the challenges is the use of HIGS system for knockdown of CcERF52A and CcERF52B in *C. campestris*. Further investigation of the relationship between CcERF52s and the cell wall enzyme genes will be needed to support our hypothesis.

Abscission processes are governed not only by cell wall enzyme activities to ensure cell separation, but also by multiple cell differentiation processes for the detachment of an organ (Maity et al., 2021). For example, a protective layer involved in the thickening and lignification of cell walls is formed to protect the newly exposed surface during abscission (Lee et al., 2018). Since multiple functions of abscission may impede the progress of haustorium development, *Cuscuta* plants inevitably select only SlERF52-dependent regulatory mechanisms for the degradation and modification of cell walls. Furthermore, in tomatoes, SlERF52 is most likely to target several genes other than cell wall enzyme genes (Ito and Nakano, 2015; Wang et al., 2021). In this respect, the high rate of non-synonymous substitution of conserved residues in CcERF52A may be associated with the evolution of specialized regulatory functions to express cell-wall enzyme genes.

CONCLUSION

The haustorium of *Cuscuta* is thought to have evolved from root tissues, based on the presence of large proportions of genes that are normally involved in root development. However, some traits of *Cuscuta* haustorium are markedly different from those of its root system. Haustorium may have evolved various parasitic traits through the recruitment of functional modules. Our findings provide valuable information for further studies exploring and understanding of haustorium evolution.

DATA AVAILABILITY STATEMENT

The datasets presented in this study can be found in online repositories. The names of the repository/repositories and accession number(s) can be found below: https://www.ddbj.nig.ac.jp/, DRR353312–DRR353329.

AUTHOR CONTRIBUTIONS

RY, TK, KA, and KN designed the research and wrote the manuscript. RY, TY, JP, and KA performed the research. RY, TK, JP, and KA analyzed the data. All authors discussed the results, reviewed the article, and approved the final article.

FUNDING

This work was supported in part by Grants-in-Aid for Challenging Research (Exploratory) (17K19374 to KN), for Scientific Research on Innovative Areas (Planned Research) (18H05489 to KN), for Scientific Research (C) (21K06235 to KN and 22K062740 to RY), for Scientific Research (A) (19H00944 to KA), and for Scientific Research on Innovative Area (Platform for Advanced Genome Science, 16H06279 to KA) from the Japan Society for the Promotion of Science.

ACKNOWLEDGMENTS

We thank the Advanced Genomics Center (Osaka Prefecture University) for the RNA quality check.

SUPPLEMENTARY MATERIAL

The Supplementary Material for this article can be found online at: https://www.frontiersin.org/articles/10.3389/fpls.2022.904313/full#supplementary-material

REFERENCES

Bawin, T. G. A., Bruckmüller, J. A., Olsen, S., and Krause, K. (2022). A host-free transcriptome for haustoriogenesis in *Cuscuta campestris*: signature gene expression identifies markers of successive development stages. *Physiol. Plant.* 174:e13628. doi: 10.1111/ppl.13628

Bolger, A. M., Lohse, M., and Usadel, B. (2014). Trimmomatic: a flexible trimmer for Illumina sequence data. *Bioinformatics* 30, 2114–2120. doi: 10.1093/bioinformatics/btu170

Dawson, J. H., Musselman, L. J., and Wolswinkel, P. (1994). Biology and control of *Cuscuta*. *Rev. Weed Sci.* 6, 265–317.

Futschik, M. E., and Carlisle, B. (2005). Noise-robust soft clustering of gene expression time-course data. *J. Bioinf. Comput. Biol.* 3, 965–988. doi: 10.1142/S0219720005001375

Hegenauer, V., Furst, U., Kaiser, B., Smoker, M., Zipfel, C., Felix, G., et al. (2016). Detection of the plant parasite *Cuscuta reflexa* by a tomato cell surface receptor. *Science* 353, 478–481. doi: 10.1126/science.aaf3919

Hegenauer, V., Slaby, P., Körner, M., Bruckmüller, J.-A., Burggraf, R., Albert, I., et al. (2020). The tomato receptor CuRe1 senses a cell wall protein to identify *Cuscuta* as a pathogen. *Nat. Commun.* 11:5299. doi: 10.1038/s41467-020-19147-4

Hozumi, A., Bera, S., Fujiwara, D., Obayashi, T., Yokoyama, R., Nishitani, K., et al. (2017). Arabinogalactan proteins accumulate in the cell walls of searching hyphae of the stem parasitic plants, *Cuscuta campestris* and *Cuscuta japonica*. *Plant Cell Physiol.* 58, 1868–1877. doi: 10.1093/pcp/pcx121

Ikeue, D., Schudoma, C., Zhang, W., Ogata, Y., Sakamoto, T., Kurata, T., et al. (2015). Bioinformatics approach to distinguish plant parasite and host transcriptomes in interface tissue by classifying RNA-Seq reads. *Plant Methods* 11:34. doi: 10.1186/s13007-015-0066-6

Ito, Y., and Nakano, T. (2015). Development and regulation of pedicel abscission in tomato. *Front. Plant Sci.* 6:442. doi: 10.3389/fpls.2015.00442

Jhu, M. Y., Farhi, M., Wang, L., Zumstein, K., and Sinha, N. R. (2022). Investigating host and parasitic plant interaction by tissue-specific gene analyses on tomato and *Cuscuta campestris* interface at three haustorial developmental stages. *Front. Plant Sci.* 12:764843. doi: 10.3389/fpls.2021.764843

Jhu, M. Y., Ichihashi, Y., Farhi, M., Wong, C., and Sinha, N. R. (2021). LATERAL ORGAN BOUNDARIES DOMAIN 25 functions as a key regulator of haustorium development in dodders. *Plant Physiol.* 186, 2093–2110. doi: 10.1093/plphys/kiab231

Johnsen, H. R., Striberny, B., Olsen, S., Vidal-melgosa, S., Fangel, J. U., Willats, W. G. T., et al. (2015). Cell wall composition profiling of parasitic giant dodder (*Cuscuta reflexa*) and its hosts: a priori differences and induced changes. *New Phytol.* 207, 805–881. doi: 10.1111/nph.13378

Kaga, Y., Yokoyama, R., Sano, R., Ohtani, M., Demura, T., Kuroha, T., et al. (2020). Interspecific signaling between the parasitic plant and the host plants regulate xylem vessel cell differentiation in haustoria of *Cuscuta campestris*. *Front. Plant Sci.* 11:193. doi: 10.3389/fpls.2020.00193

Kimura, S., and Sinha, N. (2008). Tomato (*Solanum lycopersicum*): a model fruit-bearing crop. *Cold Spring Harb. Protoc.* 3:pdb.emo105. doi: 10.1101/pdb.emo105

Lee, Y., Yoon, T. H., Lee, J., Jeon, S. Y., Lee, J. H., Lee, M. K., et al. (2018). A lignin molecular brace controls precision processing of cell walls critical for surface integrity in *Arabidopsis*. *Cell* 173, 1468–1480. doi: 10.1016/j.cell.2018.03.060

Maity, A., Lamichaney, A., Joshi, D. C., Bajwa, A., Subramanian, N., and Walsh, M. (2021). Seed shattering: a trait of evolutionary importance in plants. *Front. Plant Sci.* 12:657773. doi: 10.3389/fpls.2021.657773

Nagar, R. M., Singh, M., and Sanwal, G. C. (1984). Cell wall degrading enzymes in *Cuscuta reflexa* and its hosts. *J. Exp. Bot.* 35, 1104–1112. doi: 10.1093/jxb/35.8.1104

Nakano, T., Fujisawa, M., Shima, Y., and Ito, Y. (2014). The AP2/ERF transcription factor SlERF52 functions in flower pedicel abscission in tomato. *J. Exp. Bot.* 65, 3111–3119. doi: 10.1093/jxb/eru154

Nakano, T., Suzuki, K., Fujimura, T., and Shinshi, H. (2006). Genome-wide analysis of the ERF gene family in Arabidopsis and rice. *Plant Physiol.* 140, 411–432. doi: 10.1104/pp.105.073783

Narukawa, H., Yokoyama, R., Kuroha, T., and Nishitani, K. (2021). Host-produced ethylene is required for marked cell expansion and endoreduplication in dodder search hyphae. *Plant Physiol.* 185, 491–502. doi: 10.1093/plphys/kiaa010

Olsen, S., Striberny, B., Hollmann, J., Schwacke, R., Popper, Z., and Krause, K. (2016). Getting ready for host invasion: elevated expression and action of xyloglucan endotransglucosylases/hydrolases in developing haustoria of the holoparasitic angiosperm *Cuscuta*. *J. Exp. Bot.* 67, 695–708. doi: 10.1093/jxb/erv482

Park, S.-Y., Shimizu, K., Brown, J., Aoki, K., and Westwood, J. H. (2022). Mobile host mRNAs are translated to protein in the associated parasitic plant *Cuscuta campestris*. *Plants* 11:93. doi: 10.3390/plants11010093

Pertea, M., Pertea, G. M., Antonescu, C. M., Chang, T. C., Mendell, J. T., and Salzberg, S. L. (2015). StringTie enables improved reconstruction of a transcriptome from RNA-seq reads. *Nat. Biotechnol.* 33, 290–295. doi: 10.1038/nbt.3122

Ranjan, A., Ichihashi, Y., Farhi, M., Zumstein, K., Townsley, B., David-Schwartz, R., et al. (2014). De novo assembly and characterization of the transcriptome of the parasitic weed *Cuscuta pentagona* identifies genes associated with plant parasitism. *Plant Physiol.* 166, 1186–1199. doi: 10.1104/pp.113.234864

Sakuma, Y., Liu, Q., Dubouzet, J. G., Abe, H., Shinozaki, K., and Yamaguchi-Shinozaki, K. (2002). DNA-binding specificity of the ERF/AP2 domain of Arabidopsis DREBs, transcription factors involved in dehydration- and cold-inducible gene expression. *Biochem. Biophys. Res. Commun.* 290, 998–1009. doi: 10.1006/bbrc.2001.6299

Shimizu, K., and Aoki, K. (2019). Development of parasitic organs of a stem holoparasitic plant in Genus *Cuscuta*. *Front. Plant Sci.* 10:1435. doi: 10.3389/fpls.2019.01435

Shimizu, K., Hozumi, A., and Aoki, K. (2018). Organization of vascular cells in the haustorium of the parasitic flowering plant *Cuscuta japonica*. *Plant Cell Physiol.* 59, 715–723. doi: 10.1093/pcp/pcx197

Sun, G., Xu, Y., Liu, H., Sun, T., Zhang, J., Hettenhausen, C., et al. (2018). Large-scale gene losses underlie the genome evolution of parasitic plant *Cuscuta australis*. *Nat. Commun.* 9:2683. doi: 10.1038/s41467-018-04721-8

Tian, F., Yang, D. C., Meng, Y. Q., Jin, J. P., and Gao, G. (2019). PlantRegMap: charting functional regulatory maps in plants. *Nucleic Acids Res.* 48, D1104–D1113. doi: 10.1093/nar/gkz1020

Vaughn, K. C. (2003). Dodder hyphae invade the host: a structural and immunocytochemical characterization. *Protoplasma* 220, 189–200. doi: 10.1007/s00709-002-0038-3

Vogel, A., Schwacke, R., Denton, A. K., Usadel, B., Hollmann, J., Fischer, K., et al. (2018). Footprints of parasitism in the genome of the parasitic flowering plant *Cuscuta campestris*. *Nat. Commun.* 9:2515. doi: 10.1038/s41467-018-04344-z

Wang, R., Li, R., Chen, L., Wang, X., Fu, X., Dong, X., et al. (2021). SlERF52 regulates SlTIP1;1 expression to accelerate tomato pedicel abscission. *Plant Physiol.* 185, 1829–1846. doi: 10.1093/plphys/kiab026

Westwood, J. H., Yoder, J. I., Timko, M. P., and Depamphilis, C. W. (2010). The evolution of parasitism in plants. *Trends Plant Sci.* 15, 227–235. doi: 10.1016/j.tplants.2010.01.004

Yang, Z., Wafula, E. K., Honaas, L. A., Zhang, H., Das, M., Fernandez-Aparicio, M., et al. (2015). Comparative transcriptome analyses reveal core parasitism genes and suggest gene duplication and repurposing as sources of structural novelty. *Mol. Biol. Evol.* 32, 767–790. doi: 10.1093/molbev/msu343

Yokoyama, R. (2020). A genomic perspective on the evolutionary diversity of the plant cell wall. *Plants* 9:1195. doi: 10.3390/plants9091195

Yokoyama, R., Yokoyama, T., Kaga, Y., Oono, Y., and Nishitani, K. (2021). Characterization of Cuscuta campestris cell wall genes responsible for the haustorial invasion of host plants. *Sci. J. Kanagawa Univ.* 32, 21–26.

Yoshida, S., Cui, S., Ichihashi, Y., and Shirasu, K. (2016). The haustorium, a specialized invasive organ in parasitic plants. *Annu. Rev. Plant Biol.* 67, 643–667. doi: 10.1146/annurev-arplant-043015-111702

Zhang, L., Chen, L., Pang, S., Zheng, Q., Quan, S., Liu, Y., et al. (2022). Function analysis of the ERF and DREB subfamilies in tomato fruit development and ripening. *Front. Plant Sci.* 13:849048. doi: 10.3389/fpls.2022.849048

Conflict of Interest: The authors declare that the research was conducted in the absence of any commercial or financial relationships that could be construed as a potential conflict of interest.

Publisher's Note: All claims expressed in this article are solely those of the authors and do not necessarily represent those of their affiliated organizations, or those of the publisher, the editors and the reviewers. Any product that may be evaluated in this article, or claim that may be made by its manufacturer, is not guaranteed or endorsed by the publisher.

frontiers | Frontiers in Plant Science

TYPE Original Research
PUBLISHED 22 July 2022
DOI 10.3389/fpls.2022.940284

OPEN ACCESS

EDITED BY
Vincenzo Lionetti,
Sapienza University of Rome, Italy

REVIEWED BY
Giulia Malacarne,
Fondazione Edmund Mach, Italy
Daniele Coculo,
Sapienza University of Rome, Italy

*CORRESPONDENCE
Duoduo Wang
duoduo538@zjnu.edu.cn

†These authors have contributed equally to this work and share first authorship

SPECIALTY SECTION
This article was submitted to Plant Pathogen Interactions, a section of the journal Frontiers in Plant Science

RECEIVED 10 May 2022
ACCEPTED 30 June 2022
PUBLISHED 22 July 2022

CITATION
Wang D, Jin S, Chen Z, Shan Y and Li L (2022) Genome-wide identification of the pectin methylesterase inhibitor genes in *Brassica napus* and expression analysis of selected members. *Front. Plant Sci.* 13:940284. doi: 10.3389/fpls.2022.940284

Genome-wide identification of the pectin methylesterase inhibitor genes in *Brassica napus* and expression analysis of selected members

Duoduo Wang[1,2*†], Shunda Jin[3†], Zhe Chen[3], Yue Shan[4] and Lei Li[4]

[1]College of Chemistry and Life Sciences, Zhejiang Normal University, Jinhua, China, [2]School of Integrative Plant Science, Cornell University, Ithaca, NY, United States, [3]Key Laboratory of Tropical Fruit Tree Biology of Hainan Province, Haikou, China, [4]School of Life Sciences, Jiangsu University, Zhenjiang, China

Pectin methylesterase inhibitors (PMEIs) modulate the status of pectin methylesterification by inhibiting the activity of pectin methylesterase (PME). Recent advances indicate PMEIs play an important role in regulating plant cell wall properties and defense responses. In this study, a genome-wide analysis of *PMEI* gene family in *Brassica napus* (*B. napus*) was conducted and the expression patterns of *PMEI* genes in response to *Sclerotinia sclerotiorum* (*S. sclerotiorum*) was investigated. A total of 190 PMEI proteins were identified from the genome of *B. napus*. Chromosomal location, gene structure and properties of the PMEI family were analyzed, and these features were compared with *Arabidopsis thaliana (A. thaliana)*. A total of 123 syntenic ortholog pairs were detected from *BnPMEI* family by synteny analysis. Results showed the expansion of *BnPMEI* genes was likely predominately from whole-genome duplication (WGD) or segmental duplications. Multiple *cis*-elements related to plant growth and development, environmental stress responses, hormone responses were detected in the promoters of *BnPMEI* genes, implying they were regulated by both internal and external factors. Furthermore, expression analysis of transcriptome data combined with quantitative RT-PCR (qRT-PCR) validation identified several candidates that were strongly responsive to *S. sclerotiorum* infection. These *BnPMEI* genes are candidates for manipulation to breed novel and improved genotypes that are more resistant to sclerotinia stem rot (SSR). Extensive interactions were detected among 30 BnPMEI proteins, forming complex protein-protein interaction networks. Besides, 48 BnPMEIs showed interactions with other proteins including a range of cell wall structure-related enzymes. This study provides new insights into the evolution and function of PMEIs in *B. napus* and lays a foundation for breeding novel genotypes for crop improvement.

KEYWORDS

***Brassica napus*, genome-wide, pectin methylesterase inhibitor, evolution, plant cell wall, expression patterns, Sclerotinia sclerotiorum**

Introduction

The plant cell wall is a complex network composed of polysaccharides, including cellulose, hemicelluloses and pectin, as well as other structural proteins. Cell walls are organized into a three-dimensional matrix and play an important role in biological processes including development and disease resistance (Höfte and Voxeur, 2017; Jamet and Dunand, 2020). Pectin, the most abundant and structurally complex polysaccharide, is generally classified into three major types: homogalacturonan (HG), rhamnogalacturonan I (RG-I), and rhamnogalacturonan II (RG-II) (Mohnen, 2008). HG is highly methylesterified when secreted to cell wall matrix, and methylesters can be removed from HG by pectin methylesterases (PMEs) (Levesque-Tremblay et al., 2015). Pectin methylesterases inhibitors (PMEIs), belonging to large multigene family in plant species, inhibit the activity of PMEs by forming a reversible 1:1 complex (Giovane et al., 2004; Jolie et al., 2010). The pattern and degree of pectin methylesterification are tightly regulated by localized expression of specific PMEs and PMEIs isoforms (Coculo and Lionetti, 2022). PMEI was first discovered in kiwi fruit (Balestrieri et al., 1990) and then detected in many other plant species including members of the Brassica family such as *Arabidopsis thaliana (A. thaliana)* (Raiola et al., 2004; Wormit and Usadel, 2018).

In recent years, the plant primary cell wall model has been revised, where pectin metabolism has been proposed to play a more crucial role in influencing cell wall traits than previously thought (Park and Cosgrove, 2012; De Lorenzo et al., 2019). Pectin methylesterification status impacts the biomechanical properties of cell wall and undergoes dynamic changes during plant development and in response to various environmental stresses (Wormit and Usadel, 2018). A strong link between PMEIs and plant development and defense responses was observed in many plant species including *A. thaliana* (Lionetti et al., 2017), rice (Nguyen et al., 2017), maize (Woriedh et al., 2013), and pepper (An et al., 2008). Genome-wide identification of *PMEI* gene family has been performed in a range of plant species including dicots including Arabidopsis (Wang et al., 2013), tomato (Jeong et al., 2018), *Brassica campestris* (Liu et al., 2018a), *Brassica rapa* (Tan et al., 2018), as well as monocot plants including rice (Nguyen et al., 2016), sorghum (Ren et al., 2019), and maize (Zhang et al., 2019).

Abbreviations: HG, homogalacturonan; PMEs, pectin methylesterases; PMEIs, pectin methylesterase inhibitors; CWI, cell wall integrity; WGD, whole-genome duplication; RG-I, rhamnogalacturonan I; RG-II, rhamnogalacturonan II; SSR, sclerotinia stem rot; Cd, cadmium; HMM, Hidden Markov Model; MW, molecular weight; pI, isoelectric point; ML, maximum likelihood; DAB, 3,3′-diaminobenzidine; AA, amino acids; TEs, transposable elements; H_2O_2, hydrogen peroxide; ROS, reactive oxygen species; GO, Gene Ontology; PL, pectate lyase; ABA, abscisic acid; PTI, pattern triggered immunity; PGIPs, polygalacturonase-inhibiting proteins; PG, polygalacturonase.

Brassica napus L (B. napus), a major oil crop in the world, is susceptible to various biotic stresses including sclerotinia stem rot (SSR) a devastating disease caused by *Sclerotinia sclerotiorum* a necrotrophic fungal pathogen. It seems likely that cell wall changes involving pectin metabolism could be involved in *S. sclerotiorum* infections and *PMEI* genes may play a role in stress-induced defense response in *B. napus*, but little information is available in the literature. Very recently, lower degree of pectin methylesterification was accompanied by lower expression level of *PMEI* genes in the leaves of cadmium (Cd) - tolerant rapeseed compared to Cd-sensitive genotype (Wu et al., 2021). This suggests PMEIs might regulate cadmium-induced stress response in *B. napus* through facilitating Cd retention in the cell walls.

In this study, we conducted a genome-wide identification of *BnPMEI* genes in *B. napus*. A total of 190 *PMEI* gene members were identified. Systematic analysis of the *BnPMEI* gene family included investigating phylogenetic relationships, gene structure, conserved motif patterns, gene duplication and cis-elements. Expression analysis of *BnPMEI* genes in response to *S. sclerotiorum* infection revealed several candidate genes including *BnPMEI19*, *BnPMEI76,* and *BnPMEI127* that were likely to regulate SSR-triggered defense. The work provides key information for future function characterization of BnPMEIs and serves as a basis for breeding novel genotypes with enhanced stress tolerance.

Materials and methods

Identification of *PMEI* genes in *Brassica napus*

Brassica napus genome sequences were downloaded from EnsemblPlants[1]. Firstly, BLASTP search was conducted in the Genoscope database[2] (Chalhoub et al., 2014) to find the putative BnPMEI members using the 79 *A. thaliana* PMEI protein sequences as queries downloaded from TAIR[3]. Secondly, hmmersearch in the HMMER web server[4] was performed to screen candidate *PMEI* gene sequences using the Hidden Markov Model (HMM) profile (PF04043) from the Pfam database[5]. To check the presence of the conserved PMEI domain in each protein, sequences of the putative PMEI proteins were validated through the Simple Modular Architecture Research Tool (SMART) database[6] (Letunic et al., 2012), the NCBI Conserved Domain Database (Marchler-Bauer et al., 2011) and

1 http://plants.ensembl.org/index.html
2 http://www.genoscope.cns.fr/brassicanapus
3 https://www.arabidopsis.org/
4 https://www.ebi.ac.uk/Tools/hmmer/
5 http://pfam.janelia.org/
6 http://smart.embl-heidelberg.de/

the Pfam database (Finn et al., 2016). The *PMEI* genes identified in the genome of *B. napus* were named according to their locations and orders on the chromosomes or scaffolds (**Supplementary Table 1**). Physicochemical properties including the length of protein sequence, molecular weight (MW), and isoelectric point (pI) were predicted using ExPASy website[7]. SignalP 4.1 Server[8] was used to predict the signal peptide sequences. Trans-membrane hidden Markov model (TMHMM) Server V2.0[9] was used to explore the transmembrane helices (Krogh et al., 2001). WoLF PSORT[10] and ProtComp 9.0[11] were used to predict the subcellular localization of BnPMEI proteins (Horton et al., 2007; Jing et al., 2017).

Analysis of conserved motif and gene structure of the BnPMEI proteins

Conserved motifs of the *PMEI* gene family in *B. napus* were analyzed *via* the program MEME (Multiple Em for Motif Elicitation)[12] using full length protein sequence of each PMEI member, with default parameters except for parameters: maximum number of motifs set as 5 and motif width set as 6–100 amino acid (Bailey et al., 2009). The exon-intron structures of the *PMEI* genes were illustrated with the online tool GSDS (Gene Structure Display Server)[13] (Hu et al., 2015).

Chromosomal locations and phylogenetic analysis

The chromosomal positions of the *BnPMEI* genes were retrieved from the Genoscope database, and were visualized using the TBtools software (Chen et al., 2020). Multiple sequence alignments of PMEI amino acid sequences were performed using the Muscle algorithm in MEGA11 software. Based on alignment results, phylogenetic trees were constructed using MEGA 11 by the maximum likelihood (ML) method with the following parameters: Jones–Taylor–Thornton (JTT) model, partial deletion, site coverage cutoff was 50%, and bootstrap replications set as 1000 to define the reliability of the resulting tree. The trees were visualized *via* the online tool Interaction Tree of Life (iTOL[14]).

Gene duplication, synteny, and evolutionary analysis

The length of each chromosome and the location of each *BnPMEI* and *AtPMEI* gene were retrieved from the Genoscope and TAIR database. Multiple collinear scanning toolkits (MCScanX) were used to analyze gene replication events and synteny relationships in *B. napus* or between *B. napus* and *A. thaliana* (Wang et al., 2012). The collinearity of the paralogous gene pairs of *PMEIs* in *B. napus* was depicted using the Advanced Circos in TBTools. To illustrate the orthologous relationship of *PMEIs* between *B. napus* and *A. thaliana*, the syntenic map was constructed with the Dual Systeny Plotter in TBtools. The synonymous rate (*K*s), non-synonymous rate (*K*a), and *K*a/*K*s ratios of each gene pair were calculated using the Simple *K*a/*K*s Calculator in TBTools. The divergence time of homologous gene pairs was calculated by the following equation T = Ks/2λ (λ denotes the estimated clock-like rate of synonymous substitution that is 1.5×10^{-8} substitutions/synonymous site/year in dicots) (Blanc and Wolfe, 2004).

Cis-elements prediction

To investigate the cis regulatory elements in the promoter regions of *BnPMEI* genes. The 2000-bp genomic DNA sequence upstream the translation start codon of each gene was extracted using TBtools, and cis-acting elements were predicted using the online tool PlantCARE[15] (Lescot et al., 2002).

Plant material and pathogen inoculation

The Resistant (R)-line 'Zhen12F28' and Susceptible (S)-line 'Zhen11C11' used in this work were kindly provided by Zhenjiang Academy of Agricultural Sciences. All plants were grown in a growth room under a photoperiod of 16 h of light and 8 h of dark at 22°C and 60–80% relative humidity. Four-leaf-stage rapeseed seedlings with similar growth rate were selected for inoculation. *S. sclerotiorum* isolate was washed with sterilized water and cultured on potato dextrose agar medium. Adaxial surface of the fourth-leaf from each seedling was inoculated with 5-mm diameter mycelial agar plugs punched from the growing margin of a 3-day-old culture of *S. sclerotiorum*. Mock-inoculated plants were treated with 5-mm diameter agar plugs only. Plants were incubated in a sealed and humidified chamber for developing disease symptoms. Leaf tissue around the inoculation site

7 https://web.expasy.org/compute_pi/

8 http://www.cbs.dtu.dk/services/SignalP/

9 http://www.cbs.dtu.dk/services/TMHMM/

10 https://wolfpsort.hgc.jp/

11 http://linux1.softberry.com/berry.phtml?topic=protcomppl&group=programs&subgroup=proloc

12 http://meme-suite.org/tools/meme

13 http://gsds.cbi.pku.edu.ch

14 https://itol.embl.de/

15 http://bioinformatics.psb.ugent.be/webtools/plantcare/html/

was collected at three time points (24, 48, and 96 h post inoculation). Three biological replicates were sampled for each treatment.

Phenotyping, trypan blue and 3,3′-diaminobenzidine staining

Images of inoculated leaves were taken using a camera and lesion area was calculated using Image J. Cell viability was tested by Trypan blue staining and hydrogen peroxide (H_2O_2) *in situ* was detected by DAB (0.5 mg/ml) staining as described (Wang et al., 2009, 2014). Images were taken using a Leica DM IL LED (LEICA, Germany) invert microscope under bright-field.

Expression analysis of *BnPMEIs* using RNA-seq data and quantitative RT-PCR

Transcriptome data of *B. napus* under *S. sclerotiorum* stress was obtained from NCBI SRA database under the following projects (ID: PRJNA321917; PRJNA274853). Fold change was expressed as ratio of Fragments Per Kilobase per Million (FPKM) values in the treated group to control group, and heatmap was generated based on log 2 of fold change value using TBtools software. Tissue-specific expression profiles of the *BnPMEIs* genes was performed. Expression profiles of the 190 *BnPMEI* genes were compared between five different tissues of *B. napus* including root, stem, young leaves, petals and silique pericarp at full-bloom stage using public data obtained from Brassica EDB[16].

Quantitative RT-PCR (qRT-PCR) assays were performed to investigate the expression levels of ten selected candidates in the R-line and S line at different time points post inoculation, as well as in different tissues including root, stem, leaf, petal and silique at full-bloom stage. The 10 genes include *BnPMEI168, BnPMEI145, BnPMEI19, BnPMEI41, BnPMEI161, BnPMEI46, BnPMEI76, BnPMEI128, BnPMEI127,* and *BnPMEI64* (**Supplementary Table 2**).

For the qRT-PCR experiments, total RNA was extracted using PureLink Plant RNA Reagent (Invitrogen, Carlsbad, CA, United States) kit. First cDNA synthesis was performed using MonScript^{TM} RTIII All-in-One Mix with dsDNase (Monad). qPCR was performed using ChamQ Universal SYBR qPCR Master Mix (Vazyme Biotech Co., Ltd) according to users' guide. The qPCR cycling was set to 95°C for 3 min, 40 cycles of (95°C for 15 s, 60°C for 30 s, 72°C for 15 s) using a LightCycler480 II instrument (Roche, Ltd). Actin from *B. napus* was used as internal reference. Primers used for QPCR were list in **Supplementary Table 2**. Relative gene expression was calculated according to the $2^{-\Delta\Delta Ct}$ method (Livak and Schmittgen, 2001). Each treatment involved three biologically independent RNA samples and each qPCR assay was performed with three technical replicates.

Analysis of uronic acid contents and cell wall-bound methyl ester contents

Acetone insoluble solids (AIS) were prepared with *B. napus* root, stem, leaf, petal and silique at full-bloom stage. Tissues were homogenized with 80% of cold acetone using a Polytron Homogenizer (VWR). The insoluble residues were collected by filtering the mixture through Miracloth (VWR), followed by washed successively with 100% acetone to remove all pigment. The powder was left overnight to dry at room temperature (RT). A total amount of 100 mg AIS was used for preparing pectin enriched fractions (PEFs). Briefly, the AIS was treated with 50 mM ammonium oxalate solution for 24 h at RT, and soluble fractions were collected by centrifugation and lyophilization. The lyophilized samples were treated with 4N potassium hydroxide for 24 h at RT, and were then centrifuged and lyophilized to obtain PEFs. Uronic acid content in the PEFs was measured as described in Jeong et al. (2018). Cell wall-bound methyl ester contents were assayed by measuring the methanol released from the cell wall after saponification treatment. Methanol reacted with 2,4-Pentanedione to form product with absorbance at 412 nm. Absorbance was measured using a spectrophotometer, and methanol content was determined by interpolating from a standard curve generated with a dilution series of methanol. Degree of pectin methyl esterification of cell walls was expressed as ratio of value of cell wall-bound methanol to value of uronic acid content.

Gene ontology analysis and protein–protein interaction prediction

Each BnPMEI protein was analyzed using InterproScan 5[17] for GO category annotation (Hunter et al., 2009). Functional interaction networks of BnPMEIs were generated using the STRING database which integrates all public sources of proten–protein interactions (PPI) and computational predictions and predicts direct (physical) and indirect (functional) associations. Proteins interacting with each of the BnPMEI member were predicted using the STRING database by submitting each protein sequence independently (Szklarczyk et al., 2011).

16 https://brassica.biodb.org/

17 http://www.ebi.ac.uk/interpro/

Statistical analysis

The statistical analysis was performed with ANOVA using Graphpad Prism 5. Error bar was represented as mean ± standard error of mean (SEM). Each comparison was performed at a significance level $P = 0.05$.

Results

Identification and physicochemical properties of the *PMEI* gene family in *Brassica napus*

Using BLAST, 190 PMEIs were acquired from the reference genome of *B. napus* by BLASTP searches with 79 AtPMEI sequences from *A. thaliana* as queries. In addition, the genome annotation data of *B. napus* was searched against the global Hidden Markov Model (HMM) profile of the conserved PMEI domain (Pfam04043) using HMMER 3.0 web server. Combining the two methods, a total of 190 sequences were obtained as members of the *PMEI* gene family. The candidates were verified to cover the conserved domain of PMEI using SMART, CDD and Pfam. The *BnPMEI* genes were then renamed based on their locations and orders on the chromosomes. Detailed information of gene name, ID, chromosomal locations, protein sequence length, MW, pI and their homologs in *A. thaliana* were listed in **Supplementary Table 1**. The length of the 190 PMEI proteins ranged from 65 to 356 amino acids (AA), with an average length of 189 AA. The MW ranged from 6901.94 to 38796.47 Da with an average of 20757.24 Da. The pI ranged from 4.18 to 11.87. Signal peptide sequence and transmembrane helices of each BnPMEI were predicated using SignalP 4.1 Server and TMHMM Server V2.0, respectively. Signal peptide sequence was present in 177 BnPMEIs. A total of 70 BnPMEI were expected to possess one transmembrane helix, while only BnPMEI37 had two transmembrane helices (**Supplementary Table 3**). This suggested BnPMEIs with at least one transmembrane helix were anchored on cell membrane. The remaining BnPMEI proteins were completely exported to the extracellular matrix. Subcellular localization prediction using WoLF PSORT and ProtComp 9.0 revealed the majority of BnPMEIs were located in the extracellular cell wall matrix (**Supplementary Table 3**). In *A. thaliana*, the AtPMEI proteins were also predicted to be secreted to cell wall (Wang et al., 2013), which was consistent with the predicted locations of BnPMEIs.

Phylogenetic analysis

To understand the evolutionary relationships among the PMEIs in *B. napus*, a phylogenetic tree was constructed based on the alignment of BnPMEI protein sequences. The BnPMEIs were classified into five clades. Clade I was the largest clade with 82 members, followed by clade V which was composed of 71 members. The remaining three clades (Clade II, Clade III, and Clade IV) contained 14, 14 and 9 BnPMEIs, respectively (**Figure 1**). In order to analyze the relationship between PMEIs from *B. napus* and *A. thaliana*, an unrooted tree was constructed using the full-length amino acids of 267 PMEIs from both species (**Figure 2**). Here, the 267 PMEIs were clustered into five clades, which was consistent with the classification of BnPMEIs. Among these PMEIs, clade II contained the largest number of PMEIs (111). Besides, 22 members belonged to clade I, 34 to clade III, 12 to clade IV and 88 to clade V. Each clade contained both BnPMEIs and AtPMEIs.

Characterization of gene structure and conserved motifs of BnPMEI proteins

Gene structure plays an important role in gene function divergence (Xu et al., 2012). In this study, the exon-intron structure of the 190 *BnPMEI* genes was analyzed using the web server GSDS (Gene Structure Display Server)[18]. Results revealed most of the *BnPMEI* genes (140/190) contained only one exon in their DNA sequences without any intron disrupting the coding sequence (**Supplementary Figure 1**). The number of exons ranged from one to six with an average of 1.3 exon. *PMEI* genes in Arabidopsis contained 1.3 exons on average as well, which was in line with this study (Wang et al., 2013). Forty-seven genes were found with two exons. Three *BnPMEI* genes contained more than two exons, including *BnPMEI190* which had 3 exons, *BnPMEI166* containing 4 exons, and *BnPMEI74* with 6 exons, respectively. Conserved motifs frequently present in the BnPMEI proteins were constructed using the MEME (Multiple Em for Motif Elicitation) (**Supplementary Figure 1**). The sequence and length information of the top five motifs were shown in **Supplementary Figure 2**. Motif 2 was found in BnPMEIs from all of the five clades, whereas motif 4 was only detected in BnPMEIs from Clade V. PMEIs belonging to Clade I, Clade IV, and Clade V contained motif 1, 2, 3, 5. PMEI proteins from Clade III had motif 1, 2, 3. Motif 2 and 5 were detected in BnPMEI members from Clade II. Interestingly, BnPMEIs within the same clade had similar motif composition and exon-intron structure, strongly supporting the reliability of clade classification by the phylogenetic analysis.

Chromosomal distribution, genome synteny and gene duplication

Brassica napus (AACC, 2n = 38) is originated in the Mediterranean region about 7500 years ago by natural

18 http://gads-gao.lab-org/

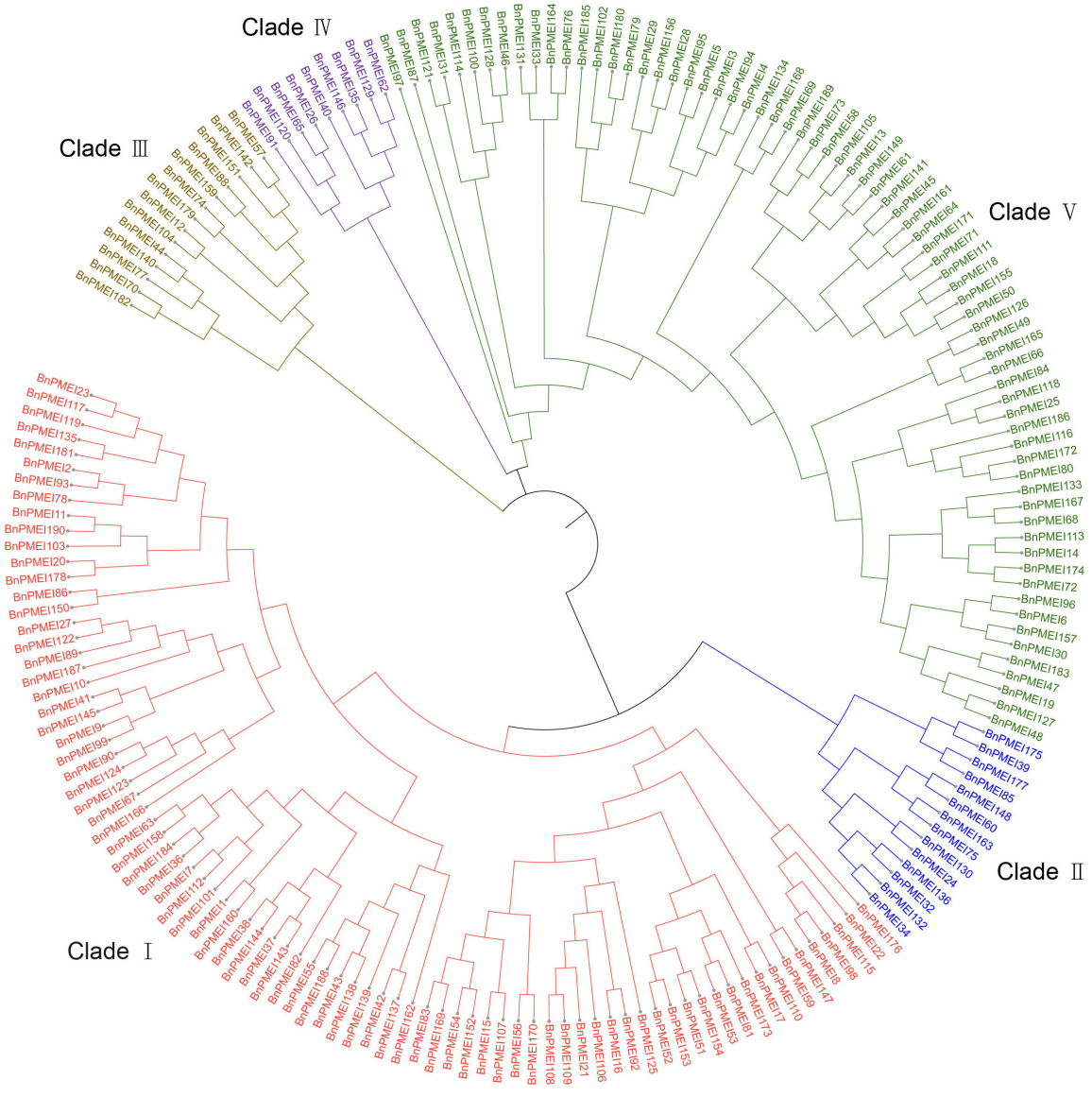

FIGURE 1
Phylogenetic tree of PMEI proteins in *B. napus*. The maximum likelihood (ML) tree was constructed using MEGA11 with full-length amino acid sequences of 190 BnPMEIs, and the bootstrap replicate was set as 1000 times. Different clades of PMEI family were represented by different colors.

hybridization between two diploid progenitors, *Brassica rapa* (AA, 2n = 20) and *Brassica oleracea* (CC, 2n = 18). *B. napus* has 19 chromosomes, of which 10 chromosomes are from An subgenome and 9 from Cn subgenome (Chalhoub et al., 2014). The smallest chromosome is A10 while the largest chromosome is C03. Both A and C subgenomes of *B. napus* have undergone duplications as reported (Chalhoub et al., 2014). Chromosomal location analysis showed the *BnPMEI* genes were unevenly distributed across 19 chromosomes. Locations of 151 *BnPMEI* genes were confirmed on the 19 chromosomes (**Figure 3**). Owing to the incomplete information of *B. napus* genome, 29 *BnPMEI* genes were assigned to random chromosomes (11 on Ann random chromosomes, 17 on Cnn random chromosomes and 1 on Unn random chromosome). In terms of the remaining *BnPMEI* genes, the chromosomes they were located on were already known but the exact locations they resided were unknown. In the *BnPMEI* gene family, 92 and 98 *BnPMEI* genes were located on A and C subgenomes, respectively. The number of *BnPMEI* genes per chromosome was from 1 to 16. The maximum number of *BnPMEIs* was discovered on chromosome C03 while the minimum number was on chromosome A04 with only one. Chromosome A01, A06, A09, C02, and C03 contained more than 10 *BnPMEI* genes. The number of *BnPMEIs* was not positively correlated

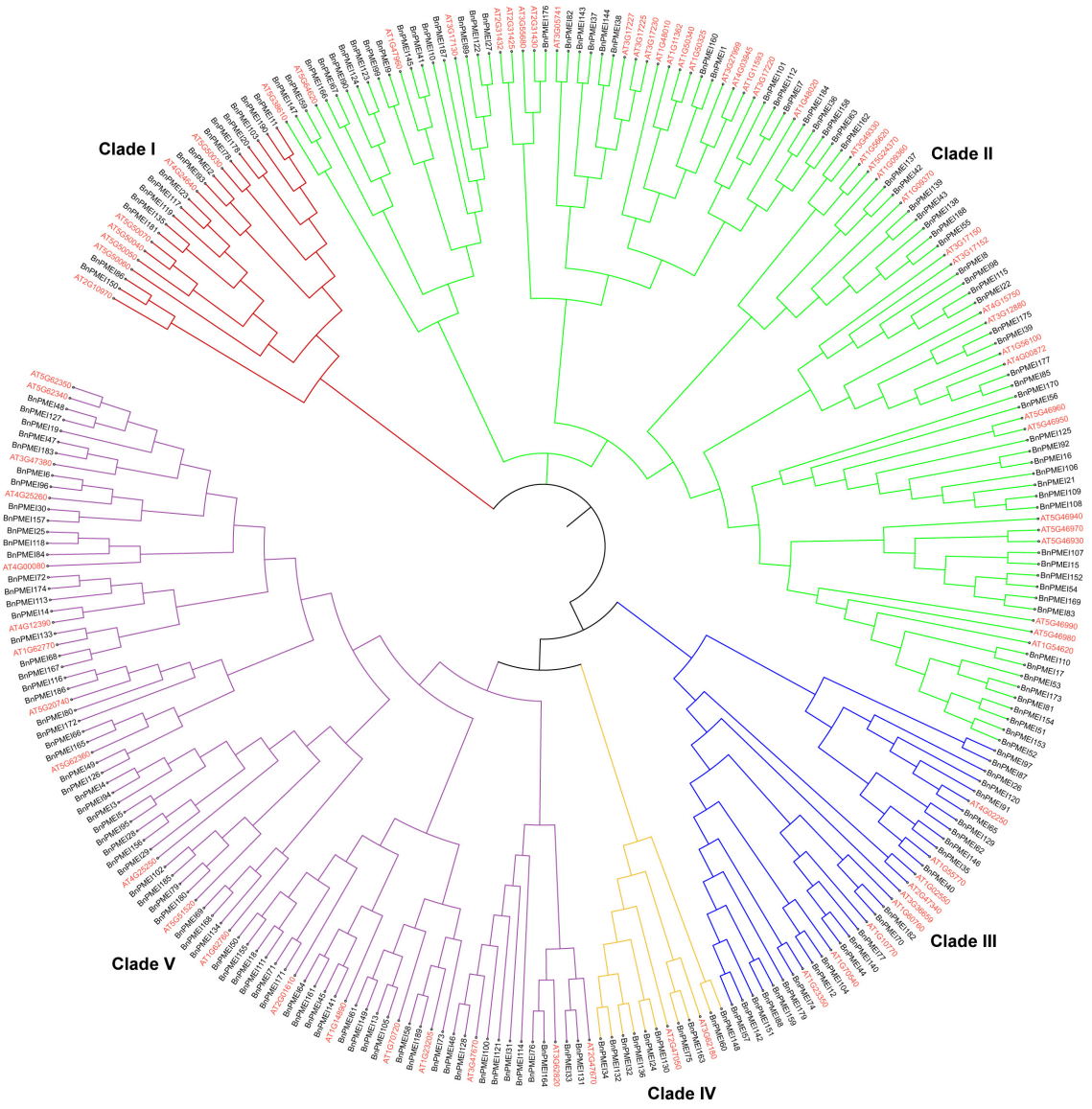

FIGURE 2
Phylogenetic analysis of PMEI proteins in *B. napus* and *A. thaliana*. The unrooted maximum likelihood (ML) phylogenetic tree was constructed using full-length amino acid sequences of 267 PMEI proteins from both species with MEGA11. Gene IDs in red color represented *PMEIs* from *A. thaliana*, and gene names in black indicated *PMEIs* from *B. napus*. The arcs in different colors indicated different clades of the PMEI proteins.

with chromosome length. Also, clusters of *BnPMEI* genes were detected on diverse chromosomes (**Figure 3**).

Gene duplication is likely essential for adaptive evolution and plays a significant role in the expansion of gene families (Panchy et al., 2016). In this study, duplication events occurred in the *B. napus PMEI* gene family were investigated. As shown in **Supplementary Table 4**, 123 *BnPMEI* genes were derived from whole-genome duplication (WGD) or segmental duplications. 49 *BnPMEI* genes evolved under dispersed duplication events which may involve repetitive sequences and/or replicative transposition by transposable elements (TEs). Only 9 *BnPMEIs* appeared as a result of tandem duplication. Using MCScanX methods, 166 paralogous gene pairs were identified. Among them, 165 gene pairs were detected across different chromosomes, while only one duplication event occurred within the same chromosome (BnaC04g00440D/BnaC04g51500D) (**Figure 4A** and **Supplementary Table 5a**). Additionally, 33 duplication events took place on the AA subgenome, 25 events occurred on the CC subgenome, and 108 across AA/CC subgenomes (**Figure 4A** and **Supplementary Table 5a**). The results suggest gene duplications, mainly driven by WGD or segmental events, play a key role in the expansion of *PMEI* gene family in *B. napus*. To characterize the selective pressure on the duplicated *BnPMEI* genes during the evolutionary process,

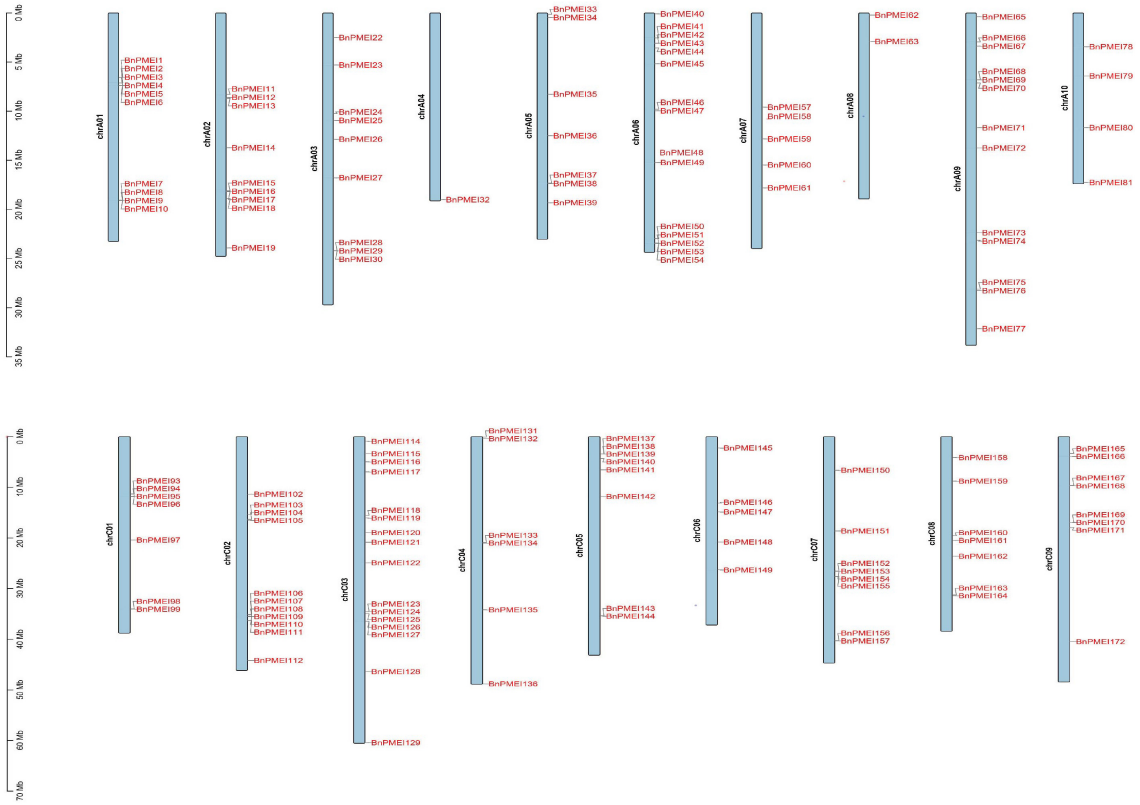

FIGURE 3
The distribution of *BnPMEI* genes on *B. napus* chromosomes. A total of 151 *BnPMEI* genes were mapped to the 19 chromosomes, and the remaining *BnPMEI* genes were unassembled scaffolds. The chromosome number was indicated on the left side of each chromosome and gene names were shown on the right side of each chromosome. The scale was megabases (Mb). Chr, chromosome.

Ka/*Ks* ratios were calculated for the paralogous gene pairs in *B. napus*. Except for one duplication event with a *Ka*/*Ks* ratio over one, the ratios of *Ka*/*Ks* for other duplication events were less than one, implying the main driving force for *BnPMEI* family evolution was the negative selection (**Supplementary Table 5a**). Estimation of divergence-time (Million Years Ago, MYA) revealed the divergence of *PMEIs* in *B. napus* occurred during ∼61.44 MYA (**Supplementary Table 5a**).

Furthermore, synteny analysis of the *PMEI* gene families between *B. napus* genome and *A. thaliana* genome was performed. Collinearity analysis revealed 105 *BnPMEIs* exhibited syntenic relationships with *AtPMEIs*, of which some *BnPMEIs* were related with more than one orthologous copy in *A. thaliana*, such as *BnPMEI2*, *BnPMEI3,* and *BnPMEI33* etc. (**Figure 4B** and **Supplementary Table 5b**). The majority of the orthologous gene pairs between *B. napus* and *A. thaliana.* had a *Ka*/*Ks* ratio of less than 0.5, implying the *PMEI* gene family might have undergone robust purifying selective pressure during evolution. Analysis of the divergence time of homologous gene pairs between *B. napus*–*A. thaliana* suggested the divergence of *PMEIs* occurred during 8.77 ∼ 69.3 MYA (**Supplementary Table 5b**).

Cis-elements in the promoters of *BnPMEI* genes

Cis-acting elements play an important role in regulating gene expression. In order to understand the potential regulatory mechanisms of *BnPMEI* genes, cis-elements within the 1.5-kb upstream from ATG for each of the *BnPMEI* gene were analyzed using PlantCARE. A wide range of cis-acting elements were identified in the promoter regions of *BnPMEI* genes, including elements related to plant growth and development, abiotic and biotic stress responses, hormones responses, and basic promoter elements in eukaryotes such as CAAT-box and TATA-box (**Supplementary Figure 3** and **Supplementary Table 6**). Plant hormone-responsive elements were detected in the promoters of a large number of *BnPMEI* genes, including GARE-motif and P-box (gibberellin-responsive elements), CGTCA-motif/TGACG-motif (MeJA-responsiveness), AuxRR-core (auxin responsiveness), ABRE motif (abscisic acid responsiveness), TCA-element (salicylic acid responsiveness), TGA-element (auxin-responsive element) and TATC-box (gibberellin-responsiveness). The most abundant ABRE-motif appeared in the promoter region of 147 *BnPMEI* genes,

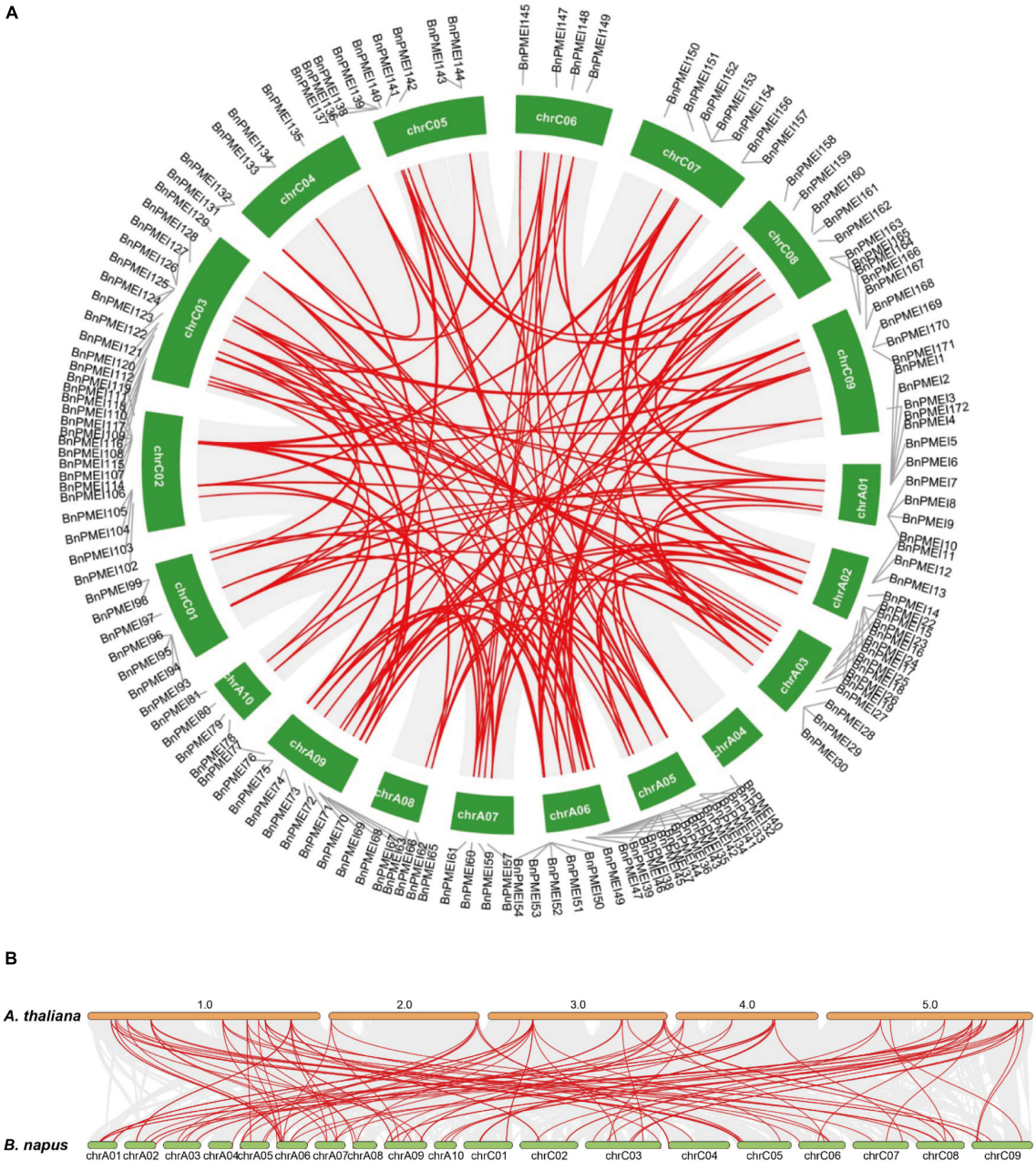

FIGURE 4

(A) Synteny analysis of *PMEI* family in *B. napus*. Gray lines indicated all synteny blocks in the *B. napus* genome, and red lines highlighted the duplicated *BnPMEI* gene pairs. ID of chromosome was indicated in the middle of each chromosome. **(B)** Synteny analysis of *PMEI* family between *B. napus* and *A. thaliana*. Gray lines in the background indicated the collinear blocks within *B. napus* and *A. thaliana* genomes, while red lines highlighted the syntenic *PMEI* gene pairs. The specie names with the prefixes '*A. thaliana*' and '*B. napus*' indicated *Arabidopsis thaliana* and *Brassica napus*, respectively. ID of the *A. thaliana* chromosome was indicated on the top of each chromosome, and ID of *B. napus* chromosome was indicated at the bottom of each chromosome.

followed by the MeJA-responsive motifs which were detected in 124 members. In contrast, auxin-related element AuxRR-core appeared in only 25 *PMEI* genes in *B. napus*, and gibberellin-responsive TATC box presented in 29 members. Another important category of cis-elements were environmental stress-responsive elements. ARE motif, essential for the anaerobic induction, appeared in 164 members from the *PMEI* family. LTR, responsive to low temperate, was occupied by 80 *BnPMEI* genes. *Cis*-element essential for drought induction was detected in the promoter region of up to 78 *BnPMEI* genes. A total of 75 *BnPMEI* genes owned TC-rich repeats which are involved in defense and stress response. 62 *BnPMEI*

genes carried MYB binding site (MRE) which is involved in light responsiveness. However, the numbers of *BnPMEI* genes containing cis-elements associated with elicitor-mediated activation, anoxic specific induction and wound responsiveness were 14, 8, and 8, respectively (**Supplementary Figure 3** and **Supplementary Table 6**).

A diversity of *cis*-elements related to plant growth and development were detected. For example, light-responsive elements were found in 157 members from the *PMEI* gene family. Another development related *cis*-element was CAAAGATATC motif which is involved in circadian control. *Cis*-elements associated with endosperm expression and meristems expression were detected, implying genes containing these elements were likely to regulate cell wall pectin methylesterase/de-methylesterase during seed germination and cell division. Elements participating in flavonoid biosynthetic gene regulation, differentiation of the palisade mesophyll cells, zein metabolism regulation, seed specific regulation and cell cycle regulation were also detected (**Supplementary Figure 3** and **Supplementary Table 6**).

Evaluation of disease development in the R-line and S-line

Disease symptoms were recorded at each time point after inoculation. For both R-line and S-line, the soft-rotting necrosis occurred as early as 12 h after inoculation with no significant difference detected for the lesion area. Disease symptoms developed rapidly as infection proceeded, and lesion size became apparent at 24 h in both lines (**Figure 5A** and **Supplementary Table 7**). Lesion area was significantly larger in the S-line than the R-line at both 24 h and 36 h post inoculation (**Figure 5A** and **Supplementary Table 7**). In order to further compare the cellular changes in both lines, trypan blue and DAB staining was performed. Trypan blue staining was conducted to examine cell viability, which was based on the principle that viable cells possessing intact cell membranes could exclude the dyes while died cells could not (Strober, 2015). Inoculated leaves from the S-line showed darker blue color than the R-line, suggesting more died cells were present in the S-line (**Figure 5B**). The presence and distribution of H_2O_2 in leaf cells were detected by DAB staining. DAB can be oxidized by H_2O_2 in the presence of some haem-containing proteins, such as peroxidases, to generate a dark brown precipitate which can be visualized as a stain using a microscope. Micrographs of the DAB-stained leaves from the S-line showed denser dark brown precipitates compared to the R-line, indicating higher level of H_2O_2 was accumulated during the infection process in the S-line (**Figure 5B**). The DAB staining result might reflect a more robust defense response associated with reactive oxygen species (ROS) in the S-line compared to the R-line. Lesion area was measured using Image J, and a significant difference ($P < 0.001$) was observed at 24 and 36 h post inoculation, respectively, between the R-line and S-line (**Figure 5C** and **Supplementary Table 7**).

Expression profiles of *BnPMEI* genes in response to *Sclerotinia sclerotiorum* infection

In order to investigate if *BnPMEI* genes were associated with resistance to *S. sclerotiorum*, expression patterns of the *PMEI* gene family were evaluated in our study. Firstly, public transcriptome data was used to evaluate the overall expression patterns of *BnPMEI* family. Transcriptome data was obtained from the NCBI SRA database under the following projects (ID PRJNA274853; PRJNA321917) (**Supplementary Table 8a**: PRJNA274853; **Supplementary Table 8b**: PRJNA321917). Wu et al. (2016) reported a global transcriptomic analysis of two *B. napus* pure lines J964 (resistant line, designated the R-line) and J902 (susceptible line, designated the S-line) at 24, 48, and 96 h post-inoculation by the *S. sclerotiorum* isolate on the primary stem; The relative differentially expressed *BnPMEI* genes between resistant and susceptible lines were characterized. In detail, transcripts of three genes including *BnPMEI161*, *BnPMEI64,* and *BnPMEI141* were strongly enhanced at 96 h post inoculation in the S line (**Supplementary Figure 4** and **Supplementary Table 8a**). The three genes were also upregulated in the R-line although to a lesser extent than the S-line at the same timepoint, while they were induced to a higher level at 48 h than 96 h in the R line (**Supplementary Figure 4** and **Supplementary Table 8a**). Expression of *BnPMEIs* were also profiled using RNA-seq data generated from leaf samples treated by *S. sclerotiorum* for 24 h in susceptible (cv. Westar) and tolerant (cv. Zhongyou 821) lines (Girard et al., 2017). A number of *PMEI* genes were up-regulated in both lines, including *BnPMEI33*, *BnPMEI41*, *BnPMEI165*, *BnPMEI164*, *BnPMEI131*, *BnPMEI167*, *BnPMEI76,* and *BnPMEI145* (**Supplementary Figure 4** and **Supplementary Table 8b**).

Expression levels of 10 *BnPMEI* genes at various infection stages in R line and S line

Based on the results of RNA-seq analysis, a total of ten *BnPMEI* genes were selected for further validation. These genes selected for qRT-PCR analysis include *BnPMEI168, BnPMEI145, BnPMEI19, BnPMEI41, BnPMEI161, BnPMEI46, BnPMEI76, BnPMEI128, BnPMEI127,* and *BnPMEI64* (**Supplementary Table 2**). We used qRT-PCR to examine their expression levels at various infection stages in our R-line and S-line. In general, several *BnPMEI* genes were responsive to *S. sclerotiorum* infection in both lines. In the R-line, *BnPMEI19* was most significantly ($P < 0.001$) induced

10.3389/fpls.2022.940284

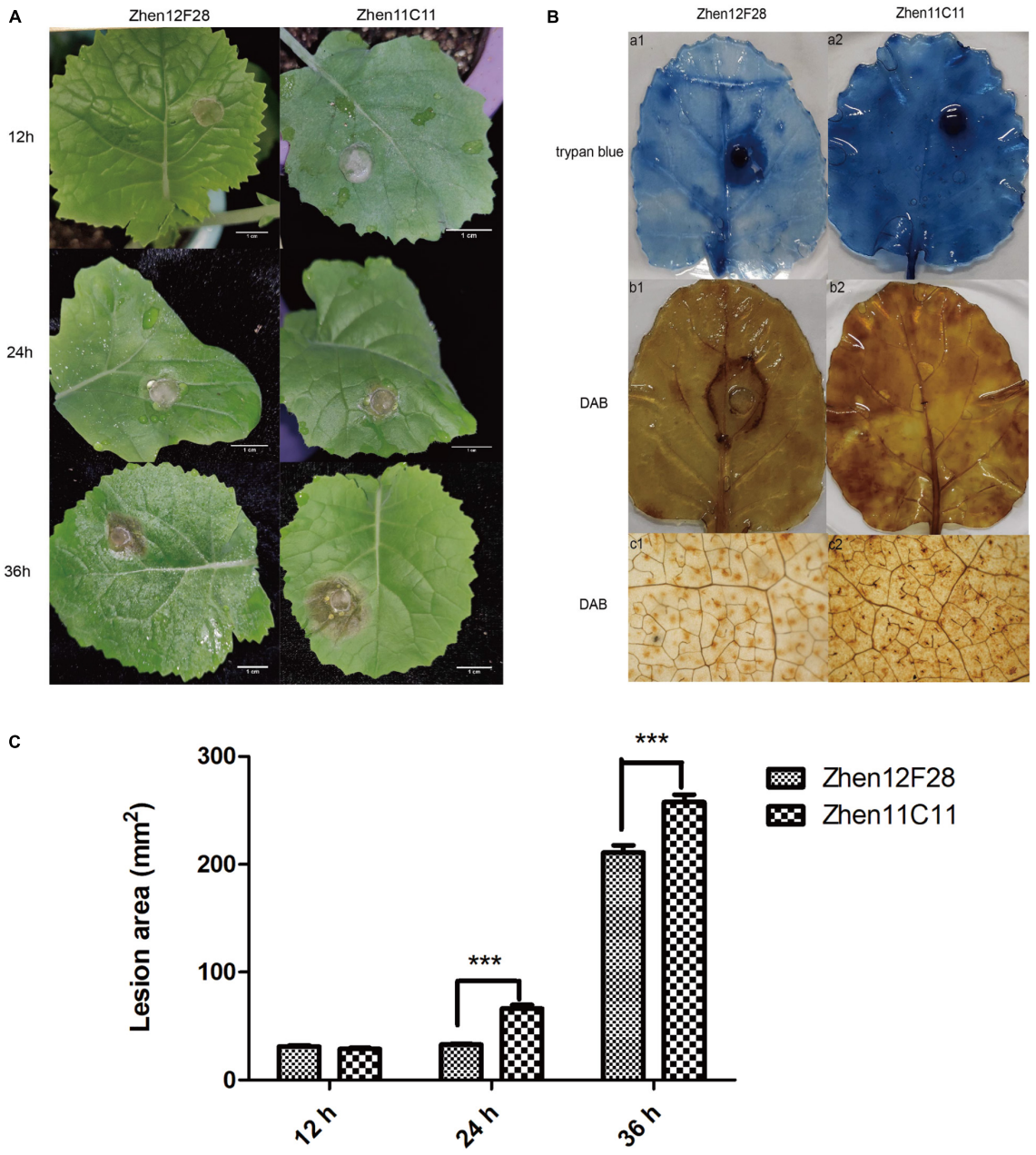

FIGURE 5
Evaluation of disease development. **(A)** Disease symptoms of leaves in Zhen12F28 (R-line) and Zhen11C11 (S-line) 12, 24, and 36 h post inoculation with *S. sclerotiorum*. Scale bar = 1 cm. **(B)** Trypan blue and DAB staining in the leaves of Zhen12F28 (R-line) and Zhen11C11 (S-line) at 36 h after inoculation. a1 and a2: Trypan blue staining; b1 and b2: DAB staining; c1 and c2: DAB staining imaged under microscope. **(C)** Lesion area of inoculated leaves in Zhen12F28 and Zhen11C11 at 12, 24, and 36 h post inoculation. Error bars are mean ± SEM, $n = 3$. Significant differences between the two lines at each time point are denoted as follows: ***$P < 0.001$.

by *S. sclerotiorum* at both 24 and 36 h after inoculation, followed by *BnPMEI127* and *BnPMEI76* (Figure 6A). In the S-line, *BnPMEI76* showed the largest fold change relative to control (0 h) at 36 h ($P < 0.001$), and transcripts of *BnPMEI127* was four times the amount of control ($P < 0.001$) (Figure 6B). Another gene *BnPMEI41* was also up-regulated in both lines, although to a lesser extent than *BnPMEI19*, *BnPMEI127*, and *BnPMEI76*. The common targets observed in both lines are likely to be vital for enlightening tolerance to SSR probably *via* strengthening cell wall mechanics and maintaining cell wall integrity (CWI). In contrast, some *BnPMEI* genes were down-regulated during infection, suggesting they might play a negative role in maintaining CWI probably through inducing cell wall loosening.

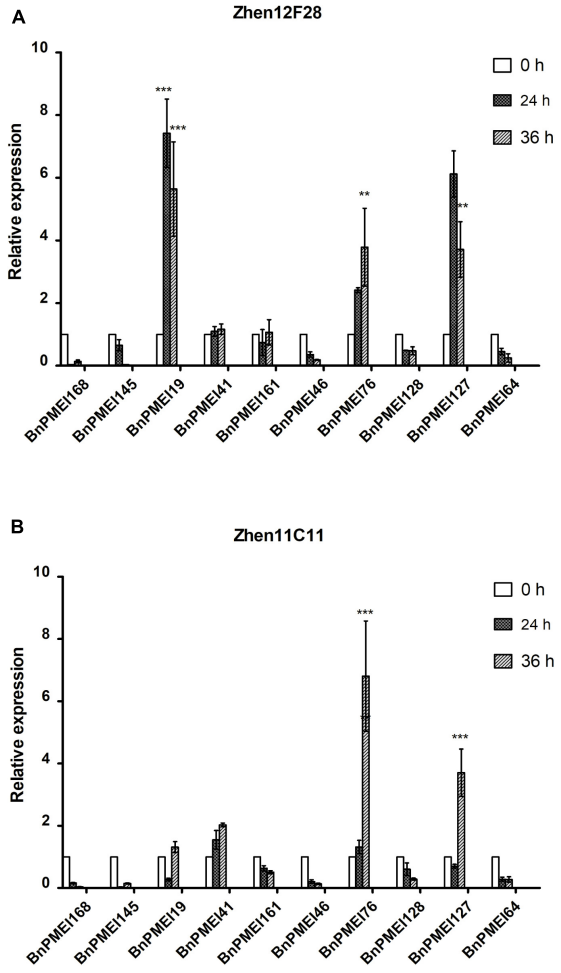

FIGURE 6
Expression profiles of selected ten *BnPMEI* genes in Zhen12F28 (R-line) **(A)** and Zhen11C11 (S-line) **(B)** after *S. sclerotiorum* infection. The relative expression levels were analyzed by qRT-PCR. Error bars are mean ± SEM, $n = 3$. Significant differences between infected lines and the control (WT) line (0 h) at each time point are denoted as follows: ***$P < 0.001$; **$P < 0.01$.

Tissue-specific expression patterns of *BnPMEI* genes

Expression profiles of *BnPMEIs* in different tissues was analyzed. The transcript levels of 190 *BnPMEI* genes in five different tissues including root, stem, leaves, petals and silique pericarp at full-bloom stage from *B. napus* cultivar ZhongShuang 11(ZS11) were obtained from public resource Brassica EDB (see footnote 16). A heatmap was constructed to illustrate the global expression patterns of the *BnPMEI* gene family (**Supplementary Figure 5**). A total of 50 *BnPMEI* genes were specifically expressed in petal with high levels while exhibited low expression levels across other tissues. Six *BnPMEI* genes were merely highly expressed in root, including *BnPMEI87*, *BnPMEI56*, *BnPMEI8*, *BnPMEI146*, *BnPMEI13*, and *BnPMEI123*. Genes that were expressed only in stem including *BnPMEI15*, *BnPMEI62*, *BnPMEI49*, *BnPMEI129*, *BnPMEI43*, and *BnPMEI175*. The numbers of *BnPMEI* genes that were detected in leaf and silique were 10 and 19, respectively. Numerous genes were expressed in more than one tissue with varying levels of transcripts. The variety of expression patterns suggested a broad range of biological functions of the *BnPMEI* genes during the development of *B. napus*.

qRT-PCR was performed to examine the expression levels of the selected *BnPMEI* genes, in various organs including root, stem, leaf, petal and silique at full-bloom stage of *B. napus* ZS11 cultivar. Significant differences were detected between different tissues for each of the ten genes. As displayed in **Figure 7**, seven out of ten *BnPMEI* genes showed the highest expression level in leaf. Two BnPMEI genes including *BnPMEI161* and *BnPMEI64* had higher levels of transcripts in root compared to other tissues, and *BnPMEI19* maintained the highest expression level in silique. Three genes including *BnPMEI19*, *BnPMEI76*, and *BnPMEI 127* were significantly induced in leaves by *S. sclerotiorum* infection, and they also maintained relatively high constitutive expression levels in leaf tissue. This suggests a role of the three *BnPMEI* genes in regulating both plant development and biotic stress. Interestingly, *BnPMEI76* was only detectable in leaf tissue, which was consistent with the public RNA-seq data. Other genes were detected in multiple tissues, suggesting they might function in various tissues during development.

Chemical analysis of pectin and its degree of methylesterification

Pectin content and degree of pectin methylesterification were compared between five different tissues from *B. napus*, including root, stem, leaf, petal and silique at full-bloom stage. Cell wall materials (AIS) was prepared from various tissues and PEFs were isolated from AISs. Pectin content was determined indirectly by measuring uronic acid content in the PEFs as uronic acid is the basic composition of pectin. Similar levels of uronic acid ($P > 0.05$) were detected in all of the five tissues, ranging from 6 to 8 μg/mg cell walls (**Figure 8A**). It is likely that the level of methyl groups bound to HG and the degree of pectin methylesterification reflects the endogenous PME/PMEI activity. As an indirect reflection of PME/PMEI activities, cell wall-bound methyl ester contents were compared between root and other tissues, respectively, by measuring methanol that was released from cell walls after chemical treatment. Resulted indicated the highest level of methanol was present in pectin fractions isolated from petal cell walls, followed by root and stem. In contrast, PEFs from silique cell walls were observed to have the lowest level of methanol (**Figure 8B**). This suggested degree of pectin methylesterification was higher in vegetative tissues

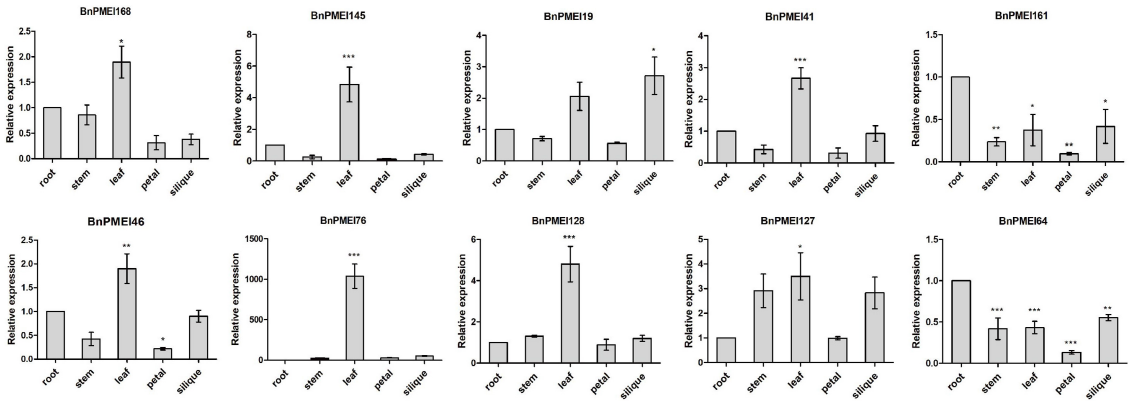

FIGURE 7
Expression profiles of the selected ten *BnPMEIs* in five different tissues including root, stem, leaf, petal, and silique at full-bloom stage of *B. napus*. The relative expression levels were analyzed by qRT-PCR and expressed as a ratio relative to that of root. Error bars are mean ± SEM, $n = 3$. Significant differences between different tissues and root are denoted as follows: ***$P < 0.001$; **$P < 0.01$; *$P < 0.05$.

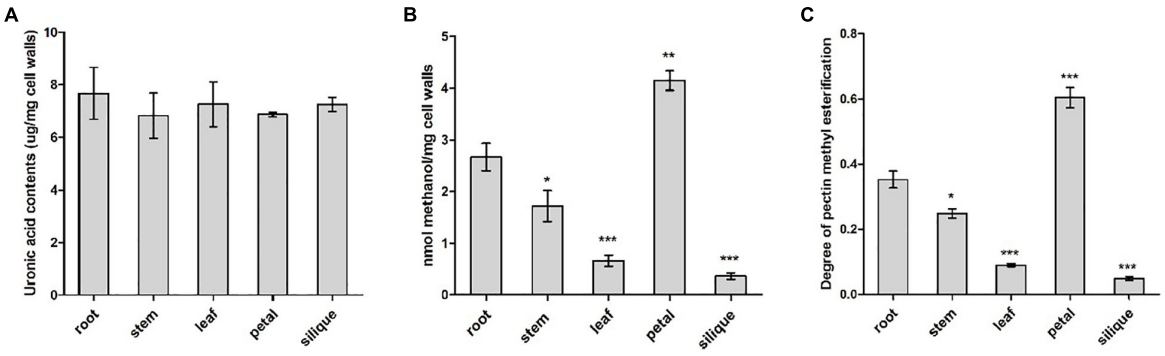

FIGURE 8
Biochemical analysis of pectin modification in various tissues including root, stem, leaf, petal and silique at full-bloom stage of *B. napus*. **(A)** Analysis of uronic acid content in pectin-enriched fractions of cell walls isolated from different tissues. **(B)** Quantification of cell wall-bound methanol in different tissues. **(C)** Degree of pectin methylesterification of cell walls in different tissues. Error bars are mean ± SEM, $n = 3$. Significant differences between different tissues and root were denoted as follows: ***$P < 0.001$; **$P < 0.01$; *$P < 0.05$.

and flower than fruit tissue. Root tissue was randomly selected as the control group for pairwise comparison. Results revealed significant differences ($P < 0.05$) between root and each of the other four tissues, in terms of both cell wall-bound methanol and degree of HG methylesterification (Figures 8B,C). The results suggested pectin methylesterification status, a major *in muro* modification of pectin, acted as a key determinant of organ and tissue development probably through regulating cell wall mechanics and integrity.

Gene ontology analysis and proten–protein interactions prediction

GO terms for each BnPMEI protein were determined using Interpro Scan 5. Each BnPMEI protein was annotated with the Molecular Function term GO:0004857, which was defined as "enzyme inhibitor activity." Part of the BnPMEI proteins were also annotated with the Biological Process term GO:0043086, a GO term defined as "negative regulation of catalytic activity" (Supplementary Table 9a). None of the BnPMEI proteins were associated to any Cellular Component GO term. The results are consistent with BnPMEI having a function related to the inhibition of the activity of PMEs.

The STRING database was used to predict potential proteins interacting with each of the BnPMEI protein as well as interaction networks between members of the *BnPMEI* gene family. A total of 30 BnPMEI proteins were involved in PPI networks and interacted with each other (Figure 9 and Supplementary Table 9b). BnPMEI86 had the highest node degree (16), meaning it interacted with 16 BnPMEI proteins, followed by BnPMEI30 with a node degree of 6. In contrast, the majority of the BnPMEIs interacted with one or three BnPMEI proteins. To be specific, 13 BnPMEIs interacted with

FIGURE 9
Protein–protein interaction networks of BnPMEIs. The networks were generated from the STRING database. Network nodes represented BnPMEI proteins. Edges represented protein-protein associations.

only one protein and 11 BnPMEIs interacted with three proteins from the *PMEI* family. In addition, each BnPMEI member was checked individually for their interaction networks. Results revealed 47 BnPMEI proteins showed interactions with various proteins in *B. napus*. Detailed information was summarized in **Supplementary Table 9c**. Numbers of BnPMEIs interacting with 10 proteins and 9 proteins were 18 and 8, respectively. However, 9 BnPMEIs had interaction with only one protein (**Supplementary Table 9c**). Interestingly, some of these BnPMEIs were detected to have associations with other cell wall structure-related enzymes, suggesting BnPMEI proteins might regulate cell wall metabolism and wall-associated biological processes through their interactions with other cell wall related enzymes. For example, BnPMEI31, BnPMEI87, BnPMEI121 were found to interact with multiple members in the *pectate lyase (PL)* gene family. BnPMEI134 alone was predicted to associate with three types of cell wall related enzymes including cellulose synthase, pectinesterase and xyloglucan endotransglucosylase/hydrolase. Other cell wall related enzymes such as alpha-galactosidase, hexosyltransferase and beta-glucosidase were also among the identifiers involved in these PPI networks (**Supplementary Table 9c**). In addition to these enzymes related to cell wall metabolism, other genes might be co-expressed with *BnPMEIs* and encode proteins which are

involved in cell wall metabolism in a coordinated way with BnPMEIs. These proteins included erecta leucine-rich-repeat receptor-like kinase, thioredoxin, cyclin, thioredoxin, CASP-like protein, bidirectional sugar transporter SWEET, 3-ketoacyl-CoA synthase, peroxidase and proteins in plant LTP family and MIP/aquaporin family (**Supplementary Table 9c**).

Discussion

Recent progress on the role of *PMEI* genes has offered new insights into our knowledge of how the degree of HGmethylesterification impacts cell wall properties, plant development, and interactions with their abiotic and biotic environments (Wormit and Usadel, 2018). In this study we have undertaken a comprehensive genome wide analysis of *PMEI* gene family in *B. napus* and have identified 190 PMEIs. This number was apparently higher than previously reported numbers of PMEIs in other dicot species including *A. thaliana* (71) (Wang et al., 2013), *Brassica campestris* (100) (Liu et al., 2018a), *Brassica rapa* (97) (Tan et al., 2018) and flax (95) (Pinzón-Latorre and Deyholos, 2013), as well as monocots such as rice (49) (Nguyen et al., 2016), *Sorghum bicolor* (37) (Ren et al., 2019), *Brachypodium distachyon* (38) (Wolf et al., 2009). *B. napus* contains more PMEI isoforms than other dicots, which might be attributed to the larger size of *B. napus* genome in comparison with other members of the Brassica family. Moreover, in monocots PMEI families are generally of smaller size with respect to number of gene members, likely due to the differences in the cell wall composition. Pectins are generally less abundant and less methylesterified in monocot species in comparison to dicot species (Mohnen, 2008).

The BnPMEIs that were identified were classified into Clades I–V, based on phylogenetic analysis. Intragroup BnPMEIs presented similar patterns of gene structure and motif composition, indicating members from the same clade might originate from a common ancestor and exhibit similar functions. Moreover, this could be a further validation on the phylogenetic classification. Having only one exon was the common pattern within *BnPMEI* genes, which was similar to *A. thaliana* (Wang et al., 2013). Gene duplication is a fundamental process in the evolution of species especially in eukaryotes and plays an important role for the creation of novel gene functions (Lynch and Conery, 2000; Tremblay Savard et al., 2011). Compared with other eukaryotic genomes, plant genomes tend to evolve at higher rates which lead to higher genome diversity (Panchy et al., 2016). Multiple mechanisms contribute to gene duplication. Duplication events are classified as singleton, dispersed, proximal, tandem and whole genome duplication or segmental. Tandem duplication, which takes place locally, results from unequal crossing-over events and leads to a cluster of two or more paralogous sequences with no or few intervening gene sequences (Zhang, 2003). In contrast to tandem duplication, other subgenomic duplication mechanisms result in dispersed duplicates. The analysis of synteny in this study showed whole genome duplication or segmental duplication was the predominant mechanism accounting for the *BnPMEI* gene family expansion. This was in line with the recognized conclusion that the major cause of expansion of gene families in many angiosperms were WGD events (Tang et al., 2008). Calculation of *K*a/*K*s values between paralogous and orthologous pairs indicated that *PMEIs* in *B. napus* and *A. thaliana* were mostly under stabilizing selection except a few sites have undergone positive selection. The only one paralogous gene pair in *BnPMEI* family with a *K*a/*K*s value higher than one could be interpreted as a consequence of very recent duplication, meaning enough time has yet to be elapsed for the related mutations to be silenced.

Cis-elements in the promoter region are fundamental in regulating gene expression. Various *cis*-elements were detected by promoter analysis. Elements that were extensively detected include light-responsive elements, hormone-responsive elements, along with those involved in developmental and environmental responses. *Cis*-elements found in *BnPMEI* genes were consistent with previously reported *PMEI* genes in *Brassica campestris, Sorghum bicolor,* and *Brassica oleracea* (Liu et al., 2018a,b; Ren et al., 2019). Multiple *cis*-elements were detected upstream each *BnPMEI* gene, suggesting each member is likely to be regulated by various factors.

Plant cell wall related genes especially those modulating pectin metabolism have been shown to regulate stress responses (Lionetti, 2015). Numerous studies have shown *PMEI* genes were involved in various environmental stresses through maintaining CWI as well as activating pattern triggered immunity (PTI) (Wormit and Usadel, 2018). *B. napus* is constantly threatened by the disease termed SSR which is caused by the fungal pathogen *S. sclerotiorum*. Cultivating disease-resistant rapeseed varieties is the most cost-effective way to prevent and control SSR.

Molecular mechanisms of *B. napus*–*S. sclerotiorum* interactions are complex, which limits the rate of molecular breeding of rapeseed. Recent studies examining the global transcriptional changes during *B. napus*–*S. sclerotiorum* interactions have revealed alterations in the expression levels of cell wall degradation-related genes (Chittem et al., 2020; Xu et al., 2021). Polygalacturonase-inhibiting proteins (PGIPs), a group of proteins inhibiting the activity of polygalacturonase (PG), could effectively enhance rapeseed immunity against *S. sclerotiorum* infection (Bashi et al., 2013; Wang et al., 2018, 2021). Both PGIPs and PMEIs are involved in regulating pectin degradation. Several studies have revealed a role of PMEIs in regulating plant immunity in *A. thaliana* and wheat (Lionetti et al., 2007; Volpi et al., 2011). A more recent study showed three PMEIs including AtPMEI10, AtPMEI11, and AtPMEI12 increased disease resistance to *Botrytis cinerea* in Arabidopsis through maintaining CWI (Lionetti et al., 2017).

Genetic analysis of loci associated with partial resistance to *S. sclerotiorum*, combined with transcriptome analysis suggested a potential role of *BnPMEIs* in regulating SSR resistance in *B. napus* (Zhao and Meng, 2003; Zhao et al., 2007, 2009).

In this study, we firstly analyzed public transcriptome data to examine the global expression profiling of *BnPMEI* genes in response to *S. sclerotiorum* infection in several rapeseed lines. A number of *BnPMEI* members responsive to infection were screened for further validation. We then investigated the expression patterns of ten selected *BnPMEIs* in local rapeseed lines including one partially resistant and one susceptible line. Prior to performing qRT-PCR, disease development, cell viability as well as H_2O_2 produced in the inoculated leaves were compared between the two lines. Significant differences in lesion area, death cell percentage and ROS were detected between R- and S- lines especially at later infection stage, suggesting defense responses were precisely regulated and vary between lines. qRT-PCR was used to test expression levels of the ten *BnPMEI* genes in the local lines 'Zhen12F28' and 'Zhen11C11." Transcripts of three genes including *BnPMEI76, BnPMEI19,* and *BnPMEI127* were significantly up-regulated during the infection process in both R-line and S-line. This was highly consistent with the results of RNA-seq analysis. However, some members were down-regulated by *S. sclerotiorum* treatment. The contrasting effects of the *BnPMEI* genes on SSR disease resistance in our study demonstrated that different PMEI isoforms are likely to modulate cell wall properties and affect the defense outcome using a range of mechanisms. Contrasting effects of genes modulating HG methylesterification degree, were shown in Arabidopsis, in particular, PME genes. AtPME3 and AtPME17 were significantly induced in A. thaliana leaves upon *B. cinerea* infection, but they had contrary impact on resistance against *B. cinerea* (Raiola et al., 2011; Del Corpo et al., 2020). Susceptibility to *B. cinerea* was significantly reduced in *pme3* homozygous mutant plants which showed decreased PME activity and methylated pectins in comparison with WT plants (Raiola et al., 2011). Further investigation indicated reduced susceptibility of pme3 mutant was mainly due to higher DM of pectin that can impair pathogen colonization rather than inducing constitutive and induced defense responses (Raiola et al., 2011). This suggested AtPME3 was a susceptibility factor required for rapid colonization of the host tissue by *B. cinerea* through modification of pectin structures. In contrast, AtPME17 has been shown to greatly trigger PME activity and significantly contributed to resistance against *B. cinerea* in *A. thaliana* (Del Corpo et al., 2020). Molecular and biochemical mechanism analysis suggested AtPME17 contributed to enhanced resistance to *B. cinerea via* activation of pathogen related defense responses, as well as affecting the rheological properties of pectin by facilitating "egg-box" formation (Del Corpo et al., 2020). Similar to *PME* genes, different PMEI isoforms function diversely during plant development and in response to various stresses. For example, tomato *PME1* was highly expressed in expanding green fruit, but not in ripening fruit. Functional characterization in transgenic plants revealed *PME1* played a negative role in regulating fruit softening probably through maintaining CWI. However, PMEIs that were highly ripening-related positively contributed to fruit softening (Liu et al., 2021). This reflects a close link between temporal-spatial expression of PMEI isoforms and their specific role.

PMEI gene expression is temporal-spatially regulated during plant-pathogen interactions. Depending on timing and location of the PMEI isoform, it is postulated that different PMEIs might make a range of contributions to disease resistance depending on mechanism and strategies they adopt. The detailed mechanisms of the regulatory role of the potential candidates need further investigation. Expression profiling of *BnPMEI* genes revealed tissue-specific patterns. The *BnPMEIs* genes were classified into seven groups based on their expression patterns. The largest group contained 50 *BnPMEI* genes which showed petal-specific patterns, indicating these genes might be involved in regulating petal development. Of the ten selected *BnPMEI* genes that were examined by qRT-PCR, significant differences were observed between various tissues for each of them.

Pectin content and level of pectin methylesterification were further examined by chemical analysis. Different tissues contained similar levels of pectin content, while degree of pectin methylesterification differed significantly between them. Strikingly, level of methylesterification in pectin fraction was the highest in petal, compared with other tissues. This was consistent with expression patterns of *BnPMEI* genes in petal, with the highest number of *BnPMEI* genes exhibited petal-specific expression. Higher level of PMEI activity is supposed to result in lower level of PME activity, which further leads to higher level of pectin methylesterification. This might account for the highest degree of pectin methylesterification in petal.

Protein–protein interaction and the associated networks are essential to the majority of cellular and biological processes, and activation of most proteins requires their interactions with other proteins (Athanasios et al., 2017). Analyzing the PPI networks allowed us to hypothesize the evolutionary relationships and predict functionally orthologous proteins between species with conserved pathways. Here, PPI network of each BnPMEI and PPI within the BnPMEI family were predicted using the STRING database. Extensive interactions were predicted to occur between different BnPMEIs, or between BnPMEI and other proteins. Interestingly, cell wall structural-related enzymes were identified in the PPI networks, especially those related to pectin metabolism such as pectate lyase, pectinesterase, and beta-glucosidase. This not only suggests pectin metabolism is regulated by the combined action of multiple enzymes, it also supports the recently revised plant cell wall model where pectin plays a much more important role in cell wall mechanics. Previously, the groups of cell wall polysaccharides and the associated enzymes are often discussed as independent entities,

but there is strong evidence for close associations among the different classes of molecules (Anderson and Kieber, 2020). Thus, future work on synergistic effect of multiple cell wall-related genes on cell wall integrity and wall associated biological processes is needed. The genome wide analysis of *PMEI* family in *B. napus* provides a theoretical basis for further function characterization and facilitates searching for candidate *PMEI* genes associated with stress response.

Data availability statement

The original contributions presented in this study are included in the article/**Supplementary Material**, further inquiries can be directed to the corresponding author.

Author contributions

DW conceived the original research plans, conducted the bioinformatic analysis, and wrote the manuscript. SJ conducted the experiments, analyzed the data, and involved in writing the manuscript. YS and LL performed the *S. sclerotiorum* inoculation experiments. DW and ZC were involved in reviewing and editing the manuscript. All authors contributed to the article and approved the submitted version.

Funding

This work was supported by the National Natural Science Foundation of China (grant number: 32101656), China Postdoctoral Science Foundation (grant number: 2021M691322), and Jiangsu Provincial Double-Innovation Doctor Program (grant number: JSSCBS20210961).

Acknowledgments

We thank Guoxu Yue at Zhenjiang Academy of Agricultural Sciences, China for kindly providing the seeds of rapeseed lines 'Zhen12F28' and 'Zhen11C11.'

Conflict of interest

The authors declare that the research was conducted in the absence of any commercial or financial relationships that could be construed as a potential conflict of interest.

Publisher's note

Supplementary material

The Supplementary Material for this article can be found online at: https://www.frontiersin.org/articles/10.3389/fpls.2022.940284/full#supplementary-material

References

An, S. H., Sohn, K. H., Choi, H. W., Hwang, I. S., Lee, S. C., and Hwang, B. K. (2008). Pepper pectin methylesterase inhibitor protein CaPMEI1 is required for antifungal activity, basal disease resistance and abiotic stress tolerance. *Planta* 228, 61–78. doi: 10.1007/s00425-008-0719-z

Anderson, C. T., and Kieber, J. J. (2020). Dynamic construction, perception, and remodeling of plant cell walls. *Annu. Rev. Plant Biol.* 71, 39–69. doi: 10.1146/annurev-arplant-081519-035846

Athanasios, A., Charalampos, V., Vasileios, T., and Ashraf, G. M. (2017). Protein-Protein Interaction (PPI) network: recent advances in drug discovery. *Curr. Drug Metab.* 18, 5–10. doi: 10.2174/1389200218011701192048 32

Bailey, T. L., Boden, M., Buske, F. A., Frith, M., Grant, C. E., Clementi, L., et al. (2009). MEME SUITE: tools for motif discovery and searching. *Nucleic Acids Res.* 37, 202–208.

Balestrieri, C., Castaldo, D., Giovane, A., Quagliuolo, L., and Servillo, L. (1990). A glycoprotein inhibitor of pectin methylesterase in kiwi fruit (Actinidia chinensis). *FEBS J.* 193, 183–187.

Bashi, Z. D., Rimmer, S. R., Khachatourians, G. G., and Hegedus, D. D. (2013). *Brassica napus* polygalacturonase inhibitor proteins inhibit *Sclerotinia sclerotiorum* polygalacturonase enzymatic and necrotizing activities and delay symptoms in transgenic plants. *Can. J. Microbiol.* 59, 79–86. doi: 10.1139/cjm-2012-0352

Blanc, G., and Wolfe, K. H. (2004). Widespread paleopolyploidy in model plant species inferred from age distributions of duplicate genes. *Plant Cell* 16, 1667–1678. doi: 10.1105/tpc.021345

Chalhoub, B., Denoeud, F., Liu, S., Parkin, I. A., Tang, H., Wang, X., et al. (2014). Plant genetics. Early allopolyploid evolution in the post-Neolithic *Brassica napus* oilseed genome. *Science* 345, 950–953. doi: 10.1126/science.1253435

Chen, C., Chen, H., Zhang, Y., Thomas, H. R., Frank, M. H., He, Y., et al. (2020). TBtools: an integrative toolkit developed for interactive analyses of big biological data. *Mol. Plant* 13, 1194–1202. doi: 10.1016/j.molp.2020.06.009

Chittem, K., Yajima, W. R., Goswami, R. S., and del Río Mendoza, L. E. (2020). Transcriptome analysis of the plant pathogen *Sclerotinia sclerotiorum* interaction with resistant and susceptible canola (*Brassica napus*) lines. *PLoS One* 15:e0229844. doi: 10.1371/journal.pone.0229844

Coculo, D., and Lionetti, V. (2022). The plant invertase/pectin methylesterase inhibitor superfamily. *Front. Plant Sci.* 13:863892. doi: 10.3389/fpls.2022.863892

De Lorenzo, G., Ferrari, S., Giovannoni, M., Mattei, B., and Cervone, F. (2019). Cell wall traits that influence plant development, immunity, and bioconversion. *Plant J.* 97, 134–147. doi: 10.1111/tpj.14196

Del Corpo, D., Fullone, M. R., Miele, R., Lafond, M., Pontiggia, D., Grisel, S., et al. (2020). AtPME17 is a functional *Arabidopsis thaliana* pectin methylesterase regulated by its PRO region that triggers PME activity in the resistance to *Botrytis cinerea*. *Mol. Plant Pathol.* 21, 1620–1633. doi: 10.1111/mpp.13002

Finn, R. D., Coggill, P., Eberhardt, R. Y., Eddy, S. R., Mistry, J., Mitchell, A. L., et al. (2016). The Pfam protein family database: towards a more sustainable future. *Nucleic Acids Res.* 44, 279–285. doi: 10.1093/nar/gkv1344

Giovane, A., Servillo, L., Balestrieri, C., Raiola, A., D'Avino, R., Tamburrini, M., et al. (2004). Pectin methylesterase inhibitor. *Biochim. Biophys. Acta* 1696, 245–252. doi: 10.1016/j.bbapap.2003.08.011

Girard, I. J., Tong, C., Becker, M. G., Mao, X., Huang, J., de Kievit, T., et al. (2017). RNA sequencing of *Brassica napus* reveals cellular redox control of *Sclerotinia* infection. *J. Exp. Bot.* 68, 5079–5091. doi: 10.1093/jxb/erx338

Höfte, H., and Voxeur, A. (2017). Plant cell walls. *Curr. Biol.* 27, R865–R870. doi: 10.1016/j.cub.2017.05.025

Horton, P., Park, K. J., Obayashi, T., Fujita, N., Harada, H., Adams-Collier, C. J., et al. (2007). WoLF PSORT: protein localization predictor. *Nucleic Acids Res.* 35, W585–W587. doi: 10.1093/nar/gkm259

Hu, B., Jin, J., Guo, A. Y., Zhang, H., Luo, J., and Gao, G. (2015). GSDS 2.0: an upgraded gene feature visualization server. *Bioinformatics* 31, 1296–1297. doi: 10.1093/bioinformatics/btu817

Hunter, S., Apweiler, R., Attwood, T. K., Bairoch, A., Bateman, A., Binns, D., et al. (2009). InterPro: the integrative protein signature database. *Nucleic Acids Res.* 37, D211–D215. doi: 10.1093/nar/gkn785

Jamet, E., and Dunand, C. (2020). Plant cell wall proteins and development. *Int. J. Mol. Sci.* 21:2731. doi: 10.3390/ijms21082731

Jeong, H. Y., Nguyen, H. P., Eom, S. H., and Lee, C. (2018). Integrative analysis of pectin methylesterase (PME) and PME inhibitors in tomato (*Solanum lycopersicum*): identification, tissue-specific expression, and biochemical characterization. *Plant Physiol. Biochem.* 132, 557–565. doi: 10.1016/j.plaphy.2018.10.006

Jing, L., Guo, D., Hu, W., and Niu, X. (2017). The prediction of a pathogenesis-related secretome of *Puccinia helianthi* through high-throughput transcriptome analysis. *BMC Bioinformatics* 18:166. doi: 10.1186/s12859-017-1577-0

Jolie, R. P., Duvetter, T., Van Loey, A. M., and Hendrickx, M. E. (2010). Pectin methylesterase and its proteinaceous inhibitor: a review. *Carbohydr. Res.* 345, 2583–2595. doi: 10.1016/j.carres.2010.10.002

Krogh, A., Larsson, B., von Heijne, G., and Sonnhammer, E. L. L. (2001). Predicting transmembrane protein topology with a hidden Markov model: application to complete genomes. *J. Mol. Biol.* 305, 567–580.

Lescot, V., De´hais, P., Thijs, G., Marchal, K., Moreau, Y., Van de Peer, Y., et al. (2002). PlantCARE, a database of plant cis-acting regulatory elements and a portal to tools for in silico analysis of promoter sequences. *Nucleic Acids Res.* 30, 325–327. doi: 10.1093/nar/30.1.325

Letunic, I., Doerks, T., and Bork, P. (2012). SMART 7: recent updates to the protein domain annotation resource. *Nucleic Acids Res.* 40, 302–305. doi: 10.1093/nar/gkr931

Levesque-Tremblay, G., Pelloux, J., Braybrook, S. A., and Müller, K. (2015). Tuning of pectin methylesterification: consequences for cell wall biomechanics and development. *Planta* 242, 791–811. doi: 10.1007/s00425-015-2358-5

Lionetti, V. (2015). PECTOPLATE: the simultaneous phenotyping of pectin methylesterases, pectinases, and oligogalacturonides in plants during biotic stresses. *Front. Plant Sci.* 6:331. doi: 10.3389/fpls.2015.00331

Lionetti, V., Fabri, E., De Caroli, M., Hansen, A. R., Willats, W. G., Piro, G., et al. (2017). Three pectin methylesterase inhibitors protect cell wall integrity for Arabidopsis immunity to Botrytis. *Plant Physiol.* 173, 1844–1863. doi: 10.1104/pp.16.01185

Lionetti, V., Raiola, A., Camardella, L., Giovane, A., Obel, N., Pauly, M., et al. (2007). Overexpression of pectin methylesterase inhibitors in Arabidopsis restricts fungal infection by *Botrytis cinerea*. *Plant Physiol.* 143, 1871–1880. doi: 10.1104/pp.106.090803

Liu, H., Liu, L., Liang, D., Zhang, M., Jia, C., Qi, M., et al. (2021). SlBES1 promotes tomato fruit softening through transcriptional inhibition of PMEU1. *iScience* 24:102926. doi: 10.1016/j.isci.2021.102926

Liu, T., Yu, H., Xiong, X., Yue, X., Yu, Y., Huang, L., et al. (2018a). Genome-wide identification, molecular evolution, and expression profiling analysis of pectin methylesterase inhibitor genes in *Brassica campestris* ssp. chinensis. *Int. J. Mol. Sci.* 19:1338. doi: 10.3390/ijms19051338

Liu, T., Yu, H., Xiong, X., Yu, Y., Yue, X., Liu, J., et al. (2018b). Genome-wide identification and characterization of pectin methylesterase inhibitor genes in *Brassica oleracea*. *Int. J. Mol. Sci.* 19:3338. doi: 10.3390/ijms19113338

Livak, K. J, and Schmittgen, T. D. (2001). Analysis of relative gene expression data using real-time quantitative PCR and the 2(-Delta Delta C(T)) method. *Methods*. 25, 402–408. doi: 10.1006/meth.2001.1262

Lynch, M., and Conery, J. S. (2000). The evolutionary fate and consequences of duplicate genes. *Science* 290, 1151–1155.

Marchler-Bauer, A., Lu, S., Anderson, J. B., Chitsaz, F., Derbyshire, M. K., DeWeeseScott, C., et al. (2011). CDD: a conserved domain database for the functional annotation of proteins. *Nucleic Acids Res.* 39, 225–229.

Mohnen, D. (2008). Pectin structure and biosynthesis. *Curr. Opin. Plant Biol.* 11, 266–277. doi: 10.1016/j.pbi.2008.03.006

Nguyen, H. P., Jeong, H. Y., Jeon, S. H., Kim, D., and Lee, C. (2017). Rice pectin methylesterase inhibitor28 (OsPMEI28) encodes a functional PMEI and its overexpression results in a dwarf phenotype through increased pectin methylesterification levels. *J. Plant Physiol.* 208, 17–25. doi: 10.1016/j.jplph.2016.11.006

Nguyen, H. P., Jeong, H. Y., Kim, H., Kim, Y. C., and Lee, C. (2016). Molecular and biochemical characterization of rice pectin methylesterase inhibitors (OsPMEIs). *Plant Physiol. Biochem.* 101, 105–112. doi: 10.1016/j.plaphy.2016.01.021

Panchy, N., Lehti-Shiu, M., and Shiu, S. H. (2016). Evolution of gene duplication in plants. *Plant Physiol.* 171, 2294–2316. doi: 10.1104/pp.16.00523

Park, Y. B., and Cosgrove, D. J. (2012). A revised architecture of primary cell walls based on biomechanical changes induced by substrate-specific endoglucanases. *Plant Physiol.* 158, 1933–1943. doi: 10.1104/pp.111.192880

Pinzón-Latorre, D., and Deyholos, M. K. (2013). Characterization and transcript profiling of the pectin methylesterase (PME) and pectin methylesterase inhibitor (PMEI) gene families in flax (*Linum usitatissimum*). *BMC Genom.* 14:742. doi: 10.1186/1471-2164-14-742

Raiola, A., Camardella, L., Giovane, A., Mattei, B., De Lorenzo, G., Cervone, F., et al. (2004). Two *Arabidopsis thaliana* genes encode functional pectin methylesterase inhibitors. *FEBS Lett.* 557, 199–203. doi: 10.1016/s0014-5793(03)01491-1

Raiola, A., Lionetti, V., Elmaghraby, I., Immerzeel, P., Mellerowicz, E. J., Salvi, G., et al. (2011). Pectin methylesterase is induced in Arabidopsis upon infection and is necessary for a successful colonization by necrotrophic pathogens. *Mol. Plant Microbe Interact.* 24, 432–440. doi: 10.1094/MPMI-07-10-0157

Ren, A., Ahmed, R. I., Chen, H., Han, L., Sun, J., Ding, A., et al. (2019). Genome-wide identification, characterization and expression patterns of the pectin methylesterase inhibitor genes in *Sorghum bicolor*. *Genes* 10:755. doi: 10.3390/genes10100755

Strober, W. (2015). Trypan blue exclusion test of cell viability. *Curr. Protoc Immunol.* 111, A3.B.1–A3.B.3. doi: 10.1002/0471142735.ima03bs111

Szklarczyk, D., Franceschini, A., Kuhn, M., Simonovic, M., Roth, A., Minguez, P., et al. (2011). The STRING database in 2011: functional interaction networks of proteins, globally integrated and scored. *Nucleic Acids Res.* 39, D561–D568. doi: 10.1093/nar/gkq973

Tan, C., Liu, Z., Huang, S., Li, C., Ren, J., Tang, X., et al. (2018). Pectin methylesterase inhibitor (PMEI) family can be related to male sterility in Chinese cabbage (*Brassica rapa* ssp. pekinensis). *Mol. Genet. Genomics* 293, 343–357. doi: 10.1007/s00438-017-1391-4

Tang, H., Bowers, J. E., Wang, X., Ming, R., Alam, M., and Paterson, A. H. (2008). Synteny and collinearity in plant genomes. *Science* 320, 486–488. doi: 10.1126/science.1153917

Tremblay Savard, O., Bertrand, D., and El-Mabrouk, N. (2011). Evolution of orthologous tandemly arrayed gene clusters. *BMC Bioinformatics* 12(Suppl. 9):S2. doi: 10.1186/1471-2105-12-S9-S2

Volpi, C., Janni, M., Lionetti, V., Bellincampi, D., Favaron, F., and D'Ovidio, R. (2011). The ectopic expression of a pectin methyl esterase inhibitor increases pectin methyl esterification and limits fungal diseases in wheat. *Mol. Plant Microbe Interact.* 24, 1012–1019. doi: 10.1094/MPMI-01-11-0021

Wang, M., Yuan, D., Gao, W., Li, Y., Tan, J., and Zhang, X. (2013). A comparative genome analysis of PME and PMEI families reveals the evolution of pectin metabolism in plant cell walls. *PLoS One* 8:e72082. doi: 10.1371/journal.pone.0072082

Wang, Y., Tang, H., DeBarry, J. D., Tan, X., Li, J., Wang, X., et al. (2012). MCScanX: a toolkit for detection and evolutionary analysis of gene synteny and collinearity. *Nucleic Acids Res.* 40:e49. doi: 10.1093/nar/gkr1293

Wang, Z., Fang, H., Chen, Y., Chen, K., Li, G., Gu, S., et al. (2014). Overexpression of BnWRKY33 in oilseed rape enhances resistance to *Sclerotinia sclerotiorum*. *Mol. Plant Pathol.* 15, 677–689. doi: 10.1111/mpp.12123

Wang, Z., Mao, H., Dong, C., Ji, R., Cai, L., Fu, H., et al. (2009). Overexpression of *Brassica napus* MPK4 enhances resistance to *Sclerotinia sclerotiorum* in oilseed rape. *Mol. Plant Microbe Interact.* 22, 235–244. doi: 10.1094/MPMI-22-3-0235

Wang, Z., Wan, L., Xin, Q., Chen, Y., Zhang, X., Dong, F., et al. (2018). Overexpression of OsPGIP2 confers *Sclerotinia sclerotiorum* resistance in *Brassica napus* through increased activation of defense mechanisms. *J. Exp. Bot.* 69, 3141–3155. doi: 10.1093/jxb/ery138

Wang, Z., Wan, L., Zhang, X., Xin, Q., Song, Y., Hong, D., et al. (2021). Interaction between *Brassica napus* polygalacturonase inhibition proteins and *Sclerotinia sclerotiorum* polygalacturonase: implications for rapeseed resistance to fungal infection. *Planta* 253:34. doi: 10.1007/s00425-020-03556-2

Wolf, S., Mouille, G., and Pelloux, J. (2009). Homogalacturonan methyl-esterification and plant development. *Mol. Plant* 2, 851–860.

Woriedh, M., Wolf, S., Marton, M. L., Hinze, A., Gahrtz, M., Becker, D., et al. (2013). External application of gametophyte-specific ZmPMEI1 induces pollen tube burst in maize. *Plant Reprod.* 26, 255–266. doi: 10.1007/s00497-013-0221-z

Wormit, A., and Usadel, B. (2018). The multifaceted role of pectin methylesterase inhibitors (PMEIs). *Int. J. Mol. Sci.* 19:2878. doi: 10.3390/ijms19102878

Wu, J., Zhao, Q., Yang, Q., Liu, H., Li, Q., Yi, X., et al. (2016). Comparative transcriptomic analysis uncovers the complex genetic network for resistance to *Sclerotinia sclerotiorum* in *Brassica napus*. *Sci. Rep.* 6:19007. doi: 10.1038/srep19007

Wu, X., Tian, H., Li, L., Guan, C., and Zhang, Z. (2021). Higher Cd-accumulating oilseed rape has stronger Cd tolerance due to stronger Cd fixation in pectin and hemicellulose and higher Cd chelation. *Environ. Pollut.* 285:117218. doi: 10.1016/j.envpol.2021.117218

Xu, B., Gong, X., Chen, S., Hu, M., Zhang, J., and Peng, Q. (2021). Transcriptome analysis reveals the complex molecular mechanisms of *Brassica napus-Sclerotinia sclerotiorum* interactions. *Front. Plant Sci.* 12:716935. doi: 10.3389/fpls.2021.716935

Xu, G., Guo, C., Shan, H., and Kong, H. (2012). Divergence of duplicate genes in exon-intron structure. *Proc. Natl. Acad. Sci. U. S. A.* 109, 1187–1192.

Zhang, H. (2003). Evolution by gene duplication: an update. *Trends Ecol. Evol.* 18:292.

Zhang, P., Wang, H., Qin, X., Chen, K., Zhao, J., Zhao, Y., et al. (2019). Genome-wide identification, phylogeny and expression analysis of the PME and PMEI gene families in maize. *Sci. Rep.* 9:19918. doi: 10.1038/s41598-019-56254-9

Zhao, J., Buchwaldt, L., Rimmer, S. R., Sharpe, A., McGregor, L., Bekkaoui, D., et al. (2009). Patterns of differential gene expression in *Brassica napus* cultivars infected with *Sclerotinia sclerotiorum*. *Mol. Plant Pathol.* 10, 635–649. doi: 10.1111/j.1364-3703.2009.00558.x

Zhao, J., and Meng, J. (2003). Genetic analysis of loci associated with partial resistance to *Sclerotinia sclerotiorum* in rapeseed (*Brassica napus* L.). *Theor. Appl. Genet.* 106, 759–764. doi: 10.1007/s00122-002-1171-2

Zhao, J., Wang, J., An, L., Doerge, R. W., Chen, Z. J., Grau, C. R., et al. (2007). Analysis of gene expression profiles in response to *Sclerotinia sclerotiorum* in *Brassica napus*. *Planta* 227, 13–24.

frontiers | Frontiers in Plant Science

TYPE Original Research
PUBLISHED 17 August 2022
DOI 10.3389/fpls.2022.958004

OPEN ACCESS

EDITED BY
Vincenzo Lionetti,
Sapienza University of Rome, Italy

REVIEWED BY
Sergio Esposito,
University of Naples Federico II, Italy
Klára Kosová,
Crop Research Institute (CRI), Czechia

*CORRESPONDENCE
Emilia Wilmowicz
emwil@umk.pl

SPECIALTY SECTION
This article was submitted to Plant Pathogen Interactions, a section of the journal Frontiers in Plant Science

RECEIVED 31 May 2022
ACCEPTED 14 July 2022
PUBLISHED 17 August 2022

CITATION
Wilmowicz E, Kućko A, Bogati K, Wolska M, Świdziński M, Burkowska-But A and Walczak M (2022) *Glomus* sp. and *Bacillus* sp. strains mitigate the adverse effects of drought on maize (*Zea mays* L.). *Front. Plant Sci.* 13:958004. doi: 10.3389/fpls.2022.958004

Glomus sp. and *Bacillus* sp. strains mitigate the adverse effects of drought on maize (*Zea mays* L.)

Emilia Wilmowicz[1]*, Agata Kućko[2], Kalisa Bogati[3], Magdalena Wolska[1], Michał Świdziński[4], Aleksandra Burkowska-But[3,5] and Maciej Walczak[3,5]

[1]Chair of Plant Physiology and Biotechnology, Faculty of Biological and Veterinary Sciences, Nicolaus Copernicus University, Toruń, Poland, [2]Department of Plant Physiology, Institute of Biology, Warsaw University of Life Sciences-SGGW, Warsaw, Poland, [3]Department of Environmental Microbiology and Biotechnology, Faculty of Biological and Veterinary Sciences, Nicolaus Copernicus University, Toruń, Poland, [4]Department of Cellular and Molecular Biology, Nicolaus Copernicus University, Toruń, Poland, [5]Bacto-Tech Sp. z o.o., Toruń, Poland

Maize (*Zea mays* L.) is an economically important source of food and feed. This species is highly sensitive to drought, which is the most limiting factor for the biomass yield of a crop. Thus, maize cultivation methods should be improved, especially by environment-friendly agricultural practices, such as microorganisms. Here, we provide evidence that *Glomus* sp. and *Bacillus* sp. modulate maize response to drought. Inoculation of maize seeds by these microorganisms restored the proper photosynthetic activity of the plant under drought and stabilized the osmoprotectant content of the leaf. The beneficial effect of *Glomus* sp. and *Bacillus* sp. was also related to the stabilization of cell redox status reflected by hydrogen peroxide content, antioxidant enzymes, and malondialdehyde level in leaves. As we revealed by several methods, shaping maize response to drought is mediated by both microorganism-mediated modifications of cell wall composition and structure of leaves, such as downregulating pectin, affecting their methylation degree, and increasing hemicellulose content. Overall, we provide new information about the mechanisms by which *Glomus* sp. and *Bacillus* sp. induce drought tolerance in maize, which is a promising approach for mitigating abiotic stresses.

KEYWORDS

***Bacillus*, drought tolerance, *Glomus*, maize, pectin, reactive oxygen species, cell wall**

Introduction

Drought is one of the greatest threats to modern agriculture. In different parts of the globe, changes evoked by anthropogenic environmental pressure may result in a significant reduction in the yield of many crops, such as *Zea mays* L. (maize). This could consequently lead to a global humanitarian crisis, given that maize is one of the most

widely cultivated grain crops worldwide. Compared to rice and wheat, the nutrient composition of maize consists of approximately 10% protein, 72% starch, 4% fat, several B vitamins, essential minerals along with fiber, and other energy-dense components of food (Dale and Fuller, 1982; Nuss and Tanumihardjo, 2010). The United States, Brazil, and China are the top maize-producing countries in the world. This species provides key substrates used in many industries, including food, paper, and fodder, as well as has great potential in bioenergy production (Tanumihardjo et al., 2019). Furthermore, gluten-free cornmeal is widely used in the allergic diet, while starch corn seeds are a valuable component for feed. The oil produced from the germ of corn kernels is a source of beneficial unsaturated fatty acids. Importantly, corn seeds contain more polyphenols and show stronger antioxidant properties compared to other grains, e.g., rice, wheat, or oats (Dewanto et al., 2002; Siyuan et al., 2018). A major portion of maize production is utilized in ethanol fuel. This is commonly used as a motor fuel, as a biofuel additive replacement for gasoline.

Maize yield, particularly at critical growth periods, can be affected by water stress conditions. Prolonged drought stress resulted in the reduction of leaf size, reduced the vitality of seedlings, and increased death of embryos after pollination, thereby leading to a drastic decline in crop yield (Kakumanu et al., 2012; Mao et al., 2015; Chen et al., 2016). To fulfill the requirements for food and nutrition all over the world, the production of maize cereal has to be improved and protected under drought conditions. For this reason, several approaches and biofertilizers are investigated to enhance drought tolerance and promote plant growth (Ullah et al., 2017, 2019). The present methods of agricultural crop production, for instance, the use of improper chemical fertilizers and pesticides, may lead to harmful production of greenhouse gases and consequently environmental and human health problems (Shams et al., 2017).

Therefore, microbes that produce beneficial compounds can protect the plants and provide a vital solution for a sustainable and environment-friendly agricultural practice for the improvement of crop yield under unfavorable environmental conditions, such as drought (Glick, 2014; Ullah et al., 2019). This can be achieved by the synthesis of natural formulations of microbiological origin. Most of the current formulations are composed of single strains of microorganisms or their consortia. Among them, special attention should be focused on *Bacillus* sp. (bacteria) and *Glomus* sp. (fungus). To date, several physiological aspects of both microorganisms have been analyzed in plants like *Zea mays* (Vardharajula et al., 2011), *Capsicum annum* (Lim and Kim, 2013), *Triticum aestivum* (Kasim et al., 2013), *Lactuca sativa* (Ruiz-Lozano et al., 1995b), and *Cucurbita pepo* (Harris-Valle et al., 2018). Generally, *Bacillus* sp. is a soil-living bacteria. Its spores are present in the environment until the optimal conditions for proliferation occur (Earl et al., 2008). *Bacillus* sp. can exist in the rhizosphere as plant growth-promoting rhizobacteria (PGPR) or as a symbiotic bacteria. It was demonstrated that they are able to produce phytohormones, such as gibberellins, cytokinins, auxins, and polyamines, and in this way directly affect the growth of root and root hairs (Joo et al., 2004; Xie et al., 2014). Most studies regarding *Bacillus* sp. focus on their role as PGPR; however, their involvement in the mediation of plant drought responses should be particularly investigated, given the high sensitivity of crops to this stress factor. It has been shown that *Bacillus subtilis* can increase water status, photosynthetic activity, and nutrient availability; promote the accumulation of osmoprotectants including sugars and amino acids; and accelerate the production of antioxidants (Arkhipova et al., 2007; Ashraf and Foolad, 2007; Vardharajula et al., 2011). There are also reports indicating that *Bacillus* sp. mediates drought resistance in *Brachypodium distachyon* through the stimulation of the expression of drought-responsive genes, accumulation of sugars and starch in leaves, and affecting DNA methylation (Gagné-Bourque et al., 2013, 2015). *Bacillus* sp. improves the growth of *Phleum pratense* L. under drought by increasing the shoot and root biomass, photosynthetic rate, and stomatal conductance, and accumulation of saccharose, fructans, and amino acids (asparagine, glutamic acid, glutamine, and non-protein amino acid γ-aminobutyric acid) (Gagné-Bourque et al., 2016).

The mediation of plant stress responses by *Glomus* sp. has also been documented. These fungi positively influenced plant growth, mineral uptake, CO_2 exchange rate, water efficiency, transpiration, stomatal conductance, photosynthetic efficiency, and proline accumulation (Ruiz-Lozano et al., 1995a). Additionally, increased content of soluble proteins and higher activity of antioxidant enzymes have been noted in plants under the action of *Glomus* sp. (Wu et al., 2007; Sohrabi et al., 2012; Gong et al., 2015). A common mechanism of a plant's response to environmental cues is the disrupted balance between the production and scavenging of reactive oxygen species (ROS). One of the most toxic ROS that is formed in every cellular compartment is superoxide anion radical ($O_2^{\bullet -}$), which is quickly scavenged by superoxide dismutase (SOD) into H_2O_2 (Mittler, 2002; Hasanuzzaman et al., 2020). This, in turn, is inactivated by the action of catalase (CAT). ROS play a key role in the modification of the cell wall, which is the first site of perception of abiotic stress and simultaneously constitutes the first protective barrier against its effects. The primary cell wall mainly consists of hemicelluloses, celluloses, and pectins (Harholt et al., 2010; Atmodjo et al., 2013). It has been shown that drought can affect its structure by altering the proportion of different components, leading consequently to decreased extensibility and plant vitality under conditions of osmotic stress (Le Gall et al., 2015). Therefore, we aimed to determine whether inoculation of maize seeds with *Glomus* sp. or *Bacillus* sp. can modify the leaf cell wall structure under drought conditions and thereby mitigate the negative impact of water deficit on the

above-ground part of the plant, which guarantees reproductive success and high yield.

In the beginning, we verified whether experimental conditions are sufficient to induce stress-related physiological responses. For this purpose, we measured photosynthetic activity, analyzed leaf structure, level of osmoprotectant (a marker of oxidative stress), the level of selected ROS, and activity of antioxidant enzymes under drought conditions and post-inoculation with *Glomus* sp. or *Bacillus* sp. Modifications in the cell wall structure were evaluated by determining the pectin methylation and hemicellulose content. Collectively, our results show that both the tested microorganisms affect the cell wall composition and reduce the adverse effects of drought in the leaves of *Z. mays*.

Materials and methods

Inoculum preparation and growth of bacteria

Glomus spp. and *Bacillus* sp. were provided by Bacto-Tech sp. z o.o. (Poland). *Glomus* sp. (the mycorrhizal inoculum) was composed of peat, spores, hyphae, and root fragments of *Plantago major* L. This mixture was stabilized by freeze-drying. Furthermore, *Bacillus* sp. were grown in nutrition broth in a 3 L bioreactor for 7 days (26°C) and then centrifuged for 5 min at 10,000 x*g*. The obtained biomass of bacteria was stabilized by freeze-drying. The number of bacteria in the obtained sample was 10^{11} colony-forming units/g (CFUs/g).

Seeds treatment, stress application, and plant cultivation

The plant material used in this study was maize (*Zea mays* L.). Seeds were moistened with water. Then, they were divided into three groups: the first group did not receive any inoculation, the second group was inoculated with the powder composed of fungal strains (*Glomus* sp.), and the third group was inoculated with the powder composed of bacterial strain (*Bacillus* sp.). We used 800 mg of inoculation powder per 10 seeds. After that, seeds were sown in pots filled with soil, and the plants were cultivated in the phytotron chambers under controlled light and temperature conditions (22 ± 1°C, 110 μmol $m^{-2}s^{-1}$, and cool white fluorescent tubes). Plants were watered for 2 weeks in optimal 70% soil water holding capacity (WHC). Subsequently, maize seedlings inoculated with bacteria were cultivated for 4 weeks (∼31 days) in 25% WHC. Non-inoculated plants were divided into two groups: the first one was cultivated for 2 weeks in 25% WHC, while the second one was grown in well-watered conditions (control). WHC calculations were made according to Chauhan and Johnson (2010) with minor modifications described by Wilmowicz et al. (2019). After 6 weeks, plants were subjected to biometric analysis and photosynthesis-related parameters. Fresh tissues were used for *in vivo* histochemical staining. Additionally, leaves were collected for further biochemical experiments, frozen in liquid nitrogen, and stored at −80°C. In turn, for all microscopy assays, leaf sections were immediately fixed.

Chlorophyll fluorescence parameter (Fv/Fm)

The maximum quantum efficiency of PS II (Fv/Fm) was measured using a portable modulated OS-30P (Opti-Sciences, Inc., Hudson, NH, United States) according to the method described by Weng (2006). For each measurement, all the leaves from the plant were clamped at the center of the leaf clip holder for dark adaptation (30 min). Analysis was made using five plants. The results are presented as mean ± SE (n = 3).

Proline determination

Proline was analyzed according to the method of Ábrahám et al. (2010). In brief, leaves (∼0.5 g) were grounded in the presence of 3% sulfuric acid (5 μl/mg fresh weight), and then the extract was centrifuged (15,000×*g*, 5 min). The reaction mixture containing 100 μl of supernatant, 0.1 ml of 3% sulfosalicylic acid, 0.2 ml of glacial acetic acid, and 0.2 ml of acidic ninhydrin was prepared and incubated at 96°C for 30 min. Then, 1 ml of toluene was added to the samples, and the absorbance of the extract was read at 520 nm. The content of proline was calculated in reference to a prepared calibration curve. Values are expressed as μg proline g^{-1} fresh weight.

Reactive oxygen species and reactive oxygen species-related enzyme analysis

Apoplastic release of $O_2^{\bullet -}$ was visually detected by incubating hand-cut leaf sections according to Rodríguez et al. (2004). We used nitroblue tetrazolium (NBT) as it reacts with $O_2^{\bullet -}$. A blue formazan precipitate was formed after the reaction. Briefly, tissue fragments were transferred to the tubes containing 0.01% NBT in 10 mM PBS (pH 7.8). After incubation in the dark (2 h at 30°C), tissues were kept in 10 mM PBS (pH 7.8) and photographed.

H_2O_2 was analyzed following the method of Loreto and Velikova (2001), which involves the oxidation of KI by H_2O_2 in an acidic solution. In brief, the collected leaves (∼0.5 g) were grounded with 3 mL of 1% (w/v) trichloroacetic acid (TCA). The obtained homogenate was centrifuged for 15 min (14,000×*g*,

4°C). After that, 0.75 ml of the supernatant was mixed with 0.75 ml of 10 mM K-phosphate buffer (pH 7.0) and 1.5 ml of 1M KI. The absorbance of the mixture was recorded at 390 nm. The concentration of H_2O_2 was calculated by comparing it with a standard curve and expressed as μmol mg^{-1} fresh weight.

Protein extracts for enzymatic activities were prepared as follows. Frozen leaves (~0.5 g) were grounded with 5 ml of extraction buffer (50 mM K-phosphate buffer (pH 7.6) and 0.1 mM Na-EDTA). The homogenate was centrifuged (12,000×*g* for 15 min), and the obtained supernatant was used for SOD and CAT analyses. The total SOD activity was assayed according to Giannopolitis and Ries (1977).

The total CAT activity was determined by monitoring the decrease in absorbance at 240 nm (following the decomposition of H_2O_2) following the method of Cakmak and Marschner (1992). The reaction was started by adding 50 μL of the substrate to a mixture composed of 50 mM K-phosphate buffer (pH 7.0) and 10 mM H_2O_2. The results are expressed as μmol of H_2O_2 s^{-1} g^{-1} fresh weight.

Staining and quantification of pectin and hemicellulose determination

Fresh leaf fragments were incubated for 30 min with 0.02% (w/v) ruthenium red ($[(NH_3)_5Ru\text{-}O\text{-}Ru(NH_3)_4\text{-}O\text{-}Ru(NH_3)_5]Cl_6$) to determine unesterified pectin (Sabba and Lulai, 2002). Additionally, fragments of leaves (~0.1 g) were immersed in 0.5 mmol L^{-1} of $CaCl_2$ solution and washed two times with water. Pectins were isolated and quantified according to Liu et al. (2019) with slight modifications, as described in our previous work (Florkiewicz et al., 2020). The hemicellulose content was analyzed following the methodology described by Florkiewicz et al. (2020).

MDA quantification

Frozen leaves (~0.5 g) were grounded in a chilled mortar, and further steps of malondialdehyde (MDA) determination were followed as described by Hodges et al. (1999) with some modifications, as presented in our recent paper (Kućko et al., 2022).

Microscopy sample preparation and histological assay

The tissue fragments were excised from the central area of the leaves and were immediately fixed in 4% paraformaldehyde and 0.2% glutaraldehyde prepared in 1 × phosphate-buffered saline (PBS, pH 7.2). After 12 h of incubation at 4°C, tissues were dehydrated, supersaturated, and embedded in BMM resin (methyl methacrylate, butyl methacrylate, 10 mM dithiothreitol, and 0.5% (w/v) benzoin ethyl ether; Fluka, Buchs, Switzerland) as described previously (Wilmowicz et al., 2016). Then, an Ultracut microtome (Reichert-Jung, Germany) was used for the preparation of semi-thin sections (1 μm). The sections were subjected to general histological observations. First, toluidine blue dye was applied at a concentration of 0.05% for 10 min. The second experiment involved staining for 30 min with 0.02% (w/v) ruthenium red (Sabba and Lulai (2002). The obtained samples were analyzed using a microscope (LM Zeiss Axioplan, Oberkochen, Germany) equipped with a ProGres C3 digital camera.

Immunofluorescent experiments for detection of high- and low-methylated pectins

Semi-thin sections, obtained as described in the previous section, were subjected to immunodetection. We analyzed low- and non-methylated pectins (31–40%), and high-methylated pectins (15–80%) using JIM5 and JIM7 antibodies, respectively (Willats et al., 2000). Our protocol published previously (Florkiewicz et al., 2020) was adopted. Additionally, for the visualization of nuclei, the sections were incubated with DAPI following the method of Florkiewicz et al. (2020). The samples were finally observed under a fluorescent microscope (DM6000B, Leica, Wetzlar, Germany).

Statistical analysis

Statistical analysis and presentation of the obtained results were performed using MS Excel 365 (Microsoft) and SigmaPlot 2001 v. 5.0. Each result was presented as the mean ± standard error (SE) of at least three replicated measurements (n = 3). The significant differences between the tested variants were compared by Student's t-test.

Results

Verification of stressful conditions in *Zea mays* leaves

In the beginning, we aimed to verify whether the drought stress conditions were sufficient to induce the response in *Z. mays* plants. The reduced water potential limits the transpiration and CO_2 flow to the cell, caused by the closing of the stomata, and consequently leads to declined photosynthetic rate (Lawlor and Tezara, 2009). The maximum quantum efficiency of PSII is reflected by the chlorophyll fluorescence parameter Fv/Fm, which is widely used to analyze the stress

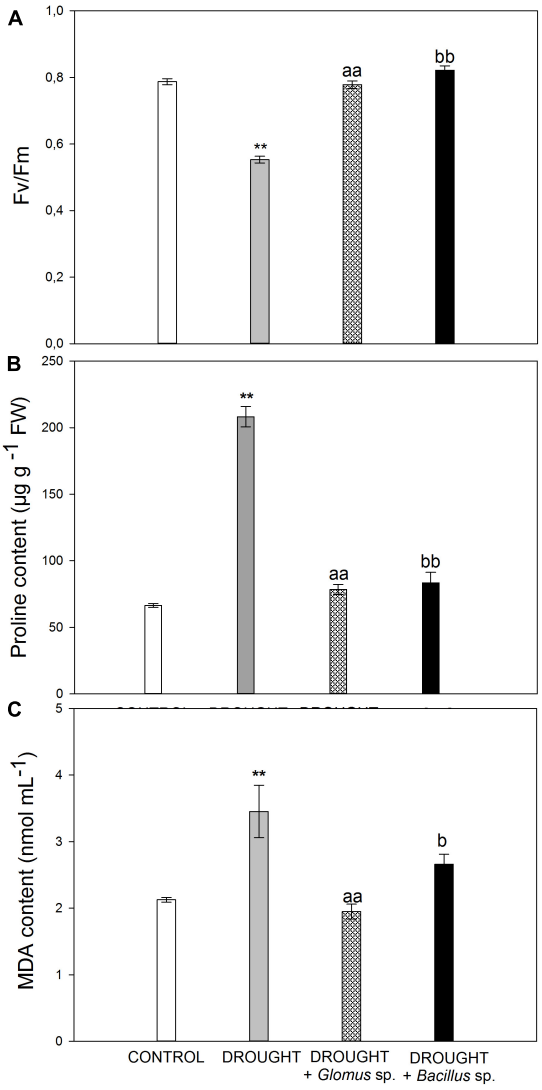

FIGURE 1
Values of maximum quantum yield efficiency of PSII (Fv/Fm) **(A)**, proline **(B)**, and MDA **(C)** content in the leaves of *Zea mays* subjected to drought conditions or inoculated with the *Glomus* sp. or *Bacillus* sp. prior to planting and drought treatment. Values for Fv/Fm are presented as mean ± SE (n = 5), while values for proline and MDA concentration are presented as mean ± SE (n = 3). Significant differences for drought-treated plants versus control are $^{**}P < 0.01$; for drought + *Glomus* sp. vs. drought $^{aa}P < 0.01$; for drought + *Bacillus* sp. vs. drought $^{b}P < 0.05$, $^{bb}P < 0.01$.

response in plants (Murchie and Lawson, 2013). Here, we show that this parameter decreased in the leaves of *Z. mays* subjected to drought conditions (**Figure 1A**), reaching a value of ∼0.55. In contrast, Fv/Fm values in the stressed plants developed from the seeds treated with *Bacillus* sp. or *Glomus* sp. were similar to those observed in the untreated control (**Figure 1A**).

One of the strategies involved in the defense mechanism of plants that is activated in drought conditions is the increased synthesis and accumulation of osmoprotectants, such as proline. These molecules are responsible for osmotic adjustment in cells, since they cause a decrease in water potential, which further improves plant tolerance to adverse environmental conditions (Ashraf and Foolad, 2007). To provide additional evidence for the drought action observed in *Z. mays* plants, we aimed to check the level of proline (**Figure 1B**). Control leaves accumulated ∼70 µg g^{-1} fresh weight, while the level of this osmoprotectant in the leaves collected from drought-stressed plants was almost higher by three times. When we subjected the plants to combined drought treatment, due to the inoculation of additional seeds prior to sowing, we observed a decrease in the content of proline when compared to the single drought treatment. Furthermore, the proline content in the samples subjected to the combined treatment was higher than that observed in the control. Water deficit in the soil leads to the generation of secondary stress-related compounds like ROS, which may affect the structure of nucleic acids, proteins, and lipids. Spontaneous action of ROS, as crucial molecules produced under stress conditions, can evoke lipid peroxidation and accumulation of toxic compounds (Gill and Tuteja, 2010). Among them, the most mutagenic is MDA, which has been recognized as a biological marker of oxidative stress (Shulaev and Oliver, 2006). The leaves of *Z. mays* cultivated under drought were characterized by an increased level of MDA (**Figure 1C**). However, when maize seeds were pretreated with *Bacillus* sp. or *Glomus* sp. strains and then the plants were subjected to drought, downregulation of MDA was observed.

Effects of *Glomus* sp. or *Bacillus* sp. treatment on the redox state in *Zea mays* leaves under drought stress

To check redox homeostasis in *Z. mays* leaves under the examined treatments, we performed staining for the $O_2^{\bullet-}$, which is one of the most toxic ROS, analyzed the activity of SOD responsible for $O_2^{\bullet-}$ dismutation, and then determined the level of H_2O_2 and the activity of the enzyme catalyzing its decomposition into H_2O – CAT. NBT staining revealed that apoplastic $O_2^{\bullet-}$ was extensively accumulated in the leaves under drought conditions (**Figure 2A**). However, when stressed plants were pretreated with *Bacillus* sp. or *Glomus* sp., the observed drought-evoked effect was reversed. In these variants, $O_2^{\bullet-}$ was detected mainly along the leaf vascular system. Importantly, almost no staining was visible in the control tissue. The SOD activity was slightly modified by water deficit, and in this case, reached a value of ∼53 units/mg of protein (**Figure 2B**). When stressed plants were pretreated with *Bacillus* sp. or *Glomus* sp., the activity of SOD was significantly lower in comparison to non-treated and drought-stressed maize plants. A minimum value of ∼2 u/mg protein was noted for plants subjected to the influence of drought and *Bacillus* sp. Water deficit in soil caused

10.3389/fpls.2022.958004

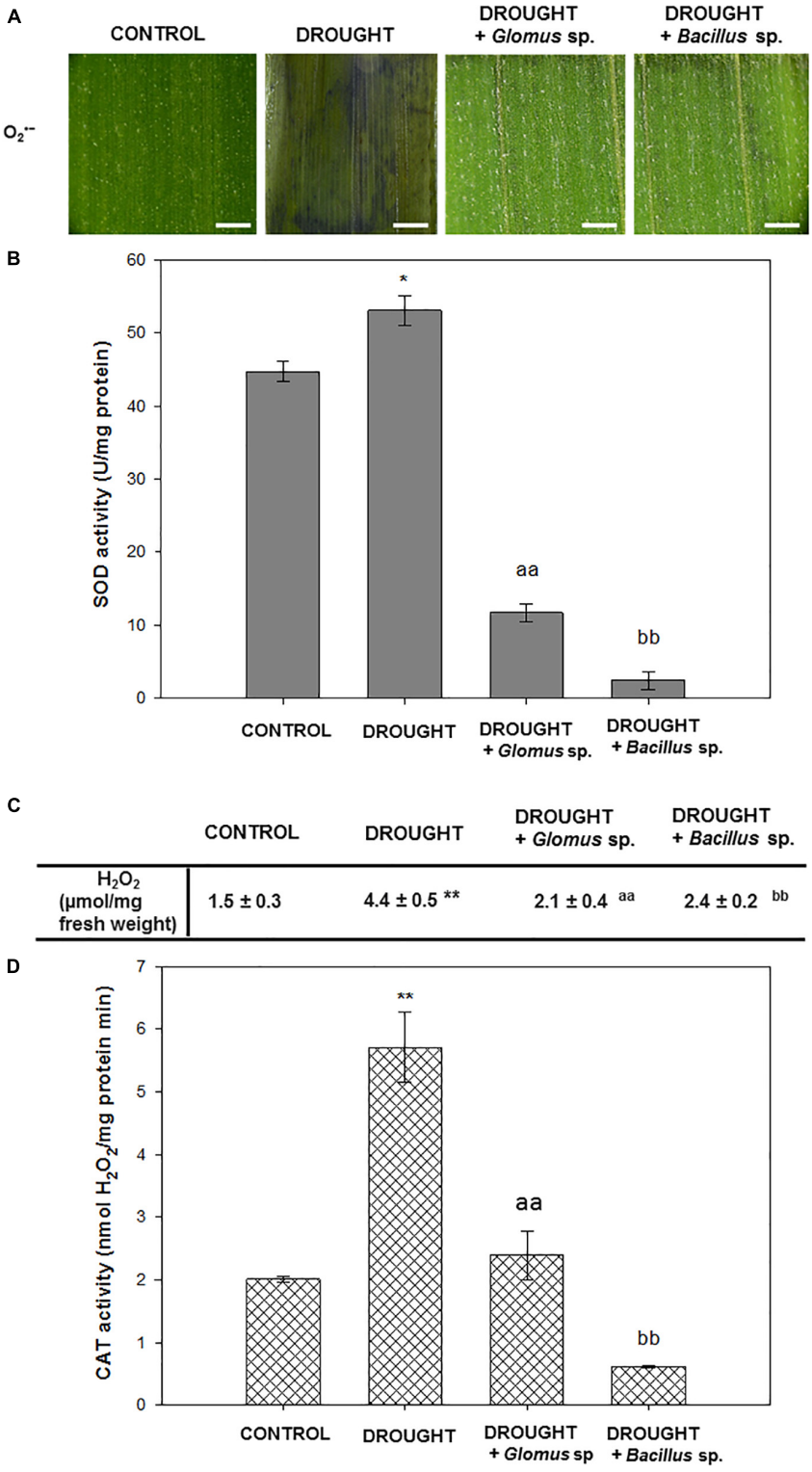

FIGURE 2
Seed inoculation combined with further drought stress affects ROS-related events in *Zea mays* leaves. Analyses have been done on leaves obtained from non-treated plants (control), drought-stressed plants, and drought-stressed *Z. mays* developed from seeds inoculated with *Glomus* sp. or *Bacillus* sp. Visualization of $O_2^{\bullet-}$ detected by histochemical staining **(A)**. The blue color corresponds to the presence of $O_2^{\bullet-}$. Bar = 1 mm. The activity of superoxide dismutase (SOD) **(B)**. The level of H_2O_2 **(C)** and activity of catalase (CAT) **(D)**. Significant differences for drought-treated plants vs. control are $^{*}P < 0.05$, $^{**}P < 0.01$; for drought + *Glomus* sp. vs. drought $^{aa}P < 0.01$; for drought + *Bacillus* sp. vs. drought $^{bb}P < 0.01$.

a strong accumulation of H_2O_2 in *Z. mays* leaves (Figure 2C). In contrast, the leaves of plants exposed to drought and *Glomus* sp. were characterized by decreased content of this ROS. In this variant, the level of H_2O_2 decreased and maintained a value similar to that observed in the non-treated plants. A different relationship was observed in the drought-stressed plants in the presence of *Bacillus* sp., where the content of H_2O_2 was higher than that observed in the well-watered plants, however, does not reach the value noted in drought-stressed plants. A high amount of this compound in the leaves of drought-treated plants was correlated with the increased activity of CAT (Figure 2D). Treatment of the stressed plants with the *Glomus* sp. strain decreased the CAT activity to the control value; however, the activity was decreased by more than half when compared to that observed during the drought. The lowest CAT activity was found in the leaves of stressed plants pretreated with *Bacillus* sp.

Effect of seed inoculation of *Glomus* sp. or *Bacillus* sp. on drought-evoked changes in the cellular structure of *Zea mays* leaves

Based on the fluctuations in the above-presented parameters. we can conclude that the application of these experimental conditions is sufficient to induce a response in the leaves. Moreover, specific cellular modifications in the leaf tissues were observed under the examined treatments (Figure 3). Water deficit in soil caused significant structural changes in leaves, such as degradation of mesophyll (Figure 3B), formation of smaller xylem vessels (Figure 3F), plasmolysis reflected by shrinkage of cells (Figures 3B,F), cell deformation (Figures 3B,F,J), and formation of several cytosolic aggregates (Figures 3B,F,J). Changes in the chloroplast location were particularly characteristic for drought-treated cells (Figures 3F,J). The structure of cells and tissues of leaves obtained from maize pretreated with *Bacillus* sp. before inducing drought conditions was similar to that observed in control (Figures 3D,H,L). More specifically, we observed well-developed vascular elements (Figure 3D), lack of plasmolysis symptoms (Figures 3D,H), properly developed mesophyll (Figure 3H), and chloroplasts positioned similar to the cells of untreated plants (Figure 3L), unlike that in drought-stressed plants (Figure 3J). Reversion of drought action by treatment with *Glomus* sp. was also manifested by cellular changes (Figures 3C,G,K). In these plants, the vascular elements were properly developed (Figures 3C,G). Nevertheless, microscopy analyses revealed that in several places protoplast gets detached from the cell wall (Figure 3C). Furthermore, some disorganization in the localization of chloroplast compared to the control section, particularly in the area surrounding the xylem, has been noted (Figure 3G). Interestingly, these areas indicated the possible presence of microorganisms (Figure 3C).

The impact of seed inoculation of *Glomus* sp. or *Bacillus* sp. on the drought-triggered cell wall remodeling of *Zea mays* leaves

Our histological analysis suggested that the cell wall might be modified under the action of drought stress. To examine the effect of both *Bacillus* bacterium and *Glomus* fungus strains on the events related to cell wall remodeling, we checked the content of hemicellulose in the maize leaves, which is the main carbohydrate in the middle lamella. As Figure 4A shows, under drought, the hemicellulose level reached a minimum value when compared to treatment groups. There was a significant increase in the content of this cell wall compound in plants inoculated with *Glomus* sp. or *Bacillus* sp. simultaneously cultivated under water deficit conditions. In such conditions, the level of hemicellulose was higher than observed in both control and plants exposed to drought.

In addition, we aimed to verify the possible changes related to the methylation level of cell wall pectin components. When maize was subjected to water deficit conditions, the total concentration of pectins drastically increased by almost three times when compared to well-watered plants (Figure 4B). Such an effect was not been observed in plants treated with drought and bacterial strains; the level of pectins was similar to that observed in the non-treated control plants. Further analyses have pointed out that the methyl esterification degree of pectins changes when plants are subjected to drought or exposed to bacteria. The intensity of red stain, which corresponds to the presence of unesterified pectin, was the highest in the drought-stressed leaves regardless of whether the plants were pre-inoculated with bacteria or not (Figure 4C).

Based on the results of ruthenium red staining, in the next step, we analyzed more comprehensively the degree of pectin methylation in the leaves of treated plants by immunolabeling with the monoclonal antibodies JIM7 (Figures 5, 6) and JIM5 (Figures 7, 8). Fluorescence indicating the presence of high-methylated pectins under control conditions was observed in the upper and lower layers of mesophyll cells located directly under the epidermis (Figure 5A). Higher magnifications revealed that the signal was emitted by cell walls (Figure 5B). Water deficit changed the localization pattern of these pectins and resulted in their distribution throughout the mesophyll area (Figure 5C). Furthermore, they accumulated more strongly when compared to the sections obtained from well-watered plants (Figure 5D). In both the control and the drought-treated leaves, no fluorescence was observed in the area of the vascular bundles (Figures 5A,C).

When *Z. mays* seeds were inoculated with *Glomus* sp. or *Bacillus* sp. and subjected to drought, highly esterified HGs were redistributed in the leaf tissues (Figure 6). In both cases, a relatively high signal after reaction with the JIM7 antibody was emitted by cell walls of the epidermis,

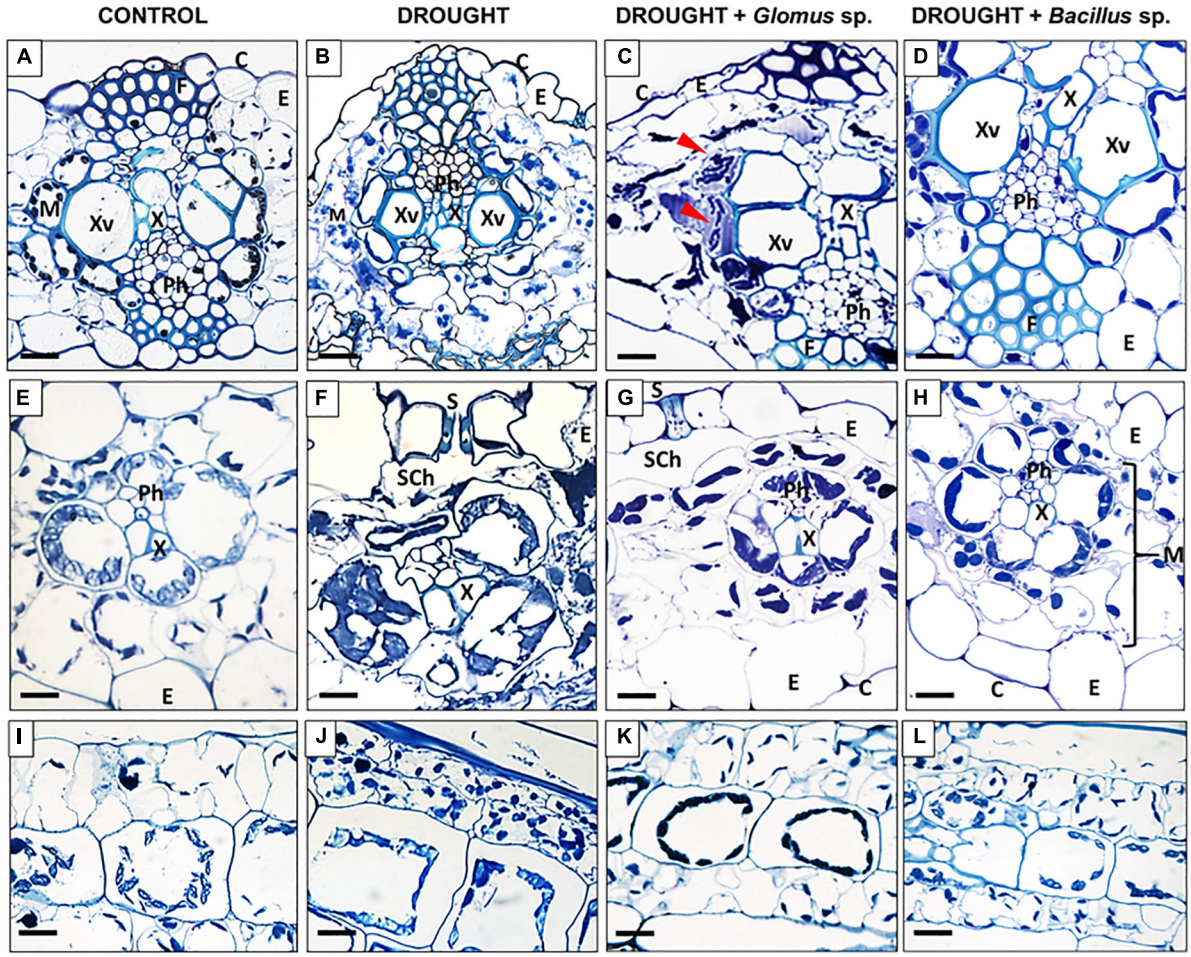

FIGURE 3
Light micrographs of cells of *Zea mays* leaves collected from plants subjected to the influence of *Glomus* sp. or *Bacillus* sp. and drought. Cross-sections were made from control **(A,E,I)**, drought-treated leaves **(B,F,J)**, and leaves collected from drought-treated plants, developed from seeds inoculated with *Glomus* sp. **(C,G,K)** or *Bacillus* sp. **(D,H,L)**. Tissue organization is described in images. The top panel shows a cross-section through the center area of the leaf, the middle panel shows the region of vascular bundles, and the bottom panel presents a longitudinal section of mesophyll cells. Possible microorganism presence was marked by red arrowheads **(C)**. C, cuticle; E, epidermis; F, fibers; M, mesophyll; Ph, phloem; S, stomata; Sch, substomatal chamber; X, xylem; Xv, xylem vessel. Bars = 15 μm.

mesophyll, and vascular tissues (Figures 6A,C). More specifically, the application of *Glomus* sp. resulted in the accumulation of JIM7-dependent fluorescence in the epidermis tissue, elements of phloem and xylem, and sclerenchyma fibers (Figure 6B). Simultaneous treatment of maize with drought and *Bacillus* sp. caused preferential localization of highly methylated pectin in mesophyll and epidermis (Figure 6C). Furthermore, strong fluorescence was detected in the cell walls of vessels, xylem and phloem, and epidermis cells adjacent to the vascular bundles (Figure 6D).

The fluorescence signals detected in the leaves after incubation with JIM5 were different under control and drought conditions (Figure 7). In general, the distribution of low-methylated pectin in the stressed leaf was homogenous throughout the mesophyll tissue adjacent to the epidermis (Figure 7C). Strong labeling was noted in the intracellular spaces of cells specifically disrupted by drought (Figure 7D). Such strong staining was not visible in the control section; however, weak fluorescence was localized in the mesophyll cell wall (Figure 7A), particularly around the vascular region (Figure 7B).

As evident in Figure 7, a similar localization pattern of low-methylated pectins characterized drought-stressed leaves of *Z. mays* subjected to the action of *Glomus* sp. or *Bacillus* sp. The highest signal density was observed in the epidermis cells (Figures 8A,C) and phloem located in the central leaf vasculature (Figures 8B,D). Low labeling, manifested by several luminous spots or short bands in the cell walls, characterized the mesophyll tissue (Figures 8A–D).

A

	CONTROL	DROUGHT	DROUGHT + *Glomus* sp.	DROUGHT + *Bacillus* sp.
Absorbance of the hemicelluloses (OD/g FW)	13.4 ± 1.2	10.3 ± 0.3 *	20.6 ± 3.4 ^{aa}	26.9 ± 4.5 ^{bb}

B

	CONTROL	DROUGHT	DROUGHT + *Glomus* sp.	DROUGHT + *Bacillus* sp.
Absorbance of the pectin (OD / g FW)	3.40 ± 0.02	8.87 ± 0.04 **	3.38 ± 0.03 ^{aa}	3.72 ± 0.04 ^{bb}

C

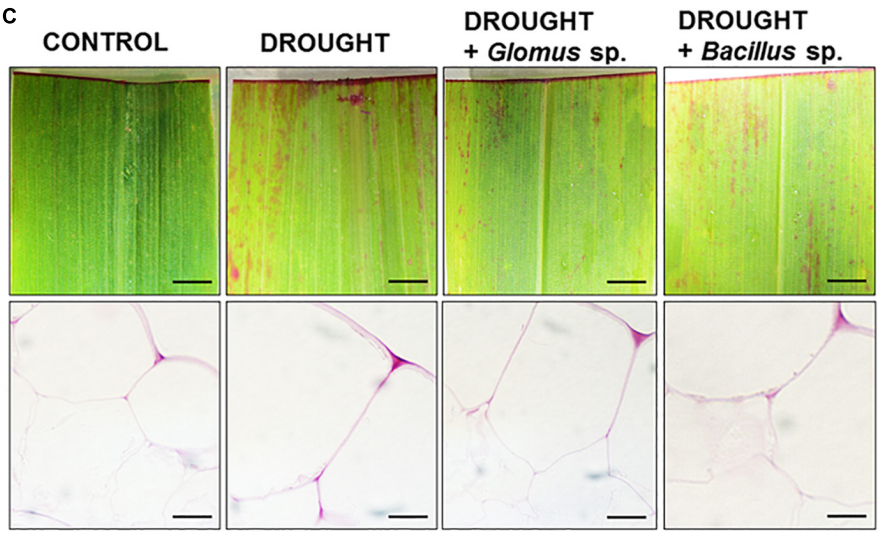

FIGURE 4
Effect of inoculation of *Glomus* sp. or *Bacillus* sp. on the pectin-related changes and hemicellulose content in maize growing under drought-stressed conditions. The analyses have been done on leaves from non-treated plants (control), drought-stressed plants, and drought-stressed maize developed from seeds inoculated with *Glomus* sp. or *Bacillus* sp. Quantitative analyses of the total pectin pool **(A)**. Visualization of de-esterified pectin (pink color corresponds to unesterified pectin presence) **(B)**. Bar = 1 mm (freshly stained leaves), 15 μm (cross-sections). Quantification of hemicelluloses **(C)**. Significant differences for drought-treated plants vs. control are $^{*}P < 0.05$, $^{**}P < 0.01$; for drought + *Glomus* sp. vs. drought $^{aa}P < 0.01$; for drought + *Bacillus* sp. vs. drought $^{bb}P < 0.01$.

Discussion

Maize is extremely sensitive to drought, given the high demand for water, particularly in the stage of vegetative development and during grain filling (Rafique, 2020). This stress leads to morphological and anatomical changes, influences cell structure, and induces multiple metabolic pathways. Water deficit reduces maize growth (Abrecht and Carberry, 1993), leaf area (NeSmith and Ritchie, 1992; Çakir, 2004), water content, and photosynthesis-related parameters (NeSmith and Ritchie, 1992). All these modifications extremely influence the yield of the crop. To improve its cultivation, we need to understand how maize recognizes drought conditions at the level of each organ and develops agrotechnical approaches aimed to improve the resistance of this species to water deficit. Nowadays, more emphasis should be given to the elimination of pesticides and the search for new biologically active, high-value substances produced by microorganisms. Among them, strains of *Glomus* sp. should be considered. Their activity in the reduction of stress effects has been proven in lettuce (Ruiz-Lozano et al., 1995b), *Lavendula spica* (Marulanda et al., 2007), and *Cinnamonum migao* (Liao et al., 2021). Another natural solution for the improvement of plant tolerance to unfavorable conditions is inoculation with different strains of *Bacillus* sp., as revealed in *Capsicum annuum* (Lim and Kim, 2013), *Z. mays* (Moreno-Galván et al., 2020), *Solanum lycopersicum* (Gowtham et al., 2020), *Glycine max* (Sheteiwy et al., 2021), *Cenchrus americanus* (Kushwaha et al., 2020), and *Helianthus annus* (Sandhya et al., 2011). Additionally, Marulanda et al. (2006) demonstrated that interactions between *Bacillus thuringiensis* and *Glomus* increase plant water uptake in *Retama sphaerocarpa* under drought. Given the high potential relevance of these microorganisms, in this paper, we checked whether inoculation of maize seeds with *Glomus* sp. or *Bacillus* sp. alleviates drought-evoked effects in leaves and, in this way, limits its negative effects on vegetative development. The changes observed in Fv/Fm

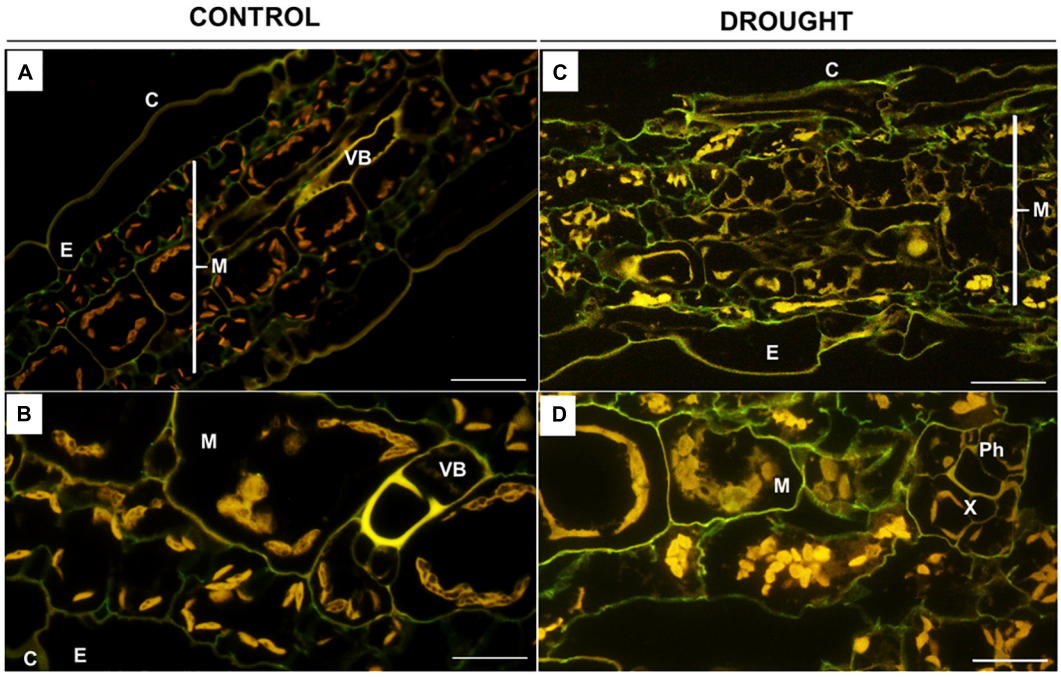

FIGURE 5
In situ immunolocalization of high-methylated homogalacturonans (HG) in *Z. mays* leaves under drought. Cross-sections of leaves from well-watered **(A,B)** and drought-stressed **(C,D)** plants were immunolabeled with the JIM7 antibody. Images were obtained by merged signals from JIM7, DAPI staining (blue color), and chlorophyll autofluorescence. Green fluorescence indicates the presence of high-methylated HG. C, cuticle; E, epidermis; M, mesophyll; Ph, phloem; Vb, vascular bundles; X, xylem. Bars = 50 μm **(A,B)**, 15 μm **(C,D)**.

in this study suggest that both microorganisms improved the efficiency of photosynthetic apparatus under drought stress (**Figure 1A**). Similar to the results of our experiment, *Glomus* increased PSII-effective efficiency in salt-stressed maize (Xu et al., 2018). Moreover, literature data provide evidence that *Bacillus* improved Fv/Fm in *Capsicum chinensis* (Samaniego-Gámez et al., 2021) and *Euterpe oleracea* (Castro et al., 2020). Furthermore, the Fv/Fm ratio of *Solanum lycopersicum* was reduced when three *Bacillus* spp. were applied (Costa-Santos et al., 2021). Furthermore, *Bacillus amyloliquefaciens* mixed with *Azospirillum brasilense* NO40 increased the photosynthetic rate of *Triticum aestivum* (Kasim et al., 2013).

Inoculation of *Z. mays* with *Glomus* sp. or *Bacillus* sp. reduces the content of proline under drought; however, its level was higher than in control (**Figure 2**). Liao et al. (2021) suggested that *Glomus* improves the growth of *Cinnamonum migao* through better absorption of nutrients and water uptake, ensuring a high turgor of tissues, and thus it is not necessary to synthesize large amounts of osmoprotectants. However, different *Bacillus* strains increased proline secretion in drought conditions in *Solanum lycopersicum* (Shintu and Jayaram, 2015), *Cicer arietinum* (Sharma et al., 2013), *Sorghum bicolor* (Grover et al., 2014), and *Cucumis sativus* (Wang et al., 2012). We propose, based on our results, that the reduced content of proline in stressed and inoculated maize when compared to drought-treated plants might be related to their increased tolerance to drought evoked by the action of *Bacillus* sp. and *Glomus* sp.

The reduced efficiency of the photosynthetic apparatus could be a result of the production of ROS due to changes in the electron transport, which is reflected by the decreased pool size of electron acceptors (Reddy et al., 2004). Moreover, ROS can initiate lipid peroxidation and induce cell membrane destruction (Sabra et al., 2012).

In *Z. mays*, water deficit in soil promoted the formation of ROS, including $O_2^{\bullet -}$ and H_2O_2 (**Figures 2A,C**), and caused membrane destabilization, which is reflected by the accumulation of MDA, as a marker (**Figure 1C**). Inoculation of seeds with *Glomus* sp. or *Bacillus* sp. mitigated this harmful effect of drought (**Figure 3**), since we observed that reduced content of $O_2^{\bullet -}$ (**Figure 2A**) correlated with decreased SOD activity (**Figure 2B**). Another symptom of oxidative stress neutralization by *Glomus* sp. and *Bacillus* sp. in maize is also evident by a reduction in H_2O_2 (**Figure 2C**) level and, consequently, the activity of CAT (**Figure 2D**). Literature data suggest that *Glomus* can act on the antioxidant enzymes of plants in a species-dependent manner. Generally, these fungi accelerate the activity of antioxidant enzymes in plants under drought, for instance, POX in *Juglans* (Behrooz et al., 2019) and *Citrus tangerine* (Wu et al., 2007), CAT in *Cinnamomum*

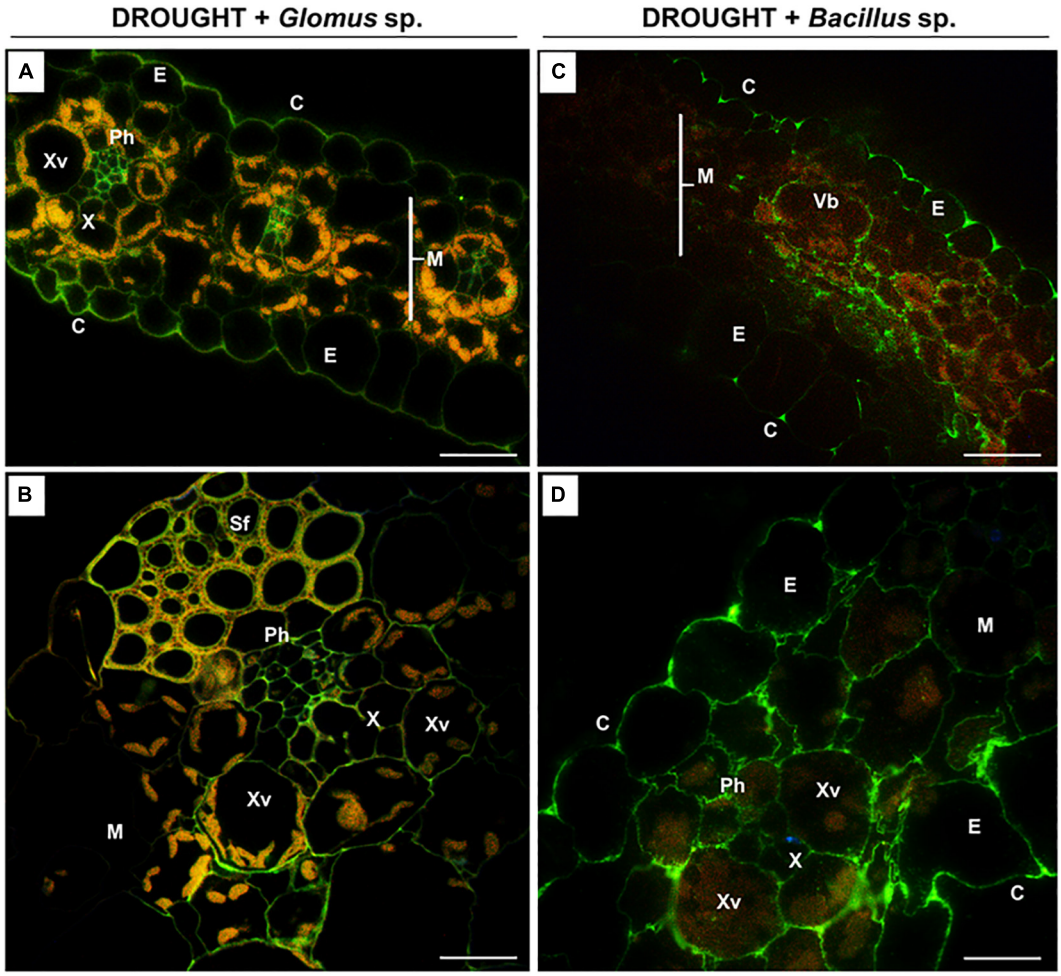

FIGURE 6
The influence of seeds inoculated with *Glomus* sp. or *Bacillus* sp. on the distribution of high-methylated pectins in the leaves of drought-stressed maize. Cross-sections of leaves from drought-stressed maize treated at the seed stage with *Glomus* sp. **(A,B)** or *Bacillus* sp. **(C,D)** were immunostained with the JIM7 antibody. Presented images were obtained by overlapping signals from JIM7, DAPI staining (blue color), and chlorophyll autofluorescence. Green fluorescence indicates the presence of high-methylated HG. C, cuticle; E, epidermis; M, mesophyll; Ph, phloem; Sf, sclerenchyma fibers; Vb, vascular bundles; X, xylem; Xv, xylem vessel. Bars = 50 μm **(A,B)**, 15 μm **(C,D)**.

migao (Liao et al., 2021), SOD and CAT in foxtail millet (Gong et al., 2015), SOD and POX in bean (Ganjeali et al., 2018), and CAT, APX, and POX in *Triticum aestivum* (Yaghoubian et al., 2014). In foxtail millet, *Glomus intraradices* decreased the concentration of H_2O_2 and $O_2^{\bullet -}$, compared with non-inoculated plants (Gong et al., 2015). Furthermore, *G. mosseae* reduced the level of H_2O_2 in wheat (Yaghoubian et al., 2014). Several studies, similar to the one presented herein, provide evidence that treatment of plants with *Bacillus* negatively influenced the activity of the antioxidant system, e.g., in *Triticum aestivum* (Kasim et al., 2013) and tomato (Arias Padró et al., 2021). Nevertheless, another relationship was observed in potatoes, in which CAT, APX, and SOD were upregulated when plants were inoculated with *Bacillus pumilus* and *Bacillus firmus* (Gururani et al., 2013). The negative impact of *Glomus* sp. and *Bacillus* sp. on the ROS content and antioxidant enzyme activities in drought-treated maize observed in this study strongly suggest that these microorganisms alleviate adverse effects of water deficit related to ROS burst. Such a hypothesis is supported by a decreased level of MDA (**Figure 1C**) in the leaf of maize inoculated with *Glomus* sp. or *Bacillus* sp., given that a high amount of MDA is derived from the lipid peroxidation of polyunsaturated fatty acids which is induced by ROS. Similar observations were noticed for MDA content in drought-stressed foxtail millet inoculated with *Glomus* (Gong et al., 2015), as well as in *Solanum lycopersicum* and cucumber treated with various *Bacillus* strains under drought conditions (Wang et al., 2012; Gowtham et al., 2020).

Lipid peroxidation indicates cell membrane rupture, which is visible in cellular structure. Indeed, microscopy analysis

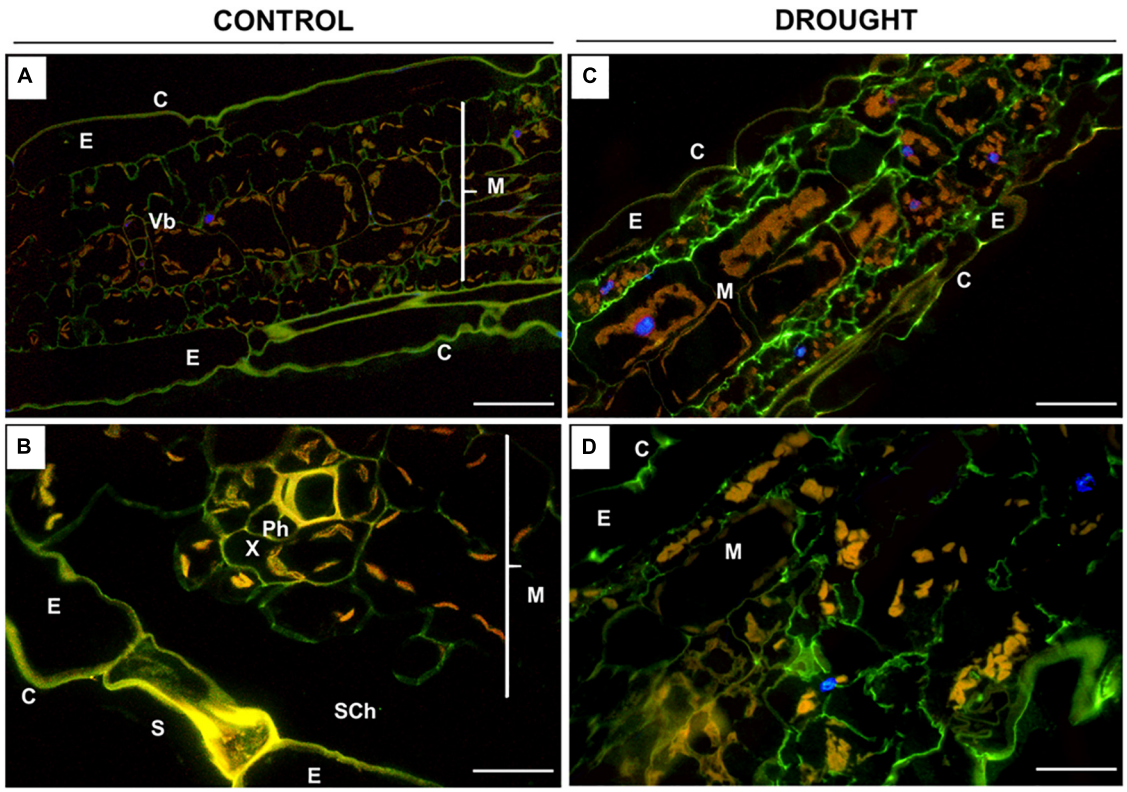

FIGURE 7
Immunolocalization of low-methylated homogalacturonans (HG) in *Z. mays* leaves under drought. Leaves from well-watered **(A,B)** and drought-stressed **(C,D)** plants were used for the preparation of cross-sections, which were stained with JIM5 antibodies. Images were obtained by merged signals from JIM5, DAPI staining (blue color), and chlorophyll autofluorescence. Green fluorescence indicates the presence of low-methylated HG. C, cuticle; E, epidermis; M, mesophyll; Ph, phloem; Sch, substomatal chamber; Vb, vascular bundles; X, xylem. Bars = 50 μm **(A,B)**, 15 μm **(C,D)**.

showed shrinking protoplasts of mesophyll cells in maize leaves (**Figure 3**) as a result of decreased water potential in cells under drought due to its limited availability. This also results in the accumulation of osmoprotective substances, such as proline (**Figure 1B**). What is more, a reduction in the diameter of the xylem vessels (**Figure 3F**) might be related to the disrupted water transport due to reduced hydraulic conductivity. The decreasing turgor pressure of mesophyll and xylem cells under drought affects their expansion, disrupting their architecture, so these tissues adapt their anatomy to environmental conditions and ensure long-distance transport (Abe et al., 2003). Reduced xylem size, as an effect of drought, was observed in *Pyrus communis* (Barss, 1930), *H. annuus, T. aestivum* (Penfound, 1931), and *Ricinus communis* L. (Penfound, 1932). The observed reduction in photosynthetic activity (**Figure 1A**) in this study might be related to drought-triggered modifications in chloroplast localization and structure (**Figures 3F,J**). The above-described symptoms were not associated with stress responses in plants inoculated with *Glomus* sp. or *Bacillus* sp., with better effects observed when bacteria were used (**Figures 3G,H**).

Modifications in the cell structure caused by drought (**Figure 3**) suggest changes in the cell wall structure. In the cell wall, hemicelluloses can bind to lignin and cellulose to improve cell wall rigidity, which strengthens this structure (Le Gall et al., 2015). So, the decrease in hemicellulose level in maize under drought might indicate a loss of cell wall integrity (**Figure 4A**). Such observations were also demonstrated in *Arabidopsis*, tobacco suspension cells, grape leaves, and wheat roots under drought (Feng et al., 2016). However, accumulated hemicelluloses may break, especially under stress conditions, thus preserving the plasticity of the wall structure (Le Gall et al., 2015; Tenhaken, 2015). Therefore, the increasing level of hemicelluloses under drought in maize inoculated with microorganisms (**Figure 4A**) may be a manifestation of a structural adjustment to combat the effects of stress.

Another manifestation of cell wall remodeling under drought is increasing pectin levels (**Figure 4B**). One of the plant's protective mechanisms under drought conditions is the synthesis of pectins, which can form protective colloids due to their ability to bind water (Wu et al., 2018). However, the content of these compounds in the inoculated maize, despite the

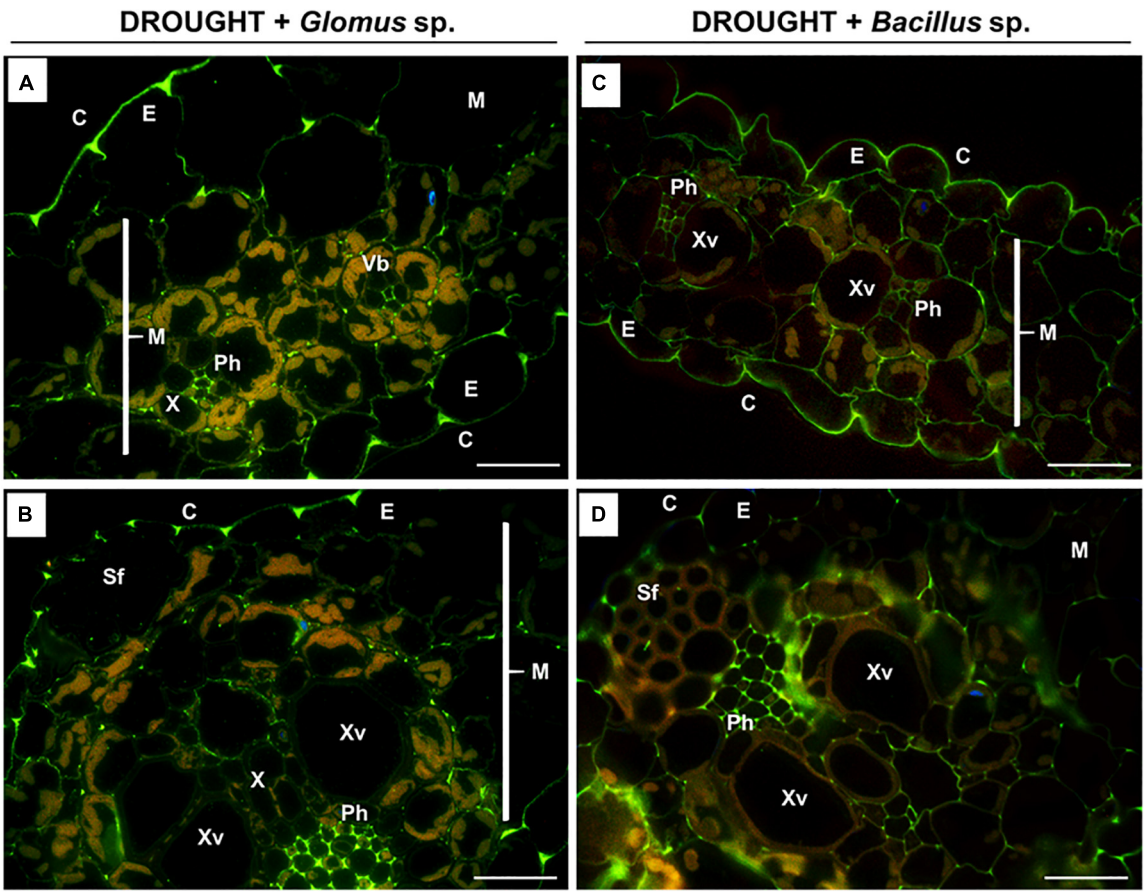

FIGURE 8
Immunodetection of low-methylated homogalacturonans (HG) in the leaves of drought-stressed *Z. mays* pretreated with *Glomus* sp. or *Bacillus* sp. strains. Reactions with monoclonal antibody JIM5 were made on leaf sections cut from drought-stressed maize treated at the seed stage with *Glomus* sp. **(A,B)** or *Bacillus* sp. **(C,D)**. Images were obtained by merged signals from JIM7, DAPI staining (blue color), and chlorophyll autofluorescence. Green fluorescence corresponds to the presence of low-methylated HG. C, cuticle; E, epidermis; M, mesophyll; Ph, phloem; Sf, sclerenchyma fibers; Vb, vascular bundles; X, xylem. Bars = 15 μm.

drought action, was the same as in the unstressed control plants (Figure 4B). A possible reason is the alleviation of drought stress by microorganisms, so the plant does not accumulate pectin.

The biomechanical properties of the cell wall, which are crucial for the modulation of its structure under drought, are determined by the methylation of pectins, e.g., homogalacturonans (HGs) (Forand et al., 2022). The synthesis of a highly esterified HG takes place in the Golgi apparatus, and then they are exported into the cell wall and de-esterified by pectin methylesterase (Willats et al., 2001). High- and low-methylated HG are accumulated in the leaves of drought-stressed maize (Figures 5, 7), indicating both the synthesis and de-esterification of these compounds. A stronger effect observed in the case of low-methylated HG under stress (Figures 7C,D) is the argument for the reduced plasticity and loosening of the wall structure. Furthermore, inoculation of maize with *Glomus* sp. or *Bacillus* sp. had not changed the general pool of pectin (Figure 4B), however, affected the degree of HG methylation and their distribution in leaf cells (Figures 6, 8). These results indicate that both microorganisms caused an intensive reorganization of the cell wall structure.

Low-methylated HG in the leaves of inoculated maize presented in the mesophyll cells, epiderm, and vascular bundles, particularly phloem (Figure 8). Pectin de-esterification could be a defense reaction of the plant leading to the generation of free carboxyl groups and the formation of gels by binding Ca^{2+} ions, which consequently leads to the appearance of a cross-link that stabilizes and mechanically strengthens cell walls (Willats et al., 2001; Braybrook et al., 2012). In the case of phloem, such a strategy enables the plant to efficiently uptake water and mineral compounds, as well as those involved in osmoregulation. High content of low-methylated HG in the phloem of stressed plants and plants inoculated with microorganisms (Figure 8) might protect against the deformation of cells characteristic of drought-treated leaves (Figures 3B,F,J). On the other hand, the accumulation of

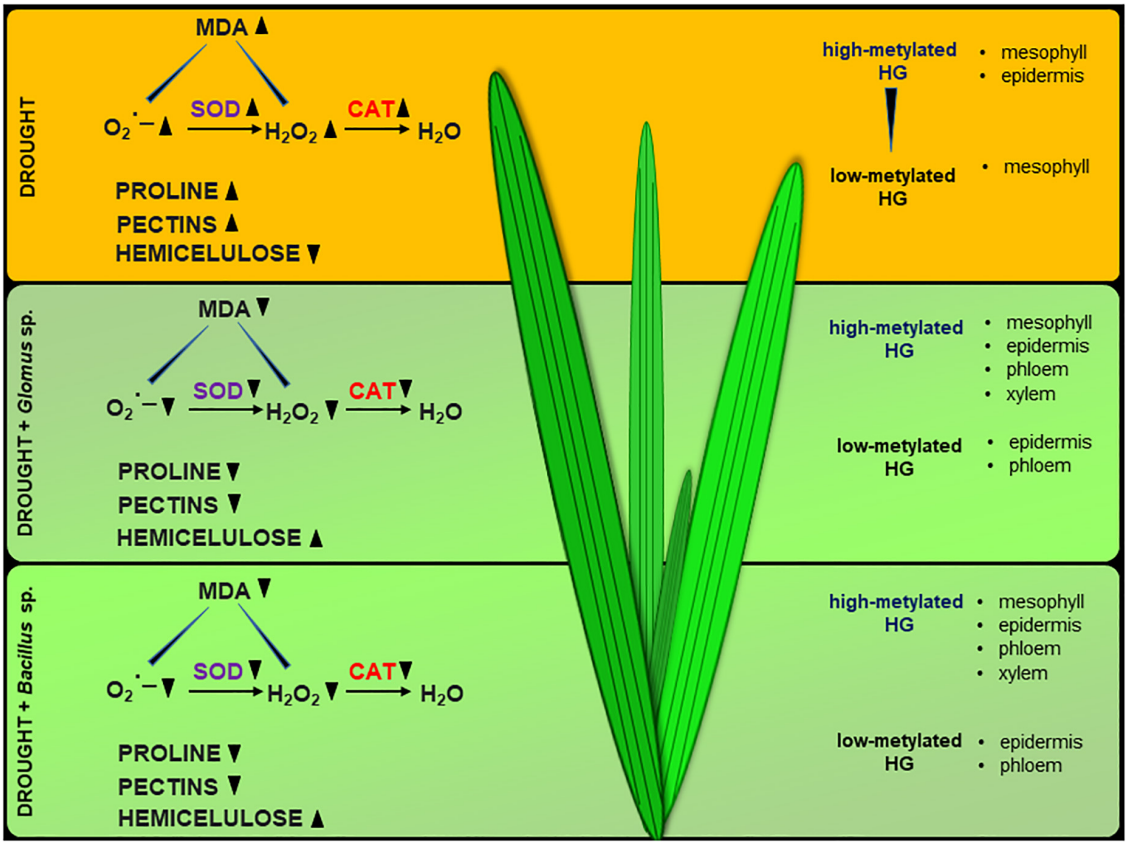

FIGURE 9
Possible action of *Glomus* sp. and *Bacillus* sp. in the improvement of soil drought tolerance in maize. The scheme was prepared based on the obtained here results.

high-methylated HG in the leaves of stressed and inoculated maize (Figure 6) supports the *de novo* formation of these compounds. There is a report showing that salt-tolerant genotypes of *Z. mays* are characterized by an increased content of these pectins (Uddin et al., 2013). The appearance of methylated HG in the epidermis ensures strength and elasticity of the cell wall, which is important in the adaptation to changing turgor pressure by stomatal movements under stress conditions (Jones et al., 2005). Therefore, maintaining the cohesion and appropriate flexibility of the cell wall mediated by the balance between high- and low-methylated pectins (Figure 6, 8) could be a part of the mechanism induced by *Glomus* sp. and *Bacillus* sp. to protect maize against drought stress consequences.

Collectively, our results support that *Glomus* sp. and *Bacillus* sp. help *Z. mays* to cope with drought stress, since inoculation of the seeds with these microorganisms prevents inhibition of photosynthesis and disruption in redox balance. Based on the presented observations, we suggest that *Glomus* sp. and *Bacillus* sp. modify the cell wall structure of maize leaves by affecting the pectin methylation level and hemicellulose content (Figure 9). It could lead to alleviation of the negative effects of drought in this species. We provide novel insight into drought stress resistance in important crop species, which could be helpful for agriculture and biotechnology development.

Data availability statement

The original contributions presented in this study are included in the article/supplementary material, further inquiries can be directed to the corresponding author.

Author contributions

EW and AK conceived and designed the research, conducted the experiments, evaluated and analyzed the data, and wrote and completed the manuscript. MWo was responsible for plant cultivation, material collection, photosynthesis analyses, and helped with spectrophotometric analyses. MŚ prepared sections for microscopy. KB was involved in the immunolocalization experiments. KB, AB-B, and MWa organized the tools and

media for microorganisms and were responsible for bacterial and fungal growth, and reviewed the manuscript. All authors contributed to the article and approved the submitted version.

Funding

This study received funding from the National Centre for Research and Development (POIR.01.01.01-00-0124/20) for Bacto-tech Sp. z o.o. The funder had the following involvement with participation in study design, microorganism inoculum preparation and interpretation of data. Bacto-tech sp. z o.o. is a spin-off company.

Acknowledgments

We acknowledged Grażyna Czeszewska-Rosiak for supporting plant cultivation.

Conflict of interest

Authors AB-B and MWa were employed by the Bacto-Tech Sp. z o.o.

The remaining authors declare that the research was conducted in the absence of any commercial or financial relationships that could be construed as a potential conflict of interest.

Publisher's note

References

Abe, H., Nakai, T., Utsumi, Y., and Kagawa, A. (2003). Temporal water deficit and wood formation in *Cryptomeria japonica*. *Tree Physiol.* 23, 859–863. doi: 10.1093/treephys/23.12.859

Ábrahám, E., Hourton-Cabassa, C., Erdei, L., and Szabados, L. (2010). Methods for determination of proline in plants. *Methods Mol. Biol.* 639, 317–331. doi: 10.1007/978-1-60761-702-0_20

Abrecht, D. G., and Carberry, P. S. (1993). The influence of water deficit prior to tassel initiation on maize growth, development and yield. *Field Crops Res.* 31, 55–69. doi: 10.1016/0378-4290(93)90050-W

Arias Padró, M. D., Caboni, E., Salazar Morin, K. A., Meraz Mercado, M. A., and Olalde-Portugal, V. (2021). Effect of *Bacillus subtilis* on antioxidant enzyme activities in tomato grafting. *PeerJ* 12:e10984. doi: 10.7717/peerj.10984

Arkhipova, T., Prinsen, E., Veselov, S., Martinenko, E., Melentiev, A., and Kudoyarova, G. (2007). Cytokinin producing bacteria enhance plant growth in drying soil. *Plant Soil* 292, 305–315. doi: 10.1007/s11104-007-9233-5

Ashraf, M., and Foolad, M. R. (2007a). Roles of glycine betaine and proline in improving plant abiotic stress resistance. *Environ. Exp. Bot.* 59, 206–216. doi: 10.1016/j.envexpbot.2005.12.006

Atmodjo, M. A., Hao, Z., and Mohnen, D. (2013). Evolving views of pectin biosynthesis. *Annu. Rev. Plant Biol.* 64, 747–779. doi: 10.1146/annurev-arplant-042811-105534

Barss, A. F. (1930). Effect of moisture supply on development of *Pyrus communis*. *Bot. Gaz.* 90, 151–176. doi: 10.1086/334092

Behrooz, A., Vahdati, K., Rejali, F., Lotfi, M., Sarikhani, S., and Leslie, C. (2019). Arbuscular mycorrhiza and plant growth-promoting bacteria alleviate drought stress in walnut. *Hortic. Sci.* 54, 1087–1092. doi: 10.21273/HORTSCI13961-19

Braybrook, S. A., Hofte, H., and Peaucelle, A. (2012). Probing the mechanical contributions of the pectin matrix: Insights for cell growth. *Plant Signal. Behav.* 7, 1037–1041. doi: 10.4161/psb.20768

Çakir, R. (2004). Effect of water stress at different development stages on vegetative and reproductive growth of corn. *Field Crops Res.* 89, 1–16. doi: 10.1016/j.fcr.2004.01.005

Cakmak, I., and Marschner, H. (1992). Magnesium deficiency and high light intensity enhance activities of superoxide dismutase, ascorbate peroxidase, and glutathione reductase in bean leaves. *Plant Physiol.* 98, 1222–1227. doi: 10.1104/pp.98.4.1222

Castro, D., Torres, M., Sampedro, I., Martínez-Checa, F., Torres, B., and Béjar, V. (2020). Biological control of *Verticillium* wilt on olive trees by the salt-tolerant strain *Bacillus velezensis* XT1. *Microorganisms* 8:1080. doi: 10.3390/microorganisms8071080

Chauhan, B. S., and Johnson, D. E. (2010). Growth and reproduction of junglerice (*Echinochloa colona*) in response to water stress. *Weed Sci.* 58, 132–135. doi: 10.1614/WS-D-09-00016.1

Chen, Y., Zhang, Z., Wang, P., Song, X., Wei, X., and Tao, F. (2016). Identifying the impact of multi-hazards on crop yield—a case for heat stress and dry stress on winter wheat yield in northern China. *Eur. J. Agron.* 73, 55–63. doi: 10.1016/j.eja.2015.10.009

Costa-Santos, M., Mariz-Ponte, N., Dias, M. C., Moura, L., Marques, G., and Santos, C. (2021). Effect of *Bacillus* spp. and *Brevibacillus* sp. on the photosynthesis and redox status of *Solanum lycopersicum*. *Horticulturae* 7:24. doi: 10.3390/horticulturae7020024

Dale, N. M., and Fuller, H. L. (1982). Applicability of the true metabolizable energy system in practical feed formulation. *Poultry Sci.* 61, 351–356. doi: 10.3382/ps.0610351

Dewanto, V., Wu, X. Z., and Liu, R. H. (2002). Processed sweet corn has higher antioxidant activity. *J. Agric. Food Chem.* 50, 4959–4964. doi: 10.1021/jf0255937

Earl, A. M., Losick, R., and Kolter, R. (2008). Ecology and genomics of *Bacillus subtilis*. *Trends Microbiol.* 16, 269–275. doi: 10.1016/j.tim.2008.03.004

Feng, W., Lindner, H., Robbins, N. E., and Dinneny, J. R. (2016). Growing out of stress: The role of cell-and organ-scale growth control in plant water-stress responses. *Plant Cell* 28, 1769–1782. doi: 10.1105/tpc.16.00182

Florkiewicz, A. B., Kućko, A., Kapusta, M., Burchardt, S., Przywieczerski, T., Czeszewska-Rosiak, G., et al. (2020). Drought disrupts auxin localization in abscission zone and modifies cell wall structure leading to flower separation in yellow lupine. *Int. J. Mol. Sci.* 21:6848. doi: 10.3390/ijms21186848

Forand, A. D., Finfrock, Y. Z., Lavier, M., Stobbs, J., Qin, L., Wang, S., et al. (2022). With a little help from my cell wall: Structural modifications in pectin may play a role to overcome both dehydration stress and fungal pathogens. *Plants* 11:385. doi: 10.3390/plants11030385

Gagné-Bourque, F., Aliferis, K. A., Seguin, P., Rani, M., Samson, R., and Jabaji, S. (2013). Isolation and characterization of indigenous endophytic bacteria associated with leaves of switchgrass (*Panicum virgatum* L.) cultivars. *J. Appl. Microbiol.* 114, 836–853. doi: 10.1111/jam.12088

Gagné-Bourque, F., Bertrand, A., Claessens, A., Aliferis, K. A., and Jabaji, S. (2016). Alleviation of Drought Stress and Metabolic Changes in Timothy (*Phleum pratense* L.) Colonized with *Bacillus subtilis* B26. *Front. Plant Sci.* 7:584. doi: 10.3389/fpls.2016.00584

Gagné-Bourque, F., Mayer, B. F., Charron, J. B., Vali, H., Bertrand, A., and Jabaji, S. (2015). Accelerated growth rate and increased drought stress resilience of the model grass *Brachypodium distachyon* colonized by *Bacillus subtilis* B26. *PLoS One* 10:e0130456. doi: 10.1371/journal.pone.0130456

Ganjeali, A., Ashiani, E., Zare, M., and Tabasi, E. (2018). Influences of the arbuscular mycorrhizal fungus *Glomus mosseae* on morphophysiological traits and biochemical compounds of common bean (*Phaseolus vulgaris*) under drought stress. *S. Afr. J. Plant Soil* 35, 121–127. doi: 10.1080/02571862.2017.1340982

Giannopolitis, C. N., and Ries, S. K. (1977). Superoxide dismutases: I. Occurrence in higher plants. *Plant Physiol.* 59, 309–314. doi: 10.1104/pp.59.2.309

Gill, S. S., and Tuteja, N. (2010). Reactive oxygen species and antioxidant machinery in abiotic stress tolerance in crop plants. *Plant Physiol. Bioch.* 48, 909–930. doi: 10.1016/j.plaphy.2010.08.016

Glick, B. R. (2014). Bacteria with ACC deaminase can promote plant growth and help to feed the world. *Microbiol. Res.* 169, 30–39. doi: 10.1016/j.micres.2013.09.009

Gong, M., You, X., and Zhang, Q. (2015). Effects of *Glomus intraradices* on the growth and reactive oxygen metabolism of foxtail millet under drought. *Ann. Microbiol.* 65, 595–602. doi: 10.1007/s13213-014-0895-y

Gowtham, H. G., Singh, B., Murali, M., Shilpa, N., Prasad, M., Aiyaz, M., et al. (2020). Induction of drought tolerance in tomato upon the application of ACC deaminase producing plant growth promoting rhizobacterium *Bacillus subtilis* Rhizo SF 48. *Microbiol. Res.* 234:126422. doi: 10.1016/j.micres.2020.126422

Grover, M., Madhubala, R., Ali, S. Z., Yadav, S. K., and Venkateswarlu, B. (2014). Influence of *Bacillus* spp. strains on seedling growth and physiological parameters of sorghum under moisture stress conditions. *J. Basic Microbiol.* 54, 951–961. doi: 10.1002/jobm.201300250

Gururani, M. A., Upadhyaya, C. P., Baskar, V., Baskar, V., Venkatesh, J., Nookaraju, A., et al. (2013). Plant growth-promoting rhizobacteria enhance abiotic stress tolerance in *Solanum tuberosum* through inducing changes in the expression of ROS-scavenging enzymes and improved photosynthetic performance. *J. Plant Growth Regul.* 32, 245–258. doi: 10.1007/s00344-012-9292-6

Harholt, J., Suttangkakul, A., and Vibe Scheller, H. (2010). Biosynthesis of pectin. *Plant Physiol.* 153, 384–395. doi: 10.1104/pp.110.156588

Harris-Valle, C., Esqueda, M., Gutiérrez, A., Castellanos, A. E., Gardea, A. A., and Berbara, R. (2018). Physiological response of *Cucurbita pepo* var. pepo mycorrhized by *Sonoran* desert native arbuscular fungi to drought and salinity stresses. *Braz. J. Microbiol.* 49, 45–53. doi: 10.1016/j.bjm.2017.04.005

Hasanuzzaman, M., Bhuyan, M., Zulfiqar, F., Raza, A., Mohsin, S. M., Mahmud, J. A., et al. (2020). Reactive oxygen species and antioxidant defense in plants under abiotic stress: Revisiting the crucial role of a universal defense regulator. *Antioxidants* 9:681. doi: 10.3390/antiox9080681

Hodges, D., DeLong, J., Forney, C., and Prange, R. K. (1999). Improving the thiobarbituric acid-reactive-substances assay for estimating lipid peroxidation in plant tissues containing anthocyanin and other interfering compounds. *Planta* 207, 604–611. doi: 10.1007/s004250050524

Jones, L., Milne, J. L., Ashford, D., McCann, M. C., and McQueen-Mason, S. J. (2005). A conserved functional role of pectic polymers in stomatal guard cells from a range of plant species. *Planta* 221, 255–264. doi: 10.1007/s00425-004-1432-1

Joo, G. J., Kim, Y. M., Lee, I. J., Song, K. S., and Rhee, I. K. (2004). Growth promotion of red pepper plug seedlings and the production of gibberellins by *Bacillus cereus*, *Bacillus macroides* and *Bacillus pumilus*. *Biotechnol. Lett.* 26, 487–491. doi: 10.1023/b:bile.0000019555.87121.34

Kakumanu, A., Ambavaram, M. M., Klumas, C., Krishnan, A., Batlang, U., Myers, E., et al. (2012). Effects of drought on gene expression in maize reproductive and leaf meristem tissue revealed by RNA-Seq. *Plant Physiol.* 160, 846–867. doi: 10.1104/pp.112.200444

Kasim, W. A., Osman, M. E., Omar, M. N., El-Daim, A., Islam, A., Bejai, S., et al. (2013). Control of drought stress in wheat using plant-growth-promoting bacteria. *J. Plant Growth Regul.* 32, 122–130. doi: 10.1007/s00344-012-9283-7

Kućko, A., Alché, J., Tranbarger, T. J., and Wilmowicz, E. (2022). The acceleration of yellow lupine flower abscission by jasmonates is accompanied by lipid-related events in abscission zone cells. *Plant Sci.* 316:111173. doi: 10.1016/j.plantsci.2021.111173

Kushwaha, P., Kashyap, P. L., Srivastava, A. K., and Tiwari, R. K. (2020). Plant growth promoting and antifungal activity in endophytic *Bacillus* strains from pearl millet (*Pennisetum glaucum*). *Braz. J. Microbiol.* 51, 229–241. doi: 10.1007/s42770-019-00172-5

Lawlor, D. W., and Tezara, W. (2009). Causes of decreased photosynthetic rate and metabolic capacity in water-deficient leaf cells: A critical evaluation of mechanisms and integration of processes. *Ann. Bot.* 103, 561–579. doi: 10.1093/aob/mcn244

Le Gall, H., Philippe, F., Domon, J.-M., Gillet, F., Pelloux, J., and Rayon, C. (2015). Cell wall metabolism in response to abiotic stress. *Plants* 4, 112–166. doi: 10.3390/plants4010112

Liao, X., Chen, J., Guan, R., Liu, J., and Sun, Q. (2021). Two arbuscular mycorrhizal fungi alleviates drought stress and improves plant growth in *Cinnamomum migao* seedlings. *Mycobiology* 49, 396–405. doi: 10.1080/12298093.2021.1938803

Lim, J. H., and Kim, S. D. (2013). Induction of drought stress resistance by multi-functional PGPR *Bacillus licheniformis* K11 in pepper. *Plant Pathol. J.* 29:201. doi: 10.5423/PPJ.SI.02.2013.0021

Liu, Z., Pi, F., Guo, X., Guo, X., and Yu, S. (2019). Characterization of the structural and emulsifying properties of sugar beet pectins obtained by sequential extraction. *Food Hydrocol.* 88, 31–42. doi: 10.1016/j.foodhyd.2018.09.036

Loreto, F., and Velikova, V. (2001). Isoprene produced by leaves protects the photosynthetic apparatus against ozone damage, quenches ozone products and reduces lipid peroxidation of cellular membranes. *Plant Physiol.* 127, 1781–1787. doi: 10.1104/pp.010497

Mao, C., Feng, Y., Wang, X., and Ren, G. (2015). Review on research achievements of biogas from anaerobic digestion. *Renew. Sust. Energ. Rev.* 45, 540–555. doi: 10.1016/j.rser.2015.02.032

Marulanda, A., Barea, J. M., and Azcón, R. (2006). An indigenous drought-tolerant strain of *Glomus intraradices* associated with a native bacterium improves water transport and root development in *Retama sphaerocarpa*. *Microb. Ecol.* 52, 670–678. doi: 10.1007/s00248-006-9078-0

Marulanda, A., Porcel, R., Barea, J. M., and Azcón, R. (2007). Drought tolerance and antioxidant activities in lavender plants colonized by native drought-tolerant or drought-sensitive *Glomus* species. *Microb. Ecol.* 54, 543–552. doi: 10.1007/s00248-007-9237-y

Mittler, R. (2002). Oxidative stress, antioxidants and stress tolerance. *Trends Plant Sci.* 7, 405–410. doi: 10.1016/S1360-1385(02)02312-9

Moreno-Galván, A., Romero-Perdomo, F. A., Estrada-Bonilla, G., Meneses, C. H. S. G., and Bonilla, R. R. (2020). Dry-caribbean *Bacillus* spp. strains ameliorate drought stress in maize by a strain-specific antioxidant response modulation. *Microorganisms* 8:823. doi: 10.3390/microorganisms8060823

Murchie, E. H., and Lawson, T. (2013). Chlorophyll fluorescence analysis: A guide to good practice and understanding some new applications. *J. Exp. Bot.* 64, 3983–3998. doi: 10.1093/jxb/ert208

NeSmith, D. S., and Ritchie, J. T. (1992). Short-and long-term responses of corn to a pre-anthesis soil water deficit. *Agron. J.* 84, 107–113. doi: 10.2134/agronj1992.00021962008400010021x

Nuss, E. T., and Tanumihardjo, S. A. (2010). Maize: A paramount staple crop in the context of global nutrition. *Compr. Rev. Food Sci.* 9, 417–436. doi: 10.1111/j.1541-4337.2010.00117.x

Penfound, W. T. (1931). Plant anatomy as conditioned by light intensity and soil moisture. *Am. J. Bot.* 18, 558–572.

Penfound, W. T. (1932). The anatomy of the castor bean as conditioned by light intensity and soil moisture. *Am. J. Bot.* 19, 538–546.

Rafique, S. (2020). "Drought responses on physiological attributes of *Zea mays* in relation to nitrogen and source-sink relationships," in *Abiotic Stress in Plants*, ed. S. Fahad (London: IntechOpen), doi: 10.5772/intechopen.93747

Reddy, A. R., Chaitanya, K. V., and Vivekanandan, M. (2004). Drought-induced responses of photosynthesis and antioxidant metabolism in higher plants. *J. Plant Physiol.* 161, 1189–1202. doi: 10.1016/j.jplph.2004.01.013

Rodríguez, A. A., Córdoba, A. R., Ortega, L., and Taleisnik, E. (2004). Decreased reactive oxygen species concentration in the elongation zone contributes to the reduction in maize leaf growth under salinity. *J. Exp. Bot.* 55, 1383–1390. doi: 10.1093/jxb/erh148

Ruiz-Lozano, J. M., Gómez, M., and Azcón, R. (1995b). Influence of different *Glomus* species on the time-course of physiological plant responses of lettuce to progressive drought stress periods. *Plant Sci.* 110, 37–44. doi: 10.1016/0168-9452(95)04184-V

Ruiz-Lozano, J. M., Azcón, R., and Gomez, M. (1995a). Effects of arbuscular-mycorrhizal *Glomus* species on drought tolerance: Physiological and nutritional plant responses. *Appl. Environ. Microbiol.* 61, 456–460. doi: 10.1128/aem.61.2.456-460.1995

Sabba, R. P., and Lulai, E. C. (2002). Histological analysis of the maturation of native and wound periderm in potato (*Solanum tuberosum* L.) tuber. *Ann. Bot.* 90, 1–10. doi: 10.1093/aob/mcf147

Sabra, A., Daayf, F., and Renault, S. (2012). Differential physiological and biochemical responses of three *Echinacea* species to salinity stress. *Sci. Hort.* 135, 23–31. doi: 10.1016/j.scienta.2011.11.024

Samaniego-Gámez, B. Y., Garruña, R., Tun-Suárez, J. M., Moreno-Valenzuela, O. A., Reyes-Ramírez, A., Valle-Gough, R. E., et al. (2021). Healthy photosynthetic mechanism suggests ISR elicited by *Bacillus* spp. in *Capsicum chinense* plants infected with PepGMV. *Pathogens* 10:455. doi: 10.3390/pathogens10040455

Sandhya, V., Shaik, Z. A., Minakshi, G., Gopal, R., and Venkateswarlu, B. (2011). Drought-tolerant plant growth promoting *Bacillus* spp.: Effect on growth, osmolytes, and antioxidant status of maize under drought stress. *J. Plant Interact.* 6, 1–14.

Shams, S., Sahu, J. N., Rahman, S. M. S., and Ahsan, A. (2017). Sustainable waste management policy in Bangladesh for reduction of greenhouse gases. *Sustain. Cities Soc.* 33, 18–26. doi: 10.1016/j.scs.2017.05.008

Sharma, S., Yadav, N., Singh, A., and Kumar, R. (2013). Nutritional and antinutritional profile of newly developed chickpea (*Cicer arietinum* L) varieties. *Int. Food Res. J.* 20:2

Sheteiwy, M. S., Abd Elgawad, H., Xiong, Y. C., Macovei, A., Brestic, M., Skalicky, M., et al. (2021). Inoculation with *Bacillus amyloliquefaciens* and mycorrhiza confers tolerance to drought stress and improve seed yield and quality of soybean plant. *Physiol. Plant.* 172, 2153–2169. doi: 10.1111/ppl.13454

Shintu, P. V., and Jayaram, K. M. (2015). Phosphate solubilising bacteria (*Bacillus polymyxa*)-An effective approach to mitigate drought in tomato (*Lycopersicon esculentum* Mill.). *Trop. Plant Res.* 2, 17–22.

Shulaev, V., and Oliver, D. J. (2006). Metabolic and proteomic markers for oxidative stress. New tools for reactive oxygen species research. *Plant Physiol.* 14, 367–372. doi: 10.1104/pp.106.077925

Siyuan, S., Tong, L., and Rui, H. (2018). Corn phytochemicals and their health benefits. *Food Sci. Hum. Wellness* 7, 185–195. doi: 10.1016/j.fshw.2018.09.003

Sohrabi, Y., Heidari, G., Weisany, W., Golezani, K. G., and Mohammadi, K. (2012). Changes of antioxidative enzymes, lipid peroxidation and chlorophyll content in chickpea types colonized by different *Glomus* species under drought stress. *Symbiosis* 56, 5–18. doi: 10.1007/s13199-012-0152-8

Tanumihardjo, S. A., Kaliwile, C., Boy, E., Dhansay, M. A., and van Stuijvenberg, M. E. (2019). Overlapping vitamin A interventions in the United States, Guatemala, Zambia, and South Africa: Case studies. *Ann. N.Y. Acad. Sci.* 1446, 102–116. doi: 10.1111/nyas.13965

Tenhaken, R. (2015). Cell wall remodeling under abiotic stress. *Front. Plant Sci.* 7:771. doi: 10.3389/fpls.2014.00771

Uddin, M. N., Hanstein, S., Leubner, R., and Schubert, S. (2013). Leaf cell-wall components as influenced in the first phase of salt stress in three maize (*Zea mays* L.) hybrids differing in salt resistance. *J. Agron. Crop Sci.* 199, 405–415. doi: 10.1111/jac.12031

Ullah, A., Nisar, M., Ali, H., Hazrat, A., Hayat, K., Keerio, A. A., et al. (2019). Drought tolerance improvement in plants: An endophytic bacterial approach. *Appl. Microbiol. Biotechnol.* 103, 7385–7397. doi: 10.1007/s00253-019-10045-4

Ullah, A., Sun, H., Yang, X., and Zhang, X. (2017). Drought coping strategies in cotton: Increased crop per drop. *Plant Biotechnol. J.* 15, 271–284. doi: 10.1111/pbi.12688

Vardharajula, S., Zulfikar Ali, S., Grover, M., Reddy, G., and Bandi, V. (2011). Drought-tolerant plant growth promoting *Bacillus* spp.: Effect on growth, osmolytes, and antioxidant status of maize under drought stress. *J. Plant Interact.* 6, 1–14.

Wang, C. J., Yang, W., Wang, C., Gu, C., Niu, D. D., Liu, H. X., et al. (2012). Induction of drought tolerance in cucumber plants by a consortium of three plant growth-promoting rhizobacterium strains. *PLoS One* 7:e52565. doi: 10.1371/journal.pone.0052565

Weng, J. H. (2006). Underestimate of PS2 efficiency in the field due to high temperature resulting from leaf clipping and its amendment. *Photosynthetica* 44, 467–470. doi: 10.1007/s11099-006-0052-3

Willats, W. G., Limberg, G., Buchholt, H. C., Alebeek, G. J. V., Benen, J., Christensen, T. M., et al. (2000). Analysis of pectic epitopes recognised by hybridoma and phage display monoclonal antibodies using defined oligosaccharides, polysaccharides, and enzymatic degradation. *Carbohydr. Res.* 327, 309–320. doi: 10.1016/S0008-6215(00)00039-2

Willats, W. G., Orfila, C., Limberg, G., Buchholt, H. C., Van Alebeek, G. J., Voragen, A. G., et al. (2001). Modulation of the degree and pattern of methyl-esterification of pectic homogalacturonan in plant cell walls. Implications for pectin methyl esterase action, matrix properties, and cell adhesion. *J. Biol. Chem.* 276, 19404–19413. doi: 10.1074/jbc.M011242200

Wilmowicz, E., Frankowski, K., Kućko, A., Świdziński, M., Alché, J. D., Nowakowska, A., et al. (2016). The influence of abscisic acid on the ethylene biosynthesis pathway in the functioning of the flower abscission zone in *Lupinus luteus*. *J. Plant Physiol.* 206, 49–58. doi: 10.1016/j.jplph.2016.08.018

Wilmowicz, E., Kućko, A., Burchardt, S., and Przywieczerski, T. (2019). Molecular and hormonal aspects of drought-triggered flower shedding in yellow lupine. *Int. J. Mol. Sci.* 20:3731. doi: 10.3390/ijms20153731

Wu, H. C., Bulgakov, V. P., and Jinn, T. L. (2018). Pectin methylesterases: Cell wall remodeling proteins are required for plant response to heat stress. *Front. Plant Sci.* 9:1612. doi: 10.3389/fpls.2018.01612

Wu, Q. S., Zou, Y. N., Xia, R. X., and Wang, M. Y. (2007). Five *Glomus* species affect water relations of *Citrus tangerine* during drought stress. *Bot. Stud.* 48, 147–154.

Xie, S., Wu, H. J., Zang, H., Wu, L., Zhu, Q., and Gao, X. (2014). Plant growth promotion by spermidine-producing *Bacillus subtilis* OKB105. *Mol. Plant Microbe Interact.* 27, 655–663. doi: 10.1016/j.btre.2019.e00406

Xu, H., Lu, Y., and Tong, S. (2018). Effects of arbuscular mycorrhizal fungi on photosynthesis and chlorophyll fluorescence of maize seedlings under salt stress. *Emir. J. Food Agric.* 30:199. doi: 10.9755/ejfa.2018.v30.i3.1642

Yaghoubian, Y., Goltapeh, E. M., Pirdashti, H., Esfandiari, E., Feiziasl, V., Dolatabadi, H. K., et al. (2014). Effect of *Glomus mosseae* and *Piriformospora indica* on growth and antioxidant defense responses of wheat plants under drought Stress. *Agric. Res.* 3, 239–245. doi: 10.1007/s40003-014-0114-x

frontiers | Frontiers in Plant Science

TYPE Mini Review
PUBLISHED 31 May 2023
DOI 10.3389/fpls.2023.1183402

OPEN ACCESS

EDITED BY
Vincenzo Lionetti,
Sapienza University of Rome, Italy

REVIEWED BY
Luciana Renna,
University of Florence, Italy
Daniele Del Corpo,
Sapienza University of Rome, Italy

*CORRESPONDENCE
Li-Jun Huang
nghua@126.com

RECEIVED 10 March 2023
ACCEPTED 05 May 2023
PUBLISHED 31 May 2023

CITATION
Li N, Lin Z, Yu P, Zeng Y, Du S and Huang L-J (2023) The multifarious role of callose and callose synthase in plant development and environment interactions. *Front. Plant Sci.* 14:1183402. doi: 10.3389/fpls.2023.1183402

The multifarious role of callose and callose synthase in plant development and environment interactions

Ning Li [1,2], Zeng Lin [1], Peiyao Yu [1], Yanling Zeng [1], Shenxiu Du [3] and Li-Jun Huang [1*]

[1]State Key Laboratory of Cultivation and Protection for Non-Wood Forest Trees, College of Forestry, Central South University of Forestry and Technology, Changsha, China, [2]Key Laboratory of Forest Bio-resources and Integrated Pest Management for Higher Education in Hunan Province, Central South University of Forestry and Technology, Changsha, China, [3]Biotechnology Research Institute, Chinese Academy of Agricultural Sciences, Beijing, China

Callose is an important linear form of polysaccharide synthesized in plant cell walls. It is mainly composed of β-1,3-linked glucose residues with rare amount of β-1,6-linked branches. Callose can be detected in almost all plant tissues and are widely involved in various stages of plant growth and development. Callose is accumulated on plant cell plates, microspores, sieve plates, and plasmodesmata in cell walls and is inducible upon heavy metal treatment, pathogen invasion, and mechanical wounding. Callose in plant cells is synthesized by callose synthases located on the cell membrane. The chemical composition of callose and the components of callose synthases were once controversial until the application of molecular biology and genetics in the model plant *Arabidopsis thaliana* that led to the cloning of genes encoding synthases responsible for callose biosynthesis. This minireview summarizes the research progress of plant callose and its synthetizing enzymes in recent years to illustrate the important and versatile role of callose in plant life activities.

KEYWORDS

callose, glucan-synthase-like, plasmodesmata, cell wall, plant-pathogen interaction

1 Introduction

As early as more than 100 years ago, callose was first found in the phloem sieve plates, microspore mother cells and pollen tubes of plants by staining with the callose specific dye aniline blue (Kauss, 1996); however, it was not until half century later that the chemical composition and molecular structure of callose was characterized (Aspinall and Kessler, 1957). Subsequently, more evidence indicated that, unlike cellulose (β-1,4-glucan), the main component of plant cell walls, callose is a chain of β-1,3-glucan and contains a small amount of β-glucan-1,6-linkages (Meikle et al., 1991). For a long time, scientists tried to purify callose synthase through biochemical means. Paradoxically, the purified protein

complex has weak cellulose synthase activity, the molecular nature of plant callose synthase remain speculative and controversial (Verma and Hong, 2001). The successful application of genetics and molecular biology in the model plant *Arabidopsis thaliana* has made a series of important progress in the study of callose synthase, 12 members of the callose synthase family were cloned and characterized in the Arabidopsis genome. The physiological function and biochemical mechanism of callose synthase were elucidated. Members of the callose synthase family are specifically expressed in different plant tissues at different stages, or upon pathogen infection, to synthesize callose and participate in the regulation of plant development and physiological functions.

2 Chemical structure and biosynthesis of callose

In general, callose is a glucan chain composed of a raft of glucose residues via β-1,3-glycosidic bonds (Figure 1A). In different types of cell walls, the structure and chemical composition of callose may be slightly different, for example, the alcoholic hydroxyl group on the glucose residue ring can be modified by esterification (Chen and Kim, 2009). While as cellulose is mainly composed of polysaccharide chains formed by glucose residues through β-1,4-glycosidic bonds (Ellinger et al., 2014). Unlike cellulose, which has a crystalline structure, callose forms rather a helical or amorphous structure without clearly defined shape.

Callose is mainly synthesized during the specific period of cell wall formation, and is an important component of plant vascular bundles, microspore outer walls, and dividing cell plates (Figure 1B). The synthesis and degradation of callose at the plasmodesmata in the cell wall is a major way to regulate the transport of substances between symplasts. Callose is also involved in the formation of phloem sieve plates. Callose accumulates on the sieve plates and controls the pore size to regulate the transport of substances in the phloem (Barratt et al., 2011; Xie et al., 2011). It was found recently that the dynamic accumulation of callose plays an important role in regulating the bud dormancy process of perennial plants (Singh et al., 2018; Tylewicz et al., 2018; Singh et al., 2019). Under short-day conditions, abscisic acid (ABA) led to increased callose synthesis in poplar shoot tips, thereby limiting the activity of shoot tip meristems and suspending growth to avoid freezing damage. Callose plays an important role in the transmission of information between plant cells and regulates the growth and development of plants at different stages.

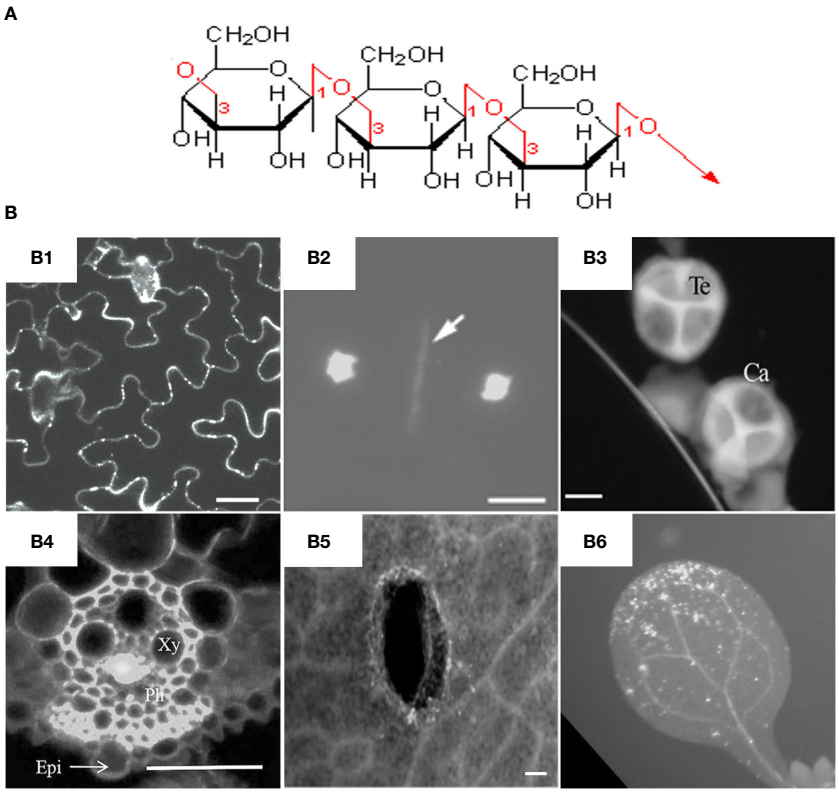

FIGURE 1
Molecular structure and fluorescent dye staining of callose. **(A)** Callose is composed of a long chain of monomer glucoses joined together by β-1,3-glycosidic bonds. **(B)** Typical images of aniline blue stained callose in different tissues and plant species. (B1) Callose deposition at the plasmodesmata of Arabidopsis leaf epidermal cells, scale bar = 20 μm (Vu et al., 2022). (B2) Callosic cell plate formation (indicated by arrow) during cytokinesis of rice pollen mother cells, scale bar = 10 μm (Zhang et al., 2018). (B3) Callose layer surrounding tetrad microspores in anther of rapeseed, Ca = callose, Te = tetrad, scale bar = 10 μm (Liu et al., 2017). (B4) Virus-induced callose deposition in rice phloem, Xy = xylem, Ph=phloem, Epi = epidermis, scale bar = 50 μm (Yi et al., 2021). (B5) Mechanical wounding-induced callose deposition in cotyledons of rapeseed, scale bar 100 μm, (Liu et al., 2018). (B6) Flg22-induced callose accumulation in Arabidopsis leaves (Keppler et al., 2018). Frames B1-B6 were reproduced with permission under the Creative Commons (CC) licenses.

Both biotic and abiotic stresses in the environment can induce plant callose synthesis. Measuring of callose accumulation in plant leaves or roots by aniline blue staining has become an important tool for detection microbial diseases or heavy metal toxicity in plants (Ellinger and Voigt, 2014). Callose is considered to be the first physical defense line of plants against environmental stress. Formation of callose at different developmental stages, in different tissue parts, and by various stresses is synthesized by callose synthase located on the cell membrane. The amount of callose in plants is jointly determined by callose synthase (CalS, also known as GSL for glucan-synthase-like) and β-1,3-glucanase (BG), the former is responsible for biosynthesis and the latter is responsible for degradation. β-1,3-glucanase is endonuclease that catalyzes the hydrolysis of β-1,3-glucosidic linkages to produce oligosaccharides with a few of glucose units and glucose monomers. Compared with synthesis, the degradation of callose is relatively less studied.

3 Expression and regulation of callose synthases

3.1 Callose synthases in model plants

Callose is synthesized by a multi-subunit protein complex on the cell membrane. The most critical catalytic subunit is callose synthase. In the model plant *Arabidopsis thaliana*, 12 callose synthase genes were identified (Verma and Hong, 2001). With the exception of *GSL1* and *GSL5*, the other *GSL* genes contain up to 50 exons. Callose synthase is composed of about 2,000 amino acids and is almost the protein with the largest molecular weight in plants, making them remarkably difficult for biochemical analysis.

Callose synthase is a large transmembrane protein with 14~16 hydrophobic transmembrane domains at the N-terminus and C-terminus of the protein, anchoring the synthase on the plasma membrane. The hydrophilic domain in the middle of the protein is located in the cytoplasm and is the main site of callose synthesis. Other major components attached to the synthase complex include sucrose synthase and UDP-glucose transferase, which provide substrates for callose synthesis (Albrecht and Mustroph, 2003). Glucosyltransferases also recruit Rop1 (Rho-related protein from plant) via protein-protein interaction. Rop1 regulates the synthesis of callose by controlling the activity of glucosyltransferase (Hong et al., 2001b). The callose synthase complex also contains annexin, which regulates the activity of the synthase complex through the concentration of calcium ions (Kauss and Jeblick, 1991). With the progress of scientific research, new components of callose synthase have been discovered, and the composition of the synthase complex has also changed according to different subcellular locations and sites of callose synthesis. High-resolution atomic force microscopy was applied to elucidate the structure of the callose synthase complex in living plants (Wu et al., 2006).

Members of the callose synthase gene family are differently expressed during developmental stages of various plant tissues, and respond specifically to various biotic and abiotic stimuli. The Arabidopsis *GSL1*, *2*, *5*, *8* and *10* are involved in the synthesis of callose during pollen development (Dong et al., 2005; Enns et al., 2005; Nishikawa et al., 2005; Huang et al., 2009; Huang et al., 2013); Both *GSL6* and *GSL8* play a role in cell plate formation during mitosis (Hong et al., 2001a; Chen et al., 2009; Saatian et al., 2018). The callose around the plasmodesmata is mainly synthesized by GSL8 and GSL12, while the callose on the phloem sieve tubes is synthesized by GSL7 (Barratt et al., 2011). GSL8 can also regulate the development and formation of leaf stomata by controlling the transport of substances between leaf cells (Guseman et al., 2010). A low-calcium condition induces the expression of *GSL10* gene in leaves that increases callose accumulation and confers plants resist cell death caused by low calcium (Shikanai et al., 2020).

Purified fungal extracts such as chitin and bacterial flagellin peptide can activate the expression and activity of *GSL5* which induces callose accumulation (Luna et al., 2011). Although these inducers can also stimulate the expression of *GSL6* and *GSL11*, so far there is no evidence that these two genes are involved in pathogen-induced callose synthesis. Therefore, callose synthases can be divided into two groups based on their biological functions, the first group including GSL1, 2, 6, 8 and 10, which are mainly responsible for the synthesis of callose during pollen development and cell division; the second group including GSL3, 4, 5, 7 and 12, which are mainly responsible for the synthesis of callose on the cell wall to defend phytopathogen infection. As for the functions of other members such as GSL9 and 11, further studies are required.

3.2 Regulation of callose synthase activity

It was once believed that callose and cellulose were synthesized by the same enzyme, and the final synthesis of callose or cellulose was specifically regulated by calcium concentration or phosphorylation level of the enzyme; further genetics and biochemical studies revealed that the two polysaccharides were biosynthesized by two different enzymes: cellulose synthase and callose synthase (Henrissat and Davies, 2000). Callose synthase protein is synthesized on the endoplasmic reticulum and then transported to the cell membrane through the trans-Golgi apparatus, therefore actin fibers are likely to participate in the distribution of callose synthase in the cell (Han et al., 2019).

Calcium ions (Ca^{2+}) play an important role in regulating callose synthesis in plants (Waldmann et al., 1988). However, merely increasing intracellular calcium is not sufficient to promote callose production. *In vitro* biochemical studies have shown that certain positively charged substances (such as polyamines and chitosan) and amphiphilic molecules (such as digitonin and phospholipids) can increase the activity of callose synthase; while some ion chelators, lanthanum ions and unsaturated fatty acids can inhibit callose synthase (Kauss and Jeblick, 1991). High-throughput proteomics analysis identified phosphorylated GSL5 protein fragment, suggesting that the activity of callose synthase can also be regulated by phosphorylation at post-translational level (Kline et al., 2010). Biochemical experiments showed that the receptor kinase CRK2 (Cys-rich receptor-like kinase) interacts with and phosphorylates GSL6, which leads to increased callose synthesis (Hunter et al., 2019).

4 Diverse role of callose function in plant development and defense

4.1 Callose and plant anther development

Callose plays an important role in the development and maturation of stamens and anthers in plant sexual reproduction. The anther primordia differentiated to form an anther structure with four independent anther cells. Each anther cell is composed of epidermis, fibrous layer, middle layer and tapetum wrapping microsporocyte. Callose begins to synthesize near the tapetum when the microspore mother cell undergoes meiosis. When meiosis is completed, four haploid microspores are isolated by the callose layer, forming a tetrad structure (tetrad). During the maturation process of microspores to pollen, callose is gradually degraded, the anther cell is continuously enlarged, and finally the cell is ruptured to release mature pollen (male gamete). Pollen outer cover pollen wall, including pollen outer wall (exine) and inner wall (intine). The composition and structure of the pollen wall change with the development of the pollen, which plays a protective role in the pollen cytoplasm. As previously mentioned, GSL2 is responsible for the synthesis of callose in the Arabidopsis tapetum and outer pollen wall (Dong et al., 2005; Nishikawa et al., 2005), and the callose in the inner wall is jointly synthesized by GSL1 and GSL5 (Enns et al., 2005). Mutants with loss of *GSL2* gene function cannot form normal pollen exine, resulting in reduced activity of male gametes. GSL8 and GSL10 play a role in the mitosis of microspores. *GSL10* loss-of-function mutants have normal tetrads, but microspore mitosis is disordered and normal pollen cannot be formed, resulting in male sterility and the inability to form homozygotes (Huang et al., 2009). Although the microspores of the *gsl8* mutant have disordered mitosis and a reduced proportion of normal pollen, they can still pollinate and form homozygotes (Töller et al., 2008; Chen et al., 2009). The role of callose in the development of female gametes remains to be studied. Recently, through genetic approach two groups independently reported that *OsGSL5* was responsible for callose deposition in anther locules; *OsGSL5* gene mutation resulted in anthers with less callose deposition, aberrant pollen mother cells and abnormal microspores (Shi et al., 2015; Somashekar et al., 2023). Global transcriptome analysis showed that expression of *OsGSL5* was downregulated in the *Osspl* (*OsSPOROCYTELESS*) mutant which was defective in meiosis-specific callose deposition (Ren et al., 2018). Whereas whether the transcription factor OsSPL directly regulates *OsGSL5* gene expression in rice requires further study, Li et al. reported that the transcription factor GhWRKY15 could bind to and repress *GhCalS4* and *GhCalS8* gene expression in cotton (Li et al., 2020).

4.2 Callose and plasmodesmata conductivity

The plasmodesmata is a unique structure in plant cells. The plasmodesmata run through the cell wall and are special channels for the transport of material and information symplasts between adjacent cells separated by the cell walls. Similar structures in animal cells are gap junctions. The plasmodesmata are tubular structures formed across the cell wall after the endoplasmic reticulum contracts across the cell plate during mitosis in plant cells. The plasmodesmata allow the passage of proteins, mRNAs, small RNAs (miRNA and siRNA) and viral genomes, and plants selectively transport substances by controlling the permeability. Deposition of callose around plasmodesmata is the main mechanism controlling plasmodesmata pore size. Through reverse genetic screening of 12 members of the Arabidopsis callose synthase family, Han et al. found that *GSL8* is responsible for callose synthesis at the plasmodesmata (Han et al., 2014). Reducing the expression of *GSL8* by RNA silencing technology reduces the callose around the plasmodesmata and causes disruption of the selective transport of auxin. In turn, auxin specifically regulates the expression of *GSL8* gene through the transcription factor ARF7 (Figure 2). It is known that auxin can be transported polarly through transport proteins on the cell membrane, but whether auxin is transported directly through plasmodesmata is still unknown. Two independent studies revealed that GSL12 is expressed in the stele and quiescent cells of plant roots and controls root development by regulating the symplast transport of transcription factor SHR and small RNA (miR165) (Vatén et al., 2011; Wu et al., 2016; Yan et al., 2019). It is worth mentioning that transport of small RNAs between plant cells was previously speculated to be through endocytosis and exocytosis; the research on *GSL12* proved directly genetic and cellular evidence that small RNAs can be transported through plasmodesmata.

The sieve pores in the phloem of vascular plants are a special form of plasmodesmata. During the development of the sieve plate, the membrane structure on the plasmodesmata degrades to form the sieve pores. Plants regulate phloem transport by controlling callose deposition around sieve pores. The specific expression of the *GSL7* in vascular tissues is responsible for the deposition of callose in the phloem. *GSL7* loss-of-function mutation leads to the inability of the phloem to transport the carbohydrate nutrients synthesized by leaves (Barratt et al., 2011; Xie et al., 2011).

4.3 Callose and plant defense response

Plant viruses spread in plants mainly through plasmodesmata. Virus-encoded movement proteins (MPs), such as the tobacco mosaic virus MP, can change the permeability of plasmodesmata and transport viral genetic material from one cell to another. The dynamic synthesis of callose at plasmodesmata is the major factor that regulates the pore size of plasmodesmata, therefore the spread of plant viruses is largely controlled by callose synthesis. It was found that the plant defense hormone salicylic acid (SA) can induce the biosynthesis of callose near plasmodesmata by activating the expression of *GSL4* and *GSL6* in Arabidopsis, and reduce the intercellular trafficking and restrict virus spreading (Wang et al., 2013; Cui and Lee, 2016) (Figure 2). Recently, Huang et al. found that plant Remorin protein-dependent plasma membrane/lipid raft

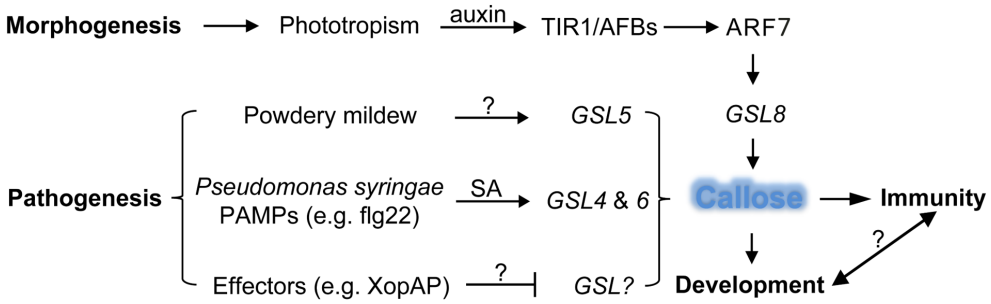

FIGURE 2
Defense and developmental pathways with respective GSLs to regulate callose synthesis in plants. The morphogen-like plant-growth regulator auxin induces *GSL8* expression through the transcriptional activator ARF7 which is released by the TIR1/AFBs auxin co-receptors to increase callose deposition and mediates plant developmental process, whereas pathogen-induced callose deposition through the activity of GSLs leads to enhanced defense response, so far the signaling crosstalk between development- and immunity-regulated callose deposition is unclear. ARF, auxin response factor; GSL, glucan synthase like; PAMP, pathogen associated molecular pattern; SA, salicylic acid; lines with arrow (↑) indicate positive effect and blunt end (T) negative, question marks (?) denote unknown genes or factors.

structures are involved in salicylic acid-induced callose synthesis (Huang et al., 2019).

Plant cell walls are the front line of defense against pests and pathogens (Swaminathan et al., 2022). Bacterial infection of plant leaves causes epidermal cells to synthesize a large amount of callose at the invasion site, and the accumulation of callose thickens the cell wall and becomes a physical barrier against bacterial infection. GSL5 (also named PMR4 for POWDERY MILDEW RESISTANT4) is mainly responsible for the synthesis of callose induced by phytopathogen invasion, so as to strengthen the cell wall of the infected or damaged part by pathogens, increase defense, *GSL5* loss-of-function mutants are unable to synthesize callose at sites of bacterial invasion (Vogel and Somerville, 2000; Jacobs et al., 2003; Nishimura et al., 2003) (Figure 2). The *GSL* gene family was expanded to 23 members in soybean (*Glycine max*); flg22 treatment upregulated the expression of *GmGSL23*, indicating the essential role of this gene and callose synthesis in the soybean defense response (Sangi et al., 2023). As broached above, not only bacterial infection, but also pathogen-associated molecular patterns (Pathogen-associated molecular patterns, PAMPs) treatment can also induce the activity of callose synthases and the accumulation of callose. The plasma membrane of plasmodesmata is characterized by enrichment of sphingolipids. The t18:0-based sphingolipids specifically facilitate the translocation of glycosylphosphatidylinositol-anchored PDLP5 protein to plasmodesmata and increase accumulation of callose, which lead to elevated resistance to the bacterium *Pseudomonas syringae* and the fungal-wilt pathogen *Verticillium dahlia* (Liu et al., 2020). The beneficial rhizobacteria *Bacillus proteolyticus* OSUB18 and *Bacillus cereus* EC9 triggered induced systemic resistance and callose deposition in host plants to protect against pathogens (Pazarlar et al., 2022; Yang et al., 2023). However, pathogen effectors, such as RxRL3 being secreted by the plant-damaging oomycete *Phytophthora brassicae*, SECP8 by citrus Huanglongbing bacterium *Candidatus* Liberibacter asiaticus and XopAP by rice bacterial blight *Xanthomonas oryzae*, could hamper callose formation (Tomczynska et al., 2020; Liu et al., 2022; Shen et al., 2022). The Avr2-Six5 effector pair of *Fusarium oxysporum* increases plasmodesmal size exclusion limit to facilitate intercellular movement of Avr2 by an unknown mechanism independent of callose deposition (Cao et al., 2018; Blekemolen et al., 2022). Interestingly, some plant-associated beneficial microorganisms, such as *Pseudozyma aphidis*, were able to repress MAMP-elicited callose synthesis to overcome the physical barriers of cell walls and penetrated into plant tissues (Alster et al., 2022). Whether those beneficial microorganisms directly secret glucanases or intervene host immune signaling pathway to reduce callose accumulation still need to be further studied, which will help to understand how plant differentiates endophytic and pathogenic colonization. Aphid infection can lead to callose synthesis. Herbivorous aphids penetrate the phloem through their stylets (needle-like mouthparts) to suck plant juice, and plants block the phloem by accumulating callose on the sieve plates (Will et al., 2013; Jaouannet et al., 2014). The *GhCalS5* gene in cotton (*Gossypium hirsutum*) was induced after aphid feeding and was involved in cotton resistance against aphid attack by mediating callose accumulation (Mbiza et al., 2022). Again, a potential effector NlG14 of the brown planthopper *Nilaparvata lugens* could trigger the accumulation of reactive oxygen species and callose to enhance rice response to both insects and microbe pathogens (Gao et al., 2022; Gao et al., 2023). Recently, Huang et al. deployed the CRISPR/Cas9-mediated gene editing approach to mutate a susceptibility gene in rice, which resulted in mutant lines resistant to root-knot nematode with increased reactive oxygen species burst and enhanced callose deposition (Huang et al., 2023). These findings provide more insights into the molecular mechanisms of plant-pathogen interaction and furnish us with potential targets for the manipulation plant immunity.

4.4 The roles of the polysaccharide callose in plant response to metals/metalloids

In addition to biotic stresses like pathogen infection, several abiotic stresses such as heavy metals, could also induce biogenesis of

callose *in planta*. The polysaccharide-based biopolymers, such as cellulose, starch and pectin, were proposed as potential biosorption agents for heavy metal removal and environmental remediation (Zhao et al., 2023). It has not escaped the scenario that the carbohydrate polymer callose plays a role in plant-metal/metalloid interactions. So far, interactions of callose and the heavy metal Aluminum and metalloid Silicon are the most well investigated exemplars, which we described in this section. Aluminum is the most abundant metallic element on Earth, accounting for approximately one-tenth of the solid mass on the Earth's surface. In acidic soils, aluminum ions affect the growth and function of plant roots and are a key factor in slowing plant growth (Ranjan et al., 2021). A growing number of experiments have shown that aluminum treatment leads to callose deposition in plant roots. Through fluorescence staining and electron microscope analysis, it was found that aluminum-induced callose synthesis in wheat roots mainly occurred in plasmodesmata. Further studies revealed that the degree of growth inhibition caused by aluminum was closely related to the decrease in plasmodesmata permeability caused by callose accumulation, which restricts root nutrient and water transport (Bhuja et al., 2004; O'Lexy et al., 2018). Excess heavy metals, such as copper, iron, zinc, and cadmium, inhibit primary root growth by enhancing callose deposition (O'Lexy et al., 2018). Wu et al. found that aluminum-induced accumulation of callose was ameliorated by elevated high pH (Wu et al., 2022a; Wu et al., 2022b). It is still unclear whether heavy metal-induced callose synthesis depends on the phytohormone signaling pathway, and the synthase responsible for aluminum-induced callose synthesis remains to be identified.

Silicon is one of the most abundant elements, accounting for a quarter of the total mass of the crust. Silicon is an essential trace element for the human body, and the silicon element in the human body mainly comes from plant diets. For plants, silicon is not an essential element, and silicon mainly exists in the form of silicon dioxide in plant cell walls (Guerriero et al., 2016). Through the study of the fern *Equisetum arvense*, it was found that plant silicification mainly occurs in callose-rich tissues, such as plant cell walls, cell plates, plasmodesmata (Law and Exley, 2011). *In vitro* biochemical experiments show that in unsaturated $Si(OH)_4$ solution, the addition of callose can cause the accumulation of silica. Using silica and callose-specific fluorescent dye analysis, it was found that the accumulation of silica occurred after callose synthesis (Guerriero et al., 2018). Genetic experiments have shown that knockout of callose synthase *GSL5* in the model plant Arabidopsis leads to loss of callose synthesis, which eventually leads to a decrease in silicon content in leaves (Brugiére and Exley, 2017). Similar findings were found in rice (*Oryza sativa* L.), where transgenic rice constitutively expressing a callose hydrolase induced changes in silicon distribution in leaves by degrading callose (Kido et al., 2015). These evidences indicate that callose in plant cell walls is related to silicification. It was hypothesized that the amorphous callose polysaccharides use the hydroxyl groups of their glucosides as a sponge to adsorb and fix granular silicon into the polysaccharide matrix (Exley, 2015; Guerriero et al., 2016). Interestingly, silicon alleviates aluminum toxicity and root growth-inhibition by reducing callose deposition in the cell walls (Jiang et al., 2022; Xiao et al., 2022). It is unclear whether callose can adsorb other chemical elements, although heavy metal ions strongly induce callose synthesis. The role of the cell wall polysaccharide callose in plant response to metals is an emerging new field that deserves more detailed investigation.

5 Concluding remarks

Callose not only plays an important role in plant development but also participates in plant defense against environmental stresses (Figure 3). Recently, progresses have been made in the biological function and biosynthesis of plant callose. Callose synthesized on the cell wall as a cellular barrier against pathogen invasion has attracted much attention. There are still many questions remained, mainly including the following aspects: Are there other components of the callose synthase complex yet to be discovered? Through which signaling pathway is callose synthesis activated during the defense against pathogen invasion? How plants differentiate endophytic friends and pathogenic foes in way of callose induction? Are callose synthases mainly regulated at the transcriptional or post-transcriptional level? Is there a connection between callose and cellulose synthesis or how are they related in the cellular membrane? How to artificially manipulate callose synthesis activity and the callose content in plants? With the development of research techniques, the answers to these key questions will be revealed.

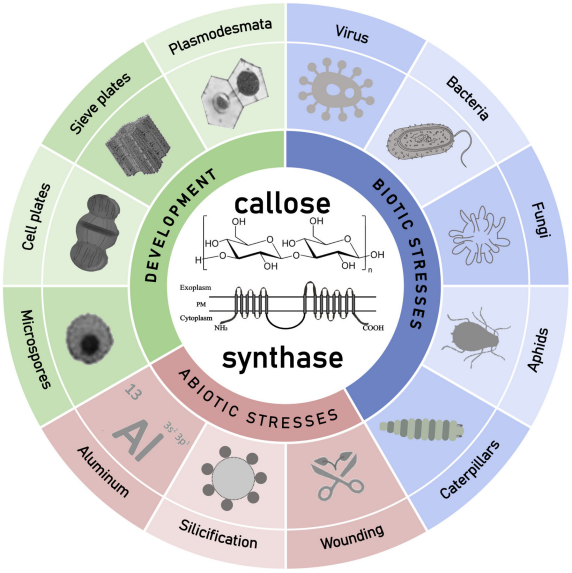

FIGURE 3
Schematic diagram about the described roles of callose and callose synthases in plant development and environment interaction with emphasis on different kind of pathogenesis. GSLs synthesized callose was found to play multiple roles in plant development, and plant response to various abiotic and biotic stresses.

The research on plant callose and its biosynthesis is still in the ascendant and has a very promising prospect.

Author contributions

NL, ZL and L-JH: conceptualization. NL and ZL: literature review. NL and ZL: writing—original preparation. NL, YZ and SD: writing—review and editing. NL, PY, YZ and L-JH: design and revision of the images. All authors contributed to the article and approved the submitted version.

Funding

This work was supported by Training Program for Excellent Young Innovators of Changsha (kq2009016), National Natural Science Foundation of China (31901345), Natural Science Foundation of Hunan Province (2021JJ31141 and 2020JJ5970), the Education Department of Hunan Province (20A517 and 22B0260), and Postgraduate Scientific Research Innovation Project (CX20210885).

Conflict of interest

The authors declare that the research was conducted in the absence of any commercial or financial relationships that could be construed as a potential conflict of interest.

Publisher's note

References

Albrecht, G., and Mustroph, A. (2003). Sucrose utilization via invertase and sucrose synthase with respect to accumulation of cellulose and callose synthesis in wheat roots under oxygen deficiency. *Russian J. Plant Physiol.* 50, 813–820. doi: 10.1023/B:RUPP.0000003280.10924.03

Alster, S., Dafa-Berger, A., Gafni, A., and Levy, M. (2022). Pseudozyma aphidis suppresses microbe-associated molecular pattern (MAMP)-triggered callose deposition and can penetrate leaf tissue. *Microbiol. Spectr.* 10, e0263821. doi: 10.1128/spectrum.02638-21

Aspinall, G. O., and Kessler, G. (1957). The structure of callose from the grape vine. *Chem. Industry*, 1296.

Barratt, D. H. P., Kölling, K., Graf, A., Pike, M., Calder, G., Findlay, K., et al. (2011). Callose synthase GSL7 is necessary for normal phloem transport and inflorescence growth in arabidopsis. *Plant Physiol.* 155, 328–341. doi: 10.1104/pp.110.166330

Bhuja, P., McLachlan, K., Stephens, J., and Taylor, G. (2004). Accumulation of 1,3-beta-D-glucans, in response to aluminum and cytosolic calcium in triticum aestivum. *Plant Cell Physiol.* 45, 543–549. doi: 10.1093/pcp/pch068

Blekemolen, M. C., Cao, L., Tintor, N., de Groot, T., Papp, D., Faulkner, C., et al. (2022). The primary function of Six5 of fusarium oxysporum is to facilitate Avr2 activity by together manipulating the size exclusion limit of plasmodesmata. *Front. Plant Sci.* 13. doi: 10.3389/fpls.2022.910594

Brugiére, T., and Exley, C. (2017). Callose-associated silica deposition in arabidopsis. *J. Trace Elements Med. Biol.* 39, 86–90. doi: 10.1016/j.jtemb.2016.08.005

Cao, L., Blekemolen, M. C., Tintor, N., Cornelissen, B. J. C., and Takken, F. L. W. (2018). The fusarium oxysporum Avr2-Six5 effector pair alters plasmodesmatal exclusion selectivity to facilitate cell-to-Cell movement of Avr2. *Mol. Plant* 11, 691–705. doi: 10.1016/j.molp.2018.02.011

Chen, X.-Y., and Kim, J.-Y. (2009). Callose synthesis in higher plants. *Plant Signaling Behav.* 4, 489–492. doi: 10.4161/psb.4.6.8359

Chen, X.-Y., Liu, L., Lee, E., Han, X., Rim, Y., Chu, H., et al. (2009). The arabidopsis callose synthase gene GSL8 is required for cytokinesis and cell patterning. *Plant Physiol.* 150, 105–113. doi: 10.1104/pp.108.133918

Cui, W., and Lee, J.-Y. (2016). Arabidopsis callose synthases CalS1/8 regulate plasmodesmal permeability during stress. *Nat. Plants* 2, 16034. doi: 10.1038/nplants.2016.34

Dong, X., Hong, Z., Sivaramakrishnan, M., Mahfouz, M., and Verma, D. P. S. (2005). Callose synthase (CalS5) is required for exine formation during microgametogenesis and for pollen viability in arabidopsis. *Plant J.: For. Cell Mol. Biol.* 42, 315–328. doi: 10.1111/j.1365-313X.2005.02379.x

Ellinger, D., Glöckner, A., Koch, J., Naumann, M., Stürtz, V., Schütt, K., et al. (2014). Interaction of the arabidopsis GTPase RabA4c with its effector PMR4 results in complete penetration resistance to powdery mildew. *Plant Cell* 26, 3185–3200. doi: 10.1105/tpc.114.127779

Ellinger, D., and Voigt, C. A. (2014). Callose biosynthesis in arabidopsis with a focus on pathogen response: what we have learned within the last decade. *Ann. Bot.* 114, 1349–1358. doi: 10.1093/aob/mcu120

Enns, L. C., Kanaoka, M. M., Torii, K. U., Comai, L., Okada, K., and Cleland, R. E. (2005). Two callose synthases, GSL1 and GSL5, play an essential and redundant role in plant and pollen development and in fertility. *Plant Mol. Biol.* 58, 333–349. doi: 10.1007/s11103-005-4526-7

Exley, C. (2015). A possible mechanism of biological silicification in plants. *Front. Plant Sci.* 6. doi: 10.3389/fpls.2015.00853

Gao, H., Zhang, H., Yuan, X., Lin, X., Zou, J., Yu, N., et al. (2023). Knockdown of the salivary protein gene NlG14 caused displacement of the lateral oviduct secreted components and inhibited ovulation in nilaparvata lugens. *PloS Genet.* 19, e1010704. doi: 10.1371/journal.pgen.1010704

Gao, H., Zou, J., Lin, X., Zhang, H., Yu, N., and Liu, Z. (2022). Nilaparvata lugens salivary protein NlG14 triggers defense response in plants. *J. Exp. Bot.* 73, 7477–7487. doi: 10.1093/jxb/erac354

Guerriero, G., Hausman, J.-F., and Legay, S. (2016). Silicon and the plant extracellular matrix. *Front. Plant Sci.* 7. doi: 10.3389/fpls.2016.00463

Guerriero, G., Stokes, I., and Exley, C. (2018). Is callose required for silicification in plants? *Biol. Lett.* 14, 20180338. doi: 10.1098/rsbl.2018.0338

Guseman, J. M., Lee, J. S., Bogenschutz, N. L., Peterson, K. M., Virata, R. E., Xie, B., et al. (2010). Dysregulation of cell-to-cell connectivity and stomatal patterning by loss-of-function mutation in arabidopsis chorus (glucan synthase-like 8). *Dev. (Cambridge England)* 137, 1731–1741. doi: 10.1242/dev.049197

Han, X., Huang, L.-J., Feng, D., Jiang, W., Miu, W., and Li, N. (2019). Plasmodesmata-related structural and functional proteins: the long sought-after secrets of a cytoplasmic channel in plant cell walls. *Int. J. Mol. Sci.* 20, 2946. doi: 10.3390/ijms20122946

Han, X., Hyun, T. K., Zhang, M., Kumar, R., Koh, E., Kang, B.-H., et al. (2014). Auxin-callose-mediated plasmodesmal gating is essential for tropic auxin gradient formation and signaling. *Dev. Cell* 28, 132–146. doi: 10.1016/j.devcel.2013.12.008

Henrissat, B., and Davies, G. J. (2000). Glycoside hydrolases and glycosyltransferases. families, modules, and implications for genomics. *Plant Physiol.* 124, 1515–1519. doi: 10.1104/pp.124.4.1515

Hong, Z., Delauney, A. J., and Verma, D. P. (2001a). A cell plate-specific callose synthase and its interaction with phragmoplastin. *Plant Cell* 13, 755–768. doi: 10.1105/tpc.13.4.755

Hong, Z., Zhang, Z., Olson, J. M., and Verma, D. P. (2001b). A novel UDP-glucose transferase is part of the callose synthase complex and interacts with phragmoplastin at the forming cell plate. *Plant Cell* 13, 769–779. doi: 10.1105/tpc.13.4.769

Huang, L., Chen, X.-Y., Rim, Y., Han, X., Cho, W. K., Kim, S.-W., et al. (2009). Arabidopsis glucan synthase-like 10 functions in male gametogenesis. *J. Plant Physiol.* 166, 344–352. doi: 10.1016/j.jplph.2008.06.010

Huang, Q., Lin, B., Cao, Y., Zhang, Y., Song, H., Huang, C., et al. (2023). CRISPR/Cas9-mediated mutagenesis of the susceptibility gene OsHPP04 in rice confers enhanced resistance to rice root-knot nematode. *Front. Plant Sci.* 14. doi: 10.3389/fpls.2023.1134653

Huang, D., Sun, Y., Ma, Z., Ke, M., Cui, Y., Chen, Z., et al. (2019). Salicylic acid-mediated plasmodesmal closure via remorin-dependent lipid organization. *Proc. Natl. Acad. Sci. United States America* 116, 21274–21284. doi: 10.1073/pnas.1911892116

Huang, H., Wang, Z., Cheng, J., Zhao, W., Li, X., Wang, H., et al. (2013). An efficient cucumber (Cucumis sativus l.) protoplast isolation and transient expression system. *Sci. Hortic.* 150, 206–212. doi: 10.1016/j.scienta.2012.11.011

Hunter, K., Kimura, S., Rokka, A., Tran, H. C., Toyota, M., Kukkonen, J. P., et al. (2019). CRK2 enhances salt tolerance by regulating callose deposition in connection with PLDα1. *Plant Physiol.* 180, 2004–2021. doi: 10.1104/pp.19.00560

Jacobs, A. K., Lipka, V., Burton, R. A., Panstruga, R., Strizhov, N., Schulze-Lefert, P., et al. (2003). An arabidopsis callose synthase, GSL5, is required for wound and papillary callose formation. *Plant Cell* 15, 2503–2513. doi: 10.1105/tpc.016097

Jaouannet, M., Rodriguez, P. A., Thorpe, P., Lenoir, C. J. G., MacLeod, R., Escudero-Martinez, C., et al. (2014). Plant immunity in plant-aphid interactions. *Front. Plant Sci.* 5. doi: 10.3389/fpls.2014.00663

Jiang, D., Wu, H., Cai, H., and Chen, G. (2022). Silicon confers aluminium tolerance in rice via cell wall modification in the root transition zone. *Plant Cell Environ.* 45, 1765–1778. doi: 10.1111/pce.14307

Kauss, H. (1996). Callose synthesis. membranes: specialized functions in plants. *Bios. Sci. Publ. Guildford UK*, 77–92.

Kauss, H., and Jeblick, W. (1991). Induced Ca2+ uptake and callose synthesis in suspension-cultured cells of catharanthus roseus are decreased by the protein phosphatase inhibitor okadaic acid. *Physiol. Plantarum* 81, 309–312. doi: 10.1111/j.1399-3054.1991.tb08737.x

Keppler, B. D., Song, J., Nyman, J., Voigt, C. A., and Bent, A. F. (2018). 3-aminobenzamide blocks MAMP-induced callose deposition independently of its Poly (ADPribosyl)ation inhibiting activity. *Front. Plant Sci.* 9. doi: 10.3389/fpls.2018.01907

Kido, N., Yokoyama, R., Yamamoto, T., Furukawa, J., Iwai, H., Satoh, S., et al. (2015). The matrix polysaccharide (1;3,1;4)-β-D-Glucan is involved in silicon-dependent strengthening of rice cell wall. *Plant Cell Physiol.* 56, 1679. doi: 10.1093/pcp/pcv099

Kline, K. G., Barrett-Wilt, G. A., and Sussman, M. R. (2010). In planta changes in protein phosphorylation induced by the plant hormone abscisic acid. *Proc. Natl. Acad. Sci. United States America* 107, 15986–15991. doi: 10.1073/pnas.1007879107

Law, C., and Exley, C. (2011). New insight into silica deposition in horsetail (Equisetum arvense). *BMC Plant Biol.* 11, 112. doi: 10.1186/1471-2229-11-112

Li, Y., Li, L., Wang, Y., Wang, Y.-C., Wang, N.-N., Lu, R., et al. (2020). Pollen-specific protein PSP231 activates callose synthesis to govern Male gametogenesis and pollen germination. *Plant Physiol.* 184, 1024–1041. doi: 10.1104/pp.20.00297

Liu, L., Li, Y., Xu, Z., Chen, H., Zhang, J., Manion, B., et al. (2022). The xanthomonas type III effector XopAP prevents stomatal closure by interfering with vacuolar acidification. *J. Integr. Plant Biol.* 64, 1994–2008. doi: 10.1111/jipb.13344

Liu, X.-Q., Liu, Z.-Q., Yu, C.-Y., Dong, J.-G., Hu, S.-W., and Xu, A.-X. (2017). TGMS in rapeseed (Brassica napus) resulted in aberrant transcriptional regulation, asynchronous microsporocyte meiosis, defective tapetum, and fused sexine. *Front. Plant Sci.* 8. doi: 10.3389/fpls.2017.01268

Liu, N.-J., Zhang, T., Liu, Z.-H., Chen, X., Guo, H.-S., Ju, B.-H., et al. (2020). Phytosphinganine affects plasmodesmata permeability via facilitating PDLP5-stimulated callose accumulation in arabidopsis. *Mol. Plant* 13, 128–143. doi: 10.1016/j.molp.2019.10.013

Liu, F., Zou, Z., and Fernando, W. G. D. (2018). Characterization of callose deposition and analysis of the callose synthase gene family of brassica napus in response to leptosphaeria maculans. *Int. J. Mol. Sci.* 19, 3769. doi: 10.3390/ijms19123769

Luna, E., Pastor, V., Robert, J., Flors, V., Mauch-Mani, B., and Ton, J. (2011). Callose deposition: a multifaceted plant defense response. *Mol. Plant-Microbe Interactions: MPMI* 24, 183–193. doi: 10.1094/MPMI-07-10-0149

Mbiza, N. I. T., Hu, Z., Zhang, H., Zhang, Y., Luo, X., Wang, Y., et al. (2022). GhCalS5 is involved in cotton response to aphid attack through mediating callose formation. *Front. Plant Sci.* 13. doi: 10.3389/fpls.2022.892630

Meikle, P. J., Bonig, I., Hoogenraad, N. J., Clarke, A. E., and Stone, B. A. (1991). The location of (1→3)-β-glucans in the walls of pollen tubes of nicotiana alata using a (1→3)-β-glucan-specific monoclonal antibody. *Planta* 185, 1–8. doi: 10.1007/BF00194507

Nishikawa, S., Zinkl, G. M., Swanson, R. J., Maruyama, D., and Preuss, D. (2005). Callose (beta-1,3 glucan) is essential for arabidopsis pollen wall patterning, but not tube growth. *BMC Plant Biol.* 5, 22. doi: 10.1186/1471-2229-5-22

Nishimura, M. T., Stein, M., Hou, B.-H., Vogel, J. P., Edwards, H., and Somerville, S. C. (2003). Loss of a callose synthase results in salicylic acid-dependent disease resistance. *Sci. (New York N.Y.)* 301, 969–972. doi: 10.1126/science.1086716

O'Lexy, R., Kasai, K., Clark, N., Fujiwara, T., Sozzani, R., and Gallagher, K. L. (2018). Exposure to heavy metal stress triggers changes in plasmodesmatal permeability via deposition and breakdown of callose. *J. Exp. Bot.* 69, 3715–3728. doi: 10.1093/jxb/ery171

Pazarlar, S., Madriz-Ordeñana, K., and Thordal-Christensen, H. (2022). Bacillus cereus EC9 protects tomato against fusarium wilt through JA/ET-activated immunity. *Front. Plant Sci.* 13. doi: 10.3389/fpls.2022.1090947

Ranjan, A., Sinha, R., Lal, S. K., Bishi, S. K., and Singh, A. K. (2021). Phytohormone signalling and cross-talk to alleviate aluminium toxicity in plants. *Plant Cell Rep.* 40, 1331–1343. doi: 10.1007/s00299-021-02724-2

Ren, L., Tang, D., Zhao, T., Zhang, F., Liu, C., Xue, Z., et al. (2018). OsSPL regulates meiotic fate acquisition in rice. *New Phytol.* 218, 789–803. doi: 10.1111/nph.15017

Saatian, B., Austin, R. S., Tian, G., Chen, C., Nguyen, V., Kohalmi, S. E., et al. (2018). Analysis of a novel mutant allele of GSL8 reveals its key roles in cytokinesis and symplastic trafficking in arabidopsis. *BMC Plant Biol.* 18, 295. doi: 10.1186/s12870-018-1515-y

Sangi, S., Olimpio, G. V., Coelho, F. S., Alexandrino, C. R., Da Cunha, M., and Grativol, C. (2023). Flagellin and mannitol modulate callose biosynthesis and deposition in soybean seedlings. *Physiol. Plantarum*, e13877. doi: 10.1111/ppl.13877

Shen, P., Li, X., Fu, S., Zhou, C., and Wang, X. (2022). A "Candidatus liberibacter asiaticus"-secreted polypeptide suppresses plant immune responses in nicotiana benthamiana and citrus sinensis. *Front. Plant Sci.* 13. doi: 10.3389/fpls.2022.997825

Shi, X., Sun, X., Zhang, Z., Feng, D., Zhang, Q., Han, L., et al. (2015). GLUCAN SYNTHASE-LIKE 5 (GSL5) plays an essential role in male fertility by regulating callose metabolism during microsporogenesis in rice. *Plant Cell Physiol.* 56, 497–509. doi: 10.1093/pcp/pcu193

Shikanai, Y., Yoshida, R., Hirano, T., Enomoto, Y., Li, B., Asada, M., et al. (2020). Callose synthesis suppresses cell death induced by low-calcium conditions in leaves. *Plant Physiol.* 182, 2199–2212. doi: 10.1104/pp.19.00784

Singh, R. K., Maurya, J. P., Azeez, A., Miskolczi, P., Tylewicz, S., Stojkovič, K., et al. (2018). A genetic network mediating the control of bud break in hybrid aspen. *Nat. Commun.* 9, 4173. doi: 10.1038/s41467-018-06696-y

Singh, R. K., Miskolczi, P., Maurya, J. P., and Bhalerao, R. P. (2019). A tree ortholog of SHORT VEGETATIVE PHASE floral repressor mediates photoperiodic control of bud dormancy. *Curr. Biol.: CB* 29, 128–133.e2. doi: 10.1016/j.cub.2018.11.006

Somashekar, H., Mimura, M., Tsuda, K., and Nonomura, K.-I. (2023). Rice GLUCAN SYNTHASE-LIKE5 promotes anther callose deposition to maintain meiosis initiation and progression. *Plant Physiol.* 191, 400–413. doi: 10.1093/plphys/kiac488

Swaminathan, S., Lionetti, V., and Zabotina, O. A. (2022). Plant cell wall integrity perturbations and priming for defense. *Plants (Basel Switzerland)* 11, 3539. doi: 10.3390/plants11243539

Töller, A., Brownfield, L., Neu, C., Twell, D., and Schulze-Lefert, P. (2008). Dual function of arabidopsis glucan synthase-like genes GSL8 and GSL10 in male gametophyte development and plant growth. *Plant J.: For. Cell Mol. Biol.* 54, 911–923. doi: 10.1111/j.1365-313X.2008.03462.x

Tomczynska, I., Stumpe, M., Doan, T. G., and Mauch, F. (2020). A phytophthora effector protein promotes symplastic cell-to-cell trafficking by physical interaction with plasmodesmata-localised callose synthases. *New Phytol.* 227, 1467–1478. doi: 10.1111/nph.16653

Tylewicz, S., Petterle, A., Marttila, S., Miskolczi, P., Azeez, A., Singh, R. K., et al. (2018). Photoperiodic control of seasonal growth is mediated by ABA acting on cell-cell communication. *Sci. (New York N.Y.)* 360, 212–215. doi: 10.1126/science.aan8576

Vatén, A., Dettmer, J., Wu, S., Stierhof, Y.-D., Miyashima, S., Yadav, S. R., et al. (2011). Callose biosynthesis regulates symplastic trafficking during root development. *Dev. Cell* 21, 1144–1155. doi: 10.1016/j.devcel.2011.10.006

Verma, D. P., and Hong, Z. (2001). Plant callose synthase complexes. *Plant Mol. Biol.* 47, 693–701. doi: 10.1023/a:1013679111111

Vogel, J., and Somerville, S. (2000). Isolation and characterization of powdery mildew-resistant arabidopsis mutants. *Proc. Natl. Acad. Sci. United States America* 97, 1897–1902. doi: 10.1073/pnas.030531997

Vu, M. H., Hyun, T. K., Bahk, S., Jo, Y., Kumar, R., Thiruppathi, D., et al. (2022). ROS-mediated plasmodesmal regulation requires a network of an arabidopsis receptor-like kinase, calmodulin-like proteins, and callose synthases. *Front. Plant Sci.* 13. doi: 10.3389/fpls.2022.1107224

Waldmann, T., Jeblick, W., and Kauss, H. (1988). Induced net Ca(2+) uptake and callose biosynthesis in suspension-cultured plant cells. *Planta* 173, 88–95. doi: 10.1007/BF00394492

Wang, X., Sager, R., Cui, W., Zhang, C., Lu, H., and Lee, J.-Y. (2013). Salicylic acid regulates plasmodesmata closure during innate immune responses in arabidopsis. *Plant Cell* 25, 2315–2329. doi: 10.1105/tpc.113.110676

Will, T., Furch, A. C. U., and Zimmermann, M. R. (2013). How phloem-feeding insects face the challenge of phloem-located defenses. *Front. Plant Sci.* 4. doi: 10.3389/fpls.2013.00336

Wu, B.-S., Lai, Y.-H., Peng, M.-Y., Ren, Q.-Q., Lai, N.-W., Wu, J., et al. (2022a). Elevated pH-mediated mitigation of aluminum-toxicity in sweet orange (Citrus sinensis) roots involved the regulation of energy-rich compounds and phytohormones. *Environ. pollut. (Barking Essex: 1987)* 311, 119982. doi: 10.1016/j.envpol.2022.119982

Wu, S., O'Lexy, R., Xu, M., Sang, Y., Chen, X., Yu, Q., et al. (2016). Symplastic signaling instructs cell division, cell expansion, and cell polarity in the ground tissue of arabidopsis thaliana roots. *Proc. Natl. Acad. Sci. United States America* 113, 11621–11626. doi: 10.1073/pnas.1610358113

Wu, B.-S., Zhang, J., Huang, W.-L., Yang, L.-T., Huang, Z.-R., Guo, J., et al. (2022b). Molecular mechanisms for pH-mediated amelioration of aluminum-toxicity revealed by conjoint analysis of transcriptome and metabolome in citrus sinensis roots. *Chemosphere* 299, 134335. doi: 10.1016/j.chemosphere.2022.134335

Wu, J., Zhang, Y., Wang, L., Xie, B., Wang, H., and Deng, S. (2006). Visualization of single and aggregated hulless oat (Avena nuda l.) (1–>3),(1–>4)-beta-D-glucan

molecules by atomic force microscopy and confocal scanning laser microscopy. *J. Agric. Food Chem.* 54, 925–934. doi: 10.1021/jf0523059

Xiao, Z., Ye, M., Gao, Z., Jiang, Y., Zhang, X., Nikolic, N., et al. (2022). Silicon reduces aluminum-induced suberization by inhibiting the uptake and transport of aluminum in rice roots and consequently promotes root growth. *Plant Cell Physiol.* 63, 340–352. doi: 10.1093/pcp/pcac001

Xie, B., Wang, X., Zhu, M., Zhang, Z., and Hong, Z. (2011). CalS7 encodes a callose synthase responsible for callose deposition in the phloem. *Plant J.: For. Cell Mol. Biol.* 65, 1–14. doi: 10.1111/j.1365-313X.2010.04399.x

Yan, D., Yadav, S. R., Paterlini, A., Nicolas, W. J., Petit, J. D., Brocard, L., et al. (2019). Sphingolipid biosynthesis modulates plasmodesmal ultrastructure and phloem unloading. *Nat. Plants* 5, 604–615. doi: 10.1038/s41477-019-0429-5

Yang, P., Zhao, Z., Fan, J., Liang, Y., Bernier, M. C., Gao, Y., et al. (2023). Bacillus proteolyticus OSUB18 triggers induced systemic resistance against bacterial and fungal pathogens in arabidopsis. *Front. Plant Sci.* 14. doi: 10.3389/fpls.2023.1078100

Yi, G., Wu, W., and Wei, T. (2021). Delivery of rice gall dwarf virus into plant phloem by its leafhopper vectors activates callose deposition to enhance viral transmission. *Front. Microbiol.* 12. doi: 10.3389/fmicb.2021.662577

Zhang, C., Shen, Y., Tang, D., Shi, W., Zhang, D., Du, G., et al. (2018). The zinc finger protein DCM1 is required for male meiotic cytokinesis by preserving callose in rice. *PloS Genet.* 14, e1007769. doi: 10.1371/journal.pgen.1007769

Zhao, C., Liu, G., Tan, Q., Gao, M., Chen, G., Huang, X., et al. (2023). Polysaccharide-based biopolymer hydrogels for heavy metal detection and adsorption. *J. Adv. Res.* 44, 53–70. doi: 10.1016/j.jare.2022.04.005

frontiers | Frontiers in Plant Science

TYPE Original Research
PUBLISHED 07 June 2023
DOI 10.3389/fpls.2023.1089011

OPEN ACCESS

EDITED BY
Vincenzo Lionetti,
Sapienza University of Rome, Italy

REVIEWED BY
Ehsan Bari,
Technical and Vocational University, Iran
Lisbeth Garbrecht Thygesen,
University of Copenhagen, Denmark

*CORRESPONDENCE
Arthur J. Ragauskas
aragausk@utk.edu

RECEIVED 03 November 2022
ACCEPTED 18 May 2023
PUBLISHED 07 June 2023

CITATION
Bryant N, Muchero W, Weber RA, Barros J, Chen J-G, Tschaplinski TJ, Pu Y and Ragauskas AJ (2023) Cell wall response of field grown *Populus* to *Septoria* infection. *Front. Plant Sci.* 14:1089011. doi: 10.3389/fpls.2023.1089011

Cell wall response of field grown *Populus* to *Septoria* infection

Nathan Bryant[1], Wellington Muchero[2,3], Rachel A. Weber[4], Jaime Barros[4], Jin-Gui Chen[2,3], Timothy J. Tschaplinski[2,3], Yunqiao Pu[2,3] and Arthur J. Ragauskas[1,2,3,5,6]*

[1]Department of Chemical and Biomolecular Engineering, University of Tennessee, Knoxville, TN, United States, [2]BioEnergy Science Center & Center for Bioenergy Innovation, Oak Ridge National Laboratory, Oak Ridge, TN, United States, [3]Biosciences Division, Oak Ridge National Laboratory, Oak Ridge, TN, United States, [4]Division of Plant Sciences and Interdisciplinary Plant Group, University of Missouri, Columbia, MO, United States, [5]Department of Chemical and Biomolecular Engineering, University of Tennessee, Center for Renewable Carbon, Knoxville, TN, United States, [6]Department of Forestry, Wildlife, and Fisheries, University of Tennessee Institute of Agriculture, Knoxville, TN, United States

Due to its ability to spread quickly and result in tree mortality, *Sphaerulina musiva (Septoria)* is one of the most severe diseases impacting *Populus*. Previous studies have identified that *Septoria* infection induces differential expression of phenylpropanoid biosynthesis genes. However, more extensive characterization of changes to lignin in response to *Septoria* infection is lacking. To study the changes of lignin due to *Septoria* infection, four field grown, naturally variant *Populus trichocarpa* exhibiting visible signs of *Septoria* infection were sampled at health, infected, and reaction zone regions for cell wall characterization. Fourier transform infrared spectroscopy (FTIR), nuclear magnetic resonance (NMR), and acid hydrolysis were applied to identify changes to the cell wall, and especially lignin. FTIR and subsequent principal component analysis revealed that infected and reaction zone regions were similar and could be distinguished from the non-infected (healthy) region. NMR results indicated the general trend that infected region had a higher syringyl:guaiacyl ratio and lower *p*-hydroxybenzoate content than the healthy regions from the same genotype. Finally, Klason lignin content in the infected and/or reaction zone regions was shown to be higher than healthy region, which is consistent with previous observations of periderm development and metabolite profiling. These results provide insights on the response of *Populus* wood characteristics to *Septoria* infection, especially between healthy and infected region within the same genotype.

KEYWORDS

***Septoria*, lignin, NMR, FTIR, PCA**

1 Introduction

Populus has garnered interest as an economically important species for applications such as biofuel production due to its rapid growth, genetic diversity, and other advantageous attributes (Sannigrahi et al., 2010). One of the most critical drivers of biofuels' economic feasibility is biomass yield (Chudy et al., 2019). Challenges to poplar growth productivity include susceptibility to fungal infections from pathogens such as *Sphaerulina musiva*, also known as *Septoria* (Feau et al., 2010). *Septoria* is particularly devastating due to its potential to be fatal to the tree and its ability to spread quickly among entire populations. Indeed, *Septoria* is considered one of the most severe diseases impacting hybrid poplar (Royle & Ostry, 1995). The two symptoms typically associated with *Septoria* infection are leaf spots and stem cankers (Cellerino, 1999). Leaf spots have a significant negative effect on photosynthesis and can lead to defoliation. Stem canker can cause broken tops, leading to severe growth penalties or death (Ostry and Mcnabb 1985; Ostry et al., 1989).

The secondary cell wall plays a role in many processes, including response to biotic and abiotic stress. It has been shown that lignin, a complex biopolymer that typically constitutes between 16 to 29% of *Populus* secondary cell walls (Bryant et al., 2020), is often synthesized and deposited at the site of fungal infections to form a periderm that prevents the spread of the pathogen. This result is consistent with previous studies of *Septoria* infection of *Populus*, with increased lignin deposition observed at the infection site. Previous transcriptome analyses of *Septoria* and other fungal infections have also identified differentially expressed genes in the phenylpropanoid and lignin biosynthesis pathway (Foster et al., 2015; Muchero et al., 2018). However, lignin content and/or structure are rarely reported in these types of studies. Additionally, these studies have evaluated response shortly after inoculation, and there is no information on the long-term effects of *Septoria* canker response in field-grown poplar. For instance, Bucciarelli et al. documented the differences in Klason lignin content and S/G ratio between susceptible and resistant *P. tremuloides* genotypes in response to *Entoleuca mammata* infection, but within 96 hrs of inoculation (Bucciarelli et al., 1998). To this effect, an exploratory study of four distinct field-grown *Populus* genotypes exhibiting signs of canker growth was conducted to determine if changes in lignin content and/or composition induced by *Septoria* infection could be elucidated. Healthy and infected region from each genotype was analyzed for Klason lignin content and composition by HSQC NMR. Additionally, whole-cell biomass was analyzed by FTIR.

2 Materials and methods

2.1 Sampling and preparation

Three-year-old *Populus trichocarpa* genotypes were sampled from a field site in Boardman, OR. The study was established in July 2016 using naturally varying genotypes from the *P. trichocarpa* genome-wide association mapping panel (Muchero et al., 2018). Samples of tree stems were taken at 20-30 cm above the soil line the form of approximately 2.5cm thick discs after 3 growing seasons in November 2018. Two hundred fifty-four out of 1,054 trees from this field site were observed to have stem and branch cankers in late summer 2018 – several months before the November 2018 harvest (Søndreli et al., 2020). Wood discs were oven-dried at 70°C for 14 days to remove moisture and prevent dry matter loss due to microbial activity. Five wood discs with noticeable signs of *Septoria* infection were selected for analysis. Two healthy discs were also selected for comparison. *Septoria* infection was previously verified at this field site using visual characterization as well as by isolation and sequencing of *S. musiva* isolates as described by Søndreli et al.(Søndreli et al., 2020). Briefly, wood from the margin between healthy and necrotic region was obtained from samples visually observed exhibiting stem canker. Region was plated on KV8 medium amended with streptomycin sulfate and chloramphenicol at 100 mg/L and 240 mg/L, respectively. The presence of *S. musiva* was confirmed by comparing the sequence of the ITS region (accession MN275180 to MN275187) to JX901814 with 99% identify. *S. musiva* infection results in a characteristic sunken stem canker that eventually leads to stem breakage. Diseased samples were selected on the basis of the severity of the infection which evident by discolorized wood.

Woody biomass for analysis was obtained by drilling the discs with a 13mm spade drill bit and collecting the wood shavings. Each disc was drilled at three locations: (1)in the healthy region of the sapwood to capture xylem with no signs of infection; (2) in the discolored *Septoria* infected region; and (3)along the reaction zone between the infected region and healthy xylem, herein referred to as the reaction zone. Each drilling location was selected to be a consistent distance from the pith to avoid the effects of radial variation. Drilling for sample material was done between the pith and the bark. The drill was cleaned between each use to mitigate cross-contamination. Each sample was Wiley-milled using a 40-mesh screen, and the mill was cleaned between each use. Milled wood samples were Soxhlet extracted with toluene/ethanol (2:1, v:v) overnight to remove extractives and then air-dried in a fume hood for at least 48 h. Extractives-free biomass was used in all further analyses.

2.2 Fourier-transform infrared spectroscopy

Extracted biomass was analyzed by FTIR *via* a Perkin Elmer Spectrum 100 FTIR spectrometer with a universal attenuated total reflection (ATR) accessory and collected *via* Spectrum software. A background scan was performed prior to sample analysis. Extracted samples were analyzed from 4,000-600 cm^{-1} with a resolution of 2 cm^{-1} and 32-scan accumulation. Each sample was analyzed in triplicate, and the three spectra were averaged for further analysis. The resulting spectra were subsequently processed and analyzed with OriginPro software. All spectra were baseline corrected manually using twelve anchor points and normalized around the 1505 cm^{-1} peak. PCA

modeling was performed within the OriginPro software environment using spectral data in the fingerprint region of 1800-600 cm^{-1}.

2.3 Heteronuclear single quantum coherence nuclear magnetic resonance spectroscopy

To prepare samples for HSQC analysis, extracted biomass was ball milled at 600 RPM for 2 hours to obtain a fine powder. Each sample was then combined with cellulase (Cellulysin) in an acetate buffer (pH 5.0) and shaken on an incubator shake at 35°C for 48h. After centrifugation, the supernatant was discarded, and the solid residue was recovered and washed with DI water three times. The solid residue was then lyophilized for at least 48h to produce enzyme lignin (EL). EL was dissolved in DMSO-d_6 in a 5mm NMR tube, sonicated for 1h, and allowed to swell overnight before analysis. For whole cell wall (WCW) analysis of BESC-335, powdered material was transferred to a 5mm NMR tube for direct dissolution with DMSO-d_6/HMPA-d_{18} (4:1). All NMR spectral data were recorded using a Bruker Avance III HD 500 MHz spectrometer. A standard hsqcetgpsip2.2 Bruker pulse sequence was used with an N_2 cryoprobe with the following specifications: ^1H spectra width of 12 ppm and 1024 data points; ^{13}C spectra width of 220 ppm with 256 increments and 32 scans. All HSQC spectra were analyzed with Bruker TopSpin 3.5pl6 software. The DMSO-d_6 solvent peak at δ_C/δ_H 39.5/2.49 was used to calibrate the spectra.

2.4 Klason lignin analysis

The Klason lignin content of each sample was determined based on modified NREL established procedures (Sluiter et al., 2008). Briefly, extracted biomass was first dried overnight at 45C in a vacuum oven. The first hydrolysis was performed with 78% sulfuric in a 30°C block heater for 1 hour with mixing every 5-10 minutes. For the second hydrolysis, the mixture was diluted to 4% sulfuric acid by adding DI water and then autoclaved at 121°C for 1 hour. The acid insoluble residue (AIR) and filtrate were separated by vacuum filtration. The AIR was dried at 105°C overnight and weighed for Klason lignin determination.

2.5 Lignin composition analysis by GC/MS

Thioacidolysis was performed on EL residues that were recovered from HSQC NMR analysis. The EL residues recovered from the NMR tube by precipitation through the addition of DI water, centrifugation, and decanting the DMSO-d_6/DIW supernatant. The recovered EL was then lyophilized for 48h. Thioacidolysis was then performed to determine the lignin monomer composition using gas chromatography mass spectrometry (GC/MS), as previously described (Barros et al., 2019; Chen et al., 2021). Briefly, 12 ml of thioacidolysis reagent was made containing 10.5 ml of 1,4-dioxane, 0.3 ml of boron trifluoride diethyl etherate, and 1.2 ml of ethanethiol. Bisphenol E in 1,4-dioxane was added as internal standard with final concentration of 1.42 mg/ml. The reagent was vortexed, and 500 µl were added to 3 mg of lyophilized EL residues. Samples were then incubated at 100°C for 2 hours and vortexed every 45 minutes. After incubation, samples were cooled to room temperature. A total of 250 µl of the supernatants were transferred to 4 ml vials and 95 µl of saturated $NaHCO_3$ was added. Samples were dried down at 40°C under a slow flow of nitrogen gas. For derivatization, a pyridine:BSTFA (1:1) solution was made, and 100 µl were added to each sample. Samples were then incubated in an orbital shaker for 30 minutes at 37°C with gentle agitation. Finally, 50 µl of each sample were transferred to GC vials and sent for GC-MS analysis. GC/MS was performed on an Agilent 6890N GC with a 5973N series MS detector with a DB-5 ms capillary column (60 m × 0.25 mm × 0.25 µm film thickness). Mass spectra were recorded in electron impact mode (70 eV) with 60–650 m/z scanning range. The ions extracted were 239, 269, 299, and 347 m/z for the thioethylated coumaryl (H), coniferyl (G), and syringyl (S) monomers, and internal standard bisphenol E, respectively.

2.6 Chemical analysis of *p*-hydroxybenzoate

The amount of *p*-hydroxybenzoate (PB) was determined by an established method (Goacher et al., 2021) with slight modifications. Briefly, 1mL of 2M sodium hydroxide and 100µL of 1mg/mL *o*-coumaric acid (internal standard) was added to 20mg of extractive-free powder. Samples were incubated at 30°C for 24h and the reaction was subsequently terminated by the addition of 100µL of 72% sulfuric acid. Samples were then incubated on ice for 5 minutes. The supernatant was collected by centrifugation and filtered through a 0.45µm nylon syringe filter prior to high-performance liquid chromatography (HPLC) analysis.

Samples were analyzed by an Agilent 1200 series HPLC. For each sample, 10µL was injected onto a Symmetry C18 column (4.6 x 50mm, 5µm particle size) maintained at 35°C. Adequate peak resolution was achieved using 75:25 (v:v) ratio of eluent B (0.1% trifluoroacetic acid in 70:30 acetonitrile:methanol) in eluent A (0.1% triflouroacetic acid in water) at a flow rate of 0.4mL/min. Spectra were integrated at the UV maxima of 255nm and a five-point calibration curve was used for quantification. The PB measurement obtained by HPLC was normalized by lignin content as determined by the Klason lignin method for comparison to HSQC NMR results.

3 Results

Careful consideration was taken when selecting the sampling locations on each wood disc. One specific concern was radial variation. It is well documented that wood structure exhibits radial variation between the pith and the bark (Lachenbruch et al., 2011). Therefore, each sample was collected at a consistent radius (between approximately 7.6cm and 10.2cm) from the center of the pith to mitigate radial differences. A total of four *Septoria* infected discs were selected for analysis, as displayed in Figure 1. Of these, two genotypes (13127 and BESC-335) exhibited more severe

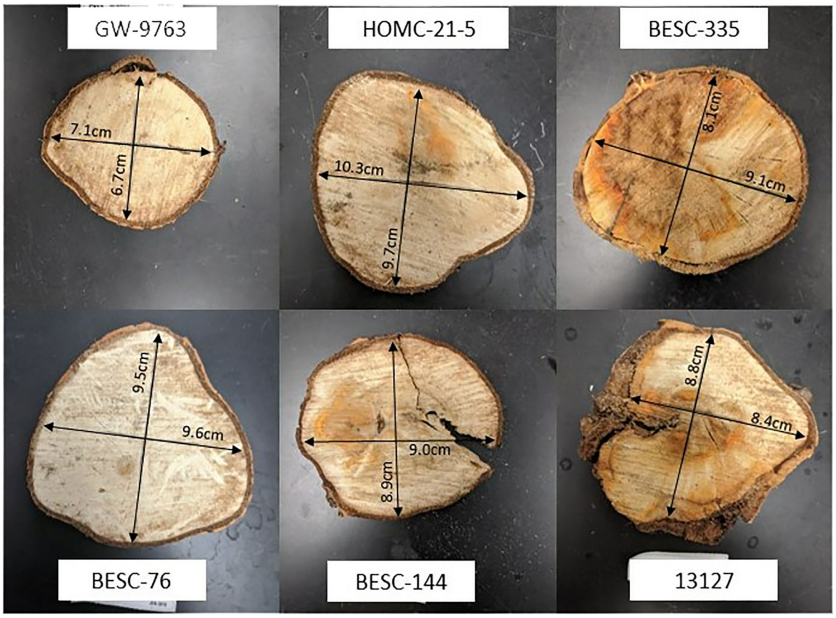

FIGURE 1
Wood discs from six lines were selected for analysis. The wood discs from four lines exhibiting signs of *Septoria* infection are 13127 (bottom right), HOMC-21-5 (top middle), BESC-144 (bottom middle), and BESC-335 (top right). Wood discs from lines GW-9763 (top left) and BESC-76 (bottom left), exhibiting no signs of *Septoria* infection, were utilized as controls.

signs of infection, covering an estimated 50-75% of the observable surface area. The other two samples (HOMC-21-5 andBESC-144) exhibited less severe signs of infection, with spots covering an estimated 25% or less of the surface area.

3.1 FTIR and PCA

FTIR analysis of extracted biomass was measured in the range of 4000-600 cm^{-1}. All samples were run in triplicate, and the three spectra were averaged to account for variability. The averaged spectra were baseline corrected and normalized around the 1505 cm^{-1} peak. Figure 2 displays spectra, pooled by region, for the fingerprint region of 1800-600 cm^{-}. The average values are represented by the solid lines, with the standard deviations represented by the surrounded bands of the same color. Peak assignments were made according to the literature and are summarized in Table 1 (Xu et al., 2005; Kline et al., 2010; Zhou et al., 2011; Akinosho et al., 2017; Shi et al., 2019; Yang et al., 2020). Several peaks typically associated with biomass and lignin are observed in this region. Notably, the large band at 1028 cm^{-1} is associated with C-O stretching vibrations from primary alcohols. Another band associated with the C=O stretching in hemicellulose (xylan) was also observed at 1735 cm^{-1}. Peaks around 1158 cm^{-1} and 897 cm^{-1} were observed, corresponding to the C-O-C vibrations of ester groups and C-H deformations of cellulose, respectively. Bands characteristic of the aromatic skeletal vibrations of lignin at 1505 cm^{-1} and 1594 cm^{-1} were also observed. Additionally, a peak at 1325 cm^{-1}, associated with syringyl ring breathing with a CO stretching, was observed in all samples. Changes in the peak intensity between healthy, reaction zone, and infected regions can provide insight to the effects of fungal degradation. As summarized in Table 2, there were several changes in the intensity ratios between the various regions. Compared to the healthy region, the reaction zone and infected regions exhibited a general increase in the 1594cm^{-1} intensity, indicating an increase in lignin content. There were also decreases in the 1157cm^{-1} peak from the healthy to reaction zone and infected regions, suggesting differences in *p*-hydroxybenzoate content. Both the 1325cm^{-1} and 1235cm^{-1} peaks also exhibited changes in intensities between the various regions. The ratio of these two peaks was correlated with the NMR S/G ratio (CC=0.54), indicating changes in the S/G ratio consistent with NMR measurements.

The spectral information from the fingerprint region of 1800-600 cm^{-1} was considered for the PCA. The resulting PC1 and PC2 explained 92.6% and 3.4% of the variation, respectively. Subsequent PCs accounted for less than 2% of the variation each. PC loadings were examined to determine which bands contributed to each principal component. For PC1, the band around 1028cm^{-1} was determined to be most significant contributor. This band has been associated with various properties of biomass and lignin, such as the C-O-C bonds in β-O-4 aryl ether linkages and other C-O bonds linked to primary and secondary alcohols. The peak around 1110 cm^{-1}, associated with the C-H deformation of S units, also contributed to PC1. Loading analysis for PC2 revealed that bands around 1640 cm^{-1} and 1735 cm^{-1} contributed most significantly to this principal component. These bands are associated with C=O stretching in lignin and xylan, respectively. The PCA output including eigenvalues, loadings, and scores are provided in the Supplementary Material.

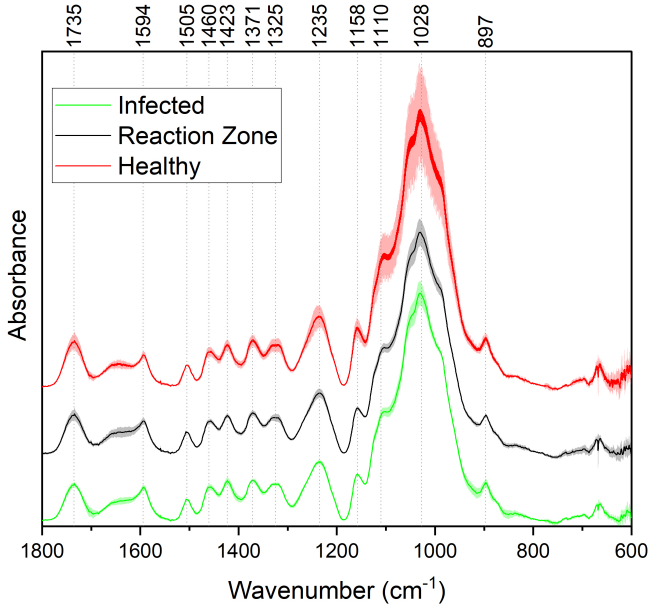

FIGURE 2
FTIR absorbance spectra of healthy (red), reaction zone (black), and infected (green) extracted biomass. For each spectrum, each of the different regions (healthy, reaction zone, infected) was pooled across the four genotypes. For each region across the four genotypes, the average values (N=4) are plotted as a solid line and the standard deviation is represented by the associated shaded area.

3.2 HSQC NMR

Each *Populus* sample was subjected to enzymatic hydrolysis, and 2D HSQC NMR was employed to analyze the resulting enzyme lignin fraction to examine lignin structure and identify differences between healthy and infected region. The aromatic region of the HSQC spectra for the healthy and infected region for each line is shown in Figure 3.

All spectra indicated the presence of the expected aromatic syringyl (S), guaiacyl (G), and p-hydroxyphenyl (H) units, as observed in Figure 3. The S units exhibited a strong $S_{2,6}$ correlation at δ_C/δ_H 103.8/6.70 ppm. Correlations associated with G units were observed at δ_C/δ_H 111.0/6.98 ppm (G_2), 115.1/6.72, 6.98 ppm (G_5), and 119.1/6.80 ppm (G_6). The $H_{2/6}$ peak was also observed at 128.2/7.17 ppm. Other correlations observed in the aromatic region include *p*-hydroxybenzoate ($PB_{2/6}$) at δ_C/δ_H

TABLE 1 Assignment of peaks in the FTIR spectra.

Observed Peak (cm^{-1})	Peak Assignment	Reference
1735	C=O stretching in lignin and hemicellulose	(Yang et al., 2020)
1594	Aromatic skeletal vibrations and C=O stretching in lignin	(Xu et al., 2005; Zhou et al., 2011; Yang et al., 2020)
1505	Aromatic C=C skeletal vibrations in lignin	(Xu et al., 2005; Zhou et al., 2011; Shi et al., 2019; Yang et al., 2020)
1460	C-H bending of methyl and methylene groups	(Kline et al., 2010; Zhou et al., 2011; Shi et al., 2019; Yang et al., 2020)
1423	C-H deformation, CH_2 bending vibration, carboxyl group stretching	(Xu et al., 2005; Kline et al., 2010; Zhou et al., 2011; Yang et al., 2020)
1371	C-H bending, stretching	(Shi et al., 2019)
1325	C=O stretching of syringyl units	(Kline et al., 2010; Zhou et al., 2011; Akinosho et al., 2017; Shi et al., 2019; Yang et al., 2020)
1235	C-C, C-O, and C=O stretching of guaiacyl unit	(Zhou et al., 2011; Akinosho et al., 2017; Yang et al., 2020)
1158	C-O stretching of ester group	(Xu et al., 2005; Kline et al., 2010; Shi et al., 2019)
1110	Aromatic C-H deformation of syringyl units	(Kline et al., 2010; Yang et al., 2020)
1028	C-O stretching of primary alcohols	(Kline et al., 2010; Shi et al., 2019; Yang et al., 2020)
897	C-H deformation vibration of cellulose	(Kline et al., 2010)

10.3389/fpls.2023.1089011

TABLE 2 The ratios of peak intensities between healthy and reaction zone/infected regions are compared to indicate changes to the cell wall upon pathogen infection.

Genotype	Region	Wavelength Ratio Compared to Healthy							
		1735 cm^{-1}	1594 cm^{-1}	1370 cm^{-1}	1325 cm^{-1}	1235 cm^{-1}	1157 cm^{-1}	1120 cm^{-1}	897 cm^{-1}
13127	Reaction Zone	0.95	1.06	0.98	1.00	0.98	0.93	0.96	0.97
	Septoria	1.05	1.12	1.04	1.05	1.06	0.98	1.07	1.01
HOMC-21-5	Reaction Zone	1.02	1.00	0.87	0.83	0.97	0.80	0.88	0.79
	Septoria	0.89	0.98	0.84	0.85	0.86	0.78	0.81	0.84
BESC-144	Reaction Zone	0.72	1.08	0.77	0.77	0.77	0.71	0.73	0.69
	Septoria	0.74	1.17	0.76	0.82	0.79	0.72	0.81	0.58
BESC-335	Reaction Zone	0.83	1.03	0.90	0.89	0.76	0.70	0.74	0.74
	Septoria	0.66	1.00	0.87	0.83	0.71	0.73	0.74	0.76

130.4/7.62 ppm and cinnamyl alcohol (I_α) at δ_C/δ_H 128.3/6.45 ppm. All spectra also exhibited peaks in the aliphatic region associated with β-O-4, β-5, β-β, and spirodienone interunit linkages. Relative abundance of each lignin structural feature is summarized in Table 3. Samples were independently analyzed by thioacidolysis for lignin composition. The ratio of S units to G units (S/G ratio) determined by thioacidolysis and HSQC NMR are highly correlated (Pearson correlated coefficient = 0.63; *p*-value < 0.01), thereby validating the S/G ratio measurements. The relative content of H units as determined by thioacidolysis and NMR were also compared. The H unit content exhibited poor correlation between the two methods (Pearson correlation coefficient = -0.1; *p*-value = 0.7). It has previously been shown that the HSQC NMR signal for $H_{2/6}$ can be overlapped by various proteins, leading to overestimation of H unit content (Kim et al., 2017). We expect this to be the case here. Therefore, careful consideration was given to results depending on the interpretation of H unit content. Thioacidolysis results are provided in the Supplementary Material.

Similarly, NMR may overestimate PB since it exists as a terminal unit. Therefore, the PB content of a subset of samples was determined *via* alkaline hydrolysis and HPLC. Due to material availability, not all samples were analyzed. However, the two samples with the highest PB content as measured by NMR (HOMC-21-5 infected, 8.22%; BESC-335 healthy, 6.42%) were included for this analysis. The PB content of each sample was normalized by its associated Klason lignin content. While HPLC measured a lower absolute value of PB (0.73%-1.44%) than NMR (1.61%-8.22%), the two measurements were highly correlated (R^2 = 0.71; *p*-value=0.002). The alkaline hydrolysis method also identified samples HOMC-21-5 infected and BESC-335 healthy as having elevated PB content (1.44% and 1.22%, respectively). To further validate this measurement, a sample that has previously been utilized as an internal reference (denoted as BESC standard poplar (Bhagia et al., 2016)), was also included in this analysis. This sample was run in duplicate *via* HPLC and in triplicate *via* HSQC NMR. The PB content of this sample was measured to be 2.13% ± 0.20% by HPLC and 16.27% ± 0.36% by HSQC NMR. This point fits the trendline established by the ten samples from this study that were analyzed, providing greater confidence of the correlation between the two measurements. Additional information regarding this comparison can be found in thesupplemental material (Figure S3, Table S2).

To explore potential changes in cell wall polysaccharides, the healthy, reaction zone, and infected regions of sample BESC-335 were subjected to whole cell wall (WCW) HSQC NMR by directly dissolving extractive free, ball milled biomass in a DMSO-d_6/HMPA-d_{18} (4:1) solvent system. Resulting spectra are included as a figure in the supplemental material (Figure S6) In the non-anomeric region (δ_C/δ_H 50-90/2-6) several cellulose signals were observed, including internal cellulose units (CI_4, CI_5, CI_6). Additionally, the non-reducing ends (CNR_3, CNR_5) of cellulose were identified. The non-anomeric region also contained many xylan related signals, such as xylan internal units (XI_2, XI_4, XI_5), reducing ends ($XR\alpha_4$, $XR\beta_4$), and non-reducing ends (XNR_2). Hardwoods contain acylated xylan, and associated acetylated xylan signals (2-*O*-Ac-β-D -Xyl, 3-*O*-Ac-β-D-Xyl) were also observed. In the anomeric (δ_C/δ_H 90-105/3.5-6) region, the signal for internal cellulose [(1→4)-β-D-Glc*p*] was observed, though the signal for the cellulose non-reducing end [(1→4)-β-D-Glc*p* (NR)] was generally better resolved. The signal associated with internal xylan units [(1→4)-β-D-Xyl*p*] was also prominent. 4-O-methyl-α-D-glucuronic acid (4-O-MeGlcA) was readily observed in the reaction zone and infected regions. This signal was present in the healthy region, though at levels very close to background. In summary, while some differences between the different

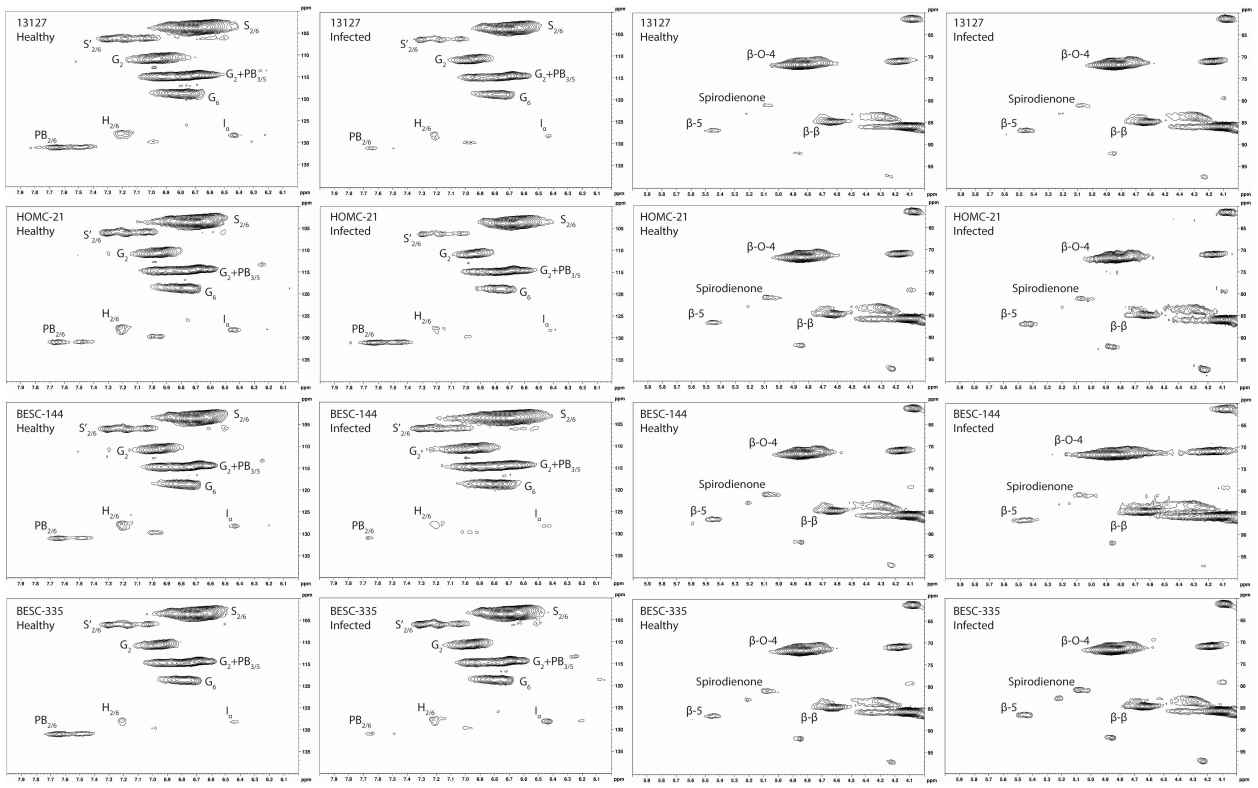

FIGURE 3
Aromatic and aliphatic region plots of the HSQC NMR spectra of the isolated lignin from each of the four analyzed lines. The first column contains the aromatic region of the healthy region from each sample. The second column contains the aromatic region of the infected region. The third column contains the aliphatic region of the healthy region. The fourth column contains the aliphatic region of the infected region. The HSQC NMR spectra of the healthy control sample GW-9763 is available in the supplementary material (Figure S3) for comparison.

regions were observed, the healthy, reaction zone, and infected regions appear to largely contain similar cellulose and hemicellulose structures.

3.3 Klason lignin analysis

The Klason lignin content the health, reaction zone, and infected regions of each sample was determined gravimetrically after two-step acid hydrolysis (Sluiter et al., 2008). As depicted in Figure 4, the lignin content was generally elevated in the reaction zone and/or infected regions compared to the healthy region. Both genotypes 13127 and BESC-144 exhibited consistent increases in lignin content from the healthy to infected regions. The lignin content of genotype 13127 increased from 27.5% (± 0.9%) in the healthy region to 31.3% (± 2.7%) and 32.8% (± 3.9%) in the reaction zone and infected regions, respectively. Similarly, the lignin content of genotype BESC-144 was measured to be 21.0% (± 0.6%) in the healthy region, 24.4% (± 1.8%) in the reaction zone region, and 27.5% (± 2.7%) in the infected region. BESC-335 also exhibited higher lignin content around the infection site (25.6% ± 1.7%) and reaction zone region (26.4% ± 0.5%) than the healthy region, which measured 21.0% (± 0.4%) lignin. While the infected region HOMC-21-5 exhibited lignin content (21.4% ± 1.6%) similar to the healthy region (19.1% ± 3.1%), the associated reaction zone region was measured to have a much higher lignin content of 24.9% (± 0.2%).

4 Discussion

4.1 FTIR and PCA

FTIR has been widely utilized as a non-destructive method of rapidly analyzing biomass properties, and the assignments of spectra peaks are well documented. Perhaps the most significant finding is the apparent S/G ratio agreement between FTIR and NMR. The ratio of the 1325cm^{-1} and 1235cm^{-1} peaks from the FTIR spectra has previously been used as a predictor for the S/G ratio (Kline et al., 2010). The ratio of these peaks across all samples were found to be correlated with the NMR S/G ratio (Table 4), supporting the relative S/G ratio measurements.

While FTIR is a convenient analytical technique, trends and differences between samples can often be difficult to elucidate. Therefore, principal component analysis (PCA) was utilized to extract additional information from the spectra. PCA is a valuable dimension reduction technique that emphasizes differences in samples based on spectral variation and has been used extensively for analyzing biomass and lignin (Xu et al., 2013). The resulting score plot (available in the supplemental material as Figure S7)

10.3389/fpls.2023.1089011

TABLE 3 Semi-quantitative results from integration of the HSQC NMR spectra.

Sample	Status	S	G	H	PB	S/G	β-O-4	β-5	β-β	Spirodienone
13127	Healthy	67.4	31.5	1.11	4.80	2.14	58.8	3.56	7.57	1.30
	Reaction Zone	67.7	31.3	1.03	2.01	2.16	60.1	3.19	8.51	1.34
	Infected	68.2	29.9	1.95	2.96	2.28	57.9	3.18	8.14	1.37
HOMC-21-5	Healthy	70.4	28.1	1.52	3.69	2.50	60.4	2.73	7.46	1.64
	Reaction Zone	69.7	29.6	1.72	2.35	2.35	62.7	2.15	7.78	0.81
	Infected	69.1	29.1	1.81	8.22	2.38	57.2	2.53	5.70	0.85
BESC-144	Healthy	68.5	29.0	2.55	4.26	2.37	56.9	3.02	7.52	1.66
	Reaction Zone	67.7	30.0	2.36	3.62	2.26	64.7	3.18	8.11	1.56
	Infected	69.4	29.4	1.18	1.98	2.36	61.3	2.87	8.08	1.28
BESC-335	Healthy	70.5	27.6	1.84	6.42	2.55	58.5	3.02	8.20	1.57
	Reaction Zone	71.1	27.6	1.35	3.94	2.58	58.0	2.48	7.81	1.47
	Infected	71.4	26.6	1.93	1.74	2.68	58.0	2.75	8.49	1.63

Signals used for volume integration are as follows: δ_C/δ_H 103.8/6.70 ppm for $S_{2/6}$, δ_C/δ_H 111.0/6.98 ppm for G_2, δ_C/δ_H 128.2/7.17 ppm for $H_{2/6}$, δ_C/δ_H 130.4/7.62 ppm for $PB_{2/6}$, δ_C/δ_H 128.3/6.45 ppm for I_α, δ_C/δ_H 71.8/4.86 for β-O-4, δ_C/δ_H 86.8/5.46 for β-5, δ_C/δ_H 84.8/4.65 for β-β, and δ_C/δ_H 81.2/5.07 for spirodienone. Results are presented relative to an S+G+H basis.

indicates that reaction zone (black) and infected (green) regions are quite similar. Additionally, PCA does a reasonable job at distinguishing the healthy region (red) from the reaction zone and infected regions, even though the healthy region of HOMC-21-5 falls just inside the 95% confidence interval (CI) of the reaction zone and infected regions. The exception is sample 13127, where the PCA identifies the healthy region to be more characteristically similar to reaction zone and infected region samples. These results suggest that sample 13127 may exhibit a cell wall structure similar to *Septoria* infection that are not immediately visible. This is supported by the Klason lignin measurements, as the healthy region of 13127 has significantly higher lignin content than the healthy region from HOMC-21-5, BESC-144, and BESC-335 (Figure 4). These FTIR and PCA results confirm that there are clear changes to cell wall structure induced by *Septoria* infection.

4.2 HSQC NMR

Changes in the S/G were observed between the healthy and infected region of the more severely infected samples. Genotype 13127 exhibited differences in S/G ratios, measuring 2.14 in the healthy region but increased to 2.43 in the infected region. The S/G ratio also increased across region condition in genotype BESC-335, measuring 2.55, 2.58, and 2.68 in the healthy, reaction zone, and infected regions, respectively. This would be consistent with the

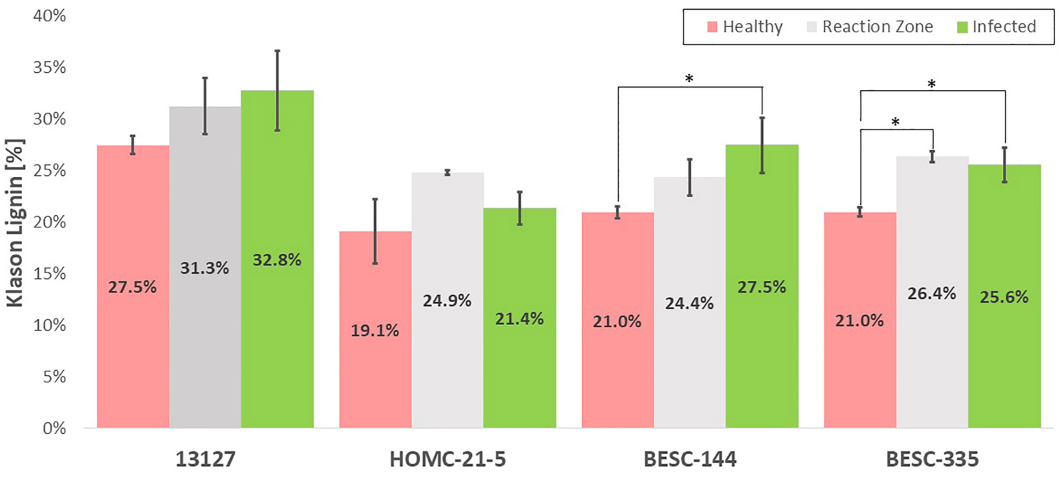

FIGURE 4
Klason lignin content of the healthy (red), reaction zone (gray), and infected (green) region of each genotype as determined by two-step acid hydrolysis. One stars (*) associated with reaction zone or infected regions indicate a statistically significant difference (p-value < 0.05) compared to the health region of the same genotype. A comparison with healthy control sample GW-9763 is available in the supplementary material (Figure S4) for comparison.

TABLE 4 The S/G ratio measured by FTIR, NMR, and HSQC NMR are summarized.

Genotype	Region	S/G ratio		
		FTIR	NMR	Thioacidolysis
13127	Healthy	0.58	2.14	1.91
	Reaction Zone	0.59	2.16	1.99
	Septoria	0.57	2.28	1.82
HOMC-21-5	Healthy	0.63	2.50	1.97
	Reaction Zone	0.53	2.35	2.03
	Septoria	0.62	2.38	1.93
BESC-144	Healthy	0.63	2.37	2.01
	Reaction Zone	0.63	2.26	1.84
	Septoria	0.66	2.36	1.83
BESC-335	Healthy	0.58	2.55	–
	Reaction Zone	0.67	2.58	1.99
	Septoria	0.68	2.68	2.15

The S/G ratio measured by HSQC NMR are correlated with FTIR and thioacidolysis as indicated by associated Pearson correlation coefficients of 0.54 and 0.62, respectively.

observed upregulation caffeate O-methyltransferase (COMT) due to *Septoria* infection (Foster et al., 2015). COMT is involved in the methylation of monolignols, and its upregulation would increase the ratio of S lignin (Do et al., 2007). However, the samples exhibiting lower severity of infection did not exhibit this trend. For the HOMC-21-5 genotype, the S/G ratio was higher in the reaction zone region (2.83) than the healthy (2.50) or infected (2.38) regions. The second low severity genotype BESC-144, exhibited a similar S/G ratio in the healthy (2.37) and infected (2.36) region, but a decreased S/G ratio (2.26) in the reaction zone region. All samples exhibited relatively low and consistent amounts of spirodienone (1.38 ± 0.26) and β-5 (2.89 ± 0.38) linkages. As expected, the most abundant interunit linkage in all samples was the β-O-4 aryl ether linkage. The variation of β-O-4 abundance was slightly more variable (σ=3.01) in the low severity genotypes (HOMC-21-5, BESC-144) than in the high severity (σ=0.86) genotypes (13127, BESC-335). The β-β and spirodienone linkages exhibited a similar trend of higher variability in the low severity genotypes. It has historically been demonstrated that β-O-4 content exhibits a strong positive correlation to the S/G ratio (Yoo et al., 2018), due in part to the propensity of S units to form this linkage. However, the four *Septoria* infected genotypes samples did not conform to this trend. Additionally, the S/G ratio was not correlated with either the β-β or spirodienone linkages. This is surprising, as both of these linkages have been shown to correlate with syringl unit content (Stewart et al., 2009). The one trend that was observed across these twelve samples was the negative correlation between the S/G ratio on the β-5 content (p-value < 0.001). This correlation is expected, as G lignin can undergo coupling at the 5-position. A lack of correlation between the S/G ratio and all linkage types was observed in the control samples. This could be contributed to relatively low abundance and limited variation in some of the linkage types. For instance, across the twelve samples taken from the infected wood discs, spirodienone linkages ranged from 0.85-1.66% and β-5 linkages ranged from 2.19-3.56% abundance. Additionally, there was generally a neutral or negative correlation between the β-5 and β-β linkages, suggesting there may be a trade-off between the abundance of condensed C-C linkages.

The PB content varied widely among the four genotypes and the region type, though the PB content was generally lower in reaction zone and/or infected region than in healthy region. This reduced PB content in the reaction zone is consistent with observed response to wounding (Frankenstein et al., 2006). In genotype BESC-144, the PB content of the infected region was approximately 50% lower than that of the healthy region. Similarly, BESC-335 showed a reduction in PB content from 6.42% in the healthy region to 1.74% in the infected region. The PB content of genotype 13127 was slightly higher in the infected region (2.96%) than the reaction zone region (2.01%), though both were lower than the healthy region (4.80%). However, HOMC-21-5 exhibited the opposite trend. While HOMC-21-5 measured a PB content of 3.69% in the healthy region and 1.76% in the reaction zone region, the infected region exhibited a PB content of 8.22%. Many aspects regarding the biosynthesis and function of PB remain a mystery. As PB primarily acylates the γ-position of S units, and it has long been hypothesized that PB promotes the formation of S-rich lignin. However, there was no correlation between S and PB abundance (p-value = 0.56). A recent study has also called this hypothesis into question (Mottiar and Mansfield, 2022). There is some evidence that PB production is associated with fungal infections (Schnitzler and Seitz, 1989), though that contradicts the trend observed here. Frankenstein et al. reported that wounding lead to decreased p-hydroxybenzoic acid content (Frankenstein et al., 2006), which is more consistent with these observations. While there appears to be appreciable PB variability among the twelve samples, based on the current knowledge (or

lack thereof) of PB biosynthesis, it is difficult to determine if variation in levels is causative or merely correlative.

4.3 Klason lignin analysis

The expected general trend of increased lignification was observed in each of the four infected *Populus* genotypes in this study by analyzing the Klason lignin content of the healthy, reaction zone, and infected region of each genotype. It has been previously shown that *Populus* forms a lignin rich periderm around the site of *Septoria* infection for containment. This is consistent with the trend observed in Figure 4, with the reaction zone and/or infected regions generally having a higher Klason lignin content than the healthy region. The most pronounced difference in Klason lignin content was observed in BESC-335, which exhibited the most severe and consistent degree of infection (Figure 1). In this sample, both the reaction zone and infected regions exhibited significantly higher lignin content (p-value < 0.05) than the healthy region. Similarly, sample BESC-144 exhibited higher lignin content in the infected region. These results signify the recruitment of lignin (or possibly lignin-like phenolics) toward a periderm to contain the fungal infection. Genotype 13127 exhibited a general increase in lignin content from healthy to reaction zone to infected region. However, this increase was determined to not be statistically significant. This is primarily driven by the high variability of the infected region (σ=3.9%) compared to the healthy region (σ=0.9%). Genotype HOMC-21-5 displayed a trend slightly different from the other three lines. The reaction zone had the highest lignin content, while the healthy and infected regions exhibited lower and similar lignin content. Increased lignin content was also an observed response from wounding of *Populus* (Frankenstein et al., 2006). From Figure 1, it appears that HOMC-21-5 had the lowest severity of infection. Poplar species exhibit various degrees of susceptibility toward *Septoria* infection. Several factors can influence the severity of *Septoria* infection. For instance, there may be pathogen interaction effects with certain *Populus* genotypes (Ward & Ostry, 2005). Additionally, environmental conditions at the time of infection can also influence severity (Ward & Ostry, 2005). These factors may influence recruitment of lignin to form a periderm to contain an infection, resulting in higher lignin content at the reaction zone between the healthy and infection region. Still, this result contrasts the trends of the other three lines, where the infected regions exhibited notably higher lignin content than the healthy regions. However, these results align with the NMR results, as the reaction zone sample exhibited both the highest S/G ratio (2.83) and the highest lignin content (24.87%) of the HOMC-21-5 line. Likewise, the healthy and infected regions had lower S/G ratios (2.50, 2.38), corresponding to their lower lignin content (19.12%, 21.36%). The area of the infected site could explain this outcome. HOMC-21-5 exhibited a less severe degree of infection which may have impacted the ability to collect the proper region. Additionally, the infection may not have been consistent throughout the thickness of the wood discs. It is therefore possible that healthy region may have been present in the infected material of HOMC-21-5 which would have an impact on the measurement. It is known that *Populus* will develop necrophylactic periderm (NP) layers around the sites of fungal infections to prevent the pathogen's spread (Qin and LeBoldus, 2014). These NP layers are created by depositing lignin and lignin-like phenolic compounds such as suberin (Mullick, 1977). A study of poplar confirmed upregulation of several lignin biosynthesis genes after being infected with *Sphaerulina*, including CoA 3-O-methyltransferase (CCoAMT), cinnamoyl CoA reductase, (CCR), and cinnamyl alcohol dehydrogenase (CAD) (Foster et al., 2015). As such, the lignin content of infected regions is expected to be higher than in the healthy regions. However, to our knowledge, increased lignification due to *Septoria* infection in poplar has not been analyzed by quantitative methods.

4.4 Conclusion

The fungus *Septoria musiva* poses a serious threat to the productivity of economically important poplar. While various studies have explored short-term changes in the days following inoculation, the long-term phenotypic changes of lignin in field-grown, naturally infected poplar stems from *Septoria* canker have not been previously reported. FTIR spectroscopy indicated there were there were likely changes to lignin content and/or structure between healthy and reaction zone/infected region, though trends were not consistent across all samples. Subsequent PCA of whole cell wall biomass samples identified that reaction zone and infected regions are similar, and can be distinguished from healthy samples. Likewise, two samples were found to have significantly higher lignin content in the infected region, and one of these also had significantly higher lignin content in the reaction zone. HSQC NMR examined differences in lignin structure. While differences in lignin structure were observed, there did not appear to be a uniform trend between region types. Two samples with elevated PB content were detected by NMR, which was validated by alkaline hydrolysis and HPLC. Whole cell wall HSQC NMR analysis of one sample suggest that polysaccharide structures remain similar across region types Additionally, the Klason lignin content trended well with the S/G ratio. These results corroborate the observations of previous studies, which noted differentially expressed lignin biosynthesis or increased lignification *via* staining after *Septoria* inoculation. A better understanding of lignin response to fungal infections can lead to improved resilience and higher biomass yield of *Populus*, which is critical for the successful implementation of biofuel production.

Notice

energy.gov/downloads/doe-public-access-plan). The views and opinions of the authors expressed herein do not necessarily state or reflect those of the United States Government or any agency thereof. Neither the United States Government nor any agency thereof, nor any of their employees, makes any warranty, expressed or implied, or assumes any legal liability or responsibility for the accuracy, completeness, or usefulness of any information, apparatus, product, or process disclosed, or represents that its use would not infringe privately owned rights.

Data availability statement

The original contributions presented in the study are included in the article/Supplementary Material. Further inquiries can be directed to the corresponding author.

Author contributions

AR and WM conceptualized the study. WM and J-GC established and maintained the field site. NB and YP prepared and analyzed the samples. RW and JB conducted the lignin analyses by GS-MS. NB drafted the manuscript. All authors contributed to the article and approved the submitted version.

Funding

Funding provided by The Center for Bioenergy Innovation, a U.S. Department of Energy Research Center supported by the Office of Biological and Environmental Research in the DOE Office of Science.

Acknowledgments

This manuscript has been authored by UT-Battelle, LLC under Contract No. DE-AC05-00OR22725 with the U.S. Department of Energy. The United States Government retains and the publisher, by accepting the article for publication, acknowledges that the United States Government retains a non-exclusive, paid-up, irrevocable, world-wide license to publish or reproduce the published form of this manuscript, or allow others to do so, for United States Government purposes. The Department of Energy will provide public access to these results of federally sponsored research in accordance with the DOE Public Access Plan (http://energy.gov/downloads/doe-public-access-plan). We thank Dr. Zhentian Lei from the University of Missouri Metabolomics Center for support with mass spectrometry analyses.

Conflict of interest

The authors declare that the research was conducted in the absence of any commercial or financial relationships that could be construed as a potential conflict of interest.

Publisher's note

All claims expressed in this article are solely those of the authors and do not necessarily represent those of their affiliated organizations, or those of the publisher, the editors and the reviewers. Any product that may be evaluated in this article, or claim that may be made by its manufacturer, is not guaranteed or endorsed by the publisher.

Author disclaimer

The views and opinions of the authors expressed herein do not necessarily state or reflect those of the United States Government or any agency thereof. Neither the United States Government nor any agency thereof, nor any of their employees, makes any warranty, expressed or implied, or assumes any legal liability or responsibility for the accuracy, completeness, or usefulness of any information, apparatus, product, or process disclosed, or represents that its use would not infringe privately owned rights.

Supplementary material

The Supplementary Material for this article can be found online at: https://www.frontiersin.org/articles/10.3389/fpls.2023.1089011/full#supplementary-material

References

Akinosho, H. O., Yoo, C. G., Dumitrache, A., Natzke, J., Muchero, W., and Brown, S. D. (2017). Elucidating the structural changes to populus lignin during consolidated bioprocessing with clostridium thermocellum. *Engineering* 5 (9), 7486–7491. doi: 10.1021/acssuschemeng.7b01203

Barros, J., Escamilla-Trevino, L., Song, L., Rao, X., Serrani-Yarce, J. C., Palacios, M. D., et al. (2019). 4-coumarate 3-hydroxylase in the lignin biosynthesis pathway is a cytosolic ascorbate peroxidase. *J. N. C.* 10 (1), 1994. doi: 10.1038/s41467-019-10082-7

Bhagia, S., Muchero, W., Kumar, R., Tuskan, G. A., and Wyman, C. E. (2016). Natural genetic variability reduces recalcitrance in poplar. *Biotechnol. Biofuels Bioprod.* 9 (1), 1–12. doi: 10.1186/s13068-016-0521-2

Bryant, N. D., Pu, Y., Tschaplinski, T. J., Tuskan, G. A., Muchero, W., Kalluri, U. C., et al. (2020). Transgenic poplar designed for biofuels. *Trends Plant Sci.* 25 (9), 881–896. doi: 10.1016/j.tplants.2020.03.008

Bucciarelli, B., Jung, H., Ostry, M., Anderson, N., and Vance, C. (1998). Wound response characteristics as related to phenylpropanoid enzyme activity and lignin deposition in resistant and susceptible populus tremuloides inoculated with entoleuca mammata (Hypoxylon mammatum). *Can. J. Bot.* 76 (7), 1282–1289. doi: 10.1139/b98-121

Cellerino, G. P. (1999). *Review of fungal diseases in poplar* Vol. AC492/E (Rome (FAO: Food and Agriculture Organization of The United Nations).

Chen, F., Zhuo, C., Xiao, X., Pendergast, T. H., and Devos, K. M. (2021). A rapid thioacidolysis method for biomass lignin composition and tricin analysis. *Biotechnol. Biofuels* 14 (1), 1–9. doi: 10.1186/s13068-020-01865-y

Chudy, R., Busby, G., Binkley, C., and Stanton, B. (2019). The economics of dedicated hybrid poplar biomass plantations in the western US. *Biomass Bioenergy* 124, 114–124. doi: 10.1016/j.biombioe.2019.03.010

Do, C.-T., Pollet, B., Thévenin, J., Sibout, R., Denoue, D., Barrière, Y., et al. (2007). Both caffeoyl coenzyme a 3-o-methyltransferase 1 and caffeic acid O-methyltransferase 1 are involved in redundant functions for lignin, flavonoids and sinapoyl malate biosynthesis in arabidopsis. *Planta* 226 (5), 1117–1129. doi: 10.1007/s00425-007-0558-3

Feau, N., Mottet, M.-J., Périnet, P., Hamelin, R. C., and Bernier, L. (2010). Recent advances related to poplar leaf spot and canker caused by septoria musiva: Minireview/ Minisynthèse. *Can. J. Plant Pathol.* 32 (2), 122–134. doi: 10.1080/07060661003740009

Foster, A. J., Pelletier, G., Tanguay, P., and Seguin, A. (2015). Transcriptome analysis of poplar during leaf spot infection with sphaerulina spp. *J. PloS One* 10 (9), e0138162. doi: 10.1371/journal.pone.0138162

Frankenstein, C., Schmitt, U., and Koch, G. (2006). Topochemical studies on modified lignin distribution in the xylem of poplar (Populus spp.) after wounding. *Ann. Bot.* 97 (2), 195–204. doi: 10.1093/aob/mcj030

Goacher, R. E., Mottiar, Y., and Mansfield, S. (2021). ToF-SIMS imaging reveals that p-hydroxybenzoate groups specifically decorate the lignin of fibres in the xylem of poplar and willow. *Holzforschung* 75 (5), 452–462. doi: 10.1515/hf-2020-0130

Kim, H., Padmakshan, D., Li, Y., Rencoret, J., Hatfield, R. D., and Ralph, J. J. B. (2017). Characterization and elimination of undesirable protein residues in plant cell wall materials for enhancing lignin analysis by solution-state nuclear magnetic resonance spectroscopy. *Biomacromolecules* 18 (12), 4184–4195. doi: 10.1021/ acs.biomac.7b01223

Kline, L. M., Hayes, D. G., Womac, A. R., and Labbé, N. J. B. (2010). Simplified determination of lignin content in hard and soft woods *via* uv-spectrophotometric analysis of biomass dissolved in ionic liquids. *BioResources* 5 (3), 1366–1383.

Lachenbruch, B., Moore, J. R., and Evans, R. (2011). "Radial variation in wood structure and function in woody plants, and hypotheses for its occurrence," in *Size- and age-related changes in tree structure and function. tree physiology*, vol. 4 . Eds. F. Meinzer, B. Lachenbruch and T. Dawson (Dordrecht: Springer). doi: 10.1007/978-94-007-1242-3_5

Mottiar, Y., and Mansfield, S. D. (2022). Lignin p-hydroxybenzoylation is negatively correlated with syringyl units in poplar. *Front. Plant Sci.* 13. doi: 10.3389/ fpls.2022.938083

Muchero, W., Sondreli, K. L., Chen, J.-G., Urbanowicz, B. R., Zhang, J., Singan, V., et al. (2018). Association mapping, transcriptomics, and transient expression identify candidate genes mediating plant–pathogen interactions in a tree. *Proc. Natl. Acad. Sci.* 115 (45), 11573–11578. doi: 10.1073/pnas.1804428115

Mullick, D. B. (1977). "The non-specific nature of defense in bark and wood during wounding, insect and pathogen attack," in *The structure, biosynthesis, and degradation of wood. recent advances in phytochemistry*, vol. 11 . Eds. F. A. Loewus and V. C. Runeckles (Boston, MA: Springer). doi: 10.1007/978-1-4615-8873-3_10

Ostry, M. E., McNabb, H. S., Jr. (1985). Susceptibility of populus species and hybrids to disease in the north central united states. *Plant Dis.* 69, 755–757. doi: 10.1094/PD-69-755

Ostry, M. E., Wilson, L. F., and Harold, S. Jr. (1989). *Impact and control of septoria musiva on hybrid poplars*. U.S. Department of Agriculture, Forest Service, North Central Forest Experiment Station. doi: 10.2737/NC-GTR-133

Qin, R., and LeBoldus, J. M. (2014). The infection biology of sphaerulina musiva: Clues to understanding a forest pathogen. *PloS One* 9 (7), e103477. doi: 10.1371/ journal.pone.0103477

Royle, D., and Ostry, M. (1995). Disease and pest control in the bioenergy crops poplar and willow. *Biomass Bioenergy* 9 (1-5), 69–79. doi: 10.1016/0961-9534(95) 00080-1

Sannigrahi, P., Ragauskas, A. J., and Tuskan, G. A. (2010). Poplar as a feedstock for biofuels: a review of compositional characteristics. *Biofuels Bioproducts Biorefining* 4 (2), 209–226. doi: 10.1002/bbb.206

Schnitzler, J.-P., and Seitz, H. U. (1989). Rapid responses of cultured carrot cells and protoplasts to an elicitor from the cell wall of pythium aphanidermatum (Edson) fitzp. *Zeitschrift für Naturforschung C* 44 (11-12), 1020–1028. doi: 10.1515/znc-1989-11-1223

Shi, Z., Xu, G., Deng, J., Dong, M., Murugadoss, V., and Liu, C. (2019). Structural characterization of lignin from d. sinicus by FTIR and NMR techniques. *Green Chem. Lett. Rev.* 12 (3), 235–243. doi: 10.1080/17518253.2019.1627428

Sluiter, A., Hames, B., Ruiz, R., Scarlata, C., Sluiter, J., Templeton, D., et al. (2008). Determination of structural carbohydrates and lignin in biomass. *Laboratory Analytical Procedure (LAP)* (Revised August 2012), Issue Date: 4/25/2008, NREL/TP-510-42618.

Søndreli, K., Keriö, S., Frost, K., Muchero, W., Chen, J.-G., Haiby, K., et al. (2020). Outbreak of septoria canker caused by sphaerulina musiva on populus trichocarpa in Eastern Oregon. *Plant Dis.* 104 (12), 3266–3266. doi: 10.1094/PDIS-03-20-0494-PDN

Stewart, J. J., Akiyama, T., Chapple, C., Ralph, J., and Mansfield, S. D. (2009). The effects on lignin structure of overexpression of ferulate 5-hydroxylase in hybrid Poplar1. *Plant Physiol.* 150 (2), 621–635. doi: 10.1104/pp.109.137059

Ward, K., and Ostry, M. (2005). Variation in septoria musiva and implications for disease resistance screening of poplars. *Plant Dis.* 89 (10), 1077–1082. doi: 10.1094/PD-89-1077

Xu, F., Sun, R.-C., Sun, J.-X., Liu, C.-F., He, B.-H., and Fan, J.-S. (2005). Determination of cell wall ferulic and p-coumaric acids in sugarcane bagasse. *Anal. Chim. Acta* 552 (1-2), 207–217. doi: 10.1016/j.aca.2005.07.037

Xu, F., Yu, J., Tesso, T., Dowell, F., and Wang, D. (2013). Qualitative and quantitative analysis of lignocellulosic biomass using infrared techniques: A mini-review. *Appl. Energy* 104, 801–, 809. doi: 10.1016/j.apenergy.2012.12.019

Yang, H., Yoo, C. G., Meng, X., Pu, Y., Muchero, W., Tuskan, G. A., et al. (2020). Structural changes of lignins in natural populus variants during different pretreatments. *Bioresour. Technol.* 295, 122240. doi: 10.1016/j.biortech.2019.122240

Yoo, C. G., Dumitrache, A., Muchero, W., Natzke, J., Akinosho, H., and Li, M. (2018). Significance of lignin S/G ratio in biomass recalcitrance of populus trichocarpa variants for bioethanol production. *ACS Sustain. Chem. Eng.* 6 (2), 2162–2168. doi: 10.1021/acssuschemeng.7b03586

Zhou, G., Taylor, G., and Polle, A. (2011). FTIR-ATR-based prediction and modelling of lignin and energy contents reveals independent intra-specific variation of these traits in bioenergy poplars. *Plant Methods* 7, 1–10. doi: 10.1186/1746-4811-7-9

Frontiers in
Plant Science

Cultivates the science of plant biology and its applications

The most cited plant science journal, which advances our understanding of plant biology for sustainable food security, functional ecosystems and human health.

Discover the latest Research Topics

See more →

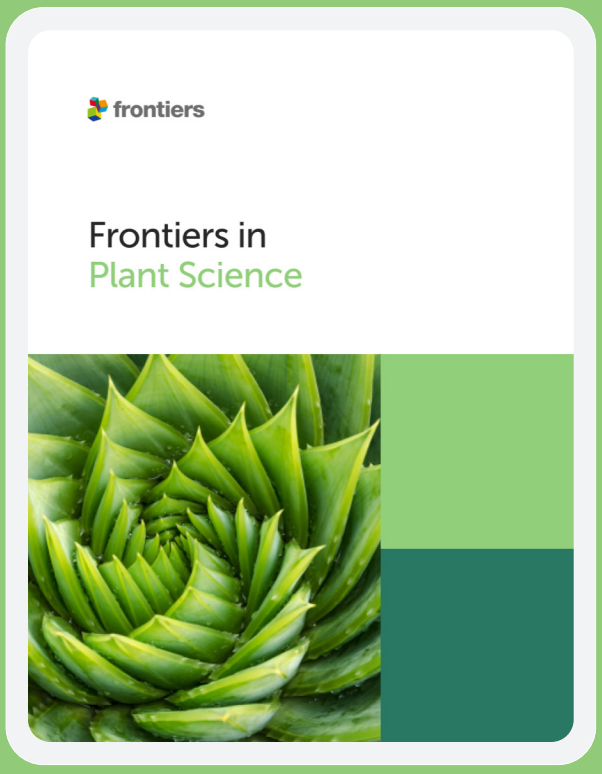

Frontiers

Avenue du Tribunal-Fédéral 34
1005 Lausanne, Switzerland
frontiersin.org

Contact us

+41 (0)21 510 17 00
frontiersin.org/about/contact